An NMR Study of Helium-3 Adsorbed on Hexagonal Boron Nitride

by
Thomas Philip Crane

A thesis submitted for the degree of
Doctor of Philosophy in the University of London

Royal Holloway University of London
1998

To my parents, Philip and Ann Crane

Acknowledgements

I would like to thank the people who have helped make this work possible. In particular I must thank my supervisor Brian Cowan, for his guidance and help − his particular approach to experimental physics has always been an inspiration to me. Thanks also go to the previous members of the research group for their friendship and inspiration; Tony Kent, Amer Husain, Laila Abou-El-Nasr and Mihail Fardis. I would like to thank the Physics Department technical support staff for their assistance, in particular Francis Greenough (liquid helium supply) and Alan Betts (Electronics Workshop). I must single out Alan Betts for special thanks − without his expertise and work in designing and building the digital based instrumentation used in this work it would not have been possible. I also thank Adrian Machiraju (Librarian) for help with on-line literature database surveys. I acknowledge use of College computing and London University supercomputing facilities. I am very grateful to my parents for their financial support.

Abstract

A Pulse-NMR study of helium-3 adsorbed on hexagonal boron-nitride (BN) powder has been performed. Structurally very similar to graphite, the exposed basal-planes present a very smooth, ideal adsorbing surface and lack its undesirable strong anisotropic diamagnetism. The relaxation times T_1 and T_2 of helium-3 have been measured as a function of coverage, temperature and frequency. A variety of two dimensional phases have been observed including: a fluid, commensurate solid, incommensurate solid plus a separate crystallite edge film. 2D melting in the incommensurate solid and an order-disorder transition in the commensurate solid have been observed. Evidence for a low temperature, low coverage fluid+commensurate solid coexistence which transforms to a single phase at higher temperatures plus a possible domain-wall phase at higher coverages has been identified.

Coupled magnetic relaxation between the helium-3 film and substrate boron-11 spins has been noted. Boron-11 relaxation times have been measured against coverage and temperature. Heteronuclear relaxation is particularly important in the commensurate phases where it can dominate homonuclear spin-lattice relaxation, providing a powerful new probe of the low coverage phases. Based on the detailed theory of coupled magnetic dipolar relaxation a model has been developed which quantitatively describes all the important features of the data many of which are unique to the BN/^{3}He system. Presented separately in chapter 8, it concludes the magnetic properties of registered helium-3 spins are dominated by $^{14}\text{N}\leftrightarrow{}^3\text{He}$ cross relaxation processes, mediated by the ^{14}N quadrupole splitting at $F_Q(^{14}\text{N})$ and driven by exchange motion in the film.

Using a computer for unattended, real-time experimental control has allowed substantial quantities of high quality relaxation data to be taken. Off-line, automated, numerical analysis of raw spin-echo and processed data has been extensively used. Modelling relaxation data with a stretched-exponential function, $h(t) = h(0)\exp(-t^a/T_{1,2})$ has provided a exceptionally sensitive indicator of physical changes in the film.

Table of Contents

List of Figures

List of Listings

List of Tables

Chapter 1
Introduction

1.1 Dimensionality

The subject of dimensionality has been of interest in physics for many years. Clearly we live in a three dimensional world. There is however considerable theoretical interest in systems with dimensionality other than 3. Cosmological theories suggest that the early universe had a large number of, typically eleven dimensions, of which all but three have shrunk to unobservable proportions. The notion of non-integer dimensionality, fractals is also of much interest. For the experimentalist creating a higher (than three) dimensional system in the laboratory is out of the question. So what of lower, ie. one or two dimensional systems? Quantum effects in 1D have been studied by confining electrons to channels cut is specially prepared slices of semiconductor. Many different types of quasi-2D systems including layered semiconductor devices, films of electrons over liquid helium and adsorbed systems have been devised and studied. This document is concerned with adsorbed systems, the others will not be considered further.

1.2 Adsorption

If a gas is allowed to come into contact with a solid or liquid surface there will be a greater concentration of gas atoms near the surface than in the volume interior due to the nett attractive potential of the surface [1]. For a small number of substances, the noble gases and a few low molecular weight non-polar gases such as CH_4 the forces of adsorption are much stronger than the adatom mutual attraction. The substrate forces then, serve only to confine the adatoms to the surface. Providing the temperature T is much lower than the energy of adsorption (E_a/k) the adatoms will largely be denied the degree of freedom in the perpendicular direction. If the surface is sufficiently smooth and fault-free the variation experienced by a mobile adatom in substrate binding potential will be low and it will move unhindered on the surface. Such an arrangement is a good approximation to an ideal 2D system. Unfortunately very few surfaces even come close to the above. One that does is graphite [2]. It has a layer structure in which the interlayer bonding is much weaker than intra-layer. This gives it its solid lubricant properties. Within the layer the carbon atoms have a hexagonal arrangement. The short intra-layer

lattice parameters keep the corrugation of the Van-der-Waals potential seen by the adatom small [3]. It is these planes when exposed that are preferred for adsorption. By heating Carbon-Black, a form of soot, to high temperatures (typically ~2000K) the adsorption surface becomes increasingly homogeneous as the ratio of exposed basal plane to *edge area* of the platelets increases [4]. The process is known as *graphitisation*. Unlike previous substrates Graphitised Carbon-Black showed steps in the vapour pressure isotherm as distinct layers of adsorbate built up [2,5]. Exfoliated graphite, a chemically modified form of the material in which some of the layers have been torn apart, show still sharper steps, as many as 7 [3], plus submonolayer features [6]. This is due to the very large basal plane area exposed by the process. Grafoil and Papyrex are commercially produced forms of exfoliated graphite.

1.3 Why Study 2D (Adsorbed Systems)?

The reduced dimensionality gives rise to striking differences between the behaviour of 3D and 2D systems. For example phenomena such as superfluidity seem to be suppressed by the reduced dimensionality [2]. By studying the dimensionally simpler 2D systems our understanding of the properties of matter in general should be enhanced. For example, by investigating monolayer helium films at low temperatures quantum mechanical effects such as intra-layer exchange can be observed without the complication of bulk inter-layer effects [7]. There is considerable similarity between the phase diagrams of 2D and 3D systems. Adsorbed films can display 2D analogues of conventional gases, liquids and solids as well as phases unique to 2D such as solids in registry with the underlying substrate [2]. It was not until the later highly homogeneous substrates were produced that 2D gases were observed. As a further attraction, a much wider range of adatom densities can be achieved in the 2D films. For example [3] to obtain a lattice spacing of 3.3Å (the monolayer density on graphite) in bulk helium-3 requires a pressure of 400bar. The question of long range crystalline order in reduced dimensions is of particularly fundamental interest [8]. It has been known for some time that true long range positional order cannot exist in 2D solids as it does in 3D [9,10]. Quasi long range order as indicated by the algebraic rather than exponential decay of the density-density correlation function does exist in 2D solids [11]. 3D solids melt with a first order phase transition due to their long range order. The nature of the melting transition in adsorbed films is the subject of much theoretical and experimental interest.

1.4 2D Melting

The KTHNY theory [11,12] describes the continuous phase transition seen when some 2D solids melt, in terms of a two stage process in which dislocation pairs in the 2D crystal unbind to leave a hexatic liquid crystal phase. The hexatic phase lacks the quasi long range positional order of its precursor but retains quasi long range order in nearest neighbour bond orientation. At higher temperatures the hexatic phase decays to an isotropic fluid in a continuous fashion. Hexagonal substrates such as graphite are believed to influence the hexatic phase by enhancing its orientational order and allowing it to persist into what would be the isotropic phase, effectively smearing out the second transition. Following is a summary of some of the experimental work performed with the noble gas/graphite systems.

1.5 Krypton on Graphite

Due to the low dimensional incompatibility (the mismatch between the lattice dimensions of the densest plane in the bulk solid and those of the adsorber) a larger number of phases have been resolved including a liquid, a commensurate solid, an incommensurate solid [13] and an intervening *re-entrant fluid* [11]. At one monolayer the solid is commensurate and melts via a lattice ordering type transition. At higher densities in the incommensurate solid melting is continuous possibly due to the effects of higher layers [11].

1.6 Argon on Graphite

Here, the dimensional incompatibility is significant (~8%). Originally it was believed to show a continuous melting transition. Later heat capacity data showed a sharp peak 47.2K and a broader one at 49.5K [14]. The sharp peak was interpreted as a weakly first order triple point melting broadened by finite-size effects or alternatively as the signature of KTHNY melting. In the latter case the broad peak was then attributed to the remnants of the substrate suppressed hexatic to isotropic transition. Later X-ray diffraction work in which the correlation length changed smoothly through melting, was taken to show the transition was continuous [15]. More X-ray diffraction work [16] showed that the solid Argon monolayer which was rotated ~3^{o} with respect to the graphite structure was still rotated by ~2^{o} in the melted fluid state − clearly indicating the ability of the substrate to maintain partial orientational order into the fluid phase. This rotational transformation may be connected with the heat capacity peak in reference **14**.

Recent 2D compressibility data from vapour pressure measurements [17] supports a KTHNY process describing melting as a 2-stage process in which the intermediate state has short ranged spatial order but solid-like properties.

1.7 Xenon on Graphite

In most of the solid region of the phase diagram melting is strongly first order. The dimensional incompatibility is ~−8%, ie. the Xe lattice structure is larger than that of graphite.

1.8 Helium on Graphite

Adsorbed films of both isotopes of helium have been studied on a wide variety of substrates [9,18,19]. Until the use of graphitised carbon black [5] and later exfoliated graphite such as Grafoil [6] the films displayed solid behaviour at all coverages due to substrate heterogeneity [19]. A simple phase diagram for the first layer of ^{3}He on Grafoil [9,20] is shown in figure 1.8.1. For ^{4}He it is very similar, differing mainly at lower coverages [21]. Most of the information for this phase diagram comes from heat capacity measurements performed by the University of Washington [18,22] and Caltech groups [19]. It can best be considered in terms of five regions based on coverage.

1.8.1 $X \leqslant 0.01$ (Very Low Coverage Regime)

At these coverages the film is believed to consist of solid patches formed at sites of preferential adsorption, for example where, the substrate is damaged or crystallites butt up against one another. The heat capacity possesses small peaks the low temperature side of which display T^2 behaviour [18,19] as expected for a 2D solid.

1.8.2 $0.1 < X < 0.5$ (2D Gas Phase)

The film displays 2D gas characteristics at these coverages [18,19,22]. An ideal classical 2D gas has a heat capacity $C/Nk = 1$ [18,19,22] independent of T. For $2\text{K} < T < 6\text{K}$ it was found that $C/Nk \sim 0.8$ at $X \sim 0.3$. The discrepancy is due to adatom interactions, successfully modelled by the second virial coefficient theory [19]. For $T > 6\text{K}$, the heat capacity rises due to thermal activation [19]. For $T < 2\text{K}$ the ^{3}He heat capacity falls off, becoming linear in T as expected for an ideal quantum (Fermi) gas [18,22,23]. After a small peak near 1K the ^{4}He heat capacity also falls off as expected for a quantum (Bose) gas. With falling density, $C/Nk \rightarrow 1$ in the $2\text{K} < T < 6\text{K}$ range as interactions become less

Figure 1.8.1, The Phase-Diagram for ^{3}He on Grafoil.

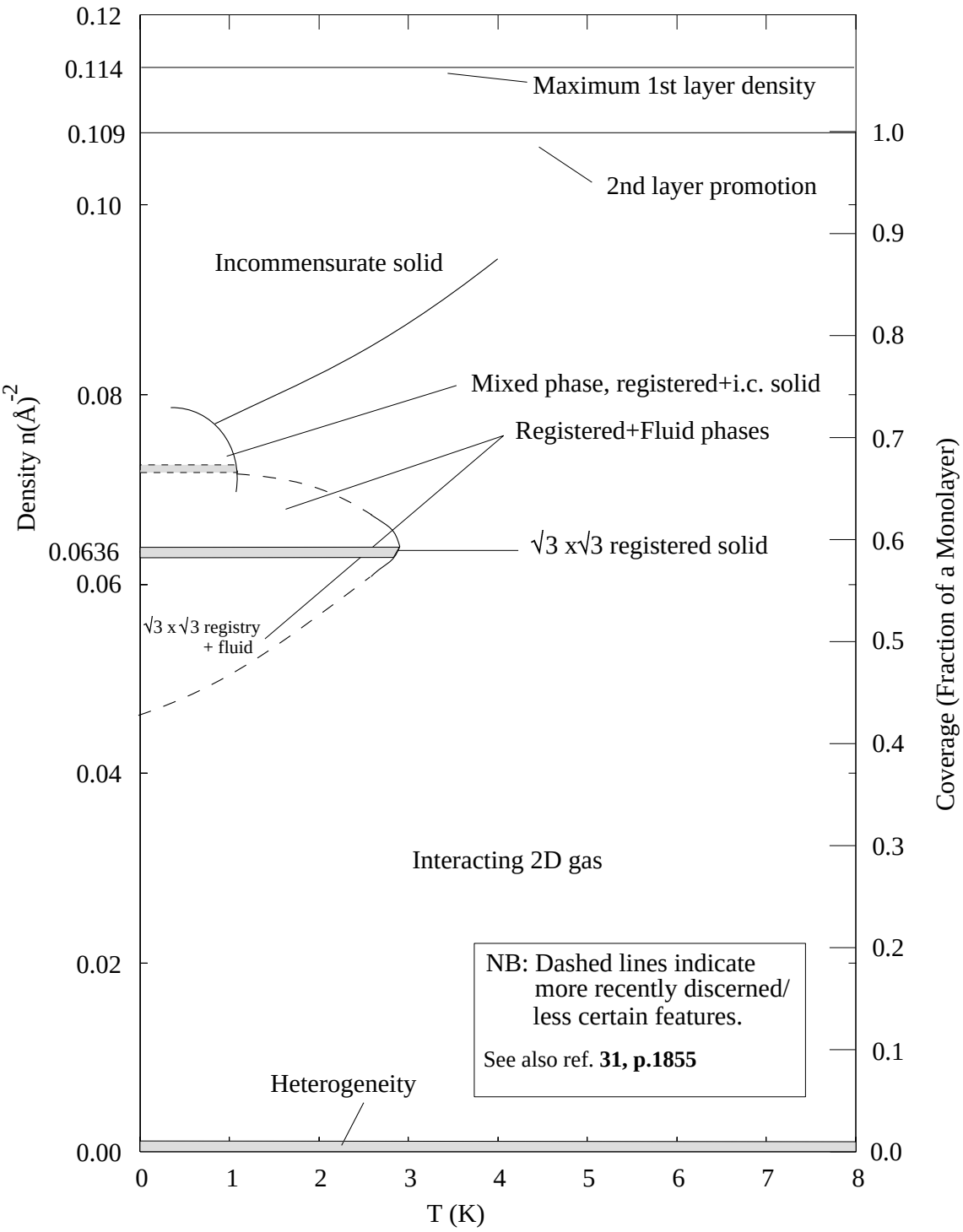

important [19] and ideal classical 2D gas behaviour increases.

1.8.3 $X \sim 0.6$ (Registered Phase)

For a narrow range of coverages ($\Delta X \sim 0.04$) centred on $X = 0.636 Å^{-2}$ [24] in which there are just enough adatoms to fill 1/3 of the basal plane graphite hexagons the film condenses into a structure in registry with the substrate [18,25]. The triangular lattice structure is designated $\sqrt{3} \times \sqrt{3}$ R30 [9] and has a lattice spacing (of 4.2Å) $\sqrt{3}$ times that of the substrate mesh. It is also known as a *Lattice Gas.* An illustration is shown in figure 1.8.3.1 and has been verified by neutron scattering experiments [26].

Figure 1.8.3.1, The $\sqrt{3} \times \sqrt{3}$ R30 Registered Adsorbate Structure on Graphite.

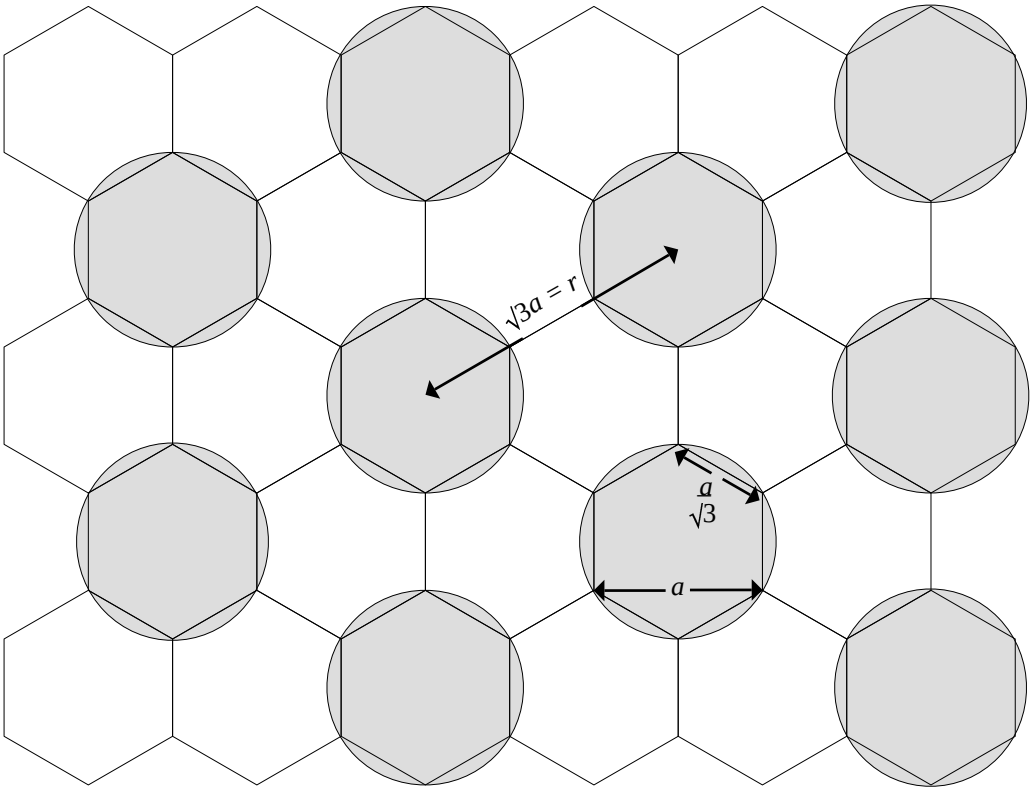

The heat capacity shows large peaks at 3K [18,22] as the registered structure undergoes a second order phase transition to a disordered structure displaying 2D gas like characteristics. The lattice gas ordering peaks indicate a transition in both spatial order and mobility [18]. Below the peak the heat capacity displays an exponential activation-law behaviour [22]. In the peak region critical behaviour occurs and the heat capacity has a logarithmic dependence [22] in reduced temperature for $0.0 < |t| < 0.1$. $C/Nk = -A \text{ Ln } |t| + B$ where $t = (T - T_c)/T_c$. T_c being the critical temperature and A & B

the critical parameters. Comparing spin states ↑↓ with lattice site occupancy (empty/ filled) the registered phase can be described by a 2D Ising model [2,18]. Campbell & Schick [27] have produced a model for a triangular lattice gas which displays an order-disorder transition at 1/3 occupancy. That it is first not second order is believed to be due to calculational approximations. Later theoretical work [8] has shown that the 3-state Potts model − a generalisation of the 2D Ising model might be more appropriate since it better reflects the 3-state degeneracy of the registered phase.

1.8.4 $0.65 < X < 0.73$ (Mixed or Partially Registered Phase)

In this narrow range of coverages the state of the film is much more complicated. It has been described as a dense fluid [18]. Later ^{4}He heat capacity measurements [28] showed a sharp peak at 1K [22] followed by a broad peak at 3K, the remnants of the registry order-disorder transition. As with the registered phase the largest ($0.75Nk$ at number density $n = 0.074$Å^{-2}) of the '1K' peaks occur at the highest T (1.23K). At lower temperatures the heat capacity decays with a T^2 (ie. 2D solid behaviour) and then exponential (ie. lattice model) characteristics. The mixed phase then, is believed to consist of a coexistence between a commensurate and incommensurate solid which is predicted by the model of Campbell & Schick [9,27].

1.8.5 $0.73 < X < 1.0$ (2D Incommensurate Solid)

In this region of the phase diagram the heat capacity displays T^2 behaviour at low temperatures [18,22,24]. This is the signature of a 2D solid. For the 2D Debye model of a solid film the heat capacity is given by $C/Nk = 28.8\,(T/\Theta_D)^2$ for $T \ll \Theta_D$ where Θ_D is the 2D Debye temperature. Calculations using 2D compressibility values derived from Θ_D verify 2D solid (the ability to resist sheer stresses and support transverse acoustic modes [19]) rather than fluid behaviour. Neutron diffraction work [8] has shown the incommensurate solid has a triangular lattice structure. As temperature is increased the heat capacity displays large peaks arising from apparently continuous phase transitions, as the solid melts, possibly via the KTHNY [12,11] mechanism. The peak heights and temperatures of occurrence rise to a maximum at monolayer completion. At coverages close to X=1 the peak narrows, indicating, according to Elgin and Goodstein [19] second layer promotion and film desorption. Neutron scattering [29] shows activation law behaviour of the defect concentration at $X \rightarrow 1$ as expected for layer promotion etc. An alternative theory by Bretz & Dash [18,30] involving the transverse acoustic modes density

of states may explain the sharpening of peaks with increasing *X*. Their model suggests that the 2D solid is in partial registry with the substrate, registered with large repeat distances. With ^{3}He, at a density $n = 0.109\text{Å}^{-2}$ the first layer is complete [9,31], the lattice spacing being 3.3Å.

1.8.6 *X* > 1.0 (The Second Layer)

With a solid first layer the second layer shows 2D gas and solid phases like the first layer but at lower melting temperatures due to the much reduced adsorption potential exerted by the first layer [8]. More recently registered phases, originally not thought to occur in the second layer [8] have been proposed [31,20] with ^{3}He. Relatively more third layer promotion occurs during the formation of the less strongly bound second layer and the first layer solid is compressed slightly to n=0.114Å^{-2} by the second layer with ^{3}He [31].

1.8.7 More Recent Work

The above description of the phase diagram for the ^{3}He/Grafoil system is now well established. However recent, detailed work has given rise to more complex phase diagrams which attempt to clarify some of the detail in the intermediate coverage region, in and around the registered phase. In the remainder of this section some of these will be mentioned. Ecke et. al. [32] have published a phase diagram for ^{4}He/Grafoil detailing the region at and below the critical point. It possesses 2D gas+commensurate coexistence, commensurate and 2D gas phases. A tri-critical point at $n = 0.039\text{Å}^{-2}/T = 1.3\text{K}$ delimits the three phases and is located by heat capacity peaks. See figure 7.6.2. Motteler [11,33] has produced a more elaborate phase diagram for the same system containing the following phases; 2D gas, 2D gas+commensurate, commensurate, incommensurate, incommensurate solid with *striped* domain walls and a hexagonal domain wall liquid similar to the re-entrant fluid of the Kr/Grafoil system.

The question of the order of the melting transition has also been re-opened. Ecke & Dash [34] claim that their data could be indicating either a KTHNY or heterogeneity broadened 1st-order melting process. Their phase diagram is more complex again, comprising the following phase designations; 2D gas, commensurate+2D gas coexistence, liquid, commensurate, commensurate+liquid coexistence, incommensurate+commensurate coexistence, liquid+incommensurate coexistence, a possible rotated liquid and the incommensurate solid. Hurlbut & Dash [35,11] proposed

that their ^{4}He heat capacity data showed weakly first-order melting but conceded the continuous KTHNY transition was also a possible explanation. Their criteria for preferring a first-order process has been questioned by several authors [11]. Recent work by Greywall & Busch [21,36] with ^{4}He has suggested that the registered region is larger than previously recognised and is in fact a fluid+registered coexistence phase. The low-temperature low-density region is designated a 2D gas+superfluid liquid coexistence phase. The C−IC region is presented as comprising a low temperature 2/5 occupancy *Striped Super Heavy Domain Wall* phase, which gives way at n=0.07Å^{-2} to a SSHDW phase+incommensurate solid coexistence. A 3/7 occupancy phase is proposed at a higher coverage, n=0.08Å^{-2} [36]. Work by the same group on ^{3}He [31,20] has produced a phase diagram (outlines included in figure 1.8.1 as dashes) in which the 1/3 occupancy $\sqrt{3} \times \sqrt{3}$ R30 registered structure is supplemented by a more dense ordered phase [28] with 2/5 occupancy, two structural arrangements of which are possible. Using neutron diffraction data Lauter, Godfrin, Frank & Schildberg [37] have reattributed the C−IC region of the ^{3}He/Grafoil phase diagram to a striped super heavy domain wall phase which transforms to a DWL and then to an isotropic fluid phase at higher temperatures, as shown in figure 7.2.2.39.

1.9 Methods of Study

Since adsorbed films have become of interest a number of interesting experimental techniques have been applied to/developed for investigating them. Some of these are [38]; Adsorption isotherms [1], Heat capacity measurements, Low energy electron diffraction (LEED) [39], Elastic and Inelastic neutron scattering [40], X-ray diffraction [41], Transmission high energy electron diffraction (THEED) [42], Atomic beam scattering [43], Mössbauer spectroscopy [44], Auger electron spectroscopy (AES) [45], Surface pressure gauge measurements [46], and NMR [3].

1.10 NMR Studies of Adsorbed Films.

NMR usefully compliments the other techniques mentioned. It is unusual in being able to provide dynamical as well as spatial information about the film [3]. By measuring the precessing nuclear magnetic moment, a macroscopically observable entity, information on the microscopic details of the system can be probed [47]. The basic requirements for an experiment are; a nucleus with a magnetic moment, preferably spin $\boldsymbol{I}$=½ to avoid quadrupolar effects and a large gyromagnetic ratio. A substrate with a

large surface area (typ.~tens m^2) to obtain enough signal, good homogeneity and a low magnetic impurity concentration is also needed. ^{3}He has been the most used nucleus for the above reasons. See Appendix 1. Its small mass makes it a quantum adsorbate providing additional interest.

In 1963 the first experimental work using ^{3}He was published **[48]**. It used Zeolite, a molecular sieve material consisting of a network of interconnecting ~13Å diameter pores. More work on Zeolite **[49,50,51]** and Vycor, a porous glass with ~70Å diameter pores followed **[52,53,54]**. Unfortunately these substrates suffered from severe heterogeneity giving universal *patchy solid* behaviour despite providing a large surface area and usably low magnetic impurity levels. In CW NMR work on graphitised carbon black by Rollefson **[55]** at 20MHz, broad lines whose width varied as a function of coverage and temperature were observed. At X~0.6 the change in linewidth at T~3K was taken to indicate ordering, the ordered phase corresponding to a classical 2D rigid lattice solid with lattice parameter of 4.3Å. It is now known that the low temperature solid is dominated by exchange processes **[3]**, ensuring the rigid lattice value is never reached.

This section describes some of the results and analyses of NMR studies of ^{3}He on Grafoil for later comparison with Boron Nitride data. Early pulsed NMR work by Grimmer & Luczszynski **[56,57]** indicated that, for sufficiently mobile spins the strong anisotropic substrate diamagnetic fields dominate the ^{3}He−^{3}He dipolar interaction leading to broad NMR lines. The 'c' axis susceptibility value is 1.73×10^{-5} emu/gr **[58]**. When a spin diffuses into the void at the edge of a platelet it experiences a large magnetic field gradient in which it relaxes. Daunt et. al. **[56]** obtained results showing that Curies law was obeyed in the high coverage solid phase down to 0.1K whereas the low coverage gas showed reductions in nuclear magnetic susceptibility, χ for $T \leqslant 1$K due to the onset of Fermi degeneracy. This onset appears to be delayed by spin independent interactions **[57]**, best modelled by the second virial coefficient theory **[59]**. Figure 1.10.1 shows a plot of T_1 and T_2 against X from pulsed NMR measurements **[60]** at 1.2K, 5.1MHz and $\beta=90^o$. β being the angle between the magnetic field B_0 and the substrate normal.

1.10.1 General Features

From low coverages to around X=0.3 (the exact position is temperature dependent) T_2 rises monotonically, a result in conflict with a homogeneous film becoming more dense with attendant motional slowdown. This is explained by an *Augmentation Factor* model described in the next section. The explanation of the turn-over at ~0.3 monolayers is not certain but is believed to be due to growth of the solid

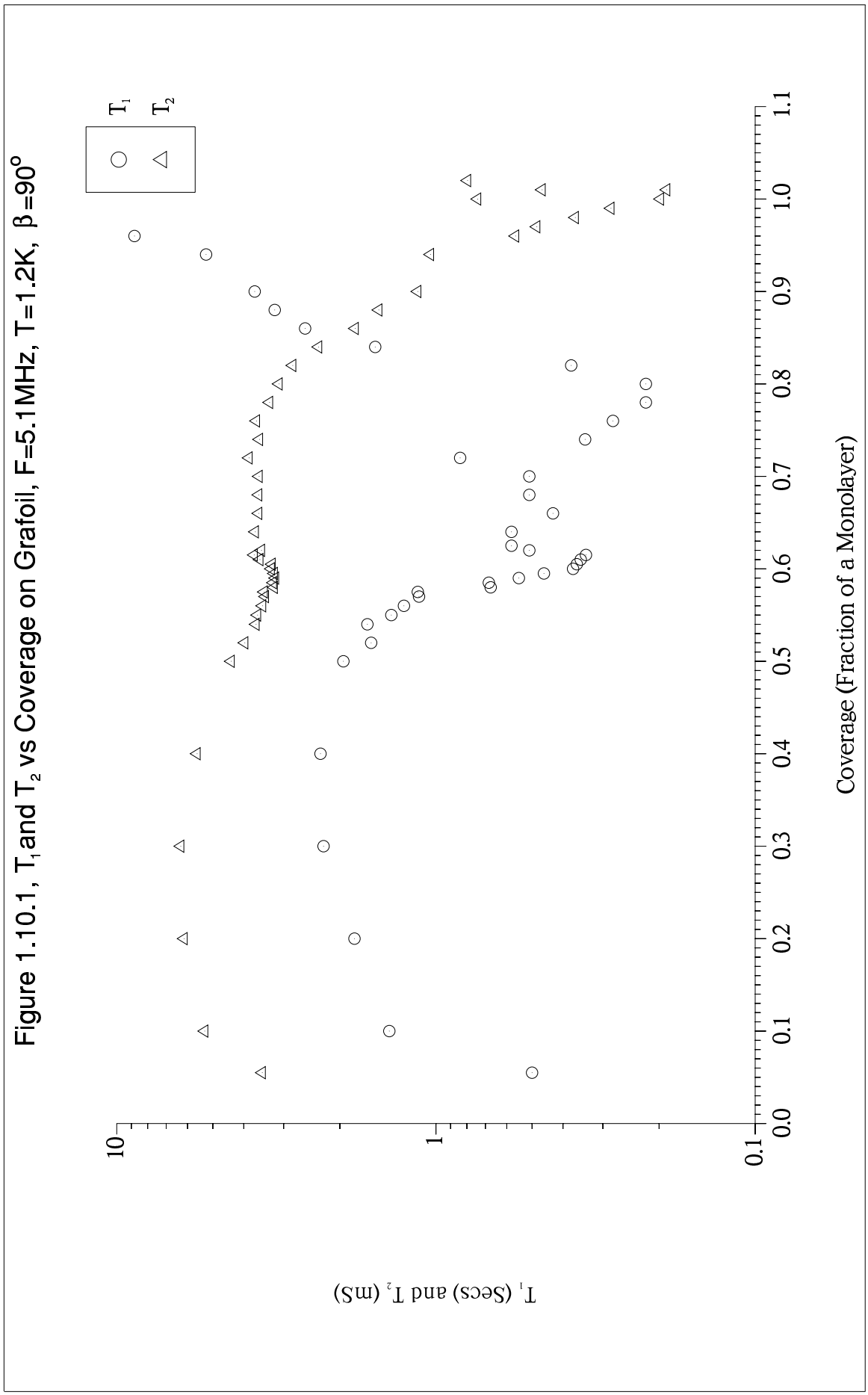
Figure 1.10.1, T1 and T2 vs Coverage on Grafoil, F=5.1MHz, T=1.2K, β=90°
T1
T2
10
1
0.1
0.0
0.1
0.2
0.3
0.4
0.5
0.6
0.7
0.8
0.9
1.0
1.1
T1 (Secs) and T2 (mS)
Coverage (Fraction of a Monolayer)

patches under increasing lateral pressure in the film [61]. From this point T_2 falls slowly as the film thickens and motion slows, until a distinct minimum forms at X~0.6 (registry). Essentially constant in the mixed phase, T_2 falls off rapidly reaching a minimum at X≈1 where density and correlation time are greatest. At 4K both minima are smaller features [60], reflecting less ordered states due to thermal activation. T_1 rises to a shallow maximum at X≈0.4, similarly to T_2, again falling off rapidly to a distinct minimum at registry. Similarly there is little variation in the mixed phase followed by a deeper parabolic minimum at X~0.8 as motion in the solid slows monotonically to fulfil the $\omega_0\tau_c$≈1 condition. Thereafter T_1 continues to rise monotonically through X=1. At 4K T_1 increases continuously with X as far as the reduced depth minimum at X~0.6 [60]. The rest of this section considers the NMR results in terms of the five phase regions previously described.

1.10.2 $X \leqslant 0.01$ (Very Low Coverage Regime)

As already mentioned, substrate heterogeneity leads to a patchy solid forming at sites of preferential adsorption. Pulsed NMR work [62] at this coverage suggests, for the particular sample used that ~0.5% of the substrate area is occupied by a high density solid with ~1.5% being covered by a lower density localised adsorbate. Below X=0.015 T_2=370μS independent of X, the X=1 incommensurate solid value [61]. For X=0.015 to 0.07, $T_2 \propto X$. This behaviour can also be explained in terms of the *Augmentation Factor* model [61] in which the preferential sites are filled at X=0.015, the remaining adatoms forming a 2D gas whose atoms undergo collisions and exchange with the solid patches, shortening T_2 below the 2D gas value towards that of the solid. As more adatoms are added and go into the 2D gas, T_2 lengthens as the ratio of mobile to localised spins increases. That the T_2 *vs* X data do not go through the origin demonstrates the unsurprising fact that the density of the solid patches is non-uniform and a continuous function of X [62]. For T > 2K & X=0.055, a $T_2 \propto \sqrt{T}$ relation was seen as expected for a 2D classical gas since $T_{1,2} \propto 1/\tau_c \propto \nu \propto \sqrt{T}$. $T_2 \propto \omega$ behaviour due to relaxation in the substrate local fields an apparently almost universal feature of this system [61] is seen. T_1 has a minimum in T, possibly showing melting in the solid patches [61].

1.10.3 $0.1 < X < 0.5$ (2D Gas Phase)

At X=0.3, T=1.1K, β=90°, T_2 (expt.)=6.2mS (fig. 1.10.1) whereas theory (equations 2.2.1.2, 2.2.1.6 etc.) predicts ~150 Sec for dipolar relaxation, evidently dipole-dipole relaxation is shorted out by a faster mechanism. For X<0.3 degeneracy

effects were seen [3,63] in χ below 1.5K, again the best fit to the data was the 2nd virial coefficient treatment of Siddon & Schick [59]. At 1MHz the classical 2D gas $\sqrt{T}$ relation was observed in T_1 and T_2 [3,63] over a wide range of T, eg. 0.7K < T < 4K at X=0.3. At 10MHz this behaviour was not seen, the initial component of the sub-exponential spin lattice relaxation, time T_1^i had an exponential − activation law T dependence plus little change in T_2. At 5MHz an intermediate behaviour was seen [61]. For $T \leqslant$2K $T_2 \propto \sqrt{T}$ behaviour occurred. Above this temperature T_2 levelled off, becoming more non-exponential, even as high as 10K [61]. These results have been attributed to a motionally narrowed mechanism effective at low T being shorted out at higher T by a temperature independent mechanism [61]. The fact that spin-spin relaxation becomes more non-exponential as T increases is interesting. In fact the non-exponentiality is super-exponentiality (see reference **61**). Since it is clear that no sum of exponential or sub-exponential processes can lead to super-exponential relaxation the dominant process must itself be relaxing faster than exponential. A possible candidate is the exp $(-D\gamma^2G^2t^3/12)$ spin echo decay due to (unbounded) diffusion in a field gradient [47]. Although the system may be tending towards a exp$-t^3$ relation, the expected exp$-D$ dependence is not present. In any case, since both the spin motion and the field it *sees* are bounded by the Grafoil platelets the diffusion cannot be regarded as truly unbounded. In the limit of $T_2 \gg a^2/D$ where 'a' is the typical dimension of a platelet in the direction of the external field, the relaxation should become asymptotically exponential and $1/T_2 = a^4\gamma^2G^2/120D$ can be written [64,65]. At 10MHz Satoh & Sugawara [64] report spin-spin relaxation being exponential at 4.2K but sub-exponential at lower T suggesting more than one system component or relaxation mechanism is significant. This rise in the *index* of relaxation (see listing 6.3.2.1 for explanation of *index*) with T is similar to the 5MHz data and is expected when the motion at low temperatures is slow enough such that on average each spin relaxes on a single platelet [66]. The distribution of platelet dimensions and orientations give rise to a distribution of relaxation times, the measured relaxation signal being the sub-exponential average of that distribution. They also report a small coverage independent maximum in T ~2.8K at lower coverages. Robertson's mechanism [65] predicts $1/T_2 \propto B_0^2 \propto \omega_0^2$ since $1/T_2 = \langle\gamma B_{graf}\rangle^2\tau_p$, where τ_p is the time to cross a platelet and B_{graf}, the platelet diamagnetic field, which should be $\propto B_0$. However $1/T_2 \propto B_0$ seems to be the almost universal behaviour [61,64]. Only for $\beta < 45^0$ and at higher frequencies ($F \rightarrow$ 10MHz) is there a deviation from the linear relation, possibly involving a quadratic term [61]. T_2 anisotropy measurements [61] did not agree with theoretical predictions for the diamagnetic local field relaxation. At 5MHz T_1 is only

weakly frequency dependent, being only ~20% longer at 4.2K than at 1.2K [61] in contrast with the 1MHz $\sqrt{T}$ dependence [3,63]. The measured values of T_1 are much shorter than predicted for dipolar relaxation in a 2D gas where $\tau_c \sim 10^{-12}$ Sec. Eg., At X=0.3, T=1.1K, β=90°, T_1 (expt.)=2.3 Sec (fig. 1.10.1) whereas theory (equations 2.2.16, 2.2.1.2 etc.) predicts ~130 Sec. It is possible that the solid patches which dominate the $X \lesssim 0.01$ T_2 data also mediate T_1, however there are problems with this scheme [61]. A better explanation involves paramagnetic impurities (PMIs) embedded in or close to the substrate surface. The modification of the dipolar T_1 due to relaxation via PMIs is given by [61,47],

$$\frac{1}{T_1} = \frac{1}{T_1^{d}} \left[\frac{\gamma_s}{\gamma_i}\right]^2 \frac{X_s}{X} \frac{S(S+1)}{I(I+1)} \left(\frac{a}{d}\right)^4 \qquad 1.10.3.1$$

γ_s and γ_i are respectively the gyromagnetic ratios of the electronic impurity and ^{3}He spins, X_s is the effective *coverage* of impurities. S and I are the impurity and ^{3}He spins respectively, 'a' and 'd' are the corresponding ^{3}He−^{3}He and ^{3}He−impurity internuclear separations. The d^{-4} term ensures only PMIs on or near the surface are significant relaxation centres, their efficacy is due to the large $(\gamma_s/\gamma_i) \sim 1000$. Given that the PMIs increase the relaxation rate across the board it is clearly inconsistent with the high coverage solid T_1 values where T_1 minima demonstrate that T_1(expt.) = 207mS ~ T_1^{dipolar}, (equations 2.2.16, 2.2.2.4, 2.2.2.5 and table 1.10.6.1). This paradox can be resolved by considering the effects of regions of preferential adsorption where solid patches reside. Rapid exchange of adatoms by collisions between the fast moving basal plane gas adatoms and the solid patches allow the relaxation rate of the 2D gas to be greatly increased via an augmentation factor mechanism. Using a 2D disc analogue of the wall relaxation mechanism for bulk ^{3}He by Chapman & Bloom [67] in which the disc is a model of a Grafoil platelet, the localised solid patch adsorbate being at the edge,

$$T_1 = \frac{4R}{\pi^2} \frac{n}{\lambda} T_1^{b} \qquad 1.10.3.2$$

PMI concentration needed to explain the low density 2D gas T_1 without significantly affecting the high density solid value. It may be that this mechanism is enhanced by there being a greater concentration of magnetic impurities at edge sites where crystalline impurities have increased the probability of a fissure occurring, for example during heat treatment. The spin-lattice relaxation time is weakly frequency dependent, $T_1 \propto \omega$ but does not go through the origin. This is partially in accordance with theory [68]. The long time hydrodynamic t^{-1} *tail* of the reduced correlation function $g_0(t)$ due to diffusive motion in 2D gives rise to a logarithmic divergence in the corresponding spectral density $j_0(\omega)$ in the $\omega\tau_c<1$ limit. It is this divergence which gives T_1 its low ω, ω dependence, T_1 being $\propto\omega$ and going through the origin in the above limit [68]. In this regime T_1 is expected to be approximately independent of τ_c which explains the weak temperature dependence [68]. A further consequence of the divergence is the breakdown of the $1/T_1 = 1/T_2 = (10/3)m_2\tau_c$ 3D behaviour [69] when $\omega\tau_c \ll 1$ [70]. The lack of significant anisotropy in T_1 is in accordance with PMI augmentation of the spin-lattice relaxation rate since the ^{3}He−Impurity inter-nuclear vectors do not lie in the substrate plane as the ^{3}He−^{3}He ones do [61].

1.10.4 $X \sim 0.6$ (Registered Phase)

At 1MHz sharp dips are seen in T_1 *vs* X but not in T_2 [3,71]. Whereas at 10MHz [64] little change occurs in T_1 but T_2 shows dips at the critical coverage X_c=0.58. Both relaxation times are affected through both the spatial and motional changes involved in ordering, (equation 2.2.23). NMR measurements [60,72] have shown that at perfect registry τ_c rises to $\sim 3 \times 10^{-8}$ sec, the increase in motion above and below X_c being due to interstitial and vacancy tunnelling respectively. Although a small number of thermally activated vacancies exist at 1K (~4% [64]) the dominant motion is temperature independent quantum mechanical exchange. Although the substrate potential is able to localise the adatoms it is not deep enough to *pull in* the tails of the wavefunctions and fully suppress exchange [72]. At 10MHz Satoh & Sugawara [64] observed T_1 temperature independence above the order-disorder transition at 3K and Arrhenius law behaviour below it with no abrupt change at the transition. This activation law behaviour suggests that it is the build up of thermally activated vacancies which leads to the transition. T_1 is mainly dipolar but T_2 still seems dominated by the substrate local fields [3]. Measurement of T_1 provides the activation energy (E_a) and the activation rate ($1/\tau_0$) for the film [64,73].

$$T_1 = 1.3 \times 10^{-9}\ \tau_0^{-1}\ X^{-3}\ \exp(-E_a/kT) \qquad T \gg T_{min} \qquad 1.10.4.1$$

$$T_1 = 3.3 \times 10^{-9}\ \omega^2\ \tau_0\ X^{-3}\ \exp(E_a/kT) \qquad T \ll T_{min} \qquad 1.10.4.2$$

$$\tau_c = \tau_0\ \exp(E_a/kT) \qquad 1.10.4.3$$

τ_c being the correlation time. For X=0.58, τ_0=2.9 × 10^{-10} sec. and E_a=3.8K **64**. Little change occurs in E_a around this coverage. At 1MHz **3** considerable change is seen in E_a with a cusp at X=0.58 where E_a=8K. Detailed measurements by our research group **60**,**72** have revealed additional features at registry: At 5MHz T_1 and T_2 show minima with X, centred at slightly different X **72**. Both the position and value of the T_1 minima are functions of frequency, it being deepest at the lowest frequency (1.3MHz), the position shifting to higher X at lower ω **60** as expected. As shown in figure 1.10.4.1 the size of the upward shift in X of the minimum-position with falling frequency reduces, ie. the minima bunch up, a consequence of the discontinuity in spatial and motional characteristics through ordering (cf. the incommensurate solid T_1 minima, §1.10.6). For $0.52 \leqslant X \leqslant 0.62$, $(1/T_1)$ follows a log(ω) law at 1.2K in accordance with that expected for the low frequency/fast motion side of the T_1 minimum in 2D **68**. T_2 has the familiar $1/\omega$ dependence. For 1K<T<2K, T_1 and T_2 show T independent exchange motion is dominant as in bulk helium **74**. The effect of exchange motion on the relaxation times is dramatic. Typical values of T_2 at 1K and 0.58 monolayers are 3.2mS (figure 1.10.1) and 1mS **64**, cf. the rigid lattice value $T_2^{RL} = 1/\sqrt{m_2} \approx 70\mu$S for a triangular lattice with lattice spacing 4.3Å. Values of τ_c have been extracted from T_1 and T_2. Fitting the T_1 data to a *universal curve* **75**,**76** in which a single adjustable parameter, τ_c (or equivalently J) scales the plot, τ_c may be extracted. This method relies upon fitting the data to $1/T_1 = A - B\log(\omega)$ for various X at low T, together with the fact the low frequency part of a theoretically calculated reduced spectral function $j_0(\omega)$ has (by design) the same logarithmic form. Analysis of T_2 makes use of the experimental linear law:- $1/T_2 = A + B\omega_0$. The frequency independent contribution 'A' is further decomposed:

$$\frac{1}{T_2^{\,freq.\ independent}} = \frac{1}{T_2^{\,other}} + \frac{1}{T_2^{\,dipole\text{-}dipole}} \qquad 1.10.4.4$$

T_2^{other} an asymptotically decaying quantity with decreasing X believed to be due to, for

Figure 1.10.4.1, T_1 vs Coverage on Grafoil Around the Registered Phase, T=1.2K, $\beta=90^{o}$

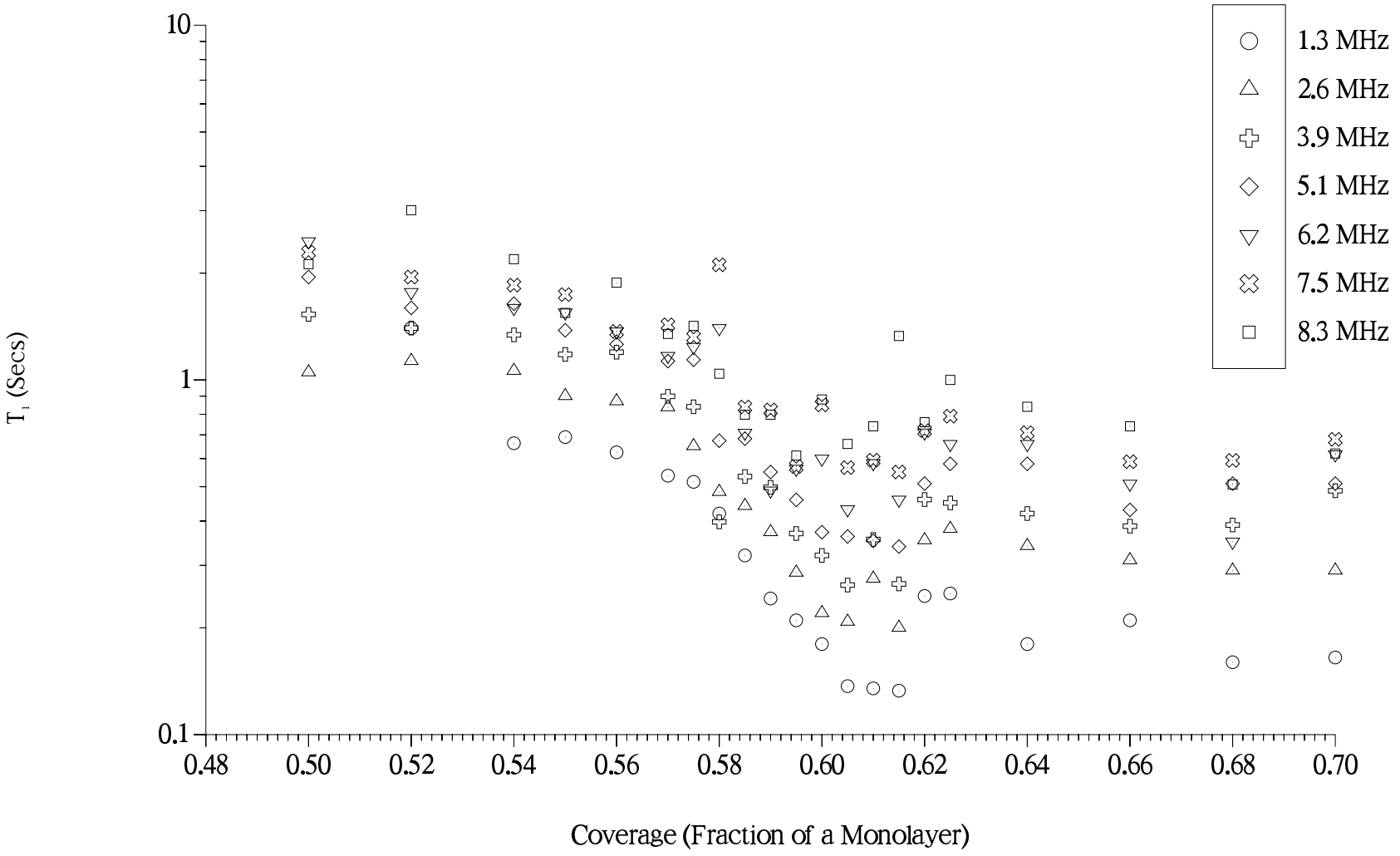

example, relaxation in solid patches can be subtracted off as a baseline. $T_2^{dipole\text{-}dipole}$, believed to be the dipolar contribution was fitted using a Kubo type expression (equation 2.2.10 with m=0 contribution only) for the adiabatic part of T_2, to obtain τ_c [60]. Using $\tau_c = a^2/2D$, where 'a' is the ^{3}He lattice spacing, the diffusion constant can be calculated. A value of 10^{-9} cm^2/sec agrees with the Sussex 1MHz result [3] but not with the Tokyo [64] one. Similarly the maximum E_a at perfect registry, 8.8K agrees and disagrees respectively. This is probably related to the fact that Sussex and London groups used Grafoil from the same batch.

1.10.5 $0.65 < X < 0.73$ (Mixed or Partially Registered Phase)

A limited amount of data has been taken here. That which has has been interpreted as a coexistence of commensurate and incommensurate solid. Assuming the phase is entirely commensurate at 0.65 monolayers and fully incommensurate at 0.74, both relaxation times have been expressed as suitably weighted sums of the above phases' limiting values. T_1 and T_2, however show little change with X [60].

1.10.6 $0.73 < X < 1$ (2D Incommensurate Solid)

The nuclear magnetic susceptibility χ obeys Curies law down to very low temperatures as expected [56] with departures being due to RF eddy current heating of the Grafoil, exacerbated by the low heat capacity of the solid. At low temperatures T_2 falls monotonically to a minimum at $X \sim 1$ monolayers as expected, with the speed of the exchange motion falling from $\tau_c = 2 \times 10^{-8}$ sec at X=0.7 to 2×10^{-5} sec at X=1 [61] which is enough to prevent the rigid lattice value being reached. Again, the increase in density leads to a reduction in exchange as in the bulk case. Maximum density at X=1 also contributes directly to the minimum in T_2. The X=1/F=5MHz/T=1K T_2 is 100μS [60]. As T is raised towards 4.2K, T_2 increases and becomes more frequency dependent as spin motion increases via thermal activation causing increased relaxation (relatively speaking) in the platelet local fields [64]. Except in the vicinity of the 10/3 effect T_2 (dipolar) should be frequency independent [77]. However it still has a significant (35 sec^{-1} MHz^{-1}) value at X=0.76/T=1.2K [77]. Only for X>0.9 does this substrate mediated component cease to be significant [60] leaving purely dipolar behaviour. The same procedure was used to extract J, the effective two-particle exchange frequency from the T_2 *vs* ω data, as at registry [60,77]. The relationship between τ_c and J is given by [70], $\tau_c = 0.267/cJ$, where 'c' is a numerical factor related to the lattice structure, originally assumed [70] and recently shown [7] to be ≈1.

T_1 in the low temperature exchange regime exhibits a series of smooth

parabolic minima in coverage with frequency demonstrating dipolar relaxation [60,8]. The positions and values of these minima are close to theoretical predictions (equations 2.2.16, 2.2.24−2.2.26, 2.2.2.4 and 2.2.2.5). At the highest coverages a kink shows another unidentified mechanism plays a part. As T is raised, the positions of the minima shift to higher X as expected. Two key statements can be made on observation of a T_1 minimum:-

- $\omega_0\tau_c \approx 1$. 1.10.6.1
- $T_1 = \omega_0/m_2$. 1.10.6.2

where m_2 is the second moment of the CW NMR line. These statements can be re-cast in a more precise way and used to extract values of J in an elegant treatment by Cowan et. al. [75]. A brief summary of the technique follows;

The dipole-dipole correlation function can be written in a general way,

$$G(t) = G(0)\, S(Jt) \qquad 1.10.6.3$$

'S' is a general description of the shape of the correlation function, being scaled by a single parameter J. Fourier transforming,

$$T_1^{-1} = J(\omega) = [G(0)/J]\, K(\omega/J) \qquad 1.10.6.4$$

'K' being the corresponding reduced spectral function. ω/T_1 will be a maximum for some value of $(\omega/J)=C$, the value of 'C' depending on the shape of 'K'. At the T_1 minimum the two statements re-cast are,

- $J = \omega^{min}/C$ 1.10.6.5
- $\omega^{min}/T_1 = G(0)CK(C) = const.$ 1.10.6.6

A plot of $T_1^{min} \times X^3$ *vs* ω^{min} will be a straight line with slope $(G(0)CK(C))^{-1}$. Scaling by X^3 renormalises the density dependence of $G(0)$, essentially the second moment. To determine 'K' a plot of J/T_1 *vs* ω/J is needed but J is not known. However for many X, ω^{min} is available and is $\propto J$. So ω^{min}/T_1 *vs* ω/ω^{min} is plotted instead. The experimental points [75,76] lie on the same line showing the correctness of the method. The logarithmic divergence at low frequencies is clearly visible [75]. An empirical expression for G(t)

having the correct short and long time behaviour determined from a moment expansion and hydrodynamic arguments respectively, is used, containing a single adjustable parameter **76**. Its Fourier transform J(ω) is calculated. By adjusting the parameter until *C*K(*C*) has the value obtained from the $T_1^{min} \times X^3$ *vs* ω^{min} plot, '*C*' is determined, hence *J* is known wherever a T_1 minimum has been observed. J/T_1 *vs* ω/J can then be plotted. *J* can be determined for those T_1 for which no minimum was seen by adjusting a trial value of *J* until the point lies on the universal curve. The procedure effectively supplements the long and short time parts of the correlation function with middle time experimental data.

Table 1.10.6.1 shows some T_1 minimum data from reference **60**. At higher coverages there is reasonable agreement between the exchange frequencies obtained from them and heat capacity measurements **31,78,76**. At lower coverages however agreement is poor, the heat capacity *J* being typically an order of magnitude lower. In more recent work **79**, low temperature NMR susceptibility data has yielded even smaller values for *J*, being down by typically another order of magnitude. It has been suggested the discrepancies are due to the presence of multiple spin exchange processes **79**. A series of T_1 minima in *T* with *X* have also been observed **3,64** as τ_c is reduced to ~$1/\omega_0$ by thermal activation. At 10MHz **64** minima were seen from *X*=0.7 at 1.8K to *X*=0.84 at 3.4K. There appears to be little correlation between the melting temperatures observed from heat capacity data and the T_1 minima. The positions of the latter designate a line of constant τ_c whereas the melting line appears to indicate constant vacancy population resulting from thermal activation. Widom et al **80** have published data showing some evidence for a two-stage KTHNY type melting process. They propose that T_c^* (5 Kat *X*=0.95), the temperature at which T_2 becomes strongly frequency dependent as the dominant mechanism changes from dipolar to relaxation via platelet local fields, and spins diffuse across the voids between the ~100Å diameter platelets, signifies the solid−hexatic transition when shear rigidity is lost. At T_c^{**} (5.9K) a kink in T_1 on the $\omega_0\tau_c<1$ side of the minimum is attributed to the hexatic−isotropic fluid phase change. See also reference **3**.

Table 1.10.6.1, Coverage of occurrence and Value of T_1 minima with Frequency on Grafoil, T=1.2K, β=90º.

Frequency (MHz)	Coverage (Monolayer)	T_1 at Minimum (Secs)
1.3	0.818	0.0499
2.6	0.805	0.0856
3.9	0.789	0.1503
5.1	0.785	0.207
6.2	0.773	0.2711
7.5	0.7676	0.2797
8.3	0.766	0.3639
10.2	0.759	0.479

1.10.7 $X > 1$ (The Second Layer)

T_1 has been observed to become sub-exponential as T falls towards 1K [64] for low second layer coverage films. The data has been analysed in terms of double exponential relaxation − The long lived component being due to the long solid first layer T_1, the faster component coming from the rapidly diffusion fluid second layer relaxing at the platelet boundaries in the presence of PMIs. Detection of sub-exponential relaxation shows the interlayer exchange rate cannot be, at most, much faster than the most rapidly decaying layer component. T_2 becomes sub-exponential as T is raised from 1K to 4.2K [64]. The short lived component coming from the short-T_2 first layer solid, the second layer + deadsorbed gas contributing the longer part. At 1K the interlayer exchange rate is fast enough to ensure exponential relaxation. It has been proposed [64] that the bulk of the relaxation takes place in this interlayer process.

Chapter 2
NMR Theory

2.1 Introduction

If an assembly of nuclear spins is placed in a static magnetic field $\boldsymbol{B}_0$, assumed to be along the $\boldsymbol{z}$ direction a magnetisation $M_z = M_0 = \chi B_0/\mu_0$ will grow parallel to B_0, where χ is the static magnetic susceptibility per unit volume and M_0 the equilibrium magnetisation. Microscopically the degenerate spin sub-levels are split by the applied field B_0, the energy difference $\Delta E = \hbar\gamma B_0$ where γ is the gyromagnetic ratio of the nucleus. For a nucleus with spin $\boldsymbol{I}$ there will be $2I+1$ magnetic sub-levels, the relative populations of which are given by Boltzmann statistics, $N_I/N_{I+1} = \exp(-\Delta E/kT_s)$ except at very low temperatures.

In the simplest case of an $\boldsymbol{I}=½$ nucleus there are only two sub-levels $I_z = -½\hbar$ and $+½\hbar$. A form of spectroscopy (NMR) exists in which RF energy is absorbed by the spins. The necessary resonance condition is that $\Delta E = \hbar\gamma B_0 = \hbar\omega_0$ where ω_0, the Larmor frequency is the angular frequency of the applied RF energy. The effect of such irradiation is to saturate the spins, destroying the magnetisation, making $N_I/N_{I+1} \to 1$, which results in the spin temperature $T_s \to \infty$. Using the continuous irradiation technique (CW NMR) the applied RF level must be kept very low to avoid saturation. In contrast, in a pulse NMR experiment a brief pulse, duration τ of an intense RF field B_1 applied perpendicular to B_0 will saturate the spins if $\gamma B_1 \tau = \pi/2$. This is termed a 90° pulse. Its effect is to tip the longitudinal magnetisation into the transverse plane where it decays to zero with a time constant T_2^*. This process, spin-spin relaxation, results from the spins dephasing after the 90° pulse, a consequence of the local inhomogeneity of the magnetic environment experienced by each spin, which therefore each precesses at a slightly different Larmor frequency, $\omega_i = \gamma(B_0 + b_i)$ for the ith spin. Typical contributions to b_i are the dipole fields of neighbouring spins and the external field inhomogeneities. If the motion of the spins is sufficiently fast such that $\omega_0\tau_c \ll 1$ where τ_c is a time characteristic of the motion, the average field seen during the Larmor period will differ little amongst spins and the dephasing time T_2^* will become long. T_2^* thus reveals information about microscopic spin motion.

After the 90° pulse, simultaneously but separately the longitudinal magnetisation M_z will grow from zero towards M_0, restoring the population difference, with a time constant T_1. Unlike spin-spin relaxation this process requires a transfer of

energy, away from the spins, $\hbar\gamma B_0$ per spin which is removed by the motion in the system to the non-spin degrees of freedom, known generically as the *lattice*. Spin-lattice relaxation therefore relies upon there being a spectral component J(ω) of the motion at the Larmor frequency to modulate the dipolar interaction. When the characteristic time of the motion $\tau_c \approx 1/\omega_0$ spin-lattice relaxation is at its most efficient and T_1 goes through a minimum in τ_c. A 180° pulse ($\gamma B_1 \tau = \pi$) inverts the longitudinal magnetisation. If the transverse magnetisation has decayed away after a 90° pulse largely under the influence of inhomogeneous broadening mechanisms such as imperfections in B_0, the spins will rephase after a 180° pulse to form a spin-echo **[81]** as shown in figure 2.1.1.

Figure 2.1.1, The 90°−180°−Spin-Echo Sequence.

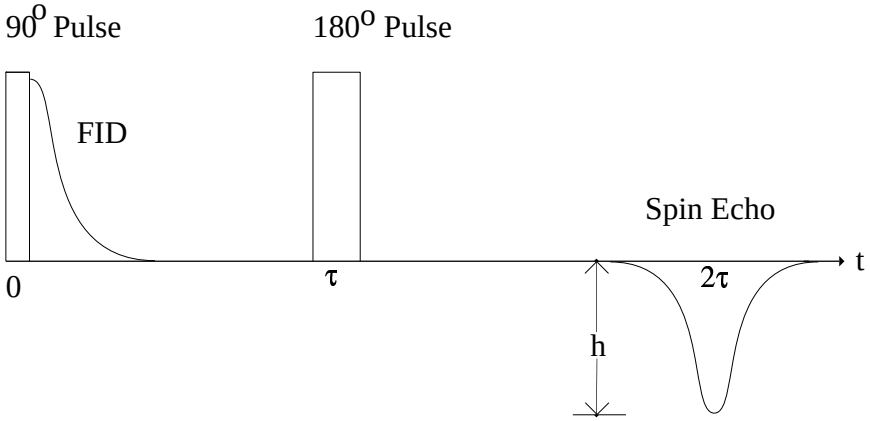

The 180° pulse reverses M_z but not the inhomogeneous field. That component of the deviance in Larmor frequency due to the inhomogeneous field is precisely reversed for each spin such that the decay of '*h*' with 'τ' is determined by homogeneous mechanisms such as the dipole-dipole interaction only. The relaxation by homogeneous mechanisms, with time constant T_2 is measured by the above *90°−180°−Echo* sequence. A 90° pulse allows the instantaneous value of the longitudinal magnetisation to be observed by tipping it into the transverse plane where it induces a voltage in the NMR coil. Throughout this work a *90°−90°−180°−Echo* sequence has been used in preference to the *180°−90°−180°−Echo* one since it does not require a spectrometer *repetition time* ≫ T_1.

In the case of nuclei with $\boldsymbol{I}>1/2$ the situation is more complicated. For example the dominant isotope in naturally abundant Boron is ^{11}B which has $\boldsymbol{I}=3/2$, (See Appendix 1). There are $2I+1=4$ energy levels corresponding to $m=3/2,\ 1/2,\ -1/2$ & $-3/2$ **[47,82]** and three allowed magnetic dipole transition $\Delta m=\pm 1$ between them. In

isolation the levels are equispaced, the transitions are degenerate and a single resonance frequency $\omega_0=\gamma B_0$ exists. All $\boldsymbol{I}>1/2$ nuclei however possess a non-zero electric quadrupole moment 'eQ'. If the spin resides in a crystal with less than cubic symmetry it will have a static crystalline electric field gradient (EFG) 'eq' to which the quadrupole moment will couple [82]. The coupling Hamiltonian is given by, [47]

$$\mathcal{H}_Q = \frac{e^2qQ}{4I(2I-1)}\left[3I_Z^2 - I(I+1) + \frac{1}{2}\eta(I_+^2 + I_-^2)\right] \qquad 2.1.1$$

where (X,Y,Z) are the principle axes of the EFG tensor V_{ij}. Choosing $|V_{ZZ}| \geq |V_{YY}| \geq |V_{XX}|$, $eq = V_{ZZ}$ and $\eta = (V_{XX}-V_{YY})/V_{ZZ}$. If the EFG has cylindrical symmetry $V_{ij} = V_{ZZ} = eq$ becomes a scalar and the asymmetry parameter $\eta=0$. This is the case with hexagonal BN which has trigonal symmetry [83,84]. $\mathcal{H}_Q$ can then be transformed into the usual NMR frame of reference in which $B_0=\boldsymbol{B}_0\boldsymbol{z}$, where θ is the angle between the direction of B_0 and 'eq' [47]. A perturbation expansion gives the splitting of the energy levels from the Larmor frequency in terms of θ and F_Q for the high field case ($\omega_0/2\pi = F_0 > F_Q$). F_Q is the quadrupolar frequency,

$$F_Q = \frac{3e^2qQ}{2hI(2I-1)} \qquad 2.1.2$$

The first order splitting F_m^1,

$$F_m^1 = \frac{E_{m-1}^1 - E_m^1}{h} = -F_Q\left(m - \frac{1}{2}\right)\frac{3\cos^2\theta - 1}{2} \qquad 2.1.3$$

For $\boldsymbol{I}=3/2$ the central $-1/2 \leftrightarrow +1/2$ transition ($m=1/2$) is unaffected but the $-3/2 \leftrightarrow -1/2$ ($m=-1/2$) and $+3/2 \leftrightarrow +1/2$ ($m=+3/2$) are, giving two symmetrically split satellite lines. Second order splitting shifts the central line ($m=1/2$) in frequency,

$$F_{½}^2 = \frac{-F_Q^2}{16F_0}\left(I(I+1) - \frac{3}{4}\right)(1 - \cos^2\theta)(9\cos^2\theta - 1) \qquad 2.1.4$$

but leaves the separation between the satellite lines unchanged. The random distribution of orientations in a powder sample such as our BN gives rise to a continuous distribution

of θ and a continuous distribution of splitting frequencies [82,47]. The resultant first order powder pattern is illustrated in figure 2.1.2 (dashed line) and shows how F_Q may be obtained from it. Second order effects smear out the central line in an asymmetric fashion around F_0 by $\approx +3F_Q^2/16F_0$ and $-F_Q^2/3F_0$ [82]. In practice the powder pattern is subject to further dipolar broadening as indicated by the solid line. The satellite peaks occur at θ=90° because the distribution of spins oriented with polar angle θ is weighted according to sin(θ) under the powder average [85].

Figure 2.1.2, The First Order Powder-Pattern for a Quadrupolar ***I***=3/2 Nucleus with Axially Symmetric Crystallites.

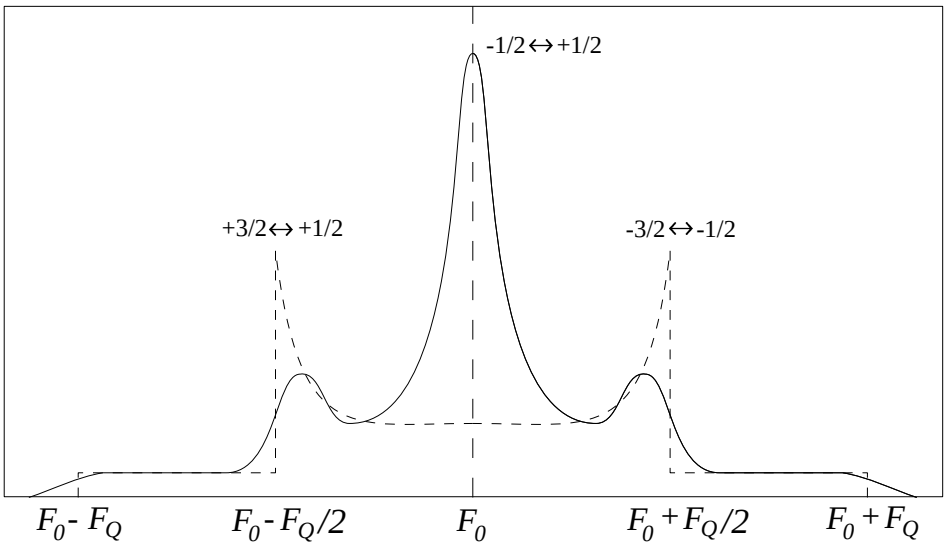

In addition to these strong broadening mechanisms the sum of the split intensities is only 55% of the unsplit line in the absence of quadrupolar effects for pulsed NMR [85], providing a poor S/N ratio and making measurements quite difficult [83,86]. Additionally at liquid helium temperatures T_1 is of the order of tens of minutes, restricting the capacity for signal averaging.

2.2 Relaxation Theory

A quantum theory of nuclear magnetic relaxation with particular reference to 2D systems has been treated in some depth [60,61,76,70,87,64,88,89]. Only the main points are considered here. Starting with a Hamiltonian describing the whole system, $\mathcal{H}$ the aim is to obtain functions describing the two relaxation processes and if possible the exponential relaxation times T_1 and T_2.

$$\mathcal{H} = \mathcal{H}_z + \mathcal{H}_d + \mathcal{H}_m \qquad 2.2.1$$

$\mathcal{H}_z$ the Zeeman Hamiltonian describes the interaction of $\boldsymbol{I}$ with $\boldsymbol{B}_0$, that is Larmor precession and the absorption of energy at $\omega_0=\gamma B_0$. In the usual frame of reference,

$$\mathcal{H}_z = -\gamma\hbar I_z B_0 = \hbar\omega_0 I_z \qquad 2.2.2$$

$\mathcal{H}_m$ the motional Hamiltonian, represents the non-spin degrees of freedom, the *lattice*, which can be for example classical bodily particle motion or exchange motion in spin-space. $\mathcal{H}_d$ the dipolar Hamiltonian describes the interactions amongst spins and acts as an intermediary between the Zeeman and motional states which would otherwise not interact. Therefore,

$$[\mathcal{H}_z,\mathcal{H}_m]=0,\ [\mathcal{H}_d,\mathcal{H}_m]\neq 0,\ [\mathcal{H}_z,\mathcal{H}_d]\neq 0 \qquad 2.2.3$$

$\mathcal{H}_d$ can usefully be expressed in terms of its spin-flip components **90**,

$$\mathcal{H}_d = \sum_{m=-2}^{2} D_m \qquad 2.2.4$$

where,

$$D_m = \frac{\mu_0}{4\pi}\hbar^2\gamma^2\sqrt{\left(\frac{4\pi}{5}\right)}\sum_{i<j} Y_2^{-m}(\Omega_{ij})\ T_{ij}^m(-1)^m/r_{ij}^3 \qquad 2.2.5$$

The Y_2^{-m} are spherical harmonics describing bodily particle motion. The Ω_{ij} represent the direction of r_{ij}, the internuclear vectors in terms of the polar θ_{ij} and azimuthal angles ϕ_{ij} with respect to B_0. The T_{ij}^m are irreducible tensor spin operators **70**. They describe motion in spin-space such as exchange and couple together eigenstates of $\mathcal{H}_z$ separated by energy $m\hbar\omega_0$, m=0 describing adiabatic processes (zero nett spin-flip) and $m\neq 0$ non adiabatic ones. The time dependence of the spin motion under the influence of $\mathcal{H}$ is given by the Heisenberg equation,

$$\frac{d}{dt}\boldsymbol{I}(t) = \frac{i}{\hbar}[\mathcal{H}, \boldsymbol{I}(t)] \qquad 2.2.6$$

Expressions for the relaxation functions in terms of $\boldsymbol{I}(t)$ are [47,70,90]; for transverse relaxation,

$$F(t) = \exp(-i\omega_0 t)\ \mathrm{Tr}\ \{I_+(t)\ I_-(0)\}/\mathrm{Tr}\ \{I_+ I_-\} \qquad 2.2.7$$

and longitudinal relaxation,

$$L(t) = \mathrm{Tr}\ \{I_z(t)\ I_z(0)\}/\mathrm{Tr}\ \{I_z^2\} \qquad 2.2.8$$

We proceed by transforming $\mathcal{H}_d$ into the *interaction representation*, a frame of reference which *moves* with the Larmor precession created by $\mathcal{H}_z$ and the spin motion due to $\mathcal{H}_m$. Replacing $\mathcal{H}$ in equation 2.2.6 by $\mathcal{H}_d^*$ the transformed $\mathcal{H}_d$, where,

$$\mathcal{H}_d^*(t) = \exp\left(\frac{i}{\hbar}(\mathcal{H}_z + \mathcal{H}_m)t\right)\ \mathcal{H}_d\ \exp\left(-\frac{i}{\hbar}(\mathcal{H}_z + \mathcal{H}_m)t\right) \qquad 2.2.9$$

The relevant components of $\boldsymbol{I}(t)$ for use in equations 2.2.7 and 2.2.8 are obtained from the solutions of the substituted equation 2.2.6. Since $\mathcal{H}_d$ is small w.r.t. $\mathcal{H}_z$+$\mathcal{H}_m$ we can perform a perturbation expansion on $\mathcal{H}_d^*(t)$ to study $L(t)$ and $F(t)$. Unfortunately even small expansions involving $\mathcal{H}_d^*(t)$ diverge at long times to any finite order of expansion [87]. The approach of Kubo [91] overcomes this problem by expanding the logarithm of the relaxation function as far as the second order term (the first non-zero one), the higher order terms are approximated by the lower order one(s). Originally developed for NMR lineshape studies it has been generalised by Cowan to treat spin-echo [87] and longitudinal relaxation [70]. The resultant expressions for the relaxation functions are;

$$F(t) = \exp\left[-\int_0^t (t-\tau) \sum_{m=-2}^{2} \left(3 - \frac{m^2}{2}\right) G_m(\tau)\ \exp(im\omega_0\tau)\ d\tau\right] \qquad 2.2.10$$

$$L(t) = \exp\left[-\int_0^t (t-\tau) \sum_{m=-2}^{2} m^2\ G_m(\tau)\ \exp(im\omega_0\tau)\ d\tau\right] \qquad 2.2.11$$

where,

$$G_m(\tau) = \mathrm{Tr}\ \{D_m(0)\ D_{-m}(\tau)\}/\ \mathrm{Tr}\ \left\{I_z^2\right\} \qquad 2.2.12$$

are the autocorrelation functions of the dipolar Hamiltonian. Using equation 2.2.5,

$$G_m(\tau) = \frac{4\pi\hbar^2\gamma^4}{5N}\left(\frac{\mu_0}{4\pi}\right)^2 \sum_{\substack{i<j \\ k<l}} \frac{Y_2^{-m}(\Omega_{ij}(0))\ Y_2^{m}(\Omega_{kl}(\tau))}{r_{ij}^3\ (0)\ r_{kl}^3\ (\tau)}\ \Gamma_{ijkl}^m(\tau) \qquad 2.2.13$$

As before the Y_2^m describe classical motion and the symmetric four-spins correlation function $\Gamma_{ijkl}^m(\tau)$ describes motion in spin-space, being written in terms of the T_{ij}^m **70**. Providing the $G_m(\tau)$ decay to zero sufficiently rapidly the integrals in equations 2.2.10 and 2.2.11 can be extended to infinity and the relaxation becomes exponential **92** and

$$L(t) \propto \exp(-t/T_1) \qquad 2.2.14$$

$$F(t) \propto \exp(-t/T_2) \qquad 2.2.15$$

and,

$$1/T_1 = J_1(\omega_0) + 4J_2(2\omega_0) \qquad 2.2.16$$

$$1/T_2 = (3/2)\ J_0(0) + (5/2)\ J_1(\omega_0) + J_2(2\omega_0) \qquad 2.2.17$$

can be written. The spectral density functions $J_m(\omega)$ describe the power density of the dipolar local field fluctuations and are the Fourier Transforms of the $G_m(\tau)$.

$$J_m(\omega) = \int_{-\infty}^{+\infty} G_m(\tau)\ \exp(i\omega\tau)\ d\tau \qquad 2.2.18$$

The oscillating exp. terms in 2.2.10 and 2.2.11 ensure that L(t) and the non-adiabatic terms of F(t) give exponential relaxation. In a 3D system the spectral densities will typically be Lorentzian,

$$J_n(\omega) = \hbar^2\gamma^4 \left\langle \frac{1}{r_{ij}^6} \right\rangle \left(\frac{\mu_0}{4\pi}\right)^2 \left(\frac{2}{3}\right) \frac{\tau_c}{1 + \omega_0^2 \tau_c^2} \qquad 2.2.19$$

resulting in exponential relaxation processes. In 2D the situation is quite different because of the reduced dimensionality. For adsorbed spins, confined to a plane the angles θ_{ij} and ϕ_{ij} on which the spherical harmonics depend are no longer independent [70]. It is convenient to transform the $G_m(\tau)$ into a frame of reference co-planar with the substrate surface,

$$G_0(t) = \frac{27}{64} \hbar^2\gamma^4 \left(\frac{\mu_0}{4\pi}\right)^2 \left[\left(\sin^2\beta - \frac{2}{3}\right)^2 g_0(t) + \frac{\sin^4\beta}{2} g_2(t) \right] \qquad 2.2.20$$

$$G_1(t) = \frac{9}{32} \hbar^2\gamma^4 \left(\frac{\mu_0}{4\pi}\right)^2 \left[\cos^2\beta \sin^2\beta \, g_0(t) + \frac{\sin^2\beta \, (1 + \cos^2\beta)}{2} g_2(t) \right] \qquad 2.2.21$$

$$G_2(t) = \frac{9}{128} \hbar^2\gamma^4 \left(\frac{\mu_0}{4\pi}\right)^2 \left[\sin^4\beta \, g_0(t) + \frac{\cos^4\beta + 6\cos^2\beta + 1}{2} g_2(t) \right] \qquad 2.2.22$$

β is the angle the substrate normal makes to B_0 and the reduced correlation functions are,

$$g_n(t) = \frac{4}{3N} \sum_{\substack{i<j \\ k<l}} \frac{\exp\left(-in\phi_{ij}(0)\right) \exp\left(in\phi_{kl}(t)\right)}{r_{ij}^3(0) \, r_{kl}^3(t)} \Gamma_{ijkl}^n(t) \qquad 2.2.23$$

Unlike $g_2(t)$, $g_0(t)$ does not depend on the fluctuating $\phi_{ij}(t)$, only on the $r_{ij}(t)$. This rotational degeneracy gives $g_0(t)$ the long time t^{-1} tail characteristic of 2D systems with $g_2(t)$ decaying asymptotically as t^{-2}. The corresponding reduced spectral densities $j_0(\omega)$ and $j_2(\omega)$ exhibit the logarithmic divergence and constant low frequency behaviour as seen in 3D systems (equn. 2.2.19), respectively. The $J_0(\omega)$, $J_1(\omega)$ and $J_2(\omega)$ are, by substitution,

$$J_0(\omega) = \frac{27}{64} \hbar^2\gamma^4 \left(\frac{\mu_0}{4\pi}\right)^2 \left[\left(\sin^2\beta - \frac{2}{3}\right)^2 j_0(\omega) + \frac{\sin^4\beta}{2} j_2(\omega) \right] \qquad 2.2.24$$

$$J_1(\omega) = \frac{9}{32}\hbar^2\gamma^4\left(\frac{\mu_0}{4\pi}\right)^2\left[\cos^2\beta\sin^2\beta\, j_0(\omega) + \frac{\sin^2\beta(1+\cos^2\beta)}{2}\, j_2(\omega)\right] \qquad 2.2.25$$

$$J_2(\omega) = \frac{9}{128}\hbar^2\gamma^4\left(\frac{\mu_0}{4\pi}\right)^2\left[\sin^4\beta\, j_0(\omega) + \frac{\cos^4\beta + 6\cos^2\beta + 1}{2}\, j_2(\omega)\right] \qquad 2.2.26$$

Cowan **[70]** has treated the case of a 2D diffusive fluid, a useful model for the low coverage 2D gas phase and a 2D triangular-lattice solid with exchange, for the higher coverage low temperature solid film (both incommensurate and commensurate). The results are summarised below.

2.2.1 (a) A 2D Diffusive Fluid

For this model the time dependence of the $g_n(t)$ comes from the $\phi_{ij}(t)$ only since the motion is purely bodily-classical. The motion of the individual spins is highly complex and it becomes necessary to replace the summation in equation 2.2.23 with an integral over a probability distribution in any practical calculation. Using a probability function appropriate for a system obeying the 2D diffusion equation **[70]**,

$$g_n(t) = \frac{2\pi\alpha}{a^4}\int_0^\infty x^3\exp\left(-\frac{tx^2}{\tau_0}\right)\left[\int_x^\infty \frac{J_n(y)}{y^2}\,dy\right]^2 dx \qquad 2.2.1.1$$

can be written. 'α' is the spin density, '*a*' the *hard core* spin radius, τ_0 is the time taken to diffuse a distance '*a*' and the $J_n(y)$ are Bessel functions.

$$\tau_0 = \left(\frac{a^2}{2D}\right) = 4Xa\sqrt{\frac{m}{2kT}} \qquad 2.2.1.2$$

where '*D*' is the 2D diffusion coefficient and '*m*' the mass of a helium atom. The above integral cannot be evaluated analytically but has been done numerically. With the corresponding reduced spectral density,

$$j_n(\omega) = \frac{2\pi\alpha}{a^4}\,\tau_0 \int_0^{\infty} \frac{2x^5}{x^4 + \omega^2\tau_0^2} \left[\int_x^{\infty} \frac{J_n(y)}{y^2}\, dy \right]^2 dx \qquad 2.2.1.3$$

the relaxation times can be calculated. T_1 (equation 2.2.16) is straightforward. However the adiabatic term in T_2 (equations 2.2.17 and 2.2.24) needs special treatment, the problem being in the low frequency logarithmic divergence of $j_0(\omega)$. Briefly, this contribution to T_2 can be written in terms of an *instantaneous* relaxation rate,

$$\frac{1}{T_2(t)} = \frac{81}{64}\,\hbar^2\gamma^4 \left(\frac{\mu_0}{4\pi}\right)^2 \left(\sin^2\beta - \frac{2}{3}\right)^2 \int_0^t g_0(\tau)\, d\tau \qquad 2.2.1.4$$

Note that '$1/T_2(t)$' increases with 't', that is, the relaxation is faster than exponential. In analogy with the NMR *rule of thumb* in 3D, $1/T_2 = m_2\tau_c$ an approximate representation for the adiabatic contributions to T_2 can be made **[70]**. It uses an empirical correlation function $g_0(t)$ having the correct long time tail and t=0 value,

$$g(t) = \frac{g(0)}{1 + t/2\tau_0} \qquad 2.2.1.5$$

giving the implicit equation,

$$1/T_2 \approx 2\ln(T_2/2\tau_0 e) \left[\frac{81}{128}\,\frac{\pi\alpha\hbar^2\gamma^4}{a^4} \left(\frac{\mu_0}{4\pi}\right)^2 \left(\sin^2\beta - \frac{2}{3}\right)^2\right]\tau_0 +$$

[..... $g_0(t)$ contribution to m_2 .....]

$$0.329 \left[\frac{81}{256}\,\frac{\pi\alpha\hbar^2\gamma^4}{a^4} \left(\frac{\mu_0}{4\pi}\right)^2 \sin^4\beta\right]\tau_0 \qquad 2.2.1.6a$$

[... $g_2(t)$ contribution to m_2 ...]

After solving the implicit equation the non-adiabatic relaxation-rate contributions (see equations 2.2.25, 2.2.26),

$$\ldots + \frac{5}{2}\, J_1(\omega_0) \;+\; J_2(2\omega_0) \qquad 2.2.1.6b$$

complete the expression for T_2.

Unfortunately having used diffusion, a concept only valid for times > τ_0, little information can be reliably expected for $\omega_0\tau_0 \gtrsim 1$ where the T_1 minimum should occur, without resorting to a microscopically more rigorous model which plays a crucial role in the short time behaviour of the correlation functions. The above results are for the simple model 'A' diffusive system which has the defect of allowing particles to glide through each other instead of bouncing at collision.

2.2.2 (b) A Solid With Exchange

A solid with exchange is in many respects fluid-like. In the hydrodynamic limit the Heisenberg exchange Hamiltonian,

$$\mathcal{H}_x \;=\; -2\hbar \sum_{i<j} J_{ij}\, \boldsymbol{I}^i.\boldsymbol{I}^j \qquad 2.2.2.1$$

leads to spin diffusion [7,87,93]. For nearest neighbour two-particle exchange $J_{ij} = J = constant$ for nearest neighbours and zero otherwise and $D = cJd^2$ can be written. 'c' depends on the lattice structure as discussed in §1.10.6 and 'd' is the nearest neighbour separation. It seems likely that three [94] or more particle exchange will be dominant for the 2D triangular lattice. These higher order processes can, however be represented in terms of an effective two-particle exchange frequency J. With no classical motion in the film the ϕ_{ij} are time independent, the time dependence of the $g_n(t)$ being due to $\Gamma^m_{ijkl}(t)$. The short time behaviour of the $g_n(t)$ can, in contrast with the fluid case, be obtained accurately from a moment expansion, the long time behaviour being obtained in analogy with the diffusive fluid which also allows a connection between τ_0 and J to be made, $\tau_0 = 0.267/J$ [70]. Armed with the long and short time behaviour, analytic empirical expressions for $g_n(t)$ can be arrived at for use in calculations which possess the correct asymptotic forms [72,76,70].

$$\frac{g_0(t)}{g(0)} \;=\; \frac{P_0}{\sqrt{1 + a_0^2\, t^2 J^2}} + \frac{Q_0}{1 + b_0^2\, t^2 J^2} \qquad 2.2.2.2$$

$$\frac{g_2(t)}{g(0)} = \frac{P_2}{1 + a_2^2 t^2 J^2} \qquad 2.2.2.3$$

Where, $P_0 = 0.524$ $a_0 = 0.9799$

$Q_0 = 0.476$ $b_0 = 3.4751$

$P_2 = 1.00$ $a_2 = 3.5355$

The values of a_0 and b_0 have been obtained from experimental data obtained on Grafoil with $\beta=90^0$ **[76]**. The corresponding spectral densities are given by **[76]**,

$$\frac{j_0(\omega)}{g(0)} = \frac{2P_0}{a_0 J} K_0\left(\frac{\omega}{a_0 J}\right) + \frac{Q_0 \pi}{b_0 J} \exp\left(-\frac{\omega}{b_0 J}\right) \qquad 2.2.2.4$$

$$\frac{j_2(\omega)}{g(0)} = \frac{P_2 \pi}{a_2 J} \exp\left(-\frac{\omega}{a_2 J}\right) \qquad 2.2.2.5$$

where $K_0(x)$ is the modified Bessel function of zero order.

Chapter 3
Boron Nitride

3.1 Introduction

As discussed in the previous chapter NMR studies of the Grafoil/^{3}He system have been very illuminating. Unfortunately Grafoil has a number of undesirable features which has motivated the search for other similar substrates. Despite the large exposed basal plane area and low proportion of higher energy adsites the average dimension of uninterrupted platelet basal plane area is only about 100Å restricting 2D dynamics to these microscopic dimensions. It may also influence 2D melting due to finite size effects [34]. From the NMR point of view the intra-planar conductivity and large anisotropic diamagnetism are much more serious. Experimentally, eddy current heating in the substrate limits the RF pulse repetition rate and prevents experiments at high frequencies or those that require long duration pulses such as in $T_{1\rho}$ measurements. Throughout most of the phase diagram T_2 is dominated by substrate diamagnetism. As the relaxation in the substrate induced field gradients is not properly understood the diffusion coefficient cannot be reliably obtained from spin-echo/applied field gradient experiments. For these reasons Boron Nitride (BN) has been investigated as an alternative substrate for ^{3}He adsorption experiments.

3.2 General Properties

BN and carbon are structurally very similar, being isoelectronic [95]. Both exist as a cubic (ie. diamond like) and hexagonal (ie. graphitic) polymorph. Like graphite the hexagonal form has solid lubricant properties and has been called *white graphite*. It is a refractory material and is stable against dissociation to 1700^{o}C in vacuo. The 3 × B−N in-plane bonds form the hexagonal array, the layers being stacked with the hexagons immediately above one another, the B−N alternation being maintained from layer to layer, (figure 3.2.1). This contrasts with graphite in which the hexagonal array of an intermediate layer has a horizontal offset [95]. There is a voluminous literature on BN, much of it relating to its physical properties such as hardness in connection with its industrial use in special coatings etc. [96]. The structural similarity with graphite was realised early on and it has been the subject of much experimental (see refs. **97**, **98**, **99**, **13**, **100**, **101**, **102**, **103**, **104**, **105**, **106**, **107**, **108**, **109**, **110**, **111**, **112**, **113**, **114**, **115**, **116**,

Figure 3.2.1, The Crystalline Structure of Graphite and Hexagonal Boron Nitride

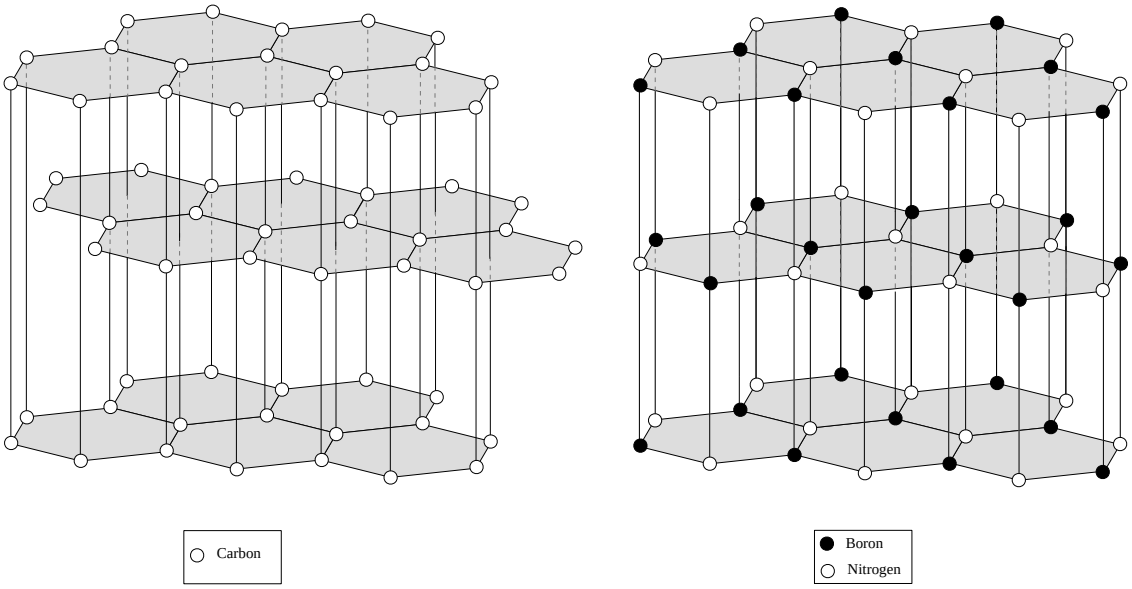

Graphite Boron Nitride

117, **118**, **119**, **120**, **121**, **122**, **123**, **124**, **125**) and theoretical (see refs. **126**, **127**, **128**, **102**, **129**, **115**, **130**, **114**) adsorption work from as far back as 1958 **[10]**. It is surprising that so little NMR adsorption work has been carried out with it. A search of the literature **[96,131]** reveals the only work that appears to have been done involves 2D phase transitions in deuterium substituted benzene and fluorobenzene at liquid nitrogen to room temperatures **[132,133]** and quite recently H_2 **[119,121,124]**, HD **[120]**. A preliminary investigation of the ^{3}He/BN system has been performed within the research group by Fardis **[76]**. His work will be discussed in §3.4. The rest of this section discusses the BN adsorption work that has been carried out allowing comparison with graphite systems to be made.

3.3 Adsorption work on BN

Hexagonal BN has been shown to possess very similar characteristics to graphite (see refs. **99**, **103**, **109**, **110**, **111**, **129**, **112**, **114**, **13**, **100**, **102**, **103**, **134**, **104**, **105**, **107**, **135**, **130**, **114**, **116**, **118**) having about the same homogeneity as graphitised carbon black graphitised at 1800^{o}C judging by adsorbed film T_2c (2D critical temperatures) values **[114]**. The smoothness of the adsorption potentials of the cleavage planes of these substrates is demonstrated by their having the lowest T_2c and T_2t (2D triple point temperatures) values **[105]**. It must be borne in mind when making

comparisons that work with several different grades of BN from at least five different manufacturers (Norton Co. [114], Carborundum Co. [13,106,108,110,111,112], Hopkins & Williams [115], Union Carbide [97,98,13,101,103,104,105,107] and Le Carbone Lorraine [13,103]) has been done. Like graphitised carbon black the resolvable features depend on heat treatment; Two features were visible after heat treatment at 300°C and three at 900°C in one case [103]. Wide variation in surface area also occurs; the three most used manufacturers samples (UC, CC [HCP-325] & LCL) having areas in the range $3m^2/g$ to $14m^2/g$ [103]. BN from Hopkins & Williams showed surface areas as high as $120m^2/g$ [115]. Our BN was Carborundum Co. HCP (high purity coarse) SHP-325. The sieve mesh number 325 indicates an average particle size of ~50μm. However electron micrographs showed that they were conglomerates of smaller flat particles with sizes between 2μm and 10μm [76]. The only article to explicitly state using an identical sample [112] found the Argon BET area to be $19.6m^2/g$ (heat treatment was to 450°C) against our $7.62 \pm 0.1m^2/g$ (heat treated to 1000°C, see §4.1.1.1). This discrepancy is in qualitative agreement with graphitised carbon black which showed a decrease in surface area after heat treatment to 1000°C [114].

Low coverage (X<0.1) films revealed deviations from Henry's law due to heterogeneity. However the heterogeneity did not prevent vertical discontinuities at 2D condensation suggesting it occurs in distinct patches [111], c.f. non-crystalline amorphous substrates such as Mylar where no phase transitions are observed [136]. A second virial coefficient calculation of adsorption potentials which assumed a single exposed surface produced values lower than experiment, again indicating the presence of higher energy adsites [110]. Analyses assuming two different adsorption areas [106,108] produce results much closer to predictions. In more recent work [116] using Ar, Kr & Xe and a second virial coefficient analysis the model misfit (the size of the minimised parameter at convergence) was 300× larger in the single surface case, unlike P33 (a graphitised carbon black). The two areas are largely the hexagonal basal planes and the higher energy crystallite edge sites [13,101,106,108,110]. The truncated polygonal bi-pyramids of P33 (2700) a high temperature graphitised carbon black lack significant edge area and demonstrate Henry's law, single surface behaviour [108,110]. Curiously a numerical inverse-problem analysis [135] of the distribution of adsorption potentials failed to reveal the presence of BN edge sites. There appears to be considerable variation in the proportion of edge area from sample to sample. Electron micrographs suggest 5-10% [106,108], an adsorption model independent two surface virial coefficient analysis claims 3.25% [106]. A simultaneous adsorption/dielectric isotherm experiment [101] in which an isotherm feature

was attributed to the filling of edge sites puts the figure at 9%. More recent work [13] suggests as much as 30% can be non-uniform, the most recent study [116] gives 3.0%. This quantity has considerable bearing on the interpretation of our data which we believe to indicate 5% non basal plane area.

BN isotherms tend to show less structure than their graphite counterparts. This is believed to be due to the lower binding energy of BN which increases the population of higher layers and not due to heterogeneity [111,112]. Evidence from the isoteric heats of adsorption suggests the nett adatom-adatom interaction is greater since the adsorbate is less strongly bound to the substrate. Some recent work [118] has indicated that there is in fact less corrugation in the BN−rare-gas adsorption potential than with graphite − a more ideal adsorber. Theoretical calculations show closer agreement with experimental data for BN than graphite once edge area is accounted for [126,108,112], due to the covalently bonded, non-polar, non-conducting nature of BN [112]. Approximately 4% of the graphite hexagon π electrons contribute to electrical conduction [112]. The graphite adsorption potential has been put at 2%−4% greater than BN [108] and more recently [127] at 10%−15%.

Increasingly detailed isotherm measurements have resolved layer completion in distinct higher layers; 2 layers for NO/BN [109], 3 for Kr/BN [101] and very recently 5 with Ar/BN [97], figures 3.3.1 (taken from reference **109**) and 3.3.2 (taken from reference **101**) show isotherm plots, demonstrating the exceptional homogeneity of the substrate adsorption potential.

Boron and Nitrogen have slightly different electronegativities making the B−N bond weakly polar, opening up the possibility that the hexagon centre may not be the preferred adsite for localised adsorption as it is on graphite. Dispersion force calculations have however, shown [115,130] that of four sites investigated (over N, over B, halfway between B−N on bond axis and over hexagon centre) the hexagon centre is energetically preferred [115,130]. Using the CNDO/2 molecular orbital procedure it has been shown in detail that for hydrogen, symmetrical adsorption about the B−N bond should occur but for the strongly electronegative oxygen atom the preferred adposition is shifted towards the nitrogen [129].

A variety of phase transitions have been observed in adsorbed films on BN. The dimerisation transition in Nitrogen Oxide (NO) is similar but not identical to graphite [105,109]. Submonolayer Argon-on-BN isotherms [98] have shown a step at X=0.95, which has been identified as possibly the signature of weakly first-order melting. The 2D isothermal compressibility shows a sharp peak at melting plus a broader peak at lower pressures which may be, due to the disappearance of an intermediate regime of

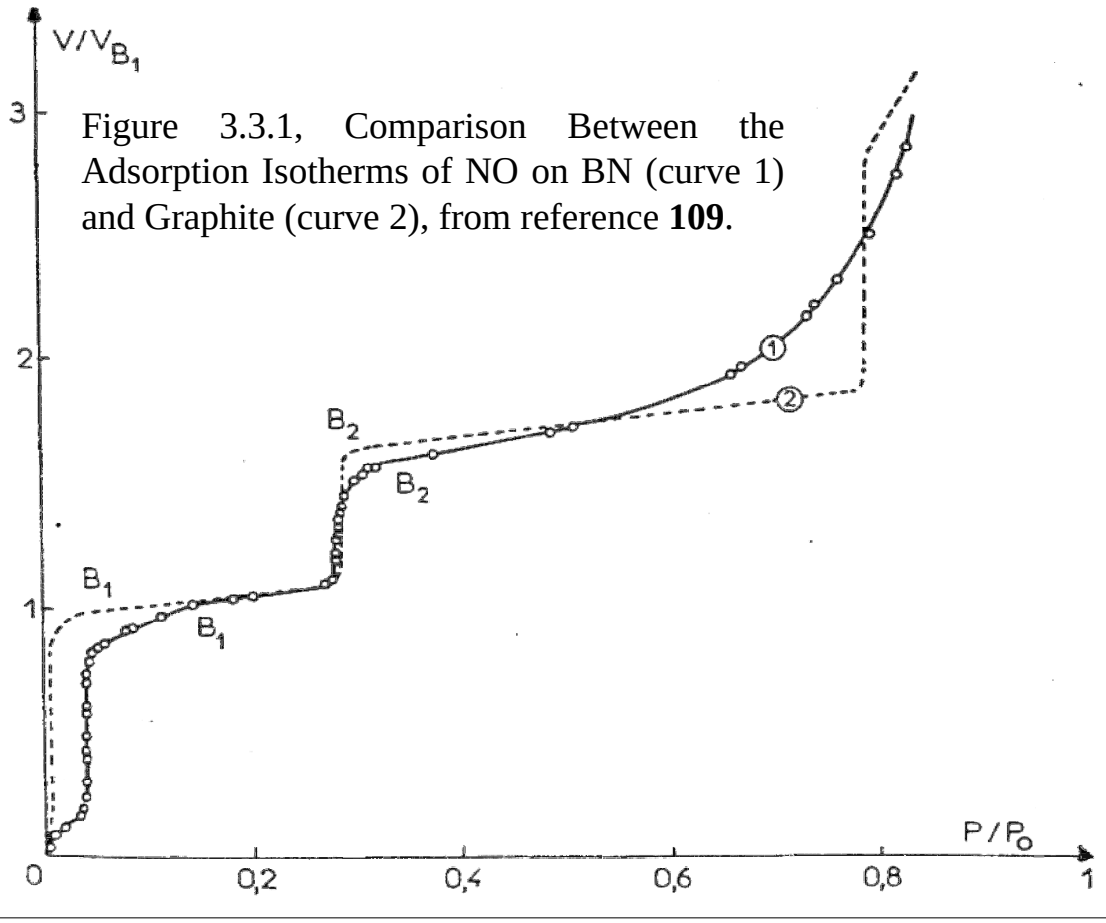

Figure 3.3.1, Comparison Between the Adsorption Isotherms of NO on BN (curve 1) and Graphite (curve 2), from reference **109**.

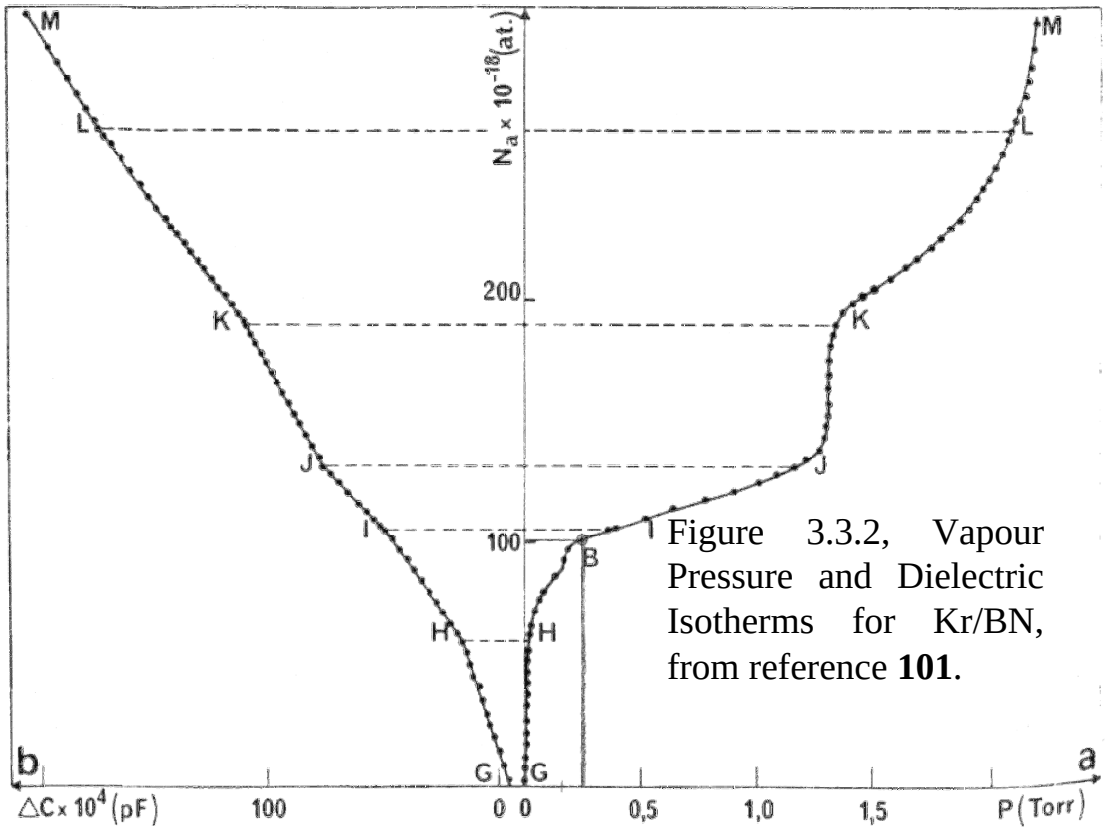

Figure 3.3.2, Vapour Pressure and Dielectric Isotherms for Kr/BN, from reference **101**.

Fig. 1. (a) Adsorption isotherm of Kr–BN at 78.30 K. (b) Dielectric isotherm of Kr–BN at 78.30 K. Capacitance variations ΔC versus the number of adsorbed atoms N_a.

short ranged solid-like domains, or due to increasing disorder with increasing temperature in a liquid phase strongly influenced by the substrate **98**. ie. a KTHNY type process. cf. the graphite results (§1.6). A corresponding multilayer adsorption study has shown reentrant layering in the 3rd and 4th layers together with two-feature melting processes in the 2nd and 3rd layers **97** and references therein.

Information on the effects of dimensional incompatibility on the phases the film is capable of supporting can be obtained by comparing BN with graphite systems: The crystalline dimensions differ by only ~2% **13**. The lattice parameters from X-ray diffraction measurements **137** are; BN (a=b=2.50Å, c=6.66Å also r=4.33Å), graphite (a=b=2.46Å, c=6.71Å also r=4.26Å) **107,112**. 'r' being the adatom separation in the registered phase, r={a,b}$\sqrt{3}$, see figure 1.8.3.1. For both substrates the largest (T_2c/T_3c) and largest liquid−solid coexistence regions (T_2c−T_2t) occur with the lowest dimensional incompatibility **134**. NB: T_3c is the bulk critical temperature. Both CH_4/Graphite and CH_4/BN show 2D gas, liquid and solid phases **104**, the dimensional incompatibility being approximately zero **134**. They also melt via first order phase transitions, a consequence of the imposition of increased spatial order by the substrate. With Kr/Graphite 2D gas, liquid, commensurate and incommensurate solids form but Kr/BN displays only a single continuous phase transition **13,134,107**. With the slightly smaller Kr atom, the dimensional incompatibility makes the 3 phase transitions for Kr/Graphite borderline, the 2% size difference of BN being enough to suppress the above phases **13,134**. For reference the following lists the BN adsorption work encountered in the literature, by adsorbate: H_2 (**119**, **121**, **124**); HD (**120**); Oxygen (**125**); Neon (refs. **108**, **110**); Argon (refs. **116**, **97**, **98**, **126**, **103**, **106**, **108**, **110**, **112**, **113**, **130**, **114**); Krypton (refs. **126**, **13**, **101**, **102**, **134**, **106**, **107**, **108**, **110**, **122**); Xenon (refs. **126**, **13**, **101**, **134**, **106**, **107**, **108**, **110**, **122**); NO (refs. **13**, **105**, **109**); Nitrogen (refs. **135**, **112**, **114**, **122**); Methane (refs. **13**, **102**, **134**, **104**); Ethylene (ref. **13**); Benzene (refs. **100**, **111**, **132**, **133**).

3.4 The ^{3}He/BN Pulse NMR Work of Fardis **76**

(The First Three Sample Chambers)

Introduction

Some of the NMR properties of ^{3}He on BN contrast starkly with ^{3}He/Graphite but in other respects are very similar.

- The signal heights are insensitive to pulse height/lengths and repetition rates due to the insulating nature of BN.

- T_2 is essentially frequency independent due to the much lower substrate diamagnetic susceptibility, Graphite: 1.73 × 10^{-5} emu/gr **[58]**, BN: 0.48 × 10^{-6} emu/gr **[138]**.
- Both relaxation processes are almost universally strongly sub-exponential. The relaxation times were characterised by Fardis using a $T_{1,2}$(1/e) measure, the time taken for the signal to relax by a factor of '1/e' from its initial value, the relaxation being modelled by a double exponential fit.

This work was performed on a series of three sample chambers. It has not been published and is summarised here together with some of the explanation given.

3.4.1 Sample Chamber 1.

A poor S/N ratio due to a low BN packing density (Monolayer capacity: 18cm^3 at STP) and short relaxation times resulting from PMI contamination of the sample during heat treatment in a stainless steel sample holder, characterised this cell. The concentration of iron impurity, amongst other metals, increased by ~50× during heat treatment. T_1 increasing as T=4K→1K was explained by a *dirty wall* mechanism **[67]** where $T_1^{\text{wall}} \propto 1/D$, the larger '$D$' the diffusion constant is the more likely a spin is to visit a PMI at the *wall* and relax, 'D' increasing with temperature. Preplating with a layer of ^{4}He produced exponential relaxation − indicating substrate responsibility for the non-exponentiality. T_2 was independent of X at low X, falling off to form the usual minimum at X=1.

3.4.2 Sample Chamber 2.

This provided a better S/N ratio (Monolayer capacity: 23.5cm^3 at STP) but also suffered from contamination. Sub-exponential relaxation times, T_2 independent of F_0 and $T_1 \propto F_0$ at intermediate coverages X~0.5 were seen. For $X \geqslant 0.7$ deviation from $T_1 \propto F_0$ occurred, a better fit being $T_1 = T_1(0)\exp(F_0/F_{\text{scale}})$. However the expected reduction in $T_1(0)$ and F_{scale} as $X \rightarrow 1$ and motion slows was not seen, pointing to non-dipolar relaxation. See also §7.2.4.1.

3.4.3 Sample Chamber 3.

Without sample-holder contamination and reasonable S/N ratio (Monolayer capacity: 22.5cm^3 at STP) a large increase in T_2 was seen indicating the previous short T_2s were due to PMI contamination. For comparison sample chamber 2 (SC#2) gave

T_2=1mS at X=0.52, T=1.2K **76, fig.7.5.1**. The corresponding SC#3 T_2=10mS and even at X=0.82, T_2=2−5mS **76, figs.7.6.2, 7.6.7, 7.6.23**. In contrast with T_2 and with the usual effect of PMIs on T_1, T_1 was little affected by the reduction in contamination. Eg. At X=0.86 and F=4.72MHz, SC#2 produced T_1=100mS, **76, fig.7.5.5**, the same as in SC#3 **76, fig.7.6.21**. T_2 was frequency independent and together with T_1, strongly sub-exponential as before. At higher coverages 0.8<X<0.9 T_1 and T_2 (just about) displayed a maximum in T at T~2K. For $T<T^{max}$ T_1 followed an Arrhenius, activation law relation before becoming temperature independent at low T as expected for dipolar relaxation in an exchange modulated solid. However for X>0.9 (eg. X=0.94) T_1 continued to rise as T fell. A possible explanation is that the maximum corresponds to melting. For $T>T^{max}$ the rapidly diffusing spins relax by interaction with impurities, giving: $T_1^{wall}\downarrow$ as $D\uparrow$ as $T\uparrow$. Whereas for $T<T^{max}$, dipolar relaxation dominates for the slow motion in the 2D solid, giving: $T_1^{dip}\downarrow$ as $\tau_c\uparrow$ as $T\downarrow$, providing $\omega_0\tau_c<1$. However the temperature of the maxima are coverage independent ruling out correspondence with melting. For $T>T^{max}$ T_1^{wall} should be frequency independent which it is not.

Given the activation law behaviour of both relaxation times below T^{max} activation energies E_a can be extracted. From T_1 data E_a decreases as X increases, suggesting that as the film thickens it becomes easier for adatoms to thermally escape from their positions − obviously unphysical for a homogeneous solid with dipolar relaxation. E_a from T_2 possesses the expected behaviour, increasing with X. [Note: This observation together with the unusual relative effect of magnetic impurities on T_1 and T_2 and the exponential 'T_1' relaxation with ^{4}He preplating show quite different explanations from those used to explain Grafoil T_1 data are needed here. As will become clearer in Chapter 7, BN with its strong ^{3}He↔Substrate-spins relaxation can be expected to have very different T_1 behaviour from but broadly similar T_2 behaviour (diamagnetism effects excluded) to the essentially spinless Grafoil]. The values are lower than on Grafoil suggesting the solid is less dense, in accordance with the known **111,112** lower BN substrate binding energy.

T_1 displays a minimum in X in the high coverage solid whose position shifts to higher X at lower frequencies as occurs for dipolar relaxation on Grafoil. A small maximum occurs at X≈0.75 immediately preceded by a small minimum at X≈0.72, the dominant minimum being at X≈0.84 for F=4.72MHz. The variation of the T_1 minima with X gives a Gruneisen ratio d(LnJ)/d(LnX) of 12 which is only half the Grafoil value. T_2 showed a similar variation with coverage to Grafoil except that there was no minimum at X=1. This is believed to be due to sample leakage into the gas handling

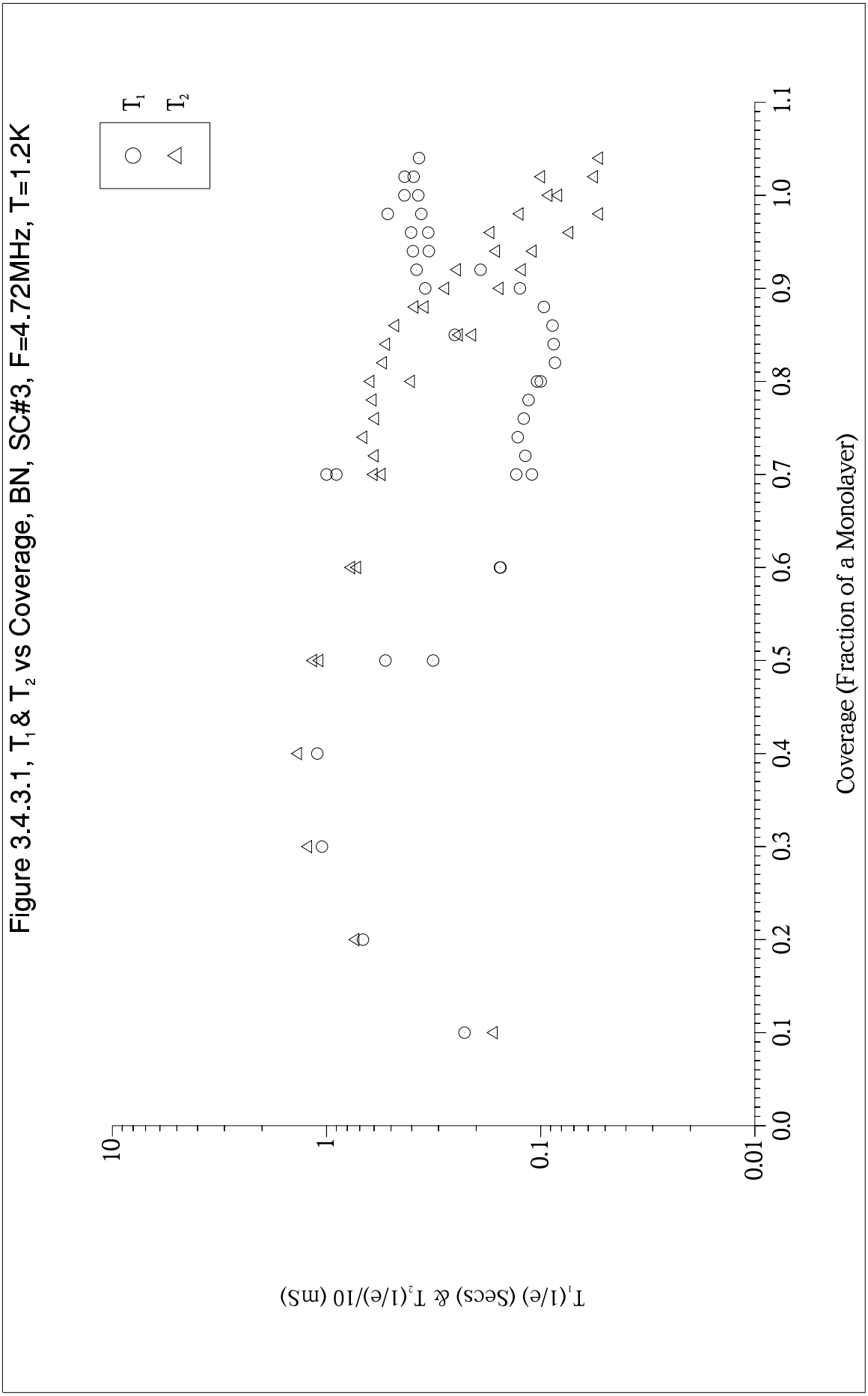
Figure 3.4.3.1, T_1 & T_2 vs Coverage, BN, SC#3, F=4.72MHz, T=1.2K
T_1
T_2
$T_1(1/e)$ (Secs) & $T_2(1/e)/10$ (mS)
10
1
0.1
0.01
0.0
0.1
0.2
0.3
0.4
0.5
0.6
0.7
0.8
0.9
1.0
1.1
Coverage (Fraction of a Monolayer)

system during annealing. Both relaxation times possess a low coverage maximum in X (at X~0.4) like Grafoil, a feature attributed to relaxation in the solid patches which grow with X for $X \geqslant 0.4$. T_1 and T_2 *vs* X are shown in figure 3.4.3.1.

3.5 The FMR Effect

The magnetic relaxation properties of ^{3}He on BN are believed to be strongly influenced by magnetic coupling of the ^{3}He spins to those of the substrate nuclei. Naturally abundant BN contains 4 spin bearing isotopes (see Appendix 1 for details) which potentially all couple with the ^{3}He.

In 1981 Friedman, Millet and Richardson **[139]** published NMR relaxation data for ^{3}He adsorbed on DLX6000 **[140]**, a solid lubricant material consisting of very small (~0.2μm diameter) spherical beads of a fluorocarbon polymer. The ^{19}F and ^{3}He were shown to be magnetically in very close mutual contact, with the ^{3}He recovery to thermal equilibrium occurring 50× more rapidly via the ^{19}F spin bath than its own lattice.

3.5.1 Magnetisation Experiments

Using a crossed coil NMR probe a series of key experiments were performed **[139,141]**;

- Inverting the ^{19}F magnetisation gave an approximately exponential recovery with $T_1 \sim 10^3$ secs, B_0=0.4T.
- Inverting the ^{19}F magnetisation and observing the ^{3}He magnetisation showed it inverting and recovering with the same 10^3 sec T_1.
- After saturating the ^{3}He magnetisation it recovered with a T_1 of only 200mS.

Moreover, applying a succession of ^{3}He 90^o pulses for a few minutes to keep the ^{3}He spins saturated, the ^{19}F magnetisation fell to ~ ½ its equilibrium value m_0, taking several ^{19}F T_1 intervals to be restored after pulsing, the ^{3}He signal being similarly degraded for a comparable period. In general on disturbing the ^{3}He magnetisation it recovered to the current ^{19}F state with the characteristic (200mS at this field) time **[142]**. Such behaviour is the signature of a two bath system **[142]**.

3.5.2 Coverage experiments

The ^{19}F relaxation rate increased by an order of magnitude on addition of approximately one monolayer of ^{3}He, showing some structure around the monolayer point **[139,141,142]**, demonstrating that the ^{19}F T_1 is a useful probe of the state of the ^{3}He

film **142**. No change in the ^{19}F T_1 occurred on addition of ^{4}He **139**. Indeed on preplating with a monolayer of ^{4}He, the preferentially adsorbed ^{4}He effectively severed the ^{3}He−^{19}F coupling, demonstrating that it is a short ranged effect **142**. Replacing the first 0.46 **142,143** of a monolayer of ^{3}He with ^{4}He did not change the ^{19}F T_1, the ^{4}He acting as 'landfill' in the preferential adsorption/heterogeneous regions of the amorphous particles where the ^{3}He−^{19}F coupling is ineffective.

3.5.3 Models

Relaxation in bulk insulating materials normally becomes astronomically slow at low temperatures as the phonon population becomes very small **141**. The dominant relaxation mechanism is believed to be scattering of phonons by nuclear spins. PMIs if present, can enhance the relaxation rate considerably **144** due to the Fourier component of their large fluctuating dipole fields at the nuclear Larmor frequency **141**. Even this mechanism becomes ineffective in very high fields/low temperatures **145** as the electronic polarisation $P_e = \tanh(\hbar\omega_e/kT) \rightarrow 1$ and detailed balance requires that the electronic spin-flip rate $\rightarrow 0$. In very small particles, however the relaxation rate remains appreciable, of the order of hours or minutes. In such particles the spin current can diffuse from/to the interior to the surface in times typically of the order of seconds **139**. If an effective relaxing agent exists at the surface all the spin are rapidly relaxed.

Shown in figure 3.5.3.1 **142** is a simple model for the ^{19}F relaxation in DLX6000. '*i*' represents the ^{3}He spins, 's' represents ^{19}F. The measured ^{19}F T_1 is 10^3 sec, the ^{3}He T_1 being 200mS (at B_0=0.4T). Since $T_{sd} \ll 10^3$ sec the ^{19}F spins remain in thermal equilibrium throughout the particle during ^{19}F relaxation. Very little relaxation takes place inside the beads as indicated by the ^{3}He absent $T_1^{\text{intrinsic}}$ value. Almost all relaxation occurs via the ^{3}He−^{19}F coupling (T_1^{is}) and the intrinsic ^{3}He spin-lattice relaxation pathway, relaxation time T_1^i in a two step process as shown by the response of the ^{3}He magnetisation to ^{19}F magnetisation disturbances. The T_1^s process operates in parallel with the two step one. Given that the measured ^{3}He $T_1 \approx T_1^{is}$ and that the ratio of ^{19}F/^{3}He spins at the surface (which determines the efficiency with which the ^{3}He relaxes the ^{19}F spins) is known the measured ^{19}F T_1 at least puts a lower limit on both T_1^i and T_1^s **142**.

Figure 3.5.3.1, A Simple Model for the Coupled $^{19}F-^{3}He$ Relaxation of DLX6000.

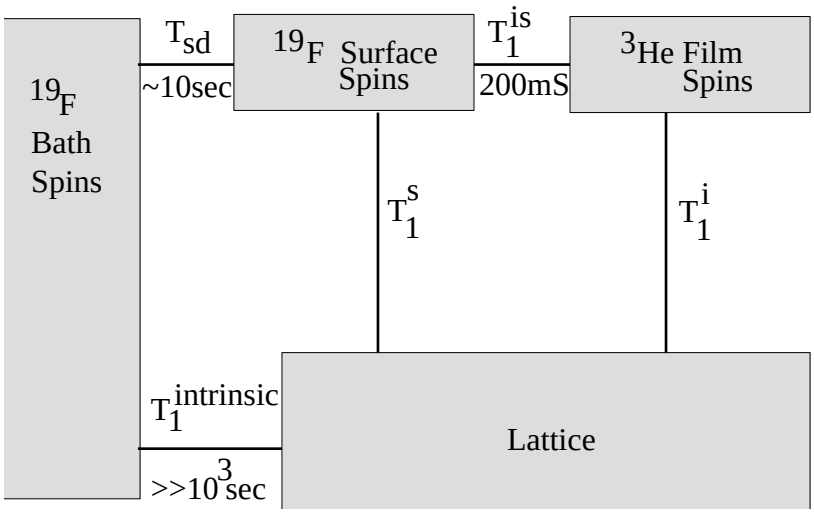

For bigger particles in which $T_{sd} \geqslant$ the measured substrate spins T_1 the recovery will be spin diffusion limited, proceeding as $(Dt)^{½}$ **[145]**. In the context of exponential least squares fitting such experimental data appears strongly sub-exponential.

The exact nature of the $^{3}He-^{19}F$ coupling is still not absolutely certain. There are three classes of model **[146,147]**:

(1) A direct coupling process in which a ^{19}F spin flip is accompanied by a simultaneous ^{3}He spin flop. However the coupling is still efficient at fields at which there is no possibility of *absorption line overlap* given the NMR line widths and difference in gyromagnetic ratios. At B_0=0.4T $F[^{3}He]$=12.6MHz, $F[^{19}F]$=15.6MHz, the respective linewidths being not more than 20KHz and 300KHz **[148]**. This scheme is a non-starter **[146,147]**.

(2) An indirect mechanism **[148]** in which the nuclear Zeeman energy gap is bridged by the dipolar line width of electronic centres **[149,150,147]** known to exist on the DLX6000 bead surfaces **[150]**. There is some evidence **[147]** that this mechanism may operate at higher temperatures (2K<T<4K) but cannot be a general explanation: In very high fields and low temperatures where the electronic polarisation $P_e \rightarrow 1$ the coupling still operates **[149,146]** efficiently. Moreover, annealing the beads near their dissociation temperature which eliminated the centres, believed to be caused by γ-irradiation in manufacture (a commercial secret **[150]**) did not affect the coupling **[146]**.

(3) A direct coupling mechanism as in (1) in which the energy difference

$\hbar(|\omega_F|-|\omega_{He}|)$ is supplied or received by the lattice **[146,150,147]**. Note that it is spin polarisation not energy (as in (2)) which flows between the two isotopes **[147]**. A simple version of this model **[151,142,146,150,147]** is illustrated in figure 3.5.3.2.

Figure 3.5.3.2, The Direct $^{19}F-^{3}He$ Coupling Mechanism.

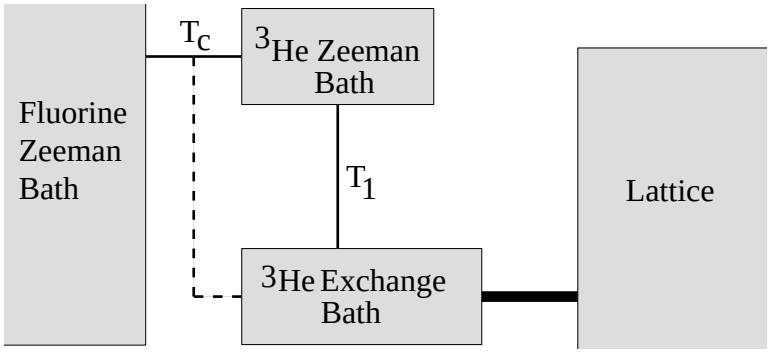

As with the ordinary intrinsic $^{3}He-^{3}He$ spin-lattice relaxation process (T_1) the $^{3}He-^{19}F$ coupling (T_c) is driven by the modulation of the internuclear dipolar interaction by spin motion (exchange in this case) in the helium film. Most but not all (dashed line in the figure) of the spins relax via the ^{3}He Zeeman bath. Using the above simple model good consistency **[146]** has been achieved with the three observables (T_1^F, T_1^{He} and R [the relative decrease in the ^{3}He magnetisation on saturation of the ^{19}F spins]) and the two model parameters T_1 and T_c.

$$\frac{1}{T_1^{He}} = \frac{1}{T_1} + \frac{1}{T_c} \qquad 3.5.3.1$$

$$\frac{1}{T_1^{F}} = \left(\frac{N_{He}}{N_F}\right)\frac{1}{T_1 + T_c} \qquad 3.5.3.2$$

$$R = 1 - \left|\frac{\gamma_F}{\gamma_{He}}\right|\frac{T_1}{T_1 + T_c} \qquad 3.5.3.3$$

(N_{He}/N_F) being the number ratio of spins.

If both relaxation times are determined by the same spectral density describing the film motion they should have the same frequency dependence **[152]**. Measurements of

the ^{3}He T_1 over three decades of frequency [153,154,150] (125KHz − 100MHz) have shown a linear relation, implying the spectral density *cut off* frequency ($\omega \sim 1/\tau_c$) > 100MHz, in conflict with the Θ_{weiss} = 0.55mK ≅ 11MHz result [152] for the exchange frequency in the case of a homogeneous film characterised by a single τ_c [150]. Cowan [68] has shown that for a single τ_c system, $T_1 \propto \omega$ can be understood in terms of the long time behaviour of the 2D correlation functions but only over approximately one order of magnitude in frequency [153,154]. At higher frequencies ($\omega > 1/\tau_c$) T_1 must diverge at least exponentially to satisfy sum rule arguments concerning the moments [68]. The ^{19}F T_1 *vs* ω is in general faster than linear [155]. In a more recent study [147] ^{19}F T_1 was $\propto \omega$ for F<100MHz, becoming quadratic above the frequency. The same measurements have been made on an Aldrich [156] substrate, again a fluorocarbon polymer but having an irregular structure described as resembling 'noodles' [157]. The circular cross section of the Aldrich powder noodles compares with the DLX6000 bead diameter but is typically an order of magnitude greater in length. The nett result of the decrease in surface area is to make $T_c \gg T_1$, suppressing the magnetisation cross flipping effects described in §3.5.1 and causing a measurement of the ^{19}F T_1 to yield T_c alone [157]. The Aldrich ^{19}F T_1 was observed [147] to follow an exp(ω) law [157]. A possible explanation of these features is to argue that T_1 follows a linear and T_c an exponential frequency law [147]. The difference in spectral density attributed to each process results from the inhomogeneity of the solid helium film on the amorphous fluorocarbon surface [153,154]. Supporting evidence comes from experiments in which bulk liquid helium-3 filled the sample chamber containing the beads. Both the diffusive motion in the body of the liquid and the liquid−surface layer solid interchange rate are very rapid [152,150], opening up an extra spectrum of fluctuations to modulate the ^{3}He−^{3}He and ^{3}He−^{19}F dipolar processes [147]. The ^{19}F T_1 is also $\propto \omega$ over three decades of frequency with bulk ^{3}He present [147].

3.5.4 Other Spins

The FMR coupling appears to be a general phenomenon not restricted to ^{3}He and ^{19}F, the only requirement being that the substrate and adsorbate possess a non zero spin species [158]. Coupling to ^{3}He has also been observed with the following substrate spins; ^{1}H [159,160,158,161], ^{2}H [158], ^{11}B [158], ^{13}C [158], ^{14}N [162], ^{29}Si [158] and ^{169}Tm [163]. Proton−fluorine coupling has also been observed using methane on DLX6000 [164]. See Appendix 1 for information on spins.

3.5.5 Context

At low temperatures the Kapitza thermal boundary resistance R_K between liquid helium-3 and certain solids is much lower than predicted by theory and measured for helium-4 **[165,142]**. This is a long standing problem **[141]**. It has been suggested that some form of magnetic coupling across the interface may be responsible for this extra channel of heat flow. The utility of these experiments is that they allow the magnetic heat flow to be studied in isolation from other channels. For further information see references **152**, **141** and **142** and references therein. In some very recent work **[166]** R_K has been measured for ^{3}He/silver-film system. At very low-T (~3mK) there is an order of magnitude increase in R_K when the silver film is preplated by a layer of ^{4}He. Varying the ^{3}He pressure and applied magnetic field demonstrates the presence of the magnetic component.

Chapter 4
The Apparatus

The consideration of the instrumentational part of this project has been split into two parts for convenience. Part-I deals with the cryostat, NMR spectrometer and analogue supporting peripherals, while part-II is concerned with the controlling computer together with those digital peripheral devices to which it is interfaced and by which it monitors/ controls the system.

4.1 Part I, (The Cryostat and Analogue Instrumentation)

4.1.1 The Cryostat

The cryostat (figure 4.1.1.1) which was built in the Physics Department's workshop has been used as a conventional pumped helium-4 system allowing temperatures in the range 1.1K to 4.2K to be achieved. Temperatures greater than 20K are reachable using a 1K/9W wirewound resistor attached to the copper helium-4 pot, when empty. With a pot capacity of ~1 litre, one fill lasts approximately 3 days. Pot filling is via a needle valve controlled inlet from the main helium bath. Temperature control below 4.2K is by regulating the pot pumping rate via a set of 4 parallel solenoid valves each with its own series valve to set its throughput. See figure 4.1.2.1. Additionally for temperatures below 2K a large Quarter Swing Valve (QSV) on the 2" diameter pumping line is used. It is driven by a motor via a worm gear, attached to a dedicated controller unit (QSV Actuator) which, like the solenoid valves is computer controlled. The controller allows three pre-setable open positions in addition to being closed. In this way the available pumping rate is graduated in seven steps.

Two copper vacuum cans isolate the sample chamber from the 4.2K bath. Both are sealed with an Indium ‘O’ ring seal. The inner vacuum can (IVC) is bolted to the pot and filled with ~1 Torr helium exchange gas to maintain thermal contact between the pot and sample chamber. The outer vacuum can (OVC) which encloses the IVC is normally pumped to a high vacuum to isolate the pot from the 4.2K bath. It attaches to the cryostat's 4.2K flange.

The 4.2K bath is contained within a specially built Oxford Instruments dewar which has a nitrogen jacket, a 40K vapour shield and superinsulation to minimise heat

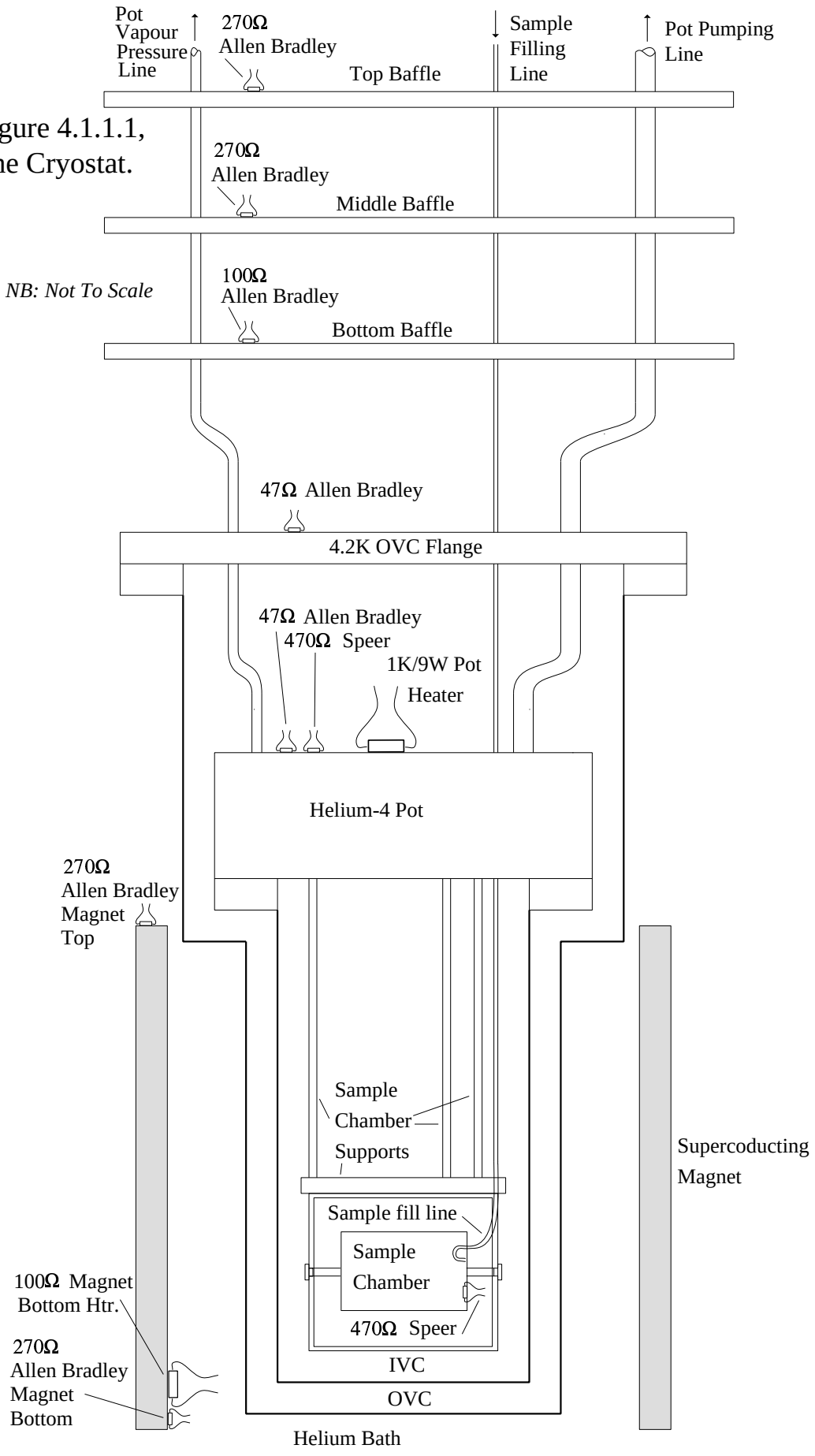

Figure 4.1.1.1,
The Cryostat.

conduction from outside. The cryostat service lines are thin walled stainless steel tube to minimise thermal conduction. Daily helium consumption is 10 litres including ~ 2 litres transfer losses.

Thermometry resistors have been placed at strategic locations in the cryostat (figure 4.1.1.1) enabling the pot, sample chamber, 4.2K flange and the vapour baffles' etc. temperatures to be monitored.

A precision gas handling system based on two 0.1 mBar resolution Druck DPI 100 digital pressure gauges allows helium-3 or other gases to be admitted to the sample chamber with a resolution of 2×10^{-3} ccs gas at STP. The gas handling system is described in detail in references **60** and **61**.

An Oxford Instruments Helium level meter model HLM2 monitors the helium bath level. A set of relay contacts in the unit open when the level becomes dangerously low, risking uncovering the top of the superconducting magnet, allowing the Magnet Controller to safely de-energise it. See figure 4.1.2.1. An Oxford Instruments Nitrogen level meter model NLM2 monitors the nitrogen jacket level, automatically topping up when necessary from a pressurised 200L Statebourne Cryogenics SV series nitrogen transport dewar.

The main magnetic field is supplied by an Oxford Instruments high homogeneity 2T persistent mode superconducting solenoid. It also has a persistent mode Z_1 shim, claimed to be capable of producing a field homogeneity of 10ppm over 1 cubic inch or if used in the opposite sense can be used to narrow the spin-echo. Finally a pair of non-persistent Helmholtz coils permit shifts and gradients to be applied. An Oxford Instruments high stability 0−75Amp magnet PSU drives the main solenoid together with its heat switch. Its output current may be adjusted either from the front panel controls or externally by the microprocessor based Magnet Controller. To reduce helium boil-off due to thermal conduction, the cryostat magnet leads are designed to carry only up to 10A which corresponds to a helium Larmor frequency of about 12MHz.

4.1.1.1 The Sample Chamber

The cylindrical sample chamber is machined from a block of Stycast 1266. It has an inner volume of 1 cubic inch. After compressing the BN powder sample into the sample chamber with a specially machined brass plug the lid was glued on with Stycast 1266. The 1/16" thin walled stainless steel tube filling line was inserted into the end of the sample chamber and sealed, again with Stycast. Inside the sample chamber the

filling line is bend over towards the wall to prevent the sample being sucked out during pumping. See figure 4.1.1.1. A 470Ω ½W Speer thermometry resistor was also embedded in the end. Along its length a 14 turn screw thread has been cut to support a 7-strand *Litz* enamelled copper wire NMR coil. The *live* side of the connection to the coil was covered in Silicon Rubber compound after soldering to avoid an electrical discharge occurring in the low pressure helium exchange gas during high voltage transmitter pulses. More information on the sample chamber's construction is given in reference **76**.

The BN sample was fired in vacuo at 1000ºC for 24 hours to remove contaminants such as water and oxygen. Once cool it was sealed into the sample chamber in a helium atmosphere. During heat treatment the BN was held in a short unused piece of Borosilicate tube rather than in the stainless steel sample holder to avoid contamination. Unfortunately it was omitted to weigh the BN in the sample chamber. However, the point-B isotherm surface area **:** sample mass ratio is highly reproducible **[76]** permitting the mass to be calculated at 10.58 ± 0.04g for a point-B helium-3 monolayer

Figure 4.1.1.1.1, 4.2K Helium-3 Adsorption Isotherm for BN Sample Chamber#4

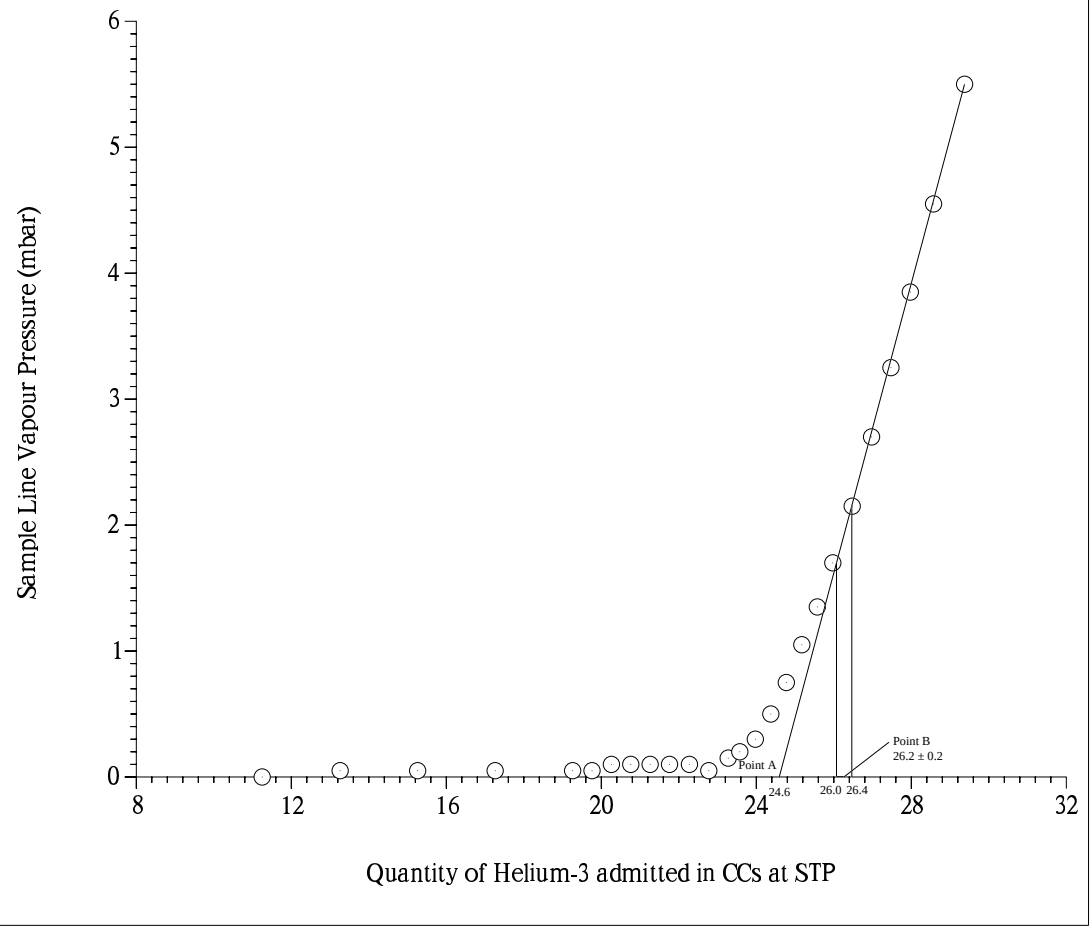

capacity of 26.2 ± 0.2 cm^3 at STP for sample chamber#4. Figure 4.1.1.1.1 shows the isotherm.

4.1.2 The Spectrometer

The pulsed NMR spectrometer was purpose designed and built within the research group and Departmental Electronics Workshop. For convenience and ease of modification it uses a modular design in which each component, eg. mixer, transmitter etc. is a separate module. The modules plug into a Radio Spares 19" rack bin system, the bin powering the modules through a connector at the back of each. A block diagram of the spectrometer together with the other cryostat ancillaries under computer control is shown in figure 4.1.2.1. It is a coherent phase, broadband design based on that described in more detail in references **60** and **61**.

The parallel resonant NMR probe consists of the NMR coil (L=6.74 ± 0.04μH, $C_{intrinsic}$=9.5 ± 0.4pF) in parallel with a nearby 33pF silvered mica capacitor (for thermal anchoring as well as capacitance) together with the capacitance of the cryostat stainless steel coaxial downline (75pF) which gives a natural resonant frequency of around 5MHz. At 4.2K the quality factor Q of the tank circuit varied between 100 and 350 or more. It was measured using a HP vector impedance meter model 4391A. The reason for the variation is unclear but may have been due to moisture entering the NMR coil coaxial downline through a leaky cryostat-top glass-metal seal. The most violent Q fluctuations occurred during and shortly after cool-down to 4.2K. At frequencies close to natural resonance the high Q caused significant spectrometer deadtime (typ. 200μS) after the pulse. Where necessary a 250kΩ potentiometer in parallel with the tank circuit was used as a Q-spoiler. Tank circuit resonant frequencies in the range 2.7MHz to 10.7MHz were obtained by parallel adding inductors or capacitors via the matching unit, the degradation in signal being typically ×4−×8 w.r.t. the ~5MHz peak. The *frequency stepper* performs this function. It consists of a wafer switch bearing 6 capacitors/inductors (plus one open position) driven by a Ledex stepping motor and has a computer interface, being designed with computer controlled spectrometer frequency changing in mind. Considerable progress has been made towards computer controlled NMR frequency changing. Automatic tank circuit re-tuning using a HP3325A frequency synthesizer and a Philips PM3311 digital storage oscilloscope has already been achieved. It is convenient to discuss the rest of the spectrometer in terms of its two sections, the transmitter (TX) and receiver (RX).

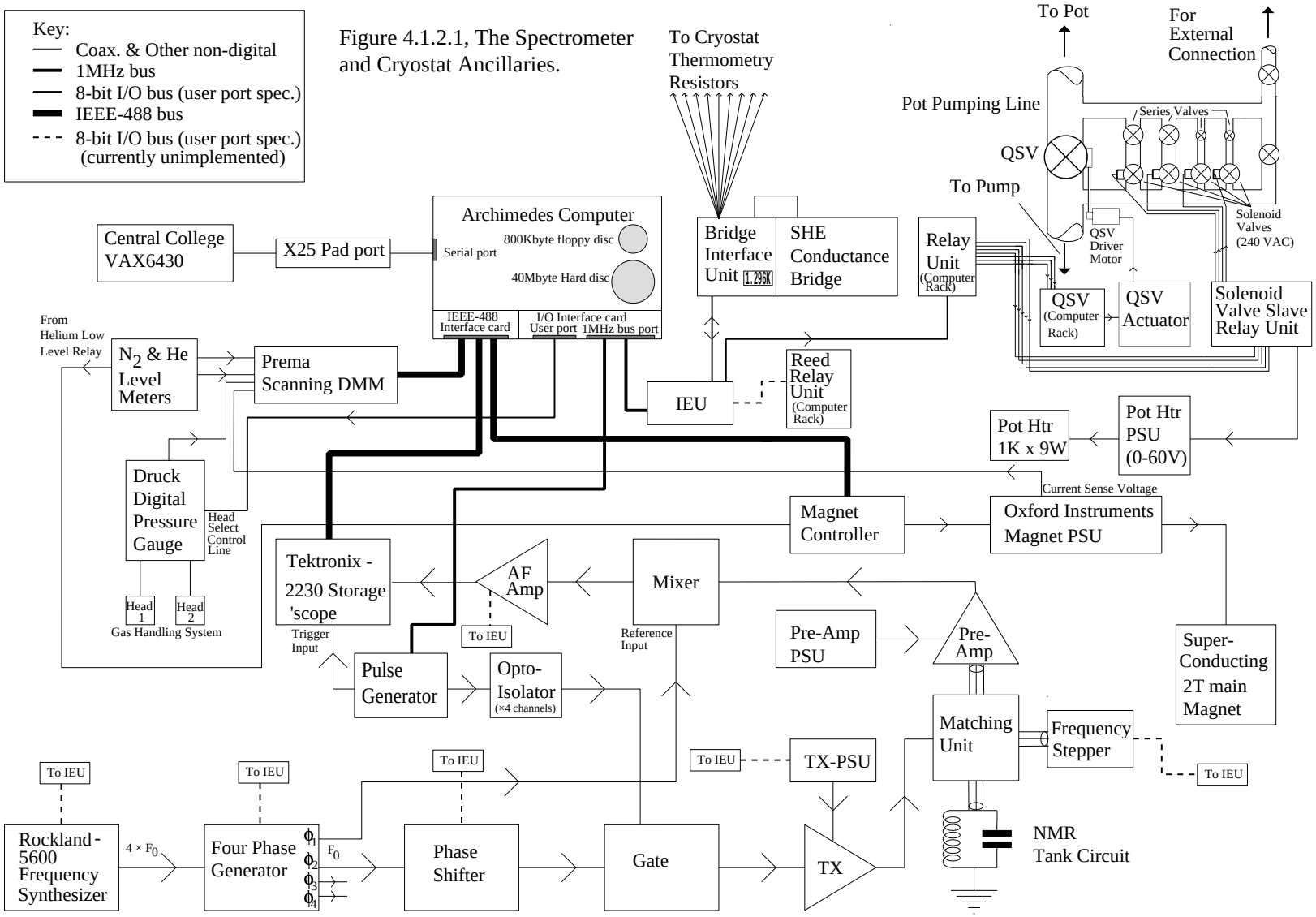

Figure 4.1.2.1, The Spectrometer and Cryostat Ancillaries.

4.1.2.1 (a) The Transmitter

The frequency standard for the experiment is produced by a Rockland 5600 synthesizer. Its output feeds the 4-phase-generator which produces 4 outputs in mutual phase quadrature and ¼ the synthesizer frequency. At this stage the signal is a square wave, the 4-phase-generator being digital in nature. This system works because the tank circuit selects the fundamental from the square wave. The phase-shifter, being fed from the 4-phase-generator provides for the phase to be quasi-continuously varied over 360°. It uses a novel design based on digital delay-lines [167]. Gated by pulses from the pulse-generator the RF is fed to the transmitter, a high power RF amplifier capable of delivering powers up to ~1kW to the tank circuit during the brief (μSecs) pulses. The output stage of the TX consists of 6 paralleled VN88AF power VMOS FETs feeding a 1:4 voltage step-up toroidal quadrifilar wound transformer. Another identical transformer in the matching unit provides a further 1:4 step-up feeding up to ~800V into 50Ω to the tank circuit. The power delivered by the TX is controlled by the TX−PSU, its output being 0−50V variable. Its 2200μF output reservoir capacitor ensures the high instantaneous current demand during pulse generation is met.

4.1.2.2 (b) The Receiver

After the TX pulse the NMR coil ringdown is damped by an arrangement of resistors and crossed-diodes in the matching unit until ~0.6V is reached. The matching unit to which the pre-amp is directly connected is located on top of the cryostat to avoid noise pickup and microphonics which can arise from long trailing cables. The tiny nuclear precession signals are coupled by the matching unit via a 33pF capacitor to the gate of a GAT 1 low noise GaAs FET for minimum noise reasons [61]. The FET is protected from destruction by TX pulses by crossed-diodes at the input. The bulk of the pre-amp gain is provided by an SL1612C variable gain broadband IC RF amplifier. Its gain control voltage comes from the pre-amp-PSU module. An emitter follower stage to buffer the signal to 50Ω completes the pre-amp. Signal detection takes place phase synchronously in the mixer, a Minicircuits SRA3 passive doubly balanced device whose reference is taken from the 4-phase-generator. It multiplies its two inputs providing sum and difference frequencies. The output AF difference frequency, the envelope of the precession signal, is fed to the AF amplifier which also optionally provides low-pass filtering for noise reduction purposes. Finally the AF signal passes to a Tektronix 2230 digital storage oscilloscope for display, storage and offline processing by computer. Oscilloscope triggering is by a special pulse from the pulse generator arranged to be

coincident with the spin-echo and to occur half-way across the oscilloscope's storage memory ensuring the echo always appears in the centre of the screen display. Computer generated *noise* leaking into the RX side of the spectrometer is a common problem. It is practically impossible to eliminate when the computer is in close physical and electrical proximity to the spectrometer/cryostat. Signal averaging while being highly effective against random noise it is often of little use against correlated computer noise. The computer's square-wave system clock is highly phase stable. Its Fourier components and those of its frequency division, a process inherent in microprocessor bus operation, result in a broad swathe in frequency of very phase stable RF emissions. Those emissions falling within the spectrometer bandwidth (typically 30KHz) of the Larmor frequency can, particularly with weak signals, produce slowly moving (from average to average) or even stationary, signal-sized beat-pattern features on the oscilloscope, effectively obliterating the signal. To combat the problem the spectrometer is powered from a filtered/line conditioned mains supply, separate from the computer/digital side of the system. Additionally the pulse generator is electrically isolated from the spectrometer gate by an opto-isolator module. The busiest and noisiest external buses, the ribbon cable 1MHz bus lines were shielded in earthed aluminium foil to cut down radiation. Of the seven most used Larmor frequencies 3.7MHz was worst afflicted by computer noise.

4.2 Part II, (The Computer and Digital Instrumentation)

4.2.1 Introduction

As shown in figure 4.1.2.1 the Acorn Archimedes computer model A440 is at the heart of the system. When unattended data taking is is progress the computer is responsible for; generating the pulses to manipulate the magnetisation, reading in plus logging-to-disk spin-echo or FID traces from the Oscilloscope and monitoring/regulating the pot temperature. Additionally the computer regularly logs general cryostat conditions such as helium and nitrogen levels with the traces for later offline diagnostic purposes. To enable automatic echo-decay as a function of field gradient measurements, the Archimedes also is able to program the Magnet Controller.

4.2.2 The Archimedes

This machine is one of the new generation of RISC (reduced instruction set computer) based computers [168]. By designing a microprocessor with a simple, streamlined instruction set the *microcode* required in a CISC processor is done away

with allowing the instructions to be executed very rapidly, often within a single *tick* of the CPU's clock [169]. This has the advantage that high processing speeds are possible without having to resort to the very high clock speeds and expensive fast RAM typical of 'high-end' CISC based systems. Archimedes is a 32-bit machine with a 26-bit address bus allowing a total of 64MBytes to be addresses in 32-bit (4 byte) words. It is based around four custom VLSI chips [170]. These are the ARM (Acorn RISC machine) − the CPU, the MEMC (Memory Management Controller), the VIDC (Video controller) and IOC (Input/Output Controller).

The ARM CPU is clocked at 8MHz, giving it a peak performance of 8MIPS for its fastest (one-tick, sequential-cycle) instructions and an average figure of ~3MIPS. The RISC concept works because in executing a typical program the CISC processor spends around 80% if its time executing ~20% of its instruction set. The RISC chip contains only those instructions used most frequently, other more complicated operations are carried out with combinations of RISC instructions in software. On the ARM all instructions are padded to 32-bits to aid *pipe-lining*. The ARM has a three stage *Fetch-Decode-Execute* pipeline ensuring a high memory ↔ CPU throughput. As an example the following assembly language instruction executes in 1 clock tick (125nS).

```
SUB r0, r0, r0, ASR#2  ; Multiply the contents of r0 by 3/4
```

This type of performance (as opposed to fast floating-point (FP) operation) makes the machine ideal for real time work in which fast, I/O and general program execution is most important.

The MEMC interfaces the CPUs address bus to the RAM and operates as a programmable lookup table allowing a distinction between physical and *logical memory* to be made. Of the addressable 64Mbytes the top 32Mbytes memory maps the ROM which contains the operating system, the physical RAM and all memory mapped peripherals including the expansion cards. To access locations in this address space the ARM must be executing in one of its three privileged modes (SVC, Supervisor Mode; IRQ, Interrupt Mode; FIQ, Fast Interrupt mode). Normally only the OS or software to drive add-on hardware such as our pulse-generator need do this. The bottom 32Mbytes goes through the address translation/lookup process. A typical machine has only 4Mbytes of RAM in it, the MEMC maps selected logical addresses to the physical ones in 128 chunks known as *pages*. Programs execute in logical memory space. In this way the bottom 32Mbytes are effectively fluid − under OS control. The ability to continually

re-map program memory has been used by the desktop/windowing system to permit *context-switching*, a simple form of *multi-tasking* − each *task* has its own logical address space starting with the same logical base address but (obviously) mapped to different physical RAM. The window manager implements multi-tasking with a *cooperative scheduling* arrangement rather than the more sophisticated *preemptive scheduling* found on multi-user operating systems such as Unix™ and VMS™. Cooperative scheduling was used by Acorn for simplicity (the OS originally had to fit in a 0.5Mbyte ROM) and to avoid the overheads of preemptive scheduling, the aim being to obtain a fast interactive response in the windowing system, ease of running intensively interactive programs such as CAD/DTP etc. in the multi-tasking *WIMP* being the machine's primary design objective. Cooperative scheduling does not allow any control over how much CPU time is consumed by the various tasks and more seriously, prevents time-critical *processes* executing when they need to. Throughout the development and use of the controlling software, we have been plagued by problems (ie. random machine crashes/ hangs etc.) associated with the attempt to get round the lack of a preemptive scheduler in order to have the machine regulate temperature independently from and asynchronously w.r.t. the main data logging program.

4.2.3 Interfacing

Two main interfacing routes have been used. For sophisticated instruments capable of many different transactions the industry standard IEEE-488 **[171]** is ideal. The Archimedes is configured as *system controller*, the Prema DMM-5000, Tektronix oscilloscope and Magnet Controller being configured as *talker-listeners*. The DMM suffered frequent *hangs* during software development. We believe this was due to its incomplete adherence to the protocol combined with the speed of the computer and its IEEE-488 interface **[172]**. In the software a series of BASIC procedures from the IEEE-488 library were replaced by lower level equivalents, the extra inter-IEEE-bus-access delays due to BASIC *interpreter* action being enough to let the Prema keep up.

For more basic transactions such as switching relays and solenoid valves etc. and reading/writing BCD digits to devices the 8-bit parallel I/O bus is ideal. The I/O card on the Archimedes like the BBC micro hardware it emulates has only one such port, the *user port*. The Interface Expansion Unit (IEU) was designed to support 28 × 8-bit I/O ports, enabling up to 28 separate devices to be interfaced to the computer. It plugs into the I/O card's 1MHz bus port and has provision for 14 plug-in cards each containing

one 6522 VIA chip [173], the VIA being the driver for the user port. The VIA contains two 8-bit bi-directional ports with handshake lines, designated ports A and B. The B side is capable of driving a reasonable load unaided, the A side can only support one standard TTL load and is too weak to be used as an output without extra buffering. The IEU contains a fairly sophisticated system of buffering for the A port. Both the port and its handshake line CA2 are separately bi-directionally buffered. Currently only the Bridge Interface Unit and Relay Unit are connected to the IEU, the allocations are; Port 1A & 1B − Bridge Interface Unit and Port 2A − Relay-Unit.

The 19" *computer-rack* uses a similar bin-system to the spectrometer. It is kept away from the spectrometer rack and has its own power-supply for noise control reasons. At the moment it is populated by only three modules the, Reed Relay Unit, Relay Unit and Quarter Swing Valve (QSV) unit, the later two being used. The Relay Unit contains 8 sub-miniature relays with front-panel LED indicators. Relay 0 slaves the Pot Heater relay, relays 1−4 the 4 pot pumping line solenoid valves and relays 5−7 feed the QSV unit which controls the QSV Actuator. It is so arranged that the latter relays correspond to the 3 QSV open positions, least-open to most-open respectively. In this way, from the software point of view, relays 1−7 seemlessly correspond to the 7 graduated pumping rates. The Solenoid Valve Slave Relay unit drives the AC mains solenoid valves and the pot heater. Mounted on its side for easy viewing/access are a series of neon indicators showing which devices are on together with manual override switches. The Reed Relay unit module comprises 8 screened reed relays with front panel *in* and *out* BNC connections, the relay connecting input to output as required. The idea being to allow the computer to re-configure the spectrometer by switching its coax. cables. As with the other connections shown in dashed type in figure 4.1.2.1 indicating unused 8-bit I/O port interfaces, the Reed Relay unit was designed when automatic frequency changing was envisaged. To enable the continuous-entry Argon isotherm [174] to be done, the Druck pressure gauge was modified to support computer selection of the head to be read/ displayed. One head measures the pressure in the standard volume store, the other the sample chamber. The switching signal comes from the I/O card user-port, the pressure reading from the Druck's analogue output via the scanning DMM.

4.2.3.1 Software Issues

One of the strong points of Archimedes is the ease and speed of driving external hardware. The data logging software ARCONTROL6, written in BASIC,

shown in Appendix 2 drives the IEEE-488 card via BASIC PROCedure calls whose definitions in the BASIC library BAS488 generate the calls to ARM SWI instruction via the BASIC SYS interface. These SWI calls are unrecognised by the operating system (OS) which passes them to the IEEE-488 card's *relocatable module* which executes them and drives the card hardware [175]. With much of the work being done at the OS/processor instruction level and not as on some systems via High Level Language (HLL) formatted I/O calls it is very fast.

Access to the I/O Interface Card's peripherals is similar, the relevant SWI "OS_Byte" calls being provided/executed by the card's relocatable module. For backwards compatibility with the BBC Micro these calls emulate access to three 256 byte pages of 8-bit memory mapped I/O locations [176]. The User Port and 1MHz bus devices appear on different emulated pages. The User Port VIA's 16 registers are accessed through 16 × 8-bit memory locations. A similar set of 16 locations exists in one of the the 1MHz bus' emulated pages for the IEU VIAs. The IEU's *latch* whose contents determines which of the 16 possible VIA's is *paged in* is mapped adjacent to the 16 byte block containing the VIA's registers. A line of 16 LEDs on the IEU front panel reflect the latch contents. The pulse generator software drives its hardware through the I/O Interface Card 1MHz bus in the ARM's privileged SVC mode directly from Assembly Language being a time-critical device.

4.2.4 The Temperature Regulation System

The cryostat's temperature regulation system originally ran on a Z80 microprocessor based Research Machines RML380Z computer and was driven through a dedicated controller/interface unit [61]. With the decision to replace the ageing machine with the then fairly new BBC microcomputer the temperature regulation software was re-written in ISO-Pascal to enable it to run as a background task, the data logging program executing in the foreground. Implementing the task switching inherent in the scheme was non trivial [177], it was never used, the decision to upgrade to Archimedes on grounds of memory and speed intervening.

The Bridge Interface unit handles all hardware aspects of temperature measurement and display. It comprises;

- A *resistor latch* to select (computer or manual) the cryostat thermometry resistor to be monitored by the SHE Conductance Bridge + front panel LED array indicating which resistor was selected.

- A front panel 4-digit 7-segment display for the temperature.
- An array of front panel LEDs and a bleeper to indicate a variety of fault conditions, (eg. bridge overflow, required resistor manually-overridden), the computer's background POTREG task being unable to write to the computer's monitor.
- A link to the bridge's BCD conductance and front panel settings output for the computer to read.

4.2.4.1 Temperature Regulation Software (POTREG)

The program operates in two modes; (1) Monitor only mode: The conductance of any resistor is monitored, the temperature calculated and displayed, (2) Regulation mode: The Pot Allen-Bradley (for T>2K) or Pot Speer (T<2K) is automatically selected by the software depending on temperature. These ranges were chosen to obtain the largest temperature coefficient of conductance from each resistor. The temperature is calculated from the conductance and displayed. If outside the specified tolerance the pot heater or a solenoid valve is operated to raise or lower the temperature. Calculation of temperature from conductance ($1/R$) is via empirical formulae [178,179];

$$\frac{1}{T} = a + b\log_{10}(R) + \frac{k}{\log_{10}(R)} \qquad 4.2.4.1.1$$

for Allen-Bradley resistors and,

$$\log_{10}(T) = A + B\log_{10}(R) + \frac{C}{\log_{10}(R)} \qquad 4.2.4.1.2$$

for Speer ones. The *'a', 'b', 'k', 'A', 'B', 'C'* are constants determined by least-squares fitting the linearised formulae to conductance *vs* temperature calibration plots, the temperature being determined from the helium-4 vapour pressure via the Helium-4 Vapour Pressure equation [180] at the start of a run. Using a Paroscientific Digiquartz Pressure Transducer ("T" series) on the pot vapour pressure line the vapour pressure was determined from the transducer's output frequency, measured by a Racal-Dana 1991 frequency counter. The calibration process (T<4.2K) was done quasi-statically by pumping the pot to its lowest temperature (~1.1K), closing off the pumping line and allowing the pot to warm up overnight while monitoring the Pot and IVC resistors

together with the pressure. Applying ~20mW heat with the pot heater to speed warming at all but the lowest temperatures the process took 20 hours and accumulated ~2400 sets of (pressure,conductance) data pairs. All cryostat thermometry resistors were roughly calibrated in the range 4.2K < *T* < Room *T* using the three available points (Room *T*, 77K and 4.2K). Separate calibrations for *T*<2K and *T*>2K were performed for the IVC and Pot resistors to avoid compromising the 3 term polynomial formulae. The fits are very good, plots revealing no perceptible systematic deviation from the experimental data. Accuracies are within a few mK. The calibration and other important parameters are read in from a file when the POTREG system is booted. Table 4.2.4.1.1 lists a set of calibration parameters.

Table 4.2.4.1.1, POTREG system calibration parameters.

	1K < *T* < 2K			2K < *T* < 4.2K			4.2K < *T* < 300K		
Resistor	*a/A*	*b/B*	*k/C*	*a/A*	*b/B*	*k/C*	*a/A*	*b/B*	*k/C*
Top Baf.	−10.5544	2.2191	12.5446	−10.5544	2.2192	12.5446	−10.5544	2.2192	12.5446
Mid. Baf.	−2.8339	0.6331	3.1548	−2.8339	0.6331	3.1548	−2.8339	0.6331	3.1548
Bot. Baf.	−1.0099	0.3416	0.6485	−1.0099	0.3416	0.6485	−1.0099	0.3416	0.6485
Flange	−0.4288	0.2611	−0.0448	−0.4288	0.2611	−0.0448	−0.4288	0.2611	−0.0448
Pot Sp.	−32.9662	4.1510	63.7542	−79.3630	11.5054	136.9312	−136.7449	20.7853	225.6249
Pot AB.	−3.1766	0.7800	3.6788	−1.8343	0.5715	1.5192	−0.5115	0.2814	0.0345
S. Cham.	−51.8467	7.3397	90.8692	−81.1510	12.1665	135.3454	−529.5734	90.4270	777.1456
ScaSp.	−49.6840	7.0079	87.3363	−77.8062	11.6380	130.0367	−309.5481	51.8981	463.3436

NB: The sample chamber anchor Speer resistor (ScaSp) is embedded in a copper rod attached to the pot inside the IVC, it was used in the past as part of a thermal anchor for the sample chamber when exchange gas could not be used due to electrical breakdown as mentioned above.

In regulation mode the POTREG software offers a number of refinements. Each of the 7 ‘solenoid valves’ is assigned a temperature range over which it will be used, the current designations are;

- 3.7K<*T*<4.2K ⇒ Solenoid valve#1
- 3.0K<*T*<3.7K ⇒ Solenoid valve#2
- 2.5K<*T*<3.0K ⇒ Solenoid valve#3
- 2.0K<*T*<2.5K ⇒ Solenoid valve#4
- 1.9K<*T*<2.0K ⇒ ‘Solenoid valve’#5
- 1.5K<*T*<1.9K ⇒ ‘Solenoid valve’#6
- 1.1K<*T*<1.5K ⇒ ‘Solenoid valve’#7

To avoid the situation in which the temperature is high (say 4.2K), a user or the data

logging program requests, a low temperature (say 1.1K) and 'solenoid valve' #7 (ie. QSV fully open) opens causing violent and wasteful boiling in the pot, a *temperature stepping system* is used. A temperature (currently 250mK) is read in from the boot time file which defines the maximum permitted single internally requestable temperature drop, the internally requested temperature being restricted to not lower than <current temperature> − <*MPSIRTD*>, and is updated continuously until the externally requested value is reached. Whenever a new resistor is selected, regulation ceases for a time related to the current SHE bridge integration time constant to allow it to settle down. This is most important because wildly spurious values of temperature calculated immediately after a resistor change can result in opening up of any 'solenoid valve' for a few seconds, which is enough to wreck a finely graduated series of higher temperature (3K−4K) temperature-dependence measurements, particularly serious if the ^{3}He film relaxation behaves hysteretically with temperature. If a faster rise in temperature than occurs by closing the solenoid valves, for T<4.2K is required, *heater out-ranging* can be requested. With this option *on* the pot heater will be used if the requested temperature is greater than the current temperature by the <*heater out-range limit*>, currently 1000mK. An analogous feature *solenoid out-ranging* is implemented for solenoid valve#1. It is used when more rapid cooling is required for temperatures $T \geqslant 4.2$K. One use is to bring the pot temperature down to 4.2K from 20K after sample annealing. The following liquid helium efficient method is used. With the pot pressure at an atmosphere after temporarily coupling the pot pumping line (pump isolated) to the cryostat helium recovery line, the pot-fill needle-valve is set ajar. The POTREG software is requested to bring the temperature to, say 4.3K and solenoid out-ranging is switched on. The very low pumping rate results in typically a helium consumption of only 100ml taking approx. 40 minutes. To avoid *solenoid valve jitter* when the (internally) requested temperature falls on the boundary between two of the above solenoid valve ranges some hysteresis has been introduced into the selection process. This hysteresis temperature is currently 26mK. Finally, since it is not easy to get the optimum matches between the software solenoid valve ranges and throughput settings on the series valves (figure 4.1.2.1) an optional facility for dynamic selection of solenoid valves has been developed. It operates by observing the rate of temperature fall, comparing it with maximum/minimum acceptable rate values and increasing or decreasing the solenoid valve number as appropriate. The maximum and minimum rates, the *on*/*off* status of the facility at boot time along with the other settings/options discussed above are contained in the boot time file. For easy modification the file uses a clear-text format. It is useful to allow a

resistor such as the sample chamber Speer to be temporarily switched in and its temperature observed during regulation, the 'ALT_R' command provides this facility. In addition to the *tolerance* specified for regulation an additional tolerance, the *in-range checking tolerance* facility also exists. It is normally assigned a larger value than the regulation tolerance, its function being to set a *System Variable* to the string "TRUE" or "FALSE" depending on whether the current temperature is within that tolerance. The foreground data-logging software can determine if the temperature is sufficiently close to that required to continue/start taking data, by reading the System Variable. ie. this implements a simple form of inter-program communication.

Listing 4.2.4.1.1 shows the POTREG *help menu* describing the system's commands.

Listing 4.2.4.1.1, The POTREG Help Menu.

```
*potreg help
****** HELP INFORMATION For Potreg Utility ******

       List Of Commands...
BOOT [calibration filename] - Boot the system & read in calibration file
SET_T <temperature>(mK) <tolerance>(mK) <acceptable tolerance>(mK)
       - Sets (1); The temperature
       - Sets (2); The tolerance used for temperature regulation
       - Sets (3); The tolerance used for in-range checking
SEL_R AUTO - Selects automatic selection of POT AB & Spear for
             temperature regulation
             - Other Effects: Enables all devices
SEL_R <n> - Selects a resistor 0<=n<=7 in the cryostat
            - Other Effects: Disables all devices
HEATER DISABLE  - Disables the heater
HEATER ENABLE   - Enables the heater
HEATER OUTRNG   - Enables the use of the heater outside its normal
                  range - ie. for T<4.2K, for quicker warming
HEATER NOOUTRNG - Disables the use of the heater outside its normal
                  operating range
                  - Other Effects: Switches all devices off
HEATER OFF      - Switches heater off, if enabled
HEATER ON       - Switches heater on, if enabled
SOLENOID OUTRNG      - Enables the use of the solenoid (0) outside its
                       normal operating range. ie. for T>4.2 for quicker
                       cooling
SOLENOID NOOUTRNG    - Disables the use of the solenoid (0) outside its
                       normal operating range
                       - Other Effects: Switches all devices off
SOLENOID ENABLE <n>  - Enables the use of the solenoid <n>, 1<=n<=7
SOLENOID DISABLE <n> - Disables the use of the solenoid <n>, 1<=n<=7
SOLENOID OFF <n>     - Switches off the solenoid <n>, 1<=n<=7, if enabled
SOLENOID ON <n>      - Switches on the solenoid <n>, 1<=n<=7, if enabled
DEV_STOP      - Causes all devices to be switched OFF & DISABLED
ACT   - Read bridge/Update temperature/Control devices etc. NB: Obsolete
DUMP  - Causes all global variables to be dumped
AUTO_IPR ON  - Allow the dynamic increase of solenoid no. if fall of T too slow
               This feature is only active for current temperature < 4.2K
AUTO_IPR OFF - Disallow the dynamic increase of solenoid no.
AUTO_DPR ON  - Allow the dynamic decrease of solenoid no. if fall of T too fast
               This feature is only active for current temperature < 4.2K
AUTO_DPR OFF - Disallow the dynamic decrease of solenoid no.
ALT_R        - Temporarily select an alternate resistor, log T & Cond. from it
HELP - Invoke this help script
```

4.2.4.2 Software Issues

Of the high level language compilers brought out for the Archimedes, 'C' was the first to support relocatable module production. For this reason and the general suitability of 'C' for programming involving both, high level operations such as floating-point arithmetic and low level features allowing efficient access to the machine hardware, the BBC/ISO-Pascal program was translated into 'C' [181]. The Archimedes 'C' compiler is ANSI conformant by default, the ANSI mode being used for programming reliability [182].

Relocatable modules occupy an area of memory separate from the main program area (the Application Workspace). Loosely speaking they are intended to operate as extensions to the operating system, providing a variety of *services* to applications. These include extra '*' OS-command line commands, extra SWIs plus the ability to attach code to various *OS-vectors* etc. so the OS will execute the code under certain circumstances. The POTREG module provides two services, a set of commands with the prefix '*Potreg' for the user to type at the keyboard or the foreground program to execute and a facility based on an internal timer-interrupt vector to execute the background regulation function every 2 seconds. The interrupt driven *thread* is executed asynchronously w.r.t. the foreground program. The 'C' package contains a tool 'cmhg' for generating the module *header* which identifies it and the services it offers to/requires from the OS. Like the 'C' compiler 'cmhg' produces *object code* which is linked to generate the executable module code, the whole process is automated by the 'amu' *make facility*.

The problems already mentioned stem from the asynchronous operation of the software. Relocatable modules being OS-extensions are usually entered by the OS with the ARM in SVC mode, this being the mode the OS carries out most of its privileged work in. The command line module entry is entered in non-privileged USR mode, the mode in which normal application code executes. The timer-interrupt call to the module is set up by a 'SWI OS_CallEvery' call, the module is in fact entered in IRQ mode, being interrupt-originated. An *IRQ-Veneer* generated transparently by 'cmhg' switches from IRQ $\rightarrow$ SVC before entering the module-proper and back again before the interrupt thread returns to the OS. Insofar as it has been possible to debug the system there appears to be two causes of the crash/hang problems: Firstly the SVC/FP one, which we believe to be fixed and secondly a timer/interrupt-time which we have been able to largely code-round.

4.2.4.2.1 The SVC/FP Problem

This arises from a potential incompatibility between SVC mode execution and Floating-Point code. The FP code in the 'C' *Run Time Library* 'SharedCLibrary' is in fact incompatible with SVC mode, a 'feature' not documented by Acorn in the 'C' package, despite the fact that the package supports both FP arithmetic and relocatable module production. To see why it is necessary to consider the *Programmers Model* of the ARM registers and the implementation of FP instructions. The ARM does not implement the complicated and therefore in the RISC context, slow FP instructions (FPIs). Instead they are executed by a software *Floating-Point-Emulator* (FPE) or optionally a dedicated maths coprocessor chip. A full set of FPIs have been defined by Acorn and some can be seen in listing 4.2.4.2.1.1 and Appendix 3.3. When the ARM encounters an instruction it does not recognise it experiences an *Undefined-Instruction-Exception*, vectoring through the *Undefined-Instruction hardware vector* to code which handles the instruction, in this case the code being the FPE module. To allow the program thread to return to the instruction following the FPI the ARM saves the value of the *Program Counter* register (R15) in R14_SVC. Table 4.2.4.2.1.1 shows the programmers model of the ARM's register map for its four modes.

Table 4.2.4.2.1.1, The Programmers Model for the ARM.

User	FIQ	IRQ	SVC
R0	R0	R0	R0
R1	R1	R1	R1
R2	R2	R2	R2
R3	R3	R3	R3
R4	R4	R4	R4
R5	R5	R5	R5
R6	R6	R6	R6
R7	R7	R7	R7
R8	R8_FIQ	R8	R8
R9	R9_FIQ	R9	R9
R10	R10_FIQ	R10	R10
R11	R11_FIQ	R11	R11
R12	R12_FIQ	R12	R12
R13	R13_FIQ	R13_IRQ	R13_SVC
R14	R14_FIQ	R14_IRQ	R14_SVC
R15 (PC)	R15 (PC)	R15 (PC)	R15 (PC)

There are 16 registers R0−R15 accessible in each mode. The three privileged modes have some private versions of the registers indicated by Rx_xxx which switch-in when that mode is selected. R15 contains the program counter plus a number of flags.

R14<generic> can be used as a general purpose register but also has a special function as the *Link Register*. A CISC CPU will normally push the program counter onto a *stack* in memory during a *jump-to-subroutine* instruction allowing it to return to the code which did the jump at the end of the subroutine's code. However memory accesses are slow compared to CPU internal register-to-register transfers and as part of its RISC design the ARM does not do this. Instead the equivalent jump instruction is BL <address>, *Branch-with-link*, the program counter is copied into R14<generic>. Return from the subroutine involves moving R14<generic> back to R15. If the subroutine does not call any others or otherwise modify the link register it need not save it anywhere. If code involving FPIs is to be executed in SVC mode it must save R14_SVC on entry to avoid corruption by the undefined-instruction-trap, failure to do so is catastrophic leading to a hang/crash etc. It is this that prevents the 'C' Run Time Library, which contains functions for logarithm and exponentiation needed in evaluating equations 4.2.4.1.1 and 4.2.4.1.2, from working in SVC mode. Unfortunately being machine code there was little scope for modifying it. A similar situation can occur with code from the 'C' compiler as shown below in listing 4.2.4.2.1.1. This is due to the *ARM Procedure Call Standard* not requiring R14 to be saved when it will not be overwritten by another subroutine call [175]. The first part is a trivial example 'C' function, below it the assembler listing produced by the compiler together with some explanatory comments relating to calling it in SVC mode;

Listing 4.2.4.2.1.1, 'C' and Assembler Listing Showing SVC/FP Problem.

```
int test(float f)  /* A function called "test" which receives an FP variable "f" */
{
  f=f+3;           /* Add 3 to "f"
  return ((int)f); /* Truncate the result to an integer and return it */
}

********************************************************************************

; generated by Norcroft RISC OS ARM C vsn 3.00 [Jul 12 1989]
a1 RN 0        ; Assign symbolic names for the 16 ARM registers
a2 RN 1
a3 RN 2
a4 RN 3

v1 RN 4
v2 RN 5
v3 RN 6
v4 RN 7
v5 RN 8
v6 RN 9
sl RN 10
fp RN 11
ip RN 12
sp RN 13
lr RN 14
pc RN 15

f0 FN 0        ; Assign symbolic names for the 8 FP registers
```

```
f1 FN 1
f2 FN 2
f3 FN 3
f4 FN 4
f5 FN 5
f6 FN 6
f7 FN 7

    AREA |C$$code|, CODE, READONLY

        IMPORT  |__main|
|x$codeseg|
        B       |__main|

        DCB     &74,&65,&73,&74
        DCB     &00,&00,&00,&00
        DCD     &ff000008

        EXPORT  test
test
        STMFD   sp!, {a1 ,a2}      ; Save registers a1 & a2 on the stack
        LDFD    f0, [sp], #8       ; Load variable "f" from caller as a'double'
        MVFS    f0, f0             ; Convert 'double' to 'float'
        ADFS    f0, f0, #3         ; Add 3 to it
        FIXSZ   a1, f0             ; Convert to integer
        MOVS    pc,lr              ; Attempt to return to caller with lr (R14_SVC)
                                   ;  corrupted by all four previous instructions.

    AREA |C$$data|
|x$dataseg|
    END
```

Fortunately such assembly code can easily be modified to preserve R14_SVC. The following steps have therefore been taken to modify the POTREG program;

- All of the POTREG 'C' source (Appendix 3.1) except one function 'absp' which evaluates equations 4.2.4.1.1 and 4.2.4.1.2 has been converted to use only integer arithmetic. Temperatures are manipulated as integer mK and the resistor calibration parameters (table 4.2.4.1.1) in the boot file are multiplied by a factor 'CALMUL', currently 1000000 and stored as integers also.

- The 'C' source for function 'absp' (Appendix 3.2) has been written without calling any routines from the run time library. Instead $\log_{10}(x)$ and 10^x are evaluated using concise empirical polynomial formulae developed for use in computer floating point implementations **[183]**. By compiling the 'C' source to assembly code (Appendix 3.3) for editing, modifications can be made, the assembly code being assembled to object code which is then linked in the normal way with the rest of the program to produce the module. After checking/exonerating the assembler code for R14_SVC corruption it was found incorrect FP results occurred although there were no crashes/hangs. It is thought this is due to some ill-defined residual

incompatibility between FP operations and SVC mode. Since the 'absp' code did not make any use of the stack (NB: Each CPU mode has its own stack) the code was modified to change from SVC → USR at the beginning, reversing the change at the end before returning to the calling code. This configuration worked.

4.2.4.2.2 The Timing Problem

Code executing under interrupt must avoid taking too long (more than a few mS) if system timing is not to be affected. This is because clocks maintained by the OS such as the *number-of-centi-seconds-since-power-on* and *time-of-year* clock*s* are updated under interrupt. Evaluating FP expressions is slow, taking ~65mS every 2Secs for one read-calculate-regulate operation. Fortunately the amount by which this causes clocks to run slow is not enough to cause problems in itself. The *clock*() function, from the 'C' library returns the number of centi-seconds since program invocation. A bug in *clock*() results in it sometimes returning spurious values, including negative ones in a largely random fashion when too much interrupt time is taken by the POTREG software. It was some time before the consequences of this were fully coded-round, part of the problem being that the asynchronous SVC code does not obey the error handlers set up to deal with errors such as integer division by zero in a controlled informative way, the result of such errors being crashes/hangs with hardware *exceptions* flagged at addresses unconnected with the POTREG software, the OS having completely lost control of the CPU. It is essentially impossible to extract any useful debugging information from such failures.

4.2.5 The Pulse Generator

A number of pulse generators have been used/developed in the course of this project. For manual data taking, spectrometer setting up and computer noise investigations when the computer must be switched off, the group's purpose built standalone microprocessor based pulse generator [61] is invaluable. In the early stages of the work when the 6502 microprocessor based BBC Microcomputer was proposed as experimental controller a pulse generator was developed for that machine. The external hardware plugged into the machine's user port and only contained a pulse demultiplexer feeding 7 pulse output channels and some pulse clean-up circuitry. Both pulse and delay timing was generated by the two 16-bit counter-timers in the 6522 VIA, driving the user

port, the rest of the design being software [184]. Despite the high degree of hardware I/O compatibility between the Archimedes and its predecessor provided by the I/O card, it has been only partially successful driving the pulse demultiplexer unit from the I/O card user port. The problem is *jitter* in the inter-pulse delays. It stems from the *refresh* of the Archimedes DRAMs which cannot be carried out during alternate cycles of the system clock as on the BBC micro but must still be done periodically. The result being small (typ. ±5μS) discrepancies in delay timing because the ARM must start and watch for the timeout of the delay counter/timer. While not making the unit useless the discrepancies are undesirable. To overcome this problem and with an eye to future needs, a new dedicated fast pulse generator was designed and built in the Department's Electronics Workshop. It comprises two mutually triggering 32-bit counter/timers clocked at up to 50MHz. The high clock speed was chosen to permit short pulses to be generated. It has 8 outputs to which any combination of pulses may be routed. Driven over the 1MHz bus from assembly language the fast I/O required to reliably generate pulses and delays as short as 140nS and 30μS respectively is attained. The pulse/delay resolution is 20nS and the maximum pulse/delay is ~40Sec with a 50MHz clock. Clock speeds of 5MHz, 500KHz, 50KHz (and an external input) are selectable providing for proportionately longer pulse/delay periods and lower resolution.

4.2.5.1 Circuit Description

A schematic diagram is shown in figure 4.2.5.1.1. The two counter/timers configured to count-down at the the system clock rate are arranged to trigger each other when they timeout eliminating the dependency of the previous design on CPU timing. All programming of the unit after pulse generation starts takes place during the delay period so that the shortest possible pulse is determined by the unit's hardware alone. The counter-timers shown consist of a 32-bit latch driving the actual counter-timer chips. In this way two sets of numbers are loaded sequentially into each before pulse generation starts. During pulse generation the latches contain the next pulse or delay value which will be read in by the counter-timer when it times-out ensuring it is programmed with the new number when its partner times-out and it must count again. Which pulse appears on which channel is determined by the *routing-latch*. *Stop/Start* and counter-timer-from-latch *pre-load* signals come from the *instruction latch*. It is vital the software keep track of the status of the pulse and delay counter-timers while running, the *pulse* and *pulse*/2 signals provided via the *status-latch* allow it to do so. By continuously reading the status-latch in a tight machine code loop, latency which puts a lower limit on delay

length is kept to a minimum. An unfortunate side effect of this mode of operation when long delays (many minutes) are required such as for the ^{11}B NMR measurements is that temperature regulation ceases since interrupts are disabled during pulse generation, leading to unacceptable temperature drift. The problem was solved by providing the software with an alternative *interrupt-driven* mode of operation. Instead of looping and reading the status-latch, the reading/checking of it (together with all other unit programming after the initial programming and start of pulse generation) is carried out under interrupt, the interrupt being generated by pulse-counter timeout via a flip-flop and reset by the program once dealt with.

Figure 4.2.5.1.1, Schematic Diagram of the Pulse Generator

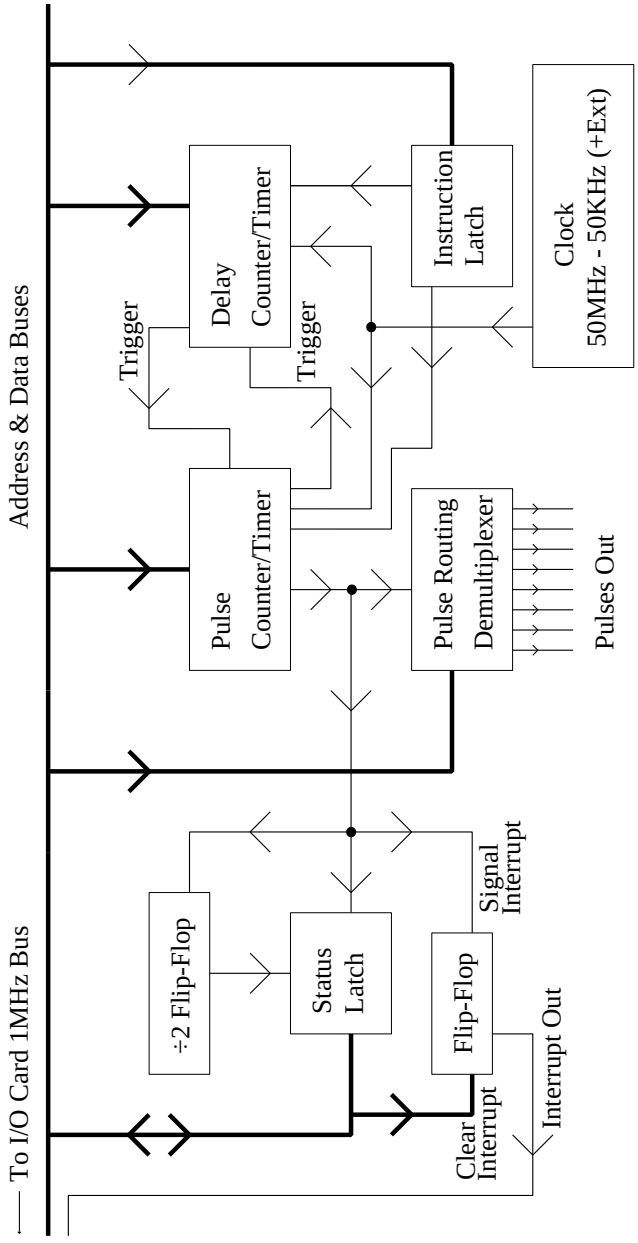

4.2.5.2 Pulse Generation Software

Two programs have been written, a dedicated pulse generator, PULSE_ARM4 and the data logging program ARCONTROL6, the later lacking the data entry/display facility [184] of the former. Both are written in BASIC and use the interpreter's built in assembler to build the machine code for each pulse sequence when run for maximum flexibility. As shown in 'PROCsetup_pulse_generator' in Appendix 2 the programmers model of the pulse generator hardware consists of 11 writable and one readable 8-bit registers. During *non-interrupt-driven* mode pulse generation both IRQs and FIQs are disabled to prevent timing interference. In the interrupt-driven mode other software such as POTREG must not disable interrupts for any significant time, 'significant' meaning of the order of the delay time. Using the system in its interrupt-mode occasional machine hangs/crashes have occurred for reasons currently unknown.

4.2.6 The Magnet Controller

The need for a versatile programmable instrument to drive the magnet PSU was conceived, along with many other parts of the spectrometer system as already discussed when computer controlled NMR frequency changing was envisaged. It has, however proved very useful especially in searching for/sweeping the ^{11}B resonance. Designed and built in the Department's Electronics Workshop with the group's new superconducting magnet in mind [185] it supports a main solenoid winding plus 9 series connected shims. After completing a skeleton design of a non-microprocessor based instrument it quickly became obvious that the features we required would make such device prohibitively complicated and expensive, so the decision to go for a microprocessor controlled instrument was made. A list of essential instrument features/ development requirements was arrived at;

(1) The need for a microprocessor development system.
(2) The need for a computer language to code in with a FP arithmetic capability.
(3) A front-panel data and instruction entry/display facility.
(4) An IEEE-488 computer interface.
(5) Some non-volatile-memory for a 'log book' facility to store the values of currents in the persisted windings with power failures etc. in mind.
(6) Some other external interfaces for connection to the helium level meter

etc.

(7) High resolution and linearity *digital-to-analogue-converters* (DACs) together with appropriate analogue driver circuitry for driving the magnet PSUs.

The following summarises the solutions/implementations of the above list;

(1) By using the same microprocessor as the BBC 'Master' series microcomputer and its *cartridge-port* memory expansion slot it was possible to map the Magnet Controller's hardware and RAM into the BBC's address space, permitting it to be used as a development system.

(2) Of the HLL compilers available at the time, there was either no support for FP arithmetic or the code produced was too large to fit in the 12K RAM available in the Magnet Controller's externally mapable address space. So coding was done in assembler for compactness and speed, the FP code being obtained from the BBC model B microcomputer's BASIC-II ROM using an intelligent disassembler **186** and other documentation **187**. After preliminary hardware testing with the BASIC interpreter's built in assembler a dedicated assembler/linker system **188** was used to develop the software.

(3) Front panel data/instruction entry is via 34 keys, interfaced to the microprocessor via a dedicated keyboard encoder chip. 35 LEDs and three rows of 5 × 7-segment displays form the instrument's display.

(4) The IEEE-488 interface uses the Texas Instruments intelligent GPIB chip set **189** based around the TMS9914 interface transceiver chip.

(5) 2Kbytes of Battery-backed CMOS RAM provide this facility, together with the command-recall and CMOS RAM integrity checksum test.

(6) The unit's two VIA chips' four 8-bit I/O ports emerge at the back of the instrument on user-port style IDC connectors. One pin drives reads the HLM2 meter's helium level relay.

(7) Two high linearity 16-bit DACs and attendant analogue output buffering circuitry based on high quality AD712 op-amps provide the drive to the magnet PSUs.

4.2.6.1 Detailed Consideration

The Magnet Controller is a standalone intelligent microprocessor controlled instrument with a purpose written operating system. It is designed to be used with two highly stable constant-current mode magnet power supplies, one for the main winding, the other for the nine shims. Control of these supplies is achieved through two analogue output signals (in the range 0 to ±5V, switchable) which specify the required current, together with a number of digital signals which control the superconducting heat-switches for the windings and current-direction switching relays. Analogue signals are derived inside the Magnet Controller from two 16-bit DACs giving a current resolution of 1 part in 65536 which comes close to the main solenoid's 0−75A PSU's front panel control resolution of 1 part in 10^5. The unit has a sophisticated front panel allowing for minimum operator intervention during magnet operations. For example by entering three numbers the unit can be instructed to do the following field sweep:

- Wind the magnet up to the current at which it was last persisted.
- Open the heat-switch to make the winding normal.
- Go to the specified sweep starting current.
- Sweep to the specified sweep stopping current at the specified rate.
- Close the switch and wind the current down to zero.

This leaves the operator free to watch for an NMR signal. It also helps prevent accidents since the Magnet Controller will not allow the superconducting heat switch to be opened unless the current in the supply equals the current in the energised winding. Alternatively while in its special *manual mode* the instrument can be instructed to open/ close switches and alter currents etc. on an individual basis allowing for a lower level of control similar to that provided by the PSU front panel controls.

4.2.6.2 Magnet Controller Design

A key feature of the Magnet Controller is its use of a BBC Master Series microcomputer as a development tool. Using the computer's cartridge port interface to map the unit's Operating System (OS) and internal peripherals into the computer's *sideways RAM* address space means that the Magnet Controller's OS and internal peripherals appear to the computer as a program stored in sideways RAM. Running the Magnet Controller is then, to the computer, like running any other sideways RAM/ROM based software (eg. a wordprocessor). This makes developing the software simpler since

it can be modified, assembled, linked and run in the same environment. By using the same CPU series as the computer (the 8-bit × 64K addressable memory, 65C00 low power CMOS) the software simply has to be re-assembled and linked to run on the unit's internal CPU. A finished version of the OS can be blown into an EPROM so as to be present whenever it is turned on. An important element of the design of the dual internal/external CPU operation is the address switching which is necessary. Owing to the fact that the 65C00 series CPUs have their hardware-vectors in the top few memory locations (addresses &FFFA to &FFFF) the instrument's OS must reside in that area when operating on the internal CPU. As part of its architecture, BBC micro sideways RAMs are mapped to a 16K block of memory in the address range &8000 to &BFFF. A result of these two features is that the unit's OS and internal memory mapped peripherals must occupy less than 16K and that these addresses must be mapped to the top but one memory quadrant (16K) when running on the external (BBC) CPU and in the top quadrant for the internal CPU. Address switching is achieved automatically by inverting the A14 line in the Magnet Controller's address bus when the specially designed link cable joining the computer to the Magnet Controller is plugged in. Unfortunately the three signals provided by the cartridge interface (ROMOE, CS, ROMQA − See reference **190** for more details) intended to produce a memory device's *chip-enable* signal result in an enable pulse ~230 nS which is too short for the Magnet Controller's comparatively slow 65C22 VIAs and is due to the computer's use of a custom memory controller chip through which the cartridge port is addressed. The slightly inelegant solution to this problem adopted was to take the computer's A14 address line directly from the CPU via a flying lead in place of ROMOE, which works well providing odd numbered sideways RAM/ROMs are disabled using an OS command. Figure 4.2.6.2.1 illustrates the logic used to convert the cartridge port address decoding signals to drive the Magnet Controller's A14 and A15 lines.

4.2.6.3 The Hardware In More Detail

Figure 4.2.6.3.1 shows a memory map for the instrument. Starting at the bottom are two 2K banks of static RAM used as workspace and stack. Following is a 2K battery backed CMOS memory for storing the currents in the magnet windings etc.

The next allocated region in the memory map is the start of the 16K block mentioned above. At address &8000 is a 2K static RAM for holding the computer's sideways RAM header when the unit is running on the external CPU. Next, is a 2K block in which all the memory mapped hardware resides. The remaining 12K is

occupied by RAM or ROM for the OS. The RAM is convenient for testing the system on either CPU without blowing an EPROM. Switching between the ROM and RAM is accomplished by a switch, in a recess in the instrument, next to these memory devices. In reality the (6+1)×2K RAMs/ROMs shown in figure 4.2.6.3.1 consists of a single 16K memory device.

Figure 4.2.6.2.1, The Cartridge-Port to Magnet-Controller Addressing logic.

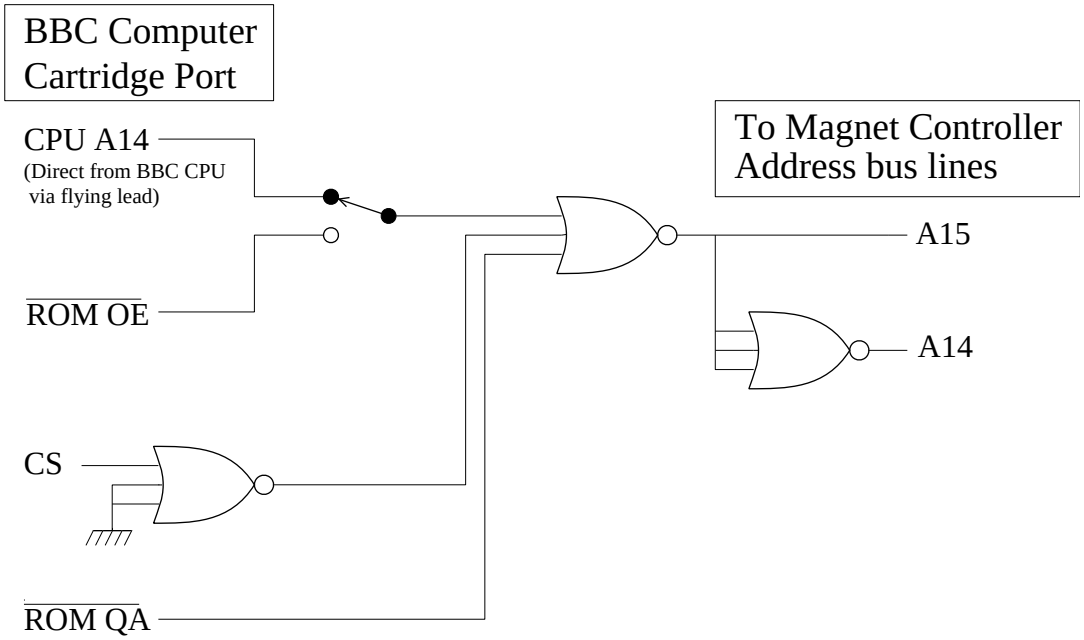

Turning to the memory mapped peripherals, the first device is a Standard Microsystems Corp. 9600-PRO keyboard encoder i.c. This is an intelligent device which alleviates the need for custom logic to interface to the keyboard. Next is the TMS9914 GPIB Adapter. This VLSI device handles all the interfacing between the microprocessor and the IEEE-488/GPIB bus. Following a previous design **[191]** made the designing of this part of the system straightforward. The 'computer' VIA **[173]** (65C22) is next in the memory map and is at the heart of the system. It is responsible for, all system timing using both its 16 bit counter/timers which are clocked at the system clock rate of 2MHz and via one of its 8 bit parallel I/O ports for connecting to the Helium low-level sensor relay in the Oxford Instruments Helium Level Meter (HLM2). The DAC board comprises the two 16 bit DACs (AD569) **[192]** and current direction switching relays. The relay board consists of eleven relays for the superconducting heat switches plus one spare and some logic which allows a complete hardware reset to be initiated under software control. The reset logic is used by the GPIB system at the end of the 'device

clear' command. Part of the reset logic is used to provide a *Watchdog* facility − A re-triggerable monostable is arranged to cause a reset on timeout, the timeout being prevented by CPU accesses to addresses within the 2K hardware page during normal instrument operation. Should hardware problems or a mains power glitch etc. cause the CPU to hang, its accesses to the hardware page should cease causing a reset and reboot. It is vital to ensure such hangs do not prevent the device de-energising the magnet when the helium level becomes low.

Figure 4.2.6.3.1, Memory Map of the Magnet-Controller.

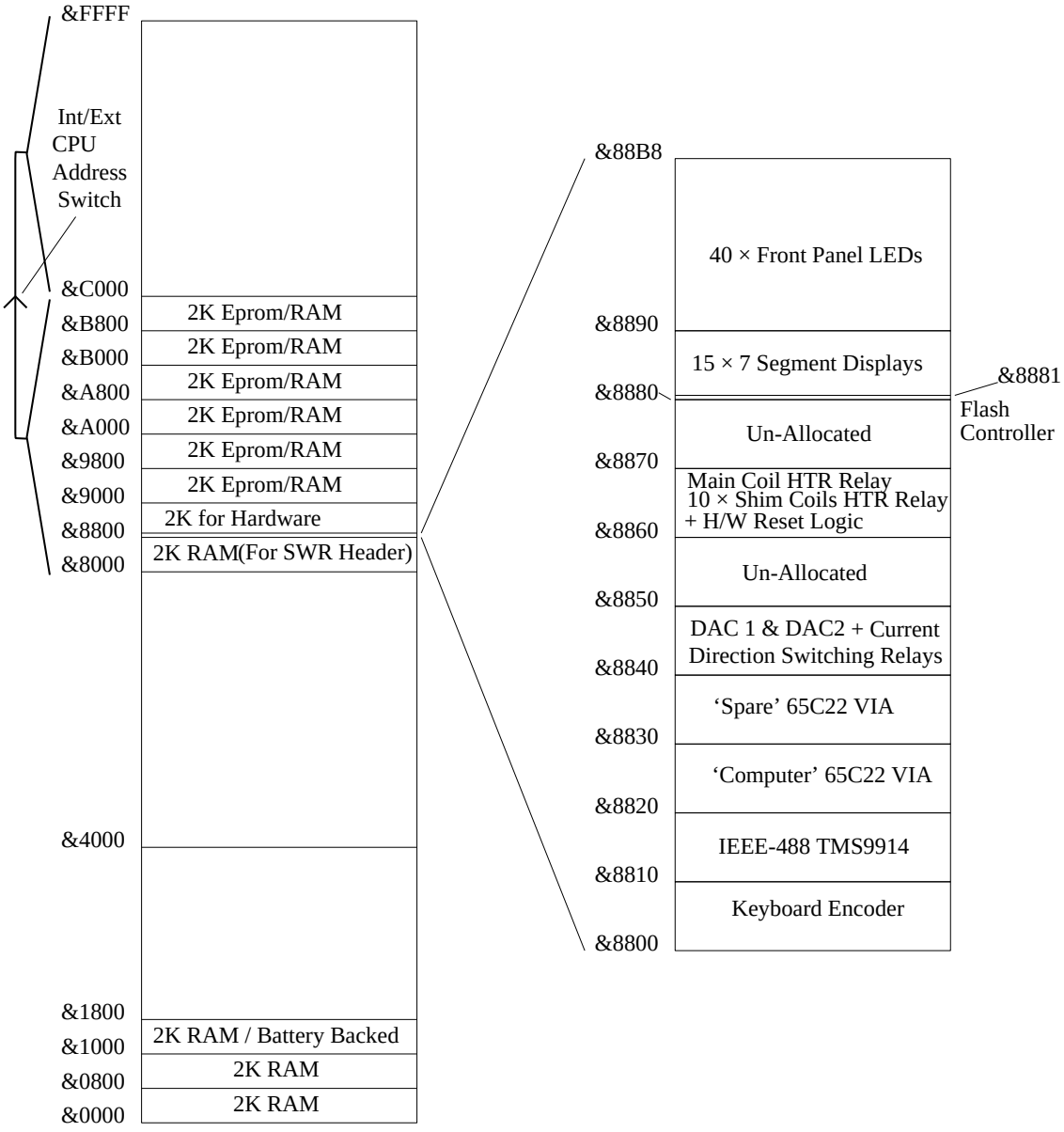

Finally comes the display driver logic. There are three types of device to consider. The flash-controller, the 7-segment displays and the LEDs. Taking the 7-

segment displays first, there are three rows of five digits. The top row echoes commands entered via the keyboard and displays messages. The middle and bottom rows reflect the currents in the PSU and magnet winding, respectively, for the currently selected magnet winding. Rather than use 7-segment display driver chips the displays are driven directly, encoding being done in software, allowing most alphabetic characters to be represented for error-message etc. purposes. At memory location &8880 is the flash-controller which consists of two 8 bit addressable latches, wherein each bit determines whether the corresponding 7-segment display digit is rendered flashing or not. By using an arrangement of a non-multiplexed display, a fast and a slow clock the flash period is determined by the slow clock. The flashing is between states of normal intensity and extra-bright, where extra-bright results when the drive to the 7-segment display is not gated by the fast clock and normal intensity when it is. The period of the slow clock is about half a second and the fast clock frequency is about 1KHz which is fast enough to eliminate any perceived flicker. A spare bit in the flash-controller is used to drive an audible alarm. The thirty five LEDs indicate the current state of the instrument.

As alluded to above there were/are hardware problems. During the developmental stage the unit was plagued by them. The problems were bus timing ones, resulting in spurious accesses to memories not addressed by the CPU and bad data being read/written by the CPU. We believe they resulted from *bus contention* in which one CPU access cycle runs into the next and capacitative bus loading/adjacent line cross-talk by/in the ribbon cable used to join the buses from board to board. The fix has been to gate the memory *chip enable* and R/$\bar{W}$ lines with the clock signal and to keep ribbon cable link lengths to a minimum. A HP1651A Logic Analyser was used to investigate these problems. On occasions the Magnet Controller still misbehaves displaying characteristic timing related symptoms. Fortunately this is now quite rare.

4.2.6.4 The Software

4.2.6.4.1 Overview

The Magnet Controller's OS has been written is assembler. It consists of more than 13000 lines of code, data and comments and is broken up into 31 modules. Using a modular approach with an assembler/linker system one module can be altered and re-assembled without having to re-assemble everything else, only re-linking is needed.

The OS is composed of two separate, independent, sets of code, the main program and interrupt code. Updating the display, checking/updating the non-volatile memory checksum and checking the helium level is carried out by the main program. It

does this continuously in a big loop. Interrupt code is executed only when one of the hardware devices in the instrument interrupts the CPU. Currently the following devices can cause interrupts; 65C22 ‘computer’ VIA, Keyboard hardware and TMS9914 GPIB transceiver. Interrupt priorities of these devices from highest to lowest are as listed above. In effect the main program has the lowest priority of all and is only executed when no devices are interrupting.

4.2.6.4.2 System Timing

The VIA's two 16 bit timers are designated T1 and T2 [173]. They work as follows: A timer is loaded with a 16 bit number. It decrements at the system clock rate and produces an interrupt when it reaches zero. In the case of T2 it then continues to decrement past zero, ie. &0000→&FFFF→&FFFE…etc. T1 is used to toggle a flag twice a second which is used by the main program to enable the LEDs to flash if required and T2 controls the DAC timing. Given the system clock rate and the fact that these timers are only 16 bits wide it can be seen that many timing operations will require multiple timer activations. In the case of the T2 it is crucial that the interrupt latency is taken account of. If it were not DAC sweep rate inaccuracies would result. The interrupt latency is the time taken between when the device interrupted the CPU and when the interrupt was serviced and can vary from occasion to occasion since the CPU may already be servicing another device's interrupt when the timer times-out. An elaborate system to deal with T2 interrupt latency has been implemented in which the latency measured from the number of counts passed zero in T2 is added to a running total of T2 latency. Each time T2 is re-programmed, as much as possible of the running total is subtracted from the original amount to be programmed. Keeping the running total across the whole of a DAC sweep ensures the best possible timing precision across that operation.

4.2.6.4.3 Arithmetic Considerations

An important part of the Magnet Controller's function involves operations on real numbers. For example a magnet current in Amps entered by the front panel in textual form (eg. 3.1415) has to be converted to a 16 binary number for use in a DAC. For maximum flexibility floating-point arithmetic must be used. Unfortunately, writing floating point arithmetic routines (addition, subtraction, multiplication and division) from scratch for an 8 bit processor such as the 65C00 series would be a long and arduous task. As mentioned above the floating point routines in the BBC Model B Micro's BASIC-II

interpreter ROM are well documented [187] and with the aid of a disassembler can be extracted. The technique has been used extensively in the software. In fact, there are two separate copies of the routines. One for the main program and one for the interrupt code. This is necessary because the two sets of code operate asynchronously w.r.t. to each other. Rounding code has been written to give the maximum accuracy of representation in the 5 digit front panel displays. To make modifications to the system floating-point constants easy they have been collected together in one module in textual not binary form. Examples of these constants are; The inverse rate a given magnet-winding will be swept at by default in Seconds/Amp, the inverse flash rate for a front panel LED in Seconds/state-change and the time the unit is to wait after reaching the desired current before closing the superconducting switch.

4.2.6.5 The Front Panel

This section discusses the key features of the front panel. Contained in the main block of keys are the numeric keys for entering data, the *clear key* and the DAC programming keys. The DAC programming keys operate by taking the number just entered into the display and acting upon it. For example hitting the *ENT−I* key after entering a number will cause the unit to do the following;

- Proceed to the energised current at the *fast* rate for the magnet-winding.
- Wait for the PSU to settle down.
- Open the switch.
- Wait for the magnet-winding to go normal.
- Go to the current just entered at the *slow* rate for the magnet-winding.
- Wait for the PSU to settle down and back EMF to die away.
- Close the switch.
- Wait for the magnet-winding to go superconducting.
- Wind the magnet-winding down to zero.

Throughout this sequence of operations the *HTR* and *CYCLE PHASE* LEDs indicate the state of progress. This mode of operation is termed the *normal* mode. *Sweep* mode as described briefly in the introduction is programmed using the *I−STP* (sweep stop current), *I−STRT* (sweep start current) and *SWP−T* (sweep time) keys. Asserting the *HOLD* function will cause the DAC to freeze until de-asserted. The *SW−HLD* (switch hold) key operates similarly. When asserted it stops the sequence of operations at the

point where the heat switch would otherwise be closed.

As well as entering a number via the numeric keys, a number can be modified using the simple editor provided by the cursor keys. The left and right arrow keys move a 'cursor' along the five digits of the top display. The cursor's presence over a digit is indicated by making that digit flash in intensity as described above. Once the cursor is present the up and down arrow keys can be used to increment or decrement the number in the display by a unit, where the size of the unit is given by the position of the digit with the cursor over it. A further refinement is provided by the *<alt> <up arrow>* and *<alt> <down arrow>* function. They work by entering the altered number immediately, in effect a combination of the *<up arrow> or <down arrow>* key followed by *ENT−I* and are most useful for trimming a current. By way of example, if it was known that there was a resonance at a current of about 1.26 Amps that needed to be located exactly, then the following shows the sequence of operations that could be used;

- Assert *SW−HLD* so that the unit will wait instead of closing the switch and winding down the current.
- Enter the number 1.26.
- Press *ENT−I* and wait for 1.26 Amps to be reached.
- Use left and right cursor keys to obtain the desired increment size.
- Use the *<alt> <up arrow>* and *<alt> <down arrow>* keys to trim the current to precisely locate the resonance.
- Deassert *SW−HLD* to make the instrument wait, close the switch and wind done the current to zero.

NB: The *<alt>* key is indicated by a triangle symbol and it is used by pressing its operand key while holding it down.

The DAC programming keys (*ENT−I*, *I−STP*, *I−STRT* and *SWP−T*) and the *COIL* key (which selects the magnet-winding) have a recall function. Whenever a number is entered by any of those keys it is stored in memory. Up to 5 entries are stored for each key and can be recalled by using the recall key together with the key in question.

An important feature of the instrument's design is the ability to program another action while the current one is still in progress and have it take effect immediately. This makes current trimming particularly flexible since if too great a current swing is programmed the current can be brought back without waiting for it to

complete.

Another useful design feature is the partitioning of the relevant instrument functions along the lines of magnet-windings. For example, if the instrument is part way through a programmed action for a magnet-winding and a new magnet-winding is selected it will remember all the details of the action which was programmed such that when that magnet-winding is re-selected the programmed action will carry on exactly as before from where it left off.

4.2.6.6 The Helium Level Monitor

To facilitate safe unattended automatic running, the main program continuously monitors the 'computer' VIA port line connected to the Helium Level meter low-level relay, (figure 4.1.2.1). If the liquid helium level inside the cryostat goes below the preset critical value just above the top of the magnet the port line will change state. On detecting this the Magnet Controller will sound its alarm and systematically de-energise all magnet windings in a controlled way, leaving the PSUs wound down to zero current.

4.2.6.7 The IEEE-488/GPIB Interface

The software has been written to permit full control of the Magnet Controller over the GPIB bus. The instrument responds to the GPIB *interface-clear*, *device-clear* and *serial-poll* (with *rsv* bit active) commands as well as 22 device dependent commands.

On receipt of the *interface-clear* command the unit software-resets the TMS9914. The *device-clear* command is used to completely reset the instrument as follows: First, the superconducting heat switches are turned off, the DACs are wound down to zero and finally the hardware-reset logic mentioned above is activated which leaves the instrument in a state equivalent to power-on.

The TMS9914's serial poll register is used in the prescribed way. Error conditions are flagged by setting the *rsv* bit together with one of the remaining 7 bits which indicate to the controlling computer what the error was. Informational level messages such as, 'the instrument is currently busy' are indicated by setting a particular bit without *rsv*.

The device dependent commands have been divided into three groups. The first group consist of ones which have no data appended to them and required no response from the instrument on the bus. An example is the "SWITCH_HOLD_ON" command which asserts the switch hold function. The second group are commands

which have a data field appended to the command and also required no response on the bus from the unit. For example, the "START_CURRENT=1.26" command tells the Magnet Controller that the next operation in sweep mode should start the timed sweep at a current of 1.26 Amps. Finally the third group are commands which have no data field but do required a response on the bus from the unit. An example of this type is "DAC?" which causes the instrument to output a string indicating the current in the PSU next time it is *talked* by the controlling computer. Appendix 4 shows one of the IEEE-488 interface source code modules, including a list of the device dependent commands.

Normally the controlling computer can cause the Magnet Controller go to remote control by asserting the GPIB *REN* bus line. Similarly the front panel <*local*> key can be used to restore local control. Should the controlling computer wish to prevent local control being reasserted it can do this using the GPIB *local-lockout* (*LLO*) command which is implemented by the unit. In a similar way a front panel remote-lockout-command key exists to prevent the GPIB interface from taking control.

Chapter 5
Experimental Techniques

5.1 Starting a Run

The first job is to leak test the sample chamber, carefully opening it to the pumping line so as not to suck out any BN powder. After checking the IVC electrics (NMR coil(s) and IVC thermometry resistors), the IVC is sealed, evacuated and leak tested. NMR coil checking is with the vector impedance meter, giving a room temperature Q(solenoid coil) = 86.8, rising to 88.9 with the IVC installed and to 109.0 with $P_{\mathrm{IVC}} \sim 10^{-4}$ mbar. Next the OVC electrics (pot heater and pot thermometry resistors) are checked before the OVC is installed, evacuated and verified leak tight. The next stage is to install the magnet, ensuring it is axially and radially centred around the sample chamber. It is necessary to electrically insulate the magnet from the cryostat chassis because the magnet has developed an electrical leak between its main winding and former. The resistance varies from run to run, the lowest recorded values being +3.703K/−−3.580K, the leak having a slight diode effect. Checks are made for electrical continuity and leakage to the former on all the windings. After checking the remaining thermometry resistors and the magnet-bottom-heater resistor, the dewar can be raised into position and its vacuum cavity pumped if necessary. After pumping the sample chamber for 1 or 2 days to a pressure < 10^{-6} mbar the cryostat is ready to pre-cool. An A.V.G. Anavac residual gas analyser is used during pumping to monitor the contaminants still outgassing from the sample. The vacuum pumping system consists of a rotary backing pump plus an Edwards 'E02' diffusion pump with a 77K trap. Round the clock pumping has been made much easier by a purpose designed automatic liquid nitrogen filler for the trap. Fed from the 200L transport dewar the filler has a coaxial plate capacitor made to fit inside the trap as a probe/level sensor. The circuit uses only 5 CMOS logic i.c.s in its head unit adjacent to the probe and slaves a mains powered cryogenic solenoid valve to admit the nitrogen. Sufficient hysteresis w.r.t. nitrogen level has been designed into the system for efficient nitrogen usage.

Approximately 1 torr of helium-4 exchange gas is admitted to each vacuum can and the pot pumping line is flushed with helium gas. A rubber football bladder attached to the pot pumping line is used to pressurise the pot with helium gas during cool down. By occasionally opening the pot-filling needle valve during the first helium transfer any contaminants in the pot filling line are blown out, protecting the needle valve from

blocking which has been a serious problem in the past. At this stage a computer program CRYOWTCHC3 is used to continuously log, the NMR tank circuit *Q* using the vector impedance meter via its IEEE-488 interface, the thermometry resistors, the dewar nitrogen and cryostat helium levels when appropriate. The data collected is used for thermometry resistor calibration and general cryostat diagnostics. Protecting the football bladder with newspaper from nitrogen splashes to which it is very sensitive, 24 litres of liquid nitrogen is poured into the cryostat to pre-cool to 77K and left overnight for thermal equilibrium to be reached. At the same time the dewar's nitrogen jacket is filled.

After blowing out the remaining liquid nitrogen, helium is transferred to 50%−60% full, 0% representing the magnet top and 100% the 4.2K flange. During the transfer the pot pumping line needs re-pressurising several times to keep the football bladder inflated. As an additional check on the magnet, its main winding resistance can be observed, falling from 1.6Ω at 77K to 0.017Ω as most of the circuit's resistance suddenly disappears when the winding becomes superconducting. Once 4.2K thermal equilibrium has been reached the OVC is evacuated, the pot is filled and pumped to ~1K using the POTREG program. At ~1K the sample is admitted to the sample chamber through the gas handling system, the gas handling system being closed off from the sample chamber when the sample line pressure has fallen to zero, the sample being cryo-pumped by the low sample chamber temperature. A sharp peak, on sample admission, in the sample chamber Speer resistor temperature verifies the sample has entered the sample chamber, ie. no sample-line blockages. The gas handling system's sample chamber valve needs to be tightened with a small wrench to prevent it through-leaking, the leak possibly being due to BN powder having previously got into its mechanism. Sample annealing is carried out at 20K for approximately ½ hour using a pot heater power of 3.6W to boil off the pot and 1.6W to maintain 20K, again under the control of the POTREG program. During this time the sample chamber Speer is monitored using POTREG's ‘ALT_R’ command until the temperature stops rising. Also monitoring the sample line pressure on the other side of the closed sample chamber valve, checks for any through leaks. It is desirable to leave the sample overnight to cool to 4.2K before starting data taking for maximum data reproducibility. Use of the gas handling system is described in more detail in references **60** and **61**.

5.2 Tuning the Spectrometer

Having put down the helium-3 sample the next step is to tune the spectrometer and look for a signal. In the case of low coverages/short T_2 leading to a weak signal, pumping down to ~1K can yield an signal increase by as much as 4 times and may be necessary to locate the signal. Tuning the tank circuit involves feeding low levels of RF from a HP3325A frequency synthesizer into the 'TX' input of the matching unit, the frequency stepper having been set to the required frequency range. Monitoring the pre-amp output on the oscilloscope and adjusting the matching unit's internal variable capacitance, the maximum RF output is obtained. Final *tweaking up* of the resonance is most conveniently done using the synthesizer's cursor-driven controls. Using the matching unit's 'TX' rather than the *monitor* connection **[61]** has the advantage of avoiding capacitative loading of the high *Q* tank circuit with resultant resonant frequency shift. Integer frequencies are avoided due to the possibility of beating with clocks in other instruments. For example NMR at exactly 10MHz, the internal frequency standard of the Rockland 5600 synthesizer, is all but impossible. Most data has been taken at the following frequencies (MHz); 2.7, 3.7, 4.5, 5.7, 6.9, 8.6 and 10.7. Having re-configured the spectrometer for NMR (see figure 4.1.2.1) and set sensible values for the TX−PSU voltage and pulse generator settings (standalone version) the Magnet Controller is used to energise the magnet and locate the resonance. Typical pulse generator settings are; 50μS for a 90^o pulse at F=4.5MHz and a *repetition time* of 1sec. With a beat free FID displayed the phase and TX−PSU voltage are adjusted for minimum signal after a correctly phased (see figure 2.1.1) 180^o pulse. Correctly eliminating the beat pattern from the FID or echo can be complicated by the fact that the signal shape is sometimes distorted in a wave-like fashion according to **[193]**,

$$M(t) = M(0)\, 2J_1(\gamma GRt)/\gamma GRt \qquad 5.2.1$$

by the effect of the residual magnet field gradient and cylindrical geometry of the sample chamber. γ is the gyromagnetic ratio, G the field gradient in the z-direction, R the sample chamber radius and $J_1(x)$ a first order Bessel function. Having obtained a fairly well tuned up 90^o−180^o−echo display as shown in figure 2.1.1 the 4-phase generator is set to modify the phase by exactly 90^o. Any Larmor − synthesizer frequency discrepancy will manifest itself as a signal which inverts about the echo centre position when the frequency discrepancy changes sign, unambiguously locating the true Larmor frequency.

The technique also allows the correct phase-shift to be set precisely. Viewing figure 4.1.2.1 and representing the precessing magnetisation signal of the spin-echo entering the mixer as, $M(t) \propto -\cos(\omega_0 t)\exp(-|t|/T_2)$ with the synthesizer reference signal, $R(t) \propto -\cos(\omega_s t + 2\phi)$, the demodulated output after low-pass filtering is,

$$M'(t) \propto -\exp(-|t|/T_2)\cos\left[\frac{(\omega_0-\omega_s)t}{2} - \phi\right] \qquad 5.2.2$$

where ϕ is the phase shift. It is evident $M'(t) = 0$ for all t only when both $\omega_0 = \omega_s$ and $\phi = 90^o$. This is illustrated in figure 5.2.1.

Figure 5.2.1, Tuning the Spectrometer Using the In-Quadrature signal.

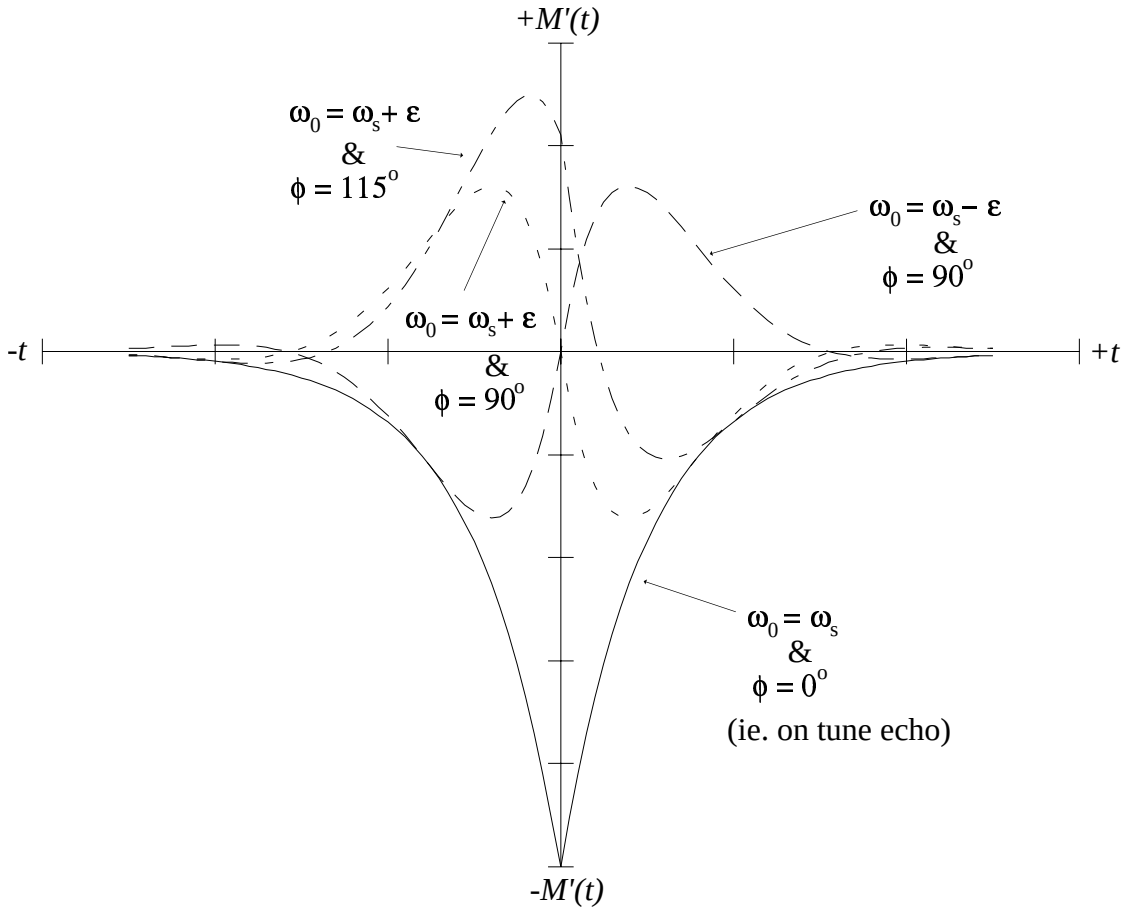

The same principle is used in *Automatic Frequency Control* (AFC) systems used in radio receivers to fine-tune a station − synchronous detection additionally involving the in-quadrature component produces a bi-directional *error voltage* which is fed back to the varicap tuner front-end to effect fine tuning.

5.3 Data Taking

Once the spectrometer is tuned up and the required temperature reached data taking can begin. Traditionally **[60,61,76]** the group's data taking has been done manually, the standalone pulse generator being programmed via its front panel with the pulse sequence and *repetition time* (where signal averaging is required), the spin echo height being measured with the aid of the TEK2230's on-screen cursors for each delay setting needed to obtain T_1 or T_2. A similar procedure involving dumping the oscilloscope trace of an FID, partially de-tuned to superimpose a beat pattern, to an X−Y plotter for later analysis was used to extract T_2^*. Naturally this is a time consuming, tedious activity and cannot be kept up 24 hours a day. Moreover, of the typically ~500 digitised points making up the echo very few are actually used in determining the signal height with the cursors. If a suitable shape function for modelling/fitting the echo or FID can be produced all the points defining it contribute to the estimate of the height, increasing the effective S/N ratio. It was for these reasons the decision to automate was made.

The current version of the data logging software ARCONTROL6 is capable of generating pulse sequences and logging signals to measure; T_2^* via partially de-tuned FIDs, T_1 and T_2 via the pulse sequences discussed in §2.1. Additionally using the Magnet Controller and the magnet's Helmholtz coils in a special configuration echo height *vs* field-gradient data can be taken. Using the background POTREG program enables ARCONTROL6 to take these data at any temperature, or more usually over a graduated range of temperatures. The system is ideally suited to measurements as a function of temperature and much use has been made of this − see §7.2.2. Instructions to the data logging software can be entered interactively or via an input-file, the file being the most flexible. The following example (listing 5.3.1) is a list of parameters describing the ARCONTROL6 input-file information and general spectrometer configuration details for a set of automatic measurements of T_1 and T_2 as a function of temperature made in Run#6 at X=0.75 monolayers;

Listing 5.3.1, Spectrometer and Computer Control Settings at X=0.75.

Run Book Symbol	Value	Explanatory notes
$4F_0$	18.169 MHz	(The Rockland synthesizer frequency)
Temperature	4.2K to 1.1K in 25 steps	
B_0	48.55mV	(The main field current, 1V ≡ 75 Amps)
B_1	2.40	(TX−PSU 'front panel' units)
P_{90}	50μS	(Length of 90° pulse)
P_{180}	100μS	(Length of 180° pulse)
Gain	×1000	(AF-AMP gain setting)
B/W	10KHz	(AF-AMP bandwidth setting)

Pre-Amp	9	(Pre-Amp PSU gain setting, 'front panel' units)
CRO	AC	(TEK2230 input coupling mode)
TB	0.5mScm^{-1} (1K)	(TEK2230 timebase setting/1K horizontal storage resolution)
YG	2.0Vcm^{-1}	(TEK2230 Y-gain setting)
Rt	3Sec for T_2	(Pulse repetition time)
	2Sec for T_1	(" " ")
Nos_ave	4	(Number of averages per trace)
Tol (reg)	10mK for T>2K	('Regulation' tolerance for Potreg)
	30mK for T<2K	
Tol (IRC)	30mK	('In-range-checking' tolerance for Potreg)
Log ScSp	Yes	(Periodically log the sample chamber Speer temperature)
Shim	0.0A	(Z_1 Shim coil not energised)
T_2 delays	500μS to 15mS in 30 linear steps	(Range of delays used to determine T_2)
T_1 delays	10mS to 4Sec→3Sec in 30 logarithmic steps	(Range of delays used to determine T_1. At 4.2K final delay in each sequence is 4Sec progressing linearly to 3Sec at 1.1K. Values of D_1 delay in 90º-D_1-90º-D_2-180º-echo sequence progresses logarithmically from 10mS to final value as determined above)
T_1 (D2)	500mS	(The T_1 D_2 delay value)
V_{PH}	5V	(Voltage for pot heater)

The TEK2230 oscilloscope has an averaging mode built into its firmware, allowing signal averaging without computer intervention. The output log file generated by ARCONTROL6 contains raw data in the form of; (1) binary screen dumps from the TEK2230 together with (2) its accompanying *waveform-preamble* which describes the instrument's settings and (3) other vital spectrometer information. The software supports both the TEK2230's horizontal digital resolutions, 1024 and 4096 samples. In averaging mode each sample has 16 bits of vertical resolution and 8 in sampling (ie. single shot trace acquisition) mode. The log file format consists of a series of *blocks* of information, the block being the basic unit of the file. Each block comprises the spectrometer information in plain text format, the waveform preamble which is also plain text followed by the binary trace. In this way data from different sets of measurements (ie. of T_1, T_2 etc.) can be concatenated together and will be decoded and analysed separately by the off-line analysis program. Below an example of a block from a set of traces for measuring T_2 is shown. Note: delay times are in μS, temperatures in mK and conductances in nMhos. The spectrometer settings start with the 'SEQUENCE' field, the waveform preamble is prefixed with 'WFM WFI:' and the binary data starts with the 'CURV %' prefix;

```
SEQUENCE=T2
READING=2
NOS_AVE=8
EDL_VAL=299
OPTIONAL_INFORMATIONVERSION=3.0.04 (Arc) (12-DEC-1991)
FREQUENCY=4.880100001
TIME=Wed,25 Dec 1991.19:15:59
PREMA ch0=+03.25014E-1VDR2A1T3S0Q0C0M0
PREMA ch1=+1.797652E-1VDR1A1T3S0Q0C0M1
T = 1105
T(req) = 1100
Tolerance {t>2k } = 30
Tolerance {t<2k } = 30
Tolerance (for in-range checking)= 30
T adjust time (min) = 1.500166667
```

```
T last update time = Wed Dec 25 19:15:53 1991
Conductance = 487100
HP5335A CH A = NOT IN USE
HP5335A CH B = NOT IN USE
T(SC Sp) = 1101
Conductance(SC Sp) = 645400
MC_DAC = N/A
WFM WFI:"ACQ, CH1, 1.0V, AC, 0.1mS, AVERAGE, CRV#
3866",NR.P:4096,PT.O:2048,PT.F:Y,XMU:1.0E+0,XOF:0,XUN:S,XIN:1.0E6,YMU:0.15625E3,YOF:0,YU-
N:V,ENC:BIN,BN.F:RP,BYT:2,BIT:16,CRV:CHK;
CURV % ÑÎÑÃÑõÑáÑÞÑÄÒÑÆÒÑáÑ™Ñ ÑçÑ•ÑÙÑHÑ{Ñ
Ð-Ñ&Ð¢Ð¢ÐÝÐ¸Ð ÐéÐÏÐ«Ð®ÐyÐ„Ð«Ð¤ÐÝÐ¬ÐÏÐÓÐ-ÐíÐÌÑTÑ Ñ4Ñ¹Ñ ÑÑ¦ÑÑ@ÑXÑ¦ÑWÑ~ÑcÑeÑjÑcÑCÑeÐéÑÐ×ÑÐ"-
Ð—Ð°ÐfiÐÐÐ¡ÐlÐ;ÐPÐÐ¢ÐbÐjÐ¤Ð°ÐwÐfÐQÐ ÐÐÐ²ÐÐflÐÐ Ð{ÐyÐyÐ
ÐJÐNÏÑÏ³ÏÓÐÐ1ÏêÐQÐÐÏòÏ‡ÐÏÃÐUÐQÐ&ÐÐ*ÏãÏÙÏÁÐ
```

.....etc.

A program called DISPLAY has been written to display the textual information and plot the TEK2230 traces on the Archimedes monitor. Equipped with a simple set of on-screen cursors for reading signal heights and times it is useful for checking raw data before uploading it to the VAX computer for analysis.

With raw data files as large as 17 Mbytes a fast reliable method of transferring them to the VAX was needed. The *Kermit* protocol for communicating between computers over a serial line is reliable but can be slow. Due to the 2048 byte *packet* size limit of the Archimedes implementation at the time, the extensive *escaping* used by the protocol and the RX−TX delays inherent in the X25 PAD through which the serial line connection goes, Kermit is painfully slow, often giving an effective throughput as low as 1000 to 2000 baud over a 9600 baud serial line. At 2000 baud (effective) 17 Mbytes takes more than 24 hours to transfer, during which time no data can be taken. Two Archimedes programs ARC2TAR and TAR2ARC have been developed to provide faster communication over the serial connection. They transfer files to and from the VAX respectively, communicating with a *server* program on the VAX not unlike Kermit. Providing full error checking and correction with the minimum escaping necessary for the two machines and using a 10 Kbyte packet length the effective throughput is often better than 8500 baud, reducing the transfer time proportionately. Multiple files can be copied in one session, the files on the VAX being in *Tar* file format which the data analysis software can read directly as a single tar file or individually after *un-tarring* on the VAX as necessary. Recently, a disc drive with an SCSI interface supporting 40Mbyte removable hard discs and a TCP/IP package giving remote file access (NFS) to the VAX over Ethernet has become available making data transfer faster and easier.

Chapter 6
Data Analysis

6.1 Introduction

This chapter deals with the mechanics of analysing raw data to provide quantities characterising the relaxation processes, eg. relaxation times. Seeking physical interpretations for the relaxation behaviour is considered elsewhere.

The first stage is to obtain sets of points of signal height *vs* time (h,t) from the sets of spin echo oscilloscope traces for T_1 and T_2 data. A similar process for getting (h,t) data from partially de-tuned FIDs also exists in the analysis software but in practice has been little used and will not be considered further.

It would have been desirable to do the analysis locally, on the data logging machine eliminating the need to transfer files off the Archimedes and be reliant on an externally provided computer service not always available. However, it was decided to do the volume processing/analysis of the raw data by batch on the VAX for a number of reasons: The scheduling restrictions discussed in §4.2.2 inherent in the Archimedes operating system RISC OS meant data taking would have to wait while the data was analysed or a second machine would be needed. The former being unacceptable as the analysis can take many hours. The VAX/VMS operating system provides a sophisticated multi-user environment ideal for developing large pieces of software. The VAX/VMS FORTRAN compiler and debugger are reliable established programs. The ability to run the analysis program as a *batch job* while monitoring its progress and doing other work interactively at a terminal has been invaluable. The VAX has a 9-track tape drive which provides an inexpensive repository for raw data should it be required for re-analysis. 460Mbytes of raw data has been produced in the course of this work and is stored on tape. Also, the Central College VAX6430, a 3−CPU symmetric multi-processing machine is significantly (typically a factor of 30 times) faster than an ARM2 CPU Archimedes where intensive FP calculations are involved.

The raw data analysis program ANALYSE consists of approximately 6700 lines of FORTRAN source code with comments. Its operation is as follows;

(a) It searches the input raw data file until a valid *block* is found, extracting the spectrometer information, TEK2230 settings and binary trace from it.

(b) Then it attempts to locate the spin echo in the trace using the algorithm described below.

(c) Next, it attempts to fit a curve through the echo using a non-linear least squares algorithm, from which it obtains the echo height.

(d) Finally, it writes out the echo height with the relevant pulse generator delay setting to a file, ie. a (t,h) data pair and starts work on the next block.

6.2 Locating and Fitting the Spin-Echo

Failure to correctly locate the position of the echo in the trace has severe consequences for the quality of the fit, so considerable trouble has been taken to get it right. The algorithm is far from infallible but has over the course of this work been developed to handle most types of anomalous echo trace encountered. It is expected to handle even very noisy echoes but to reject data containing no recognisable signal. Naturally, the dividing line can be fine and arbitrary. Two signal distortions which sometimes cause difficulties are baseline drift due to pulse/signal height differences charging the oscilloscope's input capacitance when AC input-coupled and the Bessel function distortion (§5.2).

(1) The TEK2230 is triggered to make the echo appear in the centre of the screen, §4.1.2.2. However, ringing in the high-Q NMR coil conspires to shift the echo rightwards. The coil is expected to ring for approximately Q cycles for the undamped case but the Q damping arrangement plus frequency changing etc. make reliably calculating the shift impractical. Instead the largest expected shift is calculated for the maximum Q case (5MHz unloaded tank circuit) for later use and is shown in figure 6.2.1 as the difference between *Nos_points2ex* and *Nos_points/2*, *Nos_points/2* being the screen centre where an unshifted echo should appear. *Nos_points_m2* represents the RHS end of the trace, the '*m*2' signifying that the last two points are not used for TEK2230 instrumental reasons. These rather unusual symbols have been chosen to be similar or identical to the corresponding variable names in the ANALYSE source code to aid understanding it.

(2) The next stage is to find the place where the ringing which saturates the receiver electronics ends. It is designated *End_of_sat_ringdown*. A guess value for the signal baseline height *Baseline_guess*, the average of the last *n* (currently 10) points up to *Nos_points_m2* is found. The region from *Trailing_edge_of_180* to *Half_way_bet_echo_and_180* is searched for either, the rightmost largest signal excursion measured w.r.t. the *Baseline_guess* or the TEK2230's largest (eg. 255 in

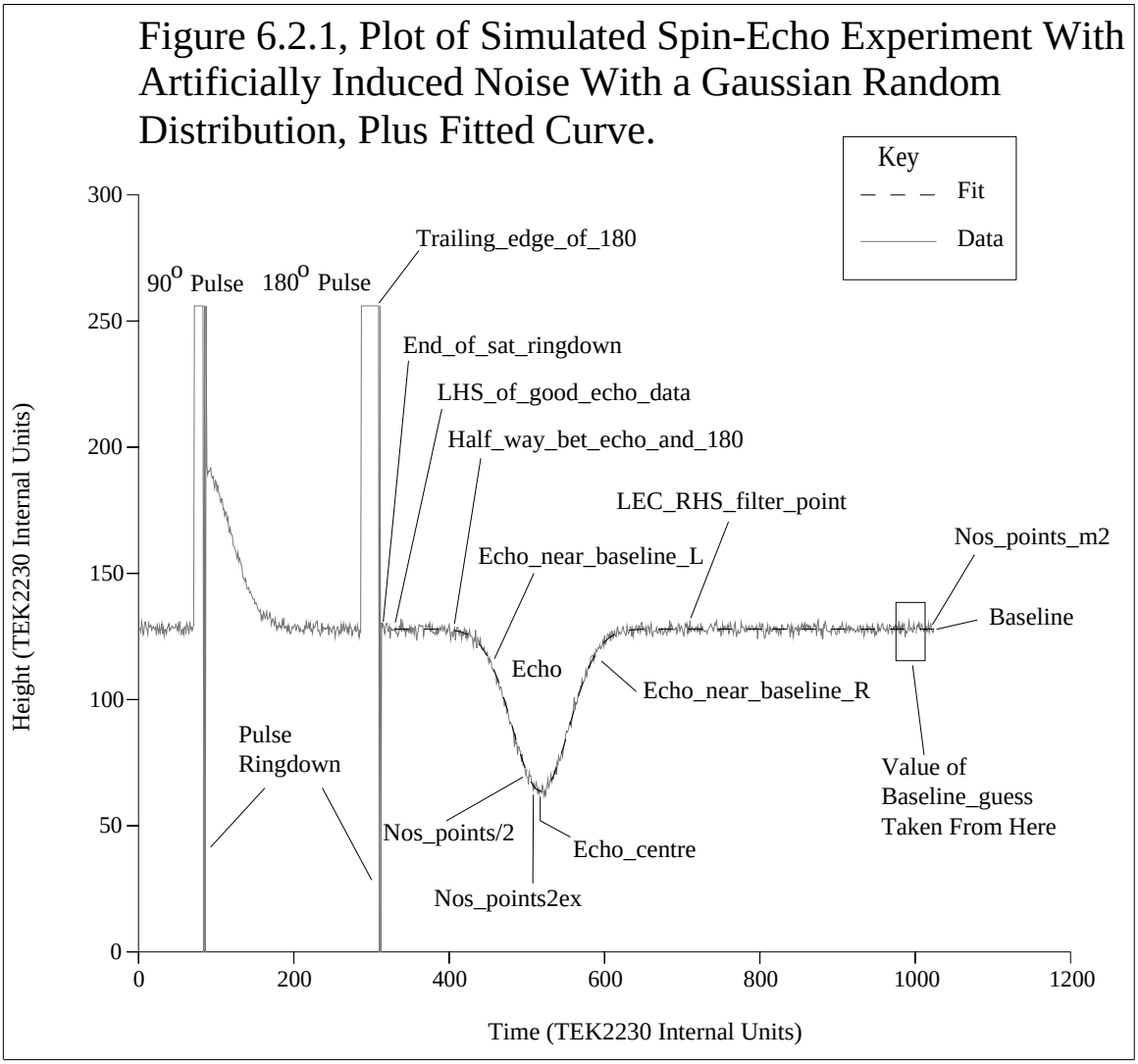

sample mode) and smallest (eg. 0) possible, rightmost sample output values. *End_of_sat_ringdown* is assigned this position. *Half_way_bet_echo_and_180* is defined as (*Trailing_edge_of_180* + *Nos_points*/*2*)/2. Occasionally, where T_2 is very short (eg. < 100μS) and with small delay settings the saturating ringdown can extend beyond *Half_way_bet_echo_and_180*, the echo being partially absorbed by it. Such data occurred in the ^{11}B work. If this is the case the rest of the trace is searched using the TEK2230's largest/smallest value criteria alone to extend rightwards the position of *End_of_sat_ringdown*. An 'Abnormal Extension' warning is issued to that effect. *End_of_sat_ringdown* is then extended rightwards until the trace meets the *Baseline_guess*. This has been done for maximum protection against any ringdown being included in the later echo region filtering processes, failure to prevent this can lead to the echo centre being improperly located. If the baseline meet is not found the rightmost search position is used and a warning issued. Locating *End_of_sat_ringdown* is the most problematic part of the entire procedure. A variety of options modifying the

rightmost position searched in the extension process and the L→R/L←R extension search direction are available for difficult sets of data and are enabled/disabled using VAX/VMS *logical names* which can be invoked/modified at will at run time, even part way through an analysis run from another *VMS process* if necessary without modifying any code.

(3) To avoid weighting the echo asymmetrically in the filtering process used to find its centre, a point *LEC_RHS_filter_point* (ie. *locate-echo-centre_…*) is defined and used as the rightmost point to be filtered with the echo. It is designated as the rightmost of; (a) A point a distance (*Nos_points*/*2* − *End_of_sat_ringdown*) right of *Nos_points*/*2* or (b) Where the trace meets the *Baseline_guess*. If the trace↔*Baseline_guess* meet is not found the trace is rejected and an error message generated. Using a digital low-pass filter function $F(i) = (F(i-2) + F(i-1) + F(i) + F(i+1) + F(i+2))/5$ for the *i*th point, a copy of the trace, from *End_of_sat_ringdown* to *LEC_RHS_filter_point* is repeatedly filtered until there is a monotonic fall from *LEC_RHS_filter_point* to *Nos_points2*ex. Before proceeding with filtering, the values determined for *LEC_RHS_filter_point* etc. are checked to ensure they are sensible. If not the trace is rejected as in error. The filtering process represents the trace as a series of real numbers, allowing an arbitrary sized, empirically determined *smoothness factor* to be used in deciding how small the deviations from monotonicity have to be for the monotonicity criterion to be satisfied. The smoothness factor is read in from a parameter file at the start of an analysis run. Should the trace be too noisy to pass the monotonicity test after the maximum permitted number (again, read from the parameter file) of filtering operations it is rejected as in error. Most of the CPU time used by the program goes on filtering and monotonicity checking. Considerable savings have been made by optimising the number of filtering operations executed before invoking the monotonicity check, the justification being the CPU-time used in a filter operation is $\propto N$ (the number of points) whereas in a monotonicity check is $\propto N^2$. The VAX−PCA utility **[194]** provides a subroutine-by-subroutine and source code line-by-line breakdown of CPU time consumption, providing detailed information for the above optimisations.

(4) Searching the filtered trace from *Half_way_bet_echo_and_180* to *LEC_RHS_filter_point*, the lowest point defines *Echo_centre*, the best estimate for the actual centre of the spin-echo.

(5) Filtering the copy of the trace with the same function, from *LEC_RHS_filter_point* to *Nos_points_m2* until there is a monotonic fall or constant level from *Nos_points_m2* to *LEC_RHS_filter_point*, the trace at *Nos_points_m2* is taken as

the value for *Baseline*, to be used as input guess-value in the non-linear least squares fit. If the fall/constant level is not found or *Baseline* < the trace at *Echo_centre*, the trace is rejected.

(6) Using the filtered trace, starting at *Echo_centre* and going right until the signal measured w.r.t. the *Baseline* has almost decayed away locates the point *Echo_near_baseline_R*. Currently this is where the echo has decayed away to 20% of its *Echo_centre* value. If the point cannot be found a warning is issued.

(7) Using the filtered trace again, going left from *Echo_centre* as far as *End_of_sat_ringdown* until either the above signal decay criterion is met or the *Baseline* is reached or the trace starts to decrease again, eg. due to the pulse ringdown tail, locates the point *Echo_near_baseline_L*.

(8) Taking *Echo_centre* as a time=0 reference and sending the portion from *Echo_near_baseline_L* to *Echo_near_baseline_R* of the unfiltered trace to a linearised gaussian least squares fitting routine estimates the echo's gaussian time constant, τ_g, where,

$$h(t) = h(0)\exp(-t^2/\tau_g^2) + Baseline \qquad 6.2.1$$

If no fit is found the trace is rejected.

(9) Using the filtered trace again, starting at *Echo_centre* and going left until either the trace rises above the *Baseline* or starts to fall again, sets the point *LHS_of_good_echo_data*. Its function is to maximise the number of points used in the non-linear least squares fit.

(10) Finally using, the unfiltered trace from *LHS_of_good_echo_data* to *Nos_points_m2*, the gaussian time constant τ_g as the time-constant input guess value, *Echo_centre* as the time=0 reference and *Baseline* as its own input guess value, the non-linear least squares routine is called to fit the echo. Currently two fit/models are available; a pure gaussian (equation 6.2.1) and an exponential-gaussian product,

$$h(t) = h(0)\exp(-t/\tau_e\ -t^2/\tau_g^2) + Baseline \qquad 6.2.2$$

The fitted echo height is (*Baseline* − *h*(0)), *Baseline* and *h*(0) are the values returned by the non-linear least squares subroutine. If no fit was possible the trace is rejected and an error flagged.

Figures 6.2.2−6.2.7 show plots of experimental spin-echo traces with fits. All

Figure 6.2.2, Plot Showing Echo Height vs Time TEK2230 Trace Plus NLLSQ Fit.

T_2 Inter-Pulse delay=0.954mS, T=4.2K, F=4.532MHz, Nos_points=4096, X=0.2, Nos_ave=16, Helium-3 on BN signal, Run#6.

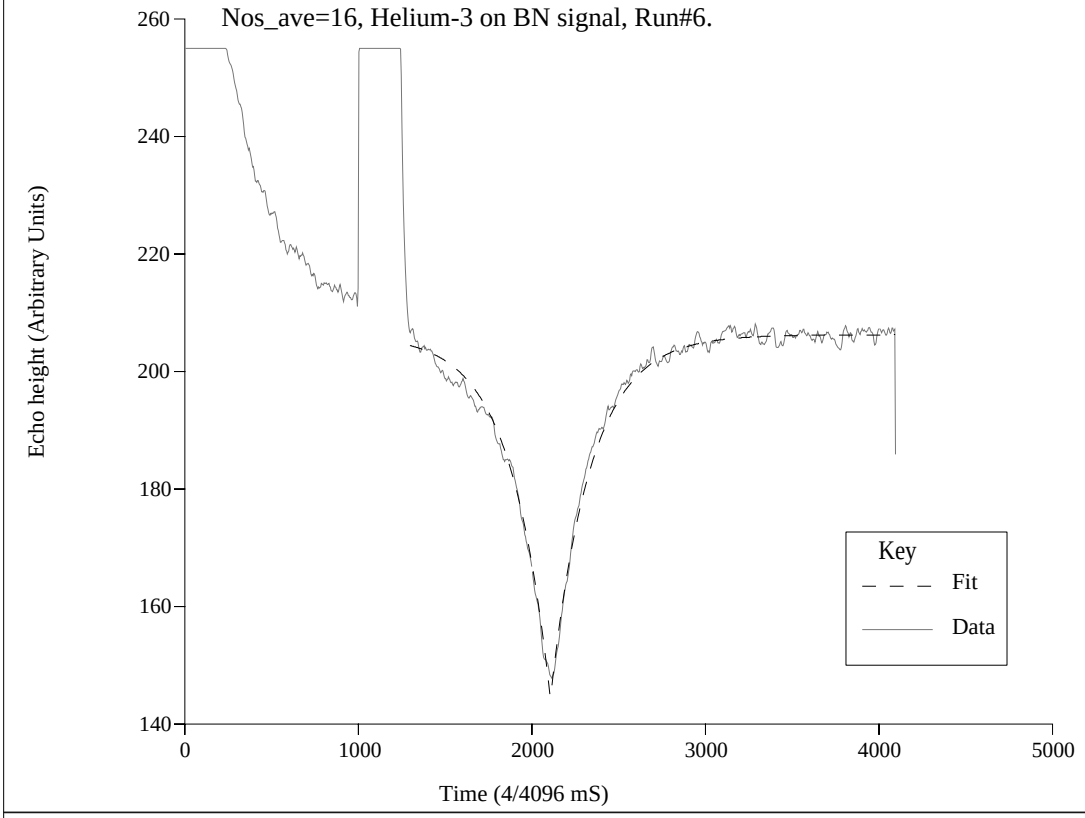

Figure 6.2.3, Plot Showing Echo Height vs Time TEK2230 Trace Plus NLLSQ Fit.

T_2 Inter-Pulse delay=5.721mS, T=4.2K, F=4.532MHz, Nos_points=4096, X=0.2, Nos_ave=16, Helium-3 on BN signal, Run#6.

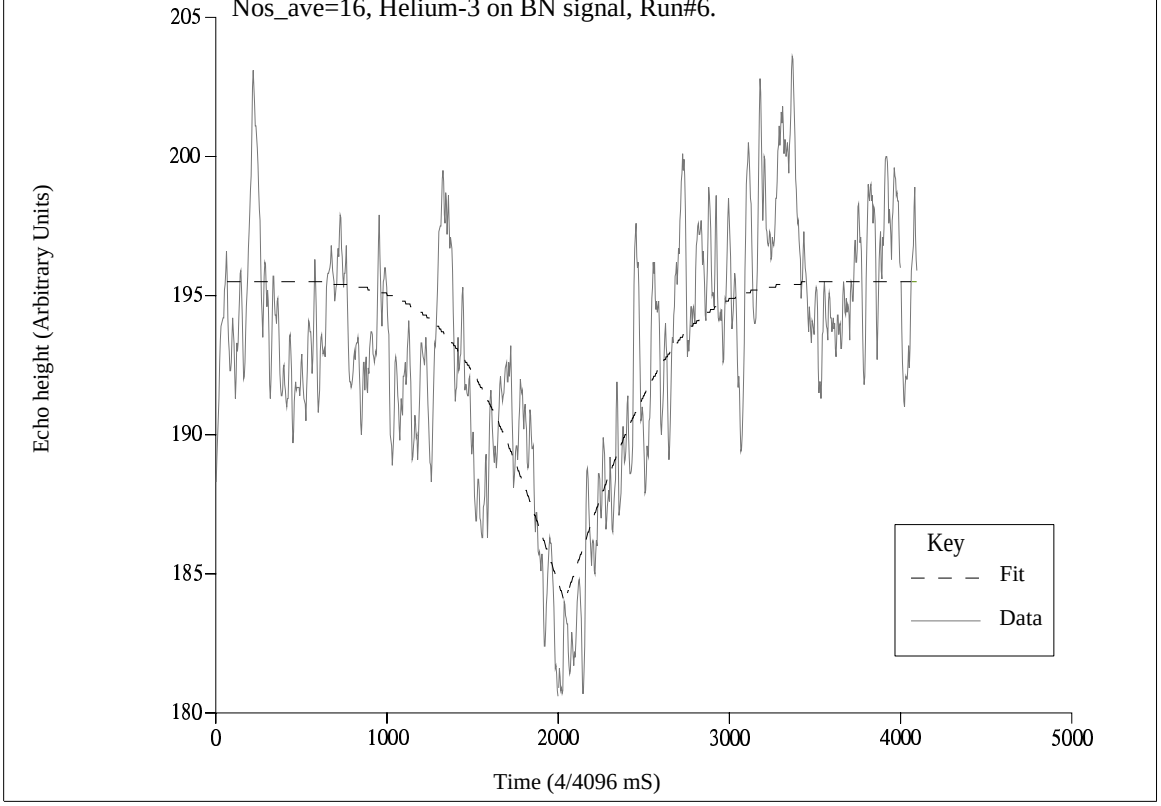

Figure 6.2.4, Plot Showing Echo Height vs Time TEK2230 Trace Plus NLLSQ Fit.

T_2 Inter-Pulse delay=1.772mS, T=4.2K, F=10.69MHz, Nos_points=4096, X=0.4, Nos_ave=16, Helium-3 on BN signal, Run#6.

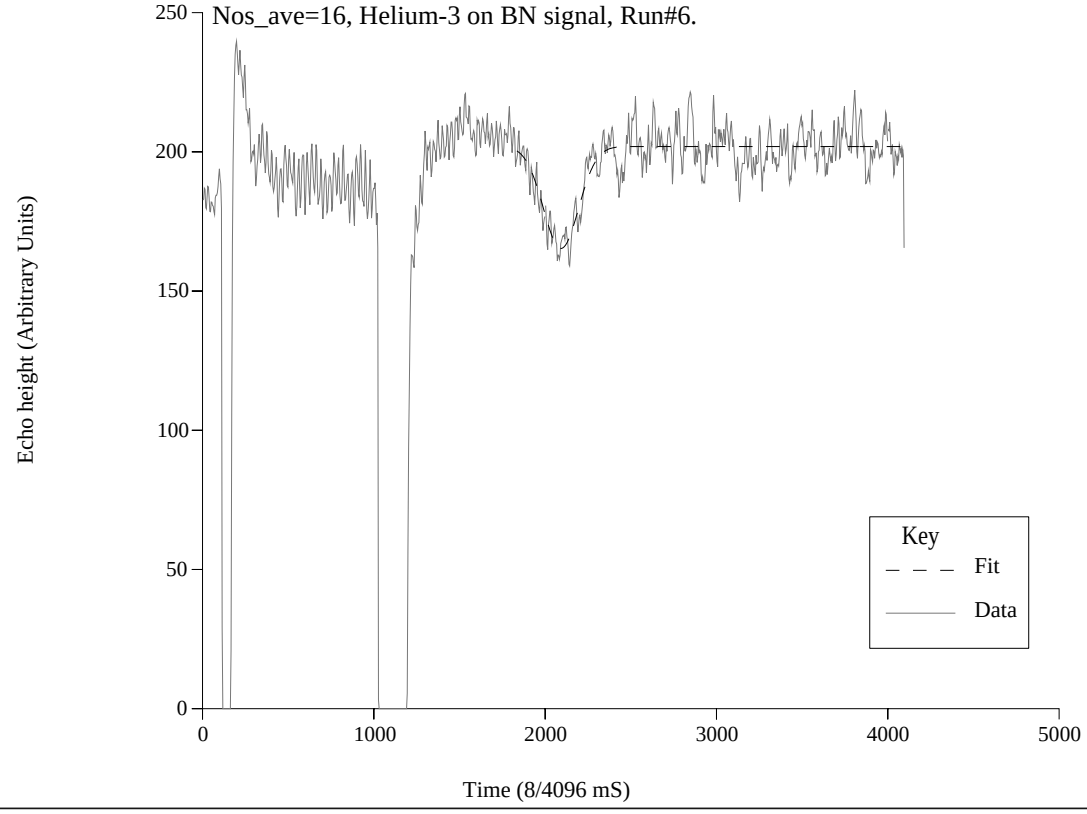

Figure 6.2.5, Plot Showing Echo Height vs Time TEK2230 Trace Plus NLLSQ Fit.

T_2 Inter-Pulse delay=3.362mS, T=4.2K, F=10.69MHz, Nos_points=4096, X=0.4, Nos_ave=16, Helium-3 on BN signal, Run#6.

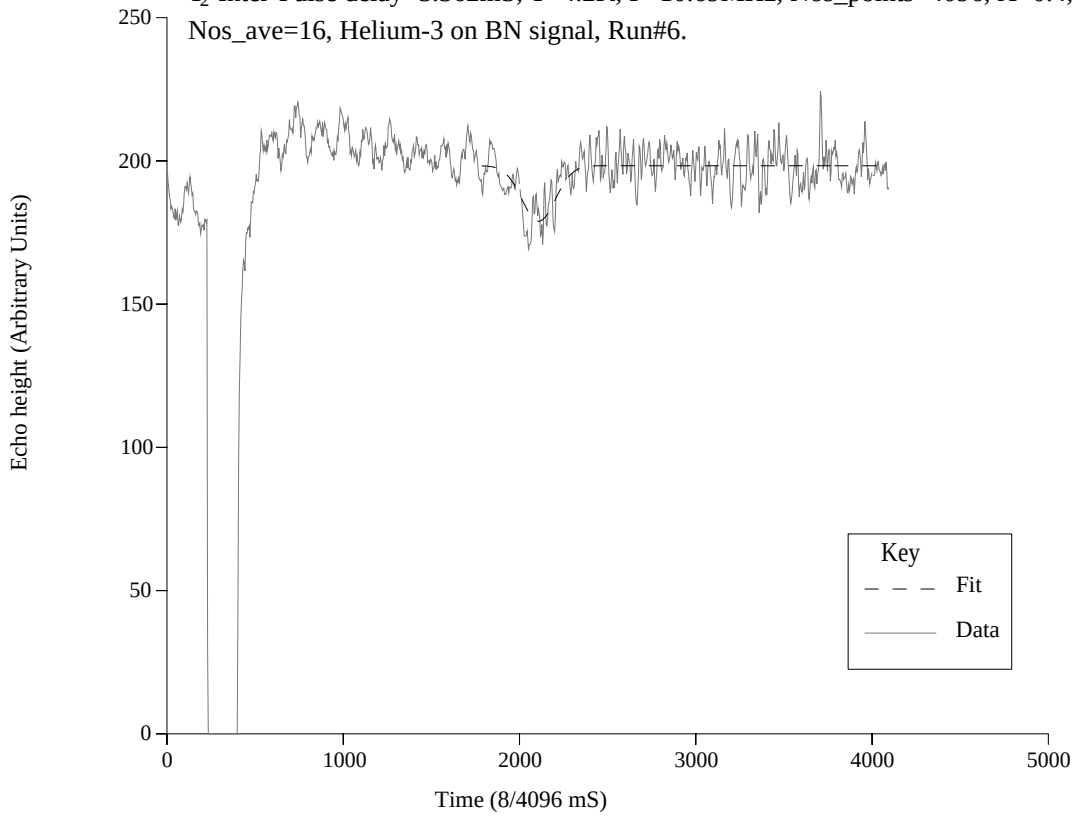

Figure 6.2.6, Plot Showing Echo Height vs Time TEK2230 Trace Plus NLLSQ Fit.

T_2 Inter-Pulse delay=0.230mS, T=1K, F=4.88MHz, Nos_points=4096, X=0.7, Nos_ave=4, Rep-time=2mins, Boron-11 signal, Run#8.

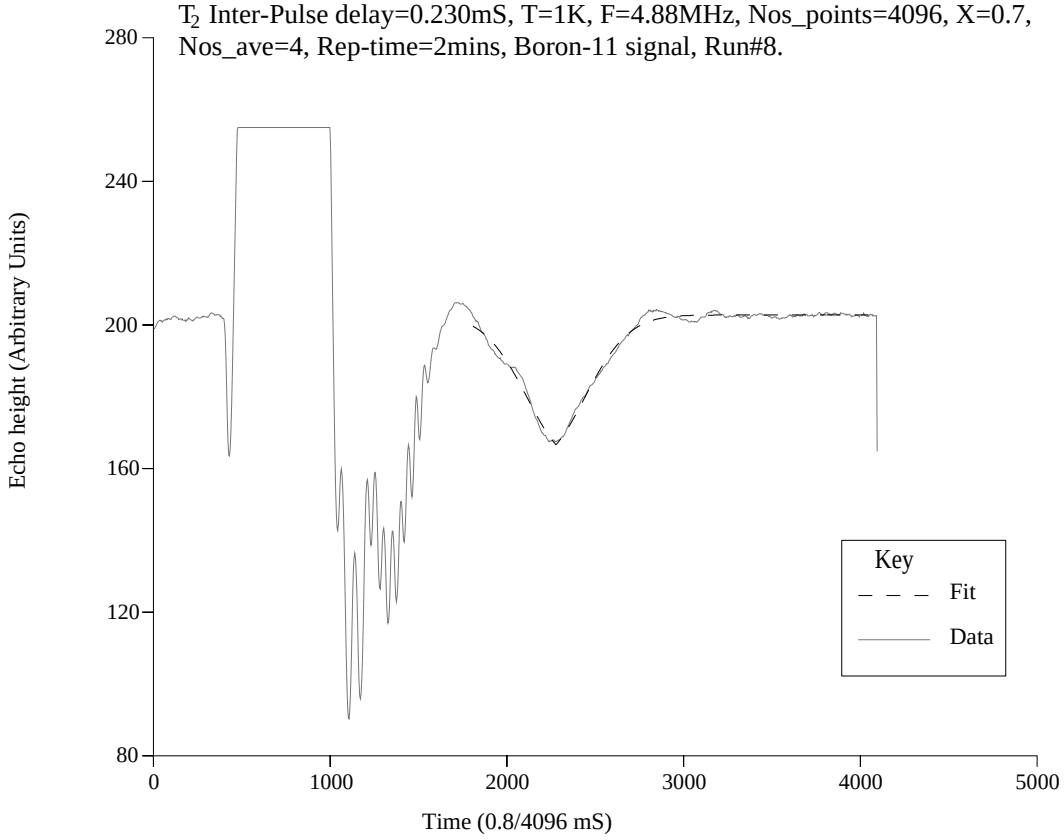

Figure 6.2.7, Plot Showing Echo Height vs Time TEK2230 Trace Plus NLLSQ Fit.

T_1, 90^o-35.7min-90^o-0.23mS-180^o-0.23mS-Echo sequence, T=1K, F=4.88MHz Nos_points=4096, X=0.7, Nos_ave=4, Rep-time=1Sec, Boron-11 signal, Run#8.

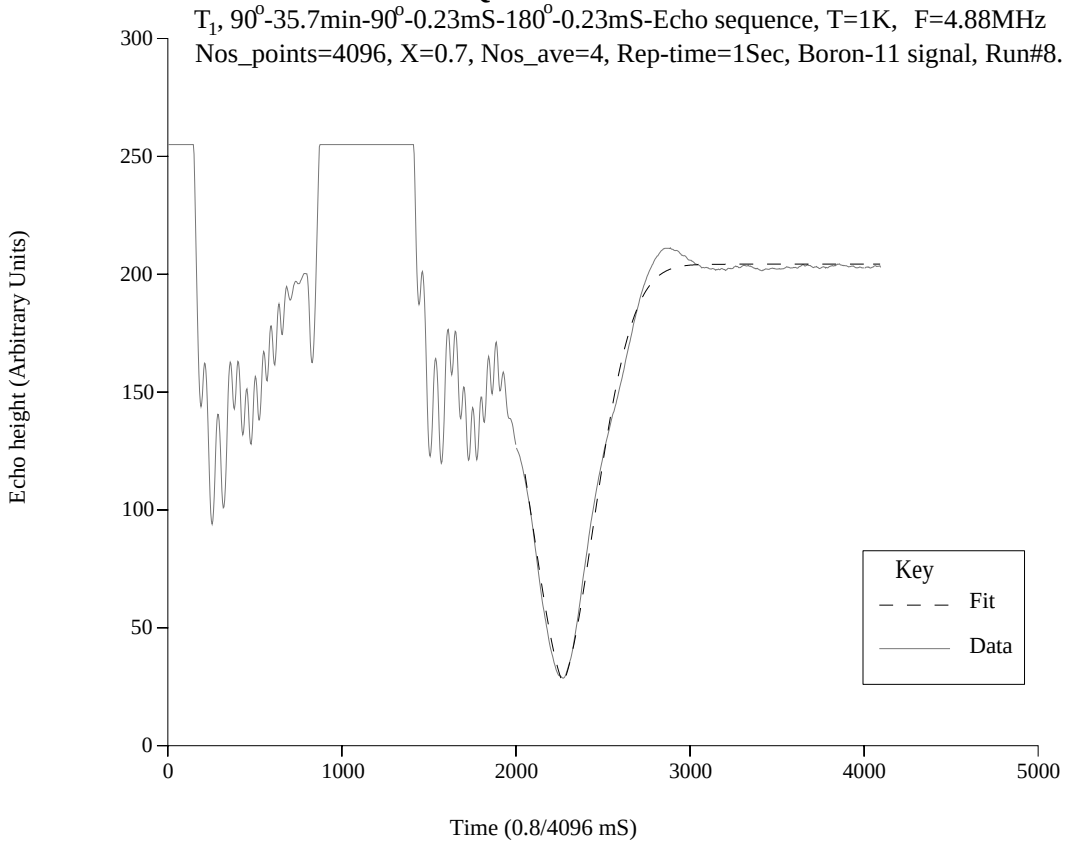

traces shown use the product function which gives a better empirical fit. Having increased the TEK2230's *y-gain* by ×2.5 w.r.t. figure 6.2.2, to better display the almost decayed-away echo, figure 6.2.3 shows the technique's power in resolving the signal. Figures 6.2.4 and 6.2.5 show traces afflicted by strong correlated computer noise, often a problem at 10.7MHz. Notice the abrupt change in the appearance of the noise at the echo centre. This is believed to be related to the pulse generator hardware and the ARM code which drives it shutting down after the last pulse in the sequence, the echo-coincident trigger pulse. Figures 6.2.6 and 6.2.7 are of Boron-11 echoes.

6.3 Regression

If we have a model believed to describe the experimental data which contains a number of adjustable parameters we need a method to find the best unbiased estimates of those parameters according to some objective criteria. If the experimental errors in the data have the expected gaussian random distribution, the method of least squares provides the best estimates. It works by minimising the square residuals. For a model function with y the dependent variable, x, the independent variable and $\theta_1 \ldots \theta_p$ the adjustable parameters,

$$y = F(x,\theta_1 \ldots \theta_p) \qquad 6.3.1$$

can be written. For the n data points $(x_1 \ldots x_n, y_1 \ldots y_n)$ we minimise $S(\theta_1 \ldots \theta_p)$ w.r.t. the $\theta_1 \ldots \theta_p$ for their best estimates, where,

$$S(\theta_1 \ldots \theta_p) = \sum_{i=1}^{n} \left(y_i - F(x_i, \theta_1 \ldots \theta_p)\right)^2 \qquad 6.3.2$$

If $F(x,\theta_1 \ldots \theta_p)$ is linear in the $\theta_1 \ldots \theta_p$,

$$F(x_i, \theta_1 \ldots \theta_p) = \sum_{j=1}^{p} \theta_j \frac{\partial F(x_i, \theta_1 \ldots \theta_p)}{\partial \theta_j} \qquad 6.3.3$$

can be written. Substituting 6.3.3 in 6.3.2 and minimising $S(\theta_1 \ldots \theta_p)$ w.r.t. θ_m,

$$\frac{\partial S(\theta_1 \ldots \theta_p)}{\partial \theta_m} = \sum_{i=1}^{n} \left(y_i - \sum_{j=1}^{p} \theta_j \frac{\partial F_i}{\partial \theta_j} \right) \frac{\partial F_i}{\partial \theta_m} = 0 \qquad 6.3.4$$

can be written, where the arguments of 'F' have been dropped for neatness. After some rearrangement,

$$\sum_{j=1}^{p} \theta_j \left(\sum_{i=1}^{n} \left[\frac{\partial F_i}{\partial \theta_j} \frac{\partial F_i}{\partial \theta_m} = y_i \frac{\partial F_i}{\partial \theta_m} \right] \right) \qquad 6.3.5$$

which describes a set of simultaneous linear equations with p unknowns, the θ_j's. Adopting a matrix notation in which the $\partial F_i / \partial \theta_j$ are the ijth elements of an $n \times p$ Jacobian matrix 'J', equation 6.3.5 can be rewritten,

$$J^T J \boldsymbol{\theta} = J^T \mathbf{Y} \qquad 6.3.6$$

By convention,

$$A \boldsymbol{\theta} = J^T \mathbf{Y} \qquad 6.3.7$$

The θ's are immediately found,

$$\boldsymbol{\theta} = A^{-1} J^T \mathbf{Y} \qquad 6.3.8$$

Many functions 'F' non-linear in a single θ_j such as a single exponential decay, $h(t) = h(0) \exp(-t/T_2)$, can be linearised by a simple transformation such as taking logs. This is bad practice however, as the errors are no longer normally distributed and the parameters will be incorrectly estimated. If 'F' is non-linear in only one of its θ_j (as with the above decay) the simultaneous equations may be solved until one is left containing only the non-linear θ_j unknown, that equation being solved by a simple iterative numerical technique such as the secant method.

6.3.1 Non-Linear Regression

If there are two or more non-linear adjustable parameters, the problem is quite different. The cases discussed above are guaranteed to find/converge to the best estimates, the following are not. The aim therefore becomes maximum reliability.

The Gauss-Newton (GN) method makes the function linear in the adjustable

parameters using a first-order Taylor expansion. Equation 6.3.7 can be re-written for the GN method,

$$A\,\boldsymbol{\Delta} = J^T [\mathbf{Y} - F_i(\boldsymbol{\theta}^{(s)})] \qquad 6.3.1.1$$

'*s*' is an index of iteration and $\boldsymbol{\Delta}$ is the function's linear correction vector. Writing $J^T [\mathbf{Y} - F_i(\boldsymbol{\theta}^{(s)})] = J^T \mathbf{r} = \mathbf{g}$ where '**r**' is the residual vector evaluated at the current iteration, ie. at $\boldsymbol{\theta}^{(s)}$,

$$A\,\boldsymbol{\Delta} = J^T \mathbf{r} = \mathbf{g} \qquad 6.3.1.2$$

the algorithm proceeds as follows,

(1) Start with some initial guess values for the $\boldsymbol{\theta}^{(s)}$

(2) Obtain the correction vector, $\boldsymbol{\Delta}^{(s)} = A^{-1}\,\mathbf{g}$

(3) Improve the values of the $\boldsymbol{\theta}$, $\boldsymbol{\theta}^{(s+1)} = \boldsymbol{\theta}^{(s)} + \boldsymbol{\Delta}^{(s)}$

(4) If $\boldsymbol{\Delta}^{(s)}$ was small enough convergence was achieved, otherwise go back to step 2.

Whether the GN converges correctly depends critically on the closeness of the initial guess $\boldsymbol{\theta}$. For good initial $\boldsymbol{\theta}$ it can converge rapidly but has a pronounced tendency to diverge when applied to practical problems [195,196].

Another scheme, the Method of Steepest Descents proceeds in a series of hops of a suitable size, starting from the initial guess values of $\boldsymbol{\theta}$, along the negative direction of the gradient of $S(\boldsymbol{\theta})$, $\boldsymbol{\Delta} g$,

$$\boldsymbol{\Delta} g = -\left(\frac{\partial S}{\partial \theta_1}, \frac{\partial S}{\partial \theta_2}, \cdots \frac{\partial S}{\partial \theta_p}\right)^T \qquad 6.3.1.3$$

re-calculating the gradient at each step. Although reliably convergent for linear functions, in the non-linear case the elliptical contours of the *p*-dimensional 'S' surface become distorted causing convergence to the global minimum to become very slow [195], indicating $\boldsymbol{\Delta} g$ may not be the best direction to take.

The Marquardt-Levenberg method is a systematic compromise between the GN and Steepest Descents, combining their respective convergence speed and reliability. Experimentally, the directions taken from the initial guess $\boldsymbol{\theta}$ were found to usually differ by ~90°. The ML algorithm [196] interpolates between the two directions by calculating the correction vector $\boldsymbol{\Delta}$,

$$\boldsymbol{\Delta}^{(s)} = [A + \lambda I]^{-1}\,\mathbf{g} \qquad 6.3.1.4$$

where I is the identity matrix and λ is a scalar varied to control the algorithmic balance. The effect of λ can be considered from the two limiting cases: For $\lambda \to 0$, the direction $\to$ GN and for $\lambda \to \infty$, $\boldsymbol{\Delta}^{(s)} \to \mathbf{g}/\lambda$ which corresponds to a small step ($\propto 1/\lambda$) along the Steepest Descent direction, $\boldsymbol{\Delta}g$. The strategy is to control λ such that the GN direction is followed as much as possible for speed but with an inclination to the Steepest Descents to prevent divergences. λ is varied by an arbitrary fixed factor ν, being scaled up or down by ν depending on whether $S(\boldsymbol{\theta})$ is improved by an iteration. Within an iteration λ is increased until a reduced sum of squares is obtained, which should always be possible. Between iterations λ is successively reduced so that as the minimum is approached the algorithm tends towards the GN direction.

6.3.2 The Marquardt-Fletcher Algorithm

Fletcher's version of the Marquardt algorithm **[197]** uses the same basic technique but is more efficient and reliable, a result of much of the arbitrariness having been removed. The main difference is in the way λ is controlled. The new value is based on the ratio of the actual reduction in the sum of squares and that predicted on a linear model. In addition to being increased or decreased by a calculated amount it can also be left unchanged by an iteration. An invaluable property of the algorithm which has been used in both the ANALYSE and NLLSQ programs, is the ability to impose constraints on the values the θ_j are permitted to take in the event of too large a correction being attempted. Eg. unphysical negative relaxation times are precluded and echo heights are prevented from straying too far from the previously determined approximate values in the ANALYSE program. In this way proper convergence may be achieved in cases where poor data or difficult functions would otherwise prevent it **[196]**. An implementation of the MF algorithm exists in the Harwell Subroutine Library under the code VA07A. At the time of software writing VA07A was not easily obtainable, so the FORTRAN source code listing in reference **197** was used to produce a partially rewritten, in structured FORTRAN, set of subroutines to implement the method. Each fitting function is implemented through two subroutines, one defining the residuals, the other their first derivatives w.r.t. the adjustable parameters. It is important to have some idea of the errors in the fitted parameters. They can be obtained to a good approximation from the diagonal elements of the inverse of the 'A' matrix at convergence **[195]** and the variance of

the parameter. For simplicity the variance is estimated by external consistency [195], $Var = S(\boldsymbol{\theta})/(n-p)$. For small sets of data where $n \not\gg p$ the assumption that the residuals are normally distributed breaks down and the 'T' distribution must be used. A good empirically determined approximation for the 'T' distribution multiplier [198] for a 50% confidence interval is, $M(n) = 0.6745/(1-[0.362/n])$. The estimated error in the jth parameter then is,

$$E(\theta_j) = M(n) * (Var * A^{-1}_{jj})^{½} \qquad 6.3.2.1$$

It is often apparent from the estimated errors if the chosen fitting equation is a poor model for a data set. Results are typically huge errors, sometimes several orders of magnitude greater than the parameter with unexpectedly large differences in estimated errors from one parameter to another. 'A' is a positive-definite symmetric matrix, Choleski's method [199] has therefore been used to invert it. To avoid program crashes due to floating-point overflows, −ve square roots etc. from ill-conditioned matrix calculations where the data and/or fit is very poor, various traps/checks have been incorporated into the Choleski subroutine and elsewhere in the software.

The NLLSQ program was written as a user-friendly interactive interface to the MF fitting routines. It is composed of >7400 lines of annotated FORTRAN source code. Listing 6.3.2.1 lists the fitting functions implemented in the current version as it appears to a user on a terminal.

Listing 6.3.2.1, The Fitting Functions Currently Implemented by the NLLSQ Program.

```
FORM TO BE FITTED ?
THE OPTIONS ARE;

    h(t)=h(0)exp(−t/T1)+h(infinity)                              (T1)
    h(t)=h(0)exp(−t^a/T1+h(infinity)                             (T1Index)
    h(t)=h(0)exp(−t/T1  −t^2/Delta)+h(infinity)                  (ExpGauss1)
    h(t)=ha(0)exp(−t/Ta)+hb(0)exp(−t/Tb)+h(infinity)             (TWOEXP)
    h(t)=ha(0)exp(−t/Ta)+hb(0)exp(−t/Tb)                         (TWOEXP2)
    h(t)=h(0)exp(−t/T2)*cos(Omega t+Phi)+Baseline                (FID)
    h(t)=h(0)exp(−t^a/T2)*cos(Omega t+Phi)+Baseline              (FIDIndex)
    h(t)=h(0)exp(−t/T2  −t^2/Delta)*cos(Omega t+Phi)+Baseline    (FIDExpGauss)
    h(t)=h(0)exp(−t/T2)                                          (T2)
    h(t)=h(0)exp(−t^a/T2)                                        (T2Index)
    h(t)=h(0)exp(−t/T2  −t^2/Delta)                              (ExpGauss)
    h(t)=h(0)exp(−t^au/T1)+h(infinity)                           (T1a)
    h(t)=ha(0)exp(−t^au/Ta)+hb(0)exp(−t^au2/Tb)+h(infinity)      (TWOEXPa)
    h(t)=ha(0)exp(−t^au/Ta)+hb(0)exp(−t^au2/Tb)                  (TWOEXP2a)
    h(t)=h(0)exp(−t^au/T2)*cos(Omega t+Phi)+Baseline             (FIDa)
    h(t)=h(0)exp(−t^au/T2)                                       (T2a)
    h(t)=h(0)exp(−[t/T2 + Ct^3])                                 (Carr-Purcell)
    h(t)=h(0)exp(−[at^au + bt^au2])                              (ExpProd)
```

```
h(t)=2*h(0)*J1(c[t+To])/(c[t+To])+Baseline                (Bessel1)
h(t)=ha(0)exp(−t^a1/Ta)+hb(0)exp(−t^a2/Tb)                (Twoexp2index)
h(t)=ha(0)exp(−t^a1/Ta)+hb(0)exp(−t^a2/Tb)+h(infinity)    (Twoexpindex)
h(t)=h(0)*t^(1−alpha)*exp(−t/T2)                          (Strexp)
h(t)=(Dt)^1/2                                             (SD)
h(t)=h(0)+(Dt)^1/2                                        (SD2)
h(t)=h(0)exp(−t/T1)+h(infinity)+(Dt)^1/2                  (SD3)
Na(x)=A*Cx/((1−x)*(1−x+cx))                               (BET)
Na(p)=A*C(p/p0)/((1−(p/p0))*(1−(p/p0)+c(p/p0)))           (BET2)
h(T)=C*exp(+Ea/T)                                         (Ea)
1/Tn=1/Tn(ex)+1/Tn(ta), where Tn(ta)=C*exp(+Ea/T)         (Ea1)
Exit This Menu                                            (Exit)

WHERE 'au' IS A USER SPECIFIED REAL CONSTANT
```

Listing 6.3.2.2 illustrates the results of three fits (‘T2’, ‘T2Index’ and ‘TWOEXP2’) to a set of helium-3 spin-spin relaxation data from; Run#6, X=0.6, F=4.54MHz, T=1.1K, below. The ‘T2’ and ‘T2Index’ fits use a linear least squares routine to provide guess parameter values for the MF routine. Some of the guess values and the associated linear correlation coefficient are printed by the software as shown.

Listing 6.3.2.2, The Result of Three Fits using the NLLSQ Program.

t (mS)	h (volts)	t (mS)	h (volts)	t (mS)	h (volts)
0.500000	13.55000	7.010000	1.536400	13.52000	0.5336000
1.151000	8.438200	7.661000	1.366300	14.17100	0.5027300
1.802000	6.094200	8.312000	1.131900	14.82200	0.4285700
2.453000	4.699100	8.963000	1.085300	15.47300	0.4820700
3.104000	3.806100	9.614000	0.9407000	16.12400	0.3958000
3.755000	3.173800	10.26500	0.9349800	16.77500	0.3263800
4.406000	2.664100	10.91600	0.8515200	17.42600	0.3491600
5.057000	2.261000	11.56700	0.7102000	18.07700	0.3823000
5.708000	2.015200	12.21800	0.6831300	18.72800	0.3170700
6.359000	1.727700	12.86900	0.5748800	19.37900	0.2427300

‘T2’ Fit

```
Correlation Coefficient =  0.947399559

T2 (guess) =    5.5512          H(0) (guess) =    6.7323

Sum of squares at convergence:    10.9938768

Fitted parameters;

H(0)   =    14.632     +/−   0.50915
T2     =    2.5331     +/−   0.11566
```

‘T2Index’ Fit

```
Sum of squares at convergence:   0.342337234E−01

Fitted parameters;

H(0)    =    47.577     +/−   0.93234
Index   =   0.38240     +/−   0.36415E−02
T2      =   0.61049     +/−   0.75577E−02
T2 (time scaled) =   0.27513     +/−   0.60260E−02
```

'TWOEXP2' Fit

```
 Sum of squares at convergence:   0.215970026

 Fitted parameters;

 Ha+b(0) =    20.090     +/-   0.36074
 Ha(0)   =    5.5072     +/-   0.16731
 Hb(0)   =    14.583     +/-   0.19344
 Ta      =    5.6994     +/-   0.13377
 Tb      =   0.91435     +/-   0.25728E-01
 T(ave)  =    1.1877     +/-   0.11313
 T(1/e)  =    1.4171
```

Where a number of sets of data, eg. a complete set of spin-spin and spin-lattice temperature dependence data, need to be analysed is is convenient to do them together as a batch. NLLSQ will accept a file of filenames, the filenames are those of the files containing the (*t*,*h*) data with one file per temperature (or frequency, coverage etc.) for spin-spin and spin-lattice relaxation data each. For spin-spin relaxation data, the fits applied are; 'T2', 'T2Index' and 'TWOEXP2' if the *index* from the 'T2Index' fit is < 1 or 'Carr-Purcell' if not. With spin-lattice data, the fits are; 'T1', 'T1Index' and 'TWOEXP'.

Finding enough disc space on the VAX6430 to store the processed (*t*,*h*) data files can be a problem. Storing the data in unformatted, binary form is more efficient and NLLSQ can read such files. The VAX/VMS *Disc Cluster Factor*, set to 3 on the VAX6430's discs causes every file, irrespective of size to consume at least 2 Kbytes of disk space. The processed data tends to consist of large numbers of small files, an inefficient use of the available disc quota. Most of the processed data has therefore been stored in VAX/VMS *Text Libraries* enabling many files to be stored in a single text library file. Additionally the text libraries have been compressed, being stored in *DCX Data Reduced Format*. A typical set of stored processed data comprised 636 files which consumed 1533 Kbytes of disc quota. Together the files contained 443 Kbytes of actual data. The text library containing the data files occupied 563 Kbytes which was reduced to 291 Kbytes when in data reduced format.

6.4 Multi-Component Relaxation Analysis

Given the strong sub-exponentiality of almost all of the helium-3 relaxation signals measured on BN and the failure to identify a sum of two distinct exponential processes in any of the data (eg. listing 6.3.2.2) we wished to see if the processes could be characterised by a sum of a higher number of exponentials as might be expected for a system with multiple-parallel relaxation pathways. Non-linear optimisation approaches such as non-linear regression become increasingly inefficient at finding unique solutions

as the number of relaxation-times sought increases. The problem is related to that of the inversion of the Laplace Transform. Small changes in a function can lead to arbitrarily large changes in its inverse, the inverse Laplace Transform is, in general terms, inherently unstable **[200]**. An alternative analysis technique involves choosing a suitable range of relaxation times encompassing any that might be present in the process and requiring the analysis to yield the amplitudes of the spectral components of the processes present at each relaxation time, in effect an inverse Laplace Transform on a set of data points. Given the finite data-set size and experimental errors, no unique solution can be expected. Fortunately, the techniques used lend themselves to permitting extra constraints (extra, that is to fitting the experimental data) to be imposed, thus reducing the possible set of solutions.

The problem is to find $h_0(T)$, from the (t,h) data, where,

$$h(t_i) = \int_{T_{min}}^{T_{max}} h_0(T)\ \exp\left(-t_i/T\right) dT \qquad 6.4.1$$

For computer analysis $h_0(T)$ must be discretised. Using a sum of '*P*' delta functions of unknown area $(h_0)_j$ at known relaxation time T_j to describe the spectrum,

$$h_0(T) = \sum_{j=1}^{P} (h_0)_j \delta\left(T - T_j\right) \qquad 6.4.2$$

can be written. The system can be represented as a set of $N \times P$ linear equations,

$$h_i = \sum_{j=1}^{P} A_{ij}\ (h_0)_j, \quad \text{where } A_{ij} = \exp\left(-t_i/T_j\right), \quad i = 1, 2 \ldots N \qquad 6.4.3$$

The problem appears soluble by simple linear least squares, $h(t_i)$ being linear in $(h_0)_j$ but a special algorithm is needed to prevent unphysical negative $(h_0)_j$'s **[201]**. Given the inherent non-uniqueness in the problem the algorithm must not be allowed to reduce the model misfit (eg. sum of square residuals in the least squares case) to a level where the noise inevitably contaminating the data manifests itself as spurious structure in the $h_0(T)$ transform. Therefore some *a priori* knowledge of the errors in the (t,h) data is needed.

Following Whittall et. al.**[201,202]** a Linear Programming (LP) approach has been

used, being the most flexible of the available techniques. It operates by solving equation 6.4.3 for the (h_0) vector together with minimising or maximising the *objective function,*

$$\sum_{j=1}^{P} W_j (h_0)_j \qquad 6.4.4$$

subject to the error-bar constraints,

$$h_i - a\sigma_i \leqslant \sum_{j=1}^{P} A_{ij}(h_0)_j \leqslant h_i + a\sigma_i , \qquad i = 1 , 2 \ldots N \qquad 6.4.5$$

which are supplied with the input data via the σ_i. The σ_i are the errors in the h_i for the (t_i,h_i) data point, 'a' is a constant (=2), empirically determined to give about the 'correct' misfit in trials with simulated data **[201]** and the 'W_j' are weights which control how the objective is optimised. Additional constraints of the form,

$$|(h_0)_j - (h_0)_{j+1}| \leqslant \beta \qquad 6.4.6$$

can be optionally applied to smooth the relaxation time spectrum, reducing the number of distinct regions of relaxation time needed to reproduce the original decay curve. β, is a scalar and is progressively reduced over a number of fits until the data is no longer consistent with the constraints, giving the smoothest possible representation. Rather than attempt to get values for the σ_i from the spin-echo fits, the 'T*Index' and 'TWOEXP*' fits generated by NLLSQ are used to place error bars on the input data. The 'T*Index' functions in particular give reliably good, smoothly decaying fits for all data tried. In contrast with the case of the errors in the heights obtained from spin-echo fits, this formulation ensures the error bounds obtained are consistent with the expected smoothly decaying form. Having produced one or more relaxation-time distribution models, some form of model appraisal is useful. LP is ideally suited to this. A spectrum such as figure 6.4.2 derived by LP from the relaxation curve shown in figure 6.4.1 has 3 peaks. We want to know the maximum and minimum signal amplitudes which must be present in the peak regions while remaining consistent with the input data. Setting the W_j to 1 in a peak region and zero elsewhere, the objective function gives the minimum signal amplitude that must be present in that relaxation-time region. Similarly setting the W_j to −1 finds the maximum signal amplitude. Repeating the process for each peak provides quantitative information with which to qualify the detailed models produced, showing on

a lower resolution scale those broad features essential and common to the models [201]. Written in FORTRAN the LP program is based around NAG library LP routine E04MBF [203].

The output from LP for the simulated spectrum (figure 6.4.1) is reproduced below (listing 6.4.1). Both *Discrete* (β constraint not applied) and and maximum smoothness models have been produced. For each peak in both spectra statistics are provided on; height, width, area, position and a measure of the peak's asymmetry together with the maximum (‘upper bound’) and minimum (‘lower bound’) acceptable signal amplitudes in the relaxation-time region encompassed by the peak. As can be seen the models are only partially successful in reproducing the original spectrum, a consequence of non-uniqueness. In particular, peaks 2 and 3 appear shifted high and peak 1 low. Peak 2's height and area (ie. the total signal amplitude in the peak) is overstated. Only with the broader peaks, broadened by smoothing are the two bounds narrowed to the point where the lower one is non-zero. Notice how deceptively good the *log-lin* straight-line fit in figure 6.4.1 looks. From the ‘T2Index’ fit, the relaxation index is 0.896, significantly non-exponential.

Listing 6.4.1, The LP Results for the Simulated Spectrum.

```
Number of points read:    500
Obj Fn (tot,no-beta,min)=    119.66
Number of peaks (discrete spectrum) found:  3

Discrete spectrum, peak  1;
Height:       11.899
Width:       0.61989
Area:         14.436
Position:     14.908
Asymmetry:   0.00000E+00

Discrete spectrum, peak  2;
Height:       37.322
Width:        1.8272
Area:         68.857
Position:     43.945
Asymmetry:   0.00000E+00

Discrete spectrum, peak  3;
Height:       32.322
Width:        1.3702
Area:         36.368
Position:     65.230
Asymmetry:   0.00000E+00

Peak:  1 Lower bound:   0.00000E+00
Peak:  1 Upper bound:   0.12526
Peak:  2 Lower bound:   0.00000E+00
Peak:  2 Upper bound:   0.61360
Peak:  3 Lower bound:   0.00000E+00
Peak:  3 Upper bound:   0.41513

Minimum beta found;
Beta:           0.22532
Iterations:     10
```

```
Beta initial:   115.36
Obj Fn (tot,beta-min,min)=    119.67
Number of peaks (smoothed spectrum) found:  3

Smooth spectrum, peak  1;
Height:       1.7220
Width:        2.4312
Area:         13.671
Position:     14.602
Asymmetry:   0.00000E+00

Smooth spectrum, peak  2;
Height:       4.3997
Width:        13.903
Area:         78.191
Position:     46.773
Asymmetry:   0.26776

Smooth spectrum, peak  3;
Height:       3.0321
Width:        12.096
Area:         30.161
Position:     61.286
Asymmetry:  −0.38853

Peak:  1 Lower bound:   0.00000E+00
Peak:  1 Upper bound:   0.11845
Peak:  2 Lower bound:   0.58786
Peak:  2 Upper bound:   0.71317
Peak:  3 Lower bound:   0.24792
Peak:  3 Upper bound:   0.30071
```

Figure 6.4.3 shows a plot of the experimental data given in listing 6.3.2.2 together with the three fits used. The fits are typical of both T_1 and T_2 relaxation at low temperatures; strongly sub-exponential with a correspondingly poor 'T*', good 'T*Index' and 'TWOEXP*' fits with 'T*Index' being the best as indicated by the sum of squares at convergence. Figure 6.4.4 illustrates the LP spectrum of the data, the error bounds were derived from the 'T2Index' fit. Again, with 3 peaks in the discrete spectrum it is typical. Listing 6.4.2 gives the LP spectrum statistics.

Listing 6.4.2, The LP Results for the Experimental Data.

```
Number of points read:     30
Obj Fn (tot,no-beta,min)=    22.108
Number of peaks (discrete spectrum) found:  3

Discrete spectrum, peak  1;
Height:       8.4348
Width:       0.16701
Area:         12.270
Position:    0.53989
Asymmetry:   0.00000E+00

Discrete spectrum, peak  2;
Height:       4.7271
Width:        1.4842
Area:         7.6983
Position:     2.7203
Asymmetry:   0.00000E+00

Discrete spectrum, peak  3;
```

Figure 6.4.1, Relaxation Plot for Simulated Triple-Exponential Decay With 1% x h(0) Added Gaussian Random Noise and Straight line fit.

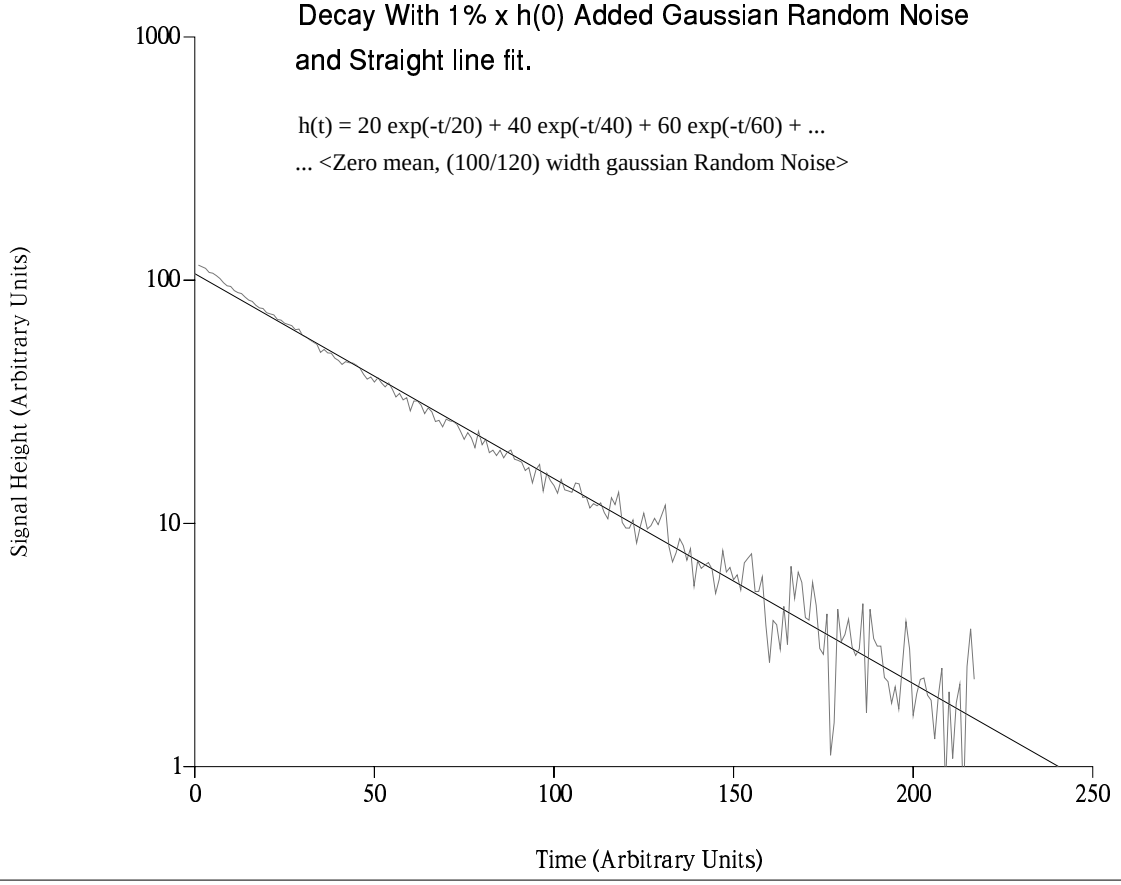

Figure 6.4.2, LP Results for Simulated Spectrum

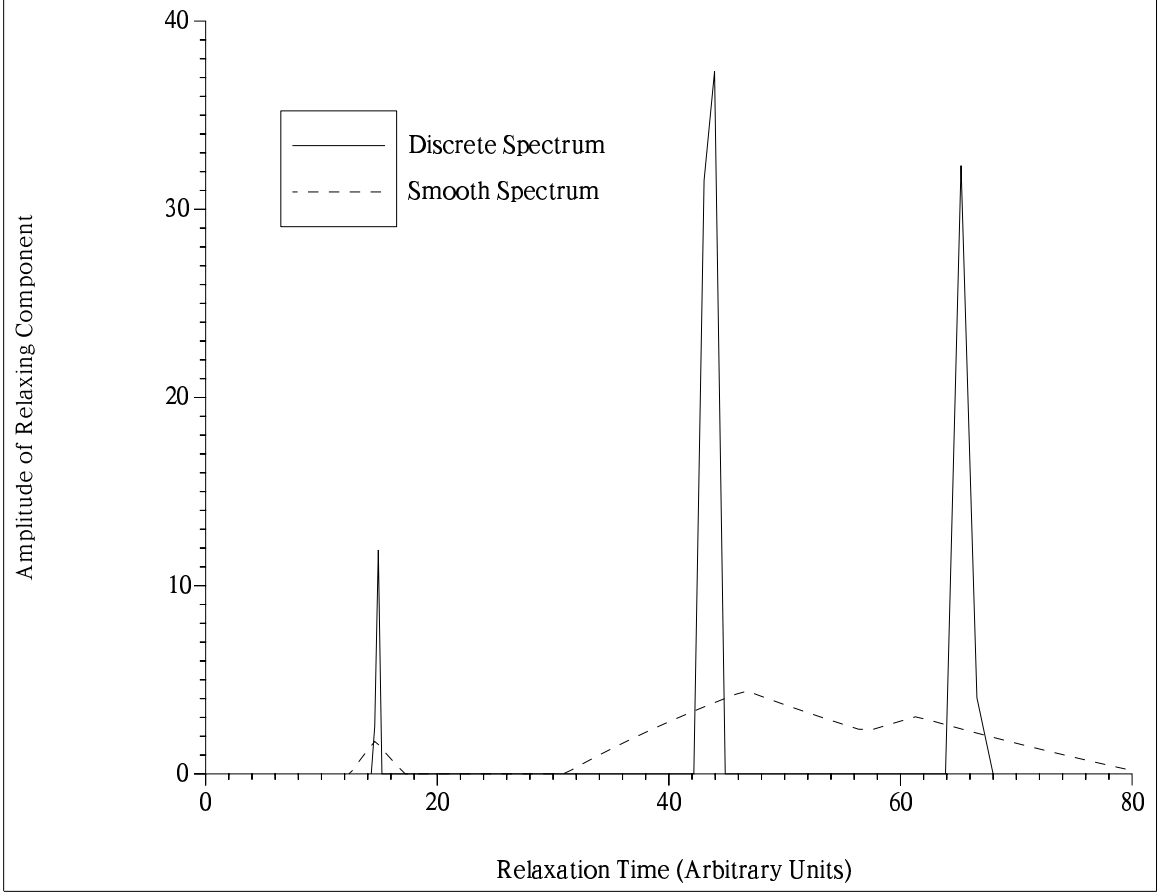

```
Height:       1.5616
Width:        5.7117
Area:         2.1390
Position:     10.469
Asymmetry:   0.00000E+00

Peak:  1 Lower bound:   0.21748
Peak:  1 Upper bound:   0.91660
Peak:  2 Lower bound:   0.21074
Peak:  2 Upper bound:   0.66911
Peak:  3 Lower bound:   0.41471E-01
Peak:  3 Upper bound:   0.25145

Minimum beta found;
Beta:           0.21172
Iterations:               7
Beta initial:    13.550
Obj Fn (tot,beta-min,min)=    28.382
Number of peaks (smoothed spectrum) found:  2

Smooth spectrum, peak  1;
Height:       2.3323
Width:        3.3782
Area:         28.306
Position:    0.70690
Asymmetry:  -0.12743

Smooth spectrum, peak  2;
Height:      0.75743E-01
Width:       0.00000E+00
Area:        0.75743E-01
Position:     155.03
Asymmetry:   0.50000

Peak:  1 Lower bound:   0.99687
Peak:  1 Upper bound:    1.3732
Peak:  2 Lower bound:   0.00000E+00
Peak:  2 Upper bound:   0.42124E-02
```

Figure 6.4.3, Plot of Echo Height vs Time, X=0.6, T=1.1K, F=4.5MHz

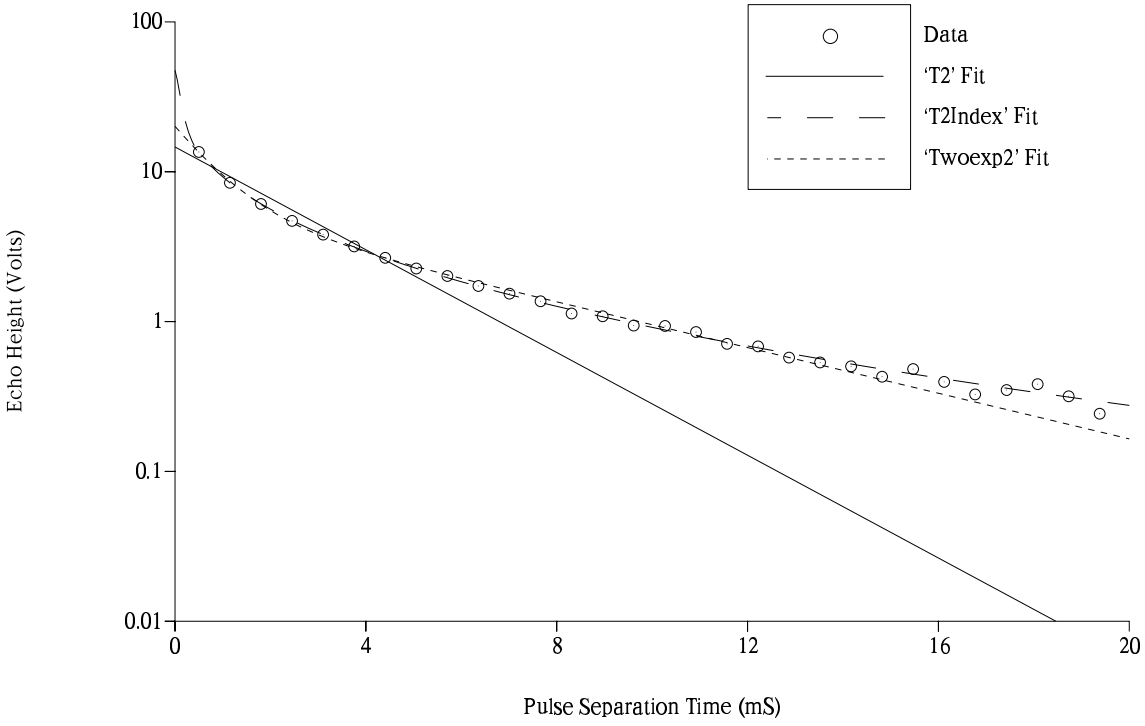

Figure 6.4.4, LP Relaxation Time Spectrum for X=0.6, T=1.1K, F=4.54MHz

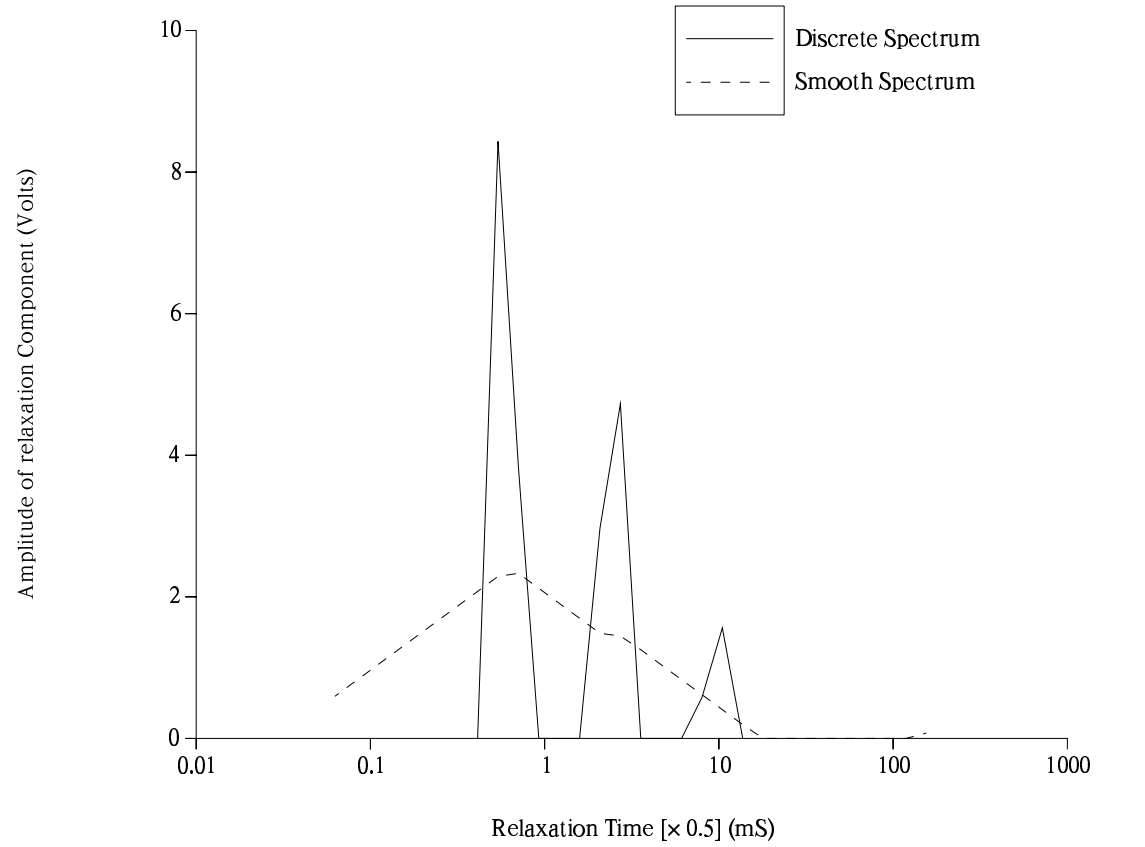

Chapter 7
The Experimental Data

7.1 Introduction

Eight experimental runs studying helium-3 on BN using pulsed NMR have been performed in the course of this work and continue the work started by Fardis discussed in §3.4 using BN sample chamber#3. Most of the results to be presented come from runs 6 to 8, the preceding ones were mainly short preliminary investigations, instrumentation trials or unsuccessful in nature. Analysis of the experimental data in this chapter is mainly presented in the order in which it was done with our understanding progressing as the analysis proceeded. It has been written this way for clarity because of the volume of data involved. For example no mention is made of the proposed DWL in the first section, §7.2.1 (Coverage Dependence Data) because the evidence for its existence did not become apparent until the analysis of §7.2.2 (Temperature Dependence Data). Cross referencing has been added to aid reading and a summary of all the data discussed in the chapter is presented in §7.6. It may also be helpful as an overview of the data and analysis to be presented here. The following summarises the important points of the runs;

RUN#1, Abandoned. Magnet could not be energised.

RUN#2, Using a coverage X=0.376 attempted pulsed gradient measurements which were unsuccessful due to the decaying magnetic field induced in the vacuum cans by the pulse-gradient coils, a pair of Maxwell configuration windings mounted about the sample chamber inside the IVC. The interest was to measure the small spin diffusion coefficient, (typ. 10^{-9}cm^2/sec) in the high coverage solid **[204]**. To investigate the effect of the can-field a *pulse-gradient-pulse* − τ − 90^o − 180^o − *spin-echo* sequence was applied and the echo height measured as a function of τ. The can field collapsed exponentially as expected for an *LR* filter arrangement with a time constant L/R of 13.5 ± 0.4 mS.

RUN#3, After removing the IVC further attempts were also fruitless, the reduced can-field was still a problem with an L/R of 8.5 ± 0.4mS. Echo height as a function of static field gradient was measured, using the pulse-gradient coils. The expected G^2 dependence (§1.10.3) was not seen. Instead it followed a G^{index} relation where $1.1 < index < 1.3$. Using equation 5.2.1 and NLLSQ's 'Bessel1' fit (listing 6.3.2.1) on FID/echo

shape *vs* gradient coils' current data, the pulse-gradient coils were calibrated, giving absolute values of '*G*' from the applied current '*I*', allowing the diffusion constant *D* to be calculated where a t^3 decay is observed. The quality of the fit is not particularly good, equation 5.2.1 only modifying the echo shape. Fortunately, the fit *homes-in* on the distortion's dominant feature, the first minimum of $J_0(x)$. The intercept of the straight-line '*G*' *vs* '*I*' plot provides the residual field gradient (dB_z/dz) for the main solenoid as $1.22 \times 10^{-3} \pm 0.04 \times 10^{-3}$ Tesla/metre at B_0=0.154 Tesla.

RUN #4, At a coverage X=0.1, T_2 was measured as a function of temperature for 4.2K < T < 14.2K. Below 9.8K the relaxation profile was sub-exponential, becoming increasingly super-exponential above it, as indicated by the *index* from the 'T2Index' fits.

RUN#5, Unfortunately sample chamber#3 met with a violent and untimely end after run#4, necessitating production of a fourth. Runs 5 to 8 used the new sample chamber discussed in §4.1.1.1. The main purpose of the run was the adsorption isotherm shown in figure 4.1.1.1.1.

RUN#6, The most extensive run, the helium-3 relaxation times were investigated at the following coverages; 0.05, 0.1, 0.2, 0.3, 0.4, 0.5, 0.6, 0.7, 0.75, 0.8, 0.85, 0.9, 0.938, 1.0, 1.05, 1.1, 1.2, 1.3, 1.4 and 1.5 monolayers. Apart from at X=0.05 where the signals were too weak and T_2 very short, temperature dependence data for T_1 and T_2 were taken at all coverages for 1.1K < T < 13.2K. For $0.85 \leqslant X \leqslant 1.2$ the relaxation times were measured in each temperature direction to look for hysteretic behaviour as might be expected at a melting transition. For $0.5 \leqslant X \leqslant 1.1$ T_1 and T_2 were measured at 1.1K at the following frequencies; 2.7, 3.7, 4.5, 5.7, 6.9, 8.6 and 10.7MHz. At most of these coverages T_1 and T_2 were measured as a function of T for 1.1K < T < 4.2K at 2.7MHz and 10.7MHz. At X=0.85 a more detailed set of frequency data was taken at 1.1K, comprising 22 frequencies between 2.64MHz and 10.7MHz. At X=0.938 the 1.1K < T < 13.2K temperature measurements were made at each of the above 7 frequencies. At X=0.3 echo height as a function of field gradient measurements were made. For X=0.4 T_2 was measured at 4 levels of deliberately applied magnet inhomogeneity, the inhomogeneity being produced by reverse driving the main solenoid's Z_1 shim. After

increasing the coverage but before annealing the sample, both relaxation times were often measured, little or no change from the previous coverage was ever observed, presumably most of the sample condensing around the filling line inlet and contributing little signal being at the extremity of the NMR coil's sensitivity. An attempt to observe a CW NMR signal using a Robinson Oscillator circuit **[205]** at 0.6 monolayers was unsuccessful. An ^{11}B signal was observed at 1.5, 0.5 and ~0.0 monolayers after pumping the sample at the end of the run.

RUN#7, After installing a saddle coil over the NMR solenoidal coil a series of double resonance/cross relaxation (^{3}He/^{11}B) experiments were performed in an attempt to directly observe the ^{3}He dipolar coupling to the substrate spins. A coverage of X=0.5 was used. No effect was clearly visible. Nothing was seen for the ^{3}He/^{14}N [Larmor Frequency] case either. See Appendix 1 for spin data. The ^{11}B T_1 and T_2 were measured as a function of T for 1.1K < T < 13.2K to investigate whether the ^{3}He T_1 minimum in T at $T \sim$ 5.1K (figure 7.2.2.18) was due to coupling with the ^{11}B spins, an ^{11}B T_1 minimum being expected at the same temperature if so. Unfortunately, the lack at the time of the pulse generator's interrupt-driven mode of operation (§4.2.5.1) and even after modifying it, bad computer noise afflicting the weak high temperature signals, prevented any firm conclusions being drawn.

RUN#8, Another set of coverage dependence data was taken in this run. Both relaxation times were measured for ^{3}He and ^{11}B at the following coverages; X=0.1, 0.2, 0.3, 0.4, 0.5, 0.6, 0.7, 0.75, 0.8, 0.85, 0.9, 0.95, 1.0, 1.1, 1.3, 1.5, ~0.0 with F=4.88MHz and T=1.1K. We wished to see if the ^{11}B relaxation times, in particular T_1 showed a similar coverage dependence to ^{3}He, revealing cross relaxation. This was the case. By slowly sweeping the field with the Magnet Controller, pulsing the sample and observing a spin-echo, a crude RF absorption spectrum was built up showing the characteristic powder pattern line-splitting for an $\boldsymbol{I}$=3/2 nucleus with a crystalline EFG, (§2.1). A further attempt to observe a CW NMR signal using the Robinson Oscillator circuit but with field modulation within the NMR line, driving a lockin-amplifier was also unsuccessful. Additionally at X=1.5 T_1 and T_2 were measured in the two ^{11}B satellite lines at F=4.88MHz and in the central line at 2.6MHz

and 3.7MHz.

A 77K Argon isotherm was performed after the helium-3 runs for another estimate of the adsorption area. Lacking the compressibility of solid helium, solid argon provides a more substrate adsorption potential independent estimate for the surface area. Using a continuous entry method enabled very detailed measurements revealing interesting features at low coverages.

7.2 RUN#6

7.2.1 Coverage Dependence Data

Figures 7.2.1.1 and 7.2.1.2 show the coverage dependence of T_2 and T_1 at the lowest temperatures. Comparing with figure 1.10.1 they have the same general form, suggesting a similar phase diagram may be appropriate. For discussion purposes the low temperature data is divided into five coverage regions; $X \leqslant 0.3$, $0.3 \leqslant X \leqslant 0.7$, $X=0.75$, $0.8 \leqslant X \leqslant 1.0$ and $X>1.0$.

$0.1 \leqslant X \leqslant 0.3$

T_2 rises for $X=0.1 \rightarrow 0.3$, which conflicts with a idea of dipolar relaxation in a homogeneous film. As on Grafoil these results can be explained in terms of an *augmentation factor model* (§1.10.2) in which the preferential sites are filled at $X \sim 0.05$, the remaining adatoms forming a 2D gas whose atoms undergo collisions and exchange with the solid patches, shortening T_2 below the 2D gas value towards that of the high density solid. As more adatoms are added and go into the 2D gas, T_2 lengthens as the ratio of mobile to localised spins increases. Providing the solid−gas interchange rate is sufficiently fast $T_2 = T_2^{\text{solid patches}} \times (X^{\text{total}}/X^{\text{solid patches}})$ is expected, which also explains why $T_2 \sim$ hundreds of seconds expected for a 2D gas is not seen [62]. $T_2^{\text{solid patches}}$ should probably be around the high coverage homogeneous solid value at $X=1$ (0.57mS) and possibly as low as the rigid lattice value ~100μS [136]. There is insufficient data for comparison purposes at $X \ll 0.3$ where $T_2 \propto X$ has been seen on Grafoil [61,62] and on Mylar [136] over a wider coverage range, however taking the $X=0.1/T=1.1$K point where T_2=1.2mS gives $T_2^{\text{solid patches}} = 0.6$mS for $X^{\text{solid patches}} = 0.05$. T_2 was found to be immeasurably short with a very poor S/N ratio at $X=0.05$ as expected for a solid-patches-only adsorbate. Supporting evidence comes from the Argon isotherm (§7.5) which has a clear substep at $X \approx 0.05$ corresponding to the filling of the preferential sites which are believed to be sited mainly at the crystallite edges [110]. The lack of significant temperature dependence in T_2, particularly obvious at $X=0.1$ also points towards the patchy solid dominating T_2, – $T_2^{\text{solid patches}}$ unlike $T_2^{\text{2D gas}}$ will be a very weak function of T, any intra-solid-patch motion present will be exchange dominated. There is little temperature dependence at any coverage implying solid dominated spin-spin relaxation of any delocalised spins.

Although for a rapidly diffusing 2D gas, $\omega_0\tau_c \ll 1$ should be valid, it appears the solid patches' contribution leads to $\omega_0\tau_c^{\text{effective}} > 1$. At constant X increasing temperature

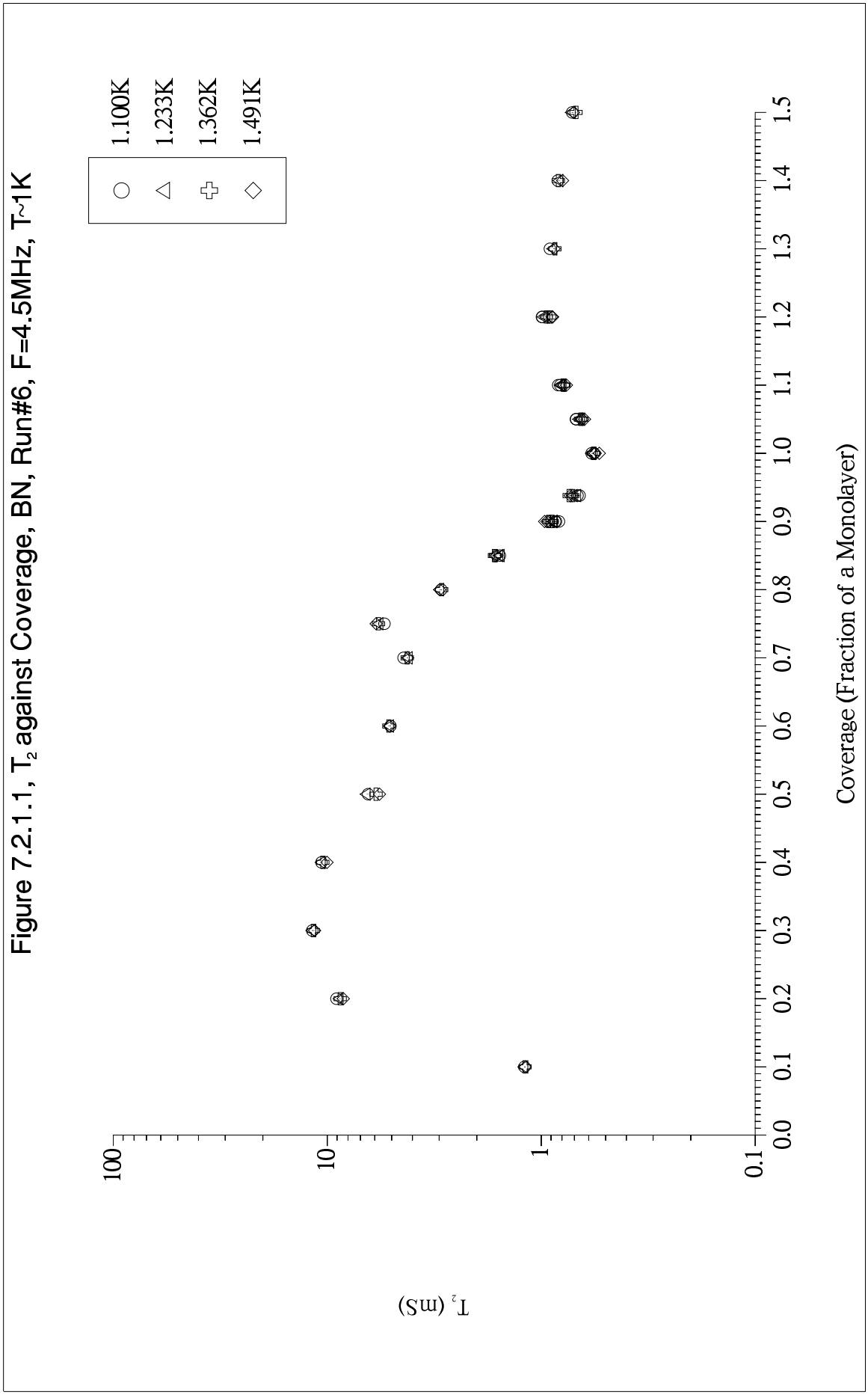
Figure 7.2.1.1, T2 against Coverage, BN, Run#6, F=4.5MHz, T~1K
1.100K
1.233K
1.362K
1.491K
T2 (mS)
100
10
1
0.1
0.0
0.1
0.2
0.3
0.4
0.5
0.6
0.7
0.8
0.9
1.0
1.1
1.2
1.3
1.4
1.5
Coverage (Fraction of a Monolayer)

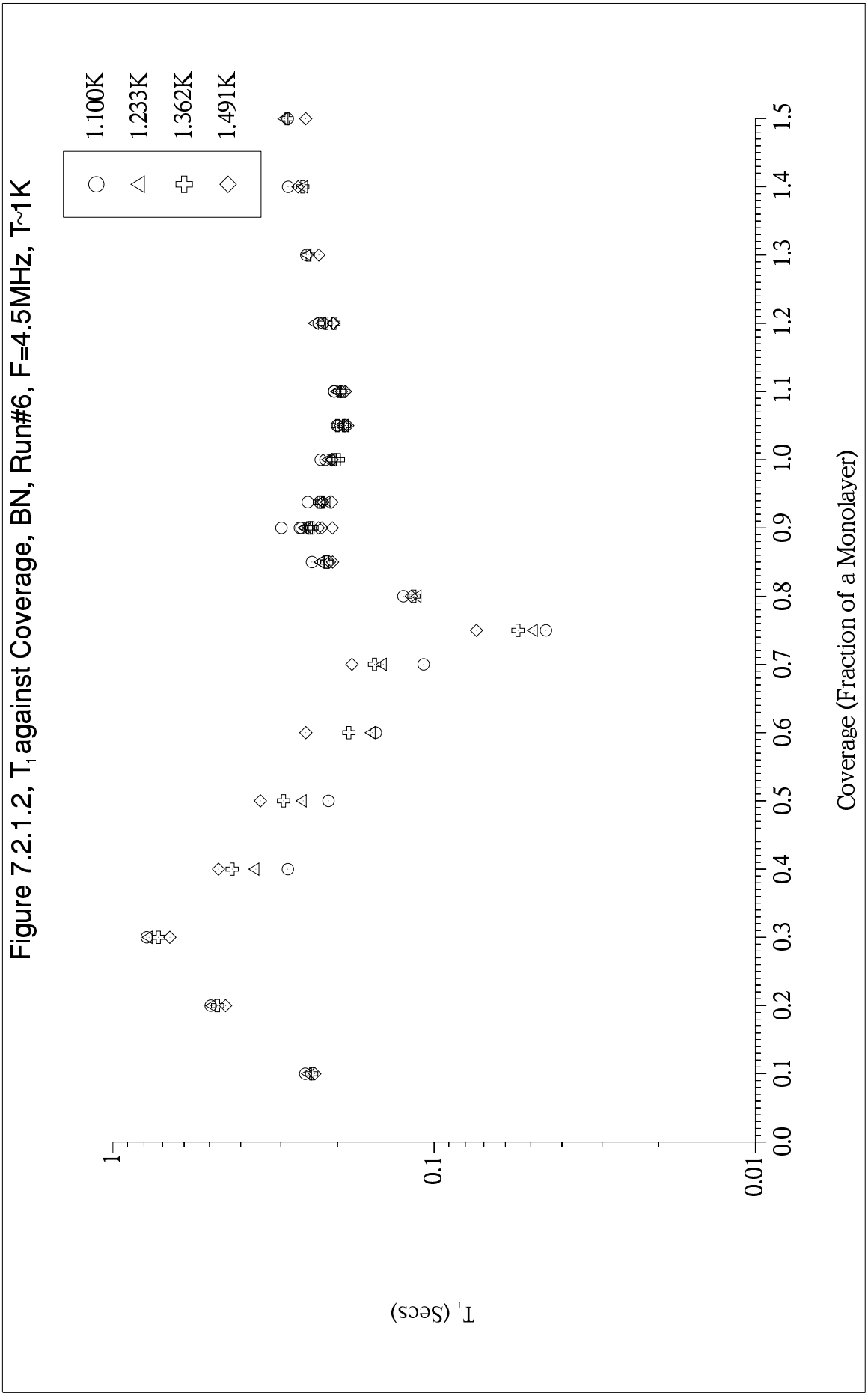
Figure 7.2.1.2, T1 against Coverage, BN, Run#6, F=4.5MHz, T~1K
1.100K
1.233K
1.362K
1.491K
T1 (Secs)
1
0.1
0.01
0.0
0.1
0.2
0.3
0.4
0.5
0.6
0.7
0.8
0.9
1.0
1.1
1.2
1.3
1.4
1.5
Coverage (Fraction of a Monolayer)

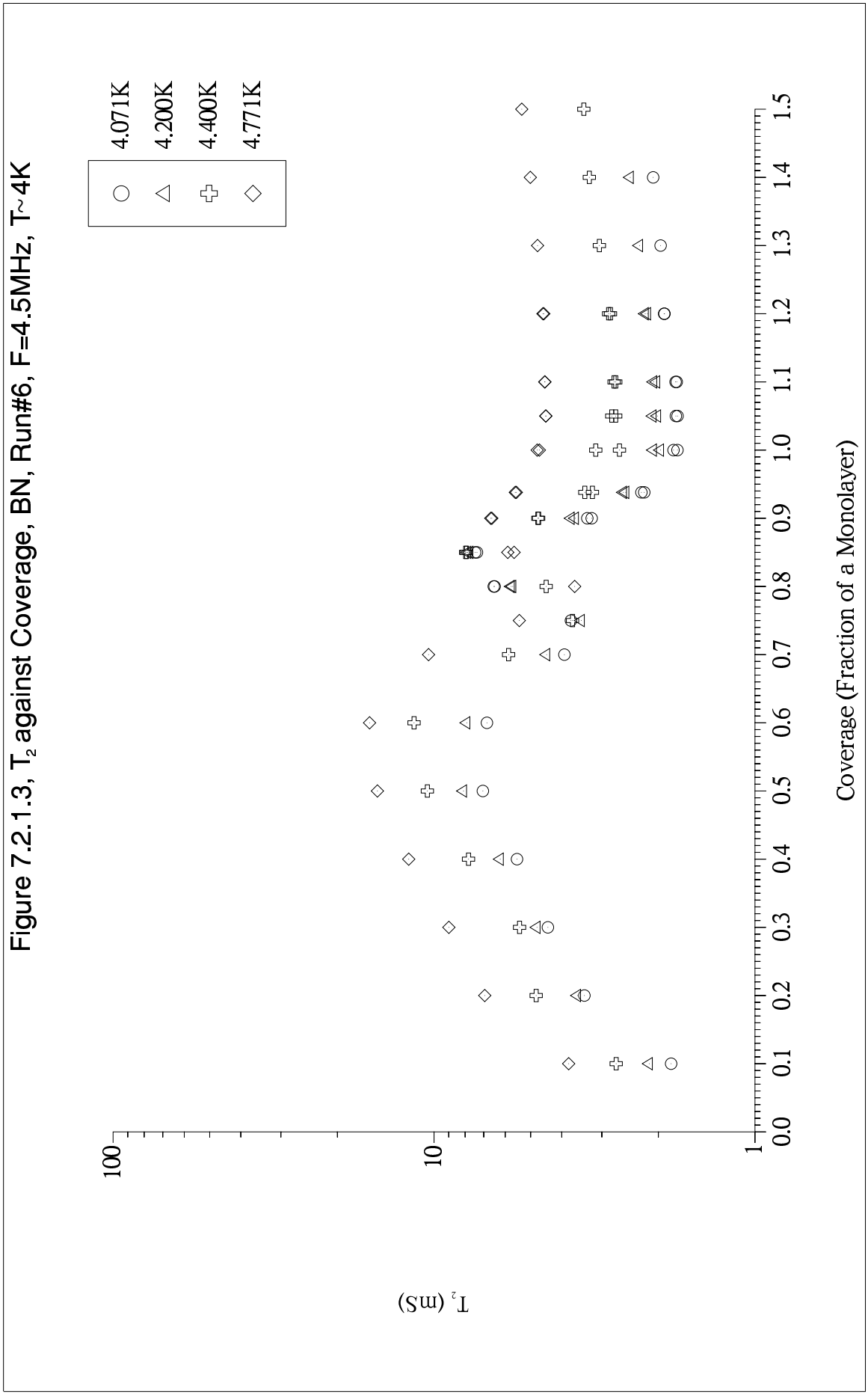
Figure 7.2.1.3, T2 against Coverage, BN, Run#6, F=4.5MHz, T~4K
4.071K
4.200K
4.400K
4.771K
T2 (mS)
100
10
1
0.0
0.1
0.2
0.3
0.4
0.5
0.6
0.7
0.8
0.9
1.0
1.1
1.2
1.3
1.4
1.5
Coverage (Fraction of a Monolayer)

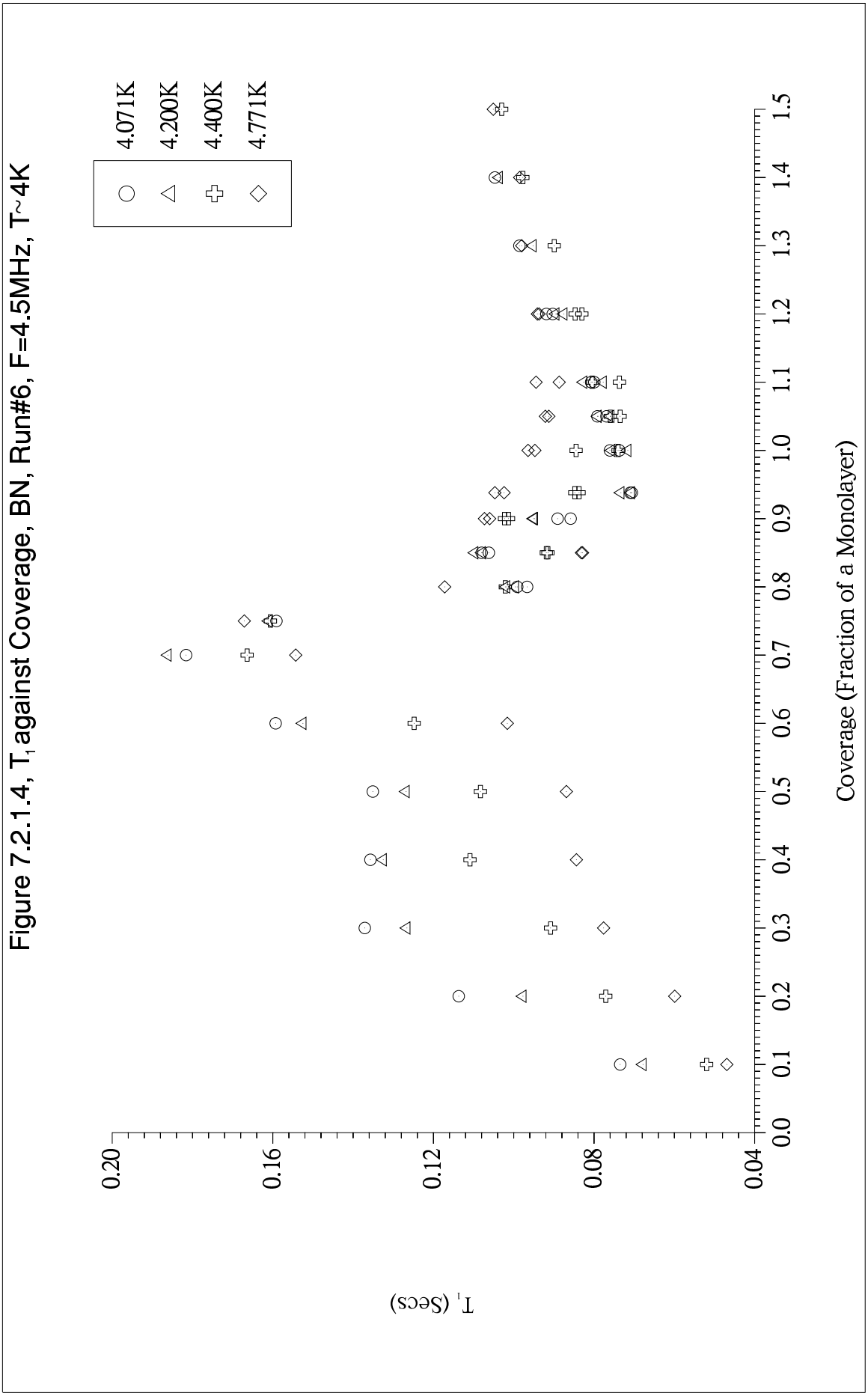
Figure 7.2.1.4, T1 against Coverage, BN, Run#6, F=4.5MHz, T~4K
4.071K
4.200K
4.400K
4.771K
T1 (Secs)
0.20
0.16
0.12
0.08
0.04
0.0
0.1
0.2
0.3
0.4
0.5
0.6
0.7
0.8
0.9
1.0
1.1
1.2
1.3
1.4
1.5
Coverage (Fraction of a Monolayer)

reduces $\omega_0\tau_c^{\text{effective}}$ towards a T_1 minimum. However, increasing the 2D gas component by increasing X has the opposite effect. A plausible explanation is that relaxation mostly takes place via the solid patches where $\omega_0\tau_c^{\text{solid patches}}$ is above ~1, that increasing temperature reduces it towards ~1 and that increasing the fluid:solid ratio by increasing X imposes a greater burden on the patches' ability to relax fluid spins by particle exchange which reduces relaxation efficiency − increasing T_1.

$0.3 \leqslant X \leqslant 0.7$

Here both relaxation times fall with increasing X. The explanation is the solid patches grow under increasing lateral pressure in the more dense film [61]. Actually, unless solid patches $\leftrightarrow$ 2D gas exchange-rate-change effects with coverage are significant here, the reduction in T_2 at X=0.3 from the X=0.1$\rightarrow$0.2 straight line extrapolation (ie. augmentation factor model relaxation) suggests solid patch expansion occurs below X=0.3. For T_1 the temperature dependence has changed direction, now increasing with temperature. This probably reflects the less dense nature of the *new growth* solid giving it a higher characteristic exchange frequency and hence smaller τ_c, resulting in $\omega_0\tau_c^{\text{new-growth-solid}} < 1$. The magnitude of the temperature dependence has also risen because the less strongly adsorbed *new growth* solid is more susceptible to thermally activated vacancy tunnelling (ie. lower activation energy) than the dense variety. There is evidence [31,206] that on Grafoil the *new growth* solid is $\sqrt{3} \times \sqrt{3}$ R30 registered which is consistent with the inferences made here from the data. An alternative (preferred, see §7.2.2) explanation for the change in direction of temperature dependence is that registered *new growth* spins are disordered by the increase in T which reduces their capacity for relaxation, particularly via substrate spins.

X=0.75

The 0.75 monolayer feature is the most interesting result in the data. Is it the result of monotonic changes in film density and correlation time in the incommensurate solid, a sign of a registered phase or something else? The $\sqrt{3} \times \sqrt{3}$ R30 registered phase is the preferred interpretation for several reasons: The 1K T_1 minimum in coverage in the 2D solid on Grafoil occurs at X=0.8 (F=5MHz) but in comparative studies (§3.3), BN has consistently been shown to present a weaker adsorption potential than graphite resulting in a less dense adsorbate which should shift the minimum towards X>0.8. The lower BN adsorption potential will also have the affect of shifting the coverage (in terms of monolayer) where registry is observed upwards from the Grafoil value (X≈0.6).

Without an independent (eg. X-ray/electron scattering etc.) value for the ^{3}He/BN monolayer lattice parameters an estimate of the registry coverage has been calculated using the Argon BET surface area. The BN basal plane hexagon area $=\sqrt{3}\,a^2/2$, where a=2.50Å for BN (§3.3). Given the effective argon molecular area as 5.30cm^3/g Ar at STP ≡ 19.6m^2/g **[112]** and our BET area (§7.2.2/X=0.75 & §7.5) 21.8 ± 0.3cm^3 STP, the number of exposed basal plane hexagons can be calculated. With the registered phase BN hexagon filling factor of 1/3 and a helium-3 4.2K point-B monolayer of 26.2 ± 0.2 cm^3 STP, registry should occur at X=0.704 ± 0.006 monolayers. As discussed above, BN contains a significant number of higher adsorption energy crystallite edge sites which preferentially adsorb the first helium-3 atoms admitted, raising the apparent basal plane coverage, and hence the phase features on it. The discrepancy $\Delta X = 0.75 - 0.704 \approx 0.05$ accords with the Argon isotherm and the NMR data with its very short T_2 at X=0.05. As discussed later in §7.4.3.2 the ^{11}B T_1 also goes though a minimum close to X=0.75 showing coupling with the substrate spins is at least partially responsible for the observed ^{3}He relaxation. This being the case, it seems highly plausible that an arrangement in which there is a well defined regular geometrical relationship between the ^{3}He spins and those of the substrate (ie. registry) will increase relaxation via this mechanism as compared with an incommensurate solid arrangement. See also §8.7.5.

For completeness another, although very much less likely explanation for the X=0.75 behaviour is either a melting transition on the basal plane film or even of an edge-sites film. The former possibility conflicts with most of the evidence already presented. An edge-sites film, more strongly adsorbed, solidifying as coverage is increased and augmenting the spin-lattice relaxation rate of the mobile basal plane spins is conceivable but how could such a process also increase T_2? In any case it is unclear why such phase changes should result in peaks in the relaxation times rather than simple monotonic changes given thermal activation is not a significant factor.

To within the resolution of the grid of coverages investigated, X=0.75 is believed to be perfect registry. Re-capping: The shift up in X from the ~0.6 Grafoil position comes from (a) The lower adsorption potential of BN which reduces the absolute film density at monolayer completion raising the registry coverage using this metric, (b) The Approximately 5% surface heterogeneity/edge-film raising the coverage at which the various phase transitions are seen by 5%, by effectively ‘taking out of circulation’ that many spins. A small shift downwards ~3% in X due to the slightly larger substrate mesh should also be present.

T_1 goes through a minimum as on Grafoil due to both motional slowdown and spatial ordering as the spins register. In contrast T_2 shows a maximum. This could be due to the loss of the fluid component as perfect registry is entered, the fast moving 2D gas spins augmenting the sub-registry T_2^{-1}, relaxing through a non-dipolar mechanism such as electron paramagnetic impurity fields. This is a little far fetched and the origin of the maximum almost certainly involves substrate spin relaxation mediated effects.

$0.8 \leqslant X \leqslant 1.0$

T_2 falls sharply from X=0.75 to the characteristic minimum at X=1.0, verifying the 4.2K ^{3}He isotherm used to determine the monolayer capacity. We attribute the fall to the formation of the incommensurate solid somewhere in $0.75<X\lesssim 1.0$ in analogy with Grafoil. T_1 rises from X=0.75 to a maximum at X=0.9 probably where second layer promotion starts, slowing the increase in first layer density (and hence τ_c) as far as X=1.05 where the overall density reaches a minimum. T_2 is dominated by the short first layer solid value here, hence the X=1.0 point probably indicates the maximum first layer density. On Grafoil the stronger substrate potential leads to a smaller coverage difference between the onset of second layer promotion and first layer maximum density. Considering the Grafoil data whose incommensurate solid T_1 minimum occurs at X=0.79 for 5.1MHz, a similar feature is expected on BN for $0.8 \leqslant X \leqslant 1.0$. A previous study of ^{3}He on BN conducted by Fardis (§3.4) using a different BN sample and a finer coverage grid around X=0.8 revealed a broad minimum at X=0.84. At X=0.75 the same temperature dependence as $X<0.75$ is apparent but for $0.8<X<1.0$ the $X \leqslant 0.3$ highest T/ lowest T_1 behaviour has reappeared, suggesting $\omega_0\tau_c>1$ for $X>0.8$. Closer inspection of the X=0.8 points reveals, by a small margin that the lowest T_1 occurs at an intermediate temperature (1.233K), the inference being a minimum is located somewhere near X=0.8 and that the small change in T has been able to *fine-tune* τ_c. See also figure 7.2.2.37.

$X>1.0$

T_2 rises to a maximum at X=1.2. In analogy with the first layer low coverage data this could be due to registering in the second layer fluid. This is probably not the case however − The maximum occurs 0.1 monolayers below the equivalent first layer localisation point, X=0.3 whereas on Grafoil registering occurs at a higher relative coverage, that is closer to the second layer's full-registry coverage **[31]**. Moreover Grafoil also has a T_2 maximum at X~1.2, well below registering in the second layer. More likely, the cause of the maximum lies in interlayer exchange effects. An analysis of

Grafoil data with its double exponential X>1.0 spin-spin relaxation has shown the ability of the solid monolayer to relax the second layer 2D gas, increasing T_2, is limited by the interlayer exchange rate which peaks at around X=1.2 **[207]**. T_2 at the maximum is more than an order of magnitude less than in the submonolayer case reflecting the ~20× more numerous solid spins. Above X=1.05 T_1 continues to rise in accordance with a fixed density first layer solid responsible for most of the relaxation plus a growing second layer fluid which it relaxes with decreasing efficiency as the fluid component grows.

At T~4K (figure 7.2.1.3) the low coverage T_2 maximum has shifted up to X=0.6, probably due to the effect of increased thermal activation working against the increasing lateral pressure in the film with coverage, from making the solid/registered patches grow, cf. §1.10.1. The X=0.75 feature has become a minimum and the X=1.0 minimum appears smeared out by thermal motion. Increased temperature dependence w.r.t. 1K is expected as thermally activated tunnelling in and gas atom collisions with, the low coverage registered/patchy and high coverage homogenous solids become the dominant mechanism, increasing T_2.

At T~4K (figure 7.2.1.4) T_1 *vs* X resembles T_2, the low coverage maximum position is raised to X=0.7, almost as far as the proposed registry transition, as with Grafoil (§1.10.1), probably via thermal motion as discussed for T_2. The $X\leqslant$0.7 data also shows the same temperature dependence as at 1K and $X\leqslant$0.3. The low temperature X=0.75 minimum is raised to ~0.8 monolayers, being all but eliminated, which is unsurprising given that on the stronger adsorbing graphite the order-disorder transition occurs at 3K. Interestingly, at X=0.75 variation with temperature is almost suppressed, a possible consequence of the substrate's ability to restrict adatom mobility, increasing the probability that an adatom will be found in a *registered position*, well above any likely order-disorder transition temperature (§1.4). The minimum at X=0.9 might be the proposed X~0.8 2D solid minimum shifted to higher X by thermally activated motion. On the other hand it may be due to second layer promotion assisted by thermal activation. The latter is more likely given the X>0.75 temperature dependence.

Further light is shed on the nature of the X=0.75 features by the coverage behaviour of the *indices* of relaxation of the two processes obtained from the *stretched exponential* 'T1Index' and 'T2Index' fits (listing 6.3.2.1) shown in figures 7.2.1.5 and 7.2.1.6 respectively. At X=0.75 the index for the T_1 process, the otherwise universally sub-exponential ^{3}He on BN low temperature relaxation gives way to a striking peak. For

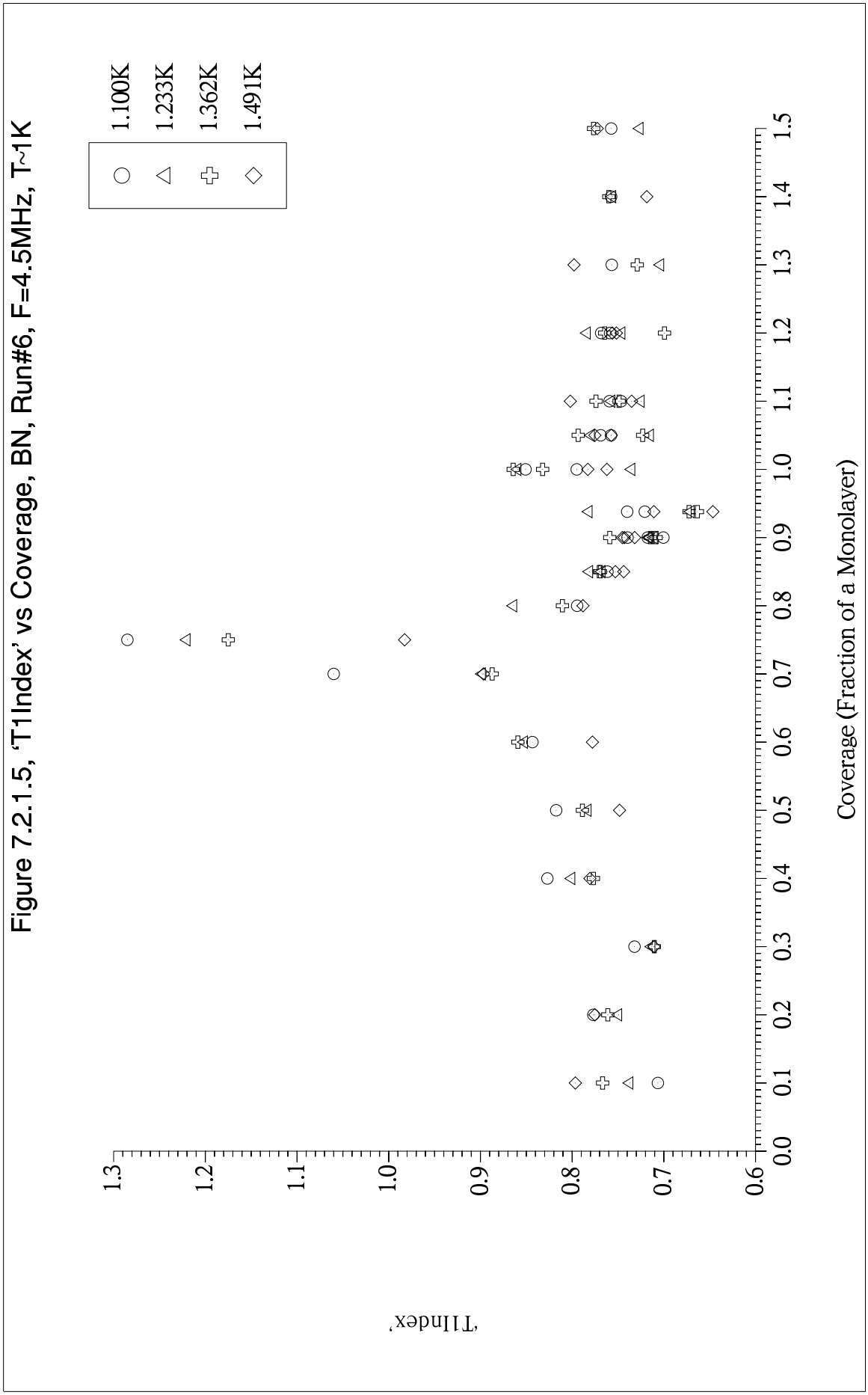
Figure 7.2.1.5, 'T1Index' vs Coverage, BN, Run#6, F=4.5MHz, T~1K
1.100K
1.233K
1.362K
1.491K
'T1Index'
Coverage (Fraction of a Monolayer)
1.3
1.2
1.1
1.0
0.9
0.8
0.7
0.6
0.0
0.1
0.2
0.3
0.4
0.5
0.6
0.7
0.8
0.9
1.0
1.1
1.2
1.3
1.4
1.5

Figure 7.2.1.6, 'T2Index' vs Coverage, BN, Run#6, F=4.5MHz, T~1K

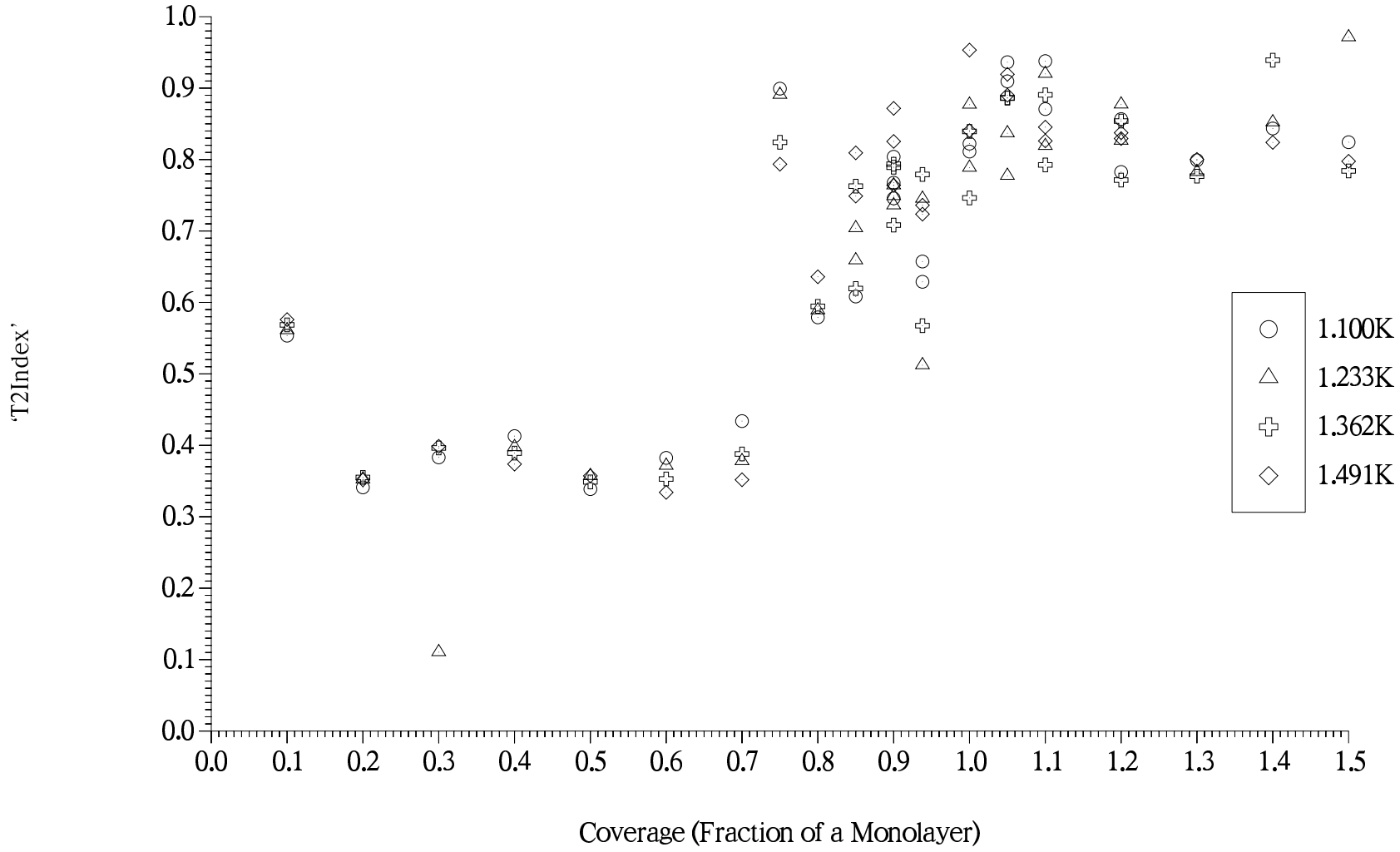

the lowest three temperatures, increasing with falling T the recovery of the magnetisation has become strongly super-exponential. Given the oscillating $\exp(-im\omega_0 t)$ term in equation 2.2.11 and the absence of an m=0 adiabatic contribution the dipolar spin-lattice relaxation process should always be exponential. Clearly something else must be responsible for this behaviour. To recap; At X=0.75 for T~1K T_1 displays a deep minimum, the lowest value for any coverage, the relaxation at the minimum is strongly super-exponential and the ^{11}B T_1 also has a minimum close by where it possesses its fastest relaxation rate in coverage, strongly suggesting relaxation via the substrate spins has become dominant. As described in §2.2.1 2D effects, a combination of the adiabatic term in F(t), the spin-spin relaxation function and the long-time tail of $g_0(t)$ cause the adiabatic part of F(t) to relax faster than exponentially. Comparing equations 2.2.16, 2.2.17 with 8.4 it is evident that the last two terms in equation 8.4 describing the heteronuclear ^{3}He−Substrate spin relaxation correspond to those in equation 2.2.16 for the ordinary homonuclear ^{3}He spin−Lattice case. The $J_0(\omega_y - \omega_x)$ term in equations 8.3−8.5 will potentially fail to describe the coupling rates $\rho_{1,2}$ and $\sigma_{1,2}$ properly, as a constant in time throughout the relaxation in the same way equation 2.2.17 fails w.r.t. '$1/T_2$' in 2D due to its adiabatic $J_0(0)$ term, requiring the separate treatment of equations 2.2.1.4−2.2.1.6 and leading to a super-exponential relaxation component. Viewing equation 2.2.18 for $J_n(\omega)$ it is evident that the oscillating exponential term in ω will ensure the integral converges and relaxation is exponential, even with the t^{-1} tail of the 2D $g_0(t)$ correlation function, provided ω>0. If $\omega=\omega_x-\omega_y\approx 0$, $J_0(\omega_x-\omega_y) \approx J_0(0)$ leading to the same situation as with F(t) and T_2 and hence a strong super-exponential relaxation component to the observed T_1. The spin-spin relaxation index also peaks at X=0.75, suggesting a multiplicity of relaxation processes have largely given way to one dominant one, possibly involving substrate spins. Note: The above points concerning $J_0(\omega_x-\omega_y)$ implicitly make the assumption, for simplicity, that ω_x & ω_y have the same sign. In reality this need not be so. Indeed, for ^{3}He and ^{11}B it is not as Appendix 1 shows and $J_2(\omega_x+\omega_y)$ replaces $J_0(\omega_x-\omega_y)$ in the above arguments.

Figure 7.2.1.7 is a plot of T_1 *vs* X at a number of frequencies. At each frequency a minimum occurs and shifts to higher X with falling frequency (mostly) as would be expected for an incommensurate solid film dipolar minimum and also observed experimentally at registry on Grafoil (§1.10.4). The minima are derived from parabolic curves fitted through three points, the lowest plus its two nearest neighbours and are presented in table 7.2.1.1.

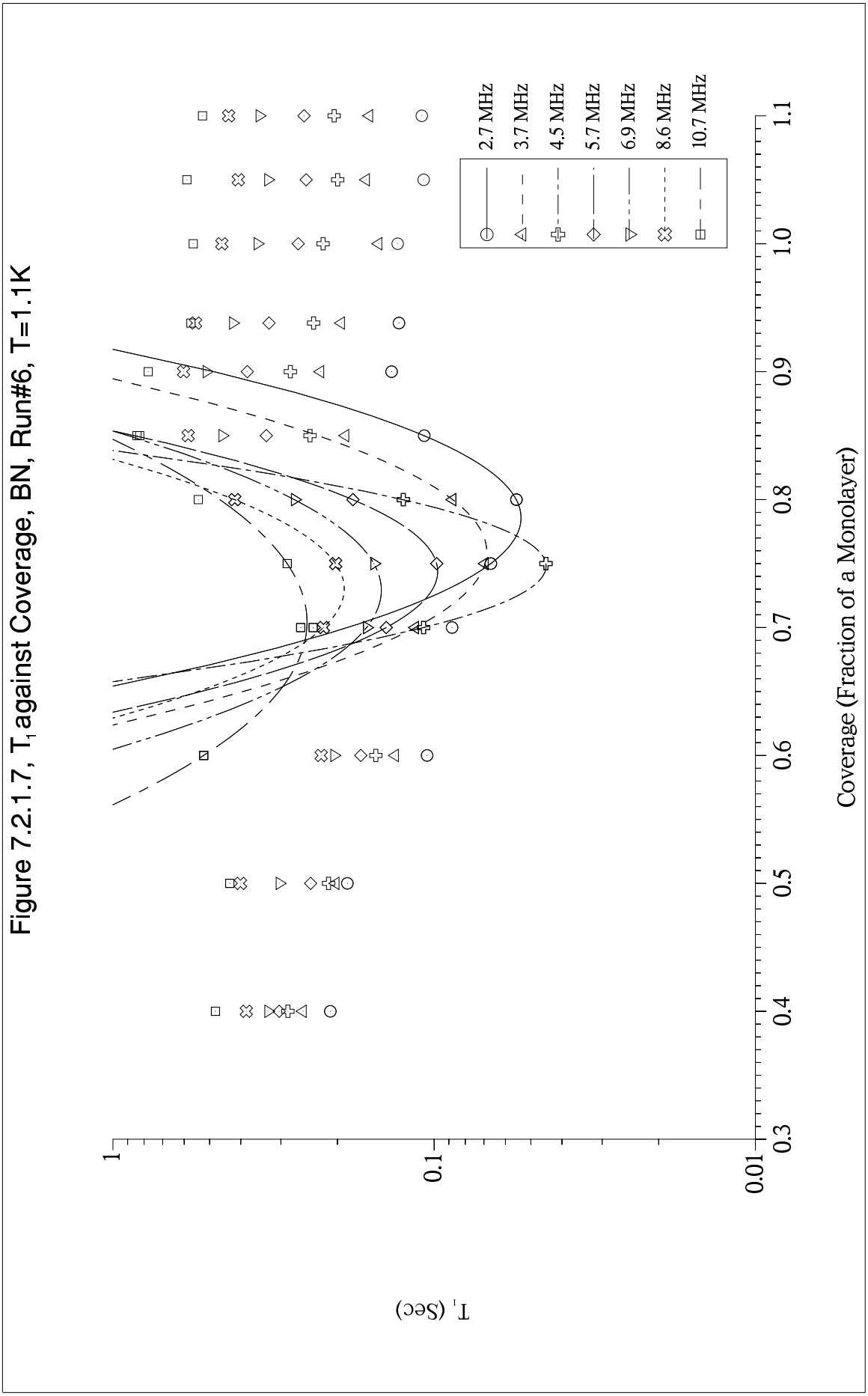

Figure 7.2.1.7, T_1 against Coverage, BN, Run#6, T=1.1K

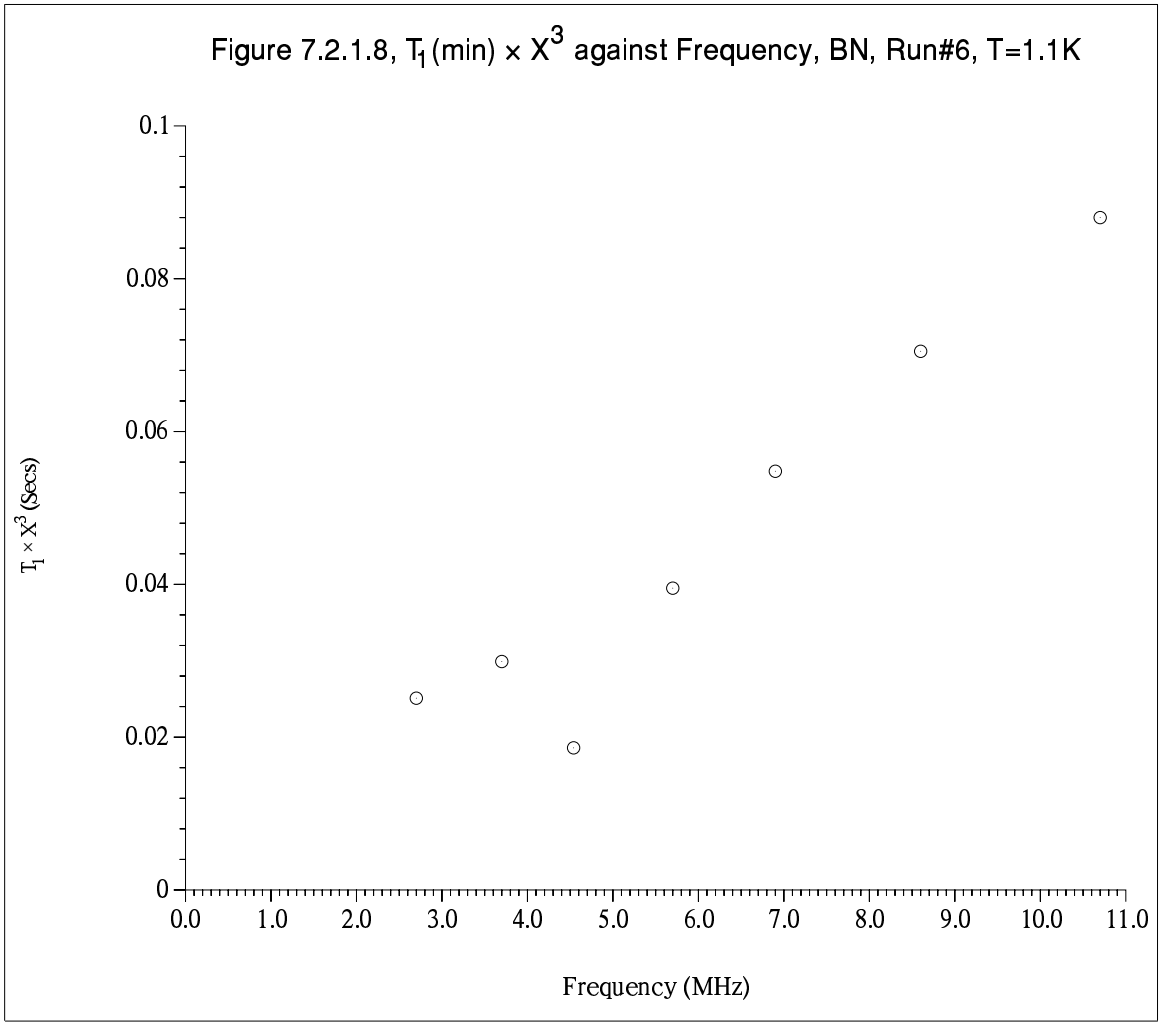

Table 7.2.1.1, Coverage of occurrence and Value of T_1 minima with Frequency on BN.

Frequency (MHz)	Coverage (Monolayer)	T_1 at Minimum (Secs)
2.7	0.784	0.0521
3.7	0.761	0.0679
4.54	0.747	0.0446
5.7	0.742	0.0967
6.9	0.728	0.142
8.6	0.729	0.182
10.7	0.709	0.247

Notice the deviations in trend at 8.6MHz in minimum coverage and at 4.54 MHz in T_1. Figure 7.2.1.8 plots $T_1 \times X^3$ against frequency which should be a straight line (§1.10.6) for homonuclear dipolar relaxation in a homogeneous solid. Evidently it is not. Neither are the deviations systematic as might be expected for edge-site adsorption offsets to the assumed basal plane coverage. Working with the assumption for a moment, that X=0.75

$\Rightarrow$ registry and relaxation is homonuclear dipolar, the occurrence of minima in coverage is due to a combination of the spin separation $\langle r_{ij} \rangle$ being monotonically reduced and τ_c increased by substrate influence to a maximum at perfect registry, providing $\omega_0\tau_c \leqslant 1$. This cannot explain the deepest minimum occurring at 4.54MHz. It is conceivable the 4.54MHz point (part of a series of temperature dependence data taken from 4.2K to 1.1K over many hours) was influenced by the extra time involved, allowing a possibly slow transition to full registry to take place. See also §7.4.3.1. NB: Most of the 1.1K frequency dependence datasets were taken after rapidly pumping down following sample annealing or T>4.2K data. However the 2.7MHz point is from a 4.2K to 1.1K temperature dependence data set and relaxed with an index of only 0.68. As discussed above at 4.54MHz relaxation was also strongly super-exponential. The inference is that at 4.54MHz the FMR coupling is intrinsically most efficient, this being due to fulfilment of a $J_n(\omega_x) \rightarrow J_n(0)$ condition which occurs at perfect registry, where ω_x involves a substrate frequency and the ^{3}He spin Larmor frequency, eg. $\omega_x = \omega_s - \omega_{He}$, in which case $\omega_s \sim 4.5$MHz.

7.2.2 Temperature Dependence Data

Included in figures 7.2.2.1 to 7.2.2.86 are the temperature dependence data in the range 1K<*X*<13.2K for each coverage investigated. Plots include several measures of T_1, T_2 and their indices of relaxation against 1/*T*. Where the spin-spin relaxation is faster than exponential ''CP' T_2' values have been included using the 'Carr-Purcell' fit (listing 6.3.2.1) modelling the magnetisation decay as $h(t) = h(0)\exp(-2t/T_2 - 8Ct^3)$. '*C*', a fit parameter reflects the decay component due to diffusion in whatever field gradients are present and '*t*' is the $90^0-t-180^0-t-$echo pulse delay time. Additionally at higher coverages where where the S/N is better $T_2(1/e)$ values have been included. For the higher coverage T_1 data $T_1(1/e)$ fits are also plotted. See §3.4 and listing 6.3.2.1. for details. Changes in the indices of relaxation show up as changes in the discrepancy between the exponential '$T_{1,2}$' and '$T_{1,2}(1/e)$' values on the relaxation time *vs* 1/*T* plots. The temperature dependence of both indices is quite illuminating, displaying features not seen clearly if at all in the relaxation time plots. Hysteretic behaviour between the up and down temperature sweeps in the build-up to the proposed melting transition in the commensurate−incommensurate transition region data and *sub-region* behaviour (see §7.2.2/*X*=0.2) are examples. The reason for the sensitivity of the indices to small changes in the film is not certain but appears to reflect the average relaxation rate remaining locally constant but with the balance between competing relaxation processes/ paths making up the sub-exponential average, changing. Where not explicitly stated the Larmor frequency used is 4.5MHz.

***X*=0.1,** T_2 (figure 7.2.2.1) shows temperature independence up to ~0.25K^{-1}, followed by an approximately logarithmic rise to a peak at ~0.12K^{-1}, then falling as *T* increases towards 13.2K. Below ~0.25K^{-1} the relaxation mechanism is believed to be exchange modulated dipolar in a patchy/edge-sites solid dominated film. The peak, which occurs at all coverages is attributed to desorption, an idea backed up by the sample-line pressure gauge readings obtained at these temperatures, from the through-leaky sample-line valve, when closed with insufficient force. The reduction in τ_c and and increasing internuclear spin separation will, bearing in mind the *NMR rule of thumb* $1/T_2 = m_2\tau_c$, increase T_2. A logarithmic rise suggests an activation law enabling an energy-of-desorption to be extracted, (see also §7.2.3.3). At temperatures above the maximum a non-dipolar mechanism which increases relaxation with motion such as, via PMIs or BN platelet diamagnetic local fields must be responsible for the turn-over. PMI *dirty-wall* relaxation, the preferred candidate is normally seen as primarily affecting T_1,

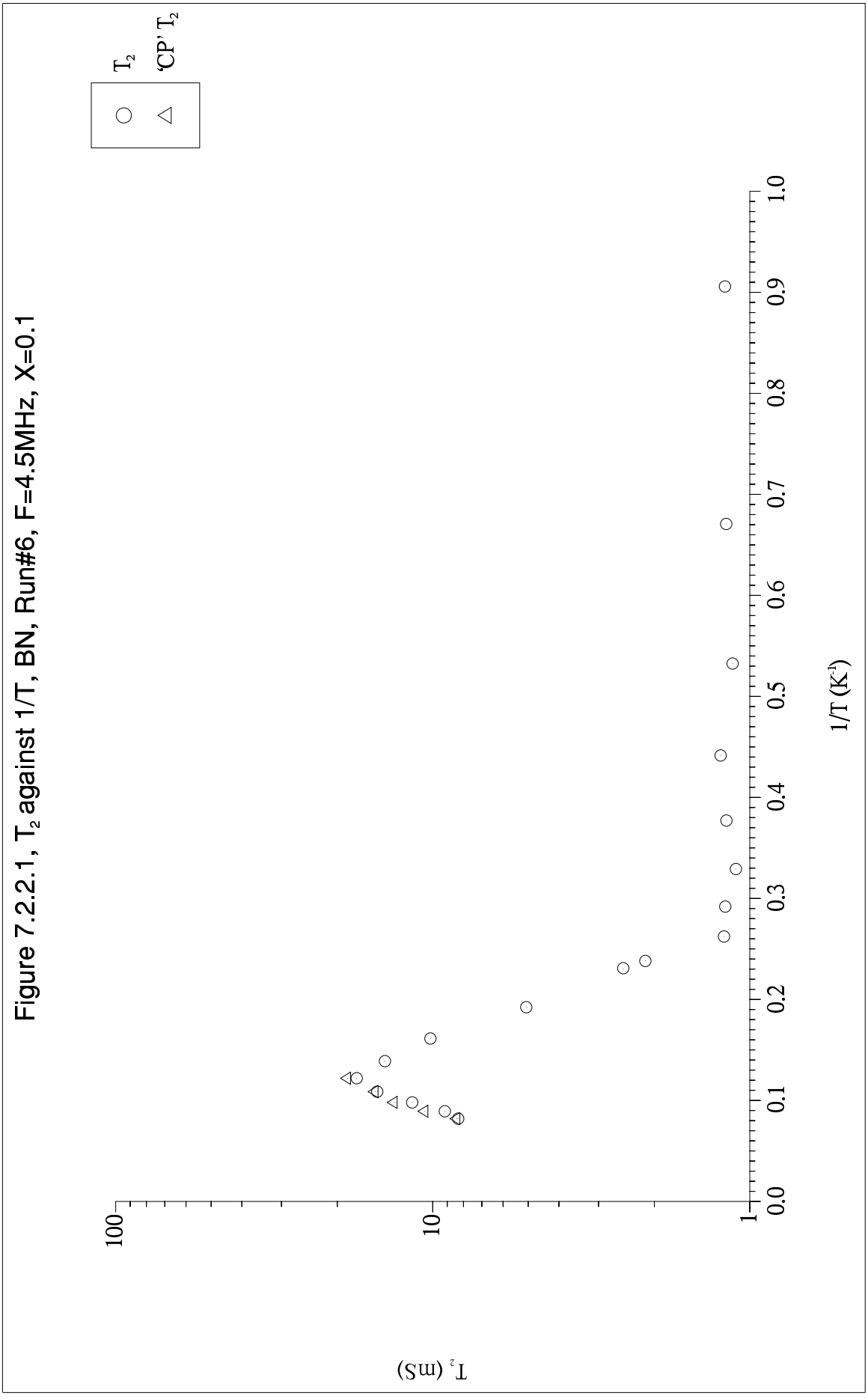
Figure 7.2.2.1, T_2 against 1/T, BN, Run#6, F=4.5MHz, X=0.1
T_2
'CP' T_2
T_2 (mS)
100
10
1
0.0
0.1
0.2
0.3
0.4
0.5
0.6
0.7
0.8
0.9
1.0
1/T (K^{-1})

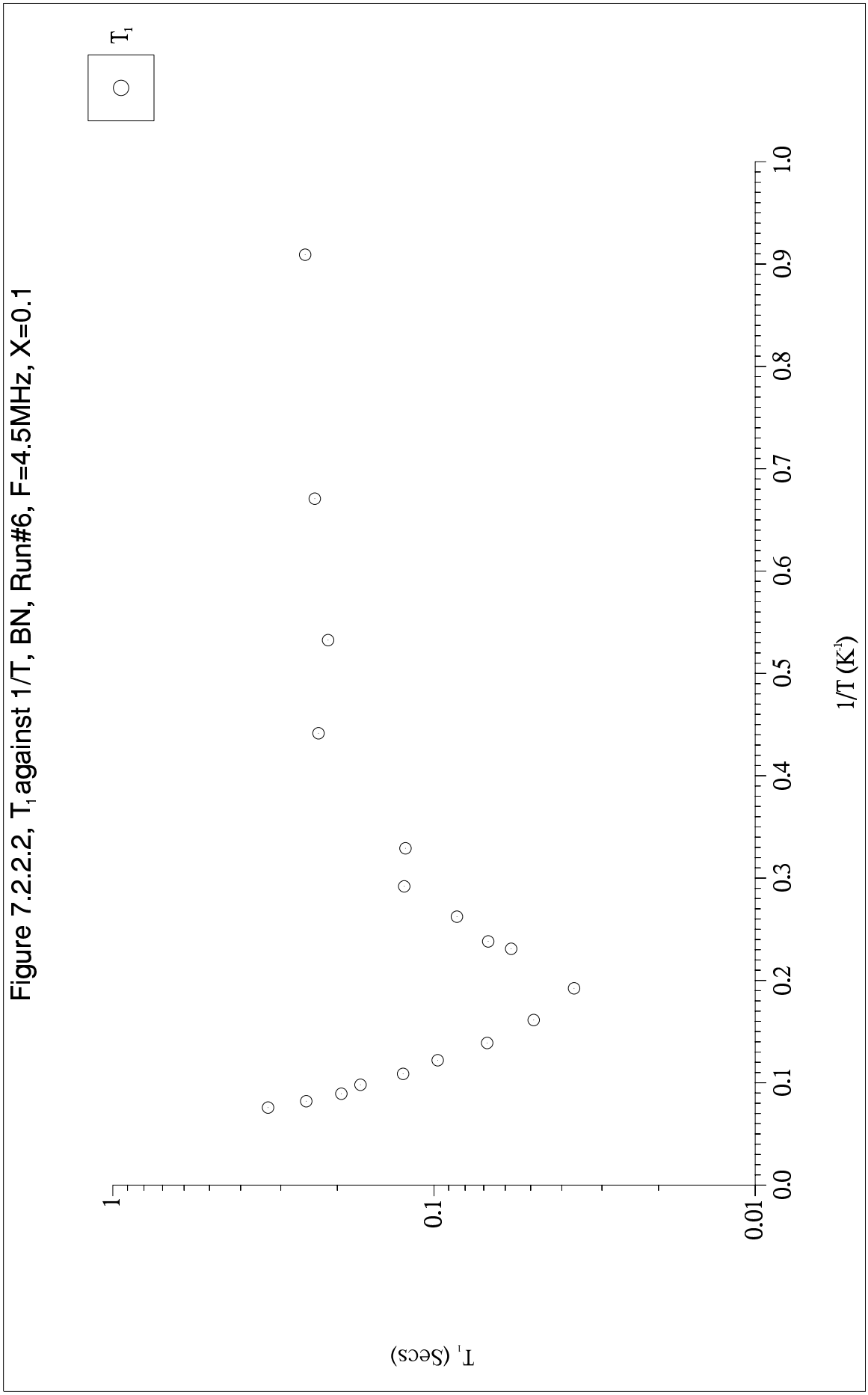

Figure 7.2.2.2, T_1 against 1/T, BN, Run#6, F=4.5MHz, X=0.1

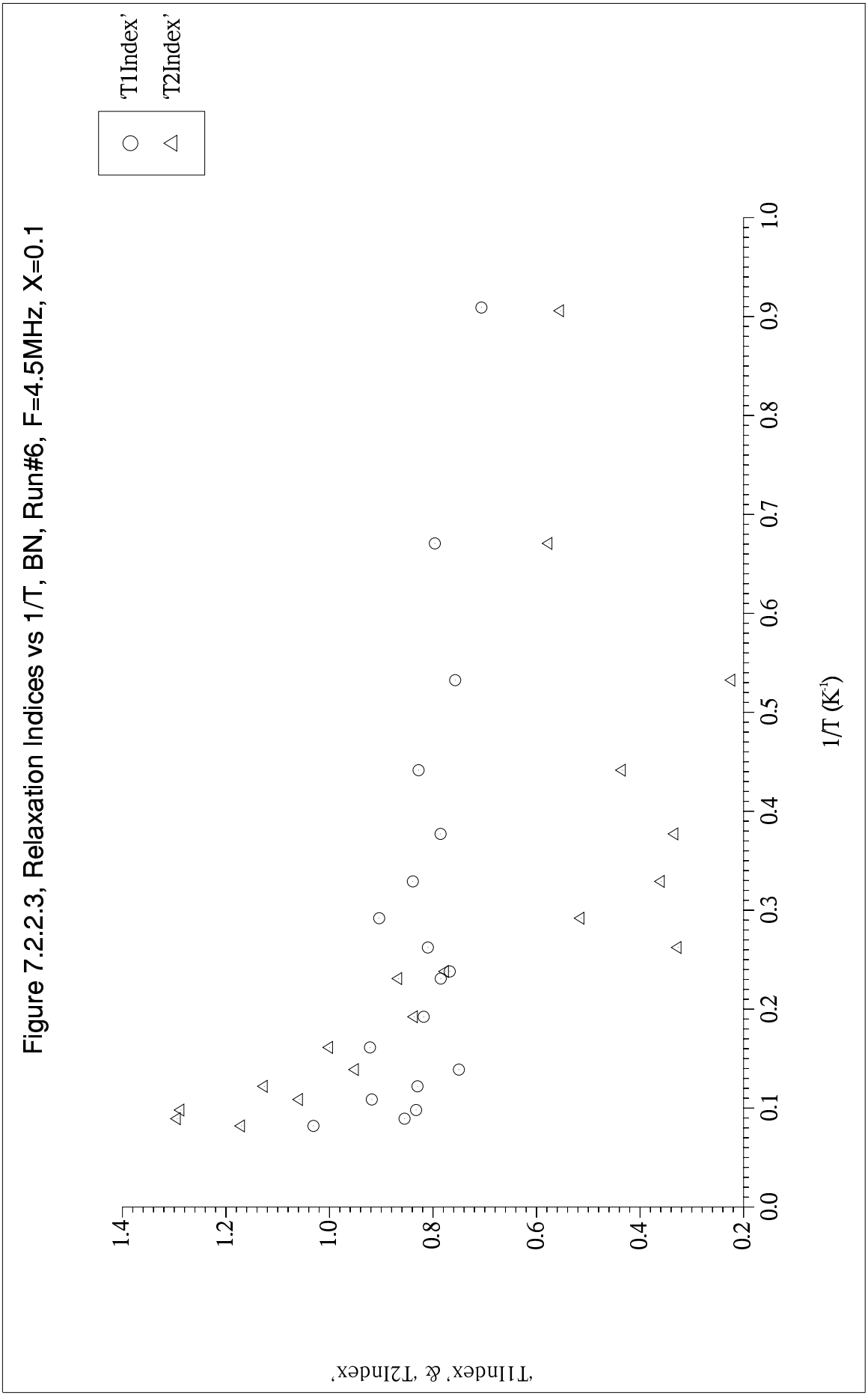
Figure 7.2.2.3, Relaxation Indices vs 1/T, BN, Run#6, F=4.5MHz, X=0.1
'T1Index'
'T2Index'
'T1Index' & 'T2Index'
1/T (K-1)
1.4
1.2
1.0
0.8
0.6
0.4
0.2
0.0
0.1
0.2
0.3
0.4
0.5
0.6
0.7
0.8
0.9
1.0

however the data of Fardis (§3.4.3) shows its effect is strongest on T_2. Desorbed spins relaxing in the electronic dipole fields of the stainless steel sample filling line may also be a significant factor here at these elevated temperatures.

T_1 (figure 7.2.2.2) possesses similar approximately temperature independent relaxation up to around $0.4K^{-1}$ followed by a distinct minimum at $\sim 0.18K^{-1}$. All coverages display at least one minimum here. On both sides of and close to the minimum T_1 fairly closely follows an activation law. The nature of the minimum is an important issue: There is no evidence at any coverage that the minimum corresponds to a phase change as reflected by a feature in T_2. As discussed later there is a conflict between the higher coverage data and a homonuclear dipolar interpretation, leaving open the novel possibility the minimum corresponds to a maximum in the ^{3}He−Substrate relaxation rate in analogy with the conventional homonuclear ^{3}He-Lattice case.

Both indices are low and approximately constant at low temperatures like the relaxation times. 'T2Index' rises with temperature in the region corresponding to the rise of T_2 towards its maximum, becoming super-exponential at the maximum. 'T1Index' remains approximately constant as far as $\sim 0.2K^{-1}$ where it become increasingly exponential. At low temperatures 'T2Index' < 'T1Index' a common feature of the data. There is unlikely to be a single cause of the sub-exponentiality of the low temperature data. Certainly, the distribution of BN platelet sizes, orientations and adsorbing surfaces is expected to lead to sub-exponential relaxation if the motion is slow enough such that $T_{1,2} < a^2/2D$, where 'a' is the average dimension of a platelet in which case most spins relax on a single surface. However the ^{4}He preplated BN (§3.4.1) and the the X=0.75 T_1 data suggest it is not the most important factor for that relaxation time. Spin-spin relaxation takes place on a time scale two orders of magnitude less than T_1 at this coverage. Its greater sub-exponentiality is therefore unsurprising. Taking T_2 = 1ms and a=5μm puts an upper limit on D, $D \leqslant 1\times10^{-4}$ cm^2/Sec if single surface relaxation is to dominate. The diffusion constant for a 2D diffusive helium-3 gas of fractional coverage X and temperature T is given by **[208]** $D = a\,(kT/m)^{½}/X4\sqrt{2}$, where '$a$' is the helium radius and 'm' its mass. At X=0.1 and T=1K gives D=3 × 10^{-4} cm^2/sec. Bearing in mind the dominance of the patchy solid T_2, the condition is easily fulfilled. Similar values for D have been inferred from a bulk helium-3/2D low coverage Grafoil comparison study **[209]**. Figure 7.2.2.4 illustrates an alternative description of the T_1 data. T_1 and $1/T_1$ are plotted against $\sqrt{T}$ for $T<T^{min}$ and $T^{min}<T<8.2$K respectively. For dipolar relaxation $T_1 \propto \tau_c$ for $T<T^{min}$ and $T_1 \propto \tau_c^{-1}$ when $T>T^{min}$. $\tau_c^{-1} \propto \sqrt{T}$ is the signature of a (2D) gas.

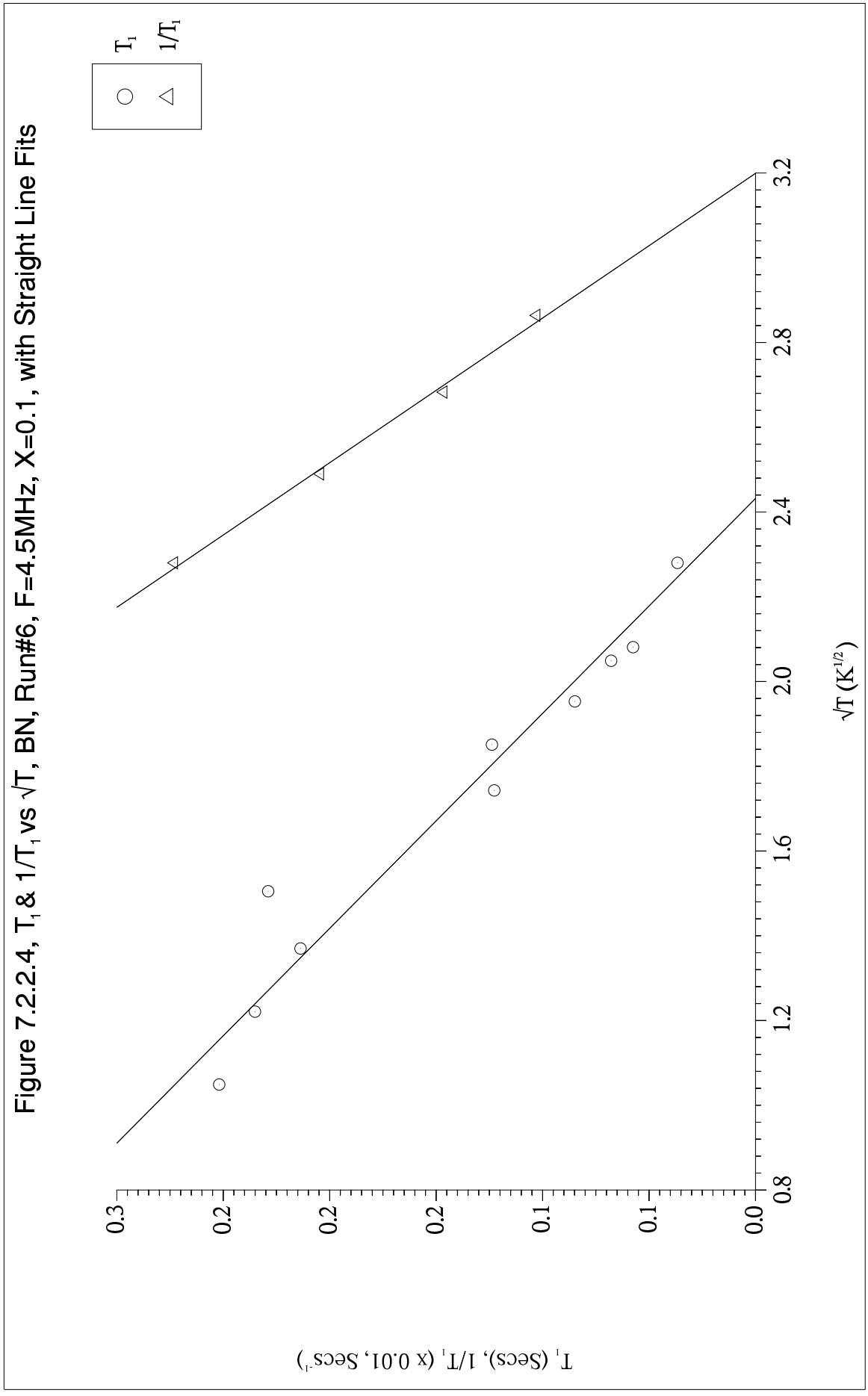
Figure 7.2.2.4, T_1 & $1/T_1$ vs $\sqrt{T}$, BN, Run#6, F=4.5MHz, X=0.1, with Straight Line Fits
T_1
$1/T_1$
T_1 (Secs), $1/T_1$ (x 0.01, $Secs^{-1}$)
$\sqrt{T}$ ($K^{1/2}$)
0.0
0.1
0.1
0.2
0.2
0.3
0.8
1.2
1.6
2.0
2.4
2.8
3.2

***X*=0.2,** T_2 (figure 7.2.2.5) falls slowly/is approximately constant up to $0.45K^{-1}$ where it falls more rapidly to a distinct minimum at $0.27K^{-1}$ followed by the desorption maximum as at X=0.1. The following interpretation is applied: With the proposed solid fraction at X=0.05 the gas:solid ratio has trebled compared with X=0.1 and relaxation in the delocalised film component is more visible, T_2 falling as temperature rises and motion increases, must be due to a non-dipolar mechanism. The preferred candidate is again via PMIs rather than by diffusion in BN diamagnetic fields or static field inhomogeneities, since the same minimum at X=0.4 does not change appreciably with frequency and the relaxation remains strongly sub-exponential. As the spins desorb the substrate embedded impurities mechanism becomes less effective, T_2 (dipolar) increases via m_2 and τ_c as discussed above and only falls again once the desorbed spin $\leftrightarrow$ substrate impurity visit-rate is high enough to short-circuit dipolar relaxation at the highest temperatures. As at X=0.1, the desorption rise is approximately logarithmic.

'T2Index' (figure 7.2.2.7) remains approximately constant at ~0.35 up to $0.25K^{-1}$ where it rises with the T_2 desorption maximum, again becoming super-exponential at the maximum. The demise of single-surface relaxation and maybe increasing spin diffusion in field gradients, as motion increases is the likely cause. Some interesting structure between $0.5K^{-1}$ and $0.3K^{-1}$ is apparent. It probably reflects subtle changes in the balance of relaxation mechanisms and the two phases present as breakup of the solid patches via thermal activation and collisions with delocalised spins increases in the build up to desorption.

T_1 (figure 7.2.2.6) lacks the nearly constant low temperature region seen at X=0.1, instead falling monotonically with increasing temperature. Logarithmic behaviour on the high T side and immediately on the low side of the minimum is apparent. A much better description of the $T<T^{min}$ T_1 data is as a 2D gas as shown in figure 7.2.2.8, plotted as for X=0.1 in figure 7.2.2.4. The deviation from the $\sqrt{T}$ law at $T\geqslant$6.5K coincides approximately with the T_2 desorption maximum and hence the loss of a 2D system.

'T1Index' is roughly constant at ~0.8 as far as ~$0.2K^{-1}$ coincident with the T_1 minimum where it drops sharply to ~0.5 before rising to and a little beyond exponentiality at high temperatures. In contrast with the T_1 *vs* X minimum at X=0.75 the sharp drop in index suggests multi-path relaxation is occurring here. Another common feature of the *index vs T* data is apparent; referred to henceforth as *sub-region* behaviour for convenience, it can be seen the data follows a clear trend over typically, a group of

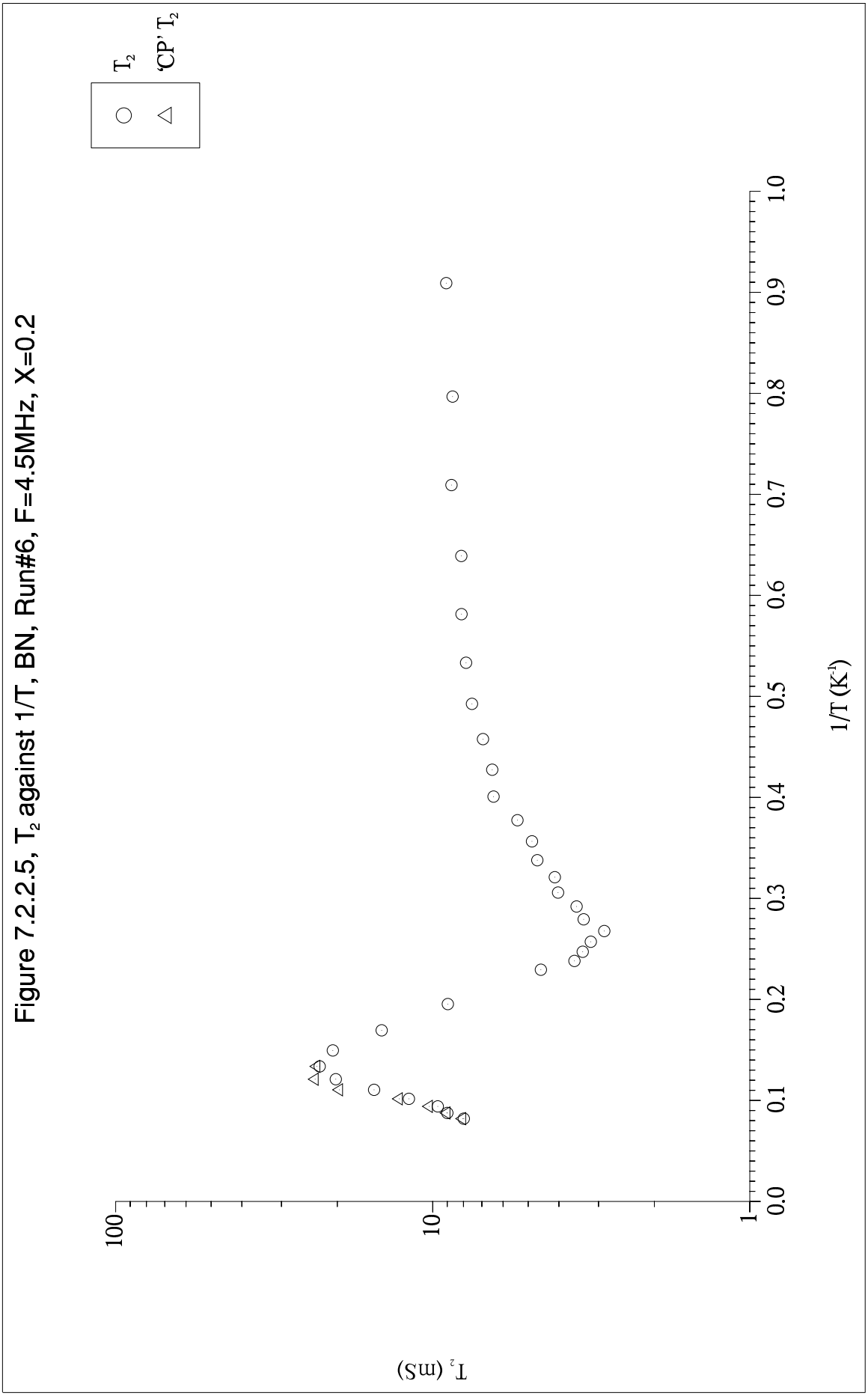
Figure 7.2.2.5, T_2 against 1/T, BN, Run#6, F=4.5MHz, X=0.2
T_2
'CP' T_2
T_2 (mS)
100
10
1
0.0
0.1
0.2
0.3
0.4
0.5
0.6
0.7
0.8
0.9
1.0
1/T (K^{-1})

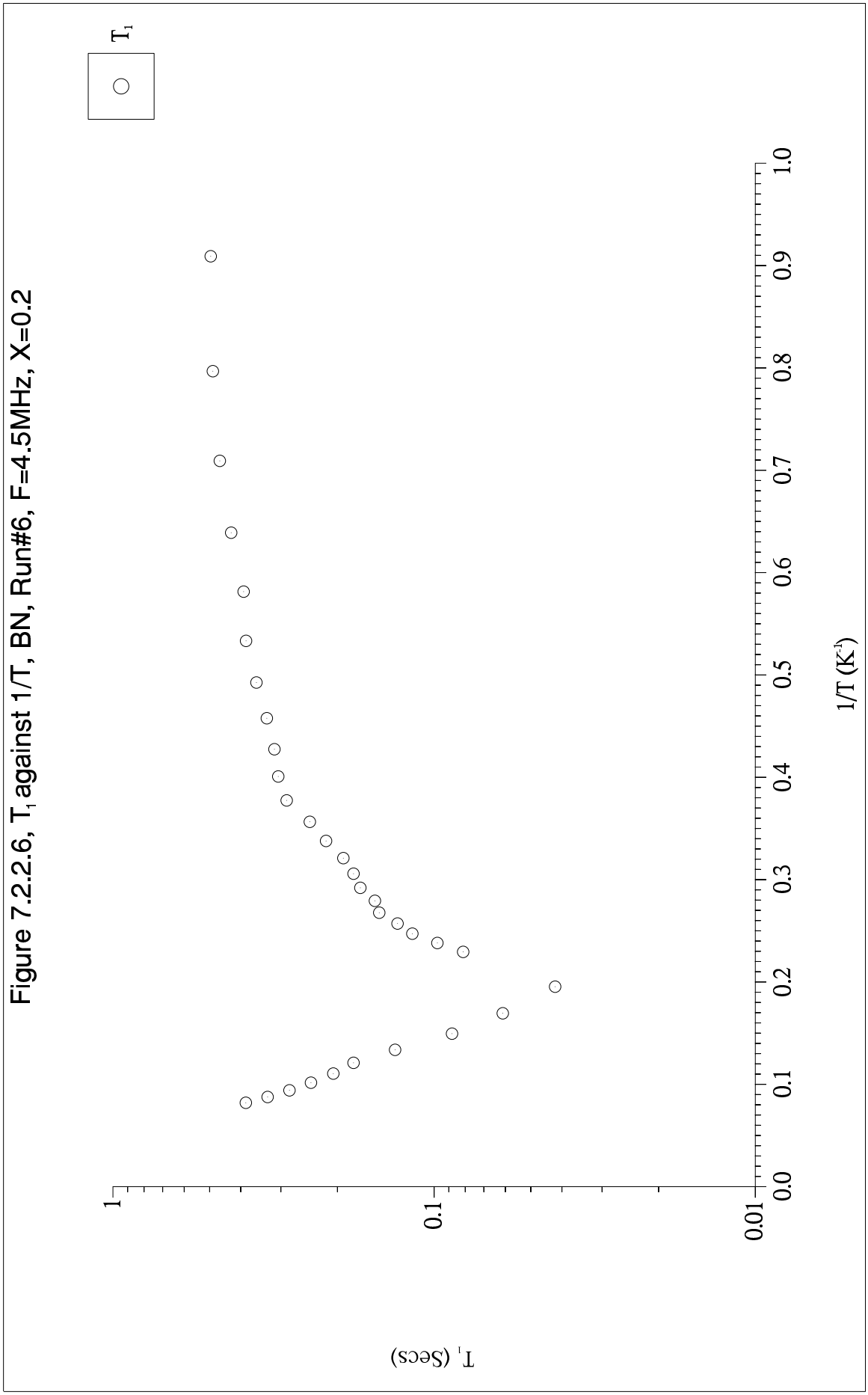
Figure 7.2.2.6, T1 against 1/T, BN, Run#6, F=4.5MHz, X=0.2
T1
T1 (Secs)
1
0.1
0.01
0.0
0.1
0.2
0.3
0.4
0.5
0.6
0.7
0.8
0.9
1.0
1/T (K-1)

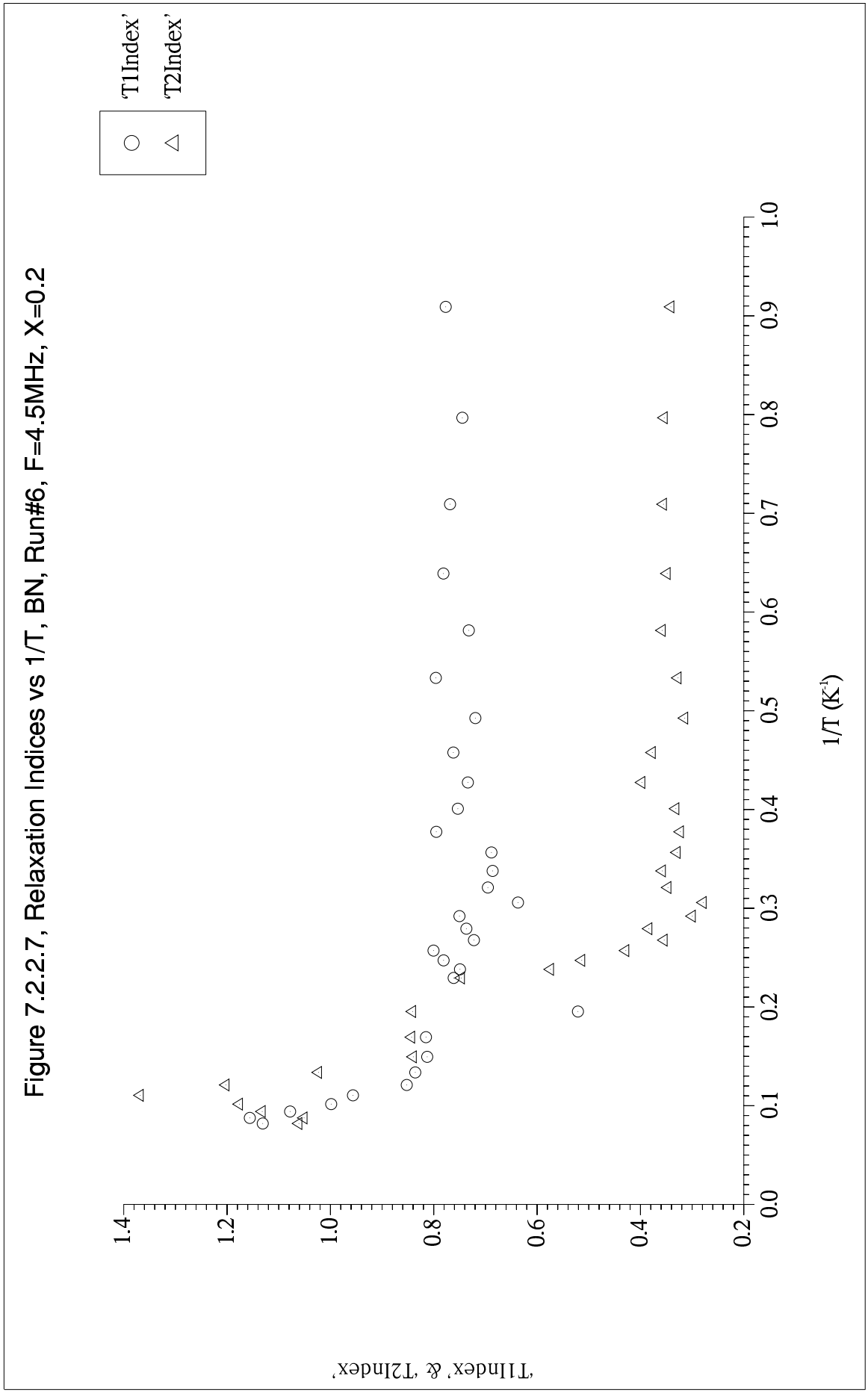
Figure 7.2.2.7, Relaxation Indices vs 1/T, BN, Run#6, F=4.5MHz, X=0.2
'T1Index'
'T2Index'
'T1Index' & 'T2Index'
1/T (K-1)
0.0
0.1
0.2
0.3
0.4
0.5
0.6
0.7
0.8
0.9
1.0
0.2
0.4
0.6
0.8
1.0
1.2
1.4

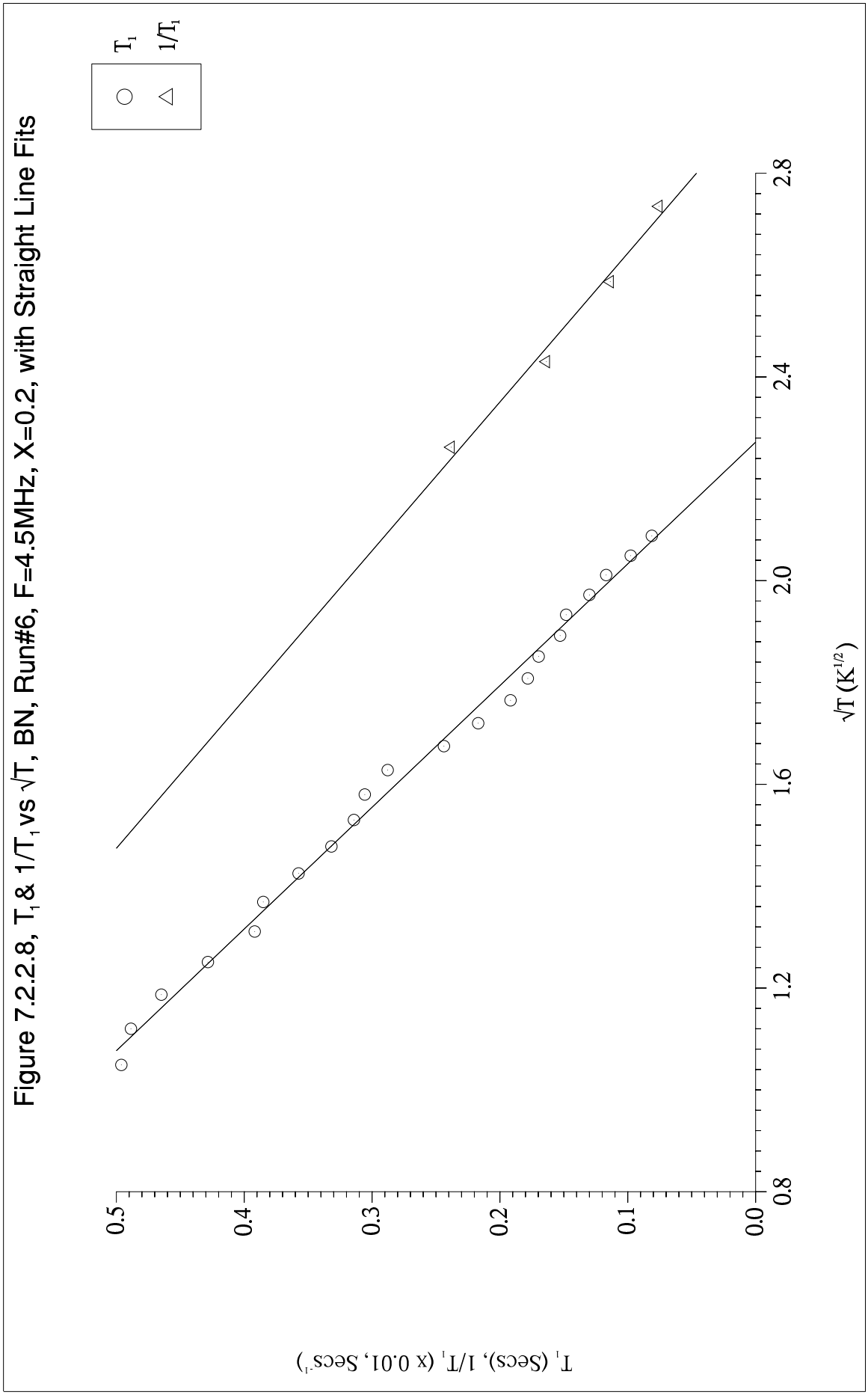
Figure 7.2.2.8, T_1 & $1/T_1$ vs √T, BN, Run#6, F=4.5MHz, X=0.2, with Straight Line Fits
T_1
$1/T_1$
T_1 (Secs), $1/T_1$ (x 0.01, $Secs^{-1}$)
√T ($K^{1/2}$)
0.0
0.1
0.2
0.3
0.4
0.5
0.8
1.2
1.6
2.0
2.4
2.8

two or three points before changing to another trend. A plausible explanation is that different regions of patchy solid formed at sites of differing binding energy, melt at different temperatures when their thermally activated vacancy concentrations reach their critical values, or more likely undergo some other less drastic change, eg. the breakup of solid patches into smaller ones. Since it is believed that much of the 'T_1' relaxation occurs through the substrate spins in addition to the ordinary spin-lattice process it is expected that the balance of relaxation channels reflected by the 'T1Index' will be a sensitive indicator of those changes. Moreover in a similar way to the substrate spin relaxation channel and registry case (§7.2.1), it is reasonable to suppose, for example, that if a solid patch were to undergo a short range *creep* in a region where there was an adsorption potential gradient, under thermal influence, that there would be a larger impact on the ^{3}He-Substrate coupling rate than the ^{3}He−^{3}He one. That is, as the patch crept across the substrate there would be larger changes in the patch's average (say) ^{3}He−^{11}B internuclear separation than the ^{3}He−^{3}He one, particularly since the ^{11}B 'coverage' seen by the ^{3}He spins is higher than its own coverage. If the solid patches are responsible for the 'T1Index' *sub-region* behaviour, it ought to increase with coverage until localisation takes place since increasing lateral pressure in the fluid film is believed to lead to solid patch growth. The data shows exactly this increase for $X \geqslant 0.3$ as the solid patches grow. It becomes apparent from the rest of the temperature dependence data to be presented that the solid patch growth is composed of registered spins.

***X*=0.3,** T_2 against $1/T$ (figure 7.2.2.9) is similar to the X=0.2 data. T_2 at the minimum and at the low temperature flat-region (figure 7.2.1.1) has increased but the relative (to the low temperature relaxation rate) increase in relaxation rate at the minimum has decreased. This is consistent with the augmentation factor description: T_2 increases as the fluid:patchy-solid spin ratio increases with X. However, relaxation due to the fluid component in the PMI fields becomes less effective as the film thickens and motion slows with coverage.

'T2Index' (figure 7.2.2.11) remains fairly constant at ~0.4 as far as ~0.3K^{-1} where it rises with the desorption maximum to super-exponentiality as before. There is a marked decrease in *sub-region* behaviour. The longest relaxation times are observed at X=0.3 (figures 7.2.1.1 and 7.2.1.2) where the solid:fluid ratio is smallest, before solid-patch growth occurs. If *sub-region* behaviour is associated with melting, thermal activation etc. in the solid patches, we may expect it to be minimal here.

T_1 (figure 7.2.2.10), as at X=0.2 lacks the low temperature flat-region, also

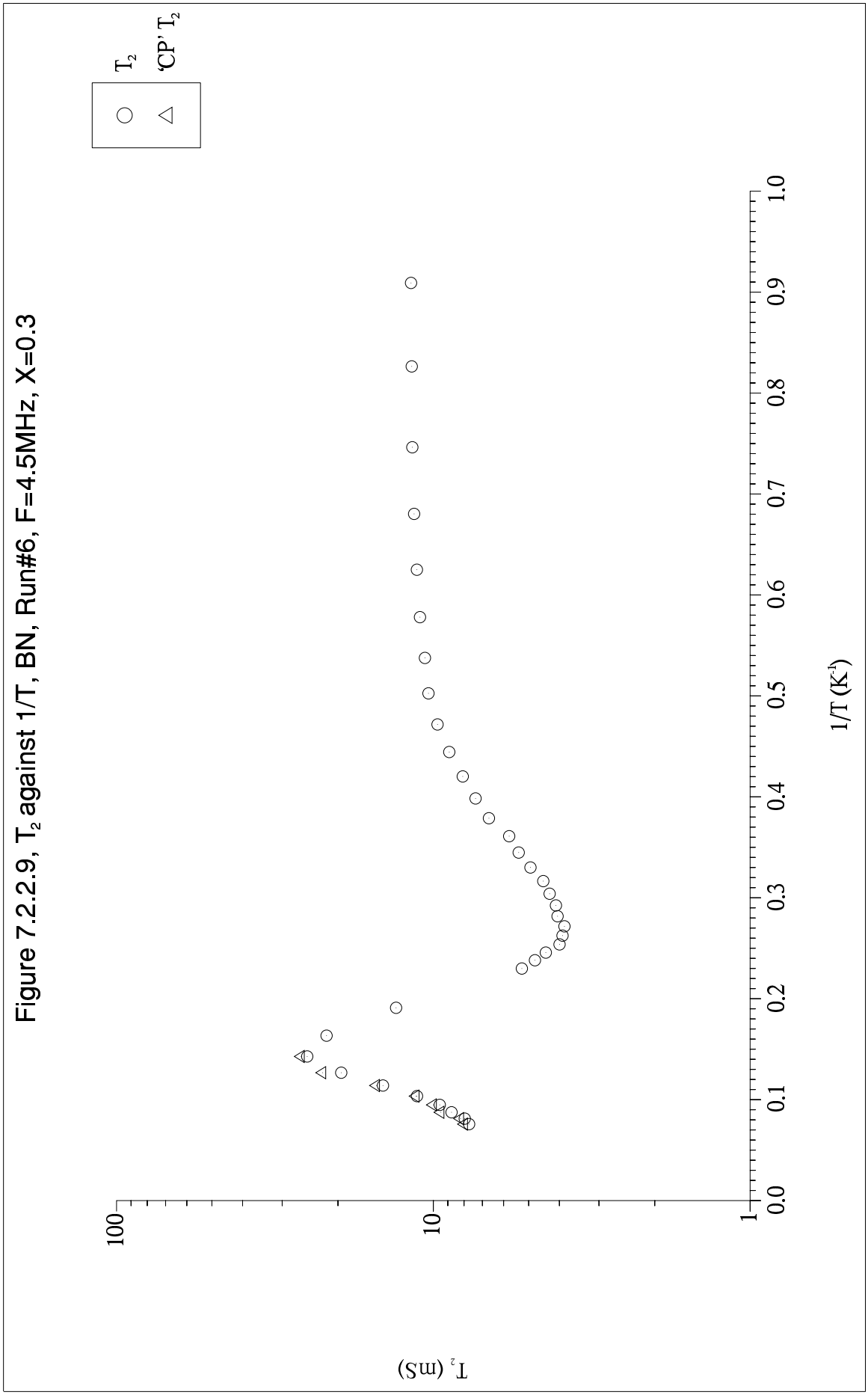
Figure 7.2.2.9, T_2 against 1/T, BN, Run#6, F=4.5MHz, X=0.3
T_2
'CP' T_2
T_2 (mS)
100
10
1
0.0
0.1
0.2
0.3
0.4
0.5
0.6
0.7
0.8
0.9
1.0
1/T (K^{-1})

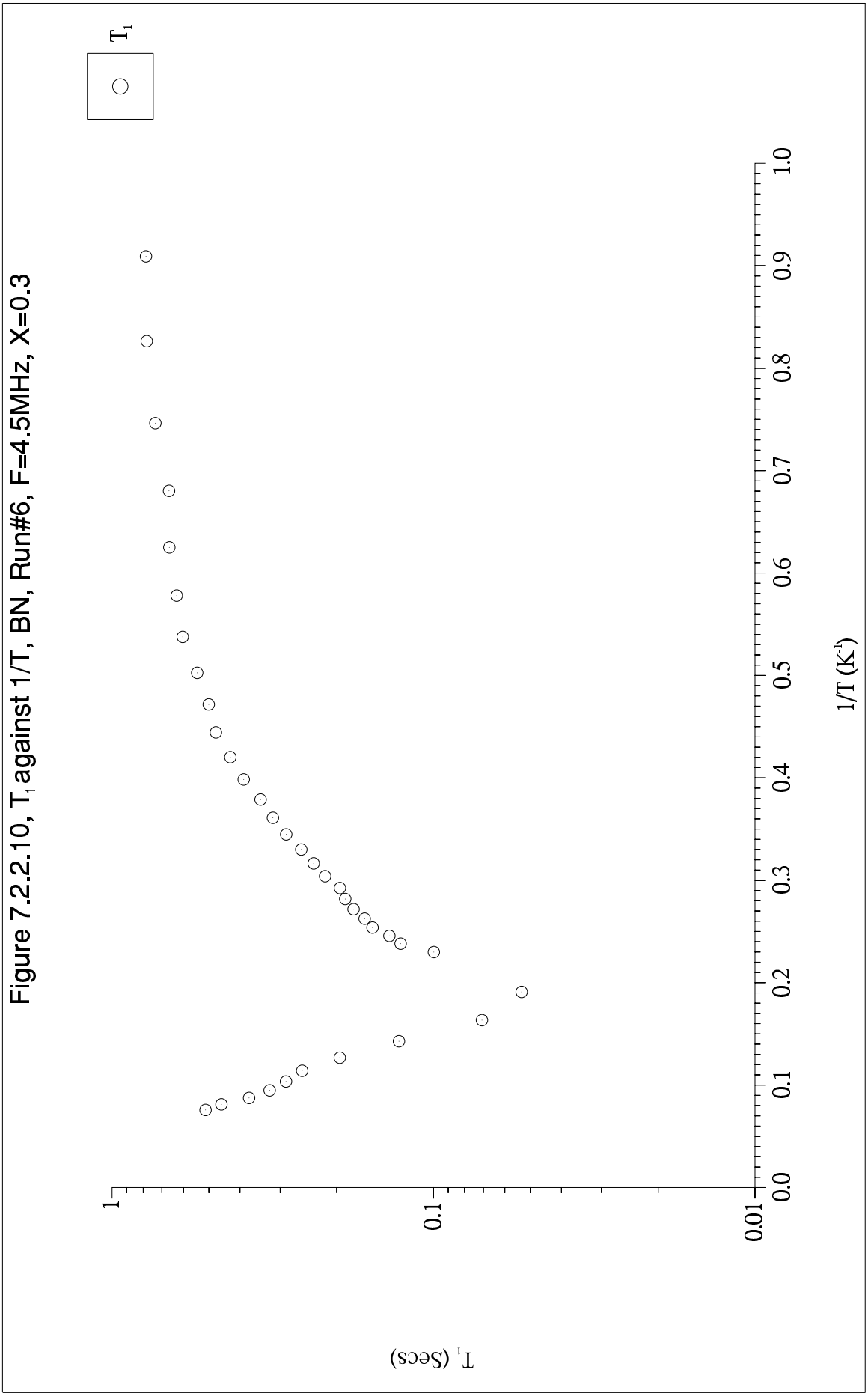

Figure 7.2.2.10, T_1 against 1/T, BN, Run#6, F=4.5MHz, X=0.3

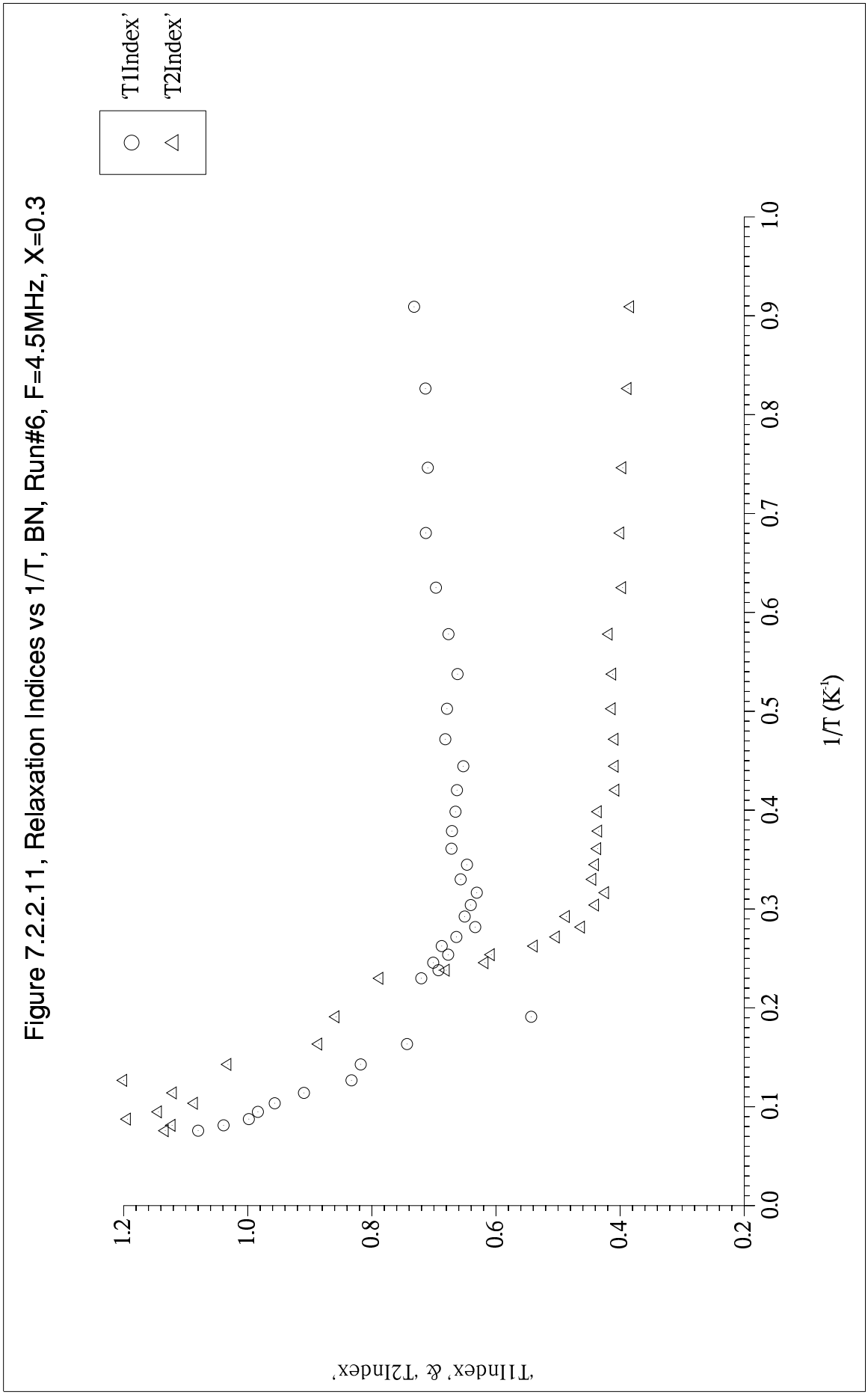
Figure 7.2.2.11, Relaxation Indices vs 1/T, BN, Run#6, F=4.5MHz, X=0.3
'T1Index'
'T2Index'
'T1Index' & 'T2Index'
1/T (K-1)
0.0
0.1
0.2
0.3
0.4
0.5
0.6
0.7
0.8
0.9
1.0
0.2
0.4
0.6
0.8
1.0
1.2

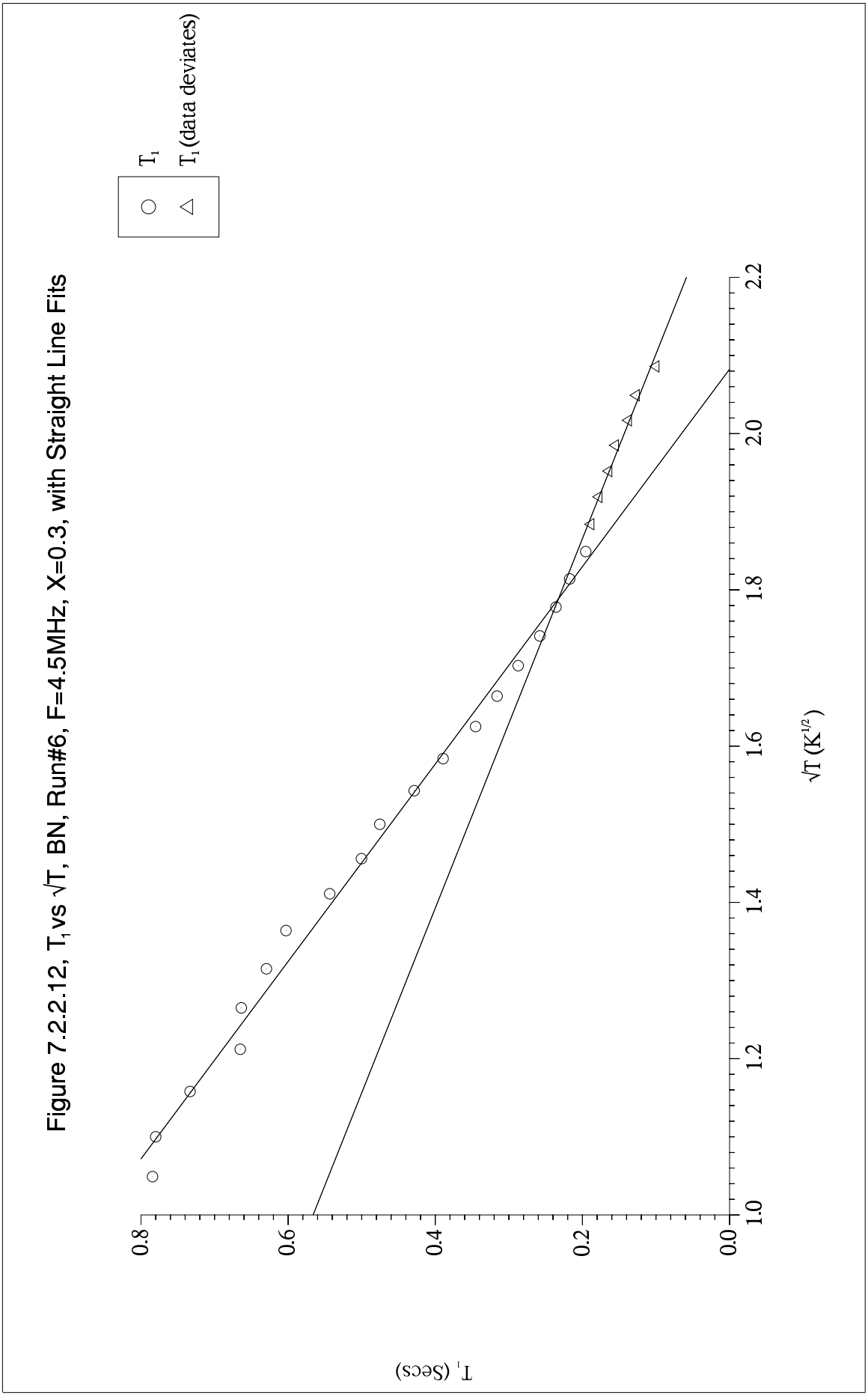
Figure 7.2.2.12, T1 vs √T, BN, Run#6, F=4.5MHz, X=0.3, with Straight Line Fits
T1
T1 (data deviates)
T1 (Secs)
√T (K1/2)
0.0
0.2
0.4
0.6
0.8
1.0
1.2
1.4
1.6
1.8
2.0
2.2

decreasing continuously with T to the minimum. Figure 7.2.2.12 shows the variation of T_1 with $\sqrt{T}$. 2D gas behaviour occurs for $T \leqslant 3.4$K, deviating at higher temperatures. Closer inspection of figure 7.2.2.8 also shows some deviation at this temperature at $X=0.2$. In the same way T_1 deviation at $X=0.2/T \sim 6.5$K was associated with the loss of two-dimensionality by desorption, $T=3.4$K coincides with the onset of desorption as indicated by 'T2Index'. Note; the $T>3.4$K data still follows an approximate $\sqrt{T}$ law as expected for a gas, the lower slope indicates less efficient relaxation as expected for desorbed spins where relaxation occurs at the surface.

'T1Index' also has less *sub-region* behaviour than at $X=0.2$ which has less than at $X=0.1$ in accordance with the above fluid:solid ratio explanation. As at $X=0.2$, 'T1Index' has a sharp minimum at the T_1 minimum.

***X*=0.4,** Figure 7.2.2.13 shows T_2 *vs* $1/T$. Included on this graph is $T_2(1/e)$ which well illustrates the strong low-temperature sub-exponentiality. Data taken at 2.7MHz for $1.1\text{K} \leqslant T \leqslant 4.2\text{K}$ appears to be identical. At both the low temperature flat-region, and minimum, T_2 has fallen with the onset of solid patch expansion. Additionally, the T_2-minimum:low-temperature relative spin-spin relaxation rate increase has fallen again as for $X=0.2 \rightarrow 0.3$ as the fluid increases in density and motion slows as discussed above. Another related trend in the data is apparent: The low temperature flat-region is progressively reduced with coverage as the minimum becomes broader. At $X=0.2$ and 0.3 the T_2 plateau extends as far as $\sim 0.45\text{K}^{-1}$. For $X=0.4$ it stops at $\sim 0.55\text{K}^{-1}$. Accepting the decrease in T_2 for $X>0.3$ in the low temperature flat-region is due to solid patch growth, the onset of the fall to the fluid minimum occurring at lower temperatures suggests the *new growth* is less dense plus less strongly bound to the substrate and therefore *melts* at a lower temperature, reducing T_2 by contributing to the non-dipolar fluid mechanism.

'T2Index' (figure 7.2.2.15) is very similar to $X=0.3$ but has increased *sub-region* behaviour.

T_1 *vs* $1/T$ (figure 7.2.2.14) is remarkably different from $X=0.3$, having a new feature, a maximum at $\sim 0.57\text{K}^{-1}$. Plotted on a linear scale T_1 for $T<T^{\min}$ is approximately proportional to $-1/T$. The following explanation is offered: T_1 rises for $0.9\text{K}^{-1}<T<0.57\text{K}^{-1}$ as the *new growth* solid undergoes thermal activation eventually *melting* at $\sim 0.57\text{K}^{-1}$. Note: $T^{\max}=0.57\text{K}^{-1}$ closely corresponds to the above onset temperature for T_2 fluid relaxation. A question that needs to be addressed is: What is the nature of the *new growth* solid? The data suggests that it $\sqrt{3} \times \sqrt{3}$ registered, the

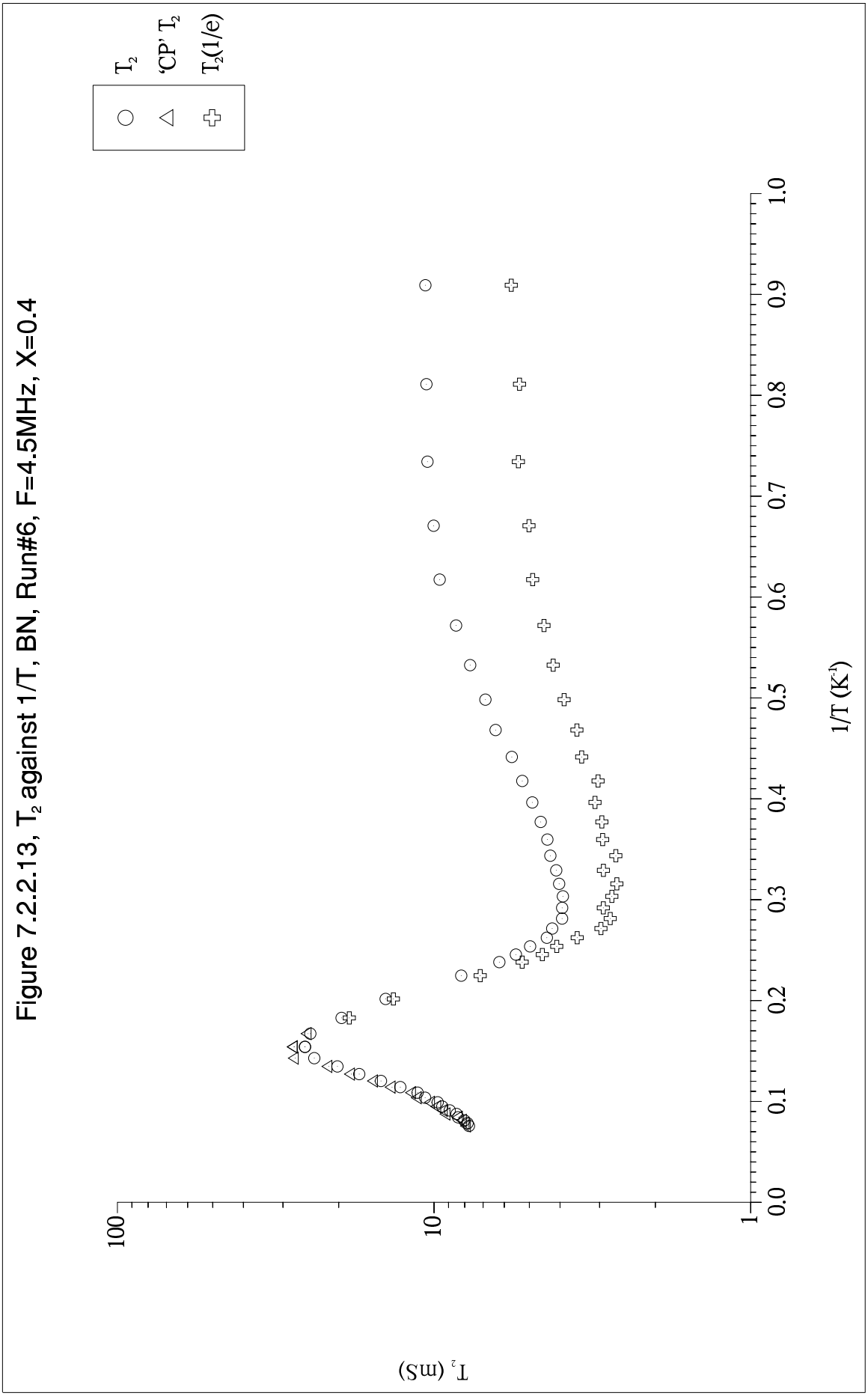
Figure 7.2.2.13, T2 against 1/T, BN, Run#6, F=4.5MHz, X=0.4
T2
'CP' T2
T2(1/e)
T2 (mS)
100
10
1
0.0
0.1
0.2
0.3
0.4
0.5
0.6
0.7
0.8
0.9
1.0
1/T (K-1)

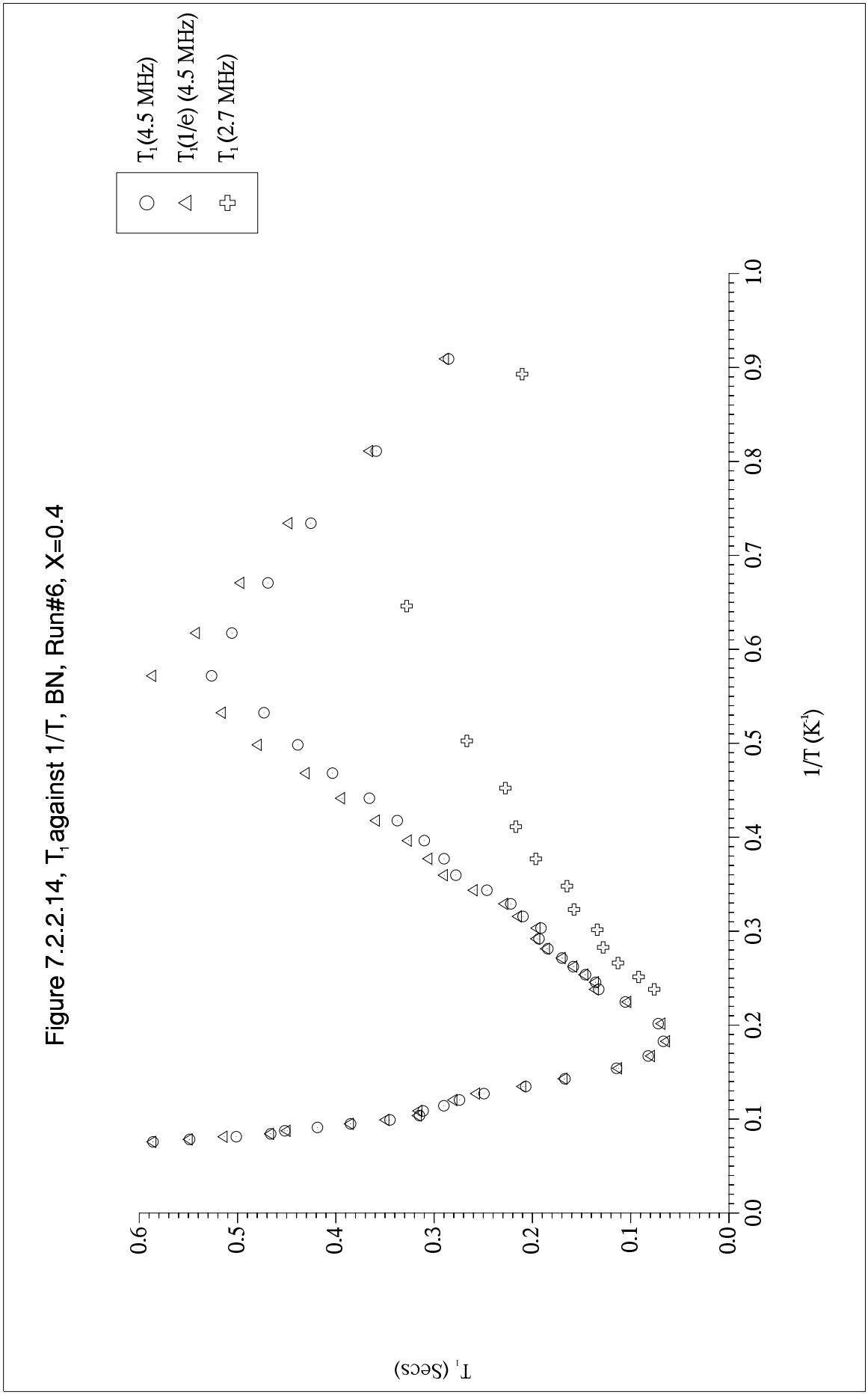

Figure 7.2.2.14, T_1 against 1/T, BN, Run#6, X=0.4

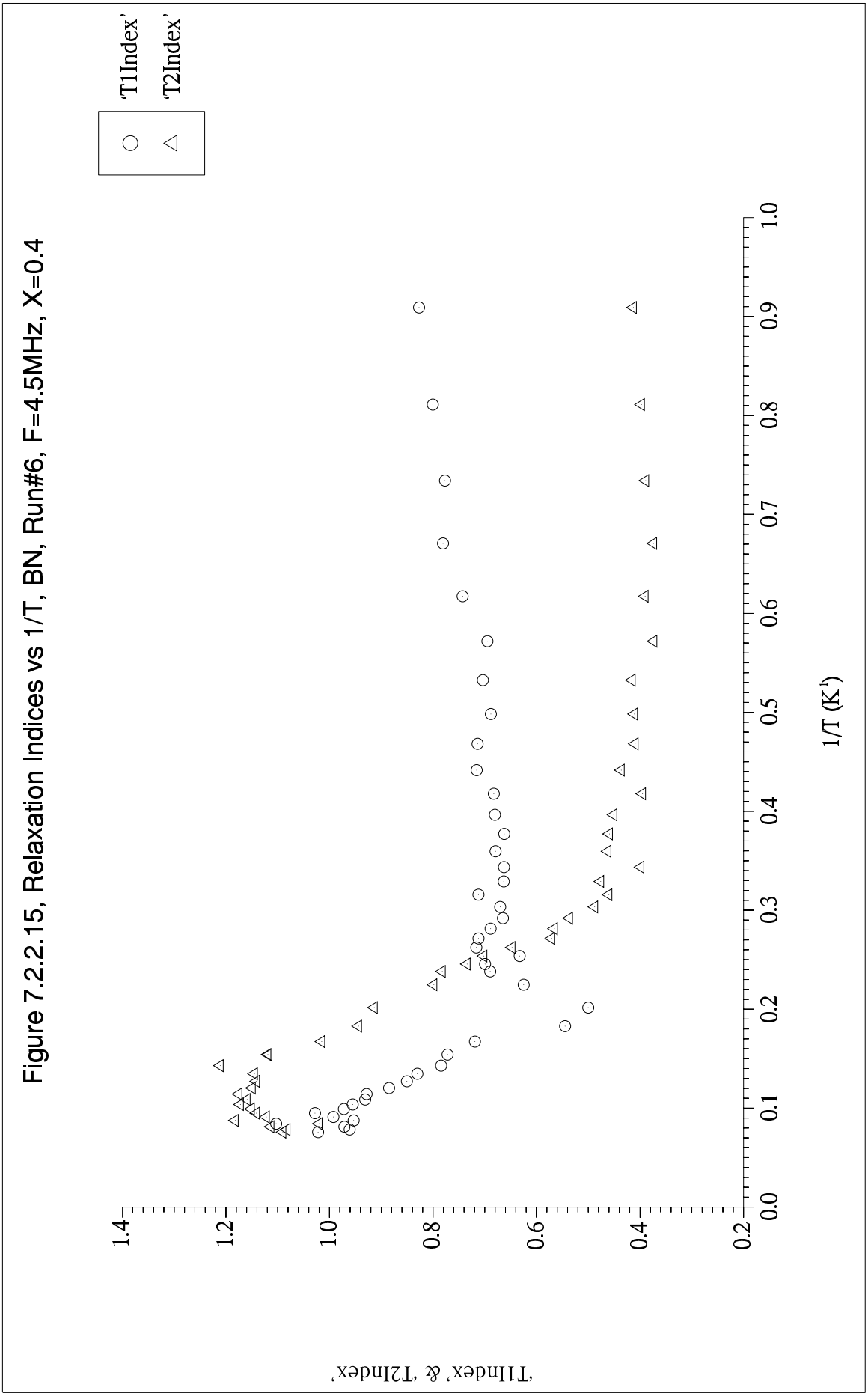
Figure 7.2.2.15, Relaxation Indices vs 1/T, BN, Run#6, F=4.5MHz, X=0.4
'T1Index'
'T2Index'
'T1Index' & 'T2Index'
1/T (K-1)
0.0
0.1
0.2
0.3
0.4
0.5
0.6
0.7
0.8
0.9
1.0
0.2
0.4
0.6
0.8
1.0
1.2
1.4

implication being *new growth* occurs once there is sufficient lateral pressure in the film but under substrate-potential influence, using the heterogeneous solid patches as nucleation sites and continues with increasing coverage until the *new growth* regions link up at X=0.75 to form perfect registry, the fluid component having disappeared. This scheme accords with the conclusions of Greywall **31** who shows a $\sqrt{3} \times \sqrt{3}$ registry+fluid coexistence phase on Grafoil extending downwards from 0.064Å^{-2} to ~0.047Å^{-2} ≡ 0.44 monolayers. Given the low temperature, $X \geqslant 0.3$ T_1 *vs* X data (figures 7.2.1.2, 7.2.1.5) is characterised by sharply falling T_1 and 'T1Index' rising to super-exponentiality at registry, we would expect to see some of the same behaviour as T falls from the proposed *new growth melting* point. The data in figures 7.2.2.14 and 7.2.2.15 show this, with T_1 falling from 0.53 Sec at 0.57K^{-1} to 0.29 Sec at 0.91K^{-1} and 'T1Index' rising from 0.69 at 0.57K^{-1} to 0.83 at 0.91K^{-1}. The rise in exponentiality below the maximum is also clearly visible from the convergence of the 'T_1' and 'T_1(1/e)' measures in figure 7.2.2.14. Insofar as it is possible to judge from the three points taken around the maximum it seems to have shifted to lower T at 2.7MHz. If so this might be an indication that the *melting* transition does not take place all at one temperature, but as in the T_1 *vs* X at X=0.75/T~1K case − with τ_c varying continuously across the registry transition, giving slightly different maximum positions as the motion is sampled at different frequencies via the spectral function describing the dipolar field fluctuations. See also §1.10.4. As in the low temperature/coverage dependence case the variation in T_1 through/up-to the transition is less at 2.7MHz than 4.5MHz, only falling from 0.33 Sec at the maximum to 0.21 Sec at the lowest temperature, as expected for dipolar relaxation. The rise in 'T1Index' below the T_1 maximum is also less pronounced at 2.7MHz, the corresponding values being 0.70 to 0.81. The nature of the *new growth* melt must also be considered. $T_1 \propto 1/T$ for $T^{\max} < T < T^{\min}$ shows T_1 falling faster than a $\sqrt{T}$ law, (figure 7.2.2.16). There is no clear explanation for this, it could have something to do with the gradual destruction of residual orientational order in the melt imposed by the substrate, with increasing temperature. On the other hand, T_1 *vs* $1/T$ for 1.1K < T < 4.2K at 2.7MHz does display the gas-type $\sqrt{T}$ relaxation for $T > T^{\max}$. Recalling the unusual behaviour of T_1 at T~1K/X=0.75/F=4.5MHz (figures 7.2.1.7, 7.2.1.8, table 7.2.1.1 and related text) including that the fastest and only super-exponential relaxation occurred at this frequency, we are tempted to speculate that the registered *new growth* patches might also be more strongly relaxing through the substrate spins at 4.5MHz, especially since the rise to the maximum is also approximately linear in $1/T$. More data for $F \neq 4.5$MHz would be necessary to test this hypothesis. Moreover, there would need to be a sufficient

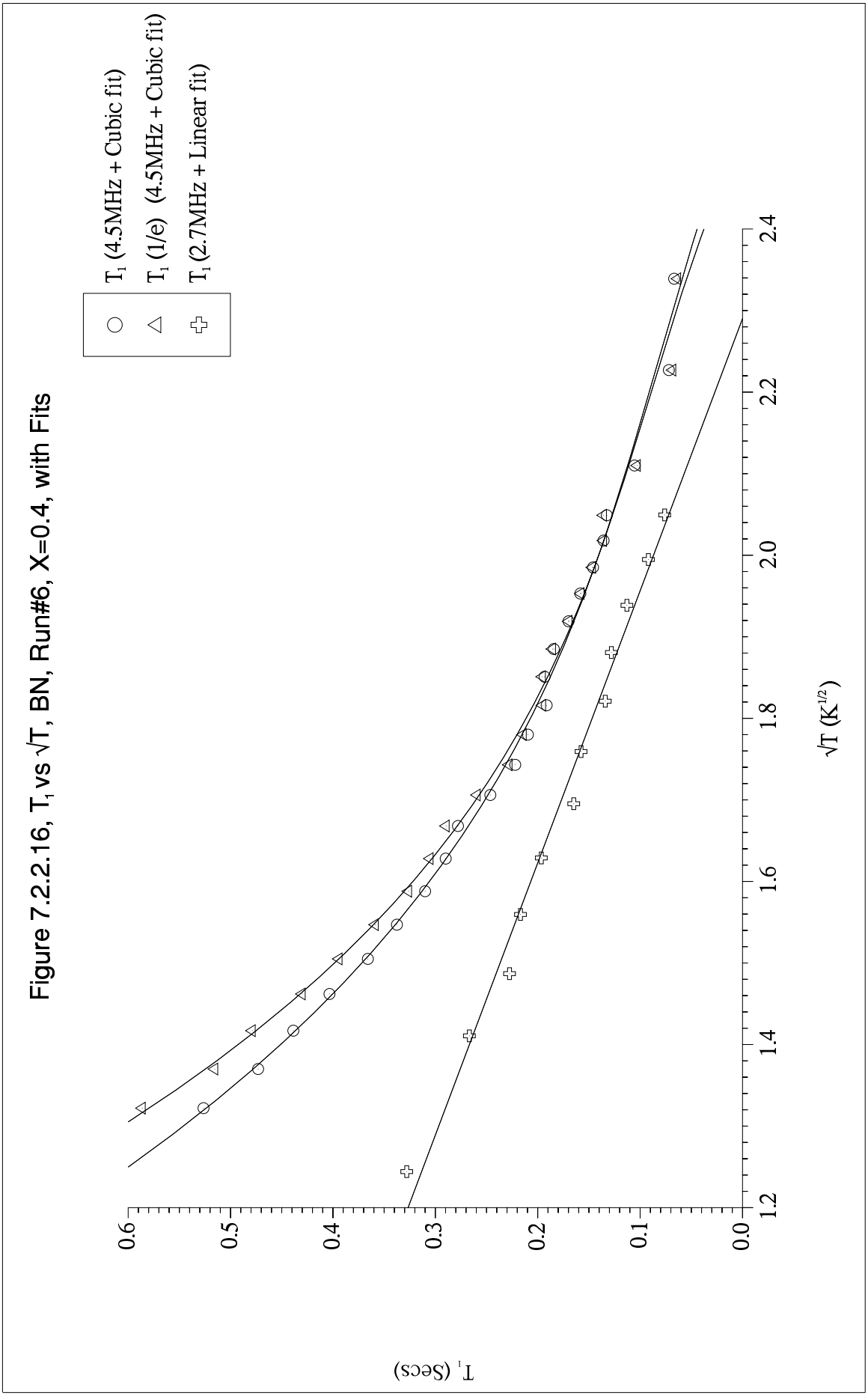
Figure 7.2.2.16, T1 vs √T, BN, Run#6, X=0.4, with Fits
T1 (4.5MHz + Cubic fit)
T1 (1/e) (4.5MHz + Cubic fit)
T1 (2.7MHz + Linear fit)
T1 (Secs)
√T (K-1/2)
0.0
0.1
0.2
0.3
0.4
0.5
0.6
1.2
1.4
1.6
1.8
2.0
2.2
2.4

registered component to allow the registered spins+4.5MHz phenomenon relaxation to dominate. See also §7.2.4. A further possibility is that the T_1-*as-a-function-of-T* behaviour simply stems from the particular combination of the Larmor frequency used plus the relative proportions of high density patchy solid, registered solid and fluid present at this coverage. With solid patch growth only having just started the patchy:registered solid ratio may be ~~1 and play a crucial role in determining T_1. This seems likely given the $T_1 \propto \pm 1/T$ relation does not appear at higher coverages approaching X=0.75 where the patchy solid should become increasingly insignificant.

Increased *sub-region* behaviour is visible in 'T1Index' (figure 7.2.2.15), particularly in the region 0.91K^{-1} to 0.57K^{-1}. Two *sub-regions* appear here, both showing a positive slope in *index vs* 1/*T*. For T>0.57K^{-1}, corresponding with the approach to the T_1 minimum, 'T1Index' remains constant around 0.7 but shows increased '*noise*' as predicted for a system with a higher solid or solid-like composition. *Noise* is this context is used to refer to fluctuations involving *sub-region* type behaviour where the *sub-regions* are too small and numerous to be individually distinguishable. Finally, the minimum at the T_1 minimum and rise to exponentiality complete the 'T1Index' data as seen at lower X.

***X*=0.5,** Figure 7.2.2.17 plots T_2 against 1/*T*. All the trends discussed at X=0.4 are apparent; The low-temperature and T_2-minimum T_2s have both fallen as has the relative rate increase. With the broader shallower minimum, the low temperature flat-region now ends at ~0.6K^{-1}. The 2.7MHz and 10.7MHz points are very similar.

'T2Index' (figure 7.2.2.19), in contrast with the predicted behaviour is smoother, rising continuously with temperature, from ~0.35 at 0.91K^{-1} to super-exponentiality. Why?

Figure 7.2.2.18 shows T_1 against 1/*T* for 4.5MHz, 2.7MHz and 10.7MHz. T_1 (4.5MHz) at the maximum has fallen compared to X=0.4 due to the increase in registering. The maximum has broadened, its position being centred at ~0.57K^{-1} which again is close to the T_2 flat-region end. As before T_1^{max} (2.7MHz) is smaller and its temperature profile flatter. Its maximum again occurs at a lower temperature (~0.65K^{-1}). The reverse occurs at 10.7MHz, with the maximum situated at ~0.55K^{-1} reaffirming dipolar relaxation. The $T_1 \propto \pm 1/T$ relationship has disappeared, $\sqrt{T}$ dependence reasserting itself again at 4.5MHz for T>T^{max}, (figure 7.2.2.20). It is consistent with the observed relaxation being due to a combination of 2D gas and the now more numerous, delocalised but still substrate-potential-influenced registry-*melt*

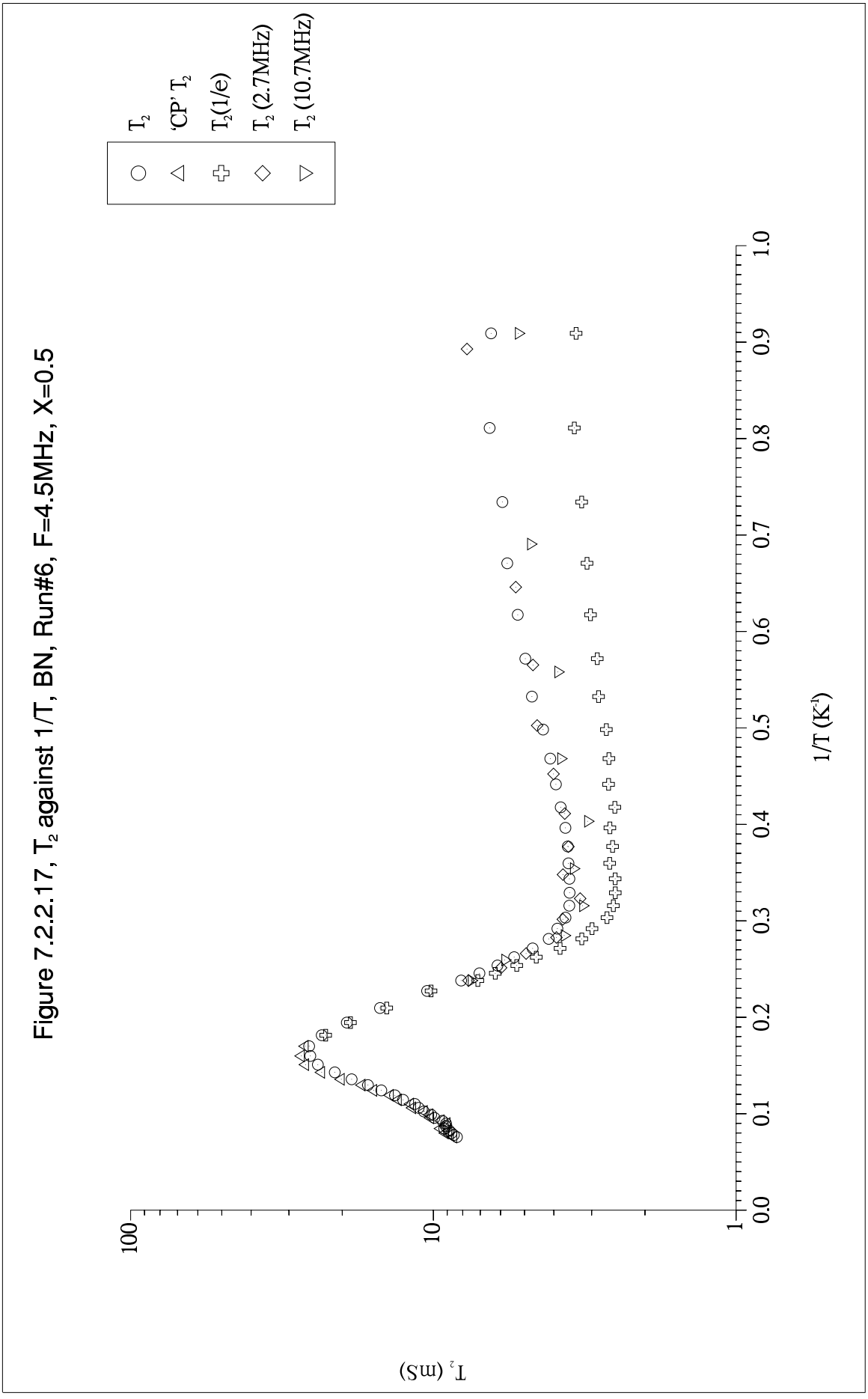
Figure 7.2.2.17, T2 against 1/T, BN, Run#6, F=4.5MHz, X=0.5
T2 (mS)
1/T (K-1)
100
10
1
0.0
0.1
0.2
0.3
0.4
0.5
0.6
0.7
0.8
0.9
1.0
T2
'CP' T2
T2(1/e)
T2 (2.7MHz)
T2 (10.7MHz)

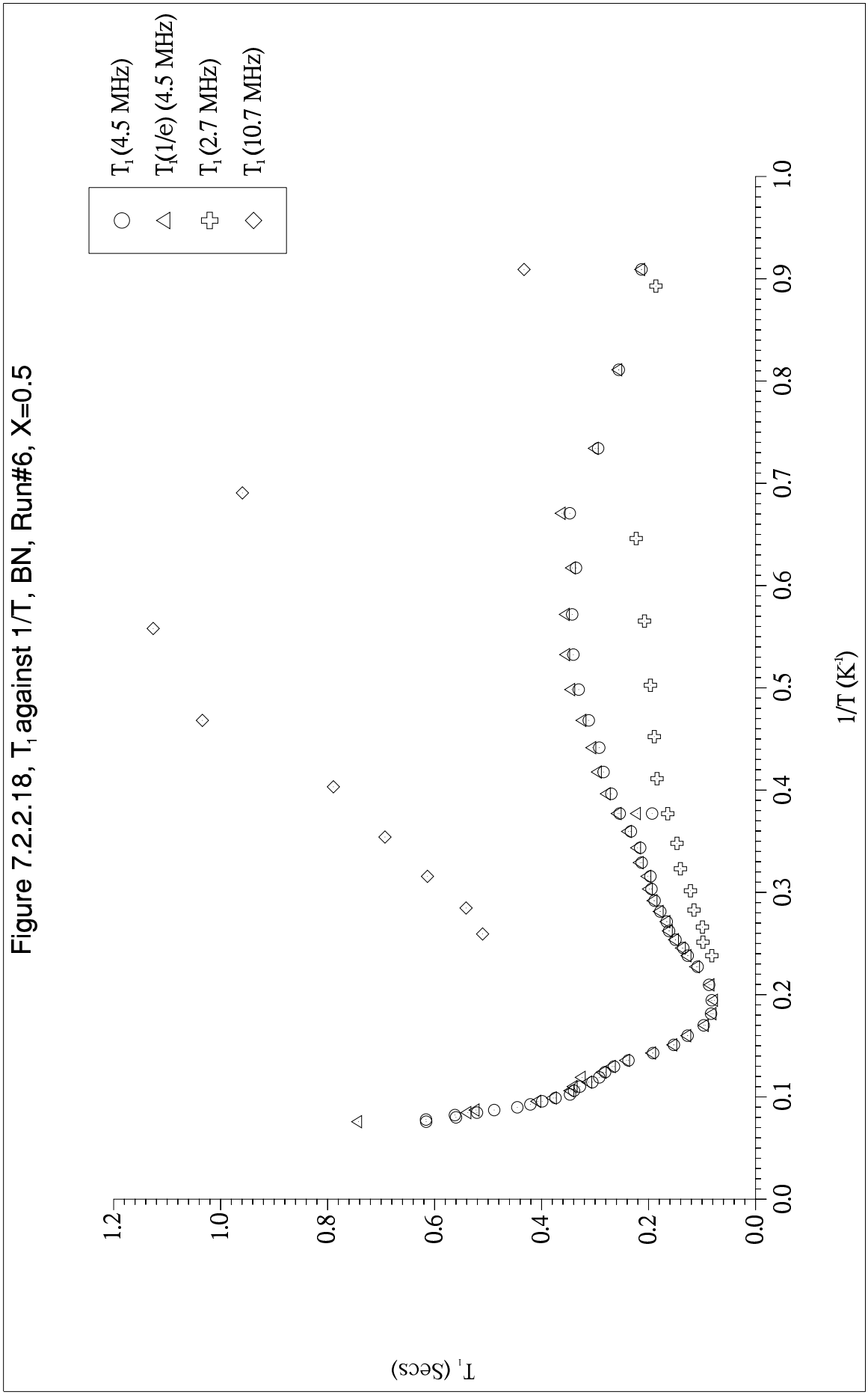
Figure 7.2.2.18, T1 against 1/T, BN, Run#6, X=0.5
T1 (4.5 MHz)
T1(1/e) (4.5 MHz)
T1 (2.7 MHz)
T1 (10.7 MHz)
T1 (Secs)
1/T (K-1)
0.0
0.2
0.4
0.6
0.8
1.0
1.2
0.0
0.1
0.2
0.3
0.4
0.5
0.6
0.7
0.8
0.9
1.0

Figure 7.2.2.19, Relaxation Indices vs 1/T, BN, Run#6, F=4.5MHz, X=0.5,
With Straight Line Fit through 'T1Index' for $0.91K^{-1}<T<0.25K,^{-1}$
(T1Index = 0.21 (1/T) + 0.62)

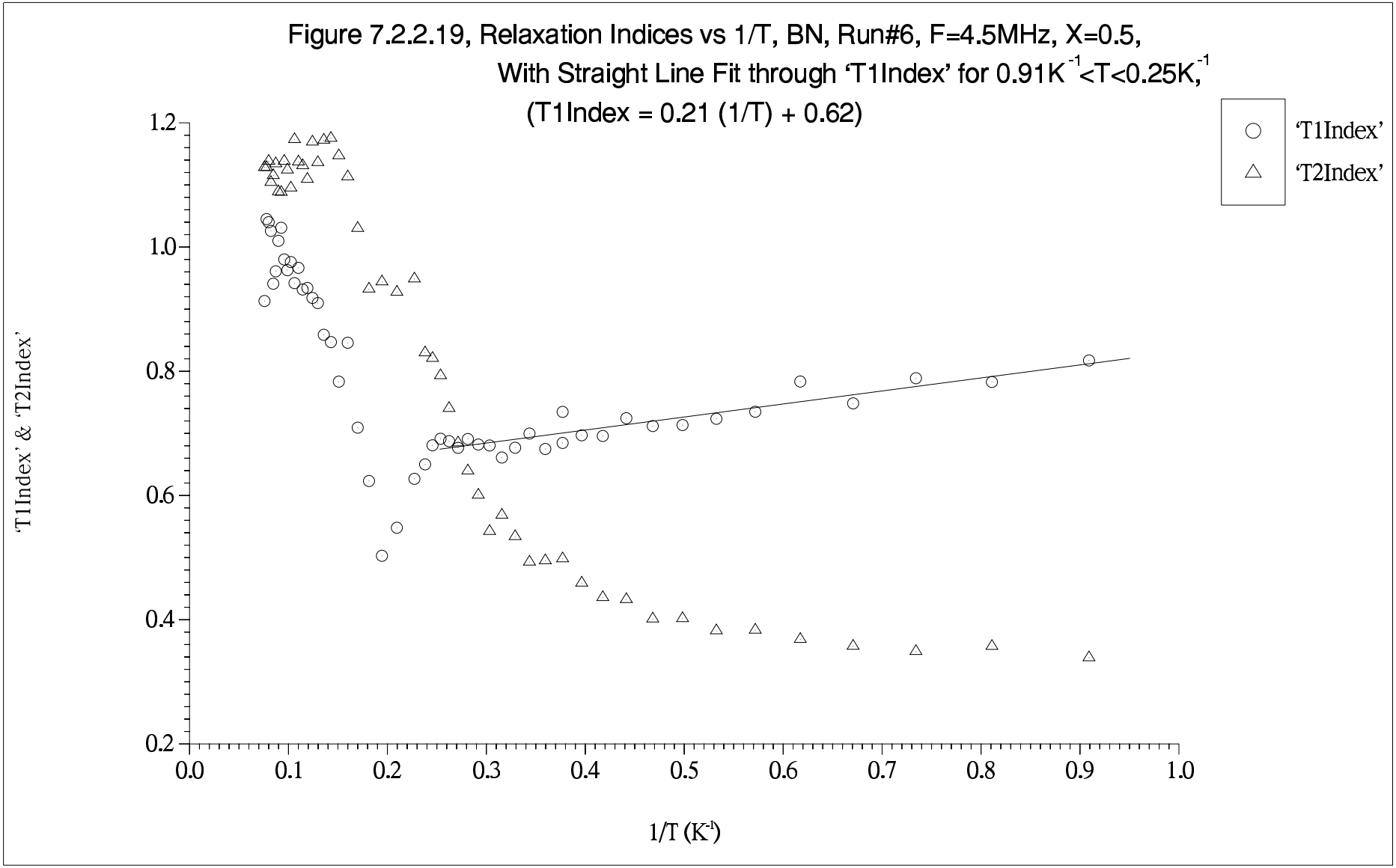

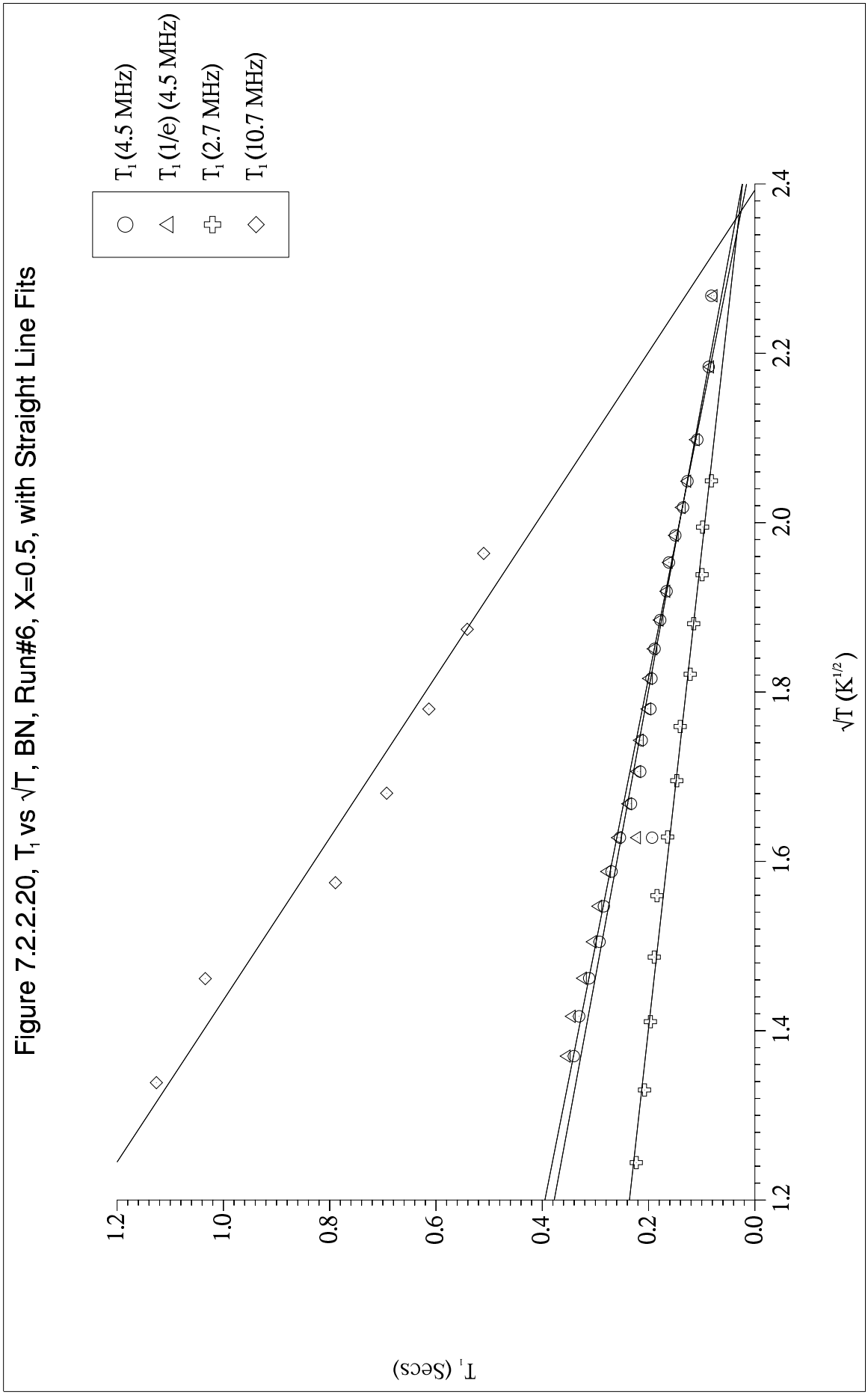
Figure 7.2.2.20, T_1 vs $\sqrt{T}$, BN, Run#6, X=0.5, with Straight Line Fits
T_1 (4.5 MHz)
T_1 (1/e) (4.5 MHz)
T_1 (2.7 MHz)
T_1 (10.7 MHz)
T_1 (Secs)
$\sqrt{T}$ ($K^{1/2}$)
0.0
0.2
0.4
0.6
0.8
1.0
1.2
1.4
1.6
1.8
2.0
2.2
2.4

spins − see below†. Recapping briefly: T_1 at $T<T^{max}$ is determined primarily by changes in the internuclear separations (in particular Substrate−^{3}He) due to registering but T_1 for $T^{max}<T<T^{min}$ is dominated by reductions in τ_c as $(\omega_x\tau_c)_{min}$ is approached, where $\omega_x=\omega_0$ in the case of a homonuclear minimum. Recalling equations 1.10.4.2 and 1.10.4.3, $T_1 \propto \omega_0^2\tau_c$ for $T<T^{min}$, we expect T_1 to be a strong function of frequency for $T \ll T^{min}$ with the maximum difference at τ_c(max) at T^{max}, as shown in figure 7.2.2.18.

'T1Index' (figure 7.2.2.19) is also slightly different from X=0.4. It shows a continuous fall from 0.91K^{-1} to ~0.25K^{-1} in addition to more *sub-region*/*noisy* behaviour. That it continues to fall above T^{max} agrees with the idea of the registry-melt component still being substrate-potential influenced, the residual orientational order gradually decaying with increasing temperature as far as ~0.25K^{-1} where desorption starts†.

***X*=0.6,** T_2 against 1/T is shown in figure 7.2.2.21. Once again, T_2 at the low temperature flat-region, T_2 at the minimum and the relative rate increase have all fallen with the increase in coverage. The flat-region end is less easy to locate in the broader minimum but is probably ~0.62K^{-1}. Included on the plot are data for 2.7MHz (1.1K<T<13.2K) and 10.7MHz (1.1K<T<4.2K) which again demonstrate the expected lack of frequency dependence. A new weak feature, a shallow maximum centred around ~0.67K^{-1} − ~0.75K^{-1} is apparent in the T_2 data. It appears in all four plots of figure 7.2.2.21 and is not an artifact as will become clearer with the rest of the $X\leqslant$0.75 data.

Figure 7.2.2.23 shows 'T2Index'. It is similar to the X=0.5 plot but more *noisy*. More interestingly, it goes through a shallow minimum at 0.67K^{-1} corresponding approximately to the T_2 maximum position.

T_1 against 1/T (figure 7.2.2.22) now shows a rise to a distinct plateau region in place of the maximum, extending from 0.62K^{-1} to 0.46K^{-1} at 4.5MHz and probably also 2.7MHz. Above the plateau region and below the minimum (0.46K^{-1}<T<0.24K^{-1}) the relaxation follows a 2D gas law (figure 7.2.2.24). Anticipating the rest of the $X\leqslant$0.75 data, we see the 'T2Index' minimum occurs at a temperature just below the low temperature side of the T_1 plateau.

'T1Index' (figure 7.2.2.23) is similar to X=0.5. It shows very clear *sub-region* behaviour at low temperatures and the continuous fall (neglecting intra-*sub-region* trends) from 1.1K to the minimum as seen before. Comparing the fits in figures 7.2.2.23 and 7.2.2.19 the slope of the fall of index with increasing temperature has risen from 0.21K to to 0.30K as the registered component grows relative to the gas.

Figure 7.2.2.21, T_2 against 1/T, BN, Run#6, X=0.6

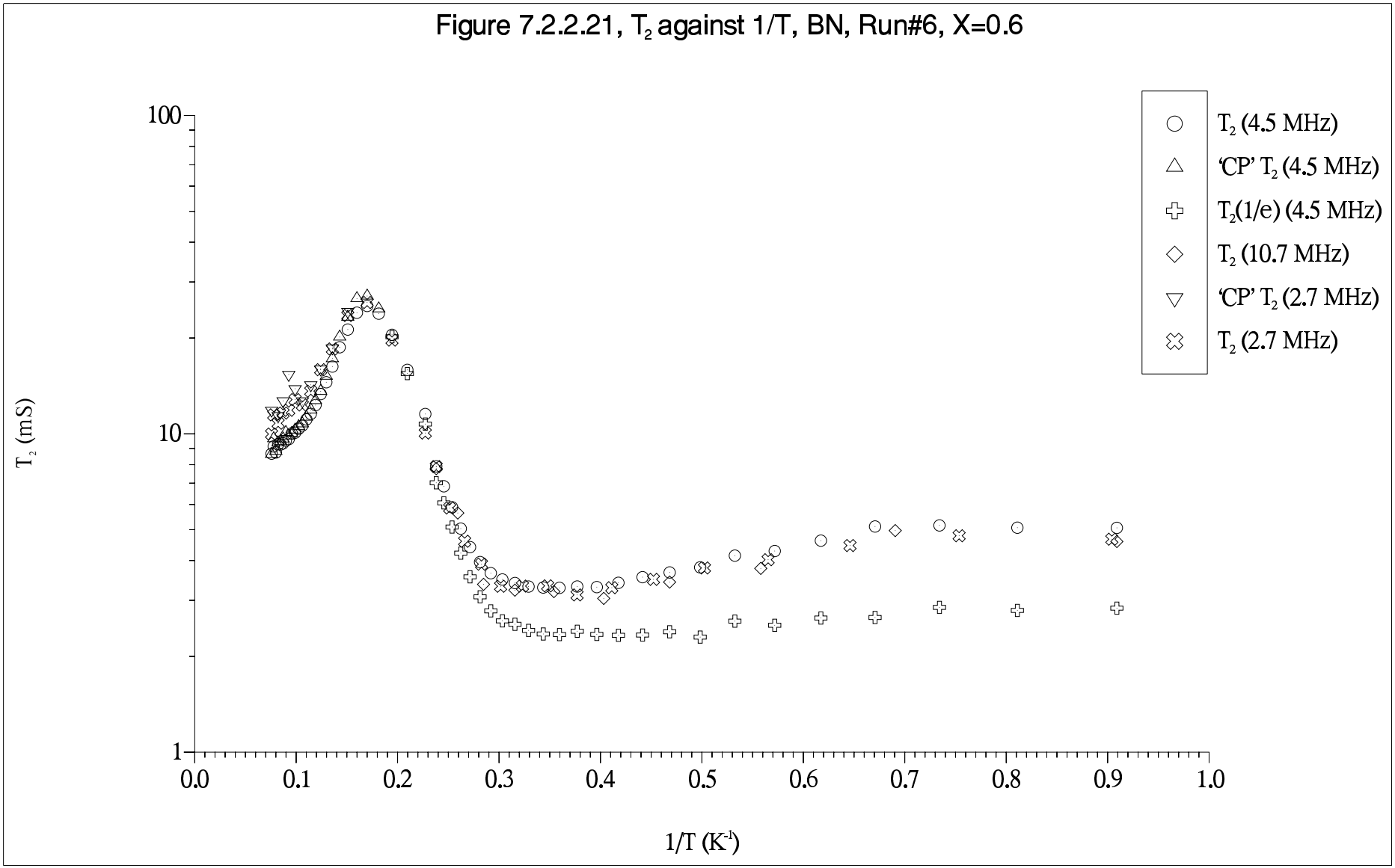

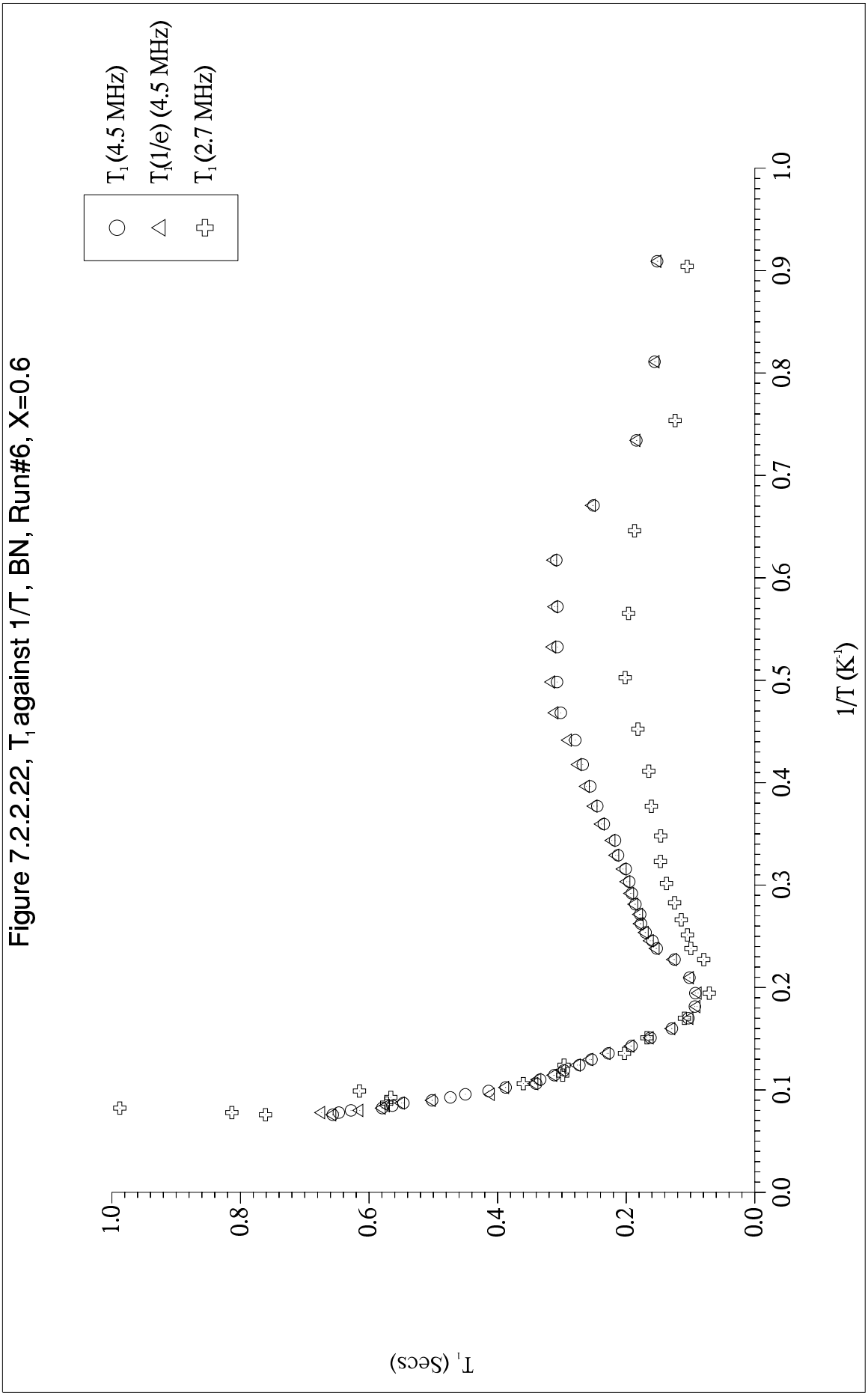
Figure 7.2.2.22, T1 against 1/T, BN, Run#6, X=0.6
T1 (4.5 MHz)
T1(1/e) (4.5 MHz)
T1 (2.7 MHz)
T1 (Secs)
1/T (K-1)
0.0
0.2
0.4
0.6
0.8
1.0
0.1
0.3
0.5
0.7
0.9

Figure 7.2.2.23, Relaxation Indices vs 1/T, BN, Run#6, X=0.6,
With Straight Line Fits through 'T1Index' for $0.91K^{-1}<T<0.25K^{-1}$,
(T1Index = 0.304 (1/T) + 0.59) [4.5 MHz]
(T1Index = 0.306 (1/T) + 0.57) [2.7 MHz]

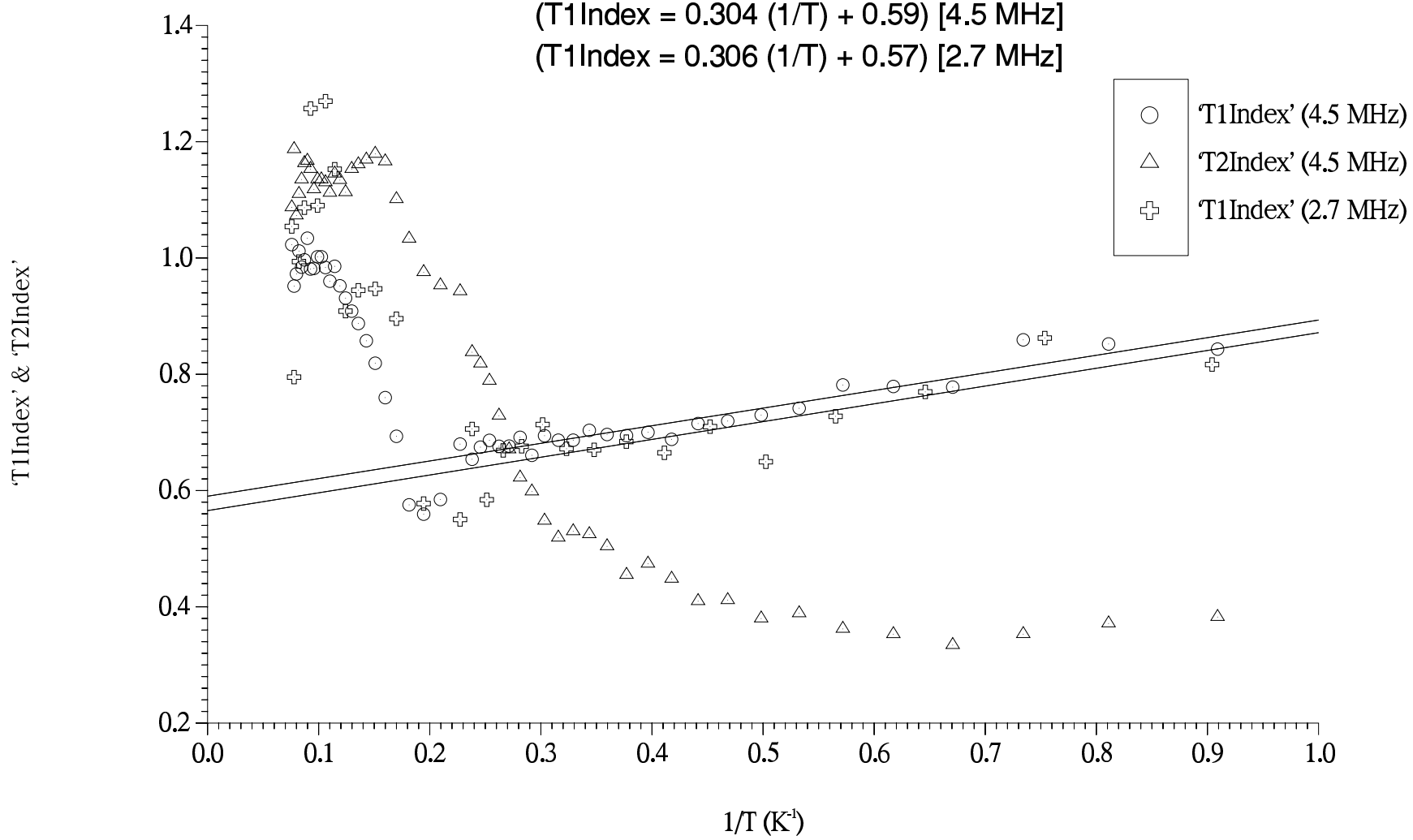

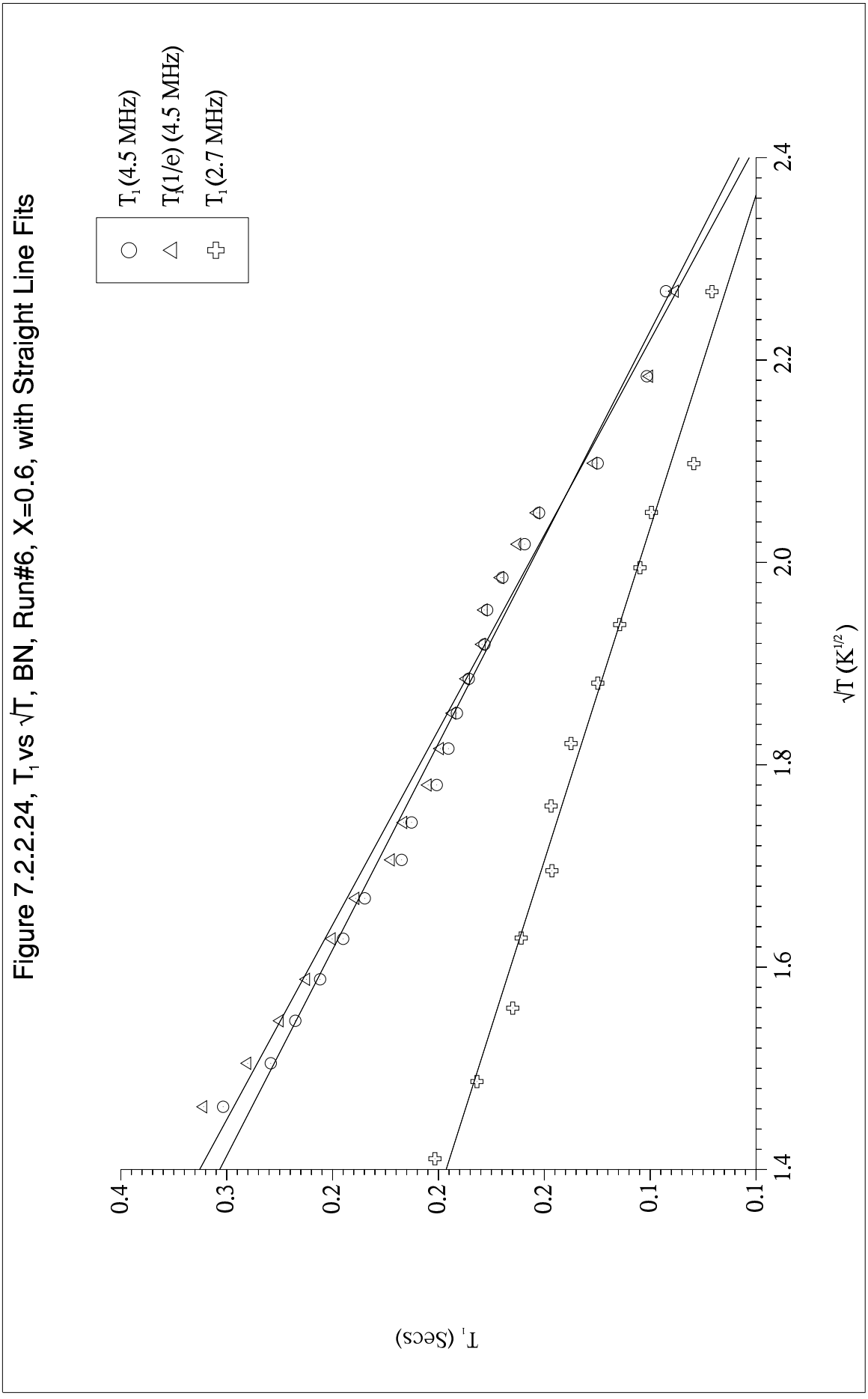
Figure 7.2.2.24, T1 vs √T, BN, Run#6, X=0.6, with Straight Line Fits
T1(4.5 MHz)
T1(1/e) (4.5 MHz)
T1(2.7 MHz)
T1 (Secs)
√T (K1/2)
0.4
0.3
0.2
0.2
0.2
0.1
0.1
1.4
1.6
1.8
2.0
2.2
2.4

A possible explanation for the data is as follows: As temperature rises to $0.62K^{-1}$ the registered solid patches undergo a change in which the long-range substrate imposed positional order is lost leaving a dense 2D fluid (liquid?) phase which, due to the substrate potentials still has considerable orientational order with an enhanced probability of a ^{3}He being found over one in every three BN hexagons. Destruction of the long-range positional order dramatically affects T_1 by disrupting magnetic coupling with the substrate spins but makes little difference to T_2 since there is little change in either $<\tau_c>$ or the ^{3}He−^{3}He $<r_{ij}>$. Moreover the mobile spins probably still experience significant relaxation by the very short-T_2 0.05 monolayer solid patches. The small T_2 maximum on the T_1 plateau's low temperature shoulder is consistent with the phase change and the limited effect it is expected to have on T_2. At the transition temperature, relaxation by a coexistence of long-range-positional-order-present (LRPOP) and long-range-positional-order-absent (LRPOA) components should reduce 'T2Index' to a minimum at that point. Above the transition temperature the rise in 'T2Index' indicates the move towards single component (ie. LRPOA) relaxation. From $0.62K^{-1}$ to $0.46K^{-1}$ T_1 is constant, there being little change in density in the substrate influenced LRPOA-registry-*melt*/dense fluid, relaxation still being mainly via the substrate spins with the dense fluid acting like the registered solid but with reduced efficiency. In this respect the LRPOA dense fluid is like the temperature-independent exchange modulated 2D solid. For $0.46K^{-1}<T<0.24K^{-1}$ T_1 decreases towards the minimum following a gas law (figure 7.2.2.24) as the orientational order disappears leaving an isotropic fluid relaxed by mechanisms driven by classical particle motion. The most striking 'T1Index' *sub-region* behaviour occurs for $T<0.62K^{-1}$ and presumably reflect the details of the process in which long-range-positional-order is lost. None of the heat capacity work on the ^{3}He/graphite system has shown heat capacity peaks around 1.7K as would be expected if the above described two-stage transition occurred there. However, the lower adsorption potential and slightly larger substrate mesh could lead to significant qualitative differences between X/BN and X/graphite systems (§3.3). Alternatively, it may simply be that the magnetic coupling with the BN substrate spins makes T_1 a uniquely sensitive probe of the registered and partially registered film's state.

***X*=0.7,** Figure 7.2.2.25 shows T_2 plotted against $1/T$. Again, T_2 at the low temperature flat-region, T_2 at the minimum and the relative rate increase have all fallen. In a reversal of trend the low temperature flat-region now appears to extend to higher temperatures, probably ending at ~$0.58K^{-1}$ with the 2D gas component influence much

reduced this close to perfect registry. The minimum position has also shifted significantly upwards in temperature butting up against the desorption edge as the PMI/ fluid relaxation only becomes effective when enough fully delocalised fluid *melt* is present. The shallow T_2 maximum around $0.7K^{-1}$ is present again, as is the corresponding but now broader minimum in 'T2Index' (figure 7.2.2.27) which now extends in temperature up to ~$0.57K^{-1}$.

The rise of 'T2Index' to super-exponentiality above the minimum is interrupted by a distinct new minimum (the beginnings of which are also just visible at X=0.6). At $0.28K^{-1}$ it is coincident with the T_2 minimum. Presumably this reflects the new abruptness of the onset of the PMI/fluid relaxation mechanism now essentially from *melt* spins only, the additional parallel non-dipolar relaxation reducing the index to a minimum until desorption takes over.

T_1 is similar to before, with the plateau low temperature shoulder at about $0.57K^{-1}$, ie. the (high temperature side of the) 'T2Index' minimum. The shift up in temperature (from $0.67K^{-1}$ at X=0.6) of the proposed first transition in which long range positional order in the registered patches is lost, is not unexpected as the patches grow and the residual energetic gas component decreases − more thermal energy is required to destroy the long range order. Figure 7.2.2.29 plots T_1 against $1/T$ with X=0.4 to 0.75 for comparison purposes. More generally the temperature of both transitions increase with coverage raising the temperature range over which the plateaux exist. T_1 plateaux rather than a $\sqrt{T}$ law indicates 2D gas spins have been incorporated into the LRPOA fluid here − ie. into a single homogeneous phase. The relaxation rates at the plateaux increase with coverage due to increasing film density. This is presumed to be realised by statistically fewer 'vacancies' in the LRPOA registered fluid which leads to enhanced homonuclear relaxation (ie. on average more ^{3}He−^{3}He nearest neighbours) and more importantly enhanced heteronuclear relaxation (ie. an improved chance of a ^{3}He spin being in a registered position). Fewer 'vacancies' in the LRPOA phase are responsible for the increase in the LRPOA→isotropic fluid transition temperature observed. Beyond the plateau ~$\sqrt{T}$ gas phase relaxation is again evident (figure 7.2.2.28). A new feature in T_1, two tiny new minima have appeared at $0.27K^{-1}$ and $0.25K^{-1}$ at 4.5MHz (figure 7.2.2.26, 7.2.2.28). One minimum is also visible in the more limited 2.7MHz data. These minima occur throughout the high coverage incommensurate solid phase. The 1.1K T_1 has, for the first time fallen below the high temperature minimum value.

As before, 'T1Index' *sub-region* behaviour has increased with the largest features again occurring below the plateau. Also the *index vs* $1/T$ ($T<T^{min}$) slope has

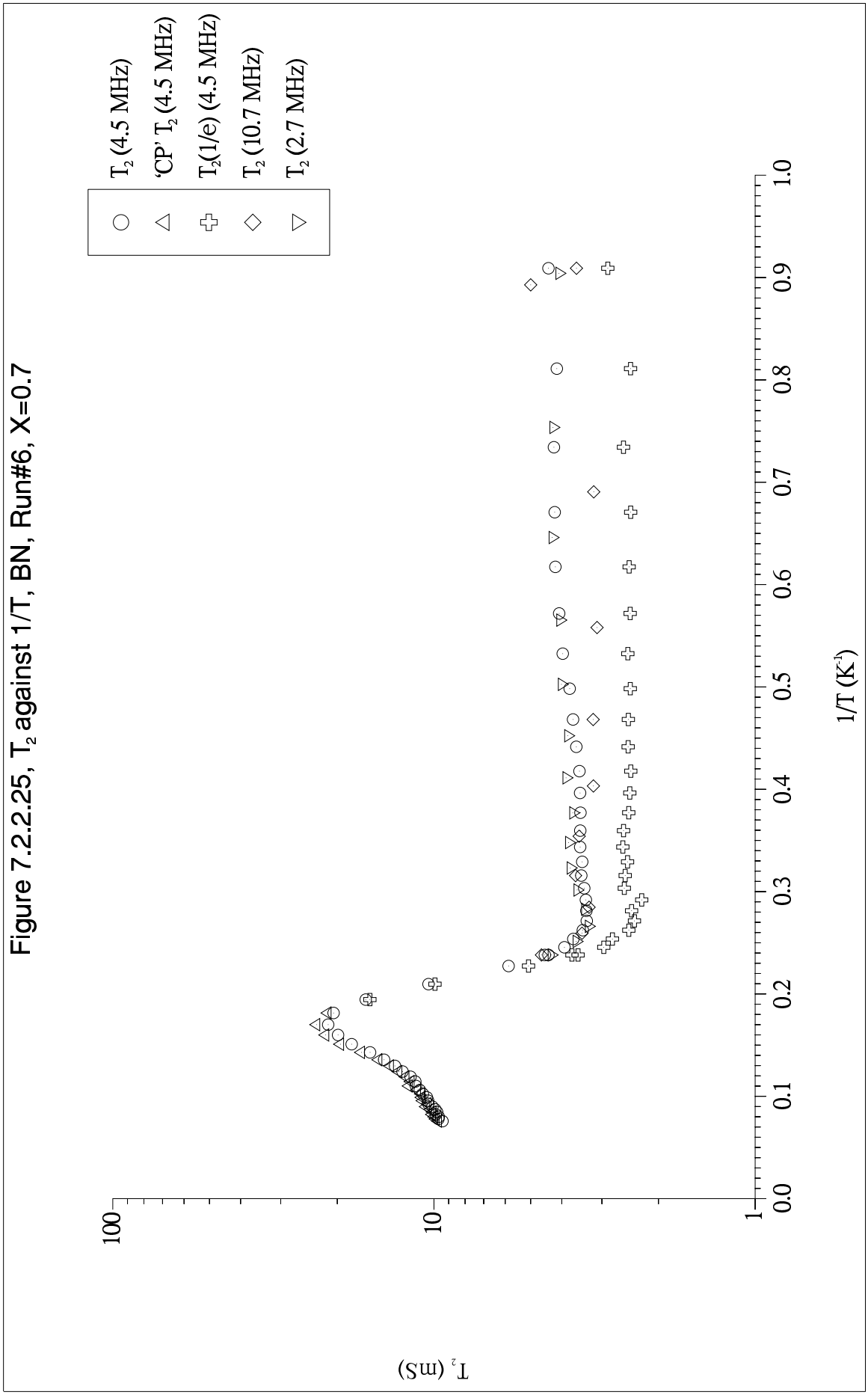

Figure 7.2.2.25, T_2 against 1/T, BN, Run#6, X=0.7

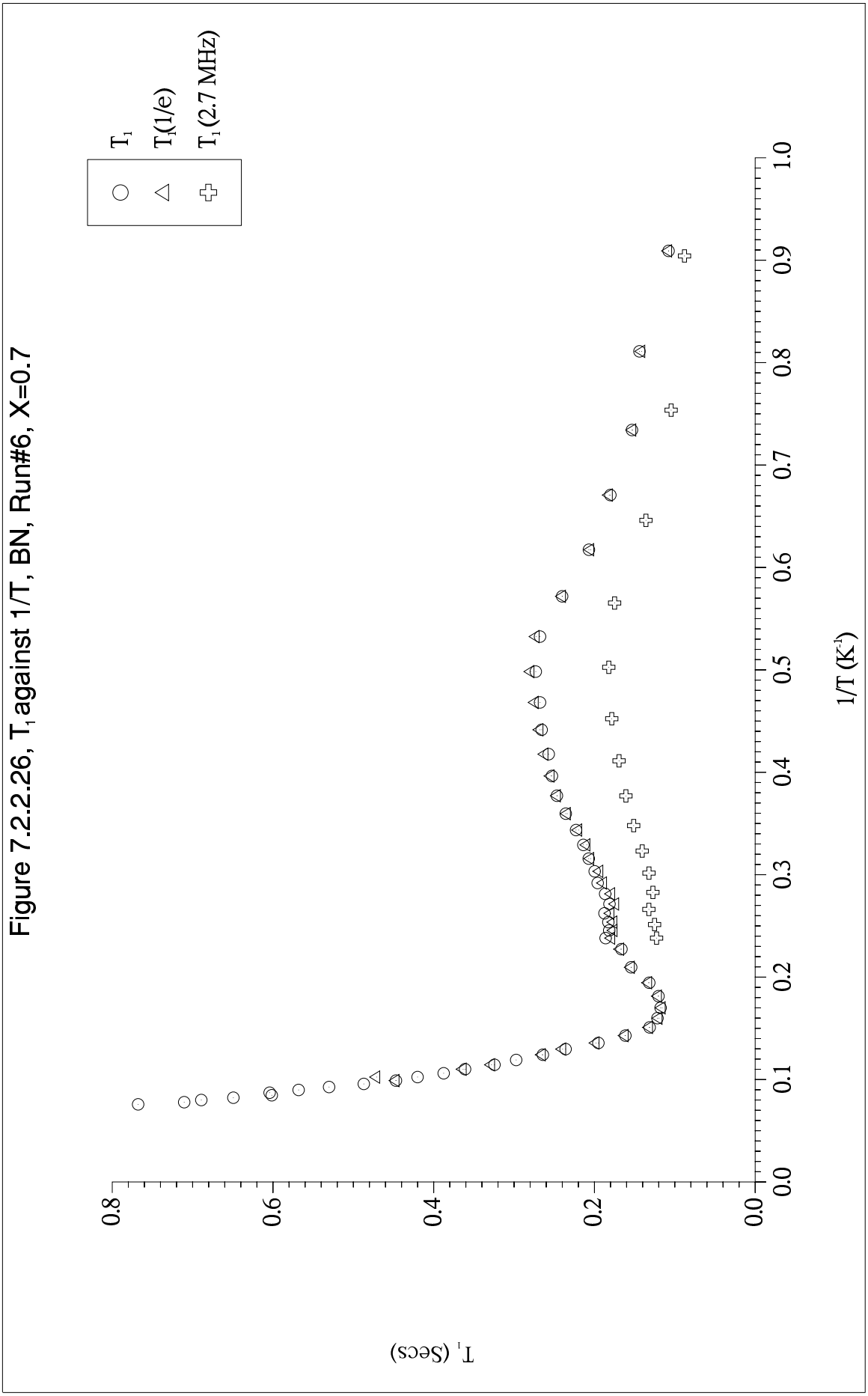
Figure 7.2.2.26, T1 against 1/T, BN, Run#6, X=0.7
T1
T1(1/e)
T1(2.7 MHz)
T1 (Secs)
1/T (K-1)
0.0
0.2
0.4
0.6
0.8
0.1
0.3
0.5
0.7
0.9
1.0

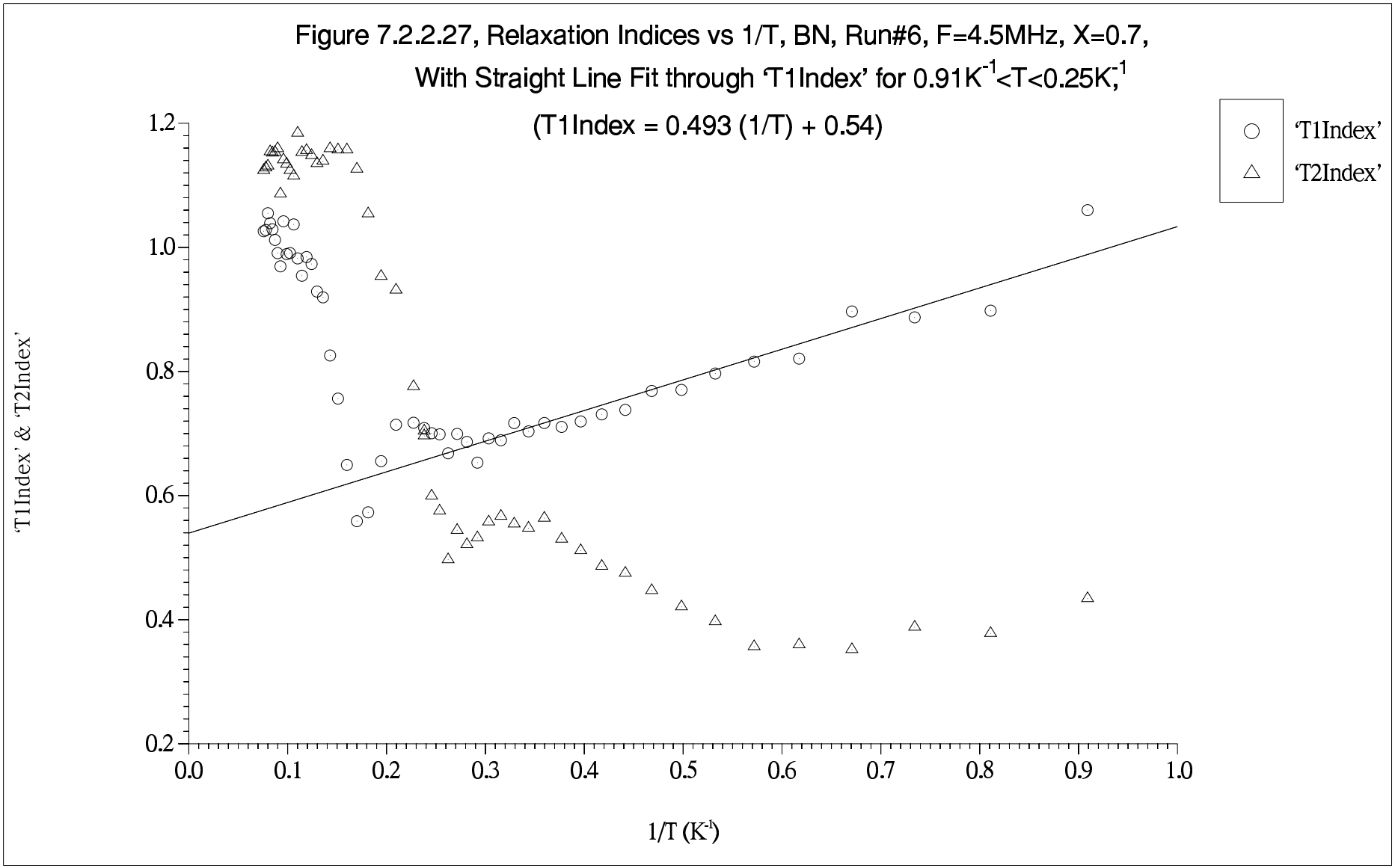
Figure 7.2.2.27, Relaxation Indices vs 1/T, BN, Run#6, F=4.5MHz, X=0.7,
With Straight Line Fit through 'T1Index' for 0.91K-1<T<0.25K-1
(T1Index = 0.493 (1/T) + 0.54)
'T1Index'
'T2Index'
'T1Index' & 'T2Index'
1/T (K-1)
1.2
1.0
0.8
0.6
0.4
0.2
0.0
0.1
0.2
0.3
0.4
0.5
0.6
0.7
0.8
0.9
1.0

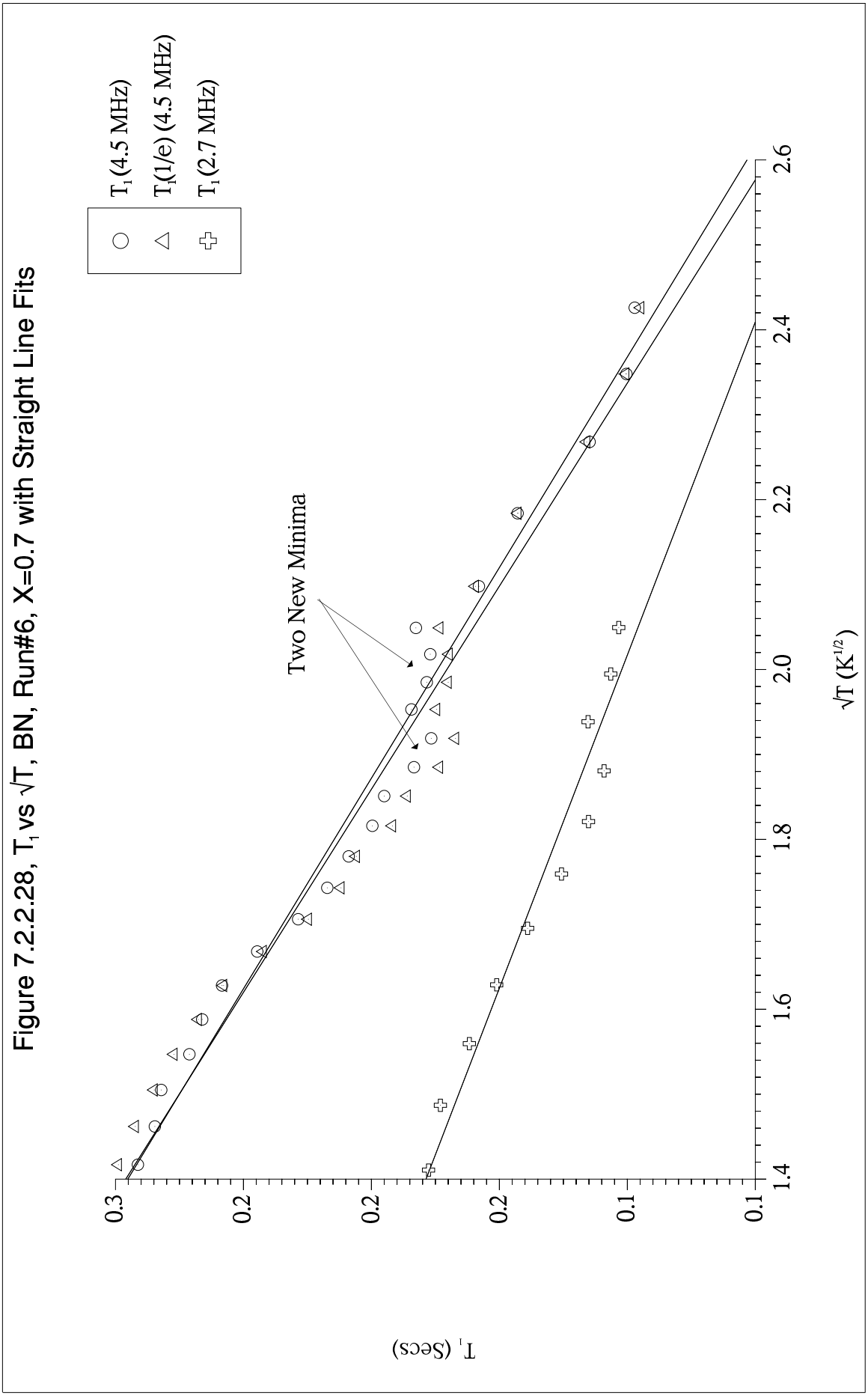

Figure 7.2.2.28, T_1 vs $\sqrt{T}$, BN, Run#6, X=0.7 with Straight Line Fits

Figure 7.2.2.29, T_1 against 1/T, BN, Run#6, F=4.5MHz, 0.4≤X≤0.75
(Lines Indicate Plateaux Regions)

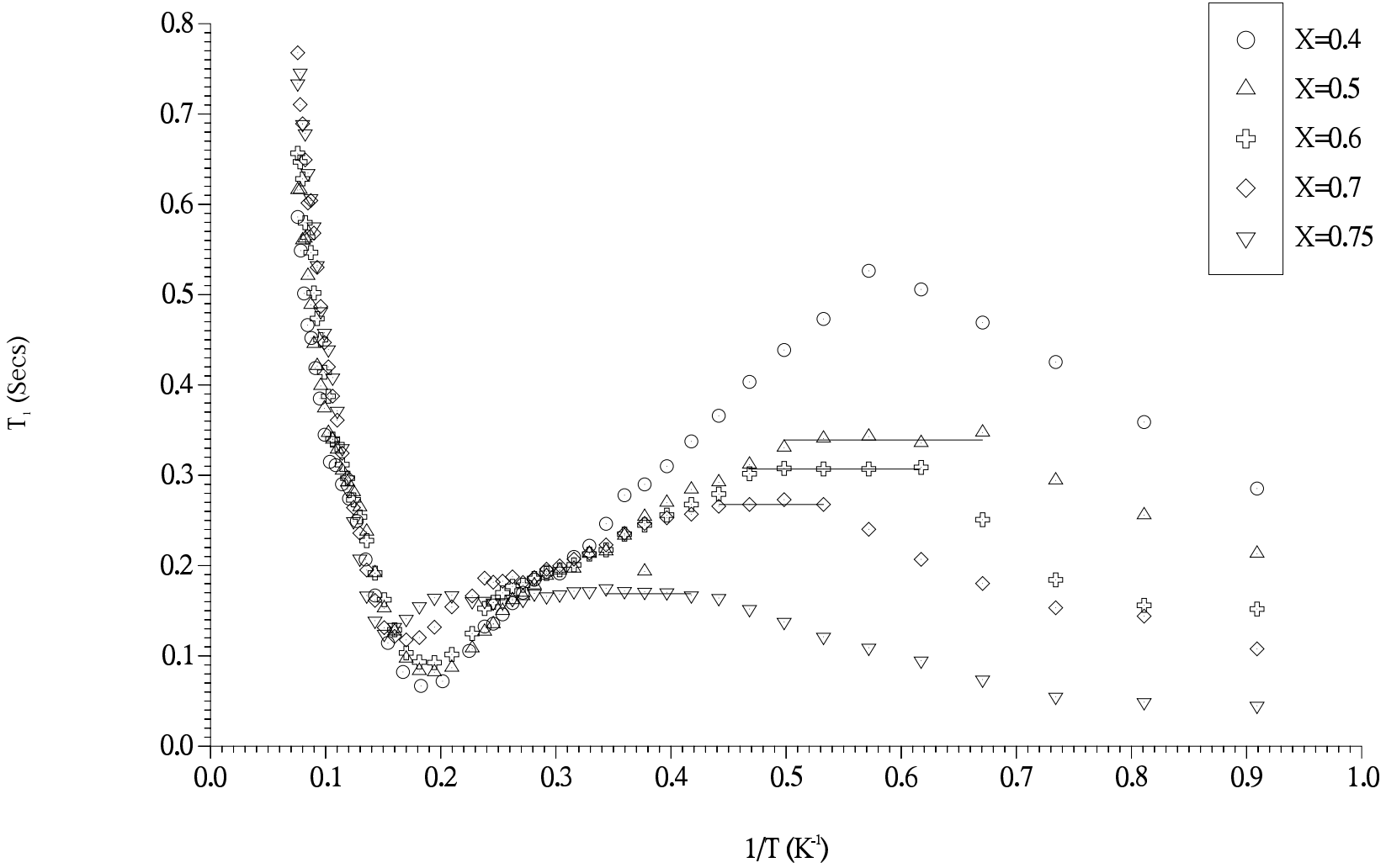

increased again as expected, from 0.30K to 0.49K.

***X*=0.75,** To within the resolution of the grid of coverages investigated, X=0.75 is believed to be perfect registry. The most dramatic set of changes in the data at any coverage w.r.t. both neighbouring coverages occur here. Starting with T_2 (figure 7.2.2.30), it has become more temperature independent at low temperatures compared with previous coverages, following the now well established trend. A distinct new minimum at an increased temperature, centred on ~0.24K^{-1} has appeared and is noticeably sharper than at X=0.2 for example. Using the inset in figure 7.2.2.30 which shows the low temperature data in greater detail, it is evident that the fall-off in T_2 starts at 0.34K^{-1} ≡ 2.9 ± 0.1K. With heat capacity measurements showing the X=0.0636Å^{-2} ^{3}He/Graphite order-disorder transition occurring at 3K (§1.8.3) we interpret the fall-off in T_2 as the onset of that transition, the resultant 2D gas spins relaxing via the PMI/fluid mechanism. Grafoil, by comparison shows little change in either relaxation time with temperature through the order-disorder transition [60,64] (see also §1.10.4). The almost temperature independence of T_2 below 3K indicates the near absence of gas phase spins expected at perfect registry. Recall figure 7.2.1.1 showed a maximum in T_2 *vs* X at X=0.75 at ~1K, a surprising feature considering the motional slowdown and spatial ordering on registering and the Grafoil results have either minima or no change. Figure 7.2.2.34 plots T_2 against 1/T for X=0.7, 0.75 & 0.8 together for comparison. T_2 at 0.75 monolayers is consistently longer than at X=0.7 as far as desorption (0.24K^{-1}) and also longer than at X=0.8 up to 0.38K^{-1} where it starts to rise in the prelude to melting of the incommensurate solid (actually DWL, see later). Similar results are obtained at 2.7 MHz. One possible cause which must be examined is the reduction of the substrate spins' magnetisation by ^{3}He RF pulses which in turn degrades the effective ^{3}He equilibrium magnetisation for a period several times T_1(substrate spins), (§3.5.1). However the data was always taken starting with the shortest inter-pulse delays after approximately 10 minutes for thermal equilibrium after changing temperature. The additional reduction in the signal height at longer delays as data collection continued would therefore shorten the observed T_2 not lengthen it. See also below‡. Without appealing to an unknown coupled relaxation effect with substrate spins, the best potential explanation here is the loss of the 2D gas/PMI relaxation channel as X=0.7→0.75 increasing T_2, followed by the decrease in the ^{3}He−^{3}He $\langle r_{ij} \rangle$ as X=0.75→0.8 when the incommensurate solid (actually DWL, see later) forms which reduces the exchange frequency and hence T_2. A quantitative analysis to determine the

Figure 7.2.2.30, T_2 against 1/T, BN, Run#6, X=0.75

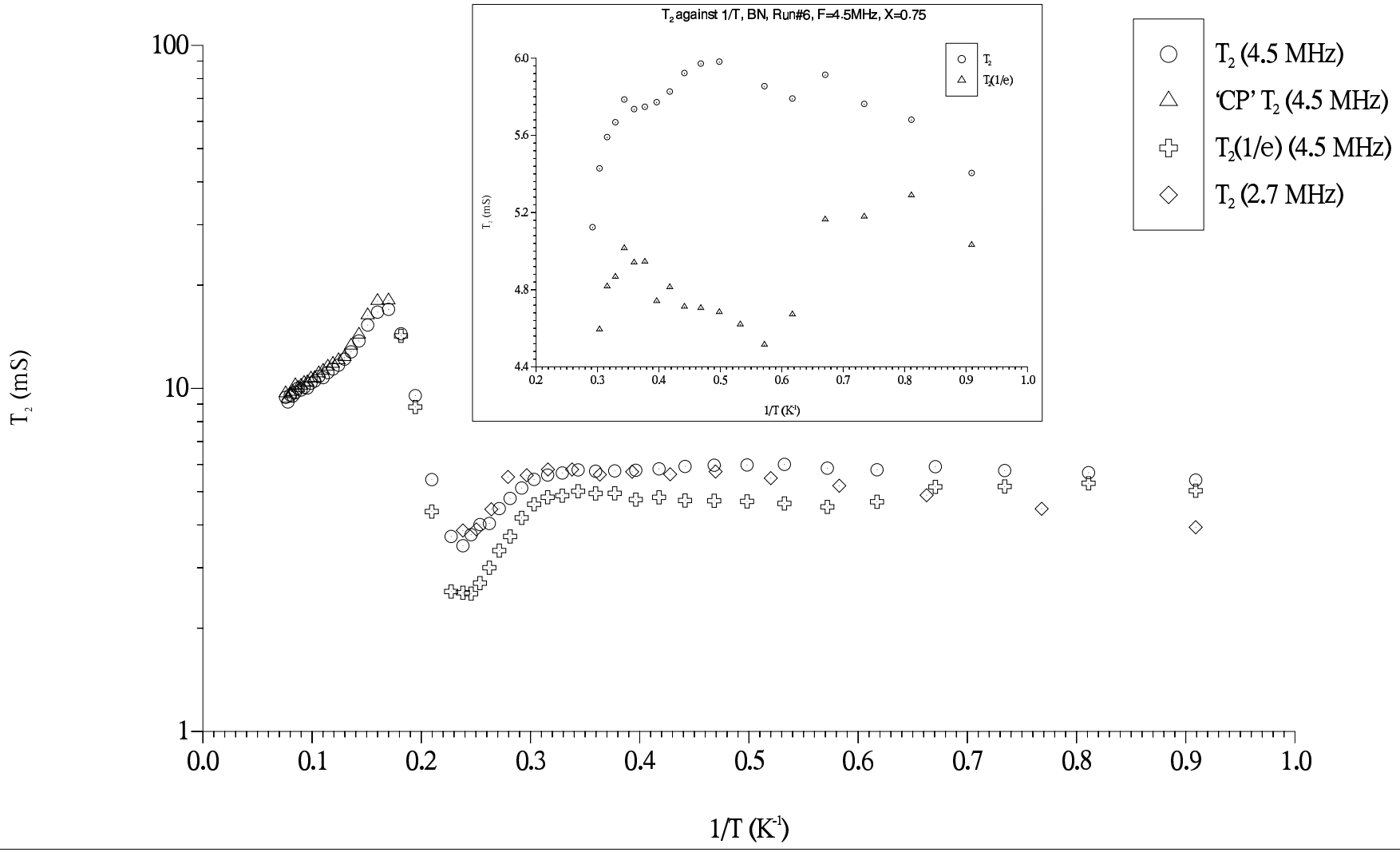

phase composition of the film as coverage approaches registry would be needed to confirm/refute this. Nuclear magnetic susceptibility measurements significantly below the 2D fluid Fermi temperature (~200mK) should provide unambiguous answers with the gas component having a Pauli law susceptibility and the registered solid a Curie one [3,206]. At X=0.75, with no 2D gas relaxation component present at low temperatures to augment T_2^{-1}, the relative relaxation rate increase at the minimum, after the order-disorder transition might be expected to have risen from its X=0.7 value. This is so.

'T2Index' against $1/T$ is plotted in figure 7.2.2.32. Features seen developing at lower coverages are fully formed here. The shallow low temperature minimum has deepened, moved up in temperature, becoming a clear, monotonically proceeding, smooth feature. Also, the higher temperature minimum coincident with the T_2 minimum at 0.24K^{-1} has deepened producing a distinct intervening flat-topped maximum. Structure in the low temperature T_2 *vs* $1/T$ data (inset, figure 7.2.2.30) falls inside the lower temperature minimum, with the largest T_2 maximum at 0.53K^{-1} coinciding with the bottom of the minimum. Using the above discussed explanations the 'T2Index' data in figure 7.2.2.32 has been annotated with the proposed phase designations. At 2.7MHz (inset, figure 7.2.2.32) 'T2Index' has the same form as 4.5MHz for $T>0.66\text{K}^{-1}$. Below this temperature however, it falls off again. T_2 at 2.7MHz, unlike at 4.5MHz, falls slowly with falling T at low temperatures. At previous coverages the temperature dependence of both T_2 and its index have been frequency independent within the quantity and quality of the data. The difference at X=0.75 is believed to be either due to insufficient time being available or the larger temperature steps used at 2.7MHz, for the long range registered structure to form properly. At 4.5MHz the 4.2K→1.1K data was taken over 13 hours in 25 equispaced steps but at 2.7MHz, in only 10 hours and 15 steps. Supporting evidence comes from 1.1K T_2-*against*-X data from Run#8 (§7.4.3.1) which was taken after rapidly pumping down to 1.1K from 4.2K following sample annealing. T_2 has the same coverage profile but its more sensitive index does not, in particular it lacks the sharp maximum at X=0.75 (figures 7.2.1.6 and 7.4.3.2). The physical reason for these differences is unknown, but could be associated with the fact that three different $\sqrt{3}\times\sqrt{3}$ R30 registered sublattices are possible. As T is lowered and long-range-positional-order is imposed by the substrate on the orientationally ordered fluid, starting in patches probably at preferential adsites, the patches will grow until their walls butt up against one other. The difference in rapidity and size of the temperature fall when a new temperature is selected by the computer may have a considerable impact on the outcome when growing mutually incompatible competing registered domains meet each other.

Figure 7.2.2.31, T_1 against 1/T, BN, Run#6, X=0.75

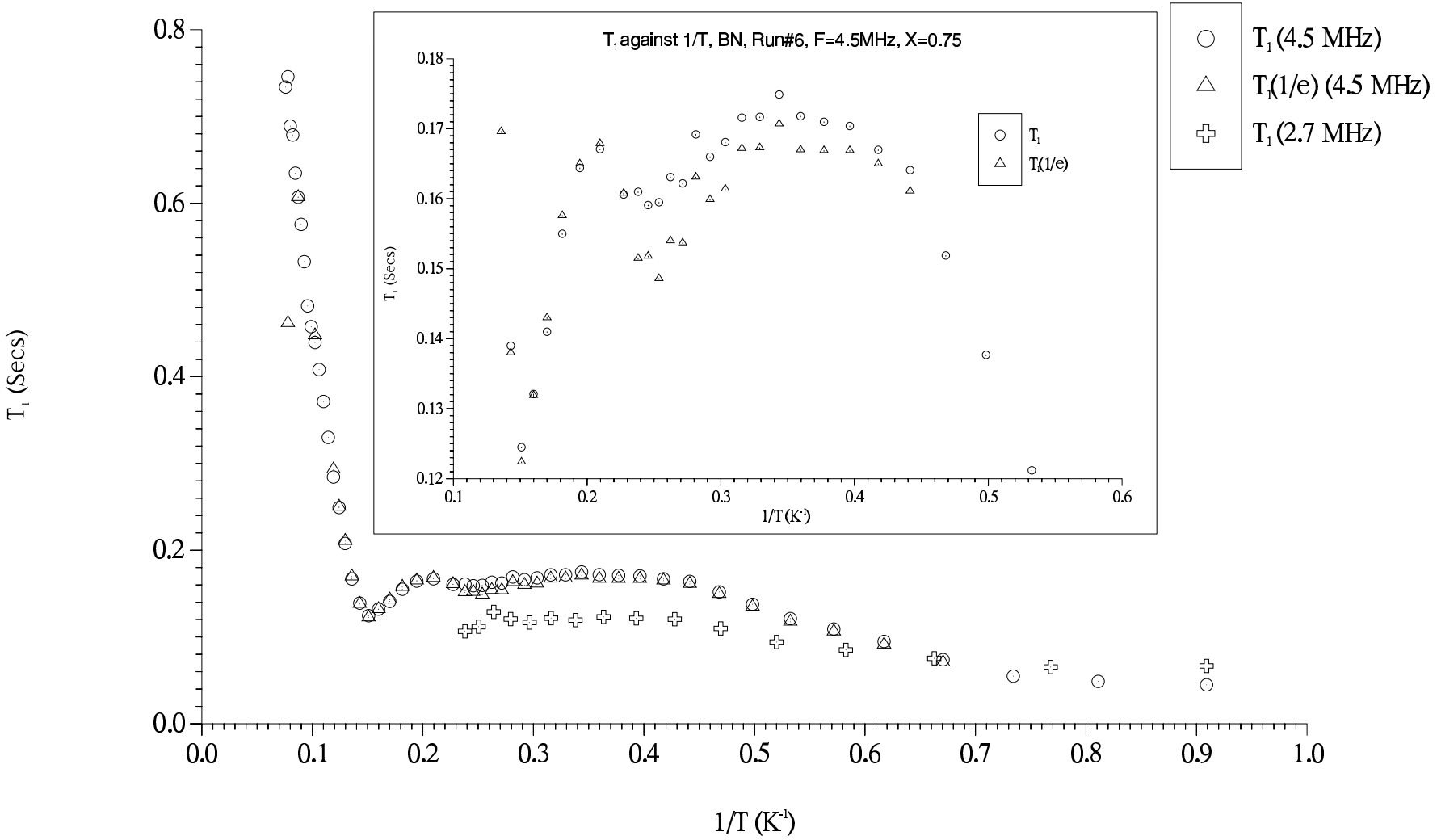

Figure 7.2.2.32, Relaxation Indices vs 1/T, BN, Run#6, F=4.5MHz, X=0.75,
Straight Line Fit Throught Data (not shown) for,
$0.91K^{-1} < T < 0.25K^{-1}$ gives,
(T1Index = 0.823 (1/T) + 0.473)

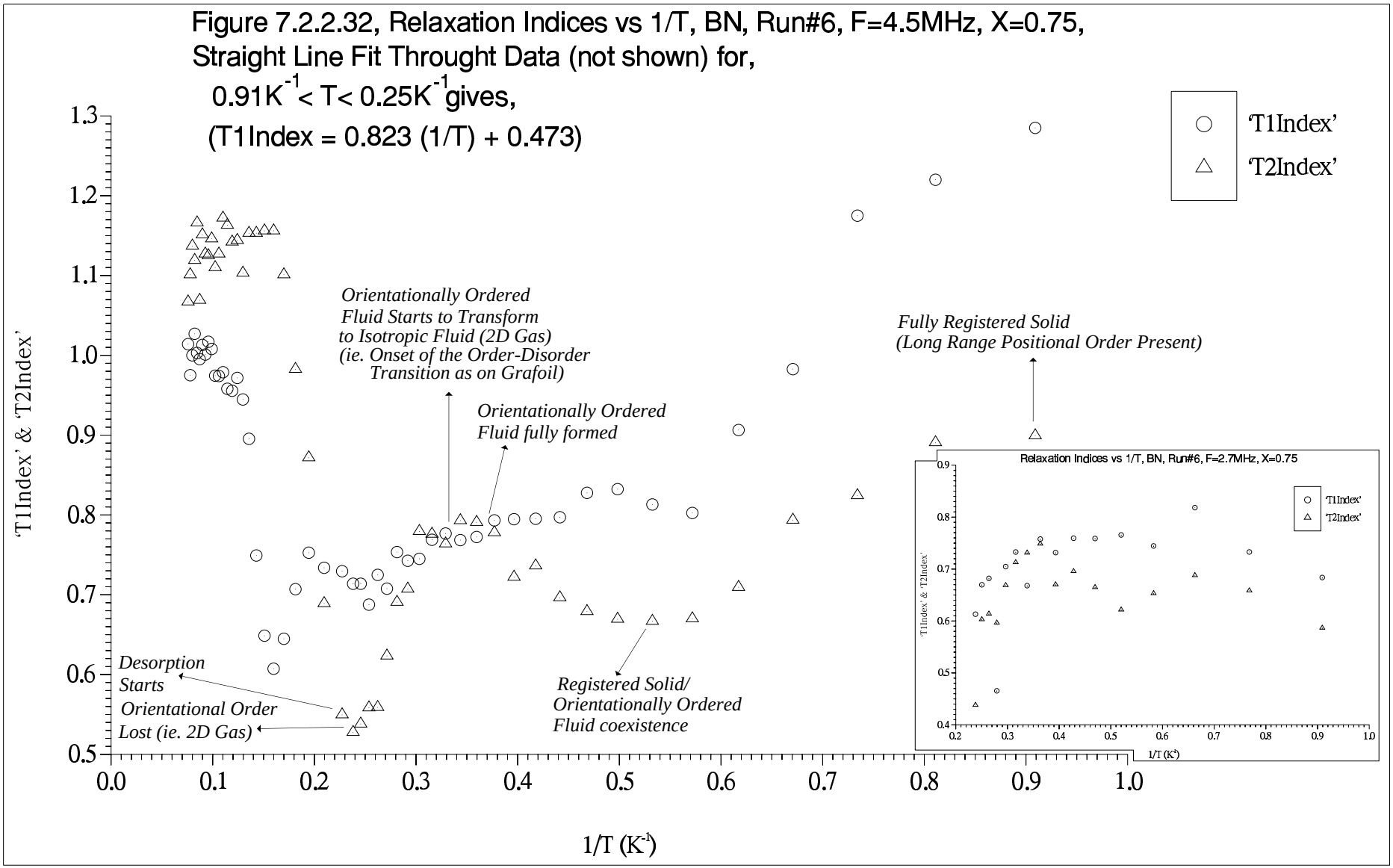

T_1 at 1.1K has fallen to 44.9mS, almost its lowest value anywhere in the run, the high temperature minimum value being 124.3mS, (figures 7.2.2.29, 7.2.2.31). With the loss of the 2D gas component the LRPOP $\rightarrow$ LRPOA transition has shifted from $0.57K^{-1}$ to much higher *T*. Again the plateau low temperature shoulder coincides with the 'T2Index' minimum. From the clearer 'T2Index' minimum it is evident its high temperature side corresponds to the high temperature end (T~$0.4K^{-1}$) of the T_1 plateau low temperature shoulder close to where the orientationally ordered fluid is believed to be fully formed (figure 7.2.2.32). Figure 7.2.2.31's inset presents the plateau region in more detail. It shows the fall off from its high temperature side also starting at $0.34K^{-1}$ in accordance with the T_2 data and its interpretation as the onset of the order-disorder transition where the orientationally ordered fluid transforms to an isotropic 2D gas. The fall off in T_1 towards the main minimum at $0.15K^{-1}$ is interrupted by the small minimum (minima?) at $0.24K^{-1}$, the T_2 minimum position. A $\sqrt{T}$ gas law relation appears to operate on both sides of this minimum (figure 7.2.2.33) but with different slopes. From $0.34K^{-1}$ ($1.7K^{½}$) to $0.24K^{-1}$ ($2.0K^{½}$) as observed at lower *X*, this occurs during the orientationally ordered fluid $\rightarrow$ 2D gas transformation when exchange motion in the orientationally ordered fluid gives way to classical particle motion in the gas. Between the small and main minima ($0.2K^{-1}$ [$2.2K^{½}$] to $0.15K^{-1}$ [$2.6K^{½}$]) the slope is increased by rapidly diffusing desorbed spins shortening the correlation time towards the main minimum. T_1 at 2.7MHz lacks the very short 1.1K value, falling to only 66.7mS which could be due in part to the faster cooling rate but is believed to be mainly due to the enhanced relaxation via the FMR mechanism at 4.5MHz as discussed in §7.2.1 and §8.

Very large *sub-region* features, the biggest at any coverage, dominate the low temperature 'T1Index' plot as T_1 falls and rises to super-exponentiality below $0.68K^{-1}$ (figure 7.2.2.32). Note also that these very large features occur for temperatures below the centre of the lowest temperature 'T2Index' minimum. This provides the clearest evidence yet that what we are seeing are the details of the establishment of the long range positionally ordered registered structure with falling temperature as the LRPOP solid dominates the LRPOA fluid and incompatible registered domains grow and meet causing discontinuities in 'T1Index'. As the proportion of fully registered spins$\rightarrow$1 relaxation via the substrate spins dominates leading to super-exponentiality (§7.2.1). Only at this coverage does the absence of 2D gas spins permit this, the average *index vs* $1/T$ slope (figure 7.2.2.32) having risen, again, from 0.493K at X=0.7 to 0.823K. Minima in 'T1Index' corresponding to both T_1 minima are again visible.

There is good evidence the magnetisation degradation effect mentioned above‡

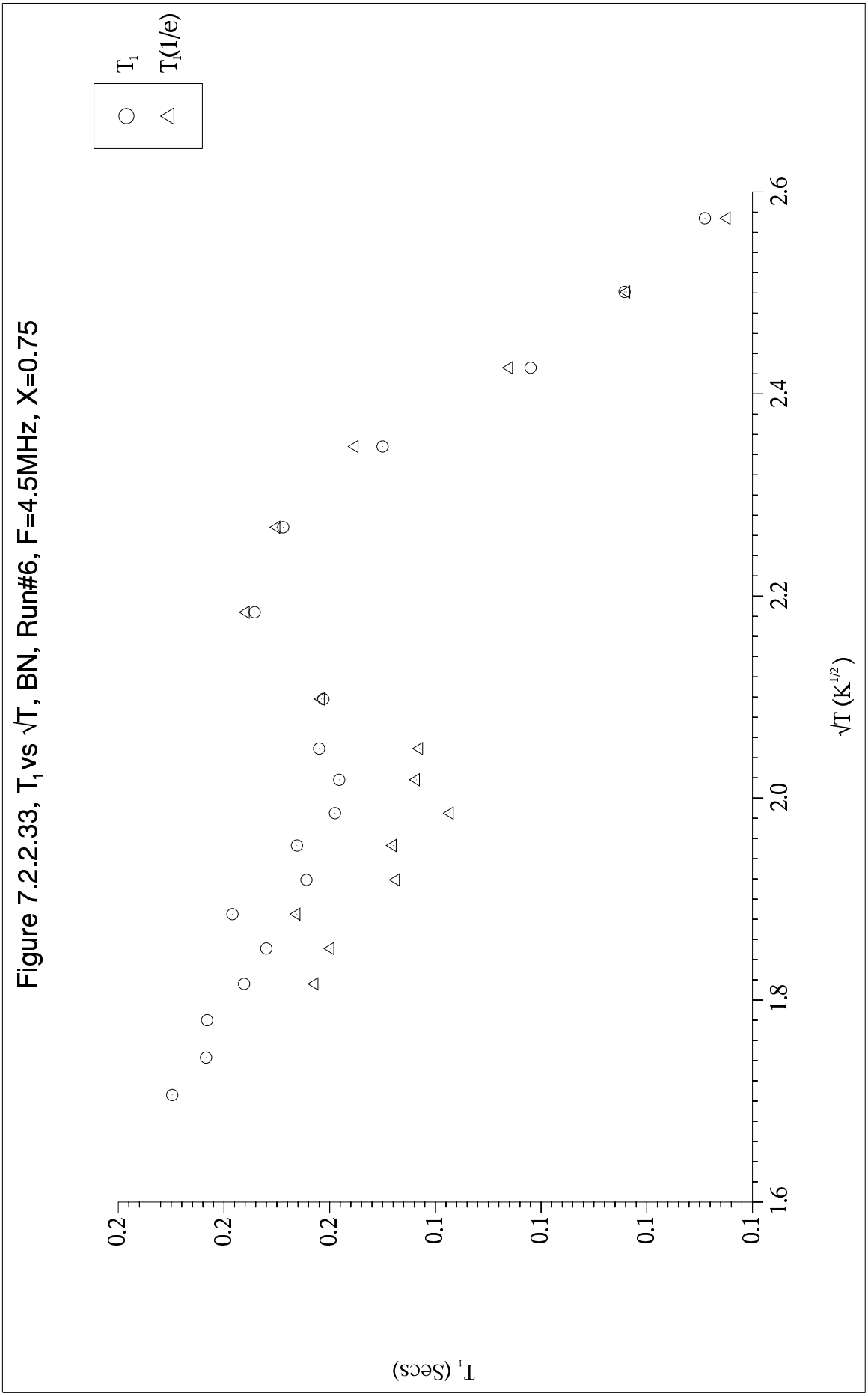
Figure 7.2.2.33, T1 vs √T, BN, Run#6, F=4.5MHz, X=0.75
T1
T1(1/e)
T1 (Secs)
√T (K1/2)
0.2
0.2
0.2
0.1
0.1
0.1
0.1
1.6
1.8
2.0
2.2
2.4
2.6

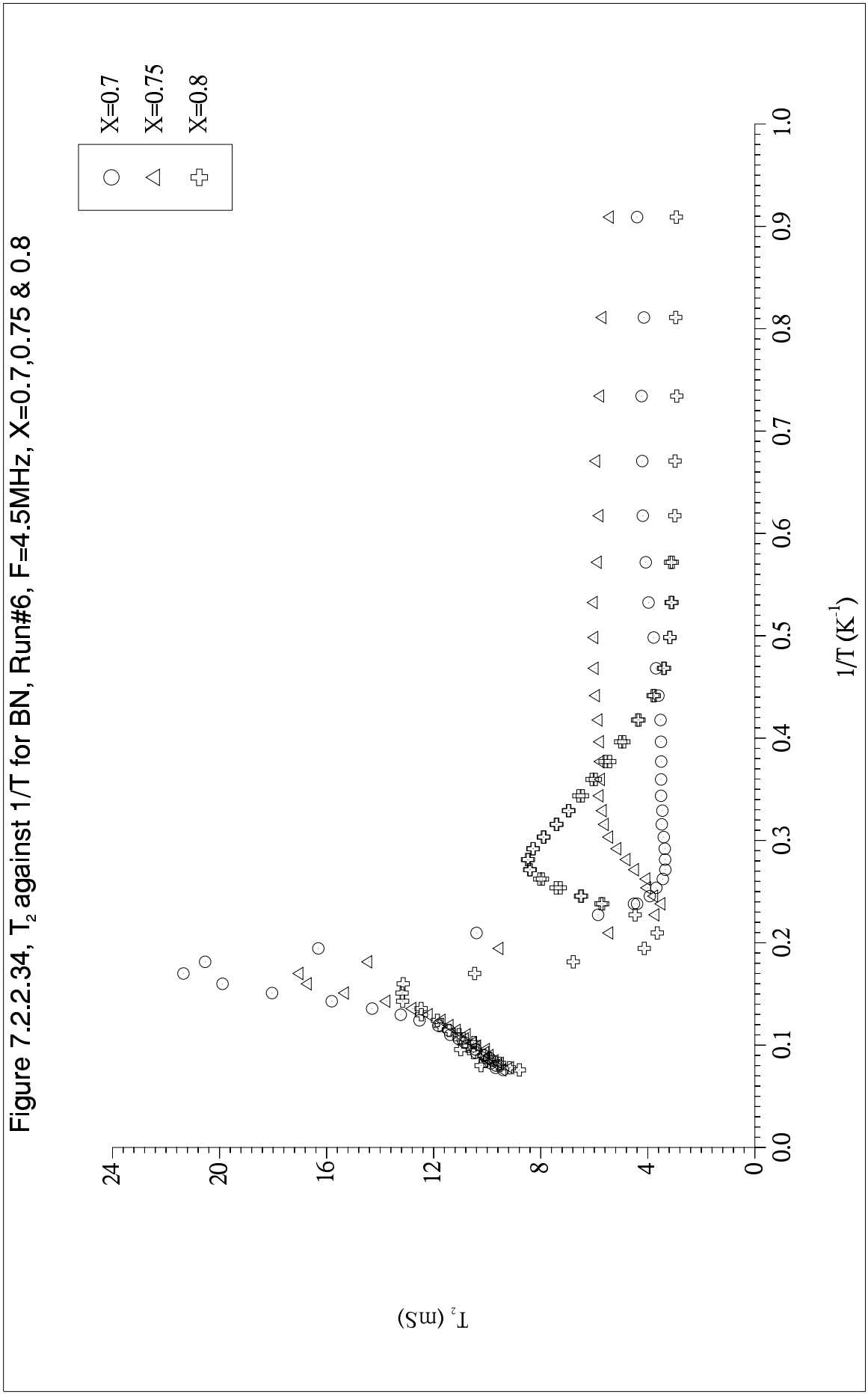

Figure 7.2.2.34, T_2 against 1/T for BN, Run#6, F=4.5MHz, X=0.7,0.75 & 0.8

Figure 7.2.2.35, 'H(0)' against 1/T for BN, Run#6, F=4.5MHz, X=0.7, 0.75 & 0.8

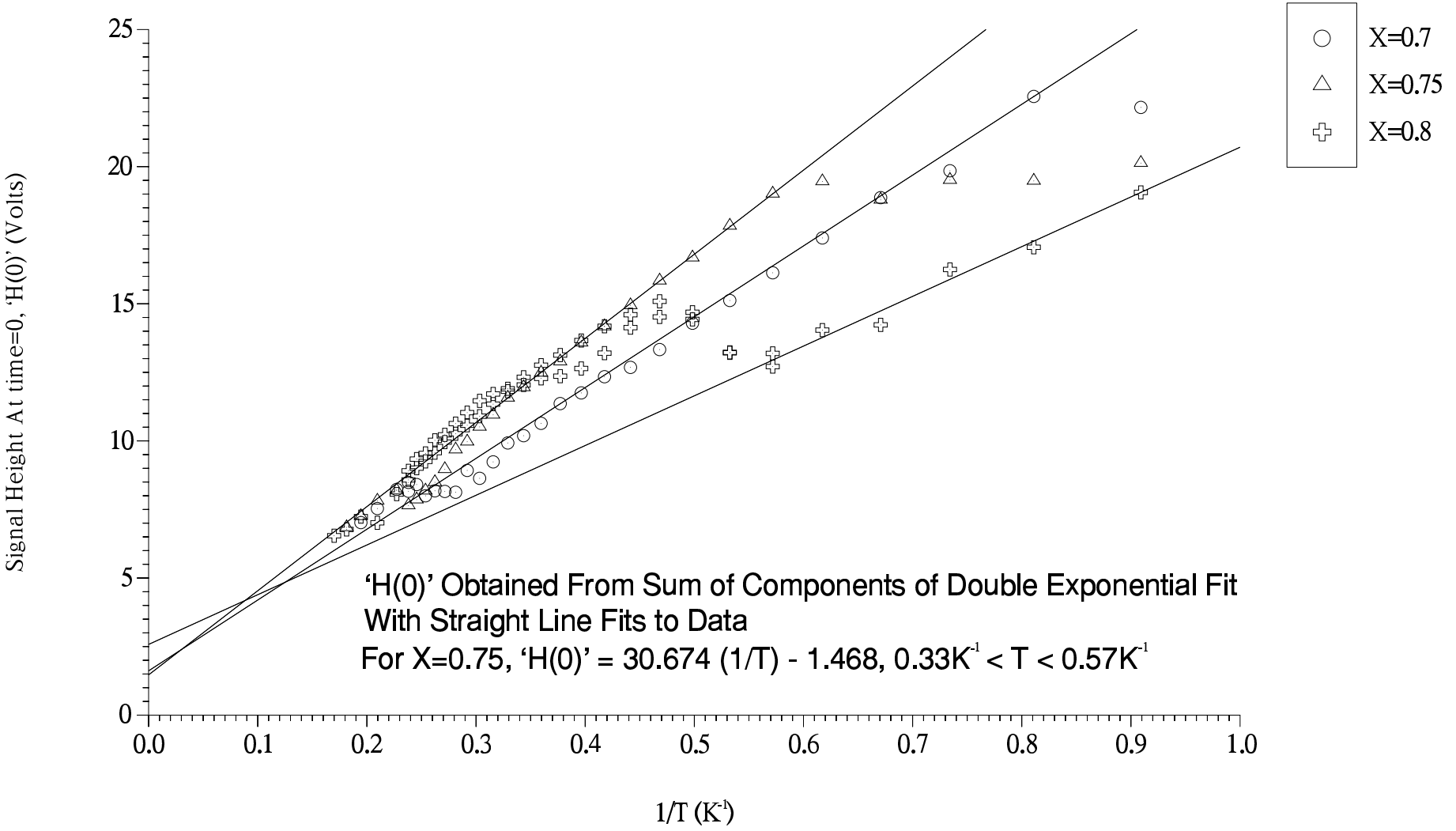

does in fact occur here. Figure 7.2.2.35 plots the equilibrium magnetisation 'H(0)'=Ha(0)+Hb(0) obtained from the double exponential fit 'TWOEXP2' (listings 6.3.2.1 and 6.3.2.2) as a function of $1/T$. It was chosen in preference to a single exponential because it produces a numerically much better fit to this low noise all-sub-exponential-decay data and lacks the unphysical behaviour of the 'T2Index' fit at the origin, the position of interest. Concerning possible effects on the relaxation times and indices the following must be borne in mind: On DLX6000 the time constant associated with producing the magnetisations depressions, the $^{3}He-^{19}F$ coupling time T_c, was short, ~200mS (at 1 Tesla). Whereas restoration of the magnetisations took several times the measured ^{19}F T_1, ~10^3 Sec. Given the way the data was taken (as shown in listing 5.3.1), namely with temperature falling, each point averaged 4 times, 30 points each per T_1 and T_2 (t,h) data set, the order the delay settings were varied in, the pulse *repetition-times* used together with the ~10 minute temperature changing time which is only of the order of $T_1(^{11}B)$, it seems likely that once significant fully registered spins are present (T=0.6K^{-1}) the magnetisation depression occurs fairly quickly and therefore has little effect on the relaxation times and their indices. T_2 *vs* $1/T$ is almost flat below 0.6K^{-1}, the onset temperature of the depression which supports the above assertion, as does 'T2Index' rising instead of falling as T falls from 0.6K^{-1} to 0.91K^{-1}. Except at X≈0.75 Curie's law is obeyed by the ^{3}He data, the apparent deviations at higher temperatures are caused by failure of the fit used to consistently estimate 'H(0)' for the non-exponential relaxation when significant changes in index take place, eg. at desorption, melting etc. Incidentally, at the highest temperatures (not shown in figure 7.2.2.35) the signal height does fall off faster with T as desorption removes spins from *view*. A reduction in magnetisation is also visible in the lowest T point at X=0.7. Applying the direct coupling model (§3.5.3) for ^{3}He/BN, for simplicity assuming; (a) only the ^{11}B spins are responsible for the ^{3}He magnetisation depression and (b) they are saturated by the flow of magnetisation from ^{3}He pulses, permits the model parameters including T_c and T_1 to be calculated. The justifications are, for (a) that $|\gamma_{^3He}| - |\gamma_{^{11}B}| \ll |\gamma_{^3He}| - |\gamma_X|$ where 'X' represents the other substrate nuclei, making coupling to ^{11}B more efficient for ^{3}He spins due to the larger spectral component of the motion modulating the dipole-dipole field fluctuations at the lower difference-frequency being more able to cause heteronuclear spin-flips, (see Appendix 1). [Note: The question of ^{3}He coupling with substrate quadrupole frequencies is being implicitly ignored here − but is treated in detail in §8], (b) is much more tenuous. Given the DLX6000 result where the ^{19}F magnetisation fell by a factor of only ~½ on ^{3}He saturation (b) is unlikely to be fulfilled.

However the data suggests it must be significantly degraded, saturation sets the lower limit for the degraded ^{11}B magnetisation. Any residual ^{11}B magnetisation will overestimate the T_c obtained (weaker through-substrate relaxation), saturation again providing the lower limit. Using the linear fit at X=0.75 provides an estimate for R at 1.1K, R=0.69±0.05. Equations 3.5.3.1, 3.5.3.3 and $T_1(^3\text{He})$=44.9mS give T_1=176mS, T_c=60.2mS indicating the ^{3}He spins are in much closer thermal contact with the ^{11}B than their own lattice, like the DLX6000 system. Equation 3.5.3.2 and $T_1(^{11}\text{B})$=7.8 minutes at X=0.75/T=1.1K (figure 7.4.3.7) yield $N(^{11}\text{B})/N(^3\text{He})$=1977. Given the mass of BN in the sample chamber together with the ^{3}He monolayer capacity (§4.1.1.1) and the BN isotopic composition (Appendix 1), $N(^{11}\text{B})/N(^3\text{He})$=391 is calculated for X=0.75. The factor of 5 discrepancy probably arises from overestimating R due to ^{11}B incomplete saturation, taking $T_1(^{11}\text{B})$=7.8 minutes, $T_1(^3\text{He})$=44.9mS and $N(^{11}\text{B})/N(^3\text{He})$=391 generates R=0.595, T_c=46.7mS and T_1=1.15Sec. The intrinsic ^{11}B relaxation rate adds an extra term $[+1/T_1(^{11}\text{B}@X=0)]$ to equation 3.5.3.2, increasing the effective $T_1(^{11}\text{B})$ value, in our case $T_1(^{11}\text{B}@X=0)$ ~20 mins increases $T_1(^{11}\text{B})$ from 7.8 to 12.8 mins. However $T_1(^{11}\text{B}@X=0)$ was measured with a maximum delay of only 35 minutes, being strongly sub-exponential, short-time measurements and exponential least squares fitting significantly underestimate it, resulting in it contributing very little to the relaxation at X=0.75. See also §7.4.3.2. A useful comparison can be made with Grafoil/registry data: At X=0.612, $T_1(^3\text{He})$=339mS (figure 1.10.1 and reference **72**). Associating the Grafoil $T_1(^3\text{He})$ with the model's T_1, the ^{3}He spin-lattice relaxation time observed in the absence of the FMR effect, taking T_c=60.2mS and using equation 3.5.3.3 gives R=0.642, the value expected if the ^{11}B spins were saturated and the registered state on BN was identical to that on Grafoil. Note, R=0.642 equals the measured BN value within experimental error despite differences in substrate mesh size and adsorption potentials which attempt to suppress exchange.

It is illuminating to compare the ^{3}He/BN data with that from other systems displaying the FMR effect. Table 7.2.2.1 lists some information on five other systems/ samples in which the FMR effect has been studied.

Table 7.2.2.1, Comparison of Systems Showing the FMR effect

Substrate & Isotope	Ref.	$F(^3He)$ (MHz)	T(K)	T_1(He) (sec)	T_1(S.) (min)	T_1(S.0) (min)	R	Size (μm¶)	T_c (sec)	T_1 (sec)	(T_c/T_1)	(N_s/N_{He})	X
DLX6000/^{19}F	**142**	16	1	0.2	16.7	~90	–	0.2	~0.2	~3.1	~0.06	~300	<1
DLX6000/^{19}F	**146**	25	0.55	0.5	9.3	–	0.14	0.2	0.7	1.7	0.42	232	1.0
DLX6000/^{19}F	**147**	100	0.4	3.7	71	–	0.09	0.2	6	15	0.4	207	1.0
Aldrich/^{19}F	**147**	110	0.4	–	113	–	1.00	See below	9	<0.5	>20	730	1.0
Nucleopore/^{1}H	**160**	9.38	1.3	0.080	3.65	5.08	1.0	~5	55	0.080	688	14	0.7
BN/^{11}B	this work	4.5	1.1	0.0449	7.8	>20	0.69	0.12	0.060	0.176	0.34	1977¶¶	0.75

'T_1(S.)' is the measured substrate T_1 with ^{3}He present.
'T_1(S.0)' is the measured substrate T_1 without ^{3}He.
¶, For DLX6000 the 'Size' ie. the typical particle dimension represents bead radius. On Aldrich powder it is ill defined. Its surface area is, however, a factor 3.5x less than DLX6000. See also §3.5.3. The BN particle size is discussed below.
¶¶, Inferred from the NMR data.

It is evident that at X=0.75 BN has more in common with DLX6000 than with the others. $(T_c/T_1) \ll 1$ occurs only on these two substrates, as the ^{3}He relaxes mostly via substrate spins, leading to $R \ll 1$. On Aldrich the larger particle size suppresses cross relaxation as a significant mechanism for ^{3}He because the time taken for magnetisation to diffuse throughout the particles becomes significant w.r.t. $T_1(^{19}F)$. Similarly for nucleopore, bigger particles and T_1(S.0) $\gg T_1$(S.) cause R=1 and $(T_c/T_1) \gg 1$. Recalling §3.3, the BN particles were observed to be 2μm to 10μm in size. For a particle (radius, *r)*, the spin diffusion time $T_{sd} = r^2/6D$, $D = (\mu_0/4\pi)\,\hbar\gamma^2/a$ (S.I. units), where '*a*' is the spin's internuclear separation. A 5μm BN particle, a=2.50Å for ^{11}B gives T_{sd} ~ 1 hour which should ensure $T_c \gg T_1$, R=1. Given the mass of BN and Argon/BET surface area (§3.3, §7.2.1/X=0.75 and §7.5) 80.6m^2, the BN surface-area:volume ratio (A/V) can be calculated. (A/V) = 171408 cm^{-1}, for spherical particles = $3/r$, giving r=0.175μm which is much too small. Recalling again §3.3, the BN particles appeared to be flat in shape and bearing in mind that ~5% of the surface is edge area, the particles have been modelled as flat square slabs. See also figure 7.3.2.6. This leads to on average 1.76×10^{12} particles with basal plane dimensions 4.67μm and slab thickness 0.123μm, the figure shown in table 7.2.2.1 and close to the DLX6000 radius. Unlike the Aldrich 'noodles' and more like DLX6000 microspheres, spin need only diffuse through one short dimension from both basal planes' adsorbed ^{3}He spins to saturate the substrate spins throughout a particle, making the results easier to explain. T_{sd} ~ 8sec for ^{11}B and r=0.123μm.

***X*=0.8,** Based on the simple model of §1.8 the film at this coverage is thought to be below the incommensurate solid, ie. in the *mixed phase*.

T_2 (figure 7.2.2.36) is temperature independent as expected for an exchange dominated system at 3mS up to $0.5K^{-1}$ (2.0K). Rising very approximately logarithmically as thermally activated vacancy tunnelling increases T_2, a maximum occurs at $0.28K^{-1}$ (3.6K) when the film *melts* and T_2 falls to a minimum at $0.21K^{-1}$ as 2D gas/PMI relaxation takes over. Thereafter the delocalised film undergoes desorption with the usual consequences for T_2. At 2.7MHz ($1.1K \leqslant T \leqslant 4.2K$) the data is the same. In the unlikely event the film were in the incommensurate solid proper rather than the *mixed phase* here there is an alternative possible explanation for the data: Considering previous coverages there can be little doubt the maximum corresponds to *melting* leaving a 2D gas but what is it that melts at the maximum? It is conceivable the rise in T_2 indicates the first part of two stage KTHNY-type process, the maximum corresponding to the hexatic orientationally ordered fluid -to- isotropic fluid transition. The loss of shear rigidity at the first transition might be expected to increase T_2 from its exchange determined low temperature value as thermally activated vacancy tunnelling suddenly becomes easier (ie. lower activation energy), in this, a low density solid lacking the strong support of the substrate potential wells in operation at registry. On Grafoil [3] at $X \approx 0.83$ the proposed, interpolated $T_c^* = 2.0K$ and $T_c^{**} = 3.4K$ (see also §1.10.6) which are similar to the proposed BN values (2.0K and 3.6K). Without heat capacity data to locate/confirm the melting peak temperature (ie. of the second transition) and supply a value for the Debye temperature from which the first transition temperature may be predicted [3,80], the evidence for KTHNY melting here must be regarded as very flimsy and speculative. There is mostly very high reproducibility between the up and down temperature sweep data. Careful inspection in the T_2−*rise* data, of the 4 points immediately to the left of $0.4K^{-1}$ reveals slight hysteretic behaviour suggesting something other than isolated vacancies tunnelling through a homogeneous film is at work here. Domain wall effects are probably responsible. Hysteresis is also just visible immediately after the proposed melting peak.

'T2Index', (figure 7.2.2.38) closely follows T_2 for $T > 0.5K^{-1}$, supporting the rise of T_2 to the maximum at $0.28K^{-1}$ being due to motional narrowing by thermally activated vacancy tunnelling since increasing motion will also better average the different platelet environments/orientations increasing the index, as it does for the higher temperature desorbed spins where the effect is sufficient to allow the 'CP' $\exp(-t^3)$ relaxation to be observed. The PMI/2D gas mechanism which generates the T_2 minimum also reduces its index by abruptly opening up an additional relaxation channel, as it did following the order-disorder transition in the registered phase/component at X=0.75, 0.7

Figure 7.2.2.36, T_2 against 1/T, BN, Run#6, F=4.5MHz, X=0.8

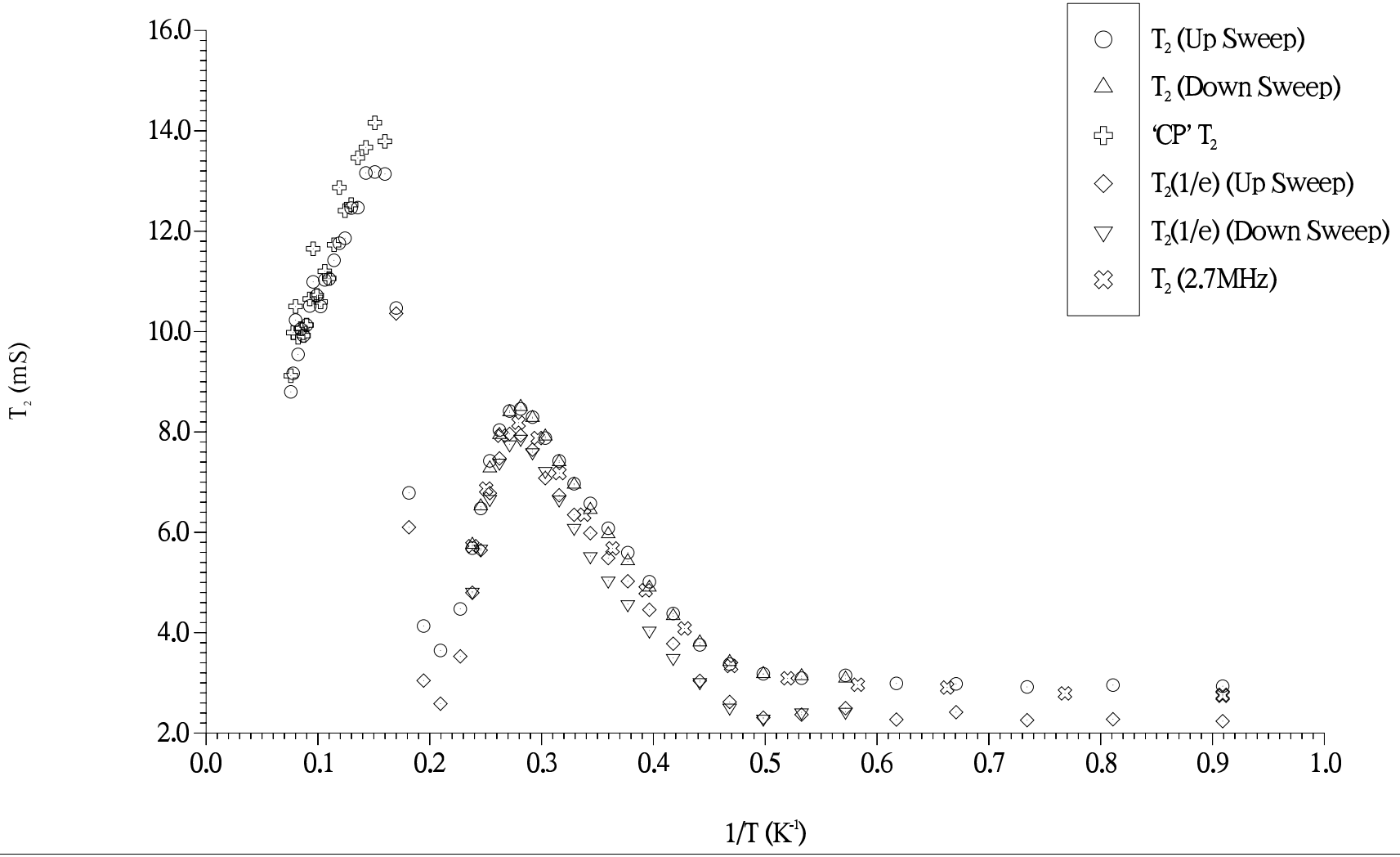

Figure 7.2.2.37, T_1 against 1/T, BN, Run#6, F=4.5MHz, X=0.8

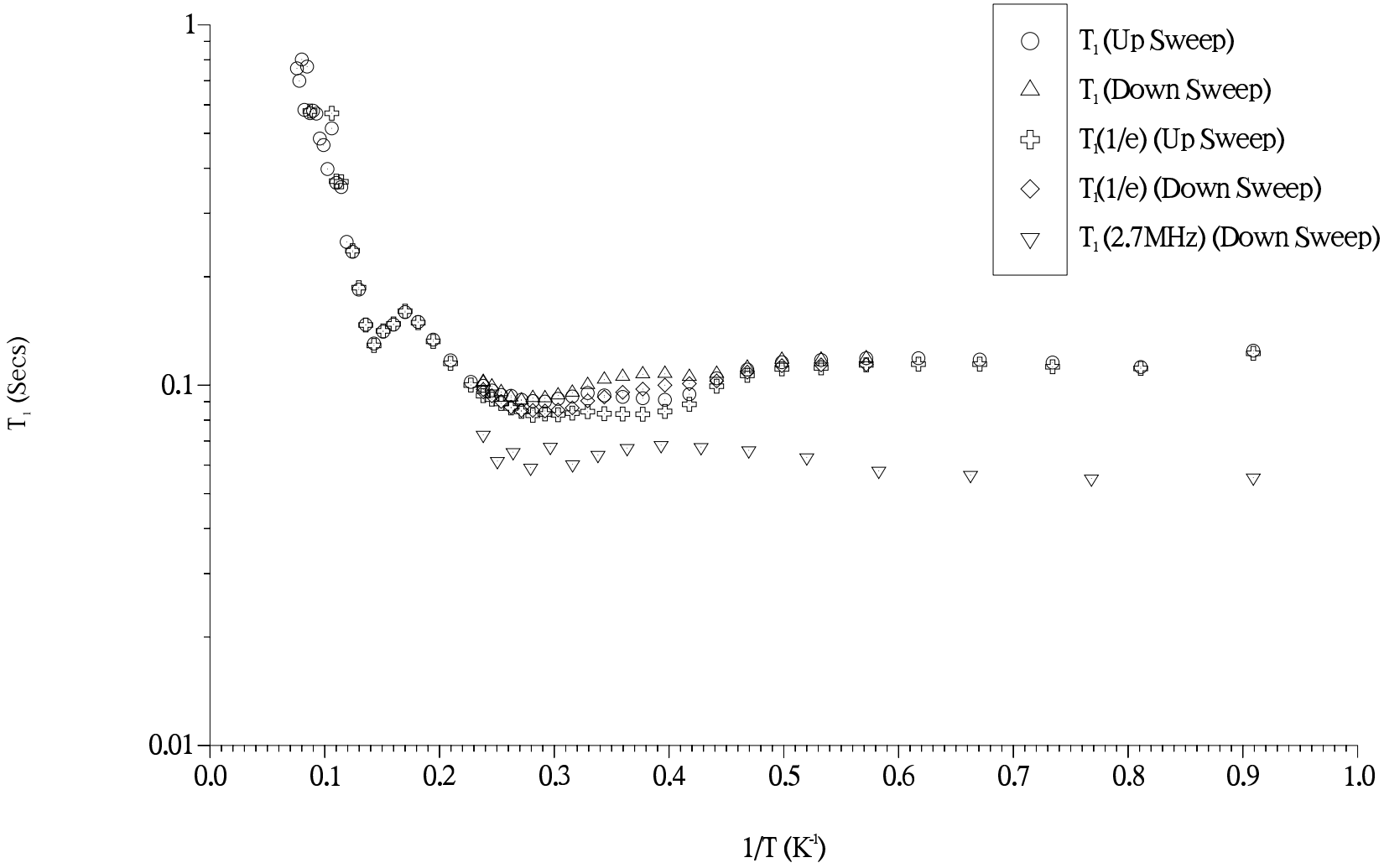

Figure 7.2.2.38, Relaxation Indices vs 1/T, BN, Run#6, F=4.5MHz, X=0.8
Straight Line Fit Throught Data (not shown) for,
$0.91K^{-1} < T < 0.47K^{-1}$ gives,
(T1Index = 0.213 (1/T) + 0.648)

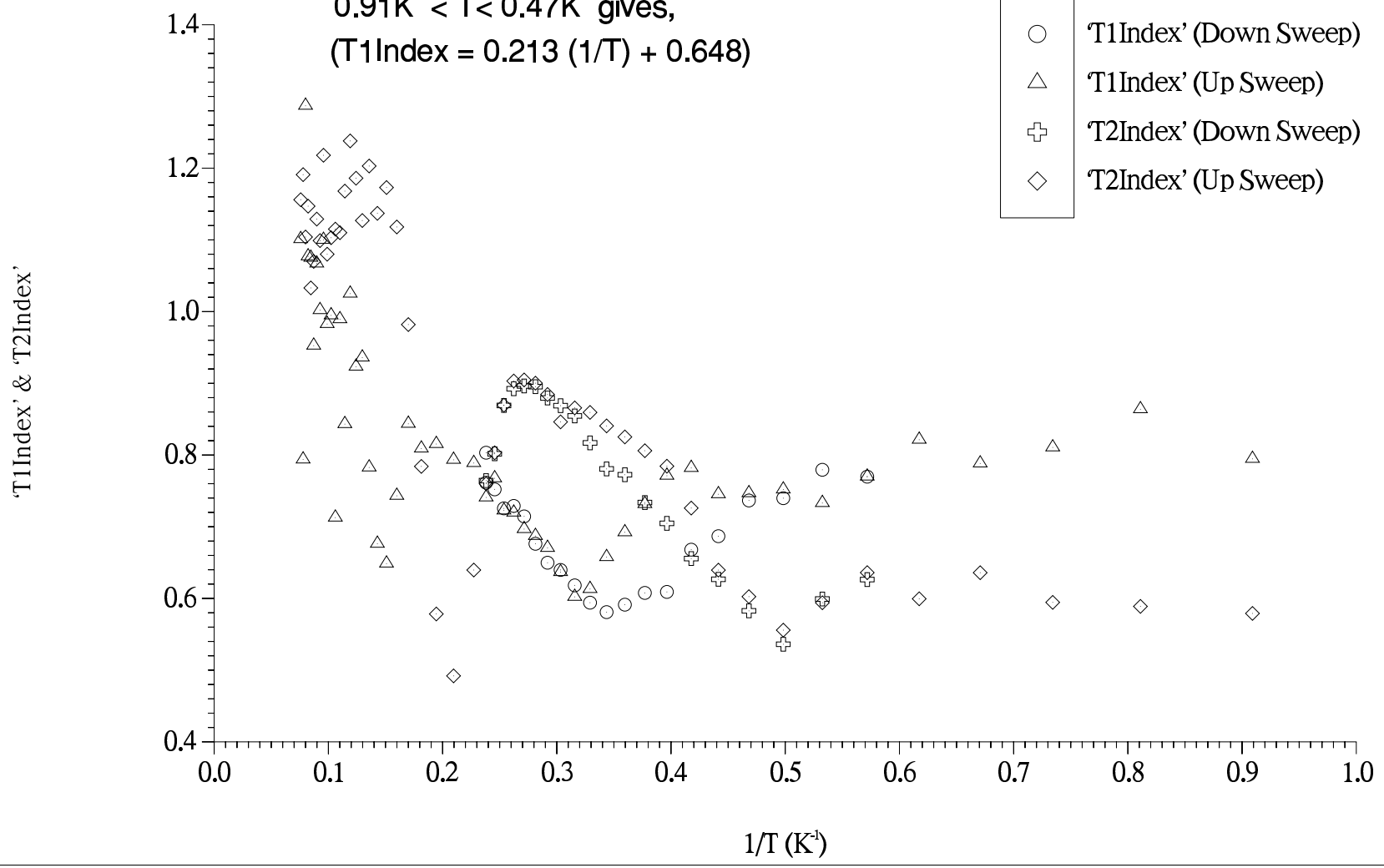

& 0.6. A distinct 'T2Index' minimum at $0.5K^{-1}$ is reminiscent of the X=0.75/0.7 data. Since it is not obviously present for the X>0.8 data we are tempted to attribute it to, in effect a small remnant registered component undergoing its LRPOP→LRPOA transition (see figure 7.2.2.32). An analogous KTHNY-type first-transition in the incommensurate solid should, of course have the same signature for the same reason. Hysteretic behaviour in T_2 in the rise to its $0.28K^{-1}$ maximum is more clearly present in the index data. The down-sweep 'T2Index' for $0.5K^{-1}\leqslant T\leqslant 0.28K^{-1}$ follows a straight line, the deviance being in the up-sweep. Temperature control/data logging was carried out in the following order; 4.2K→1.1K, 1.1K→4.2K, 4.2K→13.2K. The lack of down-sweep points below 1.75K is due to a computer crash. Evidently, the down-sweep $0.5K^{-1}\leqslant T\leqslant 0.28K^{-1}$ data has *benefited* from its 4.2K *annealing*. For both T_2 and its index the hysteretic down-sweep values are less than the up-sweep ones, suggesting the slower relaxing up-sweep values lack either a phase component or relaxation pathway available to the down-sweep ones. This is not easy to understand. Permitting insufficient time for a solid or solid-like system to *melt* fully on the up-sweep should reduce T_2 and probably its index as well, not increase them. As mentioned in the last paragraph some sort of domain wall effect may provide an explanation.

T_1 is plotted in figure 7.2.2.37 on a log scale to accentuate the minima. Without the rapid relaxation through the substrate observed at X=0.75 the low temperature T_1 has risen sharply to >100mS. After the originally proposed homogeneous-solid dipolar minimum at 1.233K (§7.2.1) it is approximately constant at low temperatures as expected for an exchange dominated solid-like system. As T rises above $0.5K^{-1}$ T_1 falls in both sweeps as far as $0.42K^{-1}$. Having passed through the originally proposed homonuclear minimum at 1.233K to its $\omega_0\tau_c<1$ side, any higher temperature minima must be due, either to phase changes, relaxation via substrate spins or some combination of the two (but see also §7.2.3.2 concerning the role of the edge-film). Hysteresis is clearly present at temperatures encompassed by the T_2-rise, being a maximum at ~$0.38K^{-1}$ (as it is for 'T2Index') where the down sweep displays a maximum, the up-sweep a minimum. The 2.7MHz '$0.38K^{-1}$' maximum appears to be shifted slightly to lower T w.r.t. 4.5MHz, pointing towards dipolar relaxation. Remembering the 'T2Index' data, it appears the down-sweep/T_1 maximum corresponds to more multi-path/component relaxation and the up-sweep T_1 minimum, the reverse. For example, if the down-sweep film is more homogeneous than the up-sweep one, any fluid/solid domains will be smaller (not having been fully solidified at low temperatures) and so possess (relative to total) more domain *wall spins*, phase changes/rearrangements

in which might explain the higher multi-component/T_1-maximum. At higher X this maximum/minimum becomes an increasingly deep minimum for both sweeps which suggests that here, it stems from or reflects very marginal changes in the film, consistent with a domain wall phase transition explanation. A detailed ^{4}He/Grafoil heat capacity survey published recently **[36]** concentrating on the phase diagram's commensurate−incommensurate (C−IC) solid transition region has suggested small 1K heat capacity peaks occurring just beyond registry (n=0.0673Å^{-2} − 0.0700Å^{-2}) indicates melting of a domain-wall-solid. On our coverage scale (by comparing the Grafoil:BN registry points alone), for BN this corresponds to X=0.79−0.82≈0.8. However, the much lower temperature of the ^{4}He/Grafoil heat capacity peaks makes this interpretation less probable. Alternatively a reattribution **[37]** of the ^{3}He/Graphite phase diagram's C−IC region **[31]** (figure 7.2.2.39) places a transition from a *striped super-heavy domain wall phase* (D) to a *domain wall liquid* (DWL) at 1K, followed by a DWL to fluid (F) transition at ~2.6K. The above He/graphite coverages corresponding to ^{3}He/BN/X~0.8 suggest the domain wall phases could only just have been entered. That is, no incommensurate solid should be present at this coverage, which is perhaps difficult to reconcile with the T_2 data, but see also below¶¶¶. It seems likely that although this type of phase diagram may be valid for ^{3}He/BN as for He/graphite and hydrogen-isotopes on graphite, the phase boundaries' positions may vary significantly from graphite to BN as they do from helium to the hydrogen isotopes on graphite **[11,210]**. The second high temperature minimum coincides with the T_2 melting maximum. Higher coverages however, suggest this is largely coincidental, although a rapid decrease in τ_c is expected and could fulfil a suitably located $\omega_x\tau_c$~1 condition, ω_x being some frequency associated with the ^{3}He and substrate Larmor frequencies. The highest temperature minimum here, the *main* minimum at X=0.7 and 0.75 and the sole minimum for X<0.7 has risen to 0.14K^{-1} and become more shallow. It roughly coincides with the T_2 desorption maximum and again this is believed to be fortuitous.

Figure 7.2.2.39, Phase Diagram for C−IC Region of ^{3}He on Graphite From Reference **37**.

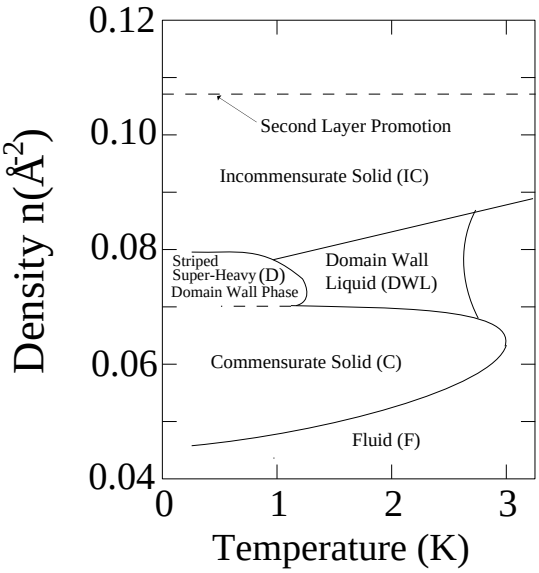

Like its T_2 counterpart 'T1Index' displays clear hysteresis (figure 7.2.2.38), the down/up-sweep discrepancy reaffirming that more multi-path/component relaxation operates during the down-sweep. *Sub-region* behaviour at low temperatures is much diminished from X=0.75 and the super-exponentiality is gone. The low temperature 'T1Index' *vs* 1/T slope has fallen from 0.82K at X=0.75 to 0.21K, the same value as at X=0.5, reaffirming little registered component is left. The minimum at the high T end of the hysteretic region ($0.32K^{-1} - 0.34K^{-1}$) does not obviously correspond to any feature in the other plots and may simply indicate a maximum in double-path relaxation as it straddles two T_1 minima. As before the $0.14K^{-1}$ minimum coincides with the highest temperature T_1 minimum.

***X*=0.85,** At low temperatures a fully incommensurate solid is believed to exist here.

T_2 (figure 7.2.2.40) starts rising from $0.8K^{-1}$ in contrast to the previous coverage where temperature independence as far as $0.5K^{-1}$ was observed. Writing $T_2 = T_2^{\text{exchange}} + T_2^{\text{tavt}}$ for the two contributions to motional narrowing and remembering the temperature independent 'T_2^{exchange}' falls off rapidly with increasing density **94**. 'T_2^{tavt}', the thermally activated vacancy tunnelling contribution also falls with increasing E_a as X rises **64** but becomes relatively more important as temperature rises, having become a stronger function of T, producing the above result. T_2 displays three distinct regions with different slopes as it rises to its maximum at $0.22K^{-1}$, a feature unique to

Figure 7.2.2.40, T_2 against 1/T, BN, Run#6, F=4.5MHz, X=0.85

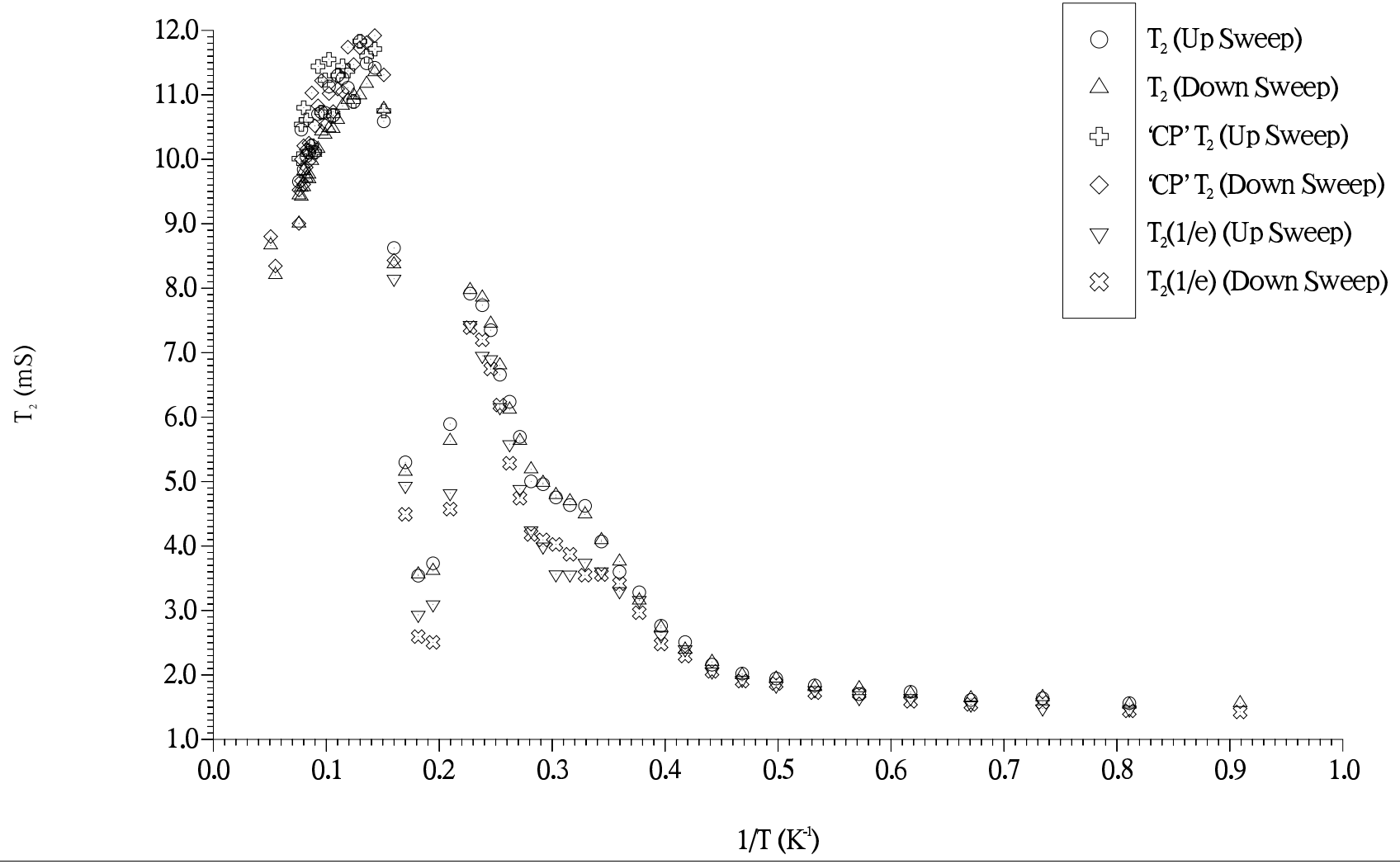

this coverage. The regions are labelled; (1) $T<0.33\text{K}^{-1}$, (2) $0.33\text{K}^{-1}\leqslant T\leqslant 0.28\text{K}^{-1}$ and (3) $0.28\text{K}^{-1}\leqslant T\leqslant 0.22\text{K}^{-1}$. Assuming the same class of phase diagram, the BN coverage to ^{3}He/graphite areal density scale conversion puts BN $X=0.85 \equiv 0.0728\text{Å}^{-2} - 0.0810\text{Å}^{-2}$ areal density on graphite. Scaling for the lower value compares only registry coverages and provides a lower limit. The upper value also takes into account monolayer completion and imposes an upper limit. A small *offset* due to the 5% edge-sites solid has been accounted for. Figure 7.2.2.39 places $X=0.85$ into the C−IC intermediate region of the phase diagram where domain wall phases exist. The following <u>possible</u> phase designations are proposed; Region (1) incommensurate solid (IC), Region (2) domain wall liquid (DWL) and Region (3) Fluid (F). However it is unclear what the 0.22K^{-1} maximum corresponds to in this scheme if *melting* to an isotropic fluid has already taken place. Again, displacement of the phase boundaries from the graphite case and/or a more complicated phase diagram eg. D_2/graphite **[210]** may explain this. Alternatively if reordering phenomena **[36]** within DWL domains could account for region (2), the 0.22K^{-1} maximum could be interpreted as DWL→F melting. Finally, if the above proposed phase designations are valid, the 0.22K^{-1} maximum could simply indicate the onset of sufficiently fast motion in the now more dense fluid melt for the PMI/fluid mechanism to start dominating dipolar relaxation. Hysteresis is visible near the proposed incommensurate solid melting point at 0.33K^{-1}. Phase transitions are clearly suggested by opposite sense hysteresis at both ends of region (2). It is noteworthy that the region (2) to region (3) transition temperature (0.28K^{-1}, 3.6K) is the same as at the $X=0.8$ *melting* peak given the DWL−F boundary in figure 7.2.2.39 is almost isothermal.

'T2Index' (figure 7.2.2.42) shows much greater low-T variation in both temperature and sweep direction compared to $X=0.8$, in contrast with T_2 which proceeds slowly and reproducibly. These trends are continued by higher coverages. The low temperature 'T2Index' values are generally slightly higher than at $X=0.8$, ruling out a '*film thickens, motion slows, single platelet relaxation increases, index falls*' type process. In any case that scheme could not explain the *noisy*, hysteretic behaviour observed. The suggestion is, index behaviour reflects the details of the thermally activated breakup of the incommensurate solid, for example into patches in the prelude to transforming to the DWL. Competition between (a) Increased patchiness which should decrease the index and (b) more thermally activated motion increasing it, as temperature is raised provides a possible explanation for the data. Being intra-incommensurate solid changes, not involving true phase transitions (hence no large changes in τ_c or the $\langle r_{ij}\rangle$) the average relaxation rate obtained by the 'T_2' and '$T_2(1/e)$' measures change only

Figure 7.2.2.41, T_1 against 1/T, BN, Run#6, F=4.5MHz, X=0.85

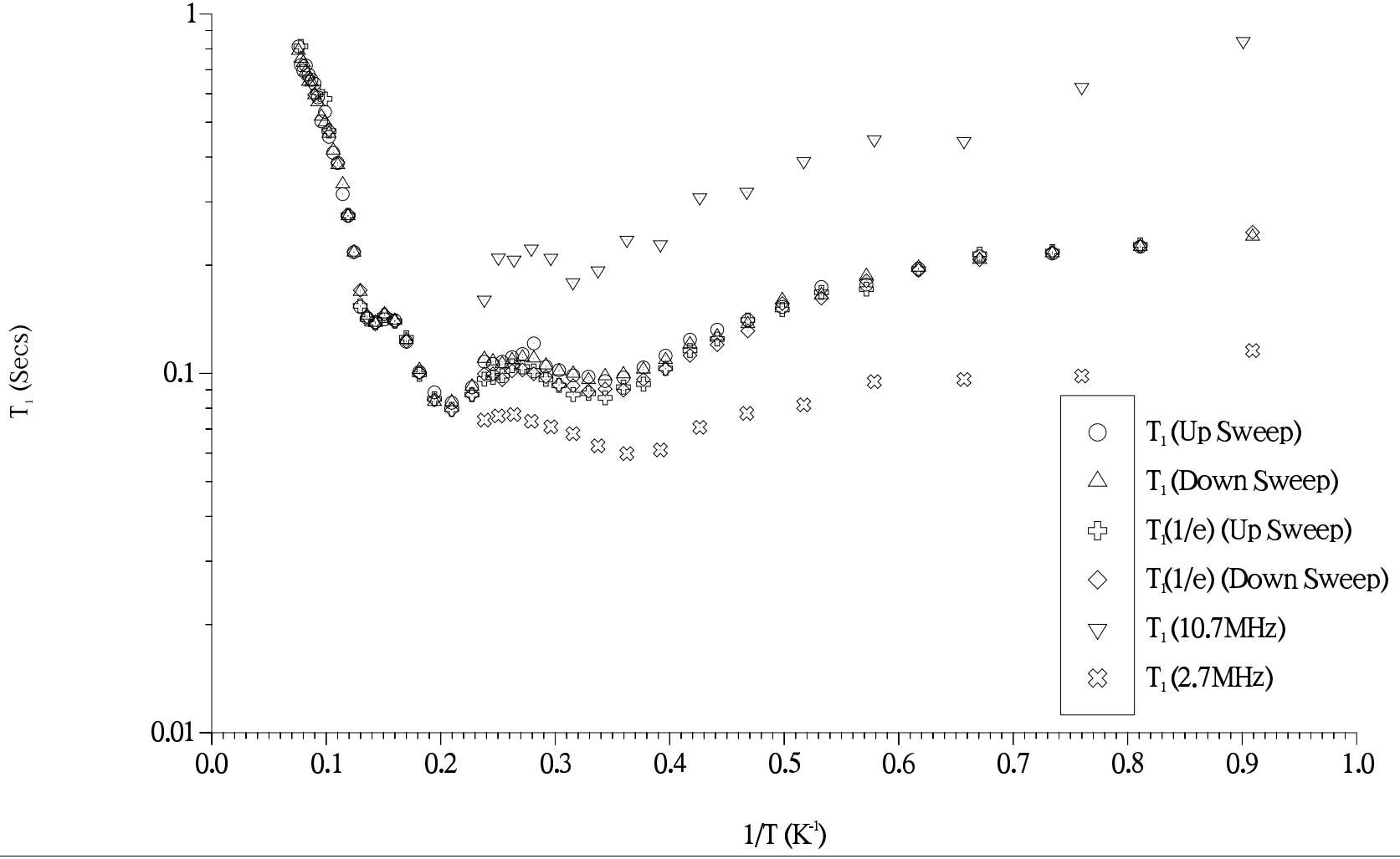

Figure 7.2.2.42, Relaxation Indices vs 1/T, BN, Run#6, F=4.5MHz, X=0.85

Straight Line Fit Throught Data (not shown) for,
$0.91K^{-1} < T < 0.30K^{-1}$ gives,
(T1Index = 0.156 (1/T) + 0.641)

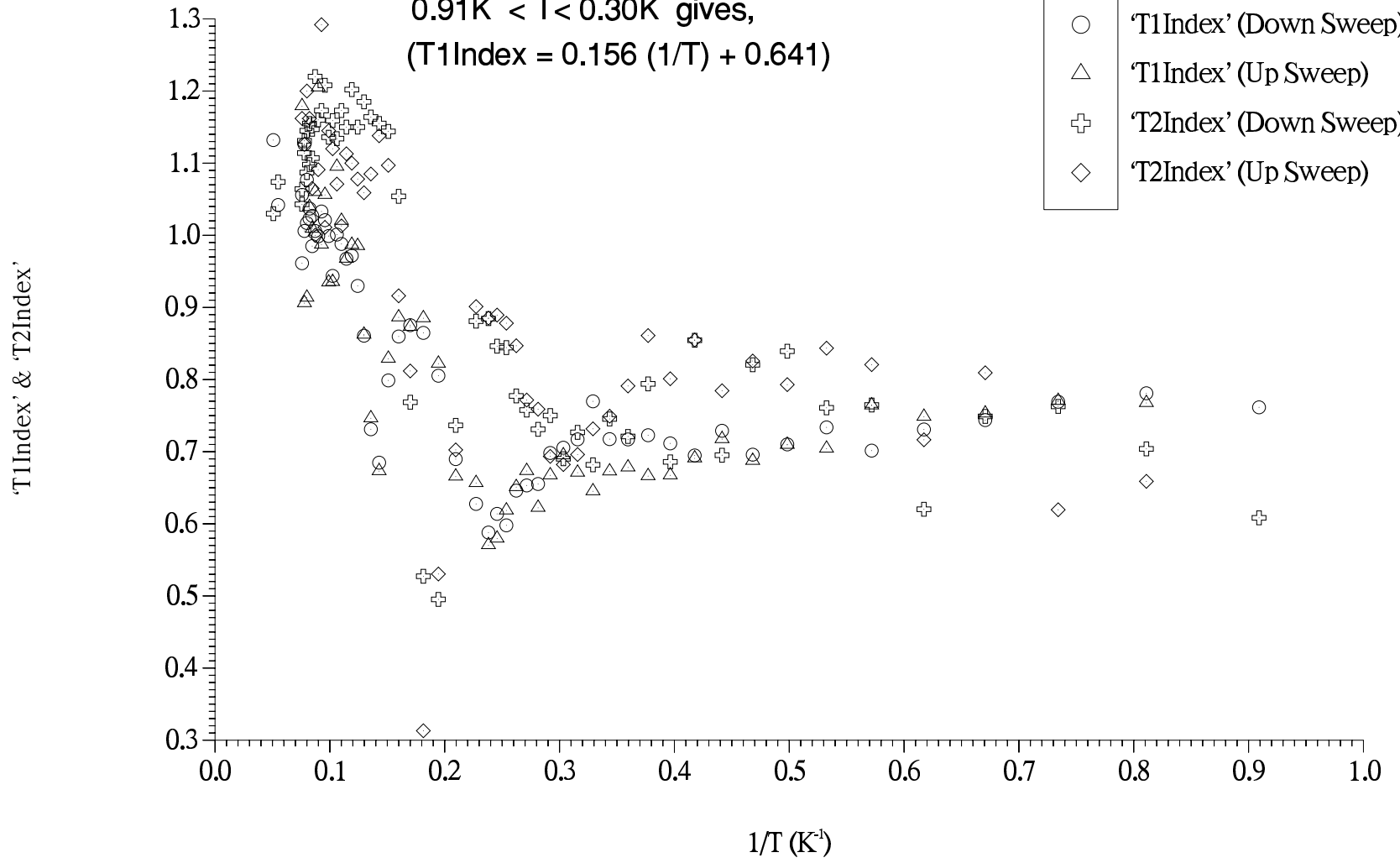

slowly. The lack of low temperature *noisy*/hysteretic 'T2Index' data at X=0.8 and its presence at $X \geqslant 0.85$ suggests as mentioned above¶¶¶, that at X=0.8 the incommensurate solid phase has not yet been entered. Instead the film is a DWL which transforms to the isotropic fluid at the T_2 melting peak. A 'T2Index' minimum (also seen at 2.7MHz) centred on region (2) (figure 7.2.2.40) at $0.3K^{-1}$ in which both sweeps converge implies an increased multiplicity of relaxation paths and an energetically favourable structural configuration. A DWL composed of small domains giving a comparable number of wall and interior spins with different relaxation rates should produce this type of signature. The familiar sharp PMI/fluid minimum at $0.19K^{-1}$ and rise to super-exponentiality completes the 'T2Index' data.

Figure 7.2.2.41 shows T_1 against $1/T$. It falls monotonically with increasing T to the first of the three high temperature minima more rapidly than at X=0.8, again because of the relatively larger thermally activated motion component. The two lower temperature minima are more distinct than at X=0.8, with the highest T one reducing in relative depth and the intermediate one increasing relatively in depth. A general trend for increasing X, $X \geqslant 0.85$ is the shift in greatest relative depth from the highest to the lowest temperature of the three minima. Dipolar relaxation is again supported by 2.7MHz and 10.7MHz data where the 4.5MHz minimum at $\sim 0.35K^{-1}$ has shifted down in T to $0.37K^{-1}$ and up to $0.32K^{-1}$ respectively. Values of (ω_0/T_1) at the minima should be frequency invariant and equal to m_2 (in the homonuclear case) providing areal density remains constant. $(\omega_0/T_1)_{min}$=373 sec^{-2} (10.7MHz), 304 sec^{-2} (4.5MHz) and 292 sec^{-2} (2.7MHz). Within experimental error the 2.7MHz and 4.5MHz points are the same. At 10.7MHz the much larger value suggests the relevant internuclear spin separation has decreased (by a factor of $(304/373)^{1/6} = 0.967$), instead of increasing, as might be expected for example because of layer promotion. Reduction of the $\langle r \rangle$ points towards structural rearrangement of spins. Inspection of figure 7.2.2.40 reveals the 10.7MHz minimum has entered T_2 region (2), the proposed DWL.

'T1Index' (figure 7.2.2.42) again displays less variation at low temperatures than the last coverage. The low temperature slope has also fallen again, to 0.16K reflecting a further reduction in effectively registered spins. The number of adatoms located over a BN hexagon and hence the FMR relaxation is expected to remain finite even at first layer maximum density where incidentally a triangular lattice *incommensurate solid* might exist as a longer range registered structure eg. 8×8 as on graphite [37]. Hysteresis is evident from $0.31K^{-1} - 0.42K^{-1}$. Its path/component multiplicity + sweep direction is in the opposite sense to 'T2Index' and the X=0.8 indices

Figure 7.2.2.43, T_2 against 1/T, BN, Run#6, F=4.5MHz, X=0.9

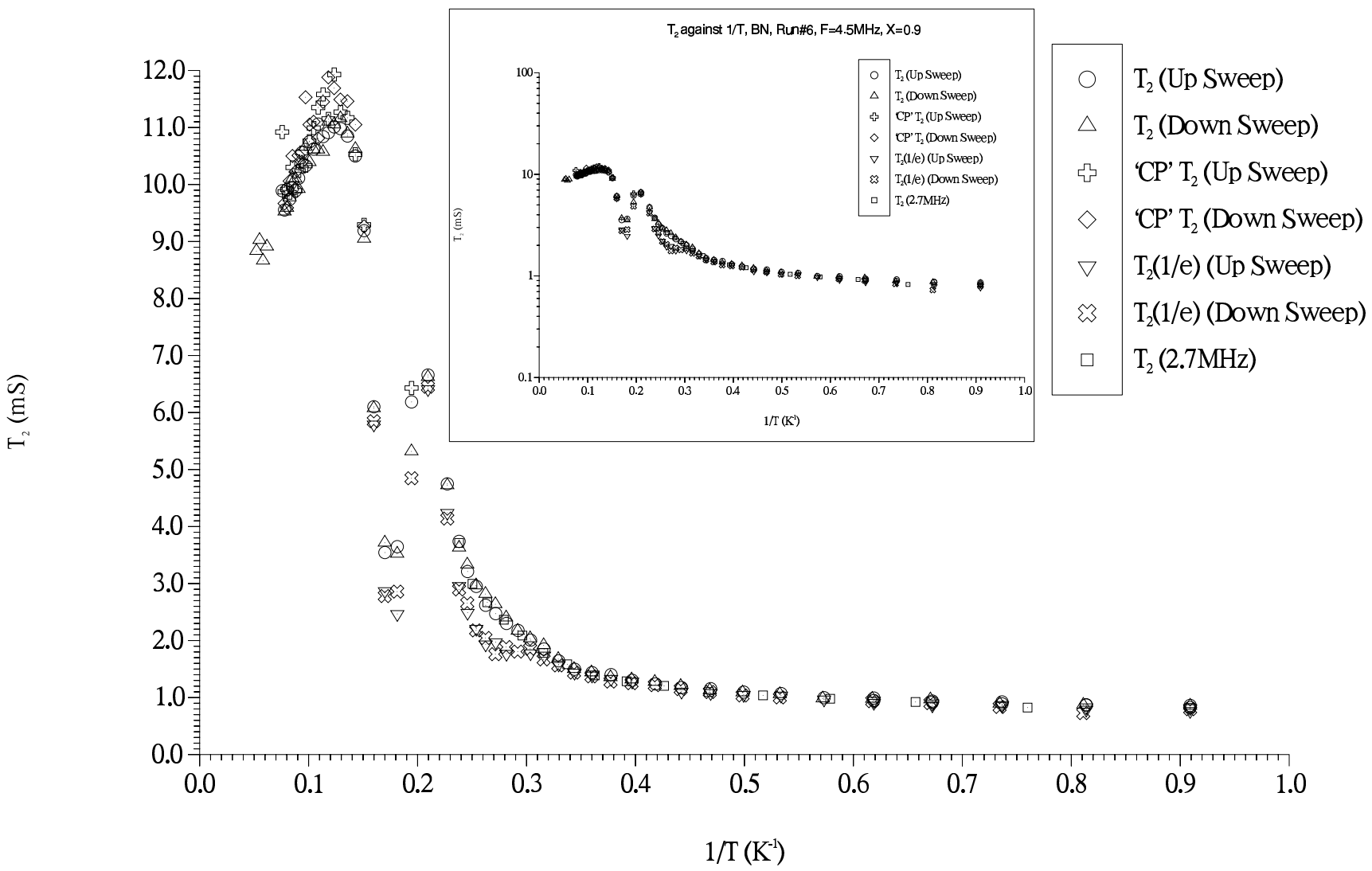

data. The change is unsurprising since this region (in contrast with X=0.8) straddles a much more distinct T_1 minimum. As at X=0.8 the 0.23K^{-1} minimum does not correspond to any particular feature in T_2, 'T2Index' or T_1 plots. It does however, shift to lower T (0.26K^{-1}) at 2.7MHz supporting the explanation given at X=0.8. The 0.14K^{-1} minimum does coincide with the highest T T_1 min, as at X=0.8.

***X*=0.9,** At low temperatures the film is believed to be incommensurate solid which melts almost directly to the fluid. There is a significant low temperature second layer population.

T_2 (figure 7.2.2.43) continues the faster rise from low temperatures (see inset) noted at X=0.85 as far as the 0.2K^{-1} maximum. In contrast with X=0.85 for $T \geqslant$0.45K^{-1} where the three regions each showed an approximately linear dependence when plotted semi-logarithmically (ie. an activation law), here T_2 rises faster. Figure 7.2.1.2 (T_1 *vs* X, T~1K) goes through a maximum at X=0.9 a probable consequence of the onset of second layer promotion. A finite 2D gas second layer population in which motion is much less restricted than in the first layer thermally activated solid, which rapidly increases with T can account for the increased rise of T_2 with T at these higher temperatures. Hysteresis ~0.27K^{-1} is visible. Just beyond the 0.2K^{-1} melting maximum super-exponential exp $-t^3$ 'CP' relaxation briefly occurs before PMI/fluid relaxation takes over. An increasing feature at higher coverages, this is believed to be caused primarily by fast moving second layer 2D gas spins diffusing in the residual applied field gradient.

'T2Index' (figure 7.2.2.45) is very similar to the X=0.85 plot. *Noisy* low temperature data as at X=0.85 is expected, here in the incommensurate solid. The first minimum at 0.27K^{-1} (2.7 MHz also) which coincides with the T_2 hysteresis is much deeper than at X=0.85, falling to ~0.4−0.5 from close to exponentiality in both sweeps. The cause of this is less certain: Recapping; the explanation offered at X=0.85 for the 0.3K^{-1} minimum was reordering phenomena within the DWL. Although the Grafoil areal density corresponding to X=0.9 lies between 0.0774Å^{-2} − 0.0897Å^{-2} which potentially places it in the domain wall phases region, there is no 'X=0.85 T_2 type' evidence for multiple phase transitions here. One possibility for an equivalent areal density ~0.086Å^{-2} is that the DWL phase region is just *clipped* (see figure 7.2.2.39), the minimum corresponding to it, being due to a sudden rapid increase in relaxing phase components over a small temperature interval. Supporting evidence comes from X=0.85 where the proposed DWL→F transition occurs at the same, or rather a slightly lower temperature (0.3K^{-1}).

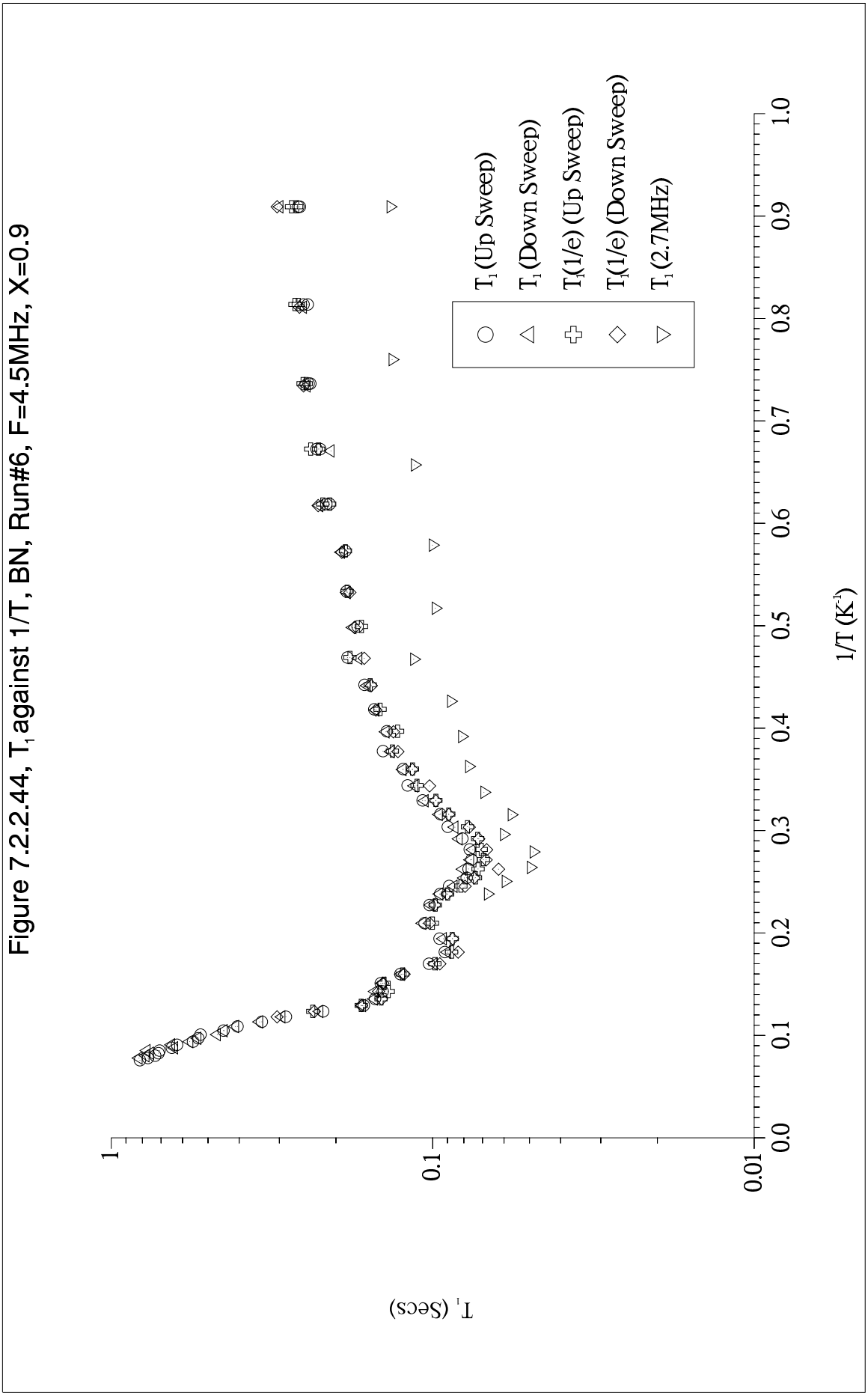
Figure 7.2.2.44, T1 against 1/T, BN, Run#6, F=4.5MHz, X=0.9
T1 (Secs)
1
0.1
0.01
0.0
0.1
0.2
0.3
0.4
0.5
0.6
0.7
0.8
0.9
1.0
1/T (K-1)
T1 (Up Sweep)
T1 (Down Sweep)
T1(1/e) (Up Sweep)
T1(1/e) (Down Sweep)
T1 (2.7MHz)

Figure 7.2.2.45, Relaxation Indices vs 1/T, BN, Run#6, F=4.5MHz, X=0.9
Straight Line Fit Throught Data (not shown) for,
$0.91K^{-1} < T < 0.45K^{-1}$ gives,
(T1Index = 0.148 (1/T) + 0.595)

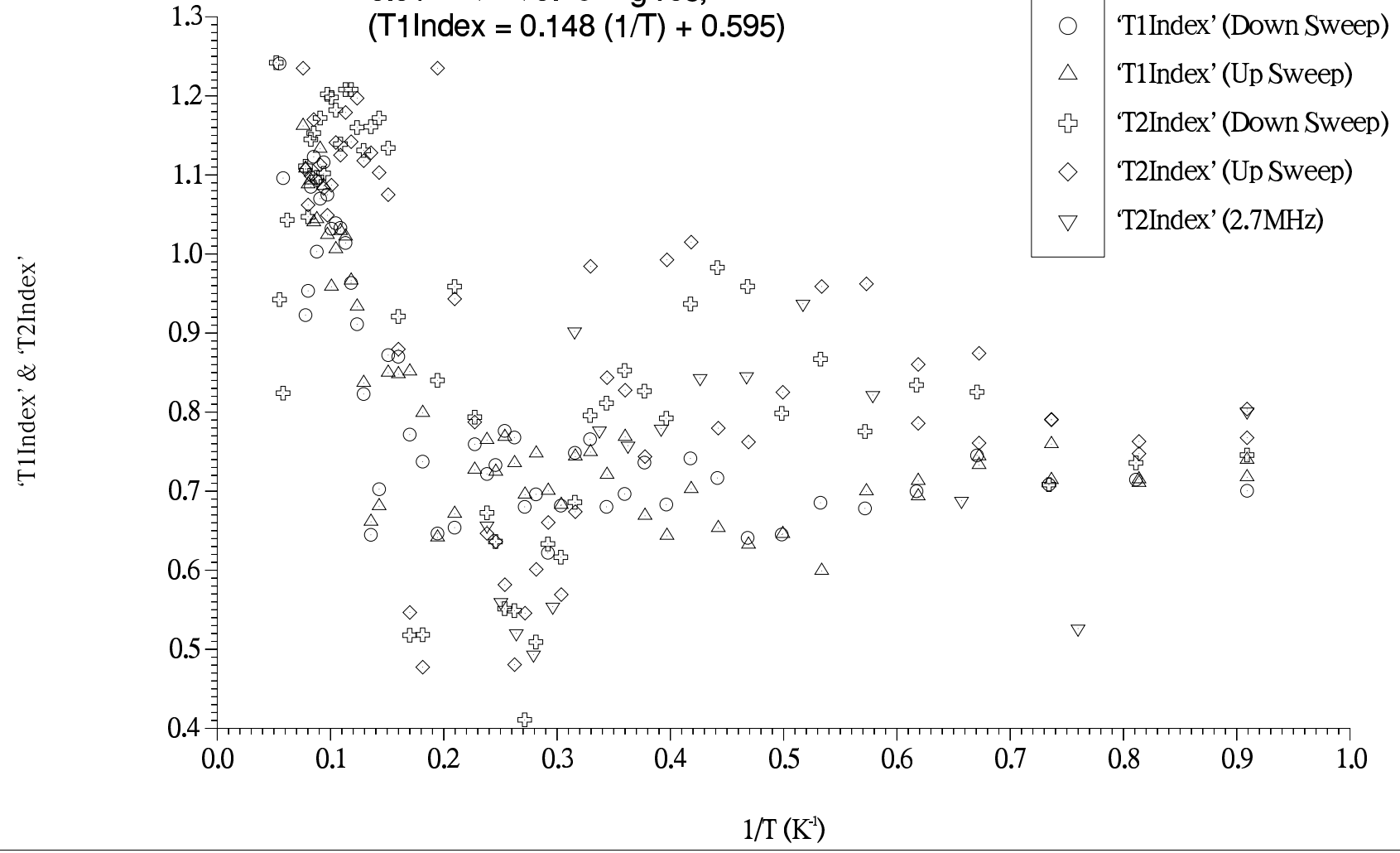

T_1 (figure 7.2.2.44) displays the same features seen at X=0.85. The first (lowest T) minimum at 0.28K^{-1} has deepened, narrowed and shifted to higher T. The second one (0.18K^{-1}) has shrunk relatively but retains approximately the same absolute value. At 0.14K^{-1} the third minimum has risen slightly in value but almost disappeared as a feature into a small inflection. At 2.7MHz the first minimum appears coincident with or a little below the 4.5MHz one. The lack of a significant downshift in T at the lower frequency as seen at lower X is probably due to the increased ($d\tau_c/dT$) expected (equn. 1.10.4.3) at the significantly higher T of the minimum at this coverage, (see figure 7.2.3.8).

'T1Index' (figure 7.2.2.45) shows considerable reproducibility at low T as at X=0.85. Presumably being far away from any T_1 minima and lacking a significant number of registered spins to relax via substrate spins, makes T_1 and its index a poor probe of the changes occurring at the proposed thermally activated breakup of the incommensurate solid into patches. This contrasts with the case of the much shorter T_2 and its index, which is dominated by its adiabatic term (equn. 2.2.17). As expected the low temperature slope has fallen again slightly, to 0.15K. Over mid-range temperatures (0.6K^{-1} – 0.2K^{-1}) 'T1Index' appears essentially random, a probably consequence of a more complicated system now involving a significant and increasing second layer population. As before the now much less distinct minima at 0.2K^{-1} and 0.14K^{-1} correspond to temperatures between the first two T_1 minima and at the third T_1 minimum respectively.

***X*=0.938,** Here the film is believed to be incommensurate solid with an increased low temperature second layer population. Melting is directly to the fluid. Firstly, for continuity with preceding coverages the relaxation times and their indices will be discussed as a function of temperature at 4.5MHz. Discussion of the data at the other 7 frequencies used follows later.

Figure 7.2.2.46 shows T_2 against $1/T$ at 4.5MHz. Unlike the previous coverage T_2 is constant as far as 0.5K^{-1} where it goes through a broad minimum centred on 0.4K^{-1} before rising to the usual maximum at ~0.2K^{-1}. The rise clearly follows an activation law (see inset). An explanation for this change in behaviour is provided by the substantial jump (~ ×2) in activation energy (E_a) (see figure 7.2.3.11) w.r.t. X=0.9 as first layer compression occurs in the approach to maximum first layer density at X=1. For 0.9K^{-1}<T<0.5K^{-1} temperature independent exchange dominance is reasserted, there now being insufficient energy to thermally create many vacancies. In analogy with the low coverage (X>0.1) 2D gas component, the 0.4K^{-1} minimum occurs as second layer 2D

Figure 7.2.2.46, T_2 against 1/T, BN, Run#6, F=4.5MHz, X=0.938

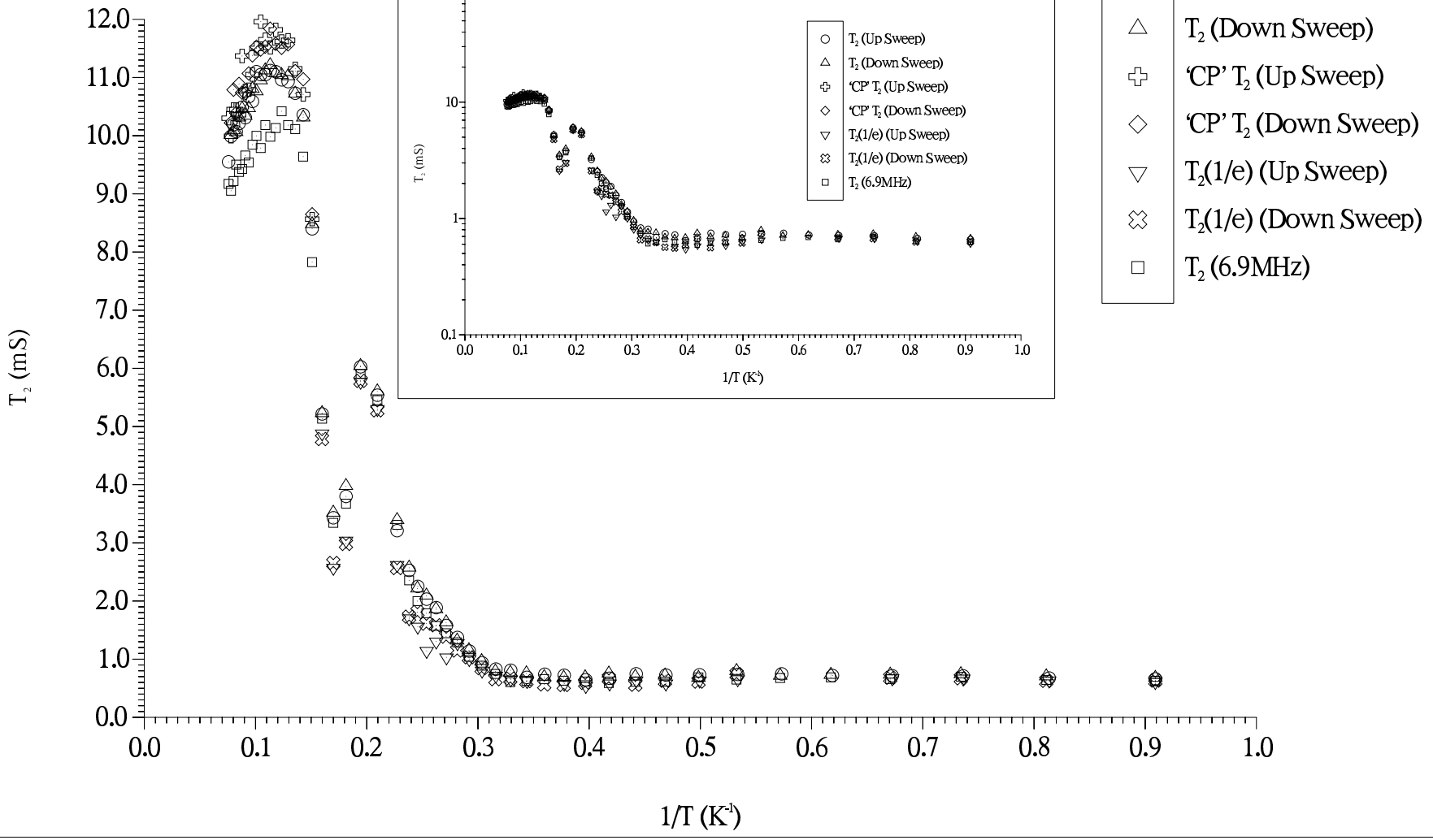

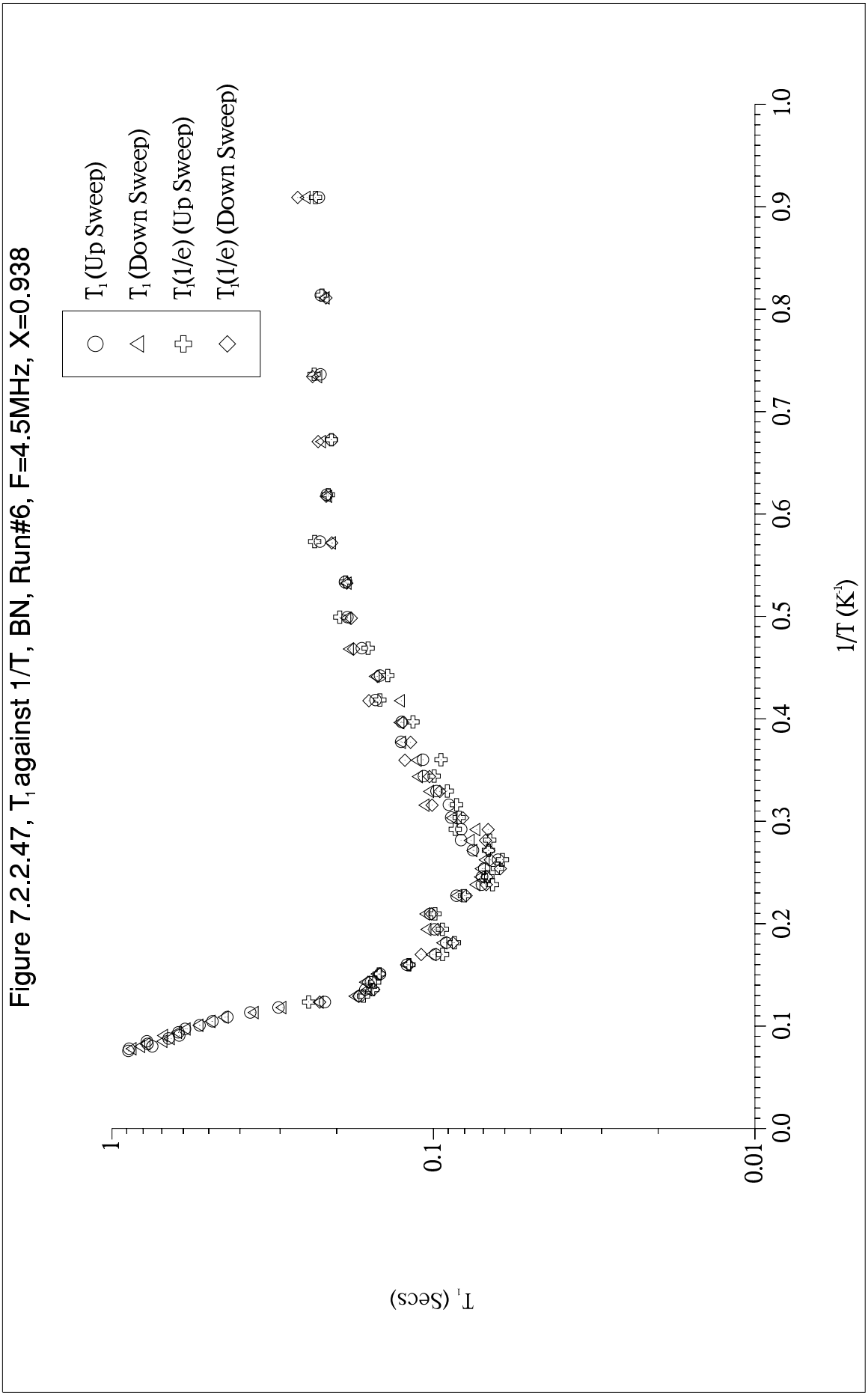
Figure 7.2.2.47, T1 against 1/T, BN, Run#6, F=4.5MHz, X=0.938
T1 (Up Sweep)
T1 (Down Sweep)
T1(1/e) (Up Sweep)
T1(1/e) (Down Sweep)
T1 (Secs)
1
0.1
0.01
0.0
0.1
0.2
0.3
0.4
0.5
0.6
0.7
0.8
0.9
1.0
1/T (K-1)

Figure 7.2.2.48, Relaxation Indices vs 1/T, BN, Run#6, F=4.5MHz, X=0.938
Straight Line Fit Throught Data (not shown) for,
$0.91K^{-1} < T < 0.45K^{-1}$ gives,
(T1Index = 0.044 (1/T) + 0.671)

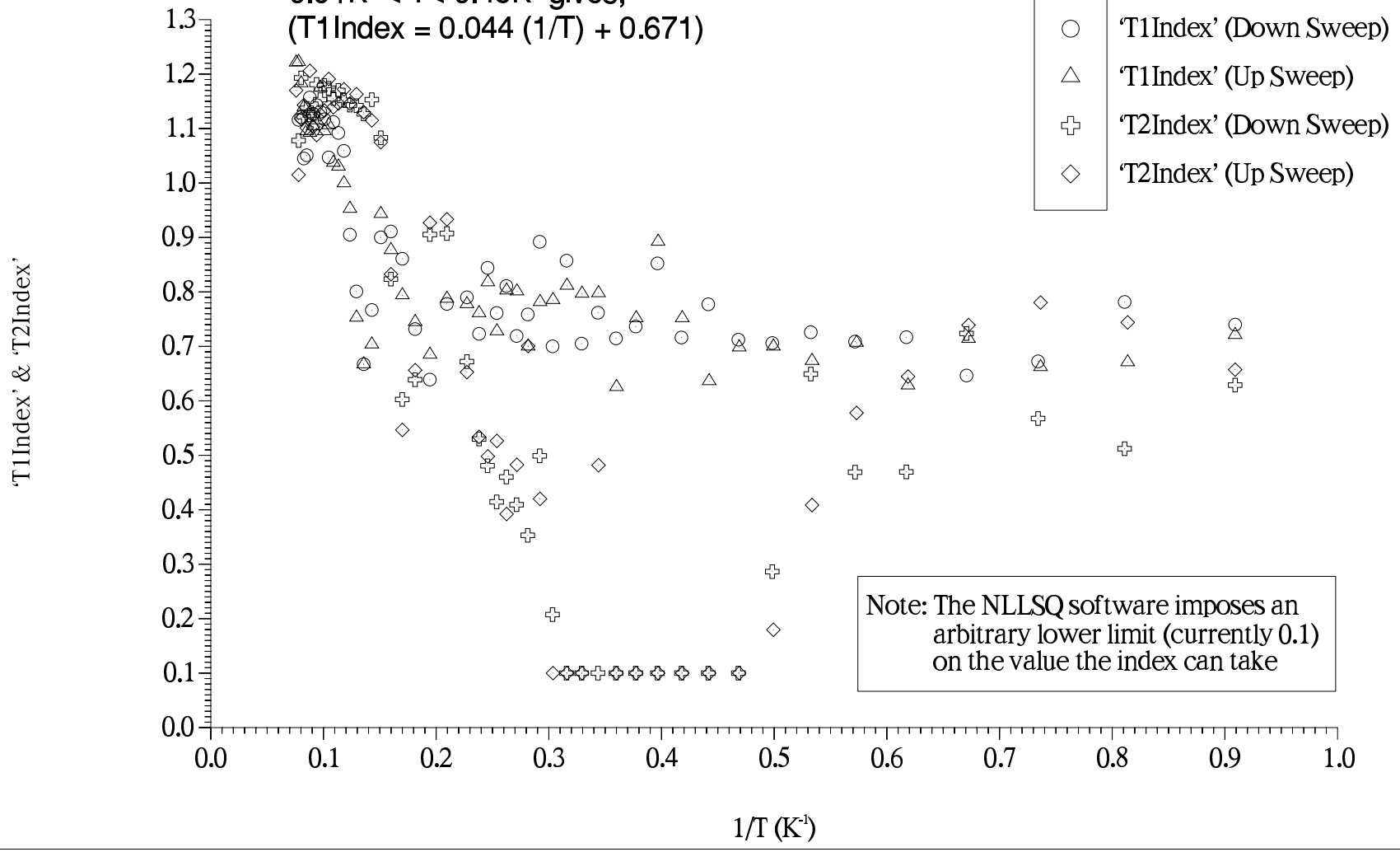

gas spins accelerate and relax via the PMI/fluid mechanism. At $0.32K^{-1}$ sufficient energy is available for thermal activation in the first layer to restore dipolar relaxation dominance, culminating in the $\sim 0.2K^{-1}$ melting maximum. Hysteresis is conspicuously almost absent in the rise, a feature repeated by the remaining coverages. With the equivalent Grafoil areal density range $X=0.938 \equiv 0.080Å^{-2} - 0.0963Å^{-2}$, the $X=0.9 \equiv 0.086Å^{-2}$ inferred for the previous coverage and the hysteresis for $0.8 \leqslant X \leqslant 0.9$ being attributed to reordering phenomena within the DWL, the $X \geqslant 0.938$ data is consistent with a first layer incommensurate solid which melts directly to the fluid.

'T2Index' (figure 7.2.2.48) shows the usual but increased *noisy* low temperature behaviour associated with the proposed thermally activated patch breakup in the incommensurate solid. The usual minimum at the T_2 melt-desorption minimum is present at $0.17K^{-1}$. As expected there is no minimum encompassed by the now hysteresis-absent T_2 rise. The most striking feature of the plot is the very strong sub-exponential relaxation centred on $0.4K^{-1}$, signalling the appearance of the strong additional relaxation channel produced by second-layer spins in PMI fields.

T_1 (figure 7.2.2.47) is very similar to $X=0.9$ apart from being temperature independent at low T like T_2. It follows the now established trend: The first minimum at $0.26K^{-1}$ has deepened, narrowed and moved to higher T. The second at $0.18K^{-1}$ has shrunk relatively, retaining approximately the same absolute value. While the third at $0.14K^{-1}$ has risen slightly, almost disappearing.

'T1Index' (figure 7.2.2.48) as at $X=0.9$ possesses the usual two high temperature minima plus mid-range-temperatures *noisy* behaviour. Unlike the $X=0.75 \rightarrow 0.9$ data where the trend was a reduction in low temperature *noisiness*, here it has increased w.r.t. $X=0.9$. There is no expectation or evidence from the 0.04K low temperature slope for an increase in registered spins. The low temperature breakup into patches of the incommensurate solid is likely to occur along substrate crystalline imperfections − the energy required for breakup depending primarily on the nature of the imperfections and not on film density. In comparison with $X=0.9$, T_1 and T_2 for $T \leqslant 0.5K^{-1}$ and the increased E_a demonstrate exchange has replaced thermally activated vacancy tunnelling as the dominant form of motion. Therefore with a large reduction in thermally activated vacancy tunnelling at low T the breakup process is increasingly unmasked and manifests itself as increased *noise* in 'T2Index' and to a lesser extent (see comments for 'T1Index' at $X=0.9$) in 'T1Index' too.

T_2 is frequency independent at low temperatures as expected for dipolar

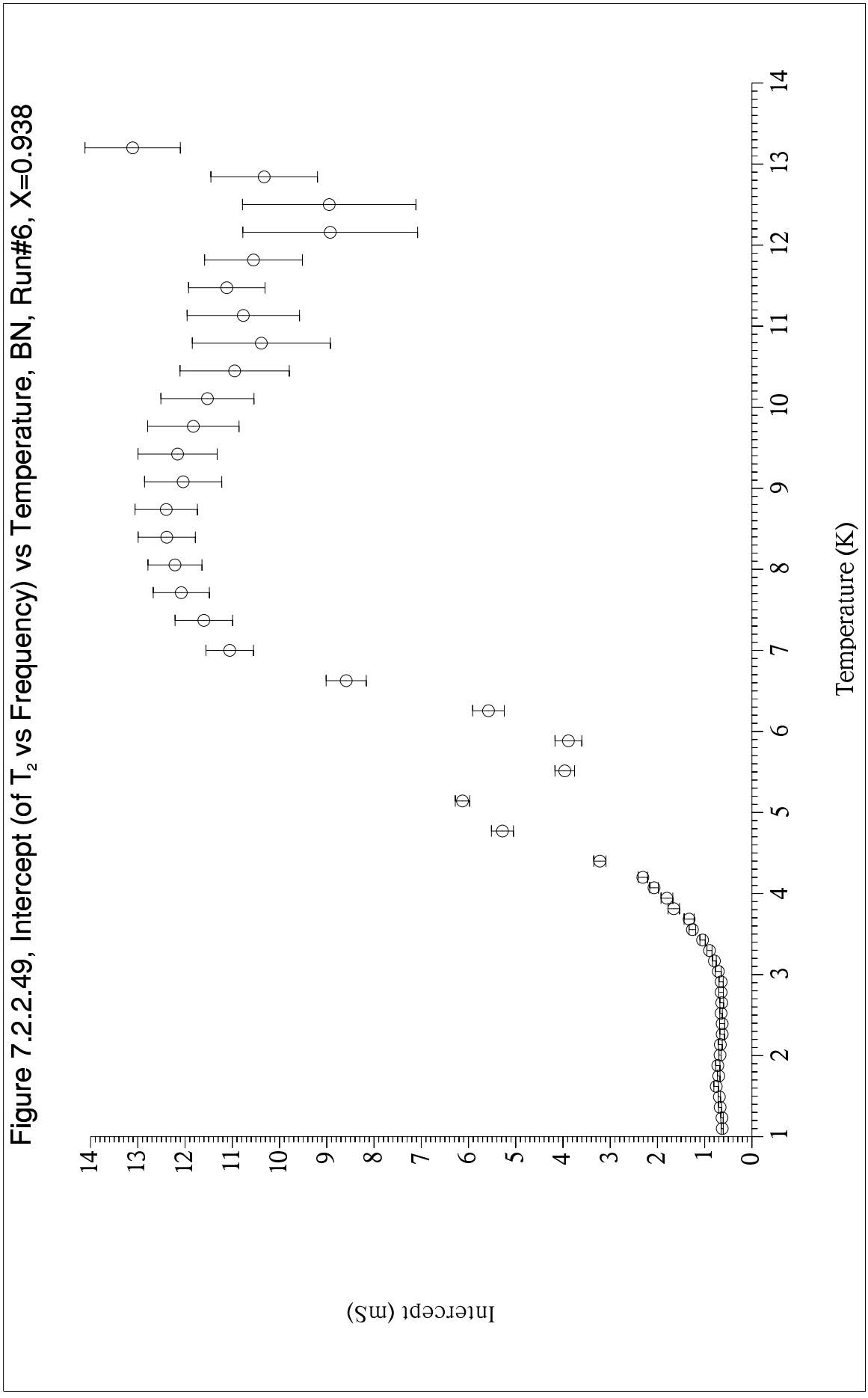
Figure 7.2.2.49, Intercept (of T_2 vs Frequency) vs Temperature, BN, Run#6, X=0.938
Intercept (mS)
Temperature (K)
0
1
2
3
4
5
6
7
8
9
10
11
12
13
14

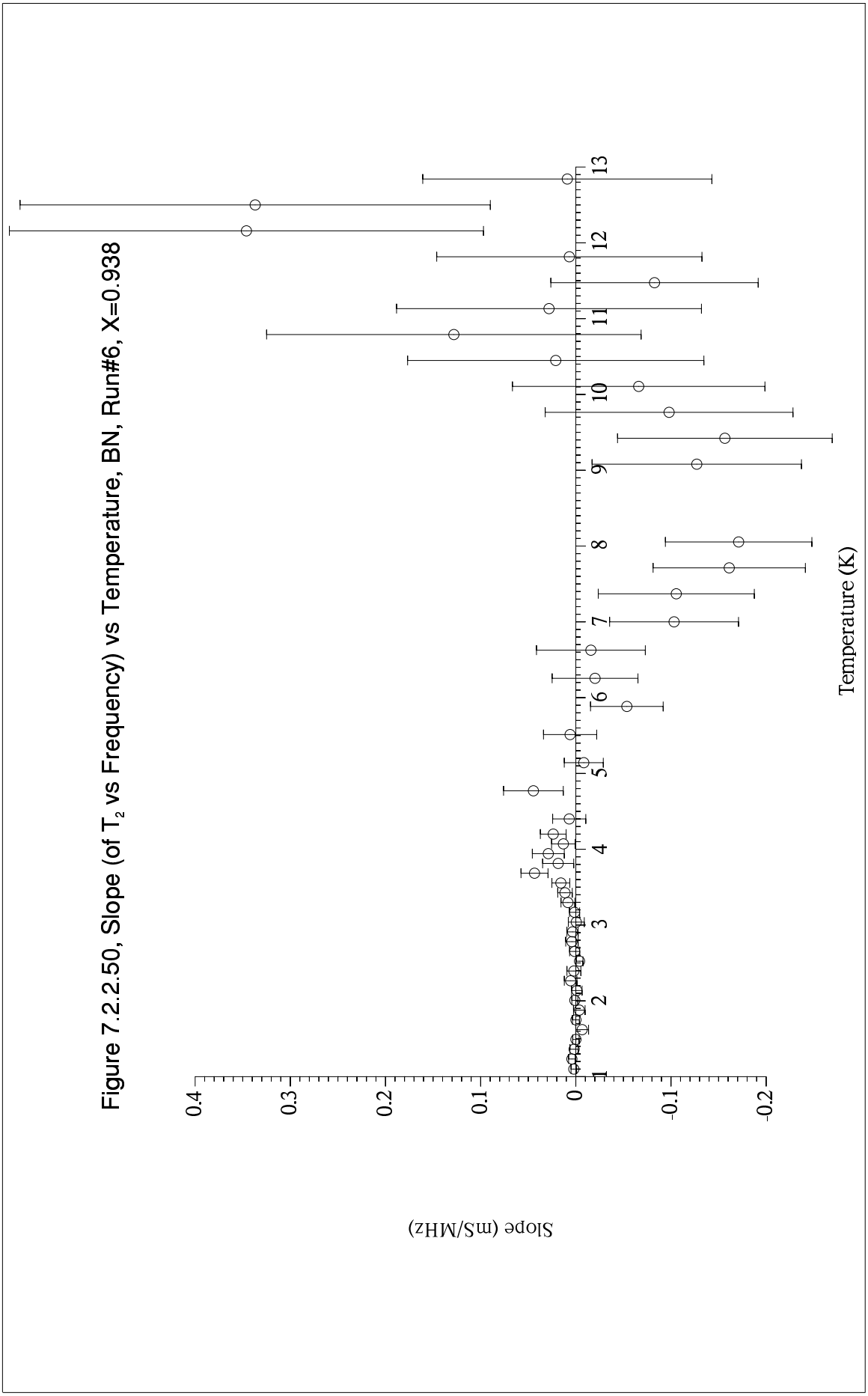
Figure 7.2.2.50, Slope (of T2 vs Frequency) vs Temperature, BN, Run#6, X=0.938
Slope (mS/MHz)
Temperature (K)
0.4
0.3
0.2
0.1
0
-0.1
-0.2
1
2
3
4
5
6
7
8
9
10
11
12
13

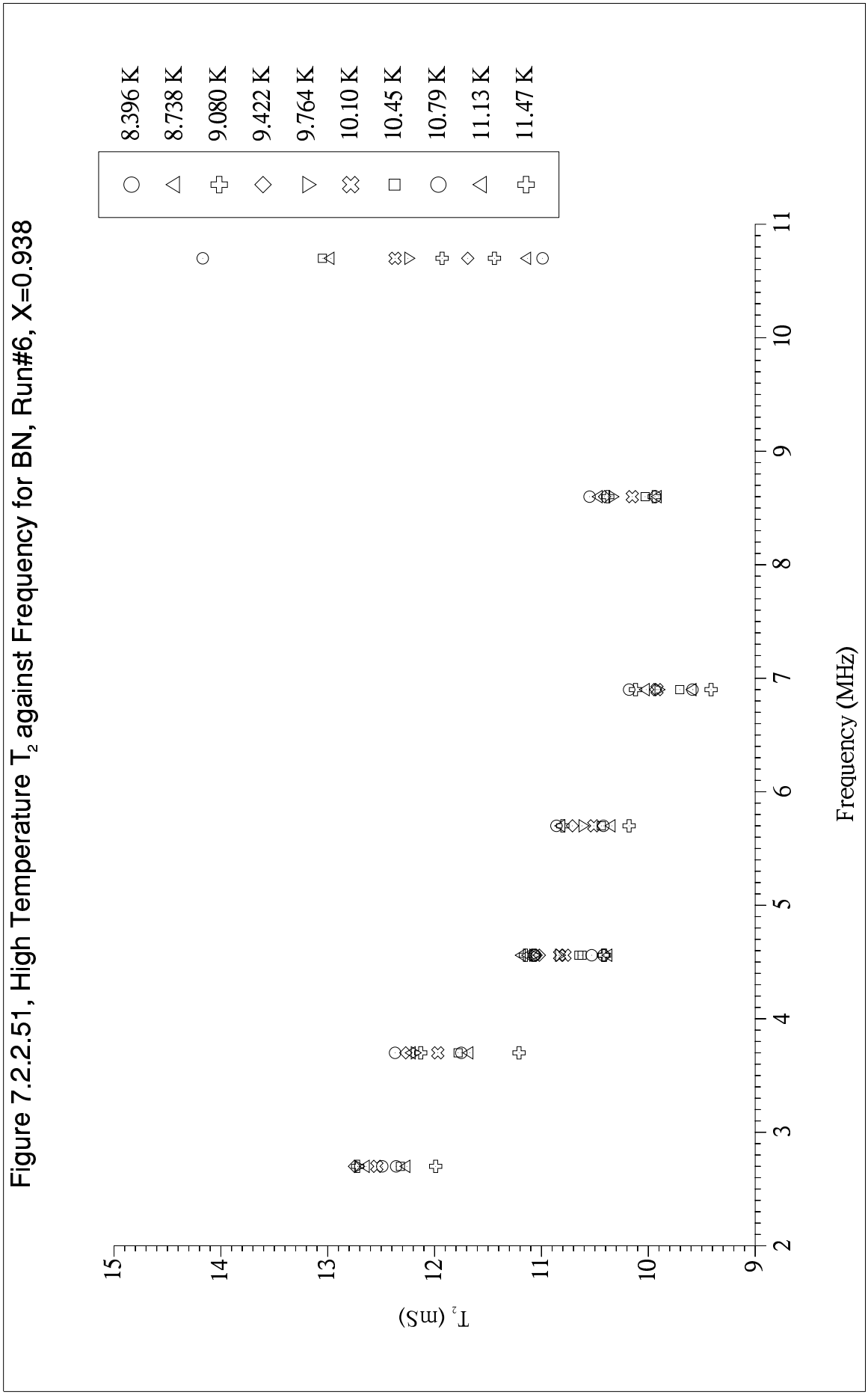

Figure 7.2.2.51, High Temperature T_2 against Frequency for BN, Run#6, X=0.938

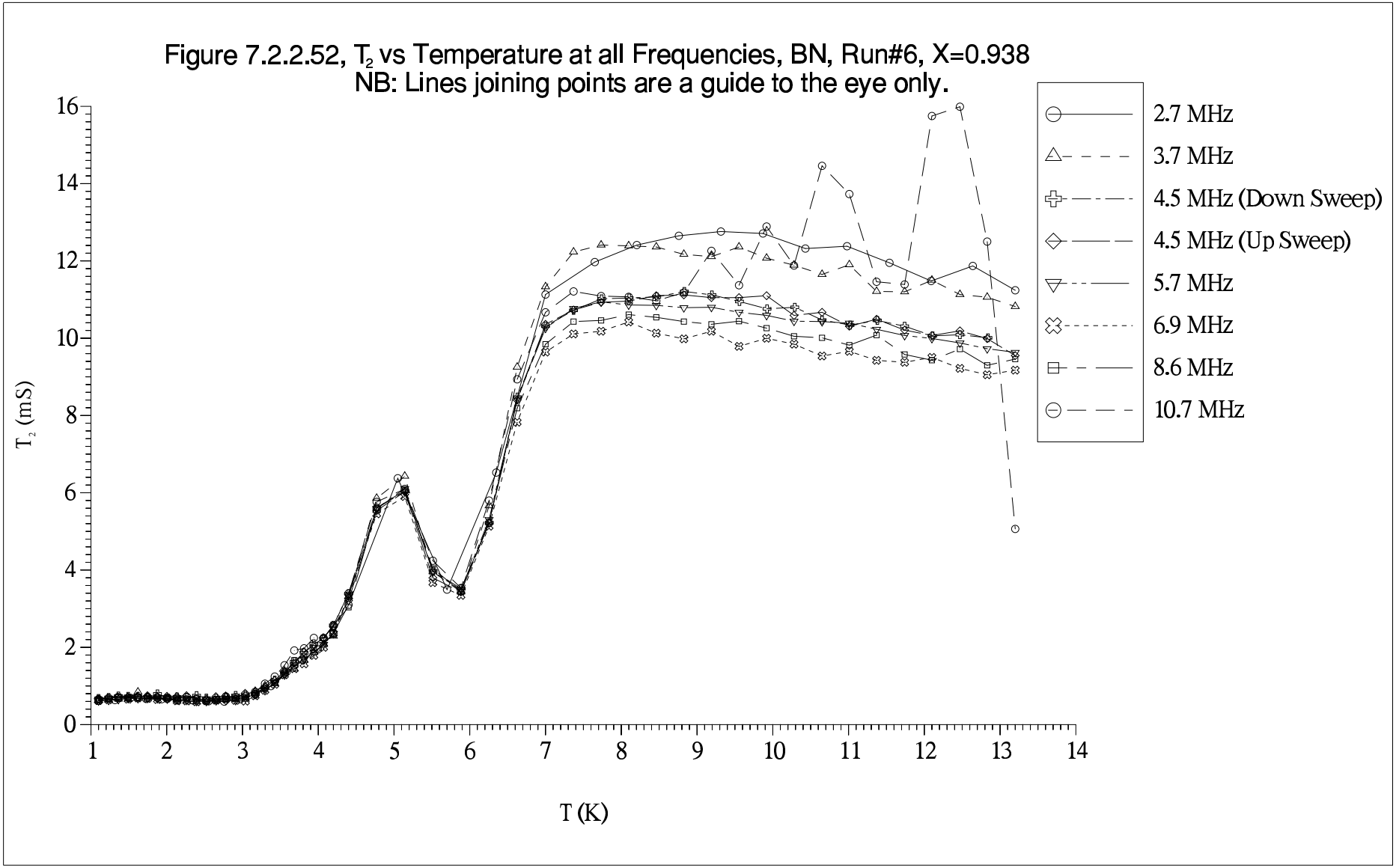
Figure 7.2.2.52, T2 vs Temperature at all Frequencies, BN, Run#6, X=0.938
NB: Lines joining points are a guide to the eye only.
T2 (mS)
T (K)
2.7 MHz
3.7 MHz
4.5 MHz (Down Sweep)
4.5 MHz (Up Sweep)
5.7 MHz
6.9 MHz
8.6 MHz
10.7 MHz

relaxation − Compare the 4.5 and 6.9MHz data in figure 7.2.2.46. Using the T_2 *vs* $1/T$ data taken at the 7 frequencies, linear least squares fits have been applied to the T_2 *vs* F data at each of the ~50 temperatures logged in the range $1.1\text{K} \leqslant T \leqslant 13.2\text{K}$. Figures 7.2.2.49 and 7.2.2.50 show the F=0 intercept and slope as a function of T respectively. The intercept appears as T_2 and accounts for almost all the relaxation at all temperatures. Below 4.5K the slope is approximately zero within experimental error indicating dipolar relaxation. A small minimum in slope at 6K is followed by a broad deep minimum centred on 8.5K which corresponds to the T_2 melt-desorption minimum and desorption maximum respectively. Just before desorption takes place and once motion including that of desorbed spins is fast enough, frequency dependent relaxation in BN diamagnetic fields should be a maximum, suggesting this mechanism. The effect is small, at 4.5MHz and 8.5K only 8% of the value of T_2 is contributed by the frequency dependent part. Noticing the increase in errors at higher temperatures it is clear the T_2 *vs* F data does not follow a linear law here. Neither does it follow the expected theoretical $1/T_2 \propto F^2$ or the experimentally observed (on Grafoil) $1/T_2 \propto F$ law for relaxation in substrate diamagnetic fields (see §1.10.3). Figures 7.2.2.51 and 7.2.2.52 show why. A clear minimum centred on 6.9MHz exists where there is a significant frequency dependence. Increased variation with temperature of T_2 at 10.7MHz, due in part to poorer S/N ratio causing the misleading high temperature slope behaviour. The cause of the minimum is uncertain. Figure 7.2.2.51 also shows the descent from 2.7MHz to the minimum at 6.9MHz is not continuous, with the hint of another minimum at 4.5MHz. In the light of this data the exp $-t^3$ 'CP' relaxation at the desorption maximum (figure 7.2.2.46) may be consistent with relaxation via spin diffusion in the applied field inhomogeneities (ie. if a quirk/feature of the main-magnet leads to its applied field inhomogeneity peaking at $6.9\text{MHz}/\gamma_{\text{He}}$) but not in BN crystallite diamagnetic fields. Features in the high-T, T_2 *vs* F data might be related to heteronuclear spin-spin relaxation, ie. the decay of the ^{3}He transverse magnetisation due to the dipolar interaction between ^{3}He and substrate spins. However equation 8.26 for the heteronuclear T_2 has the same general form as its homonuclear counterpart (equation 2.2.17) including the zero-frequency adiabatic contribution. So at least in a homogeneous system maxima or minima are not expected in τ_c (ie. in T).

In contrast with T_2, the T_1 temperature profile changes considerably with frequency, reaffirming its dipolar nature. Regarding the three T_1 minima in temperature, figures 7.2.2.53 and 7.2.2.54 respectively show the values of T_1 at the minima and their temperatures of occurrence, as a function of frequency. T_1 at the minimum increases

Figure 7.2.2.53, T_1 at T_1 Minima vs Frequency for BN, Run#6, X=0.938, with Straight Line Fits to Data

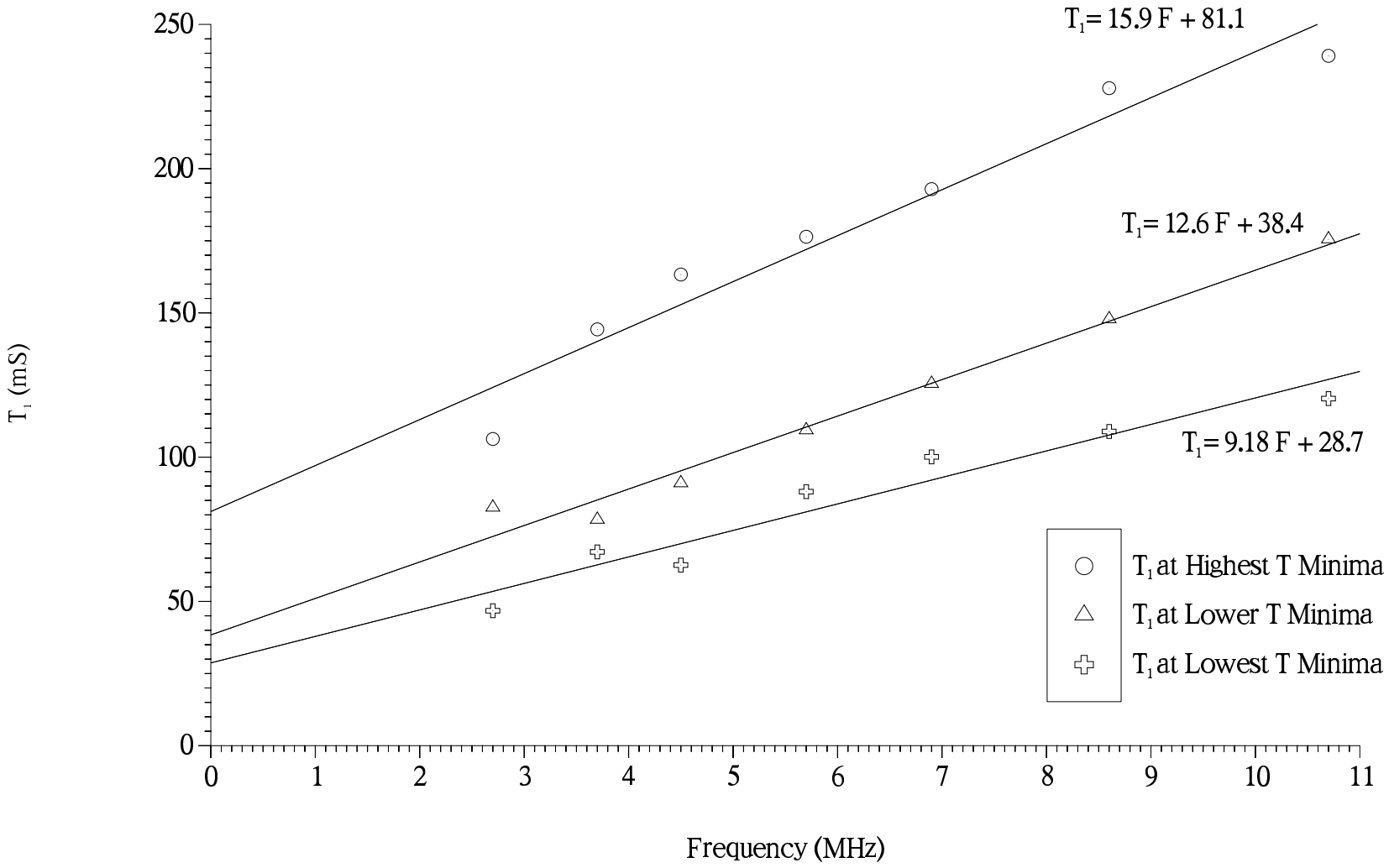

Figure 7.2.2.54, Temperature of T_1 Minima vs Frequency for BN, Run#6, X=0.938

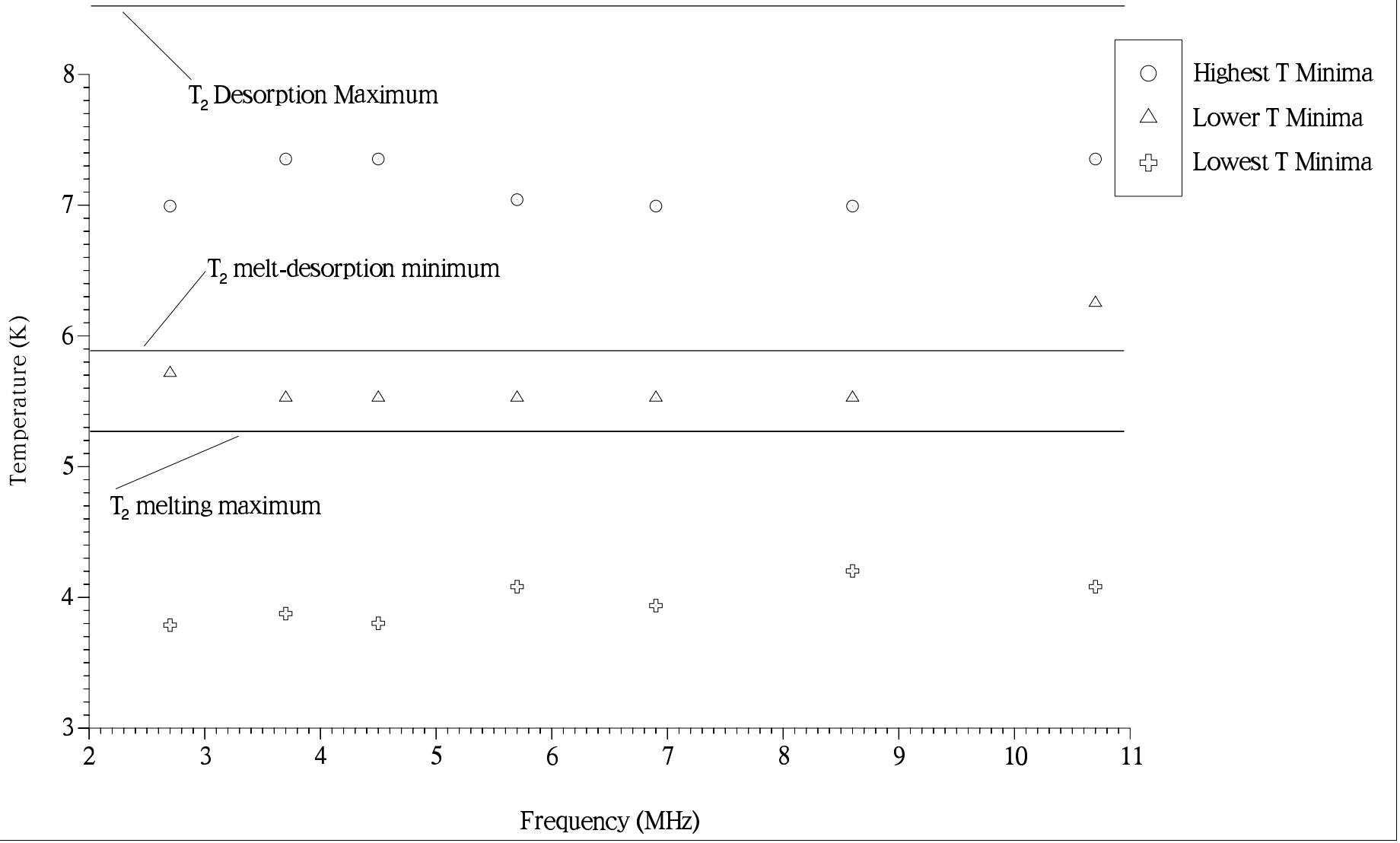

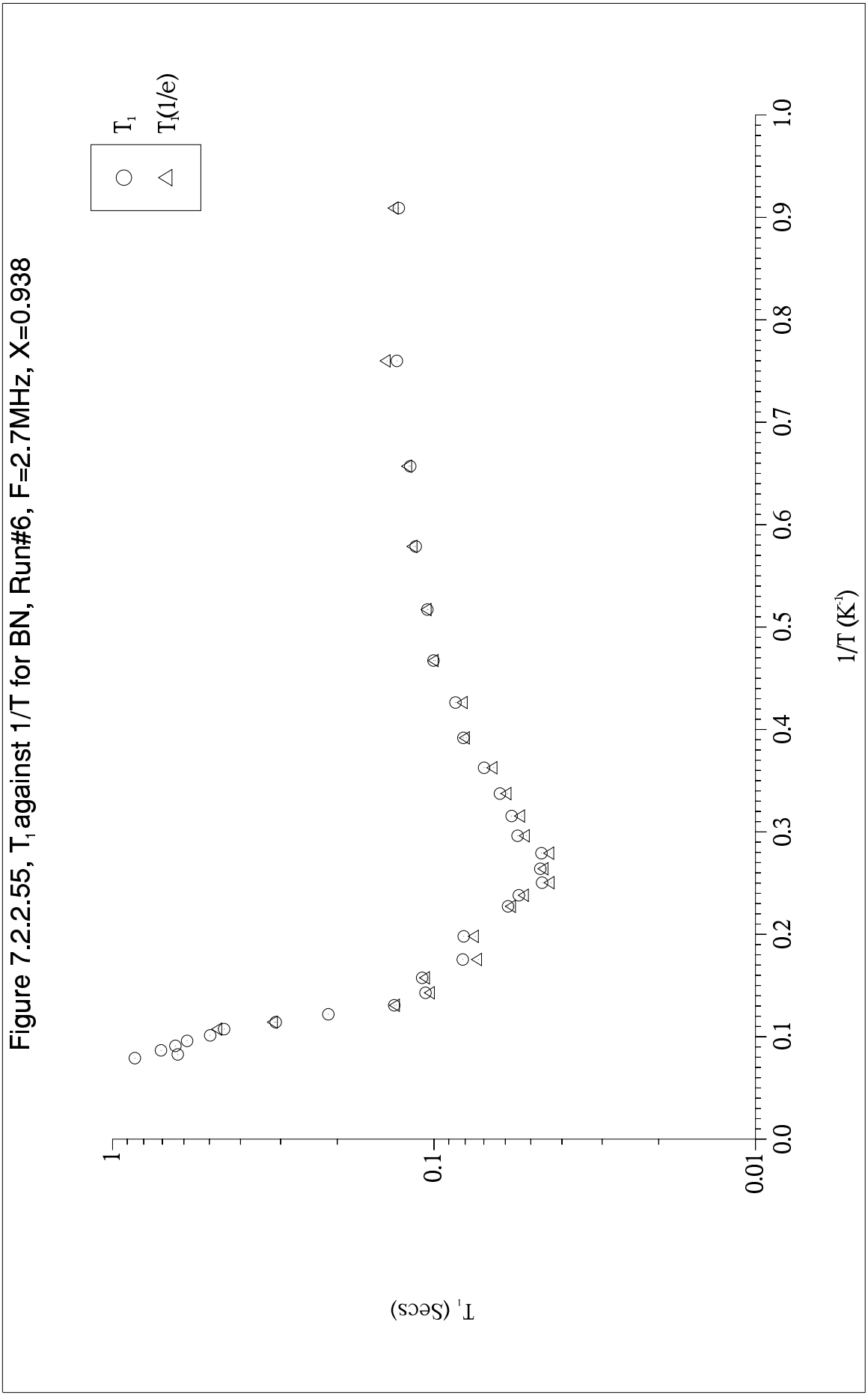
Figure 7.2.2.55, T_1 against 1/T for BN, Run#6, F=2.7MHz, X=0.938
T_1
$T_1(1/e)$
T_1 (Secs)
1
0.1
0.01
0.0
0.1
0.2
0.3
0.4
0.5
0.6
0.7
0.8
0.9
1.0
1/T (K^{-1})

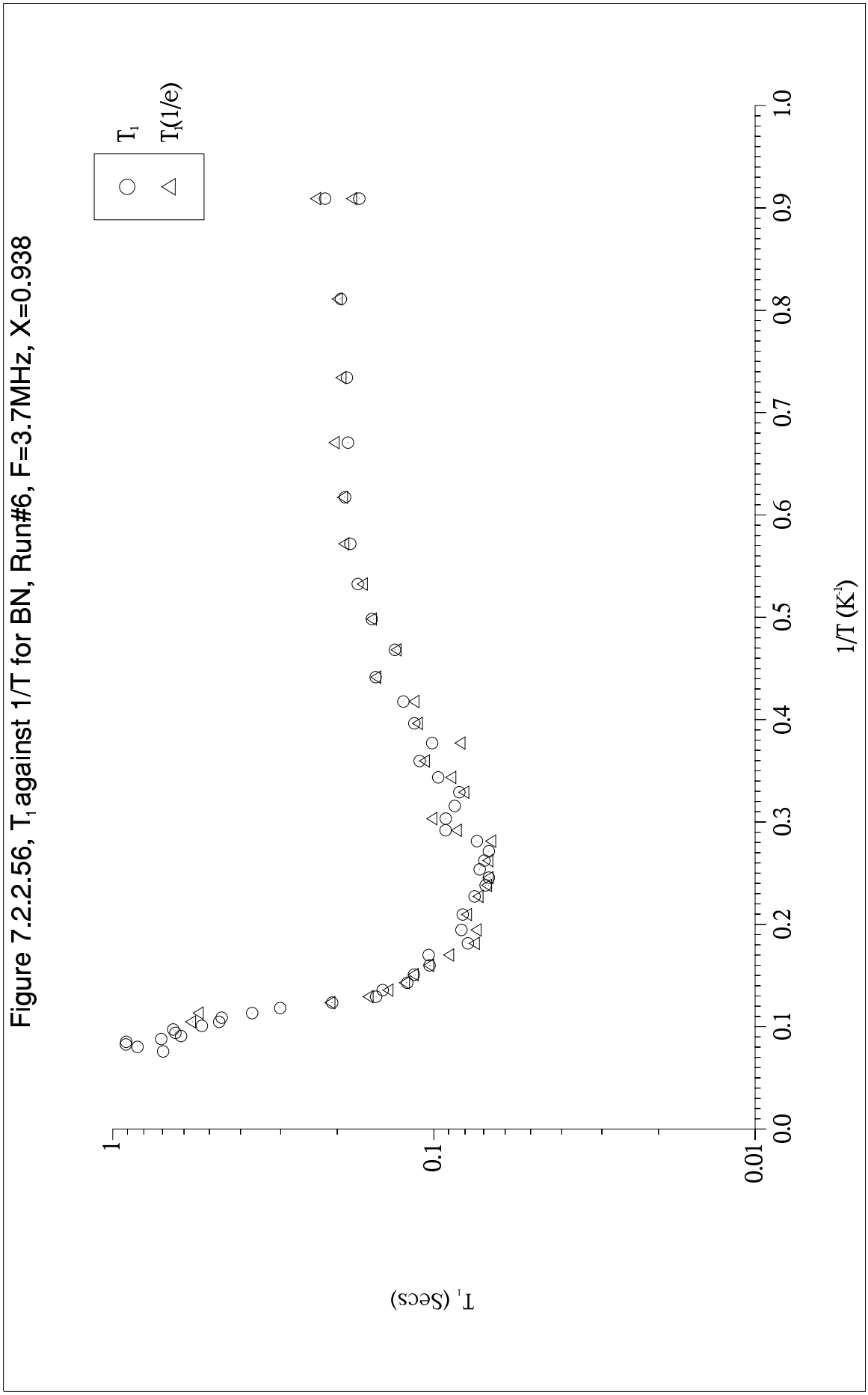
Figure 7.2.2.56, T1 against 1/T for BN, Run#6, F=3.7MHz, X=0.938
T1
T1(1/e)
T1 (Secs)
1
0.1
0.01
0.0
0.1
0.2
0.3
0.4
0.5
0.6
0.7
0.8
0.9
1.0
1/T (K-1)

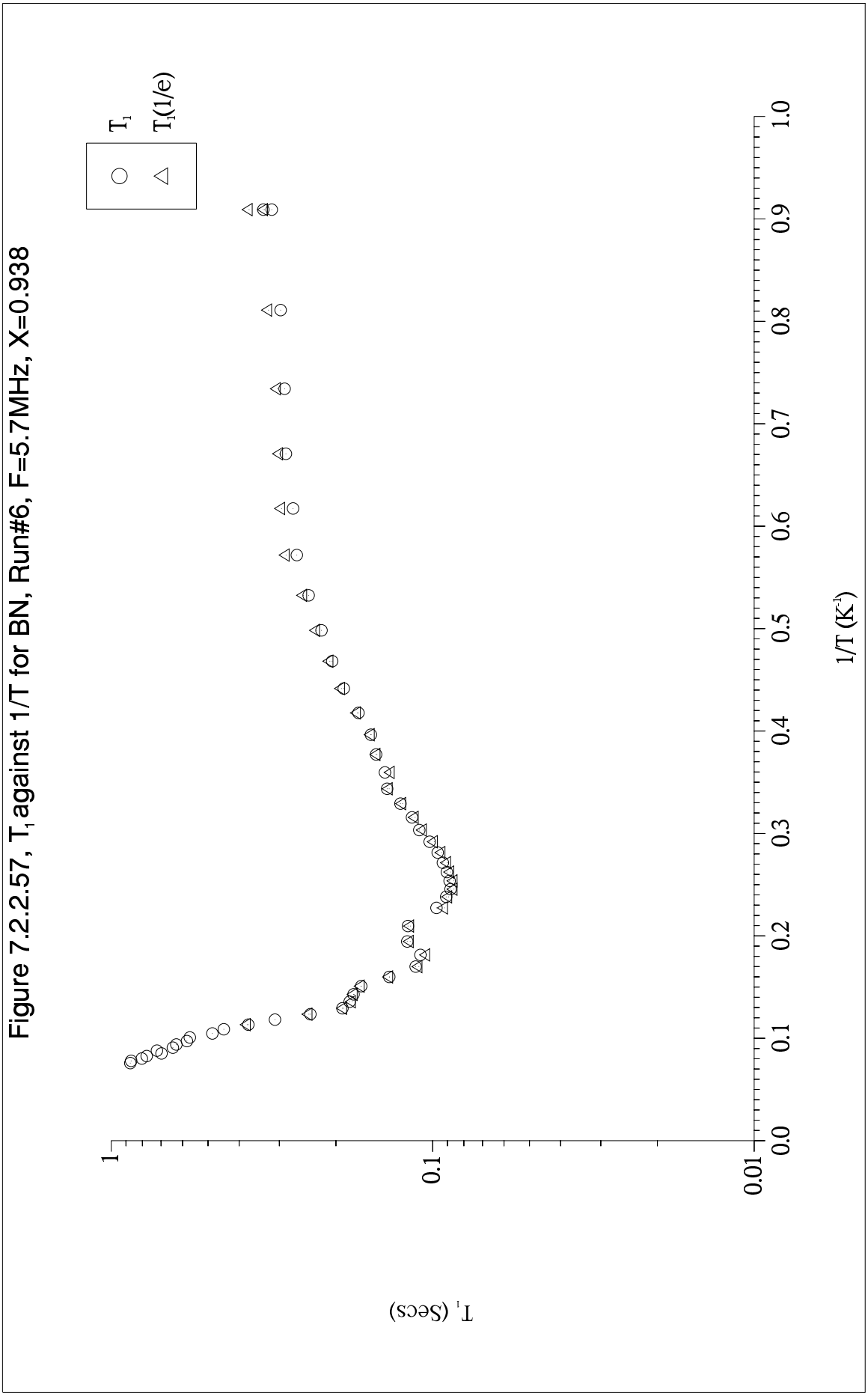
Figure 7.2.2.57, T_1 against 1/T for BN, Run#6, F=5.7MHz, X=0.938
T_1
T_1(1/e)
T_1 (Secs)
1
0.1
0.01
0.0
0.1
0.2
0.3
0.4
0.5
0.6
0.7
0.8
0.9
1.0
1/T (K^{-1})

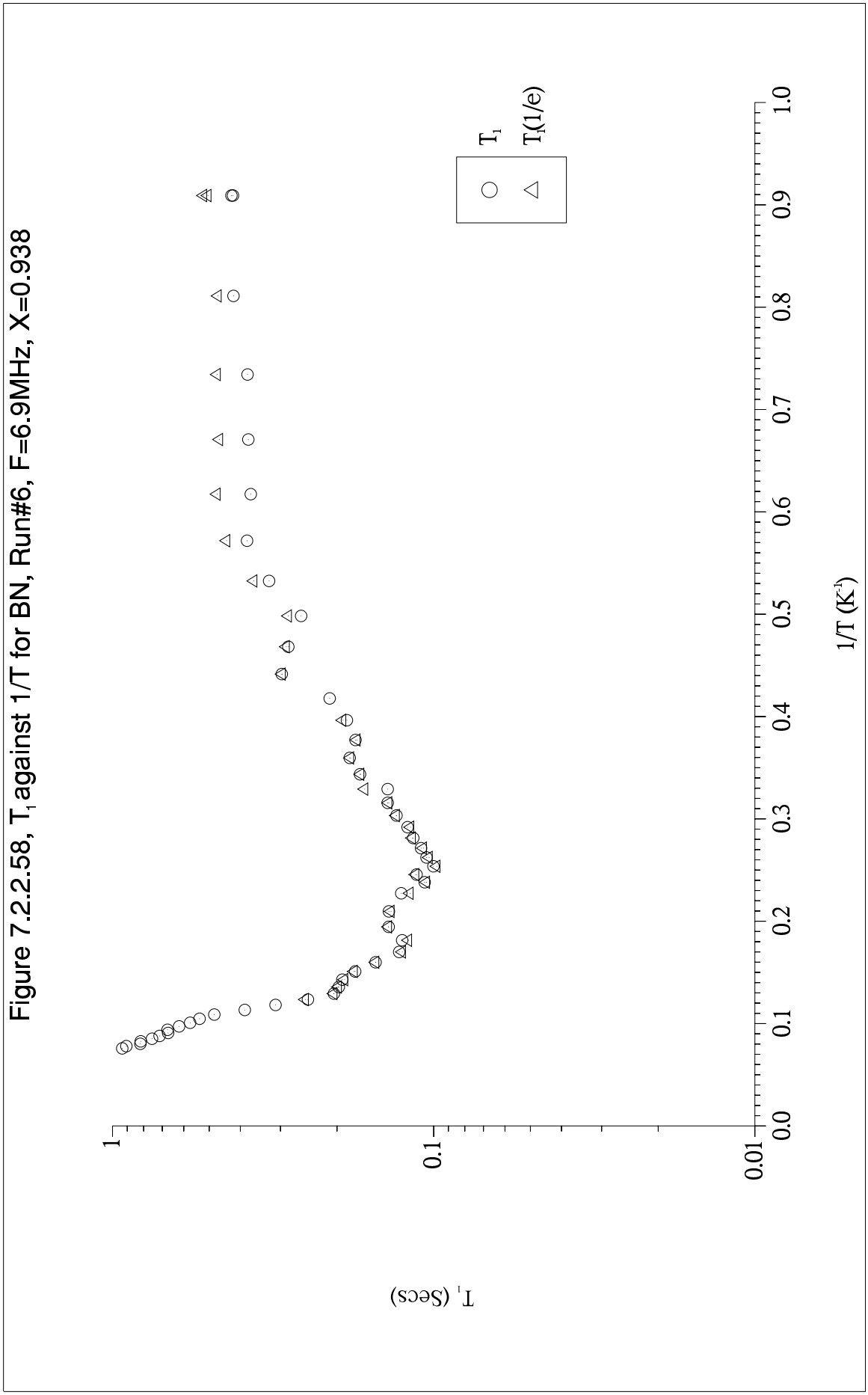
Figure 7.2.2.58, T1 against 1/T for BN, Run#6, F=6.9MHz, X=0.938
T1 (Secs)
1
0.1
0.01
0.0
0.1
0.2
0.3
0.4
0.5
0.6
0.7
0.8
0.9
1.0
1/T (K-1)
T1
T1(1/e)

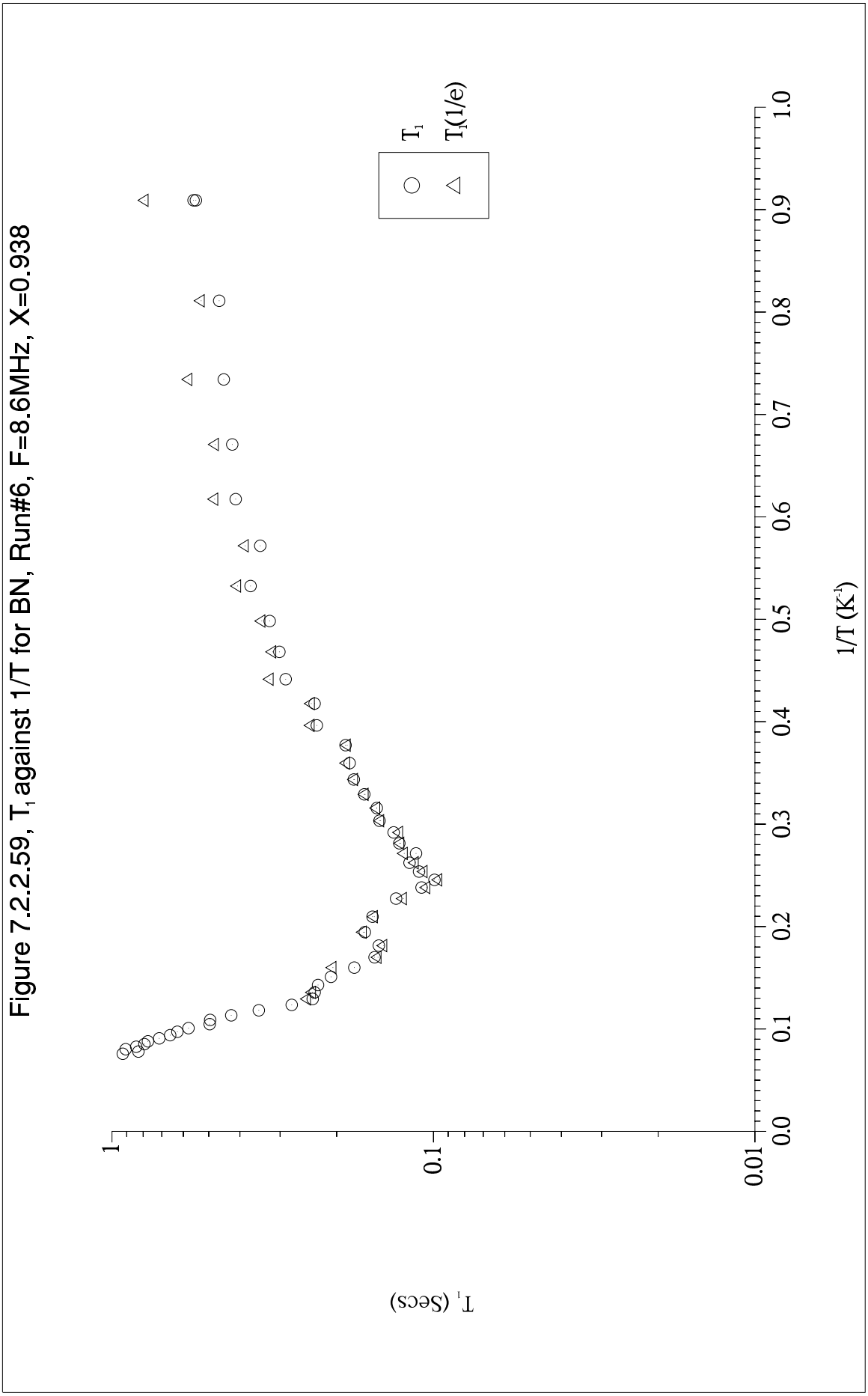
Figure 7.2.2.59, T1 against 1/T for BN, Run#6, F=8.6MHz, X=0.938
T1 (Secs)
1
0.1
0.01
0.0
0.1
0.2
0.3
0.4
0.5
0.6
0.7
0.8
0.9
1.0
1/T (K-1)
T1
T1(1/e)

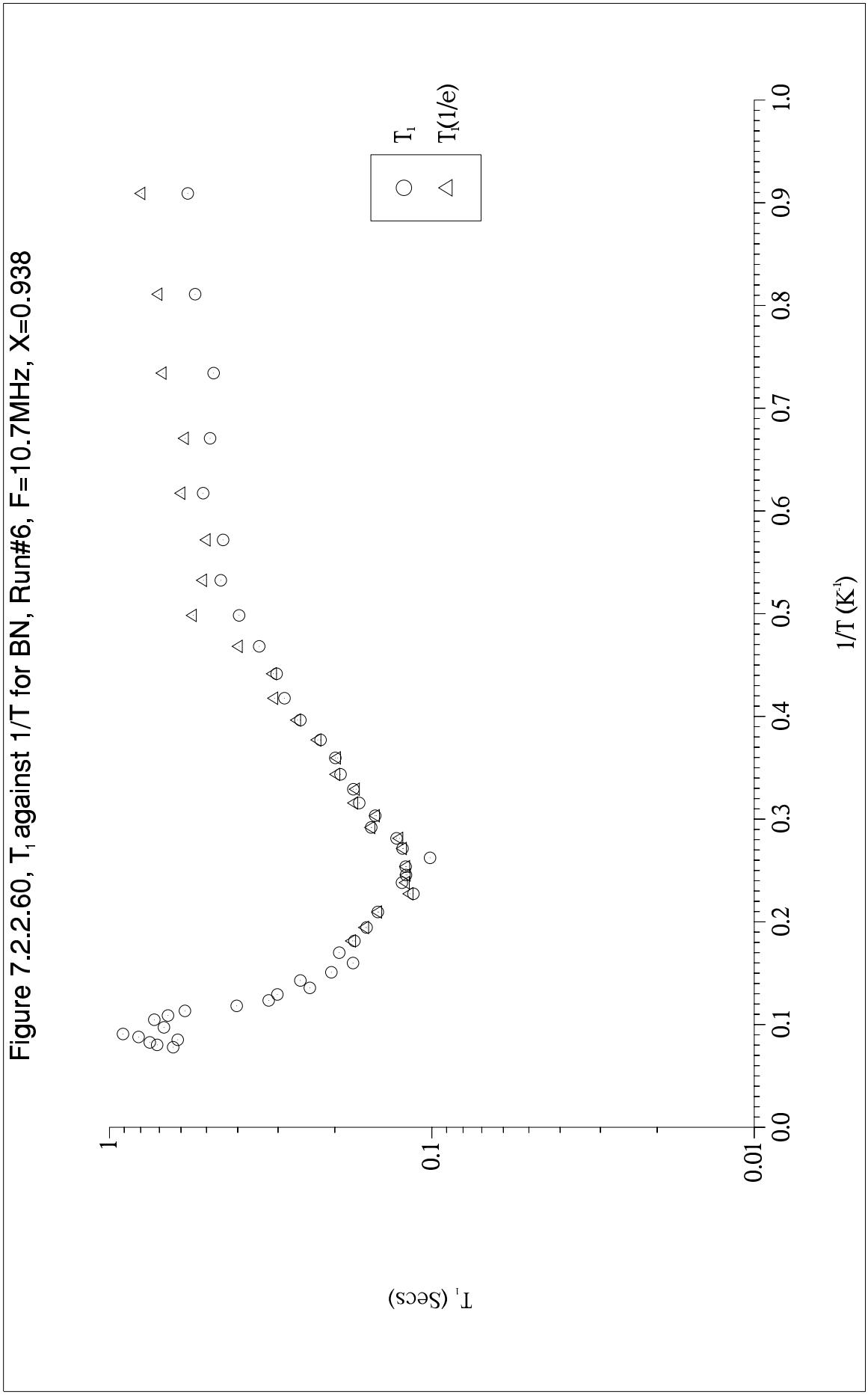
Figure 7.2.2.60, T1 against 1/T for BN, Run#6, F=10.7MHz, X=0.938
T1 (Secs)
1
0.1
0.01
0.0
0.1
0.2
0.3
0.4
0.5
0.6
0.7
0.8
0.9
1.0
1/T (K-1)
T1
T1(1/e)

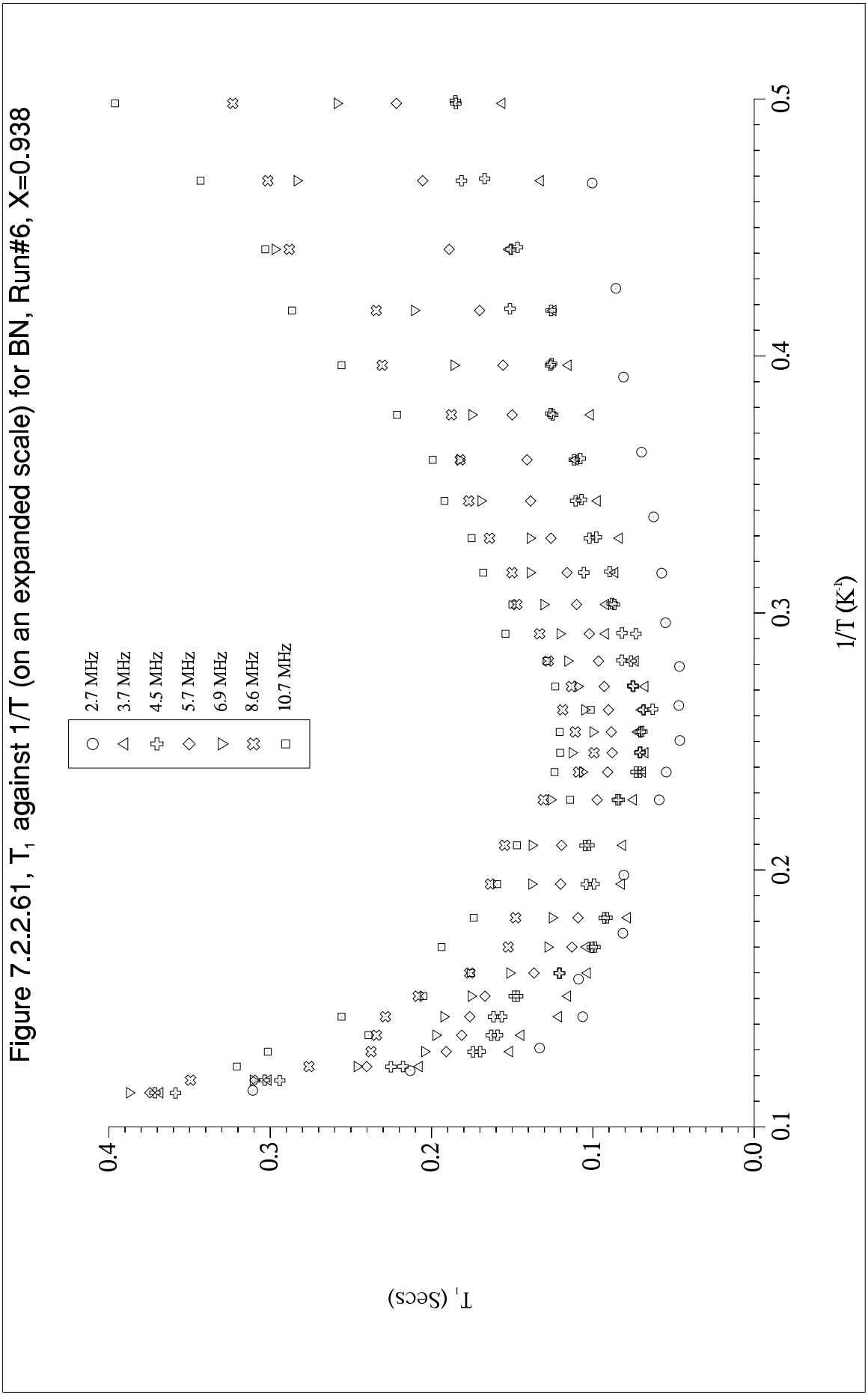
Figure 7.2.2.61, T_1 against 1/T (on an expanded scale) for BN, Run#6, X=0.938
2.7 MHz
3.7 MHz
4.5 MHz
5.7 MHz
6.9 MHz
8.6 MHz
10.7 MHz
T_1 (Secs)
1/T (K^{-1})
0.0
0.1
0.2
0.3
0.4
0.5

approximately linearly with frequency for all three minima as expected for dipolar relaxation ($T_1^{\min} = \omega_0/m_2$, in the homonuclear case). In contrast with homonuclear theory T_1 does not go anywhere near the origin. Again, this implies the frequency ω_x in the minimum condition $\omega_x\tau_c \sim 1$ is not simply the Larmor frequency. Also interesting is the increase in slope of the higher temperature minima. Layer promotion is expected to increase the slope ($1/m_2$) for simple homonuclear relaxation but the true explanation must lie in a full description including the heteronuclear mechanism. Scatter in the data is mainly due to difficulty precisely locating the minima. There is little frequency dependence in the minima's temperature-of-occurrence (figure 7.2.2.54). Assuming an activation law for τ_c (equation 1.10.4.3) and $\omega_x\tau_c = const$ within each set of minima, the small increase in temperature-of-occurrence with frequency of the lowest T minimum implies an E_a of ~40−50K. Figure 7.2.3.11 shows this activation energy compares with the Grafoil value and the BN energy of desorption but not with the BN 2D solid E_a. It is the 2D solid value which should operate here since the first T_1 minima occur well below the T_2 melting maximum as indicated in figure 7.2.2.54. Unfortunately the temperature-of-occurrence variation with frequency is shrouded in experimental scatter. If a suitable *shape-function* for the T_1 minima in T could be found, least-squares fitting through each minimum would much increase the accuracy of the (position,value) estimates as it did in the T_1 *vs* X minima case (figure 7.2.1.7).

Figures 7.2.2.55 to 7.2.2.60 plus figure 7.2.2.47 show T_1 against $1/T$ for the seven frequencies used. Additionally, in figure 7.2.2.61 the data is re-plotted together for comparison using an expanded scale over the temperature range where minima occur. Comparing the individual frequency plots, F=2.7MHz $\rightarrow$ 10.7MHz, two features are evident: (1) The low temperature T_1 increases by a factor of 4×. Approaching the minima from low temperatures, the fall-off in T_1 is much more rapid at high frequencies. This is expected since $(\omega_x\tau_c)^{\text{10.7MHz \& low } T} \gg (\omega_x\tau_c)^{\text{2.7MHz \& low } T} \gg (\omega_x\tau_c)^{\text{minima}} \sim 1$, for the respective minima. (2) The relative depth of the 3 minima in temperature increases monotonically from 2.7MHz to 8.6MHz. Abruptly at 10.7MHz the 3 minima are almost subsumed into a single broad minimum. The point is illustrated more clearly by the linear plot of figure 7.2.2.61. The reason for this not certain but the increase in T of the higher-T minimum at 10.7MHz with attendant minimum-broadening due to increased layer promotion/desorption probably plays a part.

Figures 7.2.2.62 and 7.2.2.63 plot the slope and F=0 intercept from straight line fits to the T_1 *vs* F data, as a function of T, as was done for T_2. As already alluded to, the low temperature slope falls steeply with increasing T as thermal activation in the

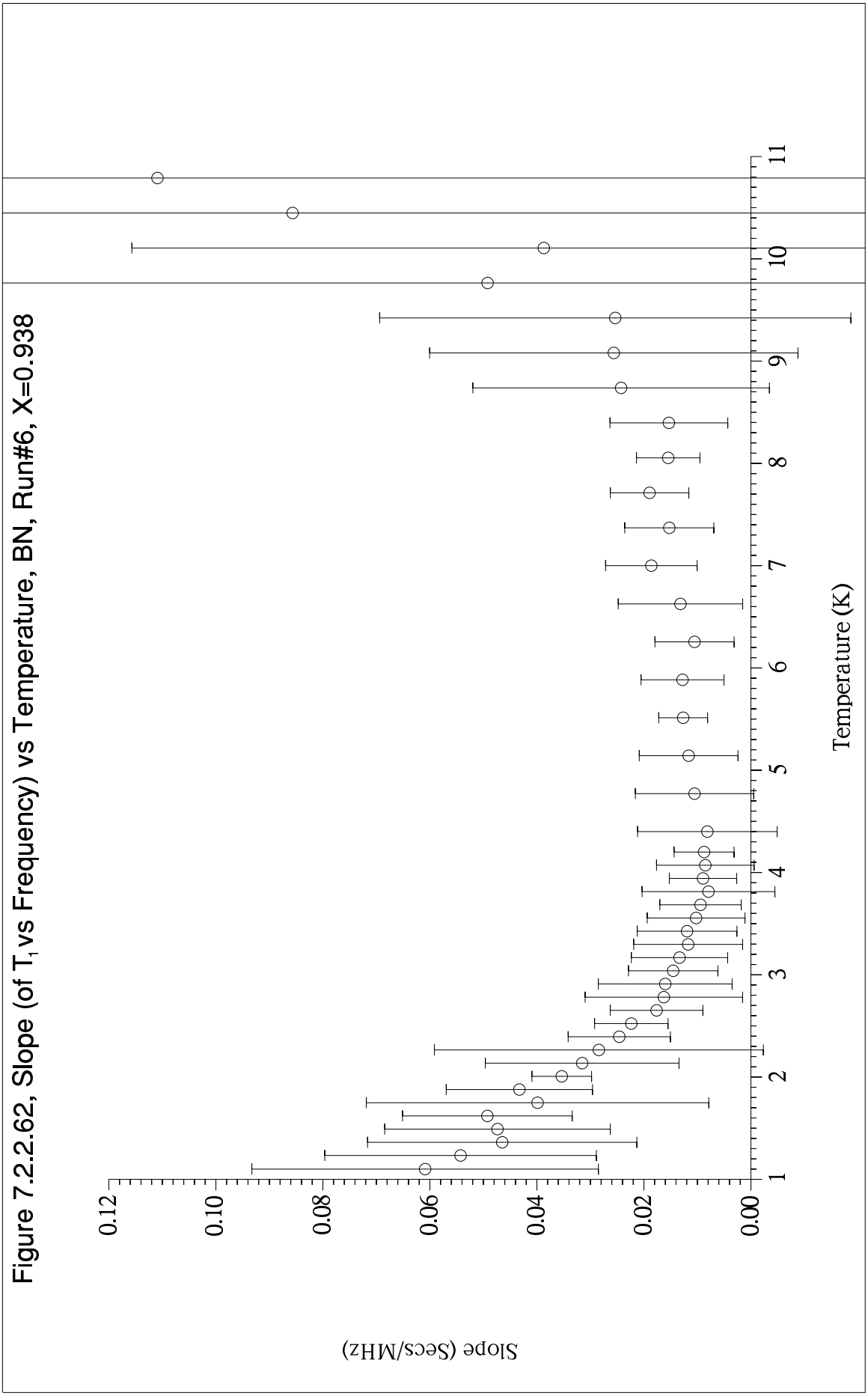
Figure 7.2.2.62, Slope (of T_1 vs Frequency) vs Temperature, BN, Run#6, X=0.938
Slope (Secs/MHz)
0.12
0.10
0.08
0.06
0.04
0.02
0.00
1
2
3
4
5
6
7
8
9
10
11
Temperature (K)

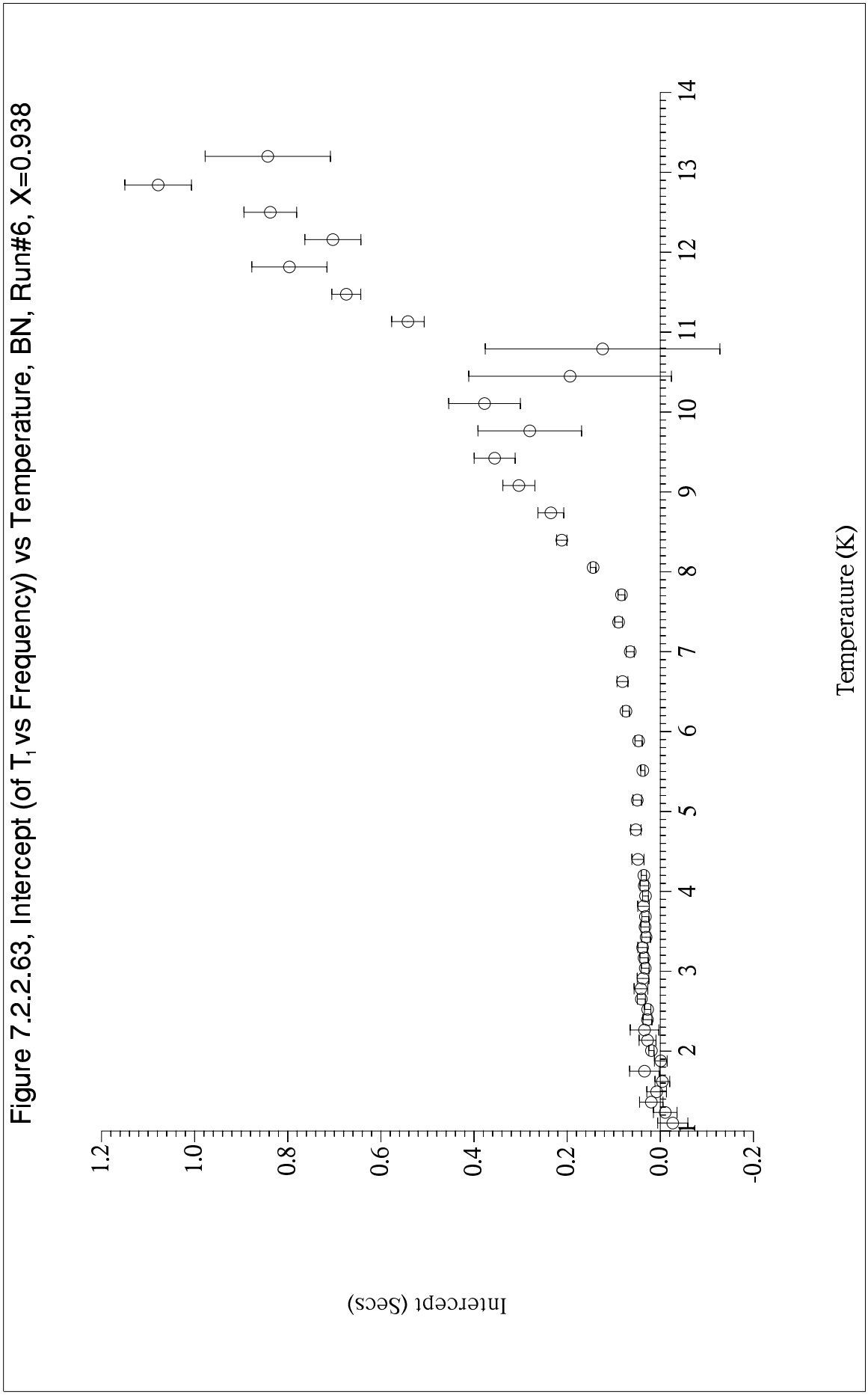
Figure 7.2.2.63, Intercept (of T1 vs Frequency) vs Temperature, BN, Run#6, X=0.938
Intercept (Secs)
1.2
1.0
0.8
0.6
0.4
0.2
0.0
-0.2
1
2
3
4
5
6
7
8
9
10
11
12
13
14
Temperature (K)

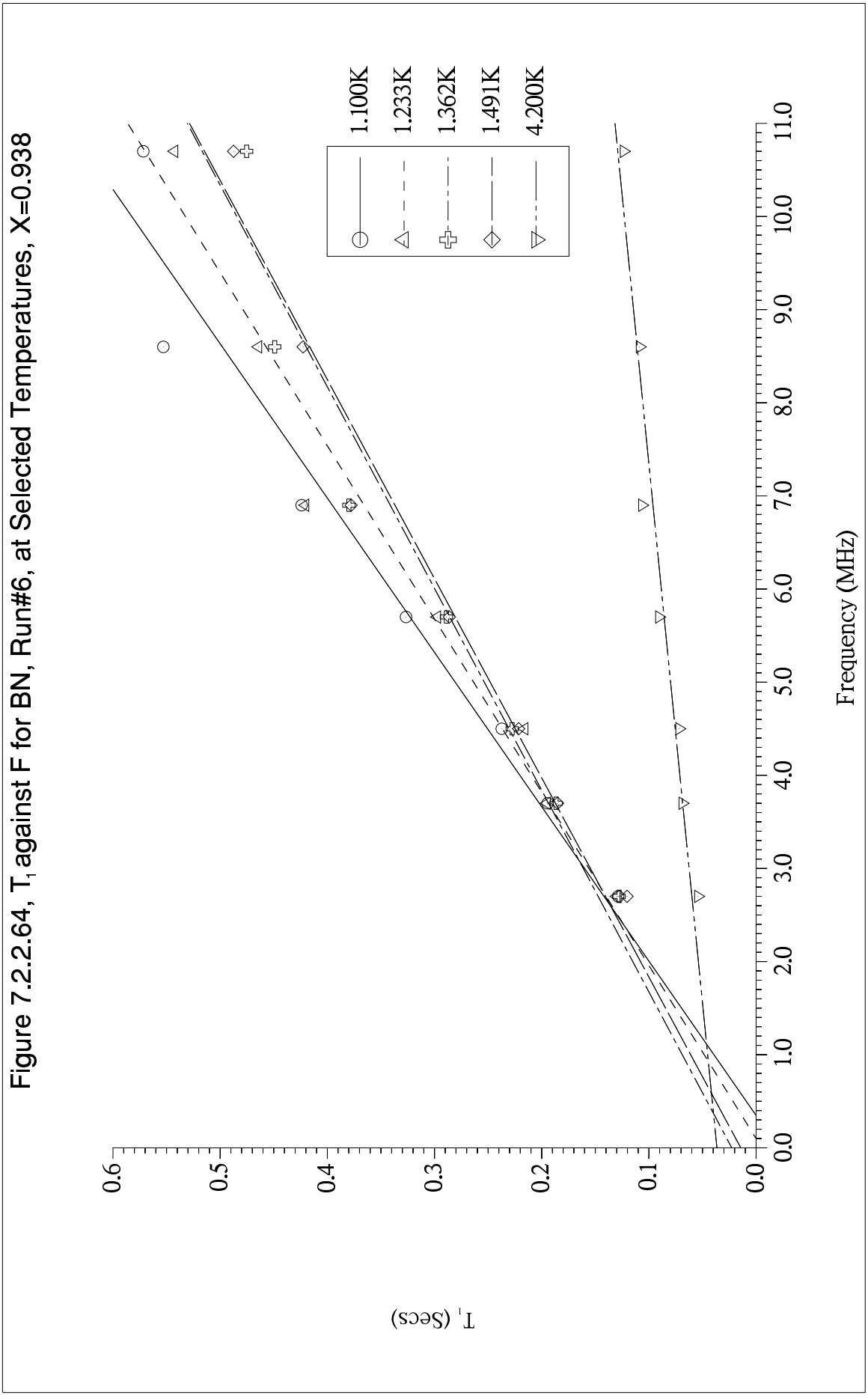

Figure 7.2.2.64, T_1 against F for BN, Run#6, at Selected Temperatures, X=0.938

incommensurate solid reduces τ_c towards the T_1 minima (equation 1.10.4.3). It is at low temperatures where the high frequency part of the spectral density ($\omega_x\tau_c>1$) determining T_1 varies most rapidly with frequency. From 1.1K to 2.6K the slope falls approximately linearly with T. Similar behaviour but with a slower fall occurs from 2.6K to the first minimum at ~3.8K (see figure 7.2.2.54). For mid-range temperatures where T_1 minima occur ($4K\leqslant T\leqslant 8K$) the slope is small and nearly constant (actually rising very slowly). Roughly speaking this is the expected behaviour where $\omega_x\tau_c\leqslant 1$. That the slope remains finite here is significant. Although we must be careful applying the successful (homonuclear) 2D relaxation theory [70] to this much more complicated system with its multiple T_1 minima etc., it must be remembered that frequency dependence on the fast side of a minimum is a known feature of the reduced dimensionality. At $T\geqslant 9K$ a combination of more rapidly increasing T_1 with T, decreasing S/N with increasing T and desorption (figures 7.2.2.46 and 7.2.2.54) leads to complete breakdown of the approximately linear relation. For $2K<T<8K$ the $F=0$ intercept remains positive and approximately constant, falling to a little below zero at $T=2K\rightarrow 1.1K$. At, for example, 4.2K where slope has become small the frequency independent contribution to T_1 $\approx$ the frequency dependent part, evaluated at 4.5MHz (see figure 7.2.2.64). Such behaviour contrasts with the homonuclear predictions in 2D [68] ($T_1 \propto \omega_0$, $0\leqslant\omega_0\tau_c\leqslant 2$) − unsurprisingly. Looking at the errors, particularly in the slopes, it is clear the fits are quite poor at low temperatures. Figure 7.2.2.64 shows some of the T_1 *vs* F data at low temperatures. The deviations from a linear law mostly consist of a faster increase of T_1 with F at the higher frequencies followed by an apparent anomalously low point at 10.7MHz. Without the 10.7MHz points the super-linear T_1 would be understandable in terms of 2D homonuclear relaxation concepts: Sum rule arguments concerning the moments preclude the linear frequency relation continuing indefinitely. Moreover, it is at the lowest temperatures where $\omega_x\tau_c$ is large because the thermally activated vacancy tunnelling rate is small, that the increased fall-off in high frequency motion leads to the increased rise in T_1 with F. If the 10.7MHz deviation could be explained by heteronuclear relaxation, itself driven by the same ^{3}He-film motion as the ^{3}He−^{3}He spin-lattice relaxation, then the above argument stands or might be generalised to include the heteronuclear relaxation channels.

***X*=1.0,** At this coverage maximum first layer density is reached. The incommensurate solid melts directly to the fluid. An increased second layer population exists at low temperatures.

Figure 7.2.2.65 ,T_2 against 1/T, BN, Run#6, F=4.5MHz, X=1.0

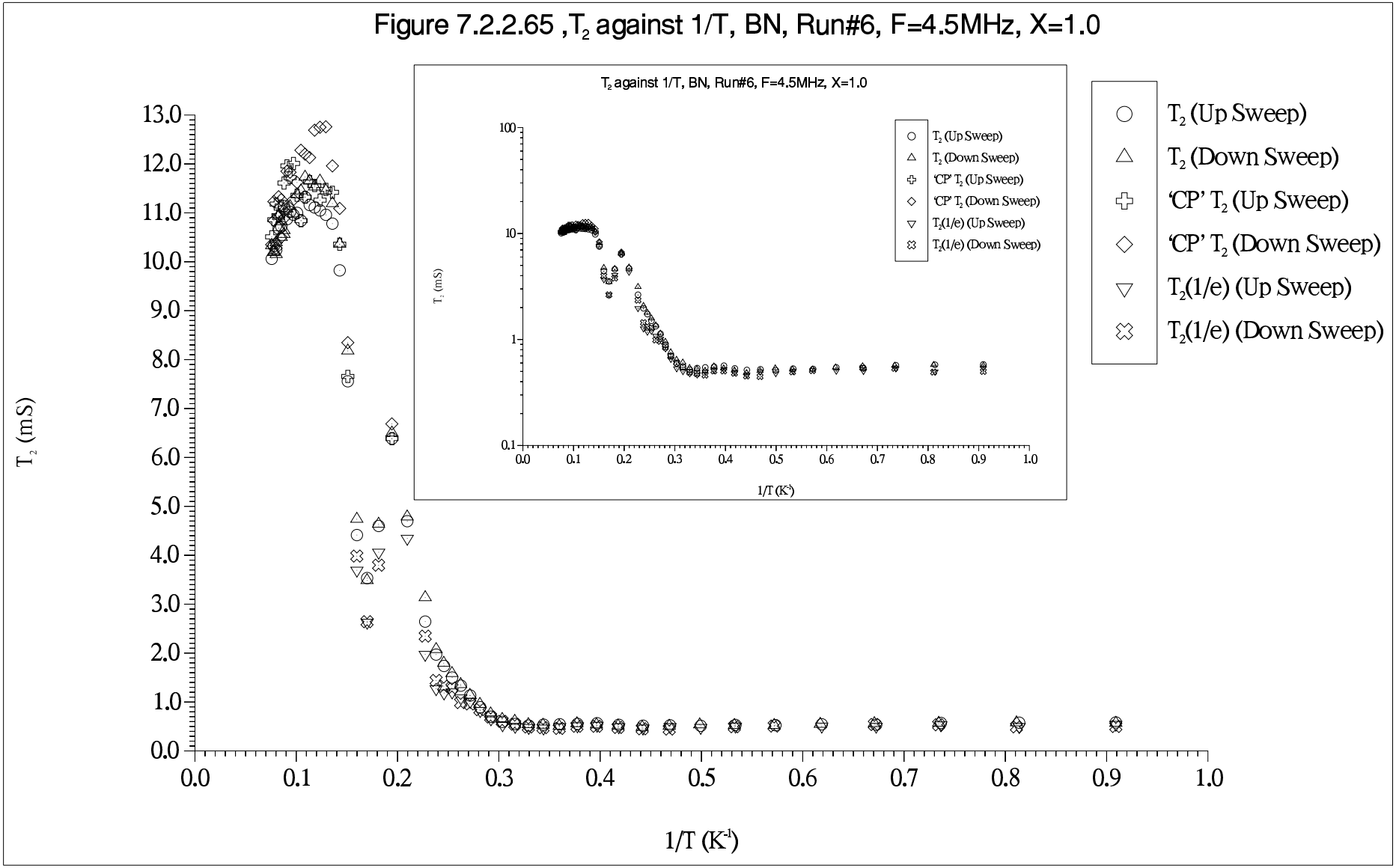

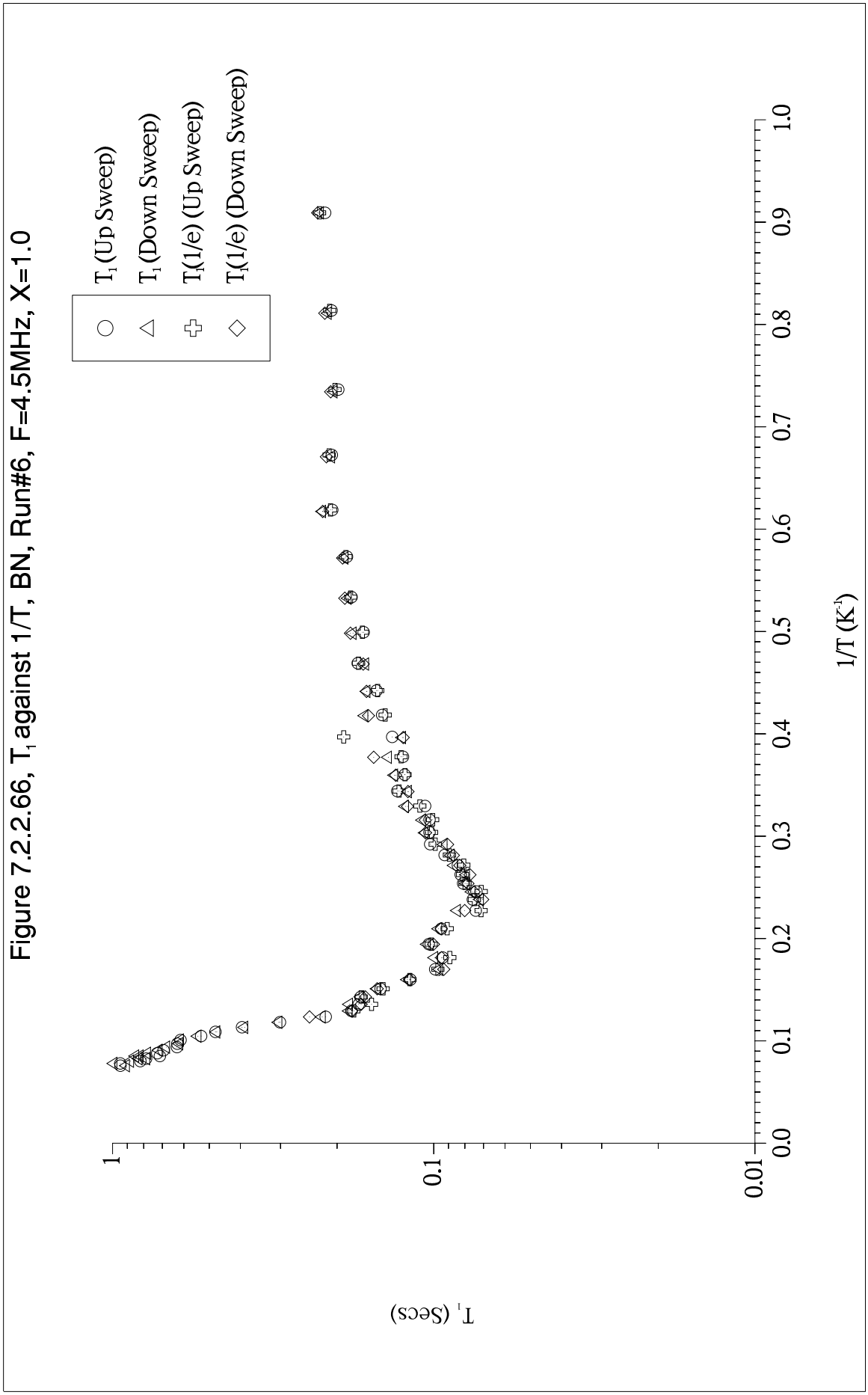
Figure 7.2.2.66, T1 against 1/T, BN, Run#6, F=4.5MHz, X=1.0
T1 (Up Sweep)
T1 (Down Sweep)
T1(1/e) (Up Sweep)
T1(1/e) (Down Sweep)
T1 (Secs)
1
0.1
0.01
0.0
0.1
0.2
0.3
0.4
0.5
0.6
0.7
0.8
0.9
1.0
1/T (K-1)

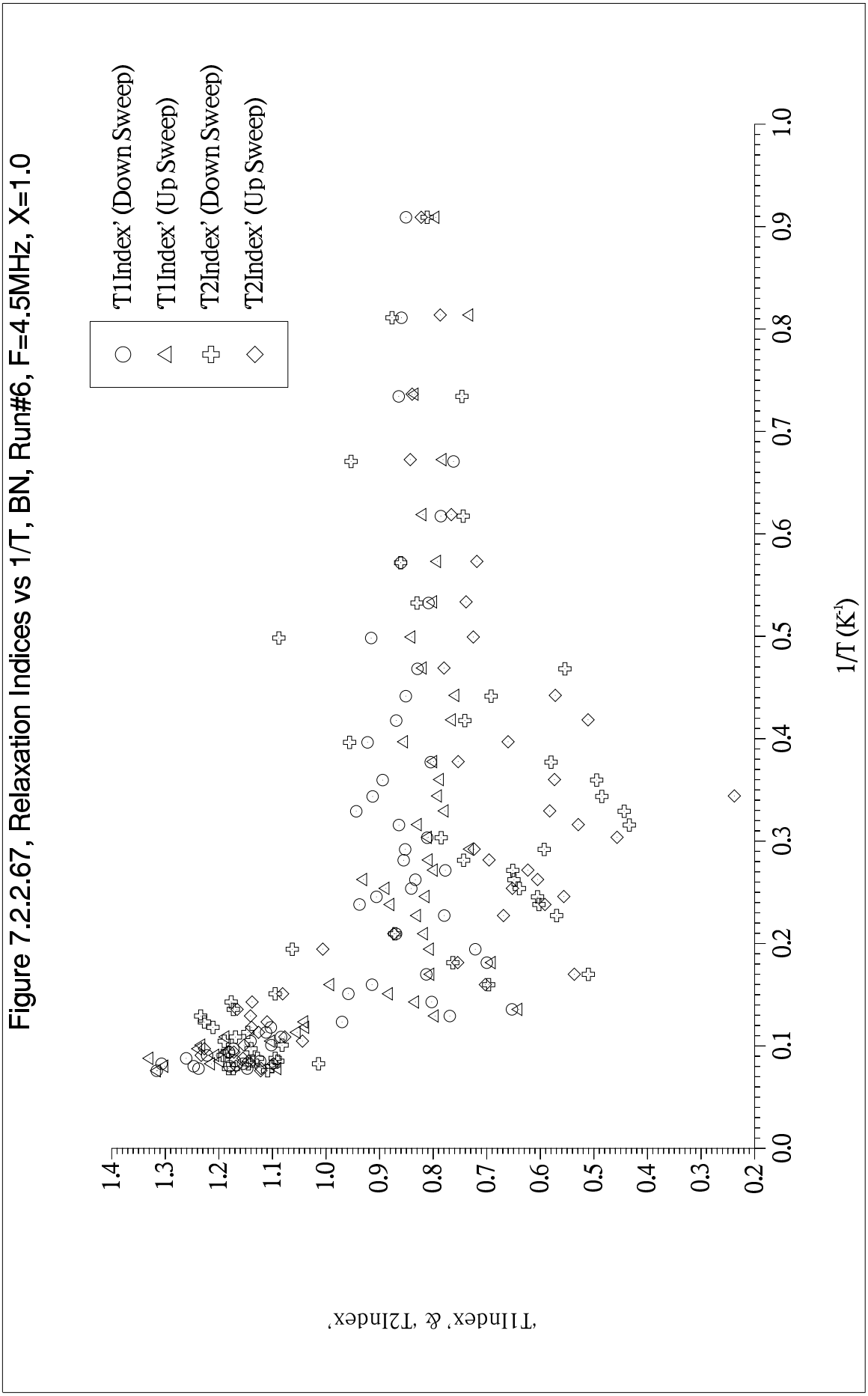
Figure 7.2.2.67, Relaxation Indices vs 1/T, BN, Run#6, F=4.5MHz, X=1.0
T1Index' (Down Sweep)
T1Index' (Up Sweep)
T2Index' (Down Sweep)
T2Index' (Up Sweep)
'T1Index' & 'T2Index'
1/T (K-1)
1.4
1.3
1.2
1.1
1.0
0.9
0.8
0.7
0.6
0.5
0.4
0.3
0.2
0.0
0.1
0.2
0.3
0.4
0.5
0.6
0.7
0.8
0.9
1.0

T_2 against $1/T$ (figure 7.2.2.65) is very similar to the 0.938 monolayer data. The X=0.938 '0.4K^{-1}' minimum has become less distinct, splitting into two smaller features centred on 0.45K^{-1} and 0.33K^{-1}. There are probably three reasons for this: (1) A decrease in T_2 at low temperatures (figure 7.2.1.1) as the film thickens and exchange slows which reduces the minimum's low temperature shoulder. (2) An increase in the low temperature second layer population together with (3) a larger E_a (figure 7.2.3.11) which makes thermal promotion into the second layer more difficult, reducing the minimum. Throughout most of the rise to the melting maximum an activation law operates as at X=0.938. Super-exponential exp$-t^3$ 'CP' relaxation is visible again at the melting maximum. With the increasing second layer fluid it is seen at all coverages $X \geqslant 1.0$.

'T2Index' (figure 7.2.2.67) is not unlike the X=0.938 data. A slight reduction in low temperature *noisiness* is probably related to the increasing low temperature second layer gas population smearing out changes in the first layer by particle exchange. The less distinct second layer T_2 PMI/fluid minimum deprives 'T2Index' of the very deep broad minimum seen at X=0.938, leaving two weaker minima corresponding to the T_2 ones. The predicted lack, again of hysteresis in the T_2 rise and the usual minimum at the T_2 melt-desorption minimum are present.

T_1 (figure 7.2.2.66) continues its trend. Like T_2 the change from X=0.938 is small compared with previous coverage-increment changes. The two higher temperature minima have again shrunk as features while the first occurs at at slightly higher temperature.

Figure 7.2.2.67 shows 'T1Index' plotted against $1/T$. Being very similar in all respects to X=0.938 the same arguments apply.

***X*=1.05,** The first layer solid should be unchanged from X=1.0. At low temperatures additional spins have entered the second layer.

T_2 (figure 7.2.2.68) is little changed from X=1.0. The minimum/minima has almost disappeared. Arguments (1) and (3) from §7.2.2/X=1.0/T_2 do not apply leaving (2) to explain the change.

'T2Index' (figure 7.2.2.70) shows less low temperature *noisiness* than at X=1.0, appearing instead as *sub-region* behaviour. A similar explanation to X=0.938→1.0 (with no increase in first layer density + more second layer fluid spins) may be appropriate. The plot is otherwise much as at X=1.0.

T_1 (figure 7.2.2.69) has changed very little from the previous coverage. Like

Figure 7.2.2.68, T_2 against 1/T, BN, Run#6, F=4.5MHz, X=1.05

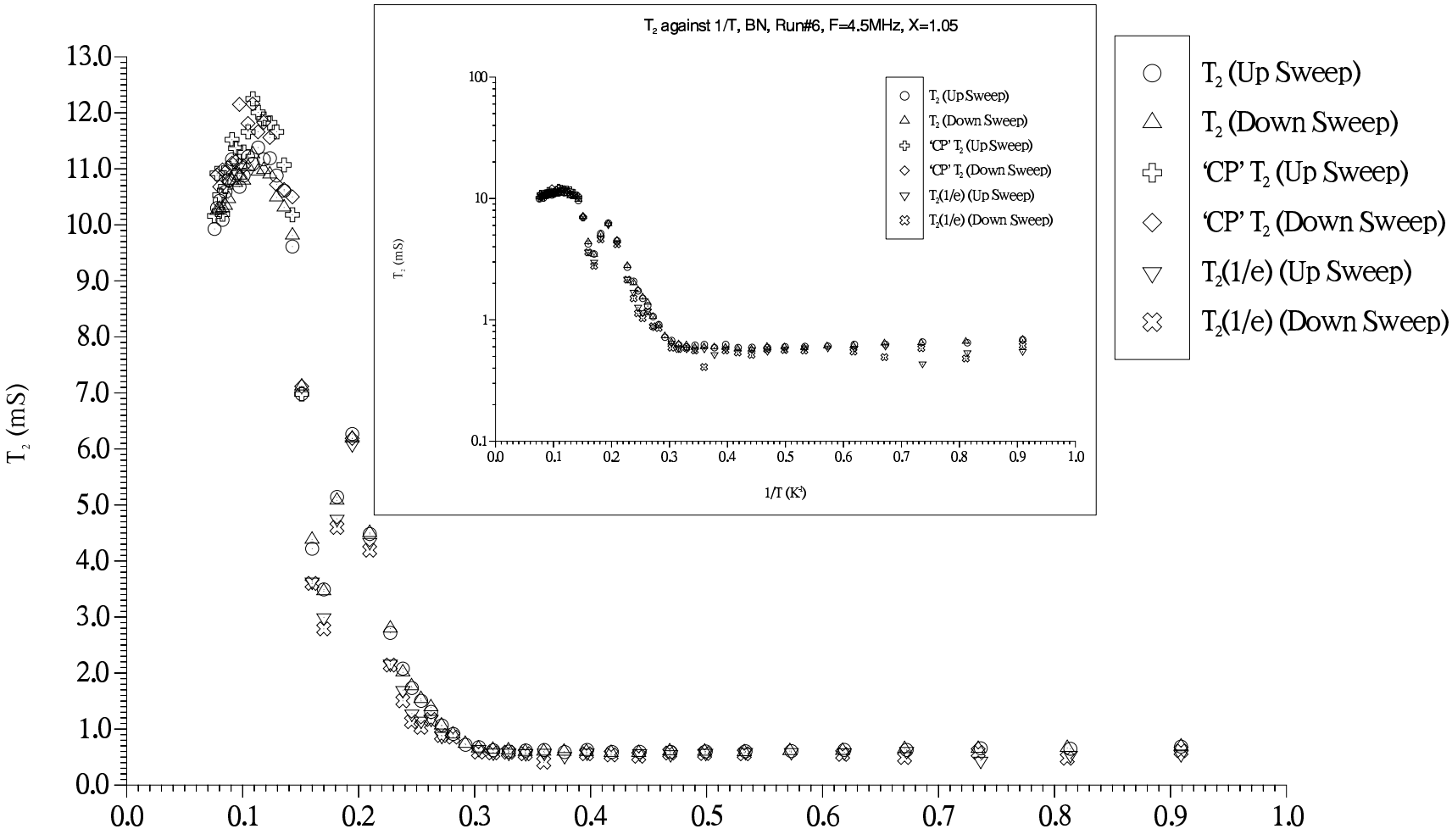

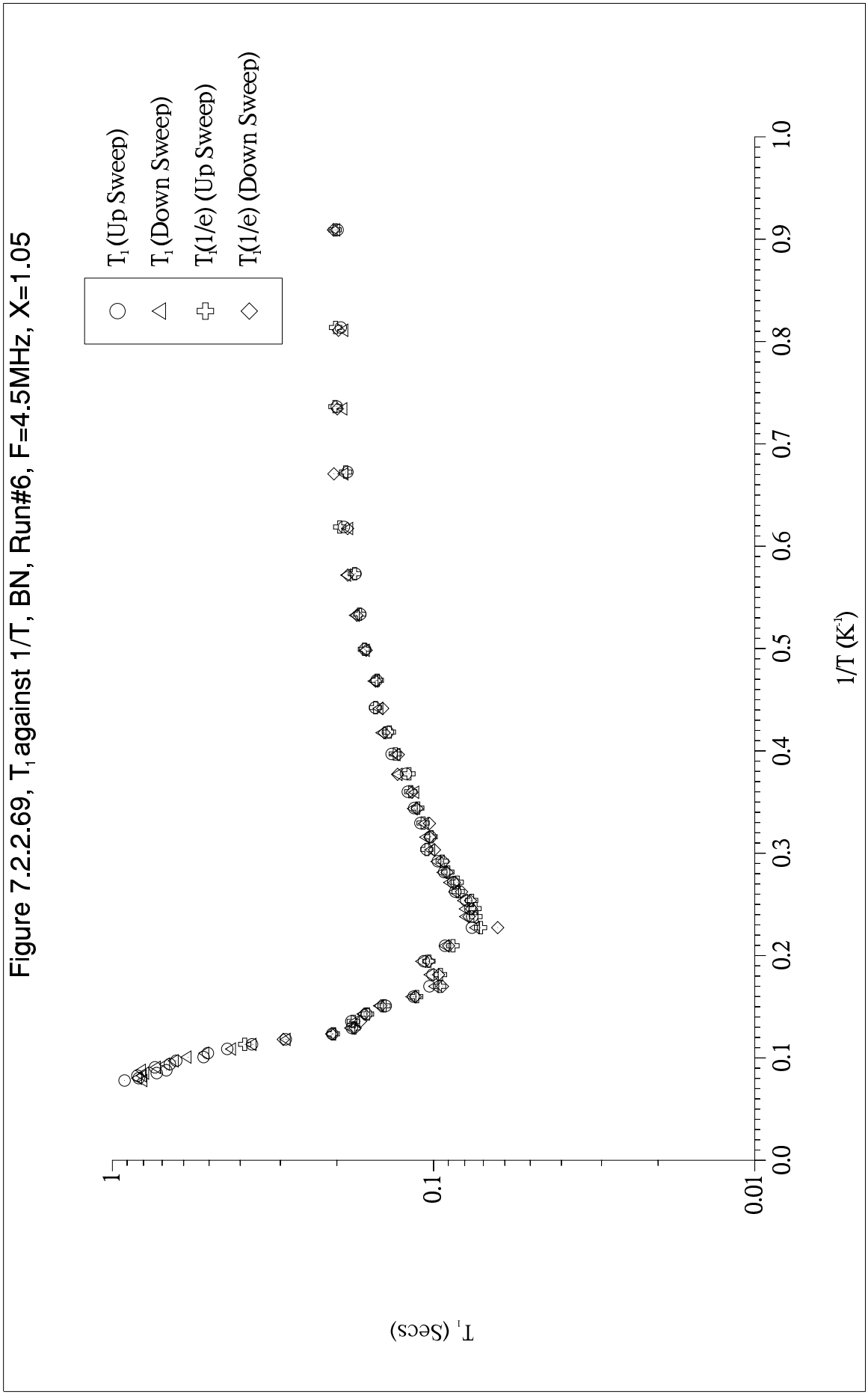
Figure 7.2.2.69, T1 against 1/T, BN, Run#6, F=4.5MHz, X=1.05
T1 (Up Sweep)
T1 (Down Sweep)
T1(1/e) (Up Sweep)
T1(1/e) (Down Sweep)
T1 (Secs)
1
0.1
0.01
0.0
0.1
0.2
0.3
0.4
0.5
0.6
0.7
0.8
0.9
1.0
1/T (K-1)

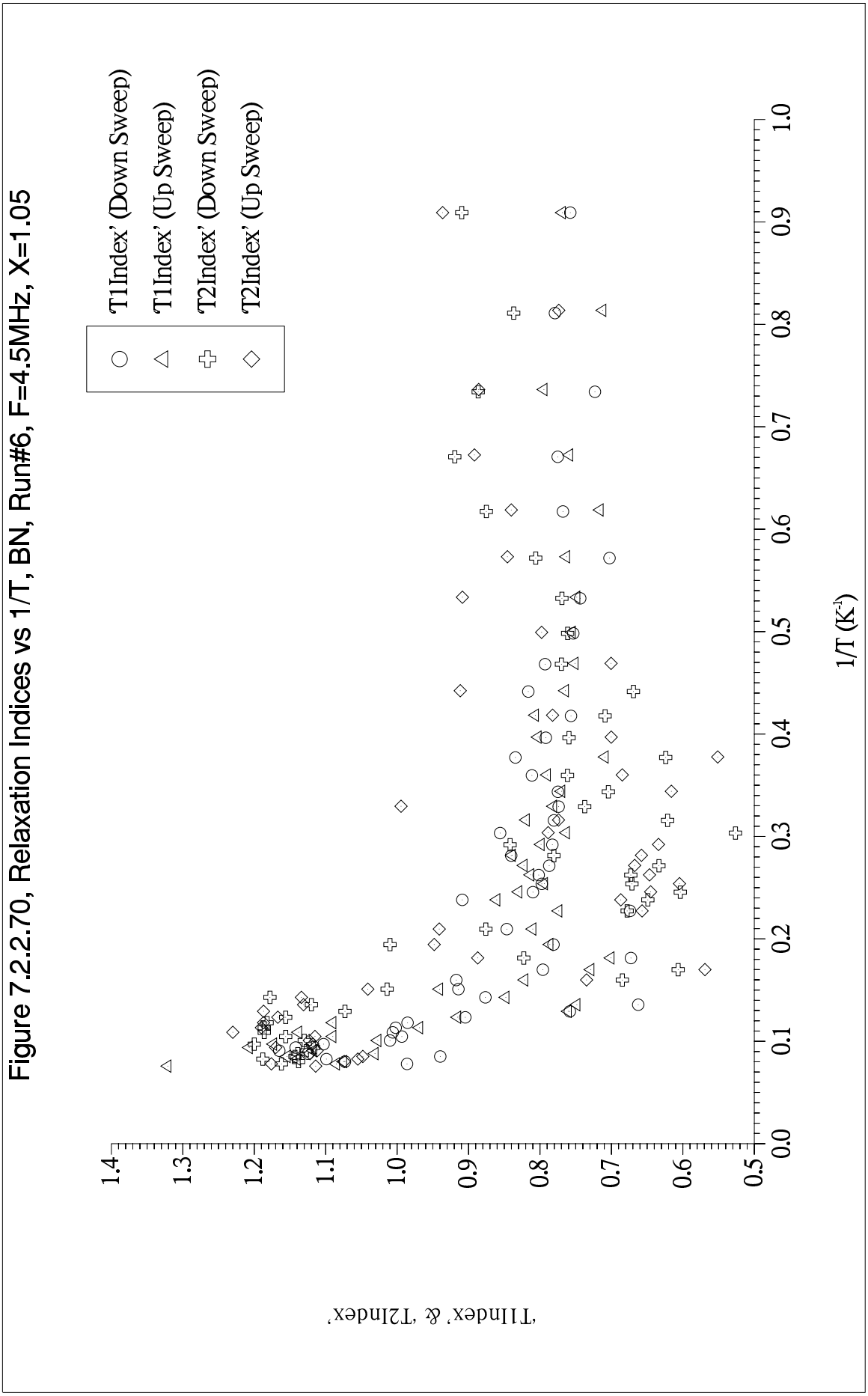
Figure 7.2.2.70, Relaxation Indices vs 1/T, BN, Run#6, F=4.5MHz, X=1.05
T1Index' (Down Sweep)
T1Index' (Up Sweep)
T2Index' (Down Sweep)
T2Index' (Up Sweep)
'T1Index' & 'T2Index'
1/T (K-1)
1.4
1.3
1.2
1.1
1.0
0.9
0.8
0.7
0.6
0.5
0.0
0.1
0.2
0.3
0.4
0.5
0.6
0.7
0.8
0.9
1.0

X=1.0 it is almost temperature independent at low temperatures. The lowest T minimum has shifted very slightly to higher temperatures, the others changing imperceptibly.

'T1Index' (figure 7.2.2.70) shows less low temperature *noisiness* than at X=1.0 but is otherwise essentially the same. As with 'T2Index' reduced low temperature *noisiness* most likely stems from interaction with the increased second layer fluid.

***X*=1.1 to 1.5,** For completeness the rest of the higher coverage data is presented in figures 7.2.2.72 to 7.2.2.86. At these coverages the first layer is believed to be unchanged from X=1.0††, melting directly to the fluid while the second layer fluid increases in density.

As second layer coverage increases the remnant of the first T_2 minimum is washed out altogether. This leaves a slow fall in T_2 as T increases from 1.1K to the onset of the T_2-rise. This slow fall must be due to the PMI/fluid mechanism. Being smooth and featureless and starting from low temperatures, suggests it is predominantly the permanent second layer spin population that is now responsible, instead of thermally promoted first layer ones. Supporting the above statement (††) is the unchanging temperature of the melting maximum and melt desorption minimum with coverage − See figure 7.2.3.1. Increased $\exp(-t^3)$ 'CP' relaxation around the melting maximum with second layer fluid coverage is particularly well illustrated by the X=1.3, 1.4 and 1.5 data sets where a finer temperature grid was used for T>4.2K. Here again it is the permanent second layer fluid spin population diffusing in field inhomogeneities, that is largely responsible. The relaxation only becomes visible once sufficient thermally activated motional narrowing is present in the first layer to stop it so strongly relaxing second layer spins. Figure 7.2.2.71 shows the $X\geqslant$1.0 T_2 temperature dependence data plotted together for comparison. The X=1.2, T_2 *vs* X maximum (see also figure 7.2.1.1) is present as far as the melting rise − that is above any temperatures at which a second layer registered structure is likely to exist, supporting the interlayer-exchange-effects interpretation mentioned in §7.2.1/$X\geqslant$1.0.

Comparing the finer temperature grid 'T2Index' data at the highest 3 coverages with lower coverages, as far back as X=0.8, two general trends are apparent regarding the melt-desorption minimum: From being a broad-deep feature at X=0.8, as X increases; (1) it narrows and (2) rises in value at the minimum. Respectively, these may be explained by increased activation energies and increased second-layer-fluid:total spins ratio diluting the melt-desorption signal. The two highest coverages have a new feature − a minimum at ~0.4K^{-1}. The reason for this is unknown.

Figure 7.2.2.71, Second Layer, T_2 against 1/T, BN, Run#6, F=4.5MHz

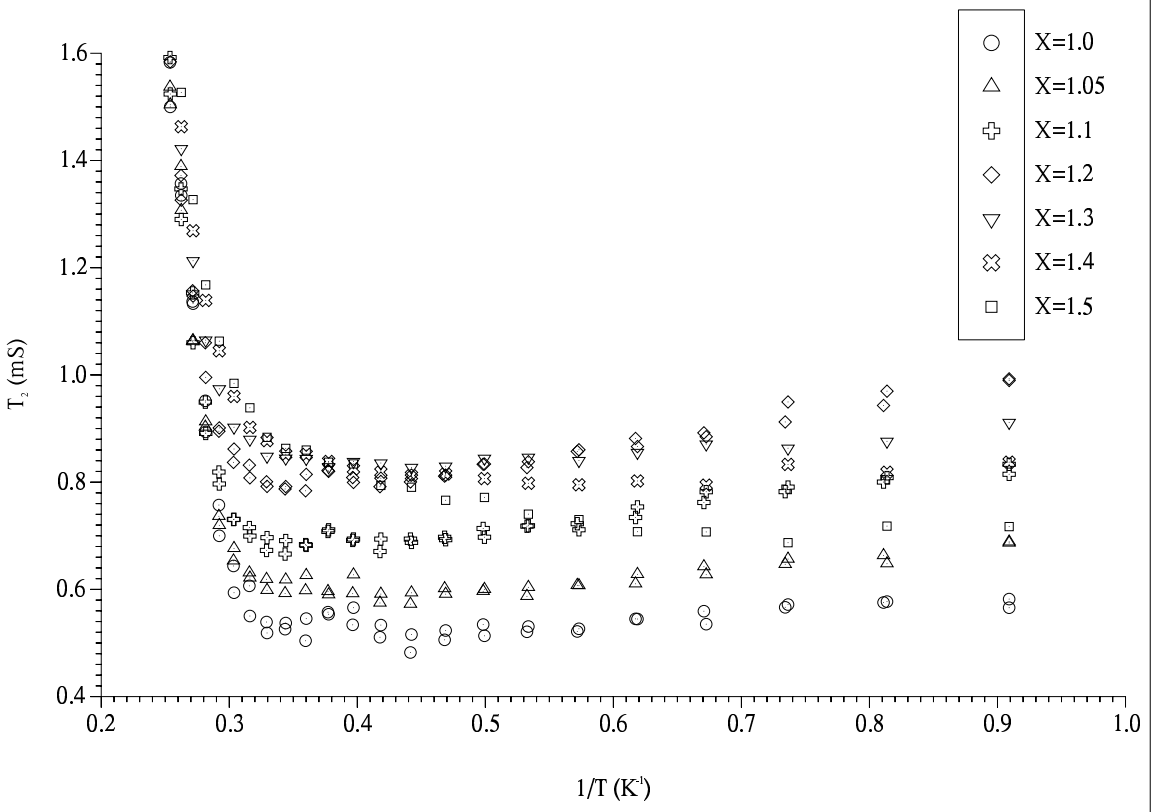

Figure 7.2.2.72, T_2 against 1/T, BN, Run#6, F=4.5MHz, X=1.1

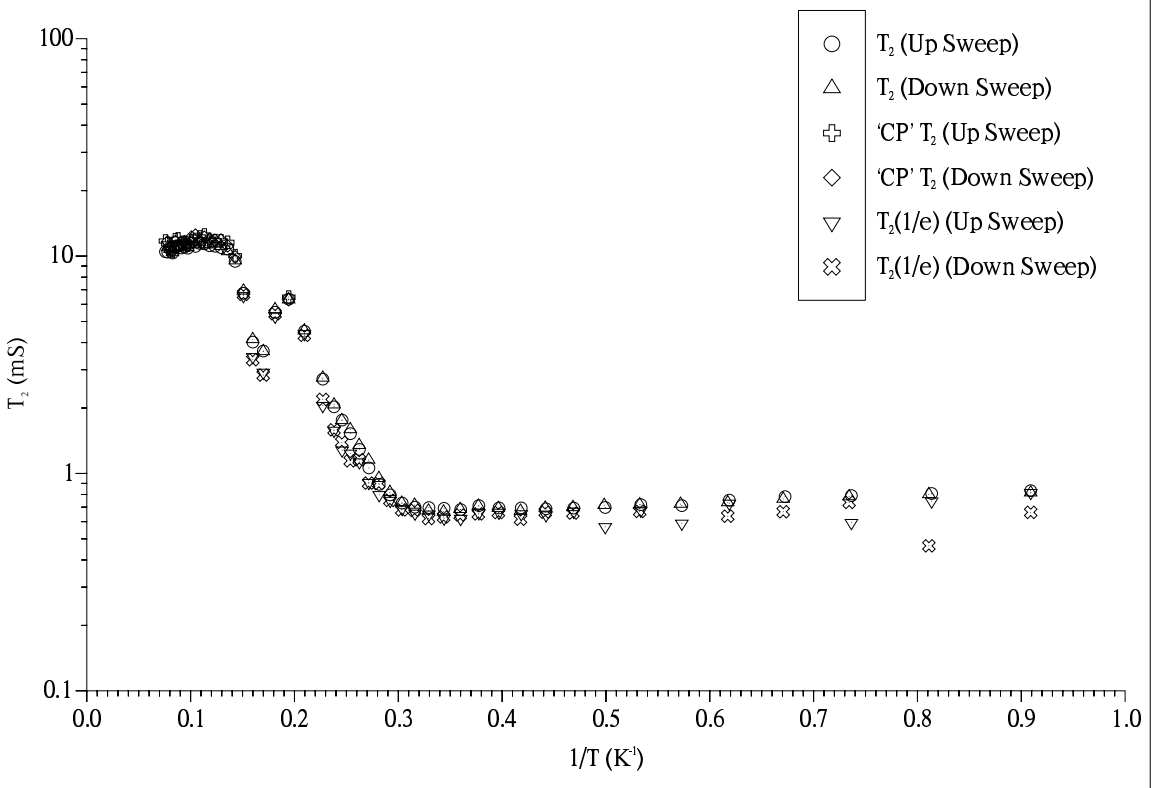

Figure 7.2.2.73, T_2 against 1/T, BN, Run#6, F=4.5MHz, X=1.2

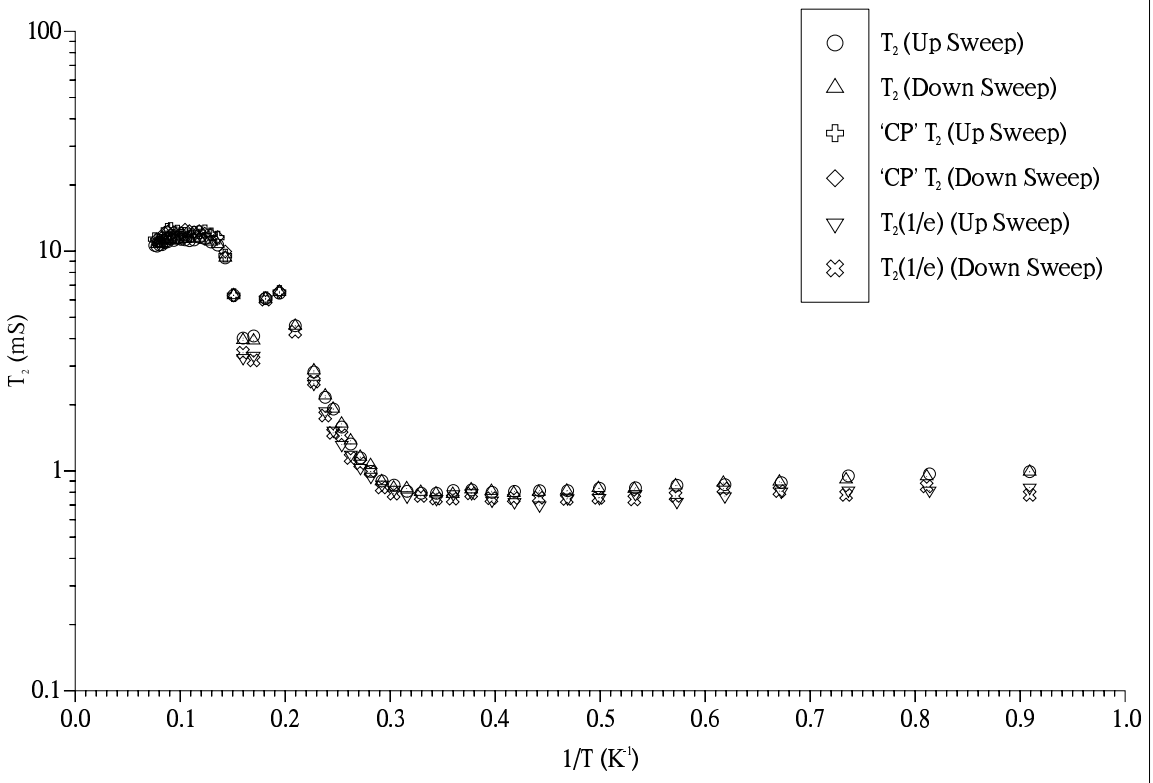

Figure 7.2.2.74, T_2 against 1/T, BN, Run#6, F=4.5MHz, X=1.3

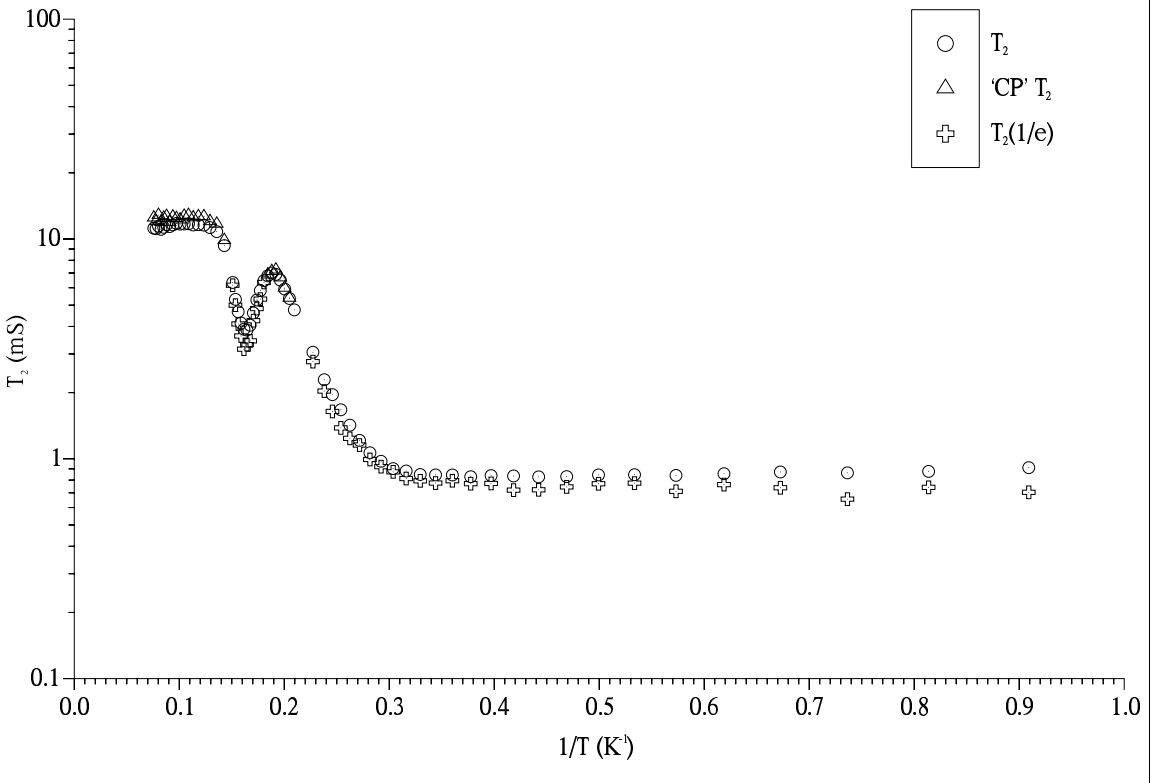

Figure 7.2.2.75, T_2 against 1/T, BN, Run#6, F=4.5MHz, X=1.4

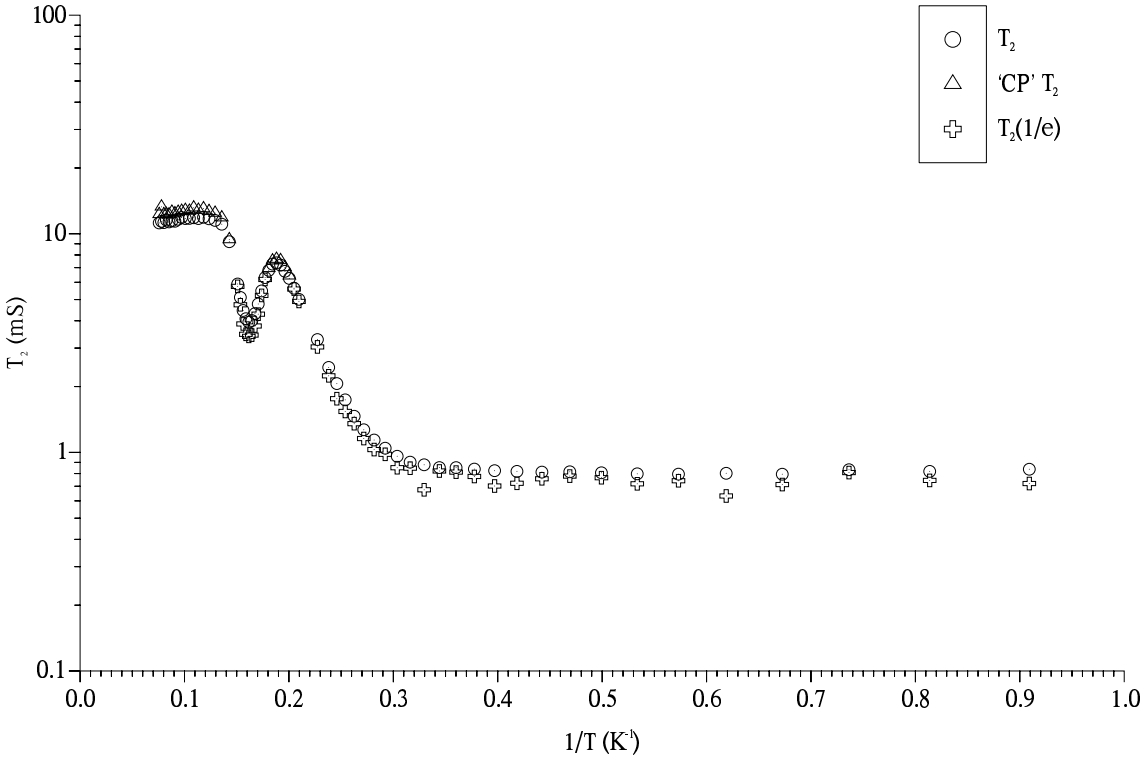

Figure 7.2.2.76, T_2 against 1/T, BN, Run#6, F=4.5MHz, X=1.5

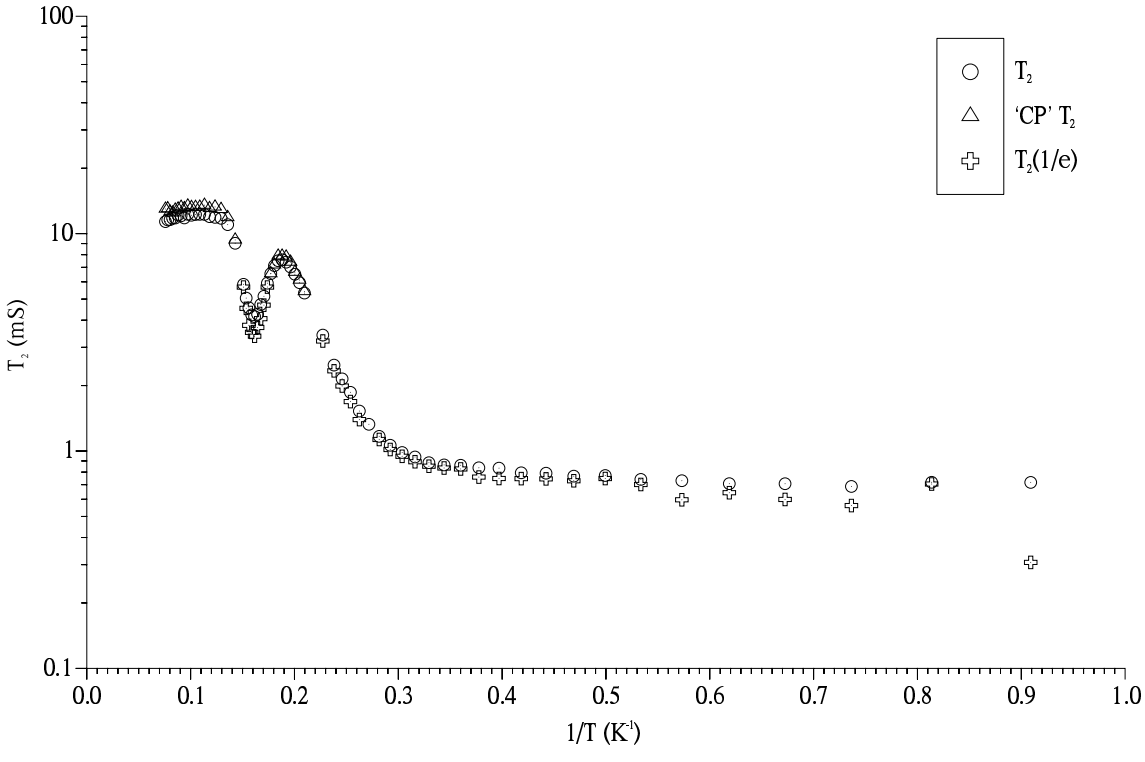

Figure 7.2.2.77, T_1 against 1/T, BN, Run#6, F=4.5MHz, X=1.1

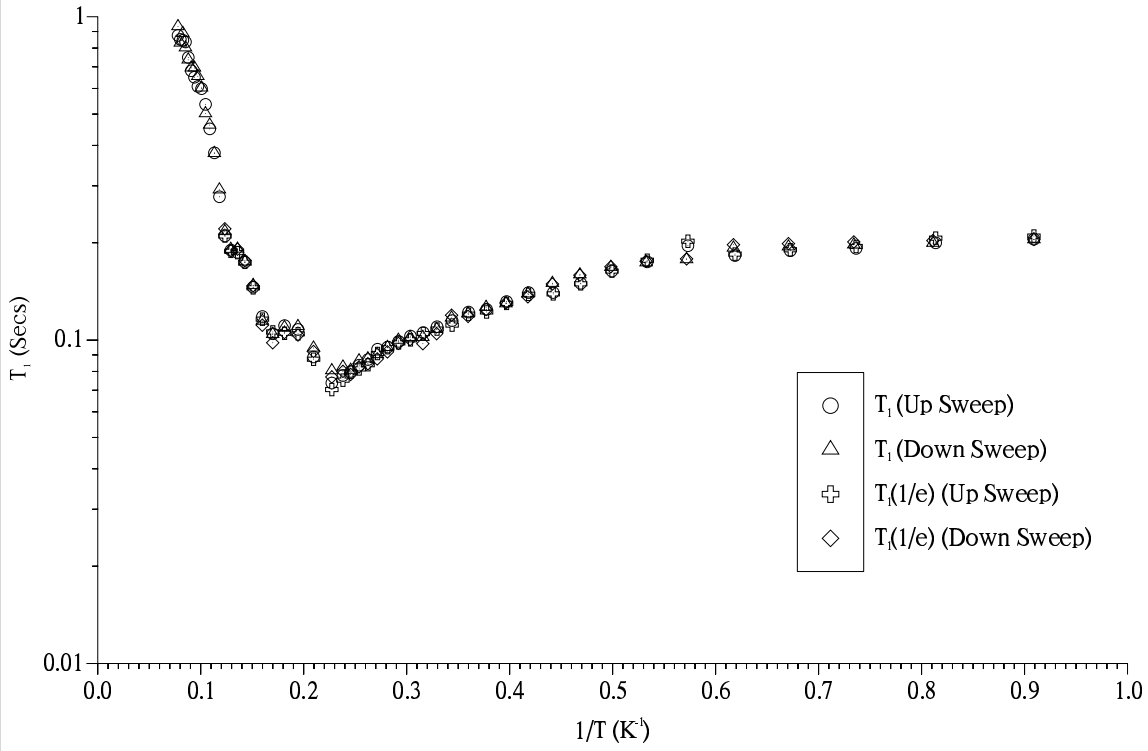

Figure 7.2.2.78, T_1 against 1/T, BN, Run#6, F=4.5MHz, X=1.2

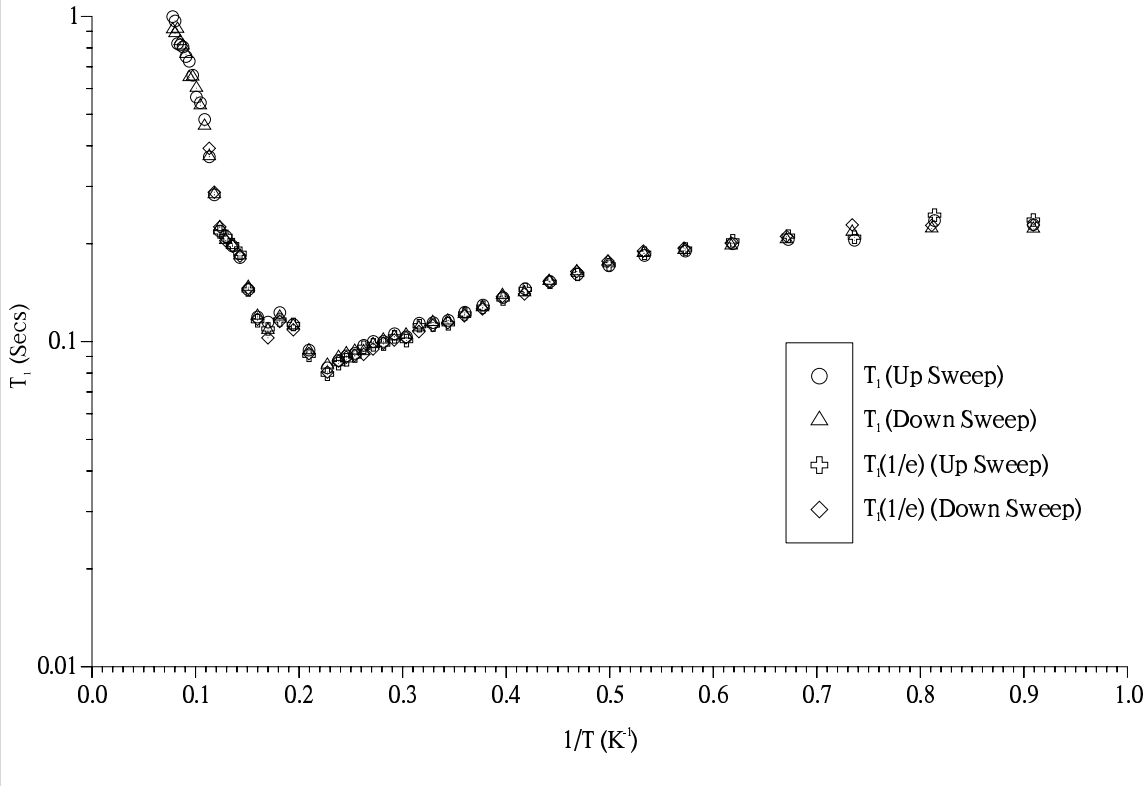

Figure 7.2.2.79, T_1 against 1/T, BN, Run#6, F=4.5MHz, X=1.3

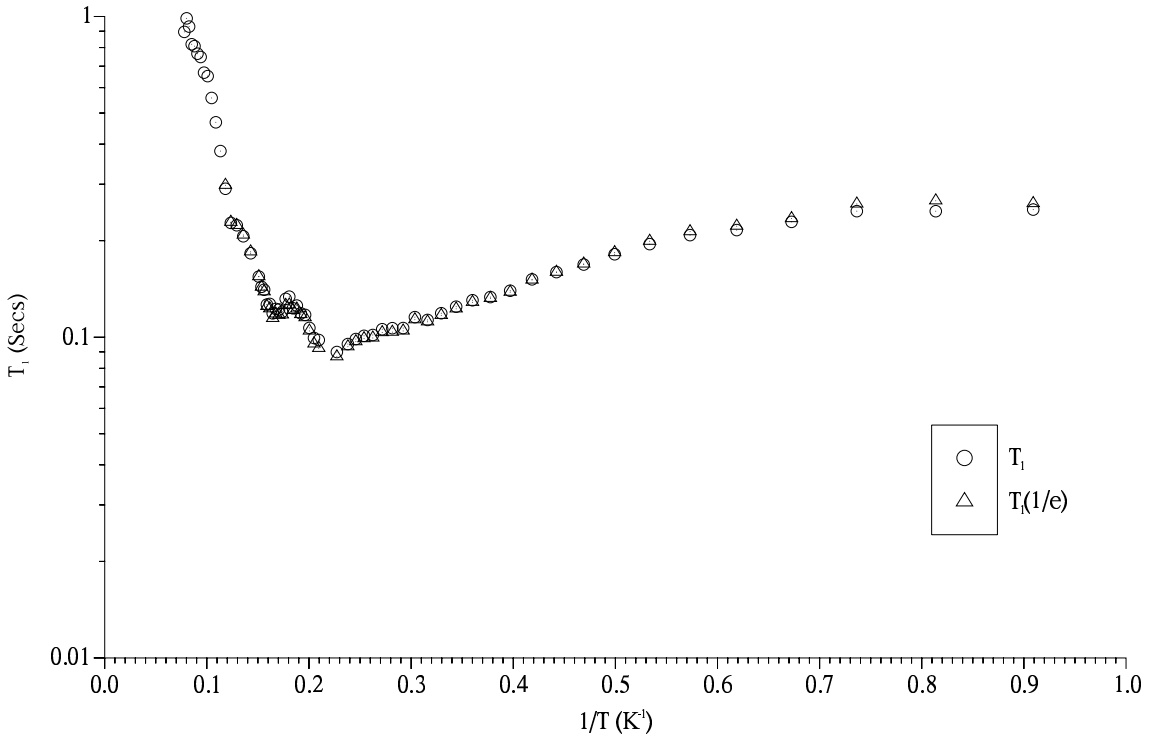

Figure 7.2.2.80, T_1 against 1/T, BN, Run#6, F=4.5MHz, X=1.4

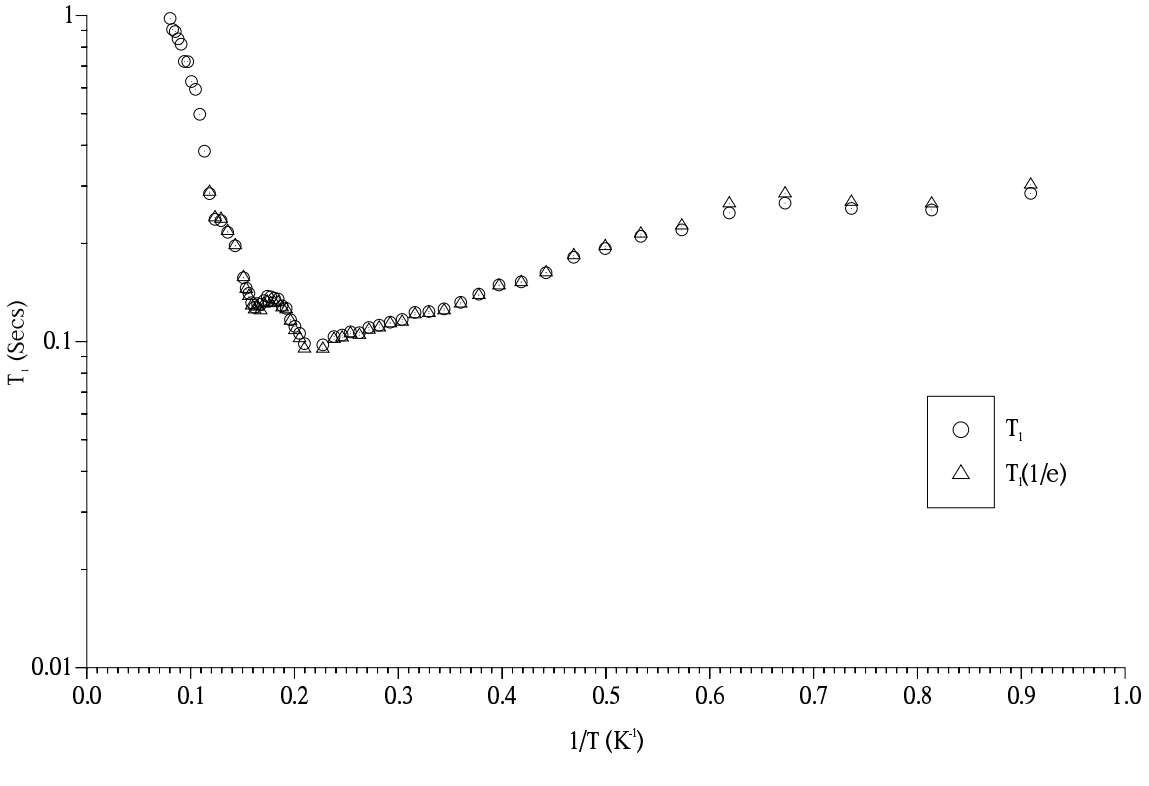

Figure 7.2.2.81, T_1 against 1/T, BN, Run#6, F=4.5MHz, X=1.5

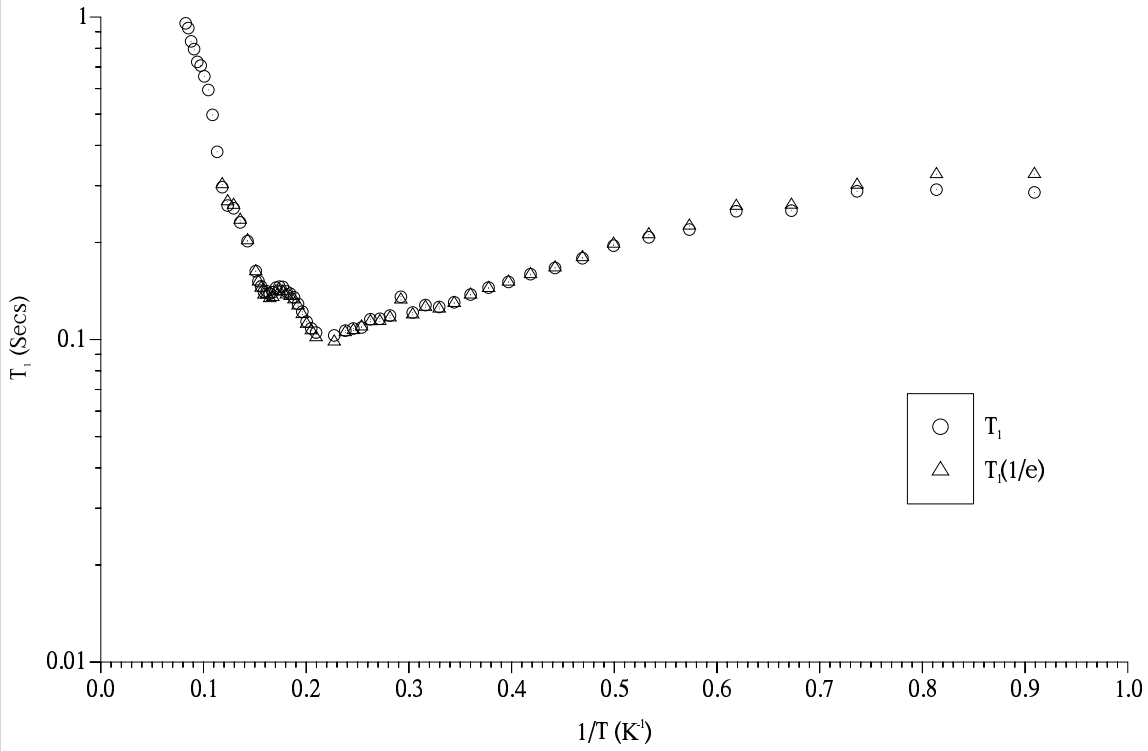

Figure 7.2.2.82, Relaxation Indices vs 1/T, BN, Run#6, F=4.5MHz, X=1.1

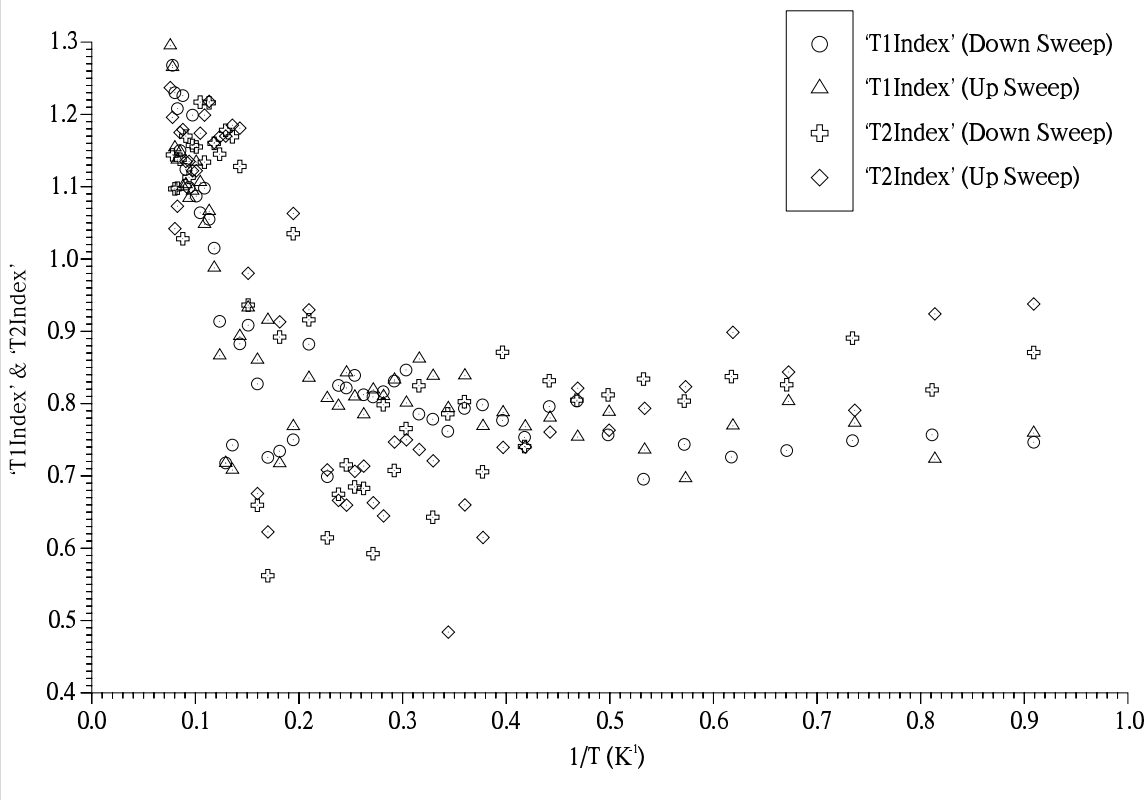

Figure 7.2.2.83, Relaxation Indices vs 1/T, BN, Run#6, F=4.5MHz, X=1.2

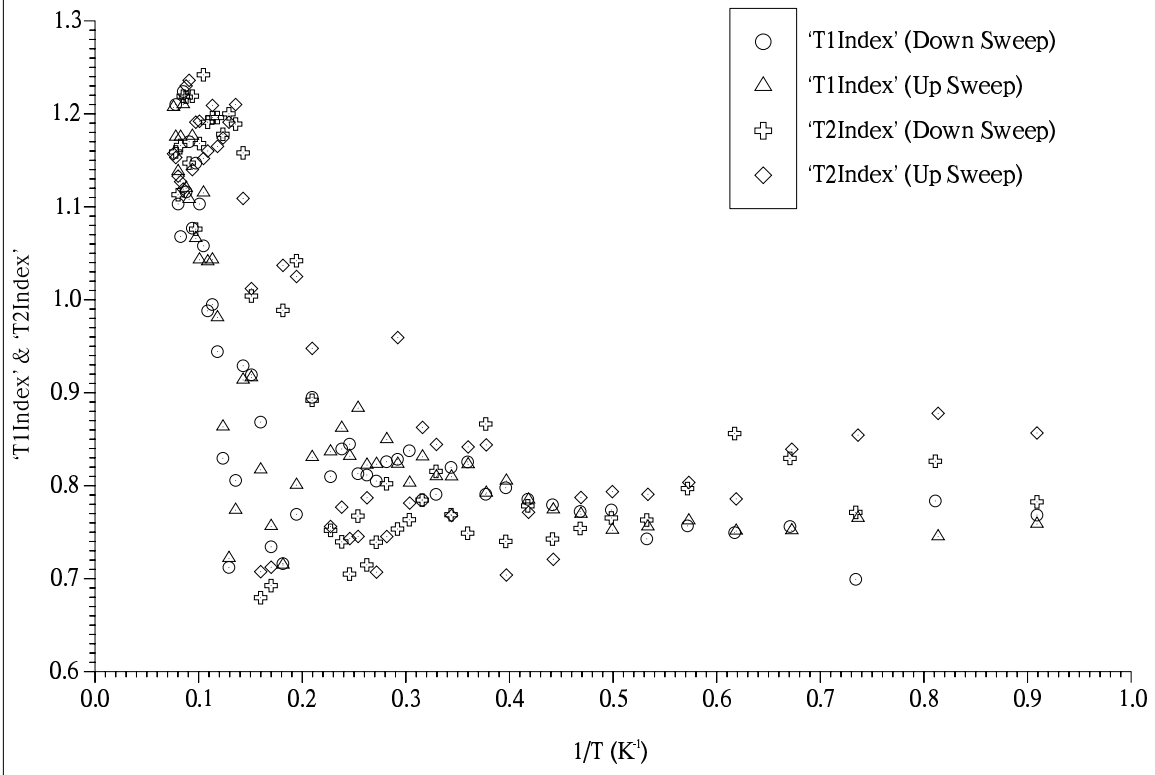

Figure 7.2.2.84, Relaxation Indices vs 1/T, BN, Run#6, F=4.5MHz, X=1.3

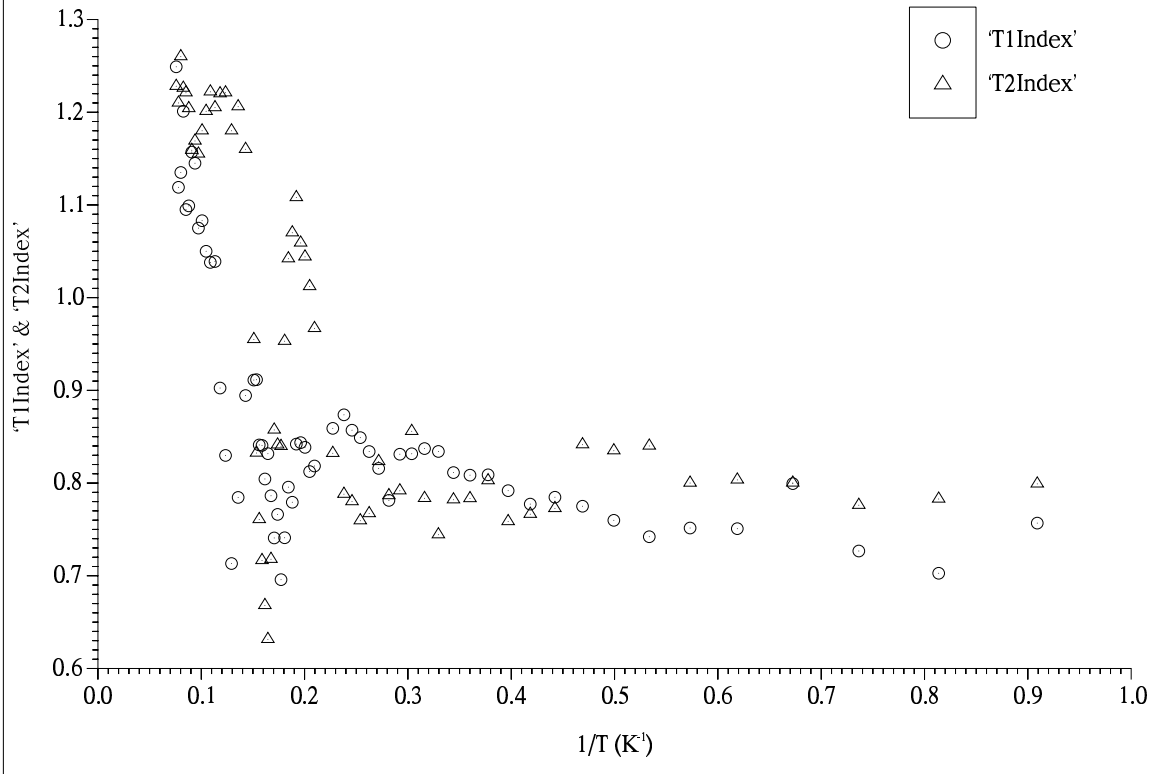

Figure 7.2.2.85, Relaxation Indices vs 1/T, BN, Run#6, F=4.5MHz, X=1.4

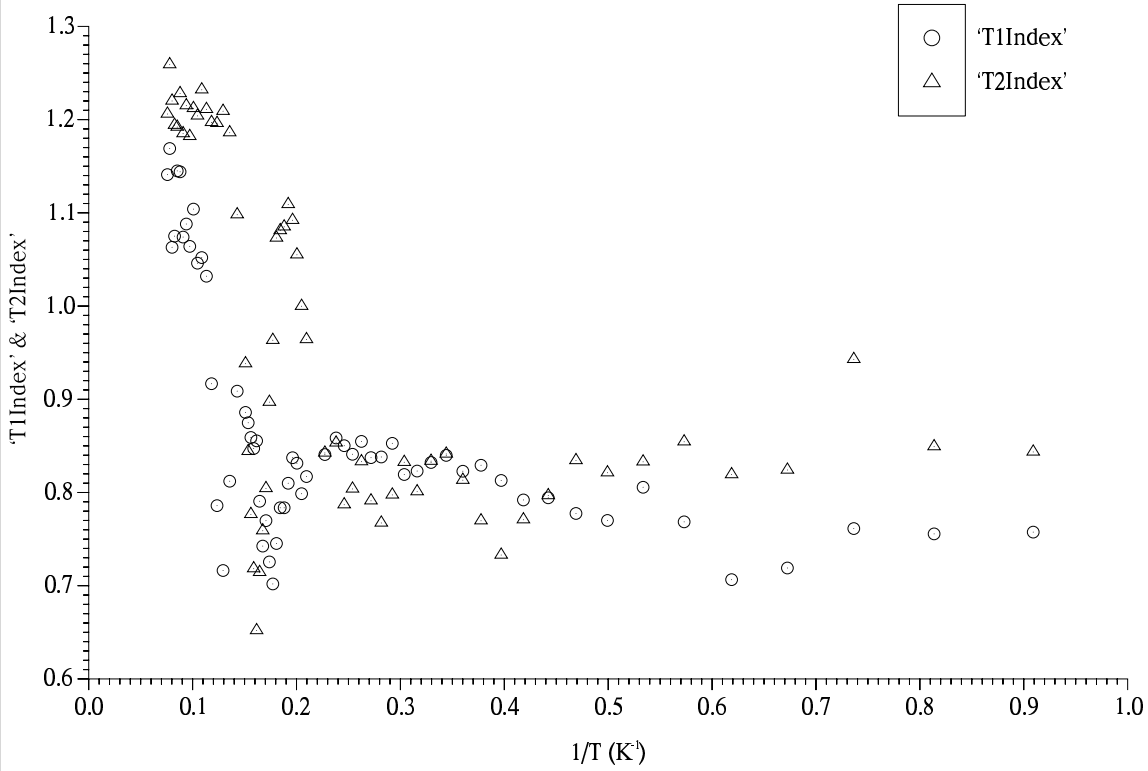

Figure 7.2.2.86, Relaxation Indices vs 1/T, BN, Run#6, F=4.5MHz, X=1.5

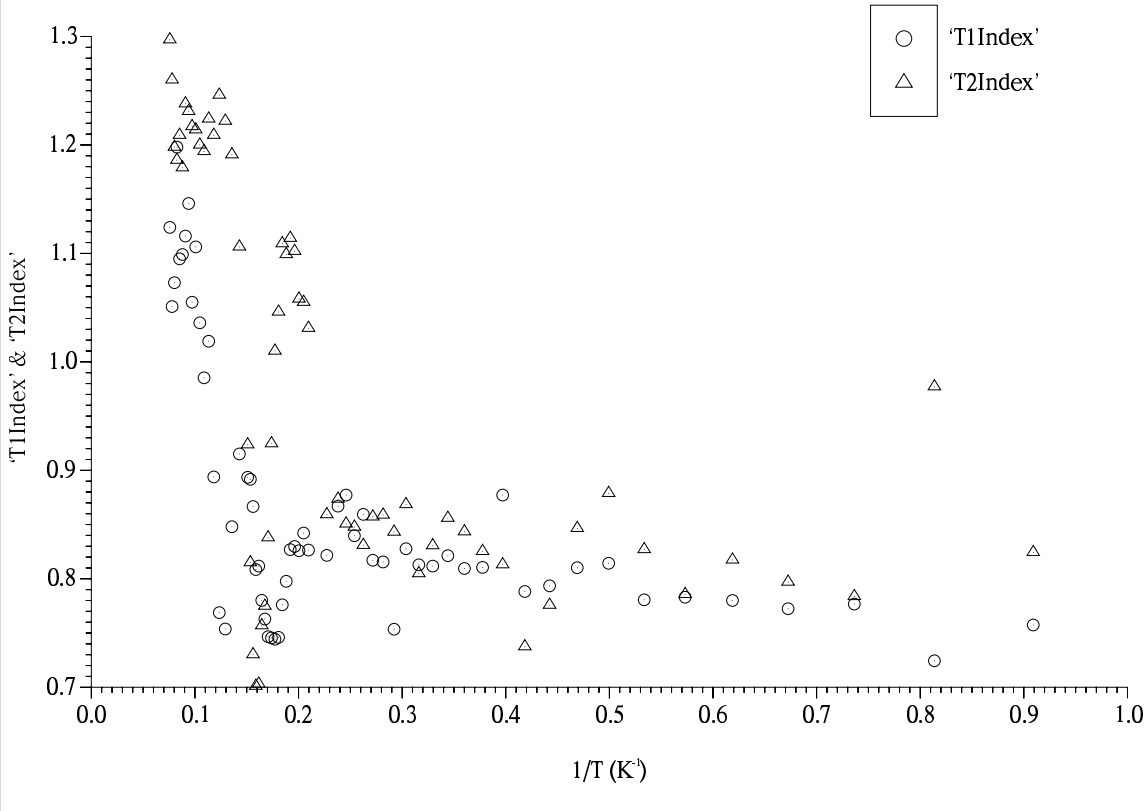

Two observations are made about T_1 *vs* $1/T$ plots at these coverages: (1) The minima's trend continues but only very slowly now since the first layer solid responsible for relaxing second layer fluid spins is unchanging. For $X>1.1$ the highest T minimum is washed out altogether. (2) The temperature independent low temperature region is progressively reduced with coverage as increasingly numerous second layer fluid spins relax by particle exchange with their solid underlayer as thermal velocities increase with T.

'T1Index' tends to show less low temperature variation with increasing coverage for the reasons discussed in §7.2.2/X=1.05. For temperatures below the usual two minima some unidentified features are present however. The two usual minima are also more clearly visible in the higher point-density X=1.3, 1.4 and 1.5 plots. They correspond to the T_1 minima in the usual way as discussed in §7.2.2/X=0.8.

7.2.3 Coverage Dependence of Temperature Data Features

7.2.3.1 T_2 Maxima and Minima

Figure 7.2.3.1 plots the temperature-of-occurrence of the two maxima and minimum against coverage. Figures 7.2.3.2−7.2.3.6 show the value of T_2 at the maxima and minimum with coverage for the three features separately and together (figure 7.2.3.3) for comparison.

Before proceeding it is worth remarking that at these temperatures, particularly with the desorption-maximum the film is in a complicated state; potentially involving a first layer, finite population second layer and desorbed spins. Moreover at low coverage the edge-sites film is likely to play an important role. Its state is difficult to be sure about and it is likely given its heterogeneous nature that it melts and desorbs in an ill-defined way over a range of temperatures. See §1.10.2, in particular the observation/model on Grafoil that the patchy-solid consisted of a small quantity of very dense strongly bound adsorbate plus a larger amount of a lower density **[62]**. See also figure 7.5.2 and related discussion. Disentangling the various contributions is not easy **[19]**.

Starting with the desorption-maximum where temperature induced desorption increases the dipolar-T_2 until the non-dipolar PMI/fluid mechanism takes over. At low coverage, $0.1 \leqslant X \leqslant 0.5$, the temperature-of-occurrence, $T^{\text{D-max}}$ falls linearly with X. For a homogeneous film $T^{\text{D-max}}$ increasing with coverage is expected as film density rises. However, a model involving a combination of desorption from an edge-sites fluid (melt) and basal-plane fluid is qualitatively consistent with the data. Here $T^{\text{D-max}}$ is determined by the relative proportions of the basal-plane to edge-sites fluid coverage, X^{ef}. X^{tot} is the total coverage, T^{efd} a characteristic edge-film fluid desorption temperature, and T^{bpd} a similar temperature characterising basal-plane fluid desorption.

$$T^{\text{D-max}} = T^{\text{efd}} \left(\frac{X^{\text{ef}}}{X^{\text{tot}}} \right) + T^{\text{bpd}} \left(\frac{X^{\text{tot}} - X^{\text{ef}}}{X^{\text{tot}}} \right) \qquad 7.2.3.1$$

Providing $T^{\text{efd}} > T^{\text{bpd}}$ and $T^{\text{D-max}}$ falling with X^{tot} is the result. With its greater binding energy the edge-film T^{efd} should certainly be greater than T^{bpd}, by how much is unclear. It is not known what fraction of spins desorb and what motional speed is required to generate the desorption-maximum. However with the edge-sites binding energy (E) estimated to be 70% stronger than on the basal-planes **[116]** and with the desorbed spin populations expected to follow a Boltzmann law ~exp ($-E/kT$) (a strong function of T)

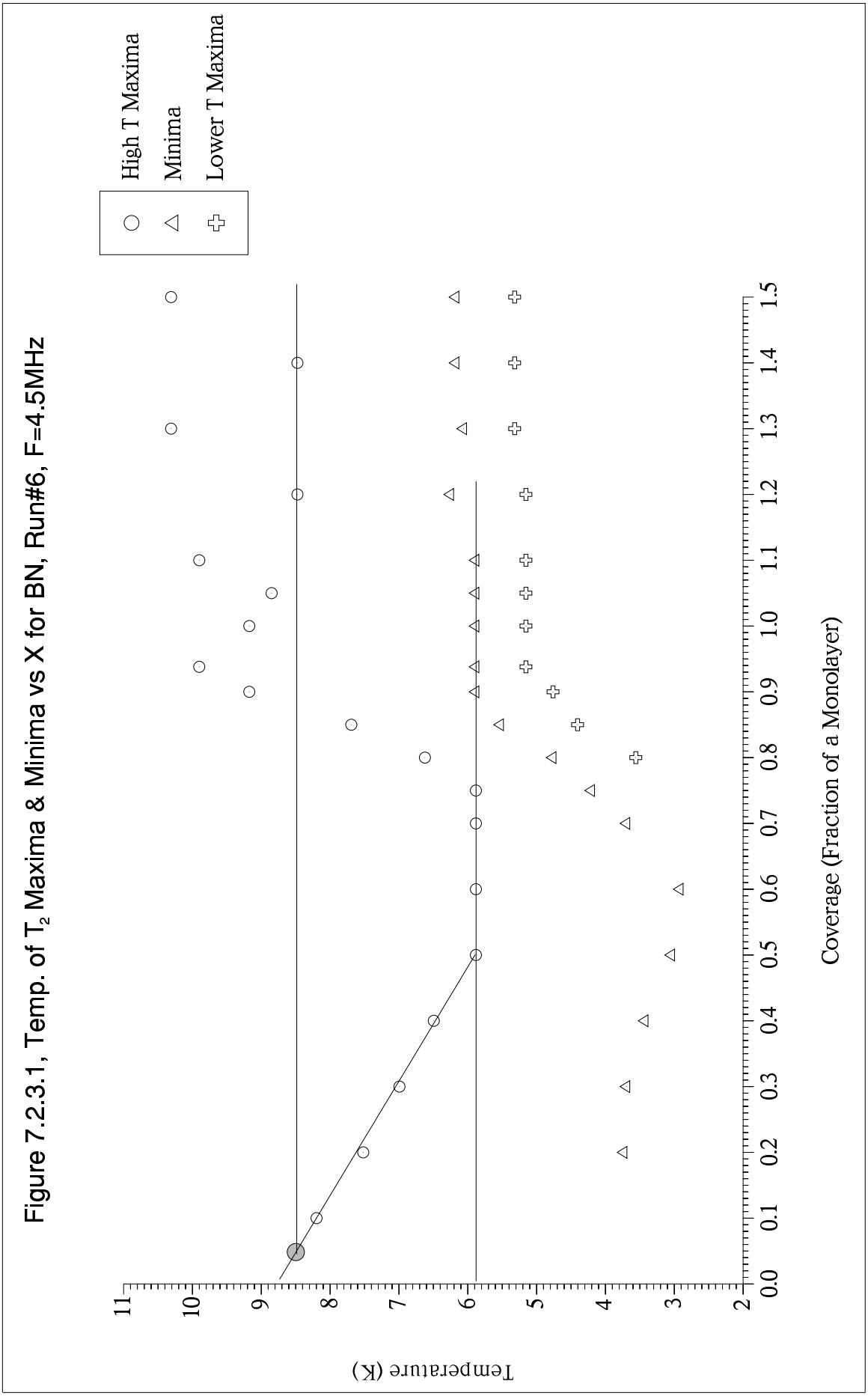
Figure 7.2.3.1, Temp. of T_2 Maxima & Minima vs X for BN, Run#6, F=4.5MHz
High T Maxima
Minima
Lower T Maxima
Temperature (K)
Coverage (Fraction of a Monolayer)
11
10
9
8
7
6
5
4
3
2
0.0
0.1
0.2
0.3
0.4
0.5
0.6
0.7
0.8
0.9
1.0
1.1
1.2
1.3
1.4
1.5

Figure 7.2.3.2, T_2 at T_2 High-T Maximum vs X for BN, Run#6, F=4.5MHz

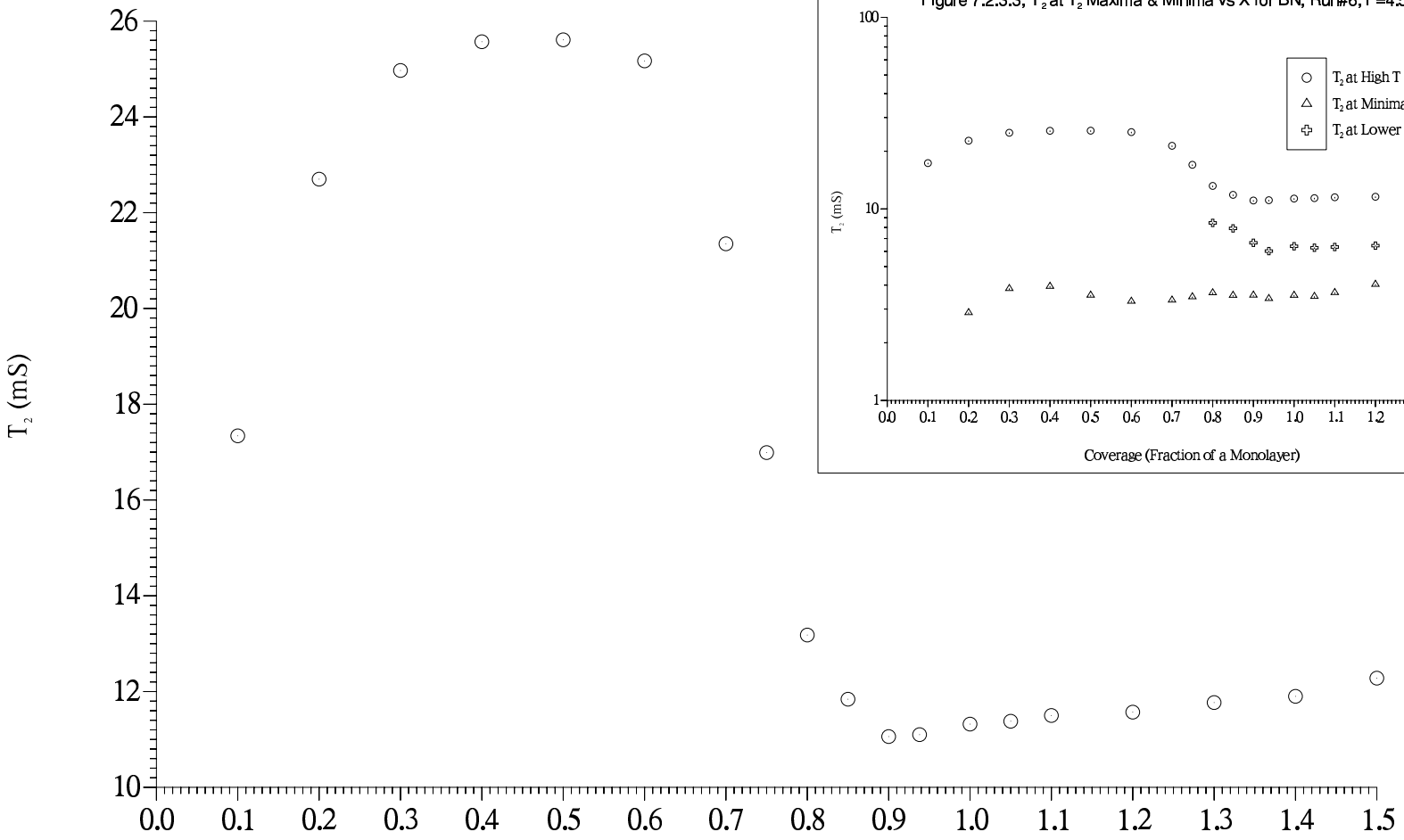

Figure 7.2.3.3, T_2 at T_2 Maxima & Minima vs X for BN, Run#6, F=4.5MHz

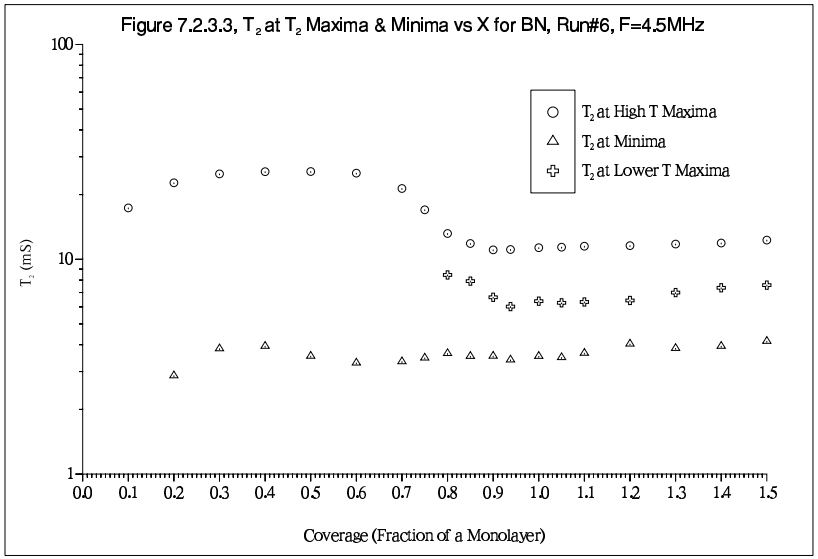

the $T^{efd} > T^{bpd}$ requirement is easily fulfilled. The model also assumes; T^{efd} independent of X^{tot}, T^{bpd} independent of X^{tot}, rapid particle exchange between the two fluids and X^{ef} constant at 0.05. That the observed behaviour is a linear law rather than the model's asymptotic $T^{D\text{-}max} \propto 1/X^{tot}$ relation probably indicates the failure of these assumptions, in particular that T^{bpd} is independent of coverage.

T_2 increases to a maximum at X=0.5 with the dense edge-sites fluid augmenting the basal plane relaxation rate (at X<0.5) as the edge-sites solid does in the low temperature case. Where T_2^{ef} and T_2^{bf} are the relaxation times for edge-film and basal-plane spins respectively, T_2 for the augmentation factor relaxation mechanism is given by,

$$\frac{1}{T_2} = \frac{1}{T_2^{ef}}\left(\frac{X^{ef}}{X^{tot}}\right) + \frac{1}{T_2^{bf}}\left(\frac{X^{tot} - X^{ef}}{X^{tot}}\right) \qquad 7.2.3.2$$

Using the X=0.1 T_2 as before gives an estimate for the edge-film relaxation time, T_2^{ef} = 17.4mS × (0.05/0.1) = 8.7mS. This is clearly too large for any type of solid even with considerable thermal activation (eg. T_2 at the melting-maximum at X=0.8 is only 8.5mS, figures 7.2.3.3, 7.2.3.6), supporting the edge-sites *fluid* assertion.

For coverages $0.5 \leqslant X \leqslant 0.75$, $T^{D\text{-}max}$ is independent of X. T_2 falls off steeply from near coverage independence around the $X \approx 0.4$ to 0.5 peak. Without the possibility at these temperatures of registering, responsible for the relaxation-time's *turn-over* with coverage seen at low T, an alternative explanation must be sought for the maximum seen here. One possibility is that as the basal-plane film thickens for $X \rightarrow 0.5$, T_2^{bf} decreases until $T_2^{ef} \approx T_2^{bf}$ which produces coverage independence via equation 7.2.3.2 over the broad maximum. With X>0.5, T_2^{bf} continues to decrease leaving, $T_2^{ef} > T_2^{bf}$ and a fall-off in the measured T_2.

Coverage independence of $T^{D\text{-}max}$ may be explained by a similar argument: From equation 7.2.3.1, both $T^{efd} \sim T^{bpd}$ and $X^{tot} \gg X^{ef}$ (providing $T^{efd} \gg T^{bpd}$) lead to $T^{D\text{-}max}$ approximately independent of X. The outlines of an additional explanation for coverage independence which obviates the need for the very sharp change in slope at $X \rightarrow 0.5$ is presented: Figure 7.2.3.1 shows that $T^{D\text{-}max}$ = 5.9K for the coverage independent $0.5 \leqslant X \leqslant 0.75$ valley is the same as the temperature of the melt-desorption-minimum monolayer-plateau. Occurrence of such regions of sustained identical

temperature independence is unlikely to be a coincidence. 5.9K might represent a type of watershed for desorption: At high-X the melt-desorption-minimum plateau could indicate sufficient thermal energy for the onset of desorption (ie. the loss of a purely 2D system) and at low-X the desorption-maximum valley might occur because there is insufficient energy below 5.9K to produce significant (ie. enough for the desorption-maximum) desorption.

In the region $0.75 \leqslant X \leqslant 0.9$ $T^{\text{D-max}}$ rises steeply. This is attributed to desorption becoming much more difficult as the energy of desorption rises with increasing film density. See figure 7.2.3.11. In contrast with the linear $X=0.1 \rightarrow 0.5$ fall-off in $T^{\text{D-max}}$ the rise here is non-linear which accords with it not being due to an augmentation effect, in accordance with the energy-of-desorption explanation.

T_2 continues to fall as monolayer density is approached.

$0.9 \leqslant X \leqslant 1.5$. $T^{\text{D-max}}$ is approximately coverage independent − as the first layer does not change. The apparent alternating/diverging behaviour seen is a consequence of the now broad ragged maxima and resultant ambiguity in maximum temperature. The ragged appearance of the maxima is believed to be due to an additional contribution, caused by the bulk of the edge-film fluid desorbing at these elevated temperatures along with the now very dense basal-plane fluid. Note the temperature coincidence, at T=8.5K of the low coverage edge-film dominated data, extrapolated back to X=0.05 and the *lower wing* of the $0.9 \leqslant X \leqslant 1.5$ data (figure 7.2.3.1), suggesting this actually locates the temperature where the bulk of the edge-film desorbs. Figure 7.2.3.4 shows the derivative of T_2 w.r.t. temperature on the high-T side of the maximum as a function of T, for $X \leqslant 0.75$. Erratic slope changes are visible for $T \geqslant 8.5$K and $X \geqslant 0.4$ where $T^{\text{efd}} \geqslant T^{\text{bpd}}$, $X^{\text{tot}} \gg X^{\text{ef}}$ such that edge-film desorption effects appear as an aberration on the otherwise smooth high-T side of the maxima. Again it is consistent with edge-film desorption.

Monolayer completion (maximum first layer density) can be seen occurring at a lower coverage (0.9) compared to the 1K data (figure 7.2.1.1) in figure 7.2.3.2, a consequence of thermally enhanced second-layer promotion. This is also seen on Grafoil **[19]**. T_2 then increases linearly with X, the sparse second layer fluid's relaxation being augmented by its dense fluid underlayer. In contrast with the low-T case (cf. figure 7.2.1.1) there is no turn-over as at X=1.2, probably because of much faster interlayer exchange.

Turning now to the melt-desorption-minimum, T_2 at which is plotted in figure

Figure 7.2.3.4, Plot of Derivative of T_2 vs T for T>T(desorption-max), BN, Run#6, F=4.5MHz, at Low Coverages.

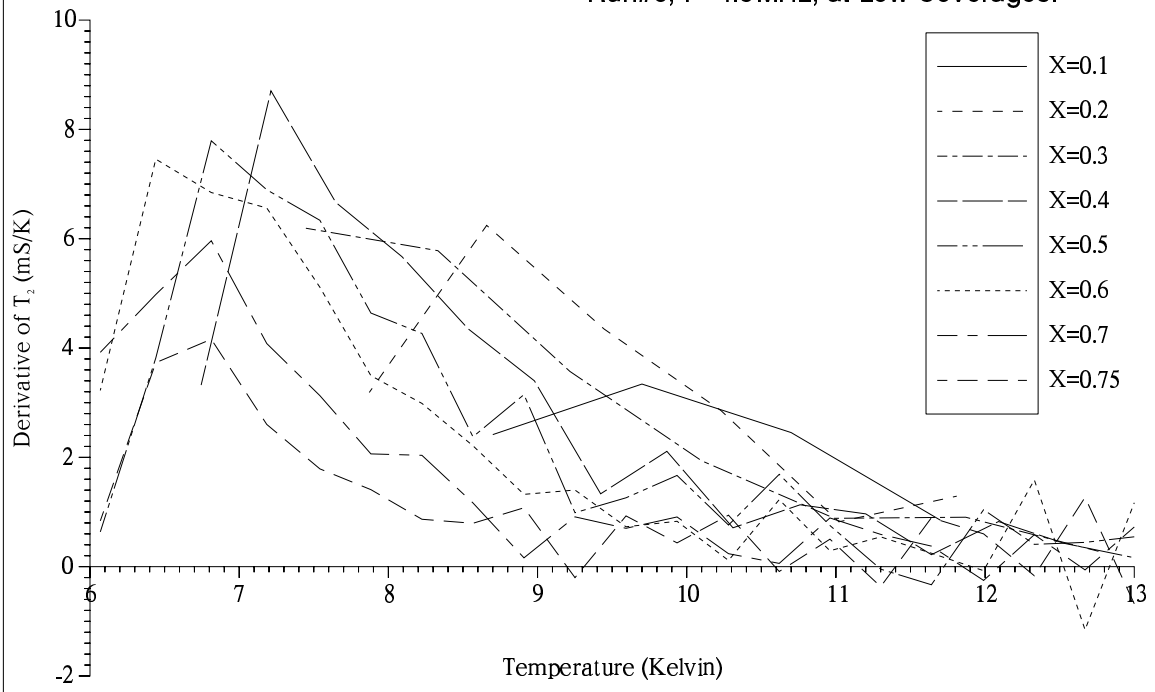

Figure 7.2.3.5, T_2 at T_2 Minimum vs X for BN, Run#6, F=4.5MHz

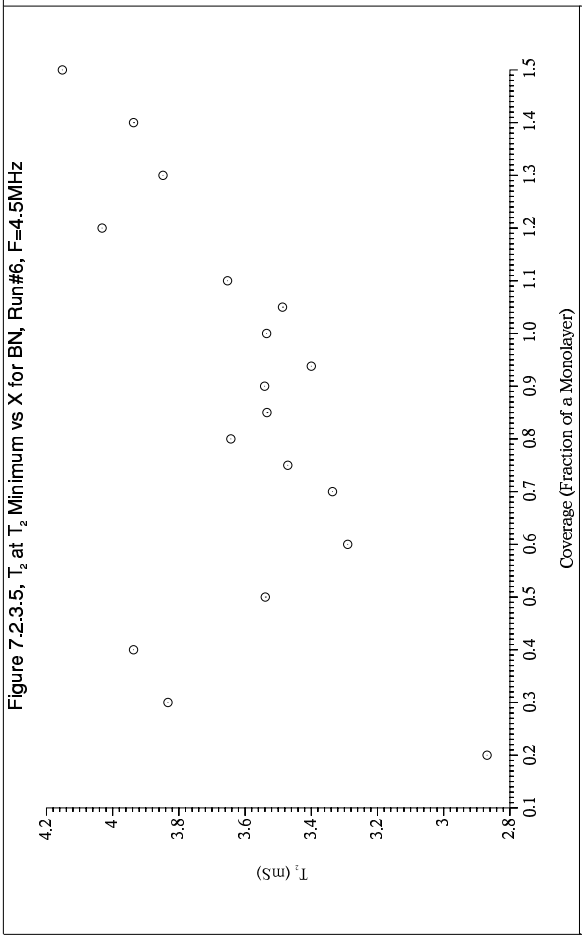

Figure 7.2.3.6, T_2 at T_2 Low-T Maximum vs X for BN, Run#6, F=4.5MHz

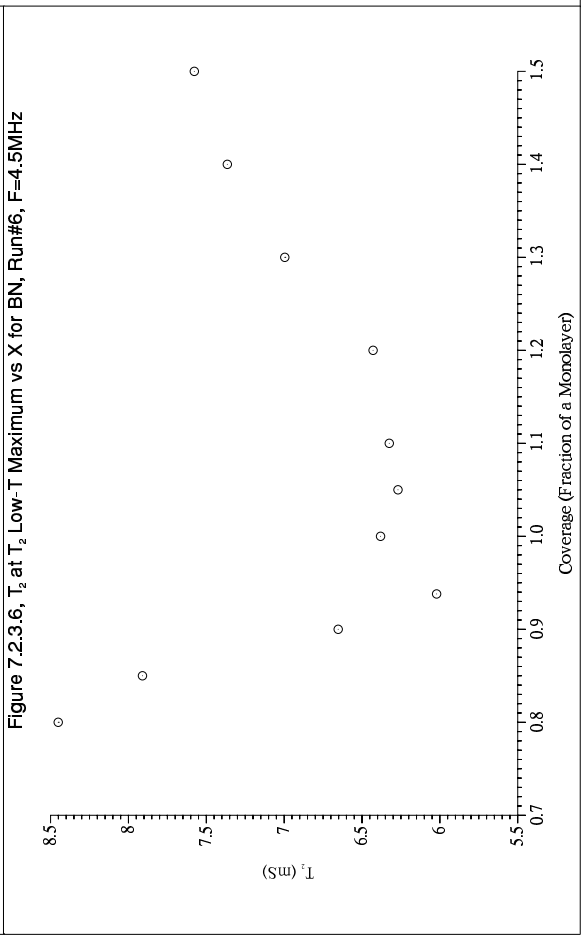

7.2.3.5. Recapping, the film is thought to be fully fluid, with rapid adsorbed thermal motion, leading to non-dipolar PMI/fluid dominated relaxation. The edge-film is probably mostly solid with considerable thermally activated vacancy tunnelling. Supporting this statement is that for $X<0.85$ $T^{\text{MD-min}} < 5.2\text{K}$, the high density basal-plane monolayer solid melting-maximum temperature. Unless the edge-film melts in the brief range $5.2\text{K} \leqslant T \leqslant 6\text{K}$ (melt-desorption-minimum monolayer temperature) it should also be solid for $X \geqslant 0.85$.

$T^{\text{MD-min}}$ falls off slowly from $X=0.2$ to a minimum at $X=0.6$. The fall does not follow a $1/X$ law, ruling out an edge+basal-plane combination/augmentation effect, unless the edge-film's state or effective motional speed change significantly over this small temperature-range (~0.8K). Instead we propose the change is due to increased (basal-plane-fluid:edge-film-solid) spins allowing PMI/fluid relaxation dominance to occur at lower temperatures. From $0.6 \leqslant X \leqslant 0.9$, $T^{\text{MD-min}}$ rises rapidly. Like the $T^{\text{D-max}}$ rise it is not linear, being faster than linear. This is attributed to (a) The rapid rise in the energy of desorption (figure 7.2.3.11) and (b) For $0.75 \leqslant X \leqslant 0.9$ the low temperature film has condensed, causing $T^{\text{MD-min}}$ to be pushed up by the increasing-with-coverage melting-temperature. For $0.9 \leqslant X \leqslant 1.1$, $T^{\text{MD-min}}$ remains constant in the unchanging monolayer film. Small unidentified second layer effects are apparent at $X>1.1$.

Although T_2 at the melt-desorption-minimum does appear vaguely similar to the desorption-maximum T_2 data (see figure 7.2.3.3) suggesting a similar explanation, the most striking observation is the relatively very limited changes with X. Between $X=0.9$ and 0.5 T_2 at the desorption-maximum increased by 130%. By comparison in the corresponding melt-desorption-minimum data ($X=0.938$ to 0.4) T_2 increased by only 15%. A dipolar T_2 should be a strong function of X, $T_2 \propto X^{-3}$, strongly suggesting T_2 here is mediated dominantly by a non-dipolar mechanism which depends primarily on spin mobility rather than internuclear separation, in accordance with the explanation given.

Finally we consider the melting-maximum. Recapping, this is believed to occur when increasing thermal activation in the solid with temperature which motionally narrows T_2, reaches a critical defect (vacancy) concentration causing melting. The melt cannot expand laterally, only out of the layer if the coverage is high enough. It then experiences a large increase in mobility with the loss of order which increases the dipolar T_2. The sharp fall off in T_2 observed above the maximum is therefore attributed to relaxation via the non-dipolar PMI/fluid mechanism.

From the onset of post-registry localisation the temperature of the melting maximum $T^{M\text{-}max}$ at X=0.8 increases towards the monolayer plateau at X=0.938. The apparent *step* at X=1.2→1.3 is probably an artifact of the finer data grid used at $X \geqslant 1.3$ more accurately locating the peak. For simplicity the melting peaks were located from the largest single T_2 point around the melting-maximum in the T_2 *vs* 1/T plots. Apparent aberrations in the $T^{M\text{-}max}$ rise to X=0.938 may also be due to peak-location inaccuracies but it must be remembered that at X=0.8 to 0.85 the film is believed to be in/entering a domain wall phase transforming to incommensurate solid at higher X. Occurring at a lower temperature than the melt-desorption-minimum the monolayer plateau starts at a higher coverage, 0.938 as against 0.9, as expected **[19]**. Figure 7.2.3.7 shows the data plotted with the melting lines of helium on Grafoil from heat capacity measurements for comparison. Helium-4 data is from reference **18** and helium-3 from **28**. Within the limits of our relatively sparse data and the lack of higher coverage ^{3}He/Grafoil data it is reassuring to see the same qualitative behaviour. A higher monolayer plateau temperature on Grafoil is due to the more dense monolayer, a consequence of that substrate's greater binding energy.

Figure 7.2.3.6, T_2 at the melting-maximum against coverage possesses the usual minimum at monolayer. Recalling that dipolar relaxation gives way to a non-dipolar mechanism at the melting-maximum, the relaxation can be expected to only partially show dipolar characteristics, hence the monolayer minimum but with limited variation in T_2 on either side.

7.2.3.2 T_1 Minima and Maxima

Figures 7.2.3.8 and 7.2.3.9 show the temperatures-of-occurrence (alone) and values of T_1 at the minima as a function of coverage. T_1 minima observed as a function of temperature are believed to be dipolar in origin, the minimum occurring as increasing temperature reduces τ_c until a $\omega_x\tau_c$=*const*. condition is fulfilled and relaxation is at its most efficient. ω_x is the Larmor frequency ω_0 if the relaxation is homonuclear or a combination of ω_0 & ω_s, where ω_s is the Larmor frequency of a substrate spin possibly incorporating quadrupolar splittings or even a substrate spin quadrupole frequency itself. The ω_x frequencies are of the order of MHz so correlation times on the order of 10^{-6} Sec. are required since '*const*' should be of the order of unity. We cannot be sure (at this stage but see §8) whether the minima are due to heteronuclear or homonuclear processes but some points can be made: A single homogenous system with homonuclear dipolar relaxation can only produce a single minimum but here there is a significant (5%) edge-

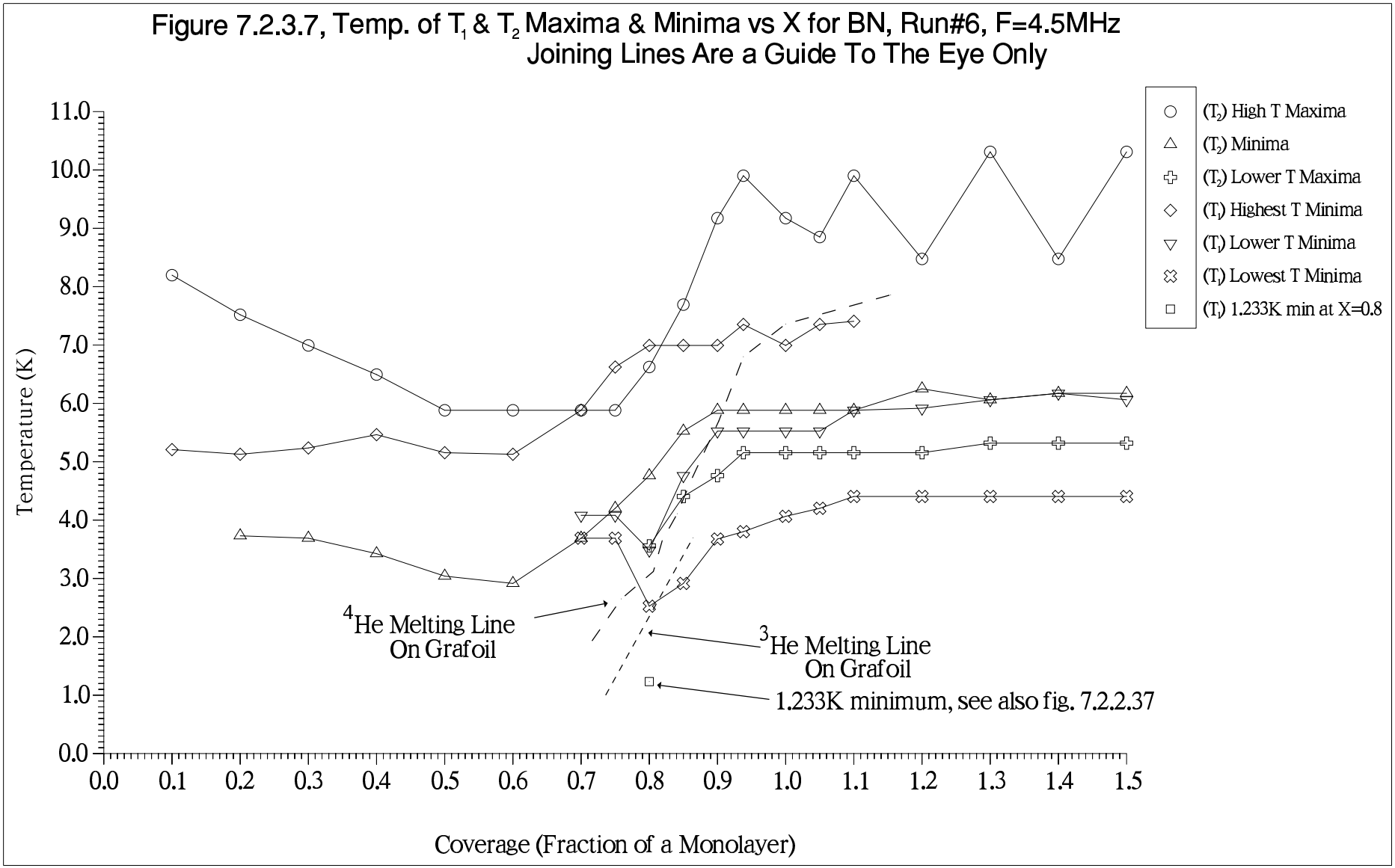
Figure 7.2.3.7, Temp. of T1 & T2 Maxima & Minima vs X for BN, Run#6, F=4.5MHz
Joining Lines Are a Guide To The Eye Only
(T2) High T Maxima
(T2) Minima
(T2) Lower T Maxima
(T1) Highest T Minima
(T1) Lower T Minima
(T1) Lowest T Minima
(T1) 1.233K min at X=0.8
4He Melting Line On Grafoil
3He Melting Line On Grafoil
1.233K minimum, see also fig. 7.2.2.37
Temperature (K)
Coverage (Fraction of a Monolayer)
11.0
10.0
9.0
8.0
7.0
6.0
5.0
4.0
3.0
2.0
1.0
0.0
0.0 0.1 0.2 0.3 0.4 0.5 0.6 0.7 0.8 0.9 1.0 1.1 1.2 1.3 1.4 1.5

Figure 7.2.3.8, Temperature of T_1 Minima vs X for BN, Run#6, F=4.5MHz
The line is a guide to the eye only

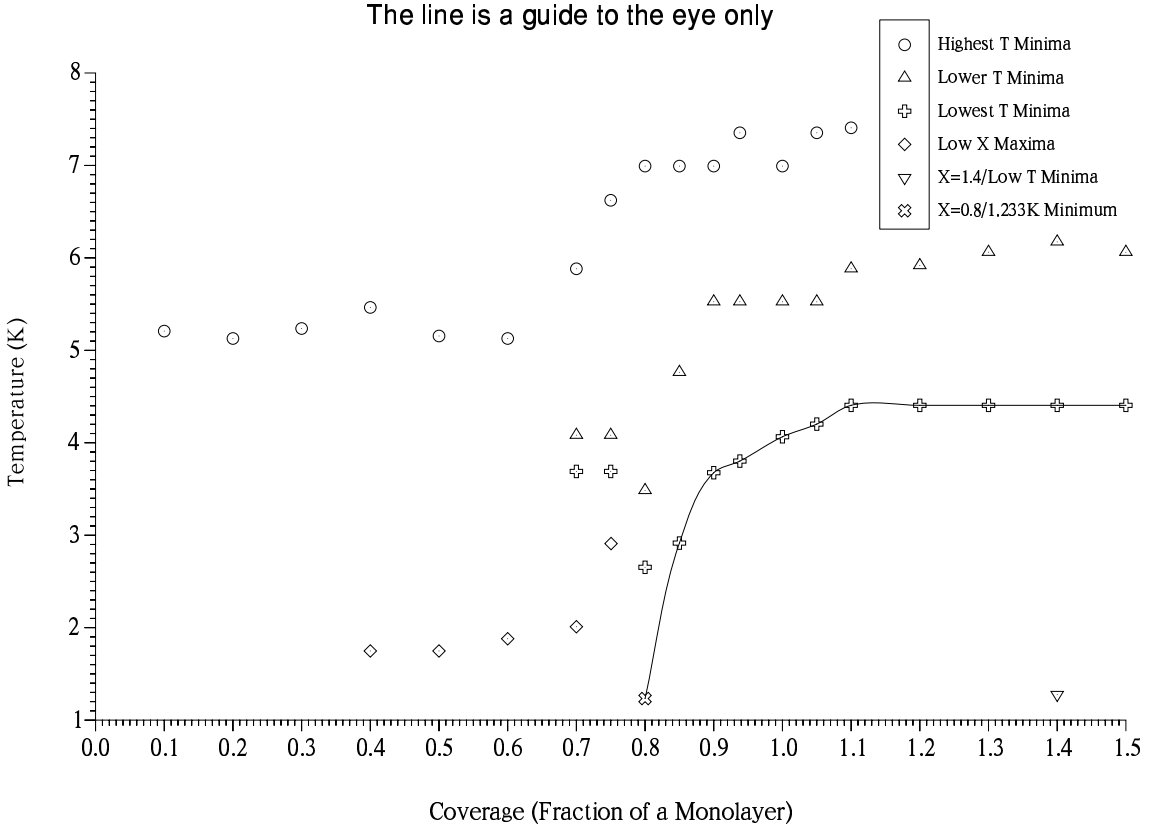

Figure 7.2.3.9, T_1 at T_1 Minima vs X for BN, Run#6, F=4.5MHz

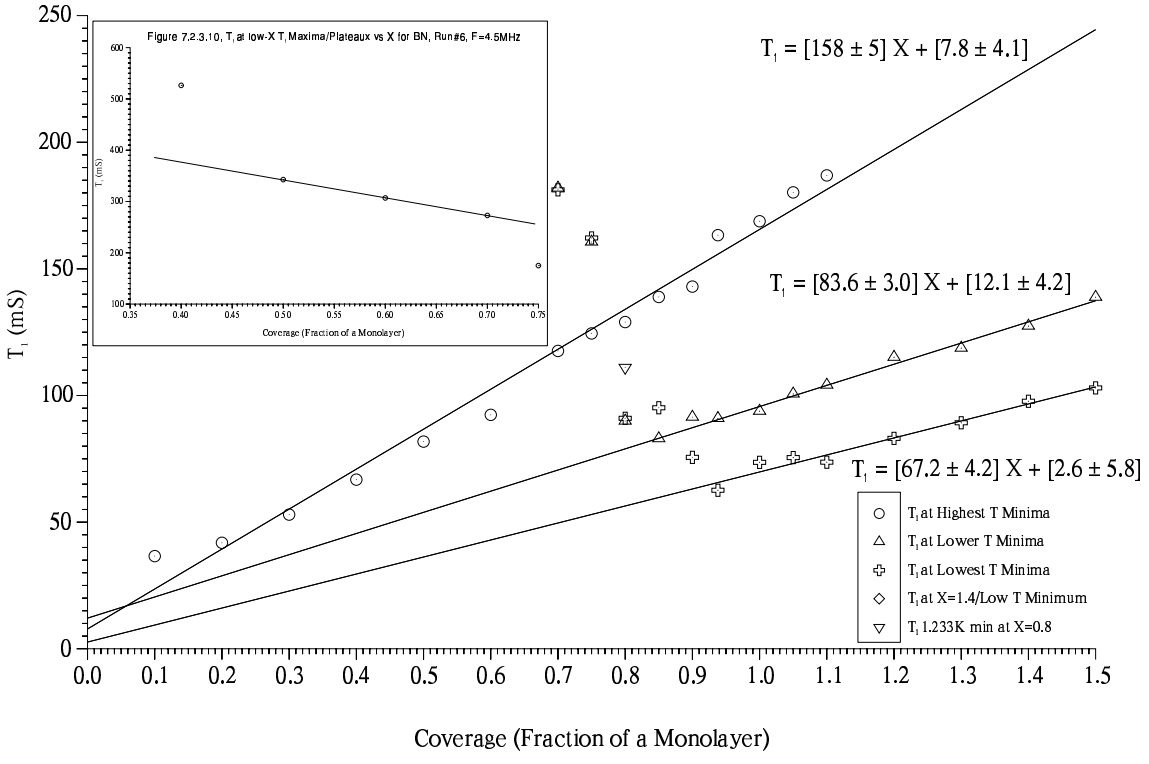

sites film. For X>0.05 two distinct systems exist and at high coverages there are three minima. Therefore at least one set of minima ought to be heteronuclear. None of the minima display a homonuclear $T_1 \propto X^{-3}$ relation anywhere which suggests that unless the relaxation occurs via the edge-film (where the mechanism could be either) it points towards relaxation through the substrate spins. Alternatively at these elevated temperatures layer promotion/desorption could explain a homonuclear minimum lacking the expected X^{-3} form.

Starting with the highest T minimum, we see that for X<0.7 this is the only minimum in T. $\tau_c \sim 10^{-12}$ Sec is expected for the low coverage basal-plane fluid (see §1.10.3) which is orders of magnitude too small to produce a minimum. Obviously something else must be responsible so the edge-film is proposed. Support comes from very low coverage Grafoil data, where the film patchy solid alone exists, which has a T_1 minimum in T, (§1.10.2). At low coverage, $T^{\min}$ occurs between $T^{\text{MD-min}}$ (T_2) and $T^{\text{D-max}}$ (T_2) where the edge-film is thought to be mostly solid and fluid respectively. A solid with sufficient thermally activated vacancy tunnelling or its melt should be able to provide the required τ_cs. In this model then, basal-plane spins relax via the edge-film through particle exchange. The signature of such augmentation-factor relaxation is $T_1^{\min} \propto X$. Figure 7.2.3.9 shows this is indeed the case. A further expected consequence of relaxation via the edge-film is temperature independence of $T^{\min}$ with X since for X>0.05 additional spins should only modify the basal-plane fluid. This is also so for $0.1 \leqslant X \leqslant 0.6$. The increase in $T^{\min}$ at $X \geqslant 0.7$ is therefore slightly surprising. It can only be assumed that at the high basal-plane fluid densities for coverages similar to those of the low temperature 2D solid, there is sufficient lateral pressure in the the basal-plane to compress the edge-film enough to require higher Ts to decrease τ_c to fulfil the necessary minimum condition. If correct this also has implications for the interpretation of the T_2 maxima/minimum data. The gradual reduction of this minimum as a feature in the high coverage data, eventually disappearing at X=1.1 is also consistent with edge-film mediated relaxation − it becomes a decreasing effect on the side of the growing lower T minima as the basal-plane fluid population increases, marginalising edge-film effects. Recalling the temperature dependence data of §7.2.2, this minimum in contrast with the lower T ones, had a corresponding minimum in ‘T1Index’ suggesting a multiplicity of relaxation channels. Again this is more suggestive of relaxation in the heterogeneous edge-film than in something more homogenous. From the slope of the $T_1^{\min}$ *vs* X plot and using $T_1^{\min} = T_1^{\text{ef(min)}} \times (X^{\text{tot}}/X^{\text{ef}})$ with $X^{\text{ef}} = 0.05$ gives $T_1^{\text{ef(min)}} = 7.9$mS. For

comparison, given the 44.9mS low temperature registry value and the low temperature incommensurate solid Grafoil minimum ~100mS **[60]**, relaxation here is evidently very efficient. This contrasts with the relatively inefficient $^{19}F-{}^{3}He$ relaxation exhibited by low coverage heterogeneous/deep-sites ^{3}He spins on DLX6000 **[141,142]**. Strong relaxation processes are favoured by both a high density edge-film (ie. short $^{3}He-{}^{3}He$ internuclear separation) and *trapped* or multiply adsorbed ^{3}He spins at the *craggy* basal plane edge-site's or where crystallites butt up against one another (ie. short and/or multiple $^{3}He-$ Substrate internuclear bonds).

Now considering the intermediate temperature minimum. Neglecting the two tiny minima at X=0.7 and 0.75 we see this feature starts at X=0.8, rising rapidly in temperature-of-occurrence to a plateau extending over $0.9\leqslant X\leqslant 1.1$ and to a lesser extent as far as X=1.5. Except at X=0.8 (where the low density solid/DWL has just formed with coverage) where it coincides with the T_2 melting-maximum, the minimum occurs at temperatures between the T_2 melting-maximum and melt-desorption-minimum. Here the basal-plane spins exist as a dense fluid. The rapid increase in T^{min} with X to the X=0.9 monolayer plateau, following the T_2 melt-desorption-minimum trend is consistent with maintaining $\omega_x\tau_c=const.$ in the increasingly dense fluid. At all but the lowest coverages $T_1^{min}\propto X$ concurs with a dense constant monolayer fluid augmenting the growing second layer fluid relaxation rate. The possibility of the edge-film being responsible for this minimum (and the lowest T one also) must also be considered: Since the more dense edge-film must be able to at least span the whole range of effective τ_c available to the basal-plane fluid with temperature, we expect that if the lower T minima were due to the edge-film, all three should occur at low coverages. Therefore we conclude the two lower T minima are due to relaxation on the basal-plane. Although the slope in figure 7.2.3.9 shows relaxation is ~2× more efficient than at the high-T minimum the edge-film:basal-plane-fluid spin ratio (0.05/0.9) makes it only ~0.1× as efficient.

Now the lowest temperature minimum is discussed. It always occurs below the T_2 melting peak, indicating a localised film. Similarly to the intermediate minimum the temperature-of-occurrence rises rapidly from X=0.8 to a plateau at 1.1 monolayers. Starting at X=0.938 where monolayer completion at the melting-maximum occurs (ie. where the melting line reaches maximum first-layer density) $T_1^{min}\propto X$ again. Relaxation is faster, by a factor of 2.6 w.r.t. the high-T minimum. Taking into account the spins ratio (0.05/0.938) the efficiency is ×0.14. More difficult to explain is the unique form of

T_1^{min} over $0.8 \leqslant X \leqslant 0.938$. Ignoring the X=0.8 point the data lies on a straight line decreasing with X, ie. $T_1^{min} \propto -X$ in contrast with the homonuclear expectation, $T_1^{min} \propto X^{-3}$. To be sure, least squares fits to both these models were done and showed the linear law was preferred. The linear regression simple correlation coefficients are 0.9984 and 0.9859 respectively. The straight line also passes through the X=0.8/1.233K point suggesting it is the *true* minimum. Looking at figure 7.2.3.8 also shows the 1.233K minimum more naturally completes the trend of the data. Heteronuclear relaxation (with a simple model, see §8.7.4) predicts T_1 independent of X here, there being no second layer fluid relaxation burden. A guess, since this minimum alone occurs in the localised film where a DWL $\rightarrow$ incommensurate solid transformation is thought to occur over the coverage range, is that the ^{3}He−Substrate geometrical arrangement changes in a way which favours progressively more efficient relaxation. See §8.7.4.

Finally the low coverage ($0.4 \leqslant X \leqslant 0.75$) T_1 maxima/plateaux plotted in figures 7.2.3.8 and 7.2.3.10 are considered. There is some ambiguity in the temperatures of the maxima for X>0.4 where broadening to plateaux occurs. In simple terms, the rise in T^{max} with coverage indicates the registered (actually orientationally-ordered-fluid) spins require more thermal energy to disorder them as the localised:2D-gas spins' ratio increases, rising to infinity at perfect registry (X=0.75). The biggest change occurs at X=0.7$\rightarrow$0.75 with the elimination of the 2D-gas. T_1^{max} falls with coverage as the proportion of spins effectively registered increases, enhancing relaxation via substrate spins. Over X=0.5 to 0.7 the fall is linear in X. This sets those points apart from X=0.4, where the onset of registering occurs, the registered spins apparently *melting* directly to the isotropic 2D-gas and X=0.75 where registry is complete. It accords with the idea that within the plateaux ($0.5 \leqslant X \leqslant 0.7$), a single phase, an orientationally ordered fluid in registry with the substrate or alternatively a commensurate solid with vacancies **[32]** exists (see also §7.6.4). The linear law suggests the number of effectively registered:non-registered spins is proportional to coverage in this phase, a result also seen on Grafoil at low temperatures at coverages below perfect registry **[206]**. Note however, in that case the film is reported to be a fluid+registered coexistence rather than the single phase proposed here.

7.2.3.3 Activation Energy Data

Figure 7.2.3.11 shows the data. There are four data sets, taken from the; T_2 desorption-maximum rise, T_2 melting-maximum rise and from T_1 on both sides of the

Figure 7.2.3.11, Activation Energies from $T_{1,2}$ vs X, BN, Run#6, F=4.5MHz
Line is a Guide to the eye only

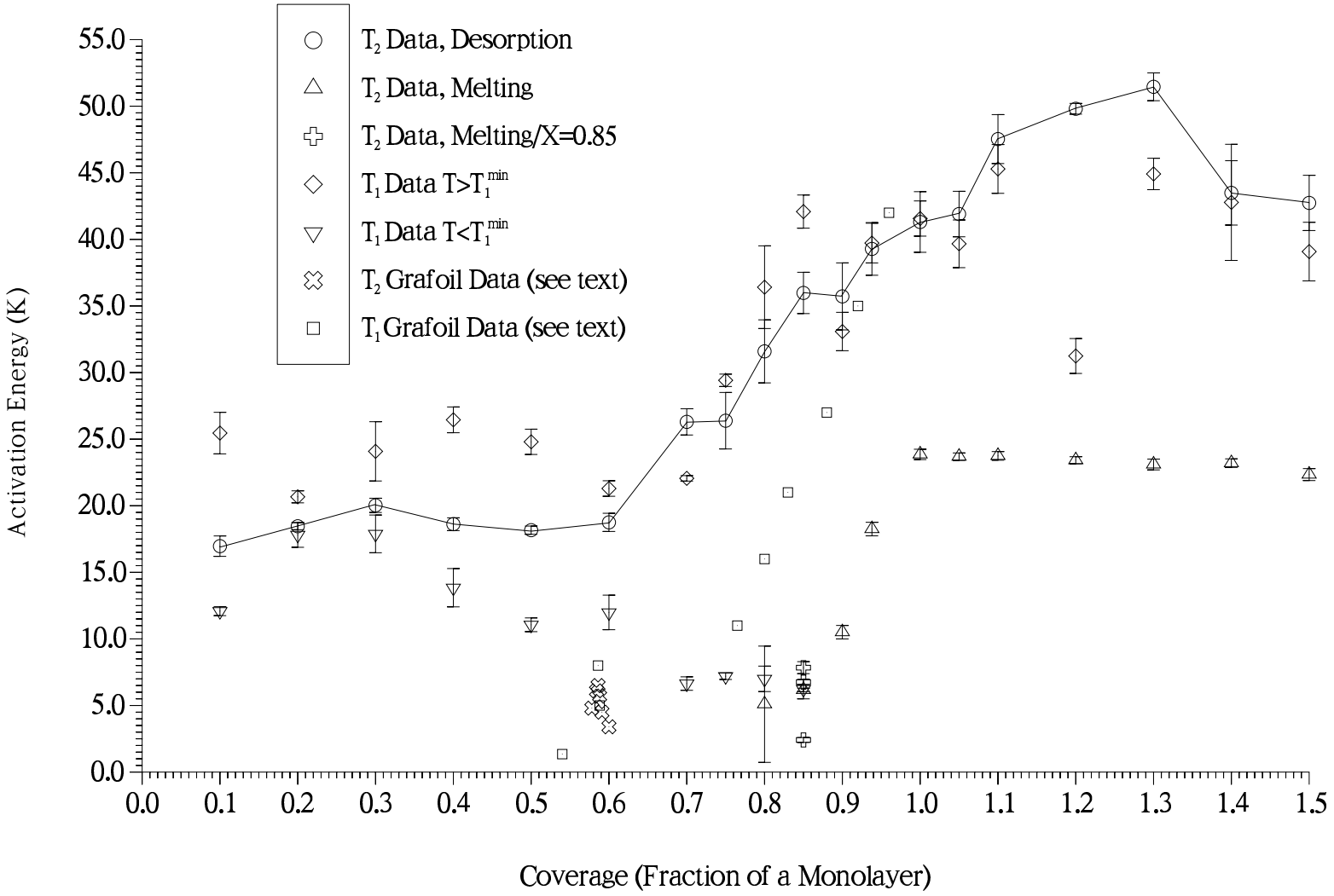

minimum where possible. At X=0.85 the 3 *sub-slopes* within the melting-maximum rise are also plotted. T_1 data has been taken from the sides of the largest maximum at each coverage. For X>0.85 at $T<T^{min}$, the T_1 data does not follow an activation law, therefore this data was not used here. Some experimental scatter on the T_1 data due to *minimum-switching* from coverage to coverage is inevitably present. Some arbitrariness is also inherent in deciding where logarithmic behaviour ceases close to the minimum. Error bars indicate the degree of non-logarithmicity rather than experimental scatter in the $T_{1,2}$ *vs* 1/T plots which is comparatively small. Remembering equations 1.10.4.1−1.10.4.3 and the NMR rule-of-thumb $1/T_2 = m_2\tau_c$, a plot of $T_{1,2}$ *vs* 1/T on a log.−lin. scale will produce a straight line where an activation law applies. Many of the graphs included in §7.2.2 are plotted this way. However, for reasons discussed in §6.3 the activation-energies E_a have been obtained from non-linear least squares fits. For comparison figure 7.2.3.11 contains some E_a values for ^{3}He/Grafoil data taken from reference **211**. T_1 derived values come from $T<T^{min}$ data. Exactly what do the energies obtained mean? This depends strongly on the temperatures over which the data was taken.

In the T_2 melting-maximum rise, E_a is the energy to thermally create and possibly, additionally, tunnel a vacancy in the solid. Note the large *errors* at X=0.8. Non-exponential behaviour at X=0.8 compared to X>0.8 accords with the DWL interpretation. E_a rises steeply to a plateau at X=1.0 as film density increases. The plateau starting-coverage X=1.0, the low temperature monolayer (maximum first layer density) point contrasts with the T_2 melting-maximum plateau onset (figure 7.2.3.7) (X=0.938). Although the melting-maximum obviously occurs at a higher temperature than most of the data used to extract the E_a, the abruptness of the E_a plateau onset suggests it is primarily the the loss of order at melting which makes second layer promotion at X<1.0 much easier. Closer inspection of the *plateau* shows E_a actually falls-off very slowly with X, suggesting particle exchange with the fast moving second layer fluid spins is contributing a little to vacancy production. However, this is not the very sharp fall-off seen on Grafoil by Satoh and Sugawara **64**.

Considering the higher temperature data from the T_2 desorption-maximum rise and T_1 at $T>T^{min}$ − They follow the same trends. Figure 7.2.3.7 shows the temperatures over which these data were taken, which are broadly similar. The data can be summarised as; Approximately coverage independent for $0.1 \leqslant X \leqslant 0.6$ at $E_a \sim 20$K ($T_2^{D\text{-}max}$) and ~ 25K (T_1^{min}) but with a shallow peak at X=0.3 (X=0.4, T_1^{min}). A rapid rise to a peak at X=1.3 over $0.6 \leqslant X \leqslant 1.5$ with a peak energy of ~ 50K ($T_2^{D\text{-}max}$), ~ 45K (T_1^{min}) follows. Unlike the $T_2^{M\text{-}max}$ case the measured energies here result from a combination

of factors which are hard to disentangle. Thermodynamic measurements using ^{4}He/ Grafoil **[19]** have inferred the following data: First-layer binding energy = −143K, First-layer first excited state (single particle substrate-normal states) = −89K and Second-layer binding energy = −30K, all referenced w.r.t. the desorbed gas. At low coverages the measured energy of desorption should approximate the binding energy. It seems very unlikely the smaller BN adsorption potential could account for a BN energy-of-desorption only ~ 20K when the Grafoil value = 143K. Even if it is excitations to the first excited state, in the low coverage fluid that are responsible the 20K is still rather too small, 143K − 89 = 54K. A more likely explanation, given the inferences already made about the low-coverage desorption-maximum behaviour, is that the 20K value mainly reflects processes such as vacancy creation, in the edge-film. Support comes from the broadly similar values in the melting-maximum monolayer plateau. The measured energy rises from X=0.7 to 1.3 as desorption becomes increasingly difficult in the now dense fluid. The cause of the X=1.3 maximum is uncertain but could be related to either edge-film desorption (§7.2.3.1) or the second layer fluid as in the case of the melting-maximum E_as.

Finally, considering the data from T_1 at $T<T^{min}$ − The data used in this measure comes from the lowest temperatures of the four. Bearing in mind the reservations about the T_1 E_as discussed at the beginning of this section, the most interesting feature here, is the fall to low values around the registry coverage (0.75) and the small peak at X=0.75. Grafoil, at registry ($X \approx 0.6$) has cusp shaped peak in E_a at very similar energies as shown in figure 7.2.3.11. However, it must be remembered that the temperatures of the T_1 at $T<T^{min}$ data ($4K \leqslant T \leqslant 7K$) are still well above the order-disorder transition ($T \approx 3K$). If not an artifact, the peak must be a residual effect from changes in the film which occurred at lower T (ie. the O-D transition). The very shallow peak (cf. Grafoil) is consistent with this idea. Support also comes from Grafoil T_1 data which still shows the remnants of the registry dip at 4K. See §1.10.1.

7.2.4 Frequency Dependence of Low Temperature Data

7.2.4.1 T_1

Measuring T_1 against frequency is of interest because it provides a direct probe of the spectral density of the dipolar local field fluctuations. If a sufficient range of experimental frequencies are available its shape may be completely mapped and compared with theoretical models for the spin motion (see §1.10.6). Figures 7.2.4.1 to 7.2.4.4 show some of the T_1 *vs* frequency plots at different coverages, conveniently divided into four qualitatively different regimes.

X=0.4 and 0.5. Here a strange double *bend* is apparent. No homogeneous film with homonuclear dipolar relaxation can produce this type of shape. Given the state of the film at these coverages, a combination of edge-film/patchy solid and basal plane registered-spins mediated relaxation should operate, the latter (at least) dominantly via substrate spins, possibly accounting for the double bend. At X=0.6, $T_1 \propto F$ for F<10.7MHz is apparent. A linear law was also seen by Fardis using sample chamber#2 at intermediate coverages (§3.4.2).

X=0.7 and 0.75. With relaxation dominated by registered spins, anomalous behaviour around 4.5MHz is apparent. Naturally, it is greatest at X=0.75. NB: See also figure 7.2.1.8. After the 4.5MHz minimum, T_1 again follows a linear law. At 0.75 monolayers the 5.7MHz point clearly lies within the minimum feature. In contrast with figure 7.2.1.8 all other variables are held constant here, eliminating any possibility of artifacts arising from ambiguity in locating the minima in coverage in figure 7.2.1.7. Note the limited variation with frequency here. It suggests $\omega_x\tau_c$ is smaller for registered spins than solid-patch ones. Also, different effective spectral density sampling frequencies ω_x may be effective in the two films.

$X \geqslant 0.8$. At lower coverages 'T1Index' $\geqslant 0.8$ and 'T_1(1/e)' $\approx$ 'T_1'. Here in the localised film where motion slows and single platelet relaxation increases the index falls causing a divergence between the two measures with 'T_1(1/e)' > 'T_1' with increasing frequency. For $X \geqslant 0.9$, 'T_1' $\propto F$ but 'T_1(1/e)' increases faster than linear. Remembering that Fardis (§3.4.2) used the T_1(1/e) metric and fitted the higher coverage data to an exponential law his data agrees at least qualitatively with the data here. At X=0.8 and 0.85 (around the proposed DWL) a different behaviour occurs with both measures increasing faster than a linear law at higher frequencies. Breakdown of $T_1 \propto F$ is predicted at higher coverage as exchange motion slows and $\omega_x\tau_c \gg 1$ becomes increasingly true. Here the high-frequency part of the spectral density, which falls-off most rapidly with frequency is sampled in a T_1 measurement. Since $1/T_1$ (homonuclear)

Figure 7.2.4.1, T_1 against Frequency, BN, Run#6, T=1.1K, X=0.4,0.5 & 0.6

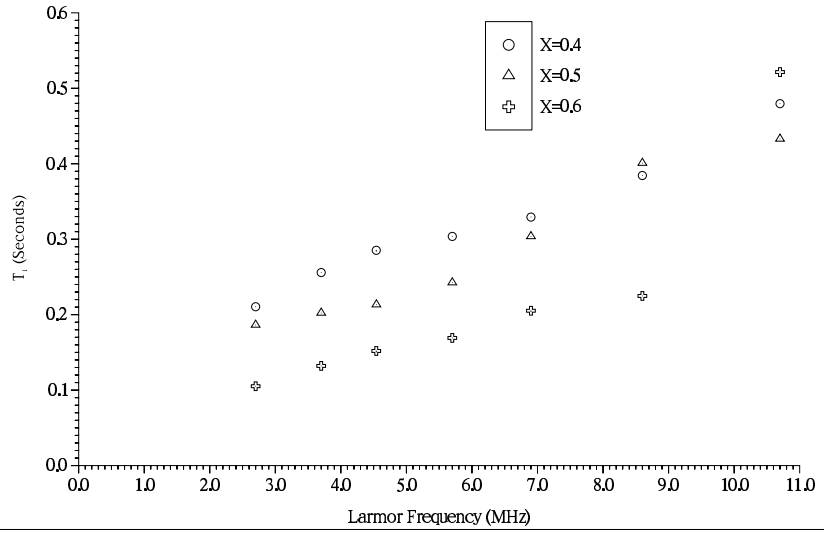

Figure 7.2.4.2, T_1 against Frequency, BN, Run#6, T=1.1K, X=0.7 & 0.75

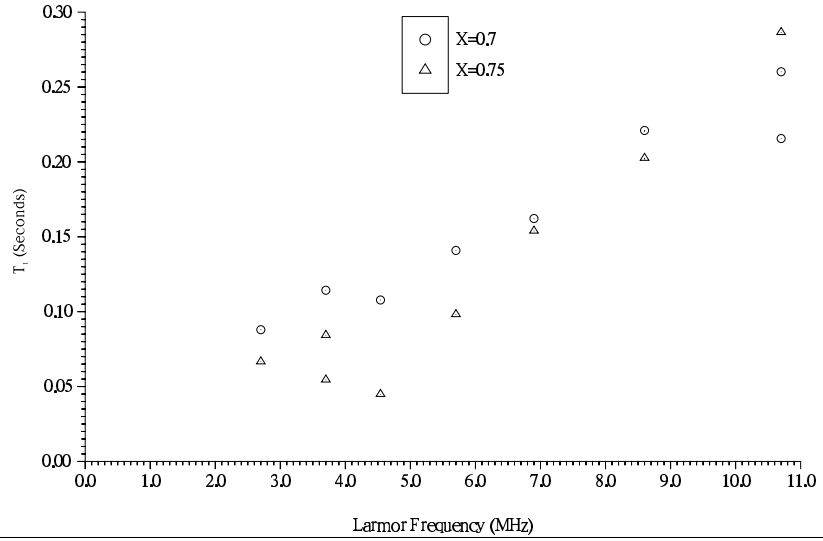

Figure 7.2.4.3, T_1 against Frequency, BN, Run#6, T=1.1K, X=0.8 & 0.85 with fits (see text)

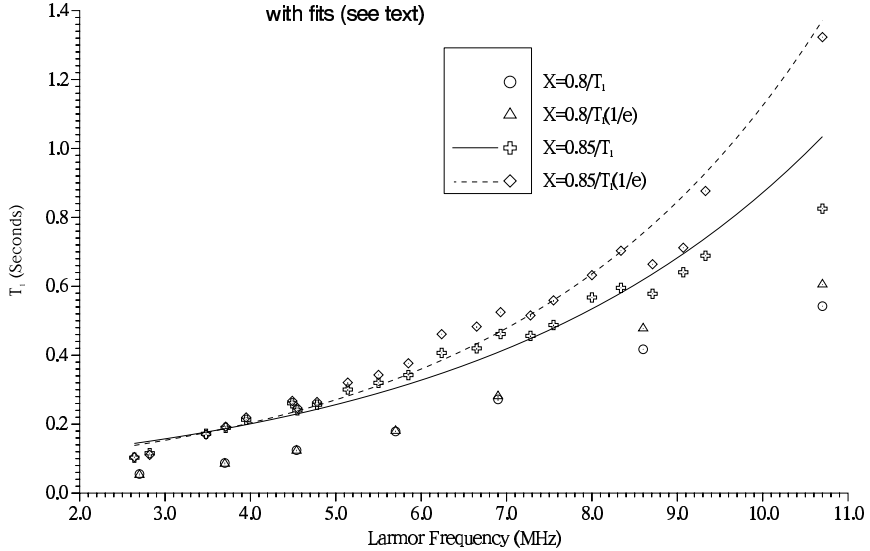

Figure 7.2.4.4, T_1 against Frequency, BN, Run#6, T=1.1K, 0.9⩽X⩽1.0 with Fits (see text)

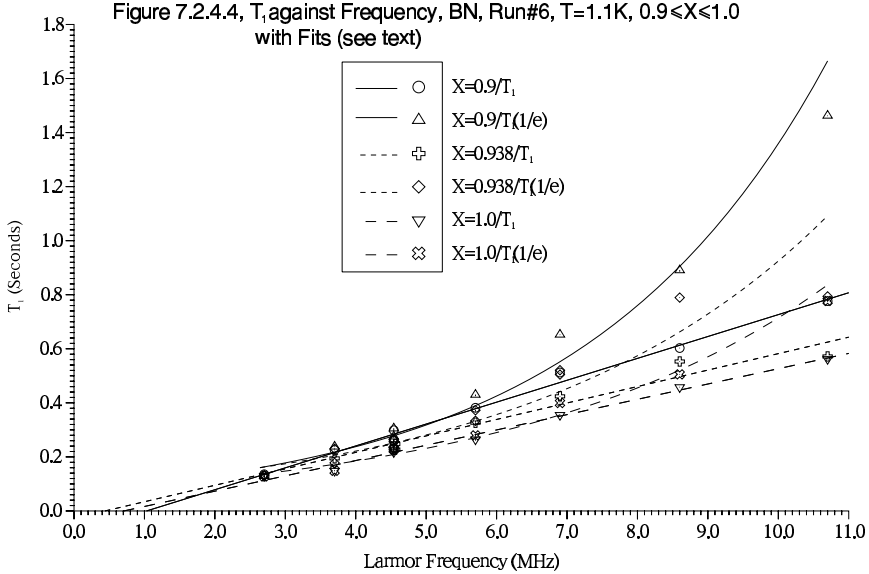

must decay at least exponentially fast [68] (see also §3.5.3) at high frequencies the data has been fitted to an exponential form,

$$T_1 = T_1(0)\ \exp\left(\frac{F}{F_{\text{scale}}}\right) \qquad 7.2.4.1$$

Some fits are shown in figures 7.2.4.3 (T_1 and T_1(1/e)) and 7.2.4.4 (curves, T_1(1/e)). Using equation 1.10.6.4, the general expression for T_1 and writing $\mathrm{K}(x) \equiv \exp(-x)$ it is evident that $T_1(0)$ and F_{scale} should both be proportional to J, the exchange frequency which falls monotonically to X=1. See also reference **76, p.153**. Table 7.2.4.1 shows $T_1(0)$ and F_{scale} obtained from the four highest coverages.

Table 7.2.4.1, Values of $T_1(0)$ and F_{scale} For The Four Highest Coverages.

X	'T_1'		'T_1(1/e)'	
	$T_1(0)$	F_{scale}	$T_1(0)$	F_{scale}
0.85	0.103	4.97	0.077	3.83
0.9	0.132	5.87	0.096	3.90
0.938	0.130	6.73	0.125	5.41
1.0	0.104	6.14	0.086	4.84

X in monolayer fraction, $T_1(0)$ in seconds, F_{scale} in MHz.

They are similar to those of Fardis [76] showing a homonuclear dipolar mechanism cannot account for the data on an exponential model. $T_1 = A + BF$ straight line fits are also plotted on figure 7.2.4.4 for the single exponential 'T_1' measure. The model due to Cowan [68] describes linear frequency law behaviour in 2D by $T_1 \propto \omega_0/m_2 \propto \omega_0/X^3$, implying the slope B should fall with X as $X \rightarrow 1$. Table 7.2.4.2 shows this is so. Unlike the model predictions however, there is a significant zero-frequency contribution A to T_1, reinforcing a non-homonuclear dipolar interpretation.

Table 7.2.4.2, Values of Linear Fit Parameters at The Three Highest Coverages.

X	B	A
0.9	0.081	−0.083
0.938	0.061	−0.027
1.0	0.057	−0.040

7.2.4.2 T_2

Fardis [76] observed T_2 independent of frequency within experimental error in contrast with Grafoil as expected with BN's much smaller demagnetising fields (§3.4). Although the bulk of the relaxation is frequency independent, some of the data here does show a noticeable frequency dependence. It is discussed for three coverage regimes ($0.4 \leqslant X \leqslant 0.7$, 0.75 and $0.8 \leqslant X \leqslant 1.0$) and is plotted in figures 7.2.4.5 and 7.2.4.6.

At the lowest coverages ($0.4 \leqslant X \leqslant 0.7$) T_2 varies with frequency in an indeterminate way, due in part to poor S/N away from 4.5MHz. Relaxation by a combination of edge-sites patchy solid and registered spins is believed to operate, as in the T_1 case.

There is a distinct maximum at 4.5MHz for X=0.75. Given the T_1 *vs* F data, it is clear the 4.5MHz T_2 maximum must be produced by a mechanism closely related to that which produces the T_1 minimum − The two graphs are even approximately mirror images of one another. It is difficult to understand how enhanced relaxation of ^{3}He spins to non-^{3}He-spin degrees of freedom (ie. a T_1 type process) at some suitable $\omega_x\tau_c \sim 1$ could also decrease the spin-spin relaxation rate. Except in the region of the 10/3 effect the homonuclear T_2 (equn. 2.2.17) is independent of frequency. A heteronuclear T_2 also exists [47] (equation 8.26) and is the time taken by ^{3}He spins to come into thermal equilibrium with each other as a result of relaxing/dephasing in the substrate spin nuclear magnetic dipolar fields. Equation 8.26 shows T_2 (heteronuclear) has the same general form as equation 2.2.17, comprising an adiabatic zero-frequency term plus several non-adiabatic ones involving both Larmor frequencies. Except possibly when the relatively small applied-field-independent ^{11}B quadrupolar frequency is taken into account, the heteronuclear relaxation rate should have a similar frequency dependence to the homonuclear case, since both Larmor frequencies are proportional to B_0 − however see §8 and the question of ^{14}N and its quadrupole frequency. Even so, a maximum is certainly not expected.

Within experimental error $T_2 \propto F$ for $0.8 \leqslant X \leqslant 0.85$. Figure 7.2.4.6 contains the least squares fit slopes and intercepts. Above 0.85 monolayers the slope has fallen to zero within the resolution of the data. This is obviously not the $T_2^{-1} \propto \omega$ (expt.) or ω^2 (theoretical) relationship, observed on Grafoil or expected for substrate platelet diamagnetism respectively. It could be due to a 10/3 type effect, involving the heteronuclear mechanism. The 10/3 effect occurs around the T_1 minimum where $\omega_0\tau_c \sim 1$. The slope is largest at the lowest non-registered localised coverage (X=0.8) where τ_c, hence $\omega_x\tau_c$ will be smallest (ie. closest to ~1). Notice that the lowest-T T_1 minimum, at

Figure 7.2.4.5, T_2 against Frequency, BN, Run#6, T=1.1K, 0.4⩽X⩽0.75

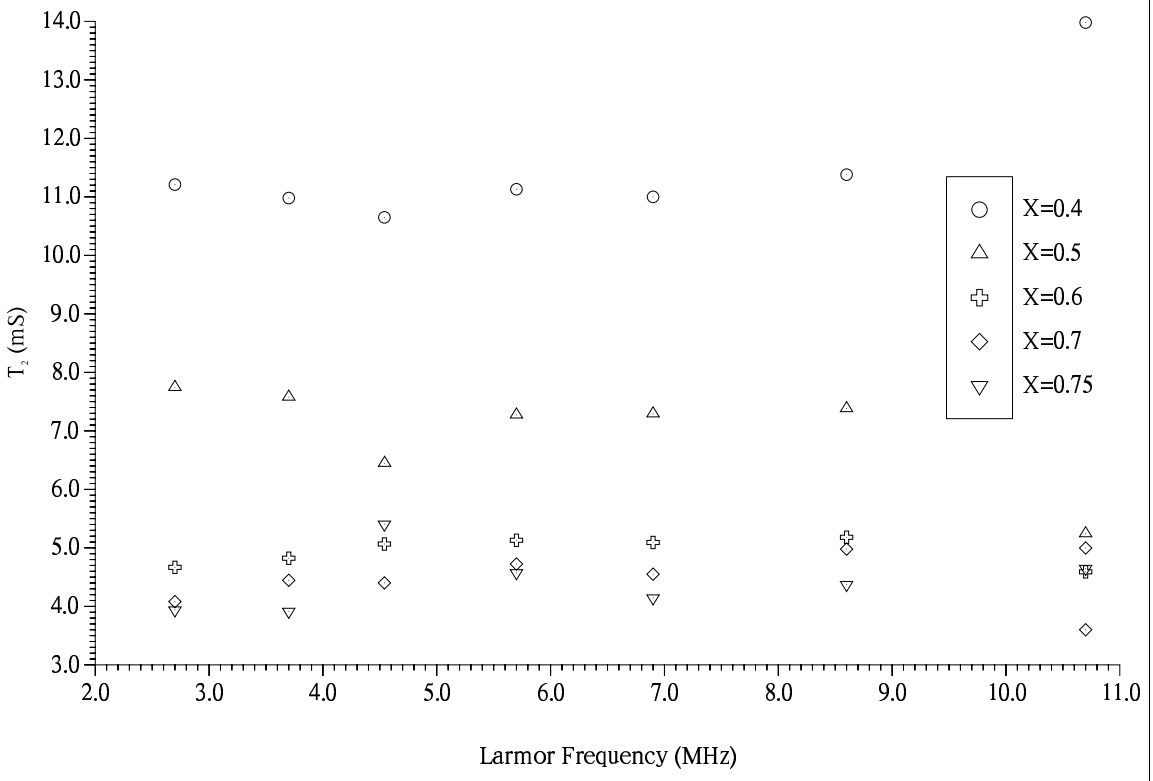

Figure 7.2.4.6, T_2 against Frequency, BN, Run#6, T=1.1K, 0.8⩽X⩽1.0

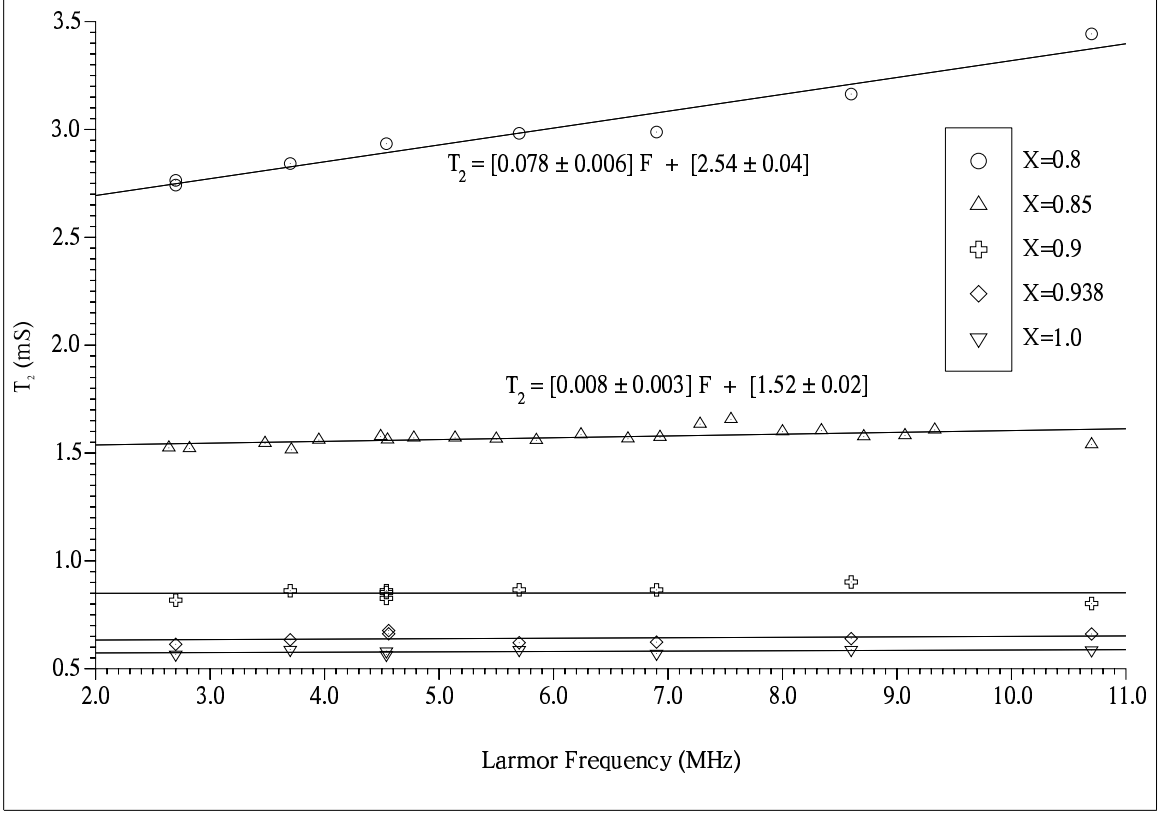

1.233K shown in figure 7.2.3.8 is at 0.8 monolayers. Comparing equations 2.2.17 and 8.26 for $^{11}B-^{3}He$ relaxation, shows the $J_2(\omega_B+\omega_{He})$ term in 8.26 will have the strongest function of frequency. See Appendix 1 for gyromagnetic ratios. The more detailed X=0.85 data set shows a small maximum feature around 7.5MHz. It is not known if this is an artifact. See §8.8.5 for the quantitative analysis of this data.

7.3 RUN#7

7.3.1 Double Resonance Experiments

We wanted to see if ^{11}B in BN would show the strong magnetic coupling to adsorbed ^{3}He spins as ^{19}F does in DLX6000. To investigate the possibility of spin cross-flipping a second NMR coil was required. A saddle coil wound on a Tufnol bobbin which fitted tightly over the sample chamber on top of its solenoidal NMR coil was constructed. The saddle geometry produces the necessary B_1 field orthogonal to both B_0 and the solenoidal B_1 field, to avoid mutual induction with it. The saddle coil consists of 2 × 9 turns of 24 SWG enamelled copper wire. Its measured electrical characteristics are $L = 11.01 \pm 0.01\mu H$, $C_{intrinsic} = 5.4 \pm 0.5pF$ giving $Q = 370$ and a natural resonant frequency of 4.8MHz at helium temperatures when installed in the cryostat. No saddle-solenoid cross-talk was detectable with a signal generator−oscilloscope arrangement. At 4.3MHz the solenoid coil produced a received signal 5.3× larger than the saddle coil and the saddle coil required a 3.9× larger TX−PSU voltage to produce the same B_1 tipping field, due to its lower filling factor. Except when tuning the spectrometer all reception was via the solenoid coil. A second separate transmitter section (Frequency synthesizer, 4-Phase generator, Phase shifter, Gate, TX, TX−PSU and Matching unit) was added to the spectrometer configuration shown in figure 4.1.2.1 to drive the saddle coil. Tuning up the ^{11}B signal is made very difficult by its short $T_2^* \sim 50\mu S$, resultant broad NMR line, long $T_1 \sim$ 10 minutes and reduction in signal intensity due to quadrupolar splitting mentioned at the end of §2.1.

All measurements were made at X=0.5. With the benefit of hindsight and the analysis of Run#6 data is is obvious X=0.75 should have been used. At X=0.5 most spins are in the 2D gas where $\omega_x\tau_c \ll 1$ precludes any useful relaxation. With limited numbers of registered spins (low temperatures only) relaxation is dominated by the edge-sites solid. None of this augurs well for observation of spin cross-flipping.

The cross-flipping experiment is a modification of the standard $180^o-90^o-180^o-$spin echo sequence (inversion recovery) used to measure T_1. The first 180^o pulse is applied by the saddle coil at the other frequency. Figure 7.3.1.1 illustrates this. If cross-flipping described in §3.5.1 does operate, the echo should at least be, reduced in height by a 90^o saddle coil pulse and doubly reduced by a 180^o one. The procedure is to monitor the echo height as a function of saddle coil TX−PSU voltage. Instrumental artifacts are eliminated with a *control* set of measurements in which the saddle coil irradiation frequency is shifted by several times $(1/T_2^*)$ of the isotope the saddle coil was tuned to irradiate, to stop resonant absorption of the RF.

Figure 7.3.1.1, An Example of a Spin Cross-Flipping Experiment Pulse Sequence.

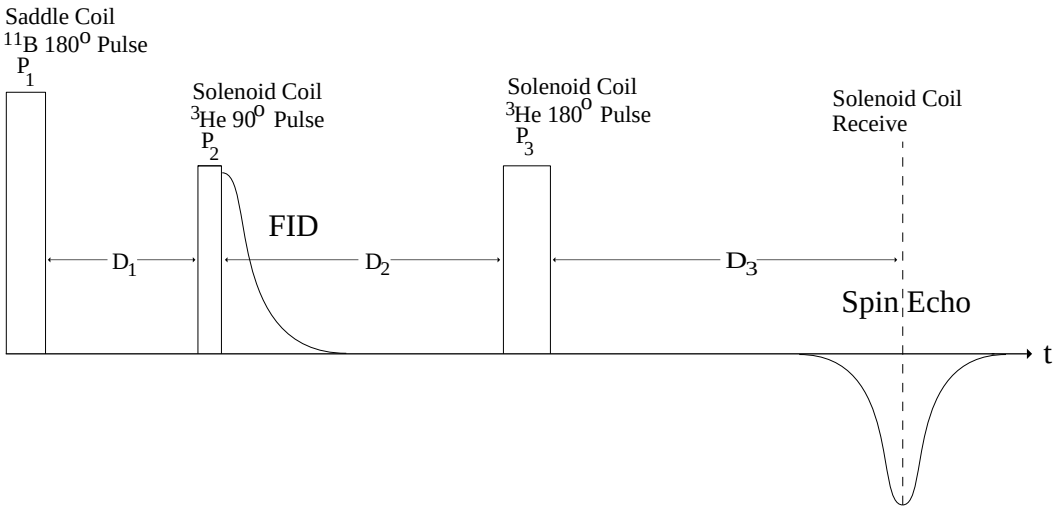

The TX−PSU voltage needed to generate a 180^{o} pulse from the saddle coil at a particular frequency was determined by tuning the solenoid coil to the same frequency and adjusting for maximum echo height with a *Solenoid 90^{o}−Saddle 180^{o}−Solenoid-RX echo* sequence. It is desirable to keep the D_1 delay short compared with the ^{3}He T_1. With strong relaxation to the substrate the ^{3}He T_1 is determined by the heteronuclear relaxation rate (§3.5.3).

Four sets of experiments were carried out to look for ^{3}He−^{11}B cross relaxation; **(1)** As shown in figure 7.3.1.1 at 1K. **(2)** The same but at 5.1K where the ^{3}He T_1 minimum occurred (figure 7.2.2.18), a marked increase in ^{11}B↔^{3}He flipping being expected if the minimum is due to heteronuclear relaxation. Experimental parameters used were P_1=100μS, P_2=170μS, P_3=300μS, D_1=100μS, D_2=1mS, *Repetition-time*=10Sec, ^{3}He F_0 = 10.29MHz, ^{11}B F_0 = 4.298MHz. The saddle coil 180^{o} pulse was on-tune at TX−PSU=24.8V. Detuning for the control data was by 3−4 × 1/T_2^* (^{11}B). T_2^* ~ 45μS. 64 averages per reading were taken. Additionally experiment (2) was repeated with D_1=250mS. **(3)** Conducted at 1K, the isotopes' roles were reversed and ^{3}He magnetisation-tipping influencing the ^{11}B spins was searched for. For each isotope the same frequency as before was used together with P_1=200μS, P_2=50μS, P_3=100μS, D_1=100μS and D_2=300μS. Detuning of the saddle coil ^{3}He frequency was by ~20× (1/T_2), T_2 (^{3}He) ~ 4mS and the ^{11}B echoes were averaged 4 times. **(4)** This is experiment (3) repeated at 5.1K.

^{3}He−^{14}N[Larmor frequency] coupling was also investigated using the same

setup as experiment (1). This corresponds to a ^{14}N Larmor frequency of 975.9KHz.

Due to computer noise the experiments were conducted with it switched off. Pulses were generated by the standalone microprocessor based pulse generator. 1K measurements were done unregulated with the QSV fully open (maximum pumping rate). The 5.1K data was temperature-regulated using a simple analogue comparator circuit based on a '741' OP-AMP driving a relay which operated the pot heater. Regulation within ±12mK was achieved using the Pot Allen-Bradley thermometry resistor. Once the storage 'scope had accumulated an echo signal, the Archimedes was switched on to log it using the ARCECHOLOG program, a cut-down version of ARCONTROL6 which does only as its name suggests.

With the exception of experiment (2) at D_1=100µS none of the results showed any sign of cross-flipping. With experiments (3) and (4) this is unsurprising given the greater relaxation burden imposed on the ^{3}He spins by the (^{11}B/^{3}He) spin ratio of ~400−2000 (§7.2.2/X=0.75 and table 7.2.2.1). Figure 7.3.1.2 shows experiment (2) data at D_1=100µS. The sharp fall around 25−30 volts appears in both plots and arises from unknown instrumentational effects. Three clear peaks are present at 7V, 12V and 22V that do not appear in the control. With the known saddle coil 180º tipping voltage, the

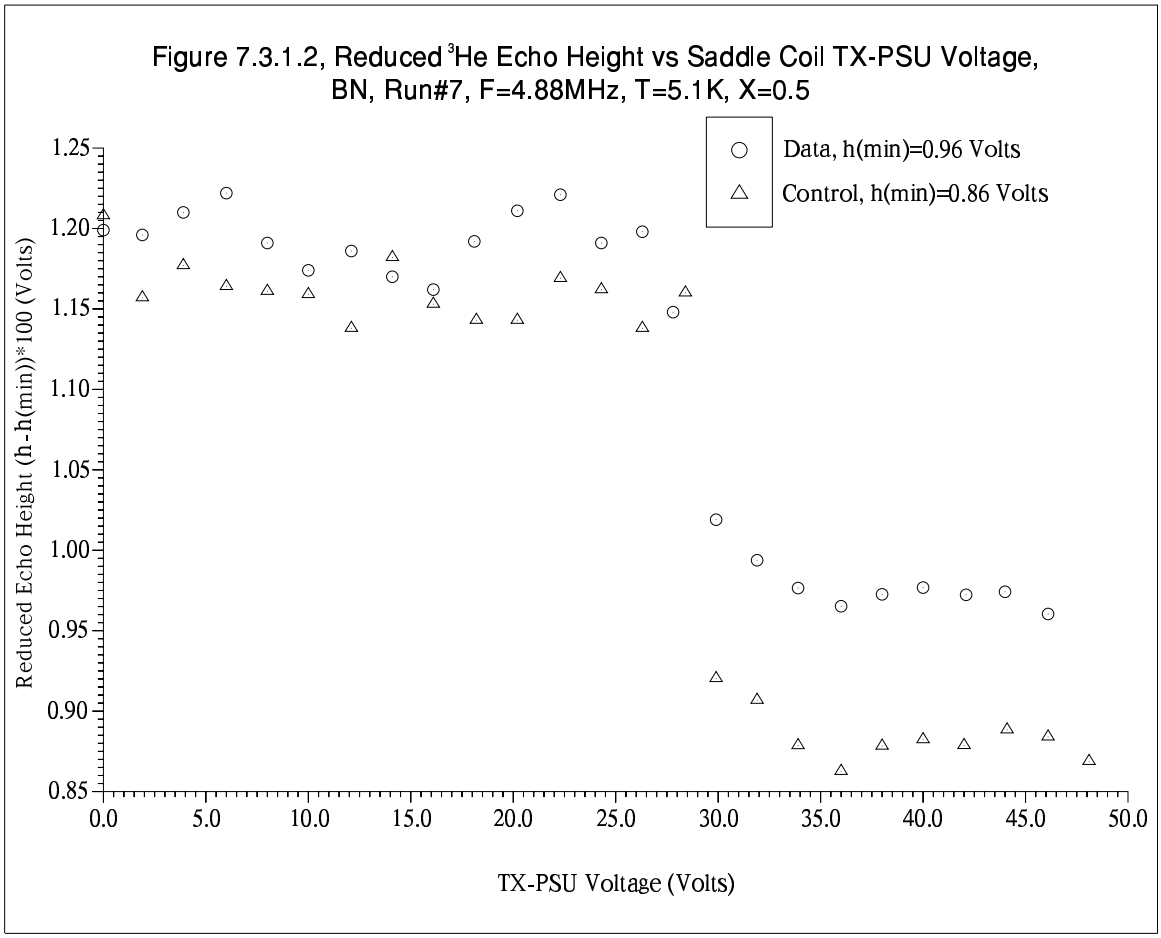

22V and smaller 12V peaks could well correspond to 180° and 90° ^{11}B magnetisation inversion and saturation respectively, influencing the ^{3}He magnetisation. However the predicted effect is to depress not enhance the magnetisation (§3.5.1). Bearing in mind the experimental pulse *repetition time* of only 10Sec and the ^{11}B $T_1 \sim 10$ minutes a spoiler factor may operate − As the experiment proceeds, starting from zero transmitter voltage and working upwards, an accumulating magnetisation of the substrate spins may conspire to mask the effects we seek. The 7V maximum may be related to this. The D_1=250mS data with no discernible features potentially supports the D_1=100μS data indicating spin-flipping and suggests the cross-relaxation time (T_1^{is} of figure 3.5.3.1) is $\ll$ 250mS. Figure 7.2.2.18 shows ^{3}He $T_1^{min} \sim$ 100mS. At X=0.1, $T_1^{min} \sim$ 40mS (figure 7.2.2.2). Moreover with a 0.05 monolayer edge-film responsible for the relaxation an effective T_1^{min} (edge-film) ~ 20mS is likely. There is an apparent contradiction between the short T_1^{is} just inferred and the DLX6000 case where the ^{3}He magnetisation stayed depressed for several × T_1 of the fluorine (§3.5.1). It must be pointed out however, the curious situation we are in here at this coverage region and temperature: A ^{11}B saddle coil 180° pulse will invert the ^{11}B magnetisation throughout the body of the BN crystallites. There is a long intrinsic ^{11}B T_1 [T_1(S.0), in table 7.2.2.1] and no possibility of significant relaxation out of the exposed basal-planes via the majority $\tau_c \sim 10^{-12}$ Sec basal-plane 2D gas ^{3}He spins. Therefore the ^{11}B magnetisation can only flow along the basal-planes by spin diffusion until it reaches the edges where the dense ^{3}He edge-film is able to relax it. The distance it has to travel is considerable (~5μm) with resultant lengthy spin diffusion time (see end of §7.2.2/X=0.75). It is tempting therefore to conclude that, (a) only those ^{11}B spins near crystallite edges are important in flipping ^{3}He spins and also, (b) with a large spin diffusion time the ^{3}He magnetisation is only significantly depressed for a time of the order of T_1^{is}. This sharply contrasts with the DLX6000 case and also BN at X=0.75/1K where the ^{11}B magnetisation only has a very short journey ~ 0.1μm through the crystallite's basal-planes to the exposed basal-planes where registered ^{3}He spins do the relaxing.

In conclusion, interesting evidence for cross magnetisation transfer has been presented but its existence is still far from proven. Observation of ^{3}He magnetisation enhancement rather than depression shows the picture is far from clear.

7.3.2 Boron-11 Temperature Dependence Data

T_1 and T_2 of ^{11}B in BN were measured as a function of temperature for 1.1K$\leqslant T \leqslant$13.2K at X=0.5. The central +½↔−½ transition (see figure 2.1.2) and a Larmor

frequency of 4.88MHz were used. The main object was to see if the ^{11}B T_1 went through a minimum at 5.1K which would have shown the ^{3}He T_1 minimum (figure 7.2.2.18) was due, at least in part, to heteronuclear relaxation. Computer noise was a serious problem, particularly at the higher temperatures where signals were small. For temperatures < 4.2K, before the pulse-generator system was modified to support operation under interrupt, during long D_1 delays (up to 35 minutes) for measuring T_1 ($90^o-D_1-90^o-D_2-180^o-echo$ sequence), the loss of POTREG temperature regulation allowed the temperature to drift by amounts ≥ the size of the temperature steps used (350mK). Drift tended to be worst at temperatures close to 4.2K where the solenoid valves need to switch more frequently to maintain the required temperature. ^{11}B spin-lattice relaxation is strongly sub-exponential and the long-delay temperature drift spoilt the best signals in each set of (*t*,*h*) data. A mitigating factor is that a point for which the temperature drifted low tended to be followed by a high-drifted (and vice-versa) one as POTREG compensated after the point was taken. For temperatures > 4.2K with pulse generation operating under interrupt the main problem was correlated computer noise which systematically polluted the signal. Signal averaging was only partially successful in getting rid of it (§4.1.2.2). In any case time constraints restricted the number of averages to 4 or 8 (T>10K). The complete set of ^{11}B temperature dependence measurements took three weeks to make. T_2 was measured using a $90^o-D_1-180^o-echo$ sequence with 150μS≤D_1≤1mS over 30 steps. A *repetition time* of 2 minutes was used. Although much less than T_1 recovery of the longitudinal magnetisation is enhanced at short times by its strong sub-exponentiality. T_1 was measured using delays; 1Sec≤D_1≤35minutes over 30 logarithmically spaced steps, D_2=150μS and a token *repetition time* of 1Sec were used. The systematic nature of some of the errors imposed on the data and the variably non-exponential relaxation make it fairly meaningless to use error values for the relaxation times obtained from NLLSQ fits to the (*t*,*h*) data. Accordingly no error-bars have been plotted on the graphs. Judging by the appearance of the T_1 echo height *vs* D_1 delay plots T-drift errors appear less serious than might have been expected, probably as a result of temperature-averaging inside the sample chamber due to its thermal equilibrium time and heat capacity. Above ~8K almost all signals had disappeared into the computer noise. At mid-range temperatures, the region of most interest, the data is borderline in validity. Figure 7.3.2.1 shows some signal recoveries from 'T_1' measurements. Three different NLLSQ fits for the 1.1K data and the single exponential 'T_1' fit for the 5.466K data are also shown. Figure 7.3.2.2 plots the normalised signal recovery *vs* D_1 delay time, that is the fitted echo height at t=∞ minus

its height at time *t*, for 1.1K. The single exponential fit is also shown, indicating the recovery's sub-exponentiality. Fit parameters from the NLLSQ program for fits shown in figures 7.3.2.1 and 7.3.2.2 are presented below;

1.1K Data;

'T_1' Fit
Sum of Squares: 0.90905
H(0) = −3.6808 +/− 0.11516
T1 = 659.15 +/− 49.812
H(inf) = 4.2302 +/− 0.11851

'T1Index' Fit
Sum of Squares: 0.36779
H(0) = −7.8202 +/− 2.4572
Index = 0.56529 +/− 0.52404E−01
T1 = 105.72 +/− 14.825
H(inf) = 8.1302 +/− 2.4212

'TWOEXP' Fit
Sum of Squares: 0.32813
Ha(0) = −0.73775 +/− 0.98729E−01
Hb(0) = −3.9257 +/− 0.21388
Ta = 57.913 +/− 14.283
Tb = 1293.8 +/− 197.51
H(inf) = 5.0623 +/− 0.27754
T(ave) = 295.66 +/− 173.73
T(1/e) = 1071.0

5.466K Data;

'T_1' Fit
H(0) = −0.72215 +/− 0.48145E−01
T1 = 697.83 +/− 109.92
H(inf) = 0.98580 +/− 0.49648E−01

Figure 7.3.2.3 shows T_1 against $1/T$. It is temperature independent up to $0.4K^{-1}$. Here the data quality is not too bad. By contrast, over the same temperature interval, figure 7.2.2.18 shows the ^{3}He T_1 rises through a plateau for F=4.5MHz as registered spins disorder. We conclude therefore, that the small number of registered ^{3}He spins do not play a significant role here, ^{11}B relaxation being dominated by the ^{3}He edge-film which is solid, changing little over these temperatures. Remembering the rapid fall-off in substrate mediated relaxation of registered spins with frequency, away from 4.5MHz (figure 7.2.4.2) the 4.88MHz Larmor frequency used here may account for this lack of registered spins' influence. As temperature rises the ^{11}B T_1 goes through a maximum at $0.35K^{-1}$ and a minimum at $0.24K^{-1}$. There is little evidence for corresponding features in the ^{3}He data. Around 5.1K ($0.19K^{-1}$) ^{11}B T_1 has a maximum not the predicted minimum. Data credibility here remains an open question.

Figure 7.3.2.4 shows T_2 against $1/T$. T_2 falls in an ill-defined way to ~$0.4K^{-1}$. Above $0.4K^{-1}$ it rises to a maximum at $0.23K^{-1}$ the rise being interrupted by a small minimum at $0.28K^{-1}$. A large minimum at $0.18K^{-1}$ follows the $0.23K^{-1}$ maximum. The values of T_2 at low temperatures are roughly consistent with a classical rigid lattice. The only motion present is due to phonons whose population is very small at these temperatures and is insufficient for motional narrowing (§3.5.3); therefore $\sqrt{m_2} \gg 1/\tau_c$ and $1/T_2 = \sqrt{m_2}$. Referring to equation 8.26 which has the same general form as equation 2.2.17 it is reasonable to suppose motion in the ^{3}He edge-film is able to motionally

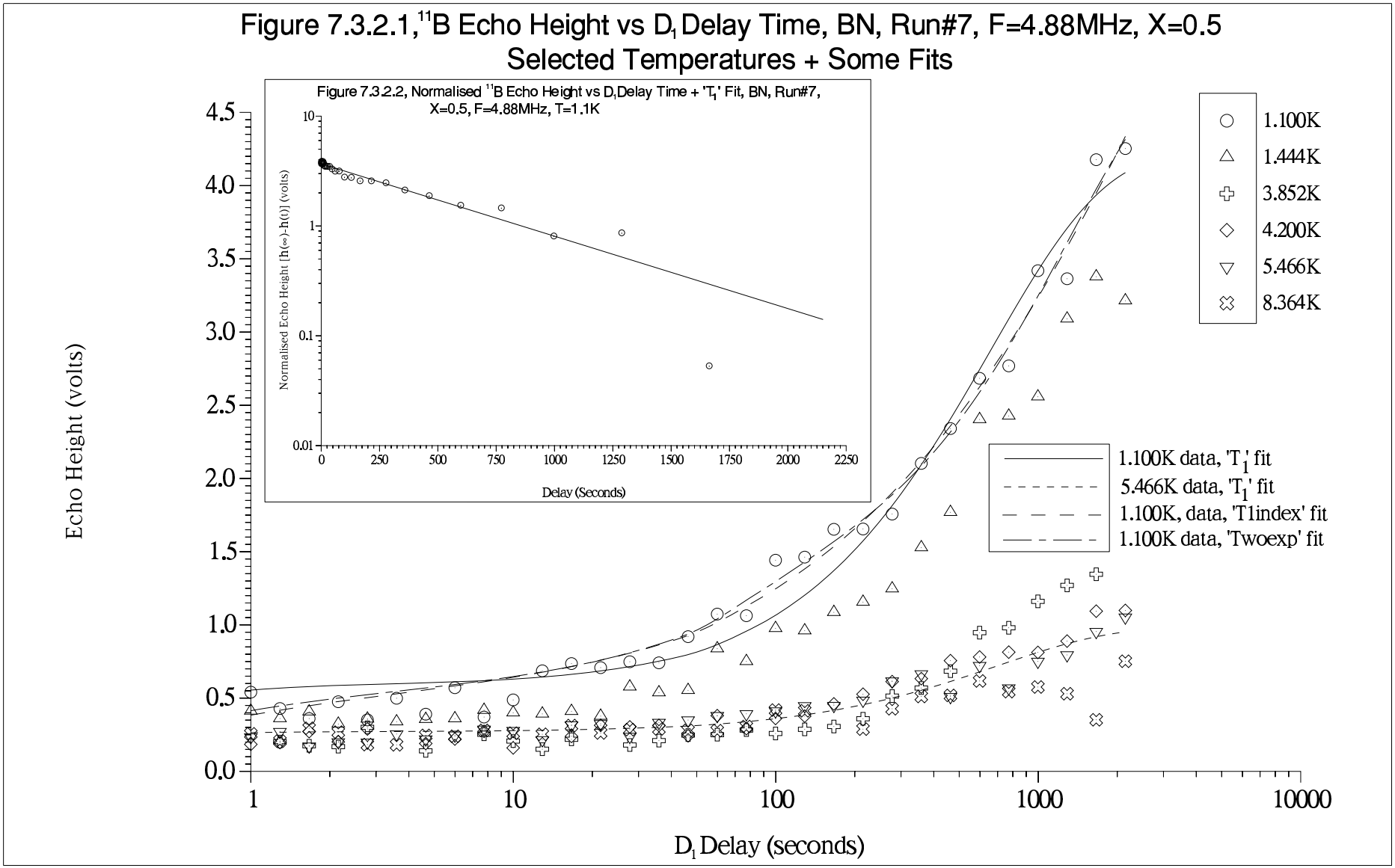
Figure 7.3.2.1, ^{11}B Echo Height vs D_1 Delay Time, BN, Run#7, F=4.88MHz, X=0.5
Selected Temperatures + Some Fits
Figure 7.3.2.2, Normalised ^{11}B Echo Height vs D_1 Delay Time + 'T_1' Fit, BN, Run#7, X=0.5, F=4.88MHz, T=1.1K
Normalised Echo Height [h(∞)-h(0)] (volts)
Delay (Seconds)
Echo Height (volts)
D_1 Delay (seconds)
1.100K
1.444K
3.852K
4.200K
5.466K
8.364K
1.100K data, 'T_1' fit
5.466K data, 'T_1' fit
1.100K, data, 'T1index' fit
1.100K data, 'Twoexp' fit

Figure 7.3.2.3, ^{11}B T_1 vs 1/T, BN, Run#7, F=4.88MHz, X=0.5

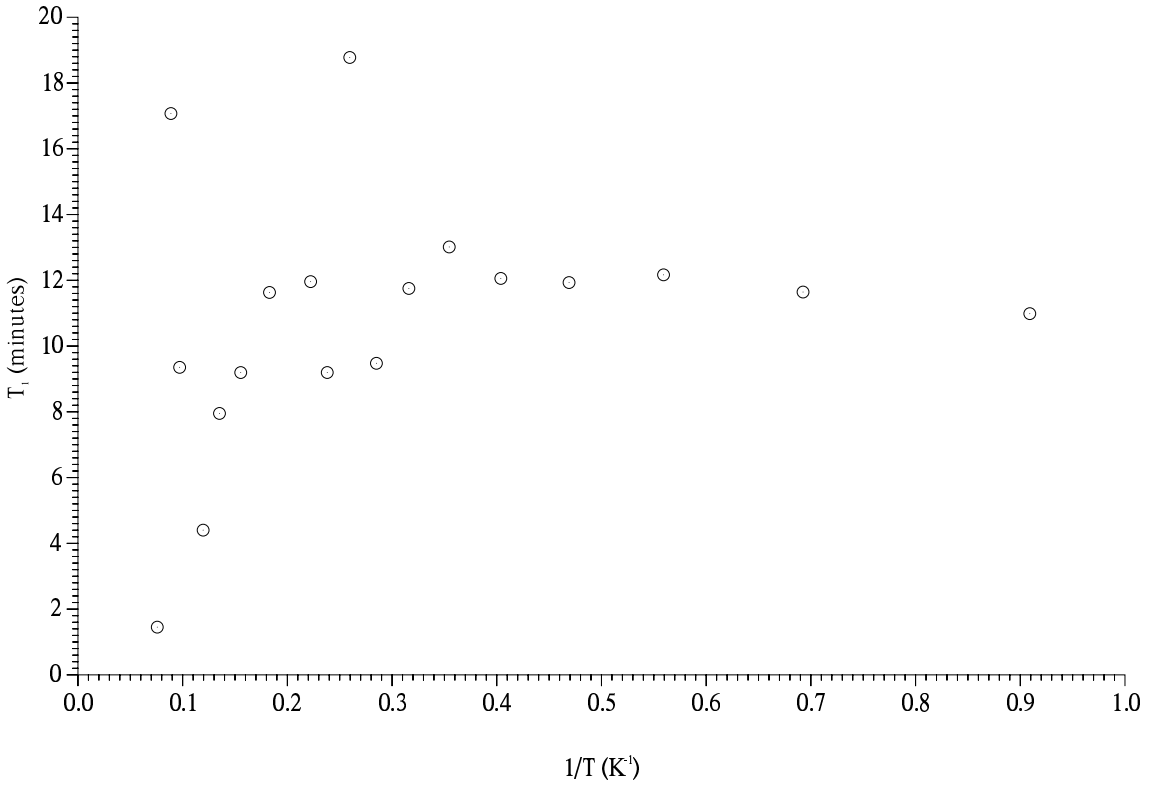

Figure 7.3.2.4, ^{11}B T_2 vs 1/T, BN, Run#7, F=4.88MHz, X=0.5

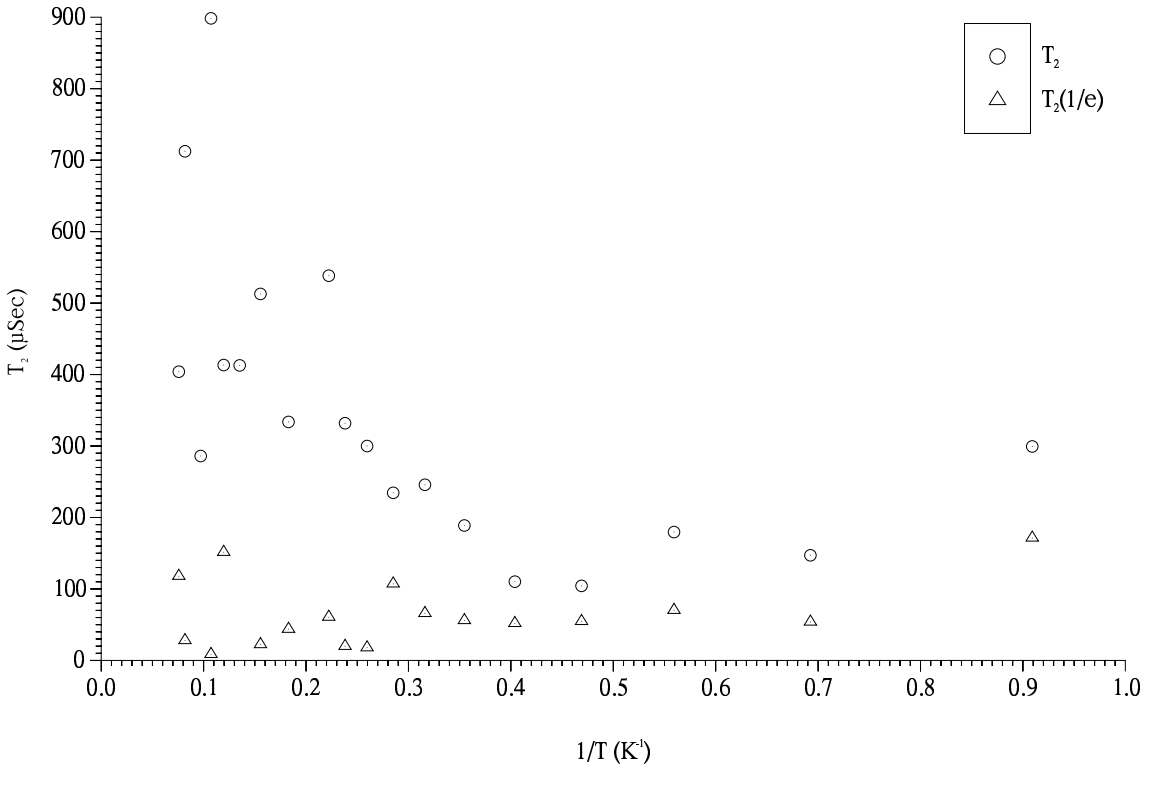

narrow ^{11}B spins to which they are adsorbed. Since only ^{11}B spins close to the crystallite edges are experimentally visible (see next paragraph) any motional narrowing present might well be detectable. The increase in T_2 for T>0.4K^{-1} could be a sign of this. It is unclear whether the features seen above 0.4K^{-1} are real effects. Most interesting is the largest minimum at 0.18K^{-1} which corresponds approximately to the ^{3}He T_1 *vs* 1/T minimum temperature. Equation 8.26, however, like equation 2.2.17 for the homonuclear case cannot produce a minimum in motional speed, ie. in temperature. As with the ^{11}B T_1 maximum this feature is at the margins of data credibility.

Figure 7.3.2.5 plots the equilibrium ^{11}B magnetisation '$h(\infty)$' obtained from the 'T1Index' fits against 1/T. Apart from the 1.1K point Curie's law is obviously obeyed. The 1.1K point which is ~1.7× larger than the extrapolated value was the first point taken in the temperature dependence data set (some time after tuning up etc.). It accords with the ideas advanced in §7.3.1; After the initial measurements the ^{11}B longitudinal magnetisation of spins far away from BN crystallite edge-sites is destroyed and is very slow to recover. ^{11}B spins close enough to the edge-sites recover their thermal equilibrium magnetisation via edge-film ^{3}He spin mediation. So only these spins are visible in subsequent measurements. Assuming this model, it is of interest to estimate

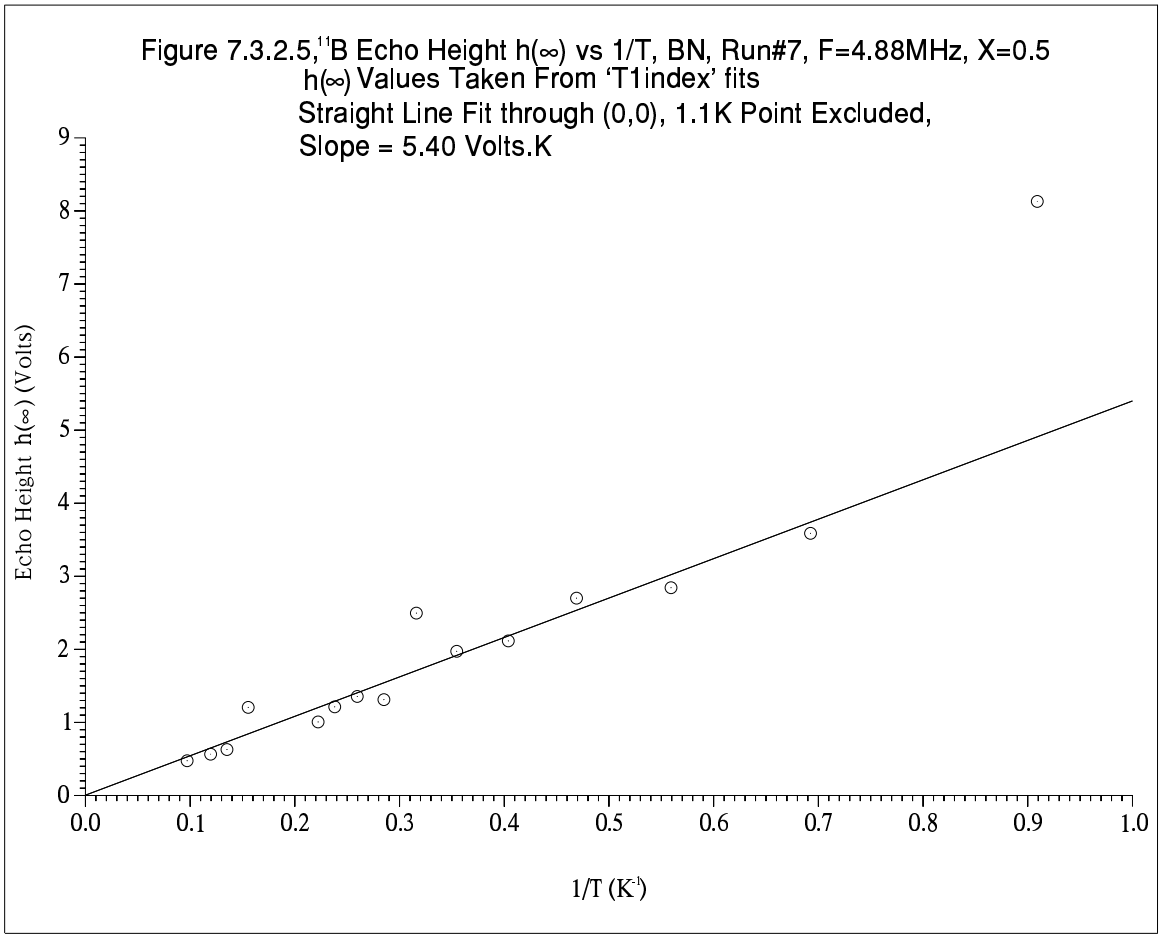

the fraction of ^{11}B spins contributing to the signal to see how far into the crystallites from the edge-sites, ^{3}He edge-film FMR mediated relaxation is effective. This has been done by comparing ^{11}B and ^{3}He static magnetic susceptibilities, obtained from the signal heights. Figure 7.3.2.6 shows a schematic model flat-square-slab BN crystallite with basal-plane dimension *x* and thickness *y*.

Figure 7.3.2.6, A Schematic Model BN Crystallite Showing ^{3}He Edge-Film Mediated Substrate Spin Relaxation.

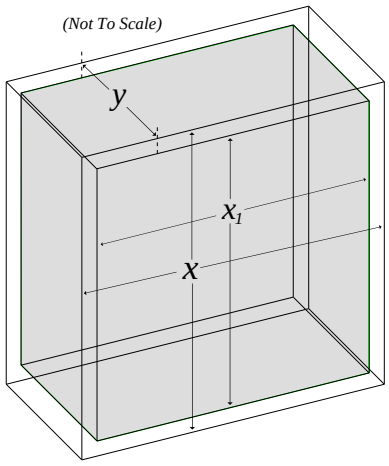

The greyed volume indicates interior spins too far from the edge-sites to be relaxed by the ^{3}He edge-film. The ^{3}He FMR relaxation penetration depth is $(x - x_1)$ and,

$$\frac{x^2y - x_1^2y}{x^2y} = \frac{N_{He}}{N_B} \times \frac{M_B}{M_{He}} \times F = C \qquad 7.3.2.1$$

can be written. $(N_{He}/N_B) \approx 1/300$ is the ^{3}He:^{11}B spin ratio at X=1.0 (see end of §7.2.2/ X=0.75). $(M_B/M_{He}) = 4.91/22$, is the ratio of the ^{11}B equilibrium magnetisation ($h(\infty)$, figure 7.3.2.5) extrapolated to 1.1K -to- the '$h(0)$' magnetisation value obtained by fitting $h(t) = h(0)\exp(-2t/T_2)$ to *90°−180°−echo* 'T_2' data for ^{3}He at X=1.0 and T=1.1K. 'F' is a collection of terms scaling the measured signal heights (M_B/M_{He}) to their magnetic susceptibilities,

$$F = \frac{1}{0.2} \times 0.471 \times \frac{600}{300} \times \frac{1}{\exp(-2\times150/172)} \qquad 7.3.2.2$$

The first terms account for the fact that in a pulse NMR experiment the signal from the central +½↔−½ transition in an $\boldsymbol{I}$=3/2 nucleus with quadrupole splittings is only 20% of the unsplit intensity **[85]**. The second term is for the ratio of the susceptibilities at constant frequency, each being $\propto I(I+1)$. The third term scales the signal heights by the ratio of the line widths as measured by the two T_2 values, the susceptibilities being proportional to the area under the NMR lines. Similar linewidth values are obtained directly from figure 7.4.2.1. The last term is needed because the ^{11}B $h(\infty)$ (from 'T_1' data) value was taken with a D_2 delay setting = 150µS. We require the t=0 signal height. Assuming exponential spin-spin relaxation for this order-of-magnitude calculation, the t=0 signal is given by dividing by $\exp(-2t/T_2)$. We obtain $C = 0.020$. $x - x_1 = x - x(1-C)^{-½}$. Taking x = 4.67µm (see end of §7.2.2/X=0.75) gives $x - x_1 = 0.047$µm. For comparison the model's BN crystallite thickness y = 0.123µm. This is quite small and corresponds to an ^{11}B spin diffusion time of only ~3.1Sec. A surprising result when the ^{11}B spins have had at least 35minutes to recover. The most likely source of significant systematic error is inadequacy of the estimate for the ^{11}B $h(0)$: Spectrometer ringdown prevents the magnetisation at short times being measured. Unfortunately, this is where most of the relaxation takes place due to strong spin-spin relaxation sub-exponentiality and the high spin-spin relaxation rate. Even double exponential fitting (which was in fact used for the $T_2(1/e)$=172µS, 'T_2' value in the last term of equation 7.3.2.2) tends to underestimate $h(0)$. Although the 'T2Index' model's behaviour is unphysical at t=0 its fit does reveal the extent of the sub-exponentiality − *index* < 0.1 was obtained.

7.4 RUN#8

7.4.1 Introduction

The purpose of this run was to study FMR relaxation as a function of ^{3}He coverage. T=1.1K was used throughout. Substrate relaxation time *vs* coverage measurements are the most sensitive technique for detecting FMR relaxation in a system (§3.5.2). Substrates such as Nucleopore **[160]** and Aldrich Powder **[147]** which showed no directly measurable DLX6000-type cross-flipping did have a substrate T_1 with coverage variation − unambiguously demonstrating the effect.

7.4.2 Field Sweep RF Absorption Spectrum

At most coverages an RF absorption spectrum was taken. This was done at constant frequency by sweeping the field. A CW method is obviously more appropriate for this type of measurement than a pulse one since saturation should not be a problem. Unfortunately we were unable to even find a signal using a CW spectrometer so the pulse system had to be used.

The method was to sweep the field using the Magnet Controller (for which it is ideal, see §4.2.6.5) while pulsing the sample with the standalone µP pulse generator and logging echo signals by computer using the ARCFIELD program. ARCFIELD is a cut-down version of ARCONTROL6. It continuously logs echo signals together with a Prema DMM voltage reading in a loop, the Prema monitoring the magnet PSU's current-sense voltage. A *90*^{o}*−180*^{o}*−echo* sequence was used. See figure 4.1.2.1 for spectrometer etc. layout. In this way a crude RF absorption *vs* magnetic field trace was built up. The three parts of the system all ran mutually asynchronously which is useful as it lessens the effects of saturation when several sweeps are done and the results averaged. Averaging was done by dividing the sweep range into ~150 equal sized *buckets*. The contents of each bucket being the average height of the echoes falling within its field range. Up and down sweeps were averaged separately because of the inherent field→echo-logging delay in the experiment. Field sweeps were done between 0 and 4250 gauss at 14 gauss/sec in both directions. The range encompasses the ^{3}He and ^{11}B resonances with both ^{11}B satellite lines. The sweep rate is a compromise between a slower sweep causing excessive helium boil-off (due to heating in the cryostat magnet supply leads) and a faster one missing resonance features. Spectrometer settings were; P_1=50µS, P_2=100µS, D_1=150µS, *repetition-time*=1Sec and B_1='^{11}B on-tune setting'. Extra partial sweeps around the ^{11}B resonances were performed, this being the main area of interest.

Figure 7.4.2.1 shows the averaged field sweeps taken at X=1.0. There are no discernible trends with coverage and this plot is typical. Key features are the ^{3}He resonance at 1504 gauss and the ^{11}B resonance with its two satellite lines at higher fields. The correspondence with figure 2.1.2 is obvious. The ragged appearance of the ^{11}B peaks is due to *hole-burning* **[69]**, a consequence of RF saturation on the inhomogeneously quadrupolar broadened lines. Incidentally, to capture the narrower ^{3}He line the field-sweep was deliberately waylaid around the ^{3}He resonant field in this data set.

The field sweep plot was used to find the quadrupolar frequency F_Q of ^{11}B in our BN sample. Referring to figure 2.1.2 and noting that the field sweeps were done at constant frequency, gives, $F_Q = 2\gamma_B |B_0^{central} - B_0^{satellite}|$, where $B_0^{central}$ and $B_0^{satellite}$ are the applied fields at the central $+1/2 \leftrightarrow -1/2$ transition and either of the two $\pm 3/2 \leftrightarrow \pm 1/2$ satellites respectively. Accurately locating the centre of the broad ragged peaks is the main difficulty. Two different criteria have been tried: (1) An average of, the down-sweep, low-field sub-peaks of the central $+1/2 \leftrightarrow -1/2$ -to- lower field $+3/2 \leftrightarrow +1/2$ satellite line separation and the up-sweep, high-field sub-peaks of the central $+1/2 \leftrightarrow -1/2$ -to- higher field $-3/2 \leftrightarrow -1/2$ satellite line separation. The advantage is, since only the central-to-satellite separation is wanted, that the sub-peaks are simple to locate. (2) After estimating the centre-of-mass of the ragged peaks an average of the separations was made. On the up-sweep both satellite lines were used with the lower satellite only in the down-sweep case.

Criterion (1) yields F_Q = 1.23MHz. Criterion (2) gives F_Q = 1.47MHz and is the preferred method.

For comparison, the four measurements of F_Q for ^{11}B in hexagonal BN found in the literature are presented: Silver and Bray **[83]** calculated $F_Q = 1.48 \pm 0.05$MHz from second order quadrupolar broadening of the $+1/2 \leftrightarrow -1/2$ central line **[212]** at room temperature in 1960 at 7.2MHz. A similar technique at 10MHz employed by Khusidman and Neshpor **[86]** in 1970 gave F_Q = 1.22MHz. A direct measurement using NQR with DC SQUID detection at 4.2K by Connor, Chang and Pines **[213]** in 1990 obtained $F_Q = 1.467 \pm 0.002$MHz. Most recently, magic angle spinning Fourier Transform Pulse NMR measurements at 192MHz by Marchetti, Kwon, Schmidt, Interrante and Maciel **[84]** in 1991 gave F_Q = 1.45MHz. MAS NMR was used because it increases resolution by narrowing the second-order quadrupolar broadened lines. Their value for F_Q comes from fitting to a computer simulation of the spun central $+1/2 \leftrightarrow -1/2$ line. With the exception of K & N our criterion (2) F_Q = 1.47MHz best agrees with the other values and will be used in the rest of this document.

Figure 7.4.2.1, Averaged Echo Height vs Applied Field in Field Sweep Expt.,
BN, Run#8, F=4.88MHz, T=1.1K, X=1.0

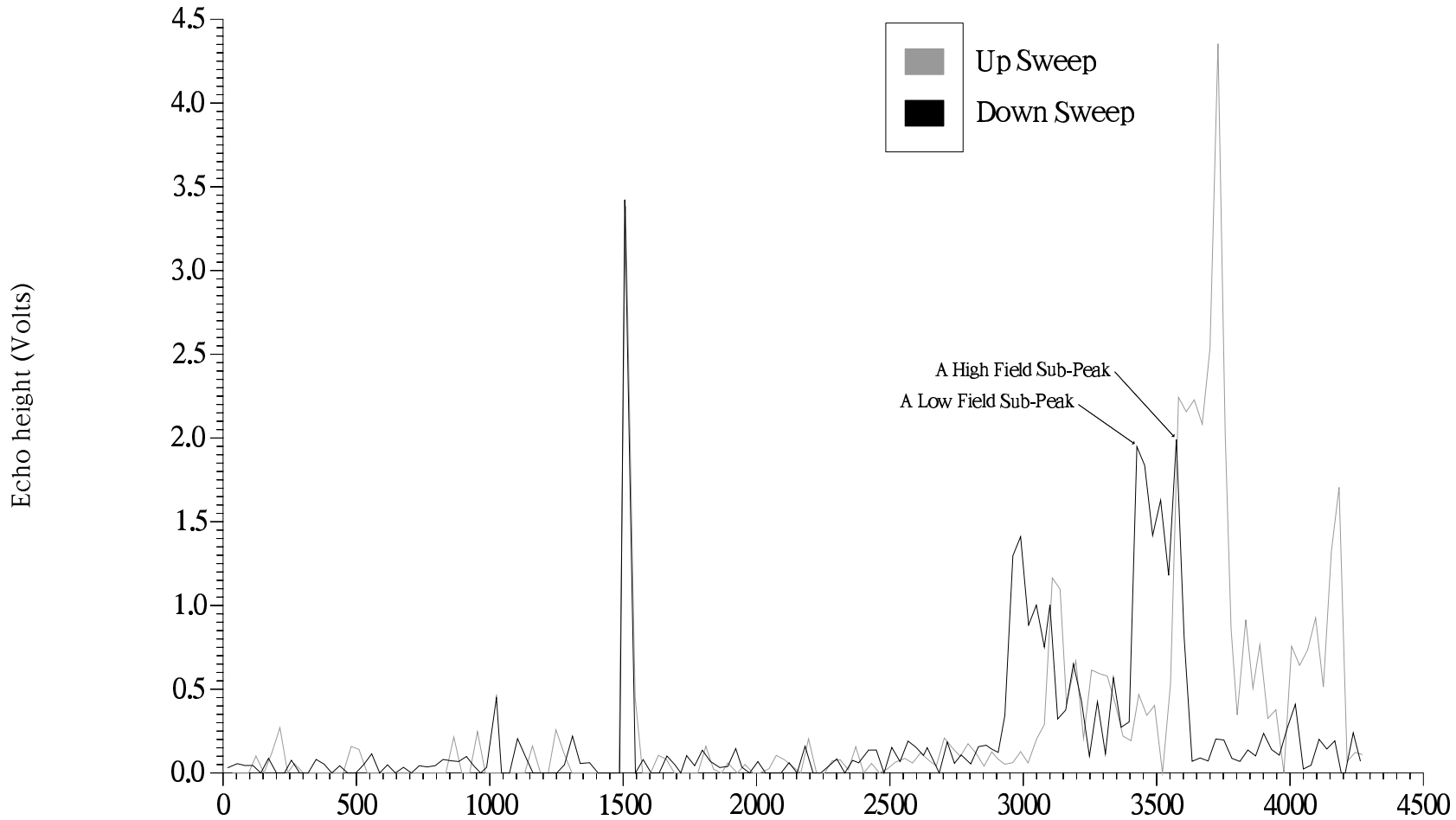

7.4.3 Coverage Dependence Data

T_1 and T_2 of ^{3}He and ^{11}B were measured as a function of coverage at 1.1K as summarised at the beginning of the chapter. Having annealed the sample to 20K after raising coverage it was pumped down to 1.1K in the minimum time, typically half an hour. Some useful comparisons with the 1K ^{3}He coverage dependence data of Run#6 (§7.2.1) are made. FMR relaxation of ^{11}B is considered in the light of the ^{3}He data.

7.4.3.1 ^{3}He Coverage Dependence Data

All the features of T_2 against X observed in Run#6 (figure 7.2.1.1) are present here. See figure 7.4.3.1. Namely, the rise to X=0.3, fall to X=0.7, maximum at X=0.75, minimum at X=1.0 and maximum at X>1.0. Quantitatively, the data differs from Run#6 over coverages $0.2 \leqslant X \leqslant 0.85$. Here Run#8 $T_2 \ll$ Run#6 T_2. The Run#6 T_2 at X=0.3 is 3× longer. At X=0.75 it is 2× longer. This is thought to be due to insufficient annealing. Run#6 ~1K data is from temperature dependence data-sets in which the relaxation times were measured from 4.2K to 1.1K over a period of ~13 hours. At certain coverages in Run#8, including X=0.3, the ^{3}He relaxation times were measured after the ^{11}B ones. The point being the ^{11}B measurements also happened to take ~13 hours. Clearly but unsurprisingly, it is the rate at which the sample is pumped down to 1K rather than the length of *settling* time at 1K that is crucial in achieving good film homogeneity. That T_2 only differs for $0.2 \leqslant X \leqslant 0.85$ implies additional Run#8-poor-anneal heterogeneity only affects those coverages where there is a significant non-edge-film component (ie. X>0.1) but before its presence is masked by a short enough T_2 in the incommensurate solid proper (ie. $X \geqslant 0.9$).

'T2Index' (figure 7.4.3.2) against coverage is broadly similar to Run#6 (figure 7.2.1.6) but the X=0.75 maximum is now only a small shoulder on the rise with coverage. More diverse relaxation at the perfect registry coverage again indicates a reduction in film homogeneity.

Like T_2, T_1 (figure 7.4.3.3) shows the same coverage features as in Run#6 (figure 7.2.1.2). The, rise to X=0.3, fall to deep minimum at X=0.75, rise to broad maximum at X<1.0 and the minimum at X>1.0 are all present. The T_1 data also differ quantitatively from Run#6, being longer than in Run#6 at all X, mostly only marginally so. The exception is around X=0.75, where T_1(Run#6) = 44.9mS but T_1(Run#8) = 110mS. Less efficient relaxation at $X \leqslant 0.3$ indicates that spins *displaced* by insufficient annealing have not joined the 0.05 monolayer edge-film where they would

Figure 7.4.3.1, ^{3}He T_2 against Coverage, BN, Run#8, F=4.88MHz, T=1.1K

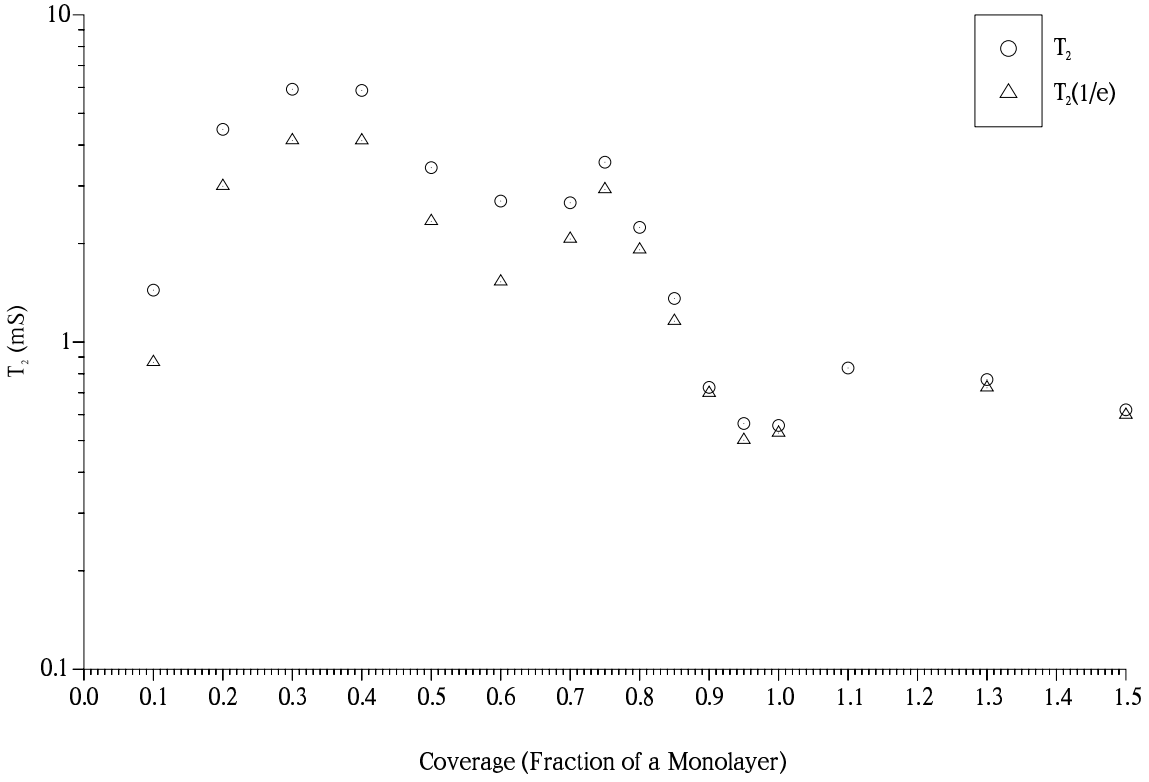

Figure 7.4.3.2, ^{3}He, 'Index' from 'T2Index' Fit vs Coverage, BN, Run#8, F=4.88MHz, T=1.1K

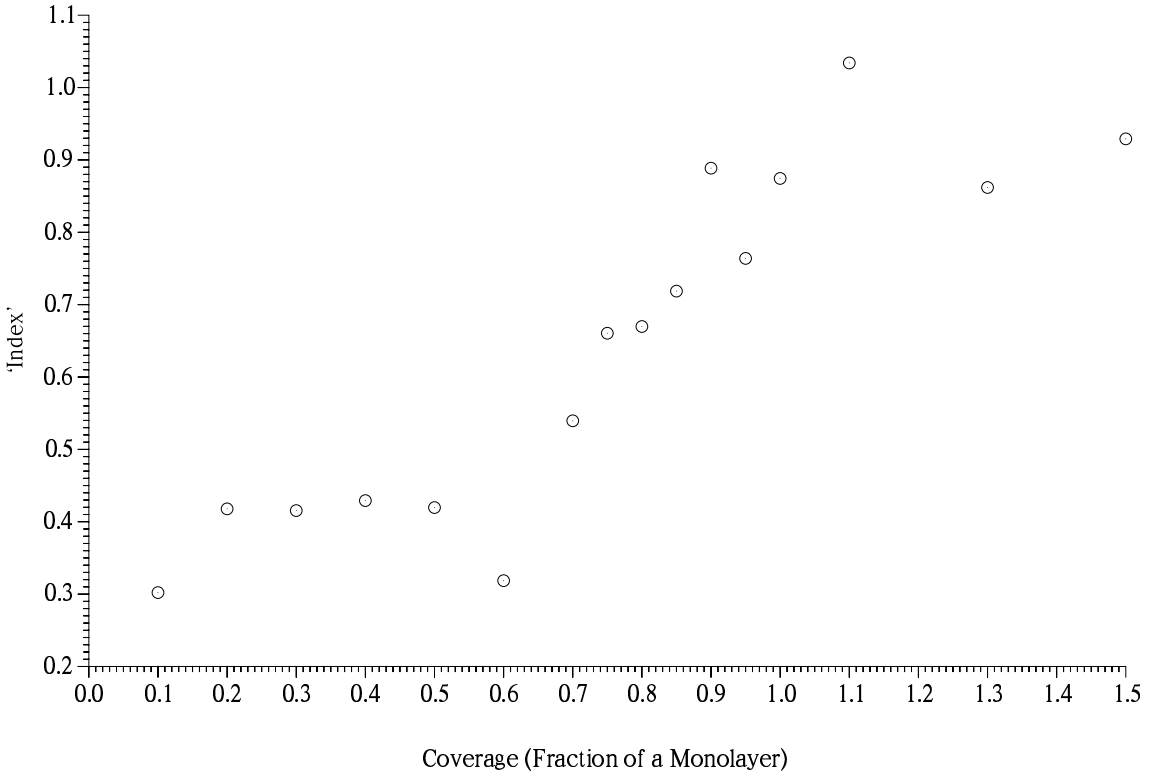

Figure 7.4.3.3, ^{3}He T_1 against Coverage, BN, Run#8, F=4.88MHz, T=1.1K

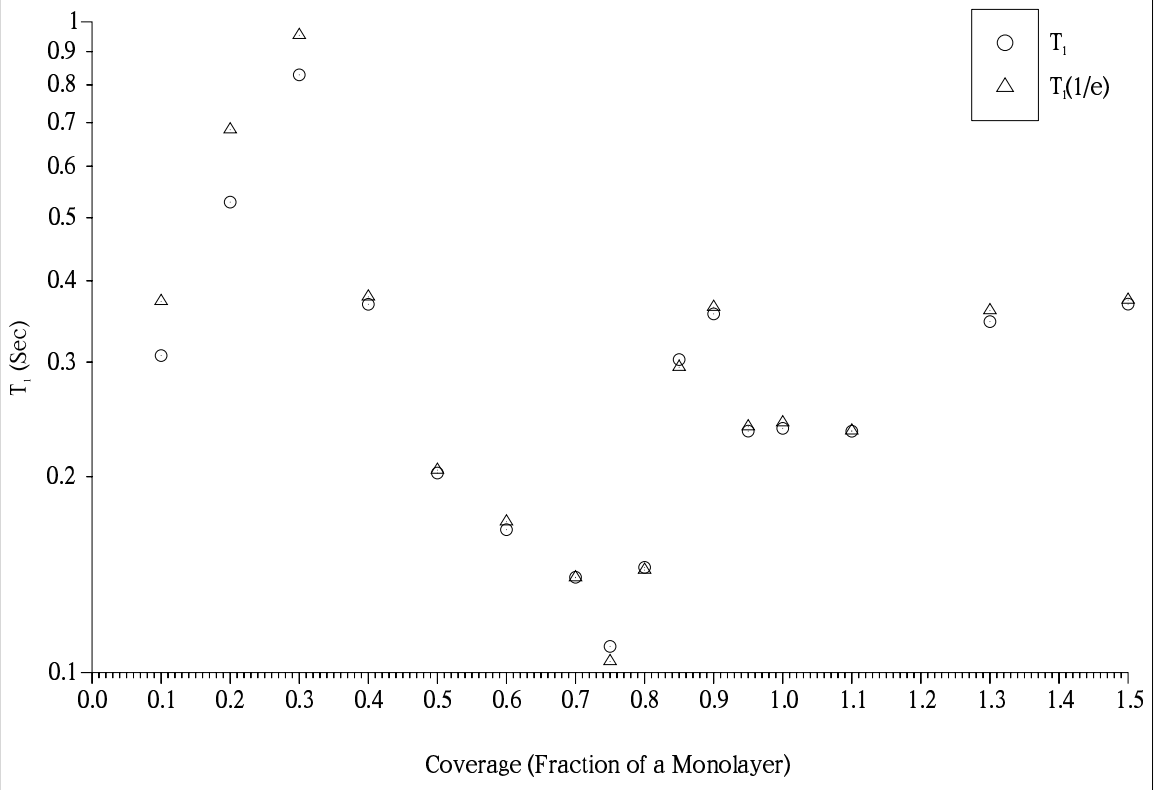

Figure 7.4.3.4, ^{3}He, 'Index' from 'T1Index' Fit vs Coverage, BN, Run#8, F=4.88MHz, T=1.1K

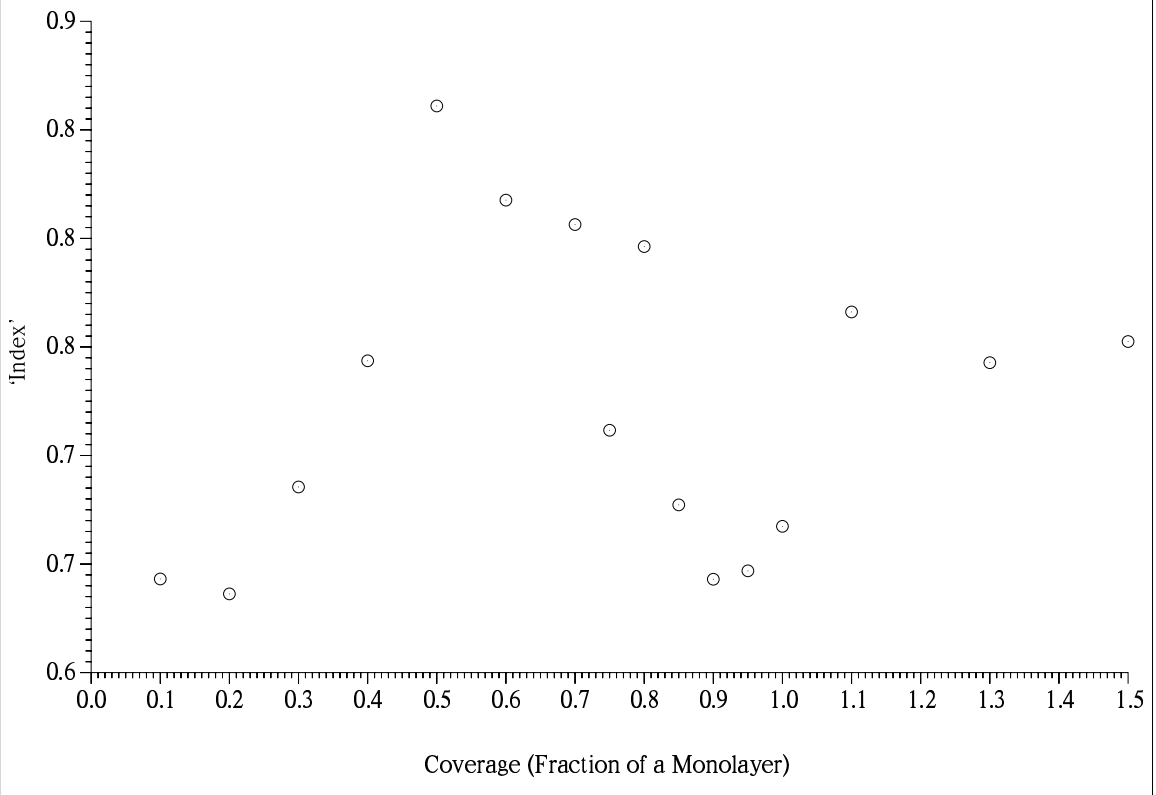

have provided enhanced relaxation for the basal-plane 2D gas. Instead it is thought they exist as heterogeneous patches elsewhere, probably on the basal-planes. X=0.75 data suggests inadequate annealing has severely disrupted registering − possibly breaking up the film into small registered regions separated by the heterogeneous patches. The higher Larmor frequency used in this run may partially account for the reduced relaxation but not by a factor of >2× (see figure 7.2.4.2). At intermediate and higher coverages slower relaxation again points towards registering and incommensurate solid formation being disrupted by random disorder in these structures. In general randomly formed dense clumps of spins away from the edge-sites can be expected to contribute towards shorter T_2s and longer T_1s at low temperatures, especially where heteronuclear relaxation operates since it obviously depends on ^{11}B−^{3}He intimacy.

'T1Index' data (figure 7.4.3.4), excluding the region around X=0.75 (ie. $0.6 \leqslant X \leqslant 0.8$), is similar to Run#6 (figure 7.2.1.5). Slightly lower values reflect increased relaxation multiplicity accompanying greater disorder. Gone is the X=0.75 super-exponential peak, replaced by a minimum. Sensitivity of the 'T1Index' probe has revealed relaxation multiplicity due to disordered/displaced spins completely obscuring super-exponential heteronuclear relaxation.

7.4.3.2 ^{11}B Coverage Dependence Data

Figure 7.4.3.5 plots the ^{11}B T_2 against helium-3 coverage. The data is strongly sub-exponential and only the *tail* of the relaxation signal is visible. This accounts for the T_2 values considerably above those expected from a rigid lattice. The key points of the data can be summarised as follows;

- $0.0 \leqslant X \leqslant 0.3$ − Roughly coverage independent.
- $0.3 \leqslant X \leqslant 0.5$ − Falls sharply.
- $0.5 \leqslant X \leqslant 0.75$ − Falls more slowly.
- $X \geqslant 0.75$ − Rises slowly.

$0.0 \leqslant X \leqslant 0.3$: With a constant 0.05 monolayer solid edge-film and most of the rest of the spins going into the basal-plane 2D gas, no coverage dependence is expected. $0.3 \leqslant X \leqslant 0.5$: As registered spins start to appear on the basal-plane the ^{11}B T_2 falls. This implies ^{3}He spins provide an additional local field contribution (primarily to their ^{11}B nearest neighbours, ie. to the 3× ^{11}B spins making up the adsorbing basal-plane hexagon) in which ^{11}B spins relax. See figures 1.8.3.1 and 3.2.1. With most of the signal coming from crystallite surface spins it is not unexpected that the effect is visible. $0.5 \leqslant X \leqslant 0.75$: The same explanation applies here. Run#8 ^{3}He T_2 falls more slowly to X=0.7, in part

Figure 7.4.3.5, ^{11}B T_2 against Coverage, BN, Run#8, F=4.88MHz, T=1.1K

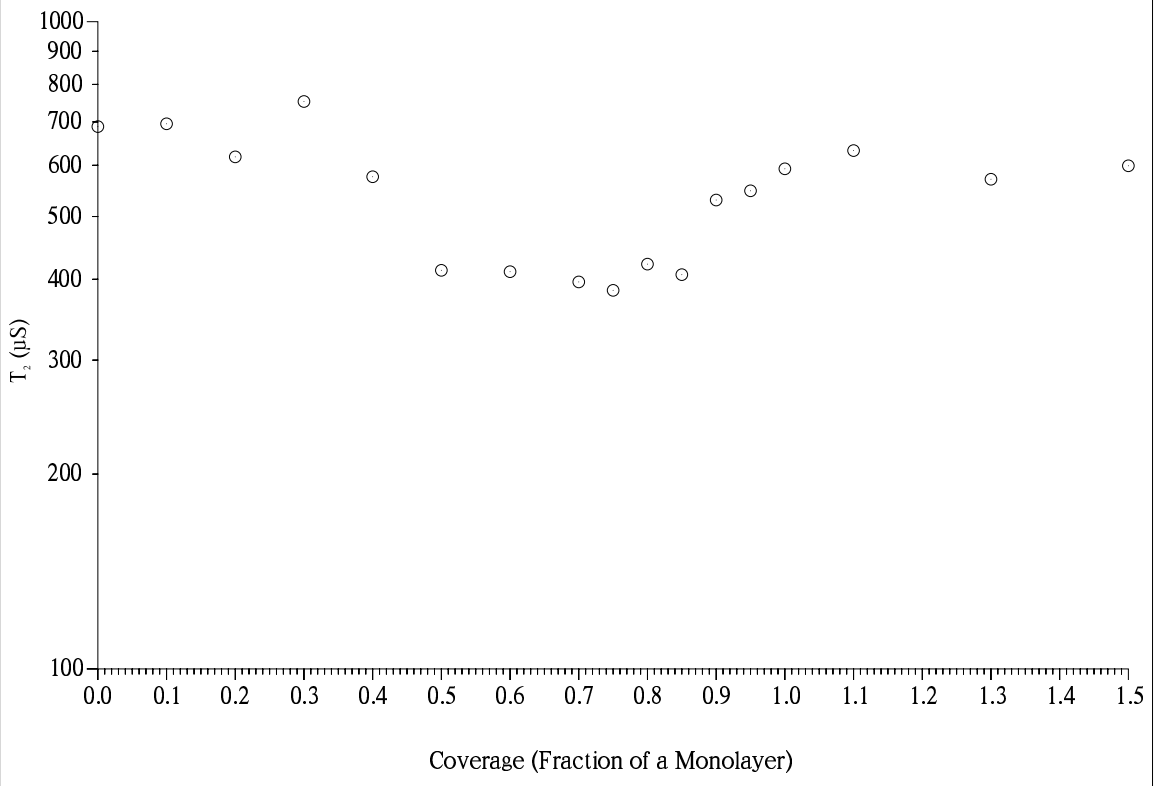

Figure 7.4.3.6, ^{11}B 'Index' from 'T2Index' Fit vs Coverage, BN, Run#8, F=4.88MHz, T=1.1K

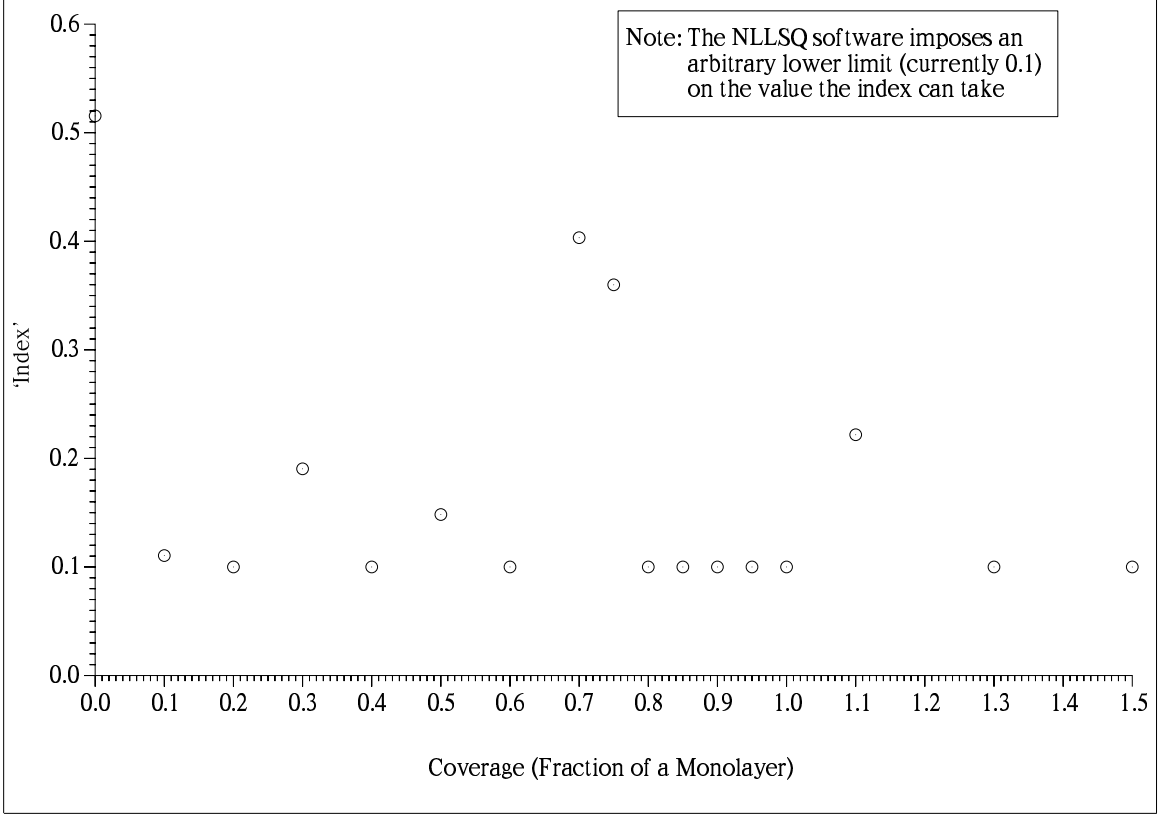

because of disruption to registering. Slow-down of the ^{11}B T_2 fall may also result from this. $X \geqslant 0.75$: At perfect registry ^3He exchange motion is partially suppressed by the localising effect of the substrate hexagon potential wells (§1.10.4). As coverage increases above $X=0.75$ the effect falls off and motional narrowing of ^{11}B spins increases, causing T_2 to rise. Initially ($0.75 \leqslant X \leqslant 0.85$) the rise is slow. This is where the DWL is thought to exist. Crudely speaking a DWL can be regarded as small patches of registered spins moving around together − So a DWL might be expected to affect substrate spins in a similar but reduced way to registry. Over $0.9 \leqslant X \leqslant 1.0$ the incommensurate solid has formed and T_2 rises to a plateau. The plateau is consistent with a fixed solid monolayer whose local field effect on ^{11}B spins is very limited − Compare T_2 values with $X \leqslant 0.3$ ones.

Figure 7.4.3.6 shows the ^{11}B 'T2Index' coverage dependence. Under a powder average the distribution of crystallite orientations is expected to give rise to a distribution of relaxation rates and therefore sub-exponential relaxation. Enhanced signal amplitude of the first measurement in a sequence together with the *shortest first→longest last* D_1 delay used when measuring T_2 probably also contributed to the sub-exponentiality. Within a crystallite, if there are ^{11}B spins in different (local) *environments* with different T_2s a further increase in sub-exponentiality can be expected. Bearing in mind the difficulty in obtaining this data and its consequent less than ideal quality the following explanation is presented: At $X=0.0$ all surface ^{11}B spins are in the same *environment* and *index*>0.5 is relatively big. Once $X=0.1$ the edge-sites are full. Exposed adsorbing edge-sites ^{11}B spins are now additionally relaxed by the ^3He edge-film and are therefore in a different *environment*. Accordingly the *index* falls off sharply. Small digression; Notice the size of the change in *index* for $X=0.0 \rightarrow 0.1$ compared with T_2, demonstrating again the sensitivity of the *index* as a probe. At $X=0.2$ the position is predictably very similar. As coverage increases from $X=0.3 \rightarrow 0.75$ registered spins increasingly appear on the exposed basal-planes, albeit erratically because of poor annealing. Consequently on the exposed basal-planes those ^{11}B spins experiencing ^3He local fields are now in a different *environment* from those that do not but in a more similar *environment* to their edge-sites counterparts. As a result *index* varies, culminating in a large peak near $X=0.75$ where all (in particular basal-plane) exposed ^{11}B spins are in a similarly ^3He-spin-intimate *environment*. Above registry, as discussed for T_2, the $^3He-^{11}B$ interaction on the basal-planes decreases leaving basal-plane and edge-sites ^{11}B spins in different *environments* again and moreover, exposed basal-plane ^{11}B spins will be in different *environments* from each other as the film becomes incommensurate, all leading to a sharp fall-off in

index.

Figure 7.4.3.7 plots the ^{11}B T_1 coverage dependence using three different measures. The dominant feature is the deep minimum near the registry coverage in the 'T_1' and 'T_1(1/e)' fit plots. It confirms all the previous suspicions based on the ^{3}He data that at registry the data is dominated by ^{3}He↔substrate cross relaxation.

Both sets of ^{3}He data (Run#6/figure 7.2.1.7 and Run#8/figure 7.4.3.3) have their 4.5−4.9MHz minima essentially at X=0.75, ie. perfect registry. So why should the ^{11}B minimum be different? Quadratic fits applied through the minima in figure 7.4.3.7 as in figure 7.2.1.7 gave ^{11}B minimum positions at X=0.686 ('T_1' fit data) and X=0.708 ('T_1(1/e)' fit data). If 2D effects were to lead to dominance of the $J_0(\omega_{He} - \omega_B)$ term in equation 8.4 as outlined in §7.2.1 in connection with the 'T1Index' data a potential explanation can be produced: Using the isotope data from Appendix 1 an ^{11}B Larmor frequency of 4.88MHz corresponds to $(\omega_{He} - \omega_B)/2\pi$ = 16.47MHz. To get the same sum frequency in a ^{3}He resonant experiment requires $\omega_{He}/2\pi$ = 11.59MHz. So as the ^{3}He Larmor frequency is increased towards 11.59MHz we should expect to see the ^{3}He T_1 minimum shift downwards in coverage towards ≈0.70 monolayers. Table 7.2.1.1 shows this is indeed the case. At 10.7MHz, X_{min} = 0.709. The problem with this argument is that $J_2(\omega_{He}+\omega_B)$ is expected to dominate $J_0(\omega_{He}-\omega_B)$ since $|\omega_{He}+\omega_B| < |\omega_{He}-\omega_B|$, unless that is, 2D angular factors intervene to make $J_0(\omega_{He} - \omega_B) > J_2(\omega_{He} + \omega_B)$. This is not entirely implausible since although $(\omega_{He} - \omega_B)/2\pi$ is 16.47MHz and $(\omega_{He} + \omega_B)/2\pi$ is only 6.71MHz both are both $\gg$0. The idea remains speculative.

At intermediate coverages ($0.3 \leqslant X \leqslant 0.7$) where registering takes place T_1 falls continuously as expected. Above X=0.75 it rises as ^{3}He↔^{11}B spin intimacy is lost, to a plateau near monolayer where the ^{3}He-solid-monolayer+basal-plane−^{11}B system is constant. T_1 is reduced by a factor of 3.6× from X=0.0→0.7 using the 'T_1(1/e)' measure which compares with an order of magnitude fall observed on DLX6000 (§3.5.2).

It is clear from the X=0.0 point that a non-negligible intrinsic relaxation mechanism exists for ^{11}B in BN. For a classical solid at these temperatures it cannot be nuclear dipole-dipole. Instead relaxation by PMIs is proposed. The PMIs are far too sparse to directly relax substrate nuclei other than their nearest neighbours because the electronic fields fall off very rapidly, as d^{-4} (equation 1.10.3.1). Instead spin diffusion allows magnetisation to flow through the crystallites from PMI sites where relaxation takes place. Such spin diffusion limited relaxation has a characteristic signature, it recovers as $h(t) \propto (Dt)^{½}$ **145**. Exponential least squares fitting will flag this as strongly

Figure 7.4.3.7, ^{11}B T_1 against Coverage, BN, Run#8, F=4.88MHz, T=1.1K

sub-exponential. Figure 7.4.3.8, 'T1Index' *vs* coverage shows the X=0.0 point is in fact strongly sub-exponential.

To further investigate the issue the 'T_1' *vs X* recoveries have also been fitted to the 'SD3' form (listing 6.3.2.1), namely,

$$h(t) = h(0)\exp(-t/T_1) + h(\infty) + (Dt)^{½} \qquad 7.4.3.1$$

where D is the diffusion coefficient. The idea being to find out how much of the relaxation is spin diffusion limited. With a ^{3}He film present there will potentially be an additional spin diffusion limited contribution as substrate spins' magnetisation diffuses through the crystallites from the relevant surfaces where ^{3}He spins relaxed it. The first two terms of equation 7.4.3.1 model relaxation of ^{11}B spins at crystallite surfaces by the ^{3}He film. Describing it as an exponential process is only an approximation: The distribution of crystallite orientations will lead to sub-exponentiality (with potential for confusion with $(Dt)^{½}$ processes) and at least for registered spins 2D effects may promote ^{11}B super-exponential recoveries as they did in the ^{3}He case (figure 7.2.1.5).

Before proceeding with the 'SD3' analysis the fitted ^{11}B equilibrium magnetisations' ($h(\infty)$, ie. magnetic susceptibility) coverage dependence is considered. It is plotted in figure 7.4.3.9. 'T1Index' fits have been used again since they represent the data well at all experimental times and are not unphysical at the time of interest, t=∞. The key observation is that around X≈0.2 to 0.3 the substrate magnetisation has fully recovered via the edge-film alone. Unless for an unknown reason some interior ^{11}B spins are being *missed out* by the diffusing magnetisation this result is in sharp conflict with the *penetration depth* estimate of §7.3.2.

Returning to the 'SD3' fit data, T_1 is included in figure 7.4.3.7. D is plotted in figure 7.4.3.10 and $h(0)$,$h(\infty)$ are plotted in figure 7.4.3.11. Starting with X=0.0, the huge value of T_1 ~ 1.3 years shows the recovery is almost entirely spin diffusion limited (§3.5.3). At 35 minutes, the longest experimental delay used the $(Dt)^{½}$ contribution accounts for 98.7% of the recovery. Figure 7.4.3.12 shows the recovery plus $(Dt)^{½}$ fit ('SD' function in listing 6.3.2.1). Only at very short times in there any noticeable deviation from the fit.

At X=0.1 the recovery profile has changed dramatically. There is now a substantial exponential contribution accounting for 92.7% of the recovery at 35 minutes. Figure 7.4.3.9 shows most of the (interior) ^{11}B spins do not recover. Those that do must be near the edge-sites given the small D contribution.

Figure 7.4.3.8, ^{11}B 'Index' from 'T1Index' Fit vs Coverage, BN, Run#8, F=4.88MHz, T=1.1K

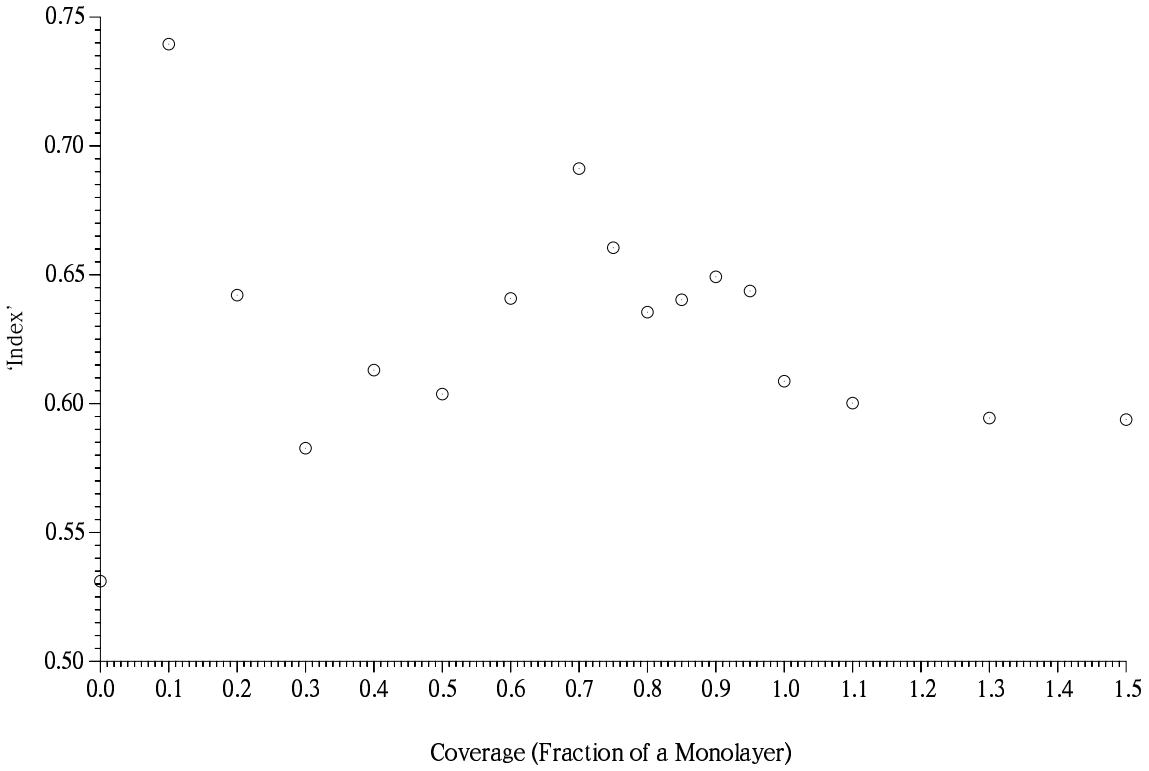

Figure 7.4.3.9, ^{11}B Echo Height h(∞) vs Coverage, BN, Run#8, F=4.88MHz, T=1.1K 'T1Index' Fit Used, NB: No Fit was possible at X=0.0.

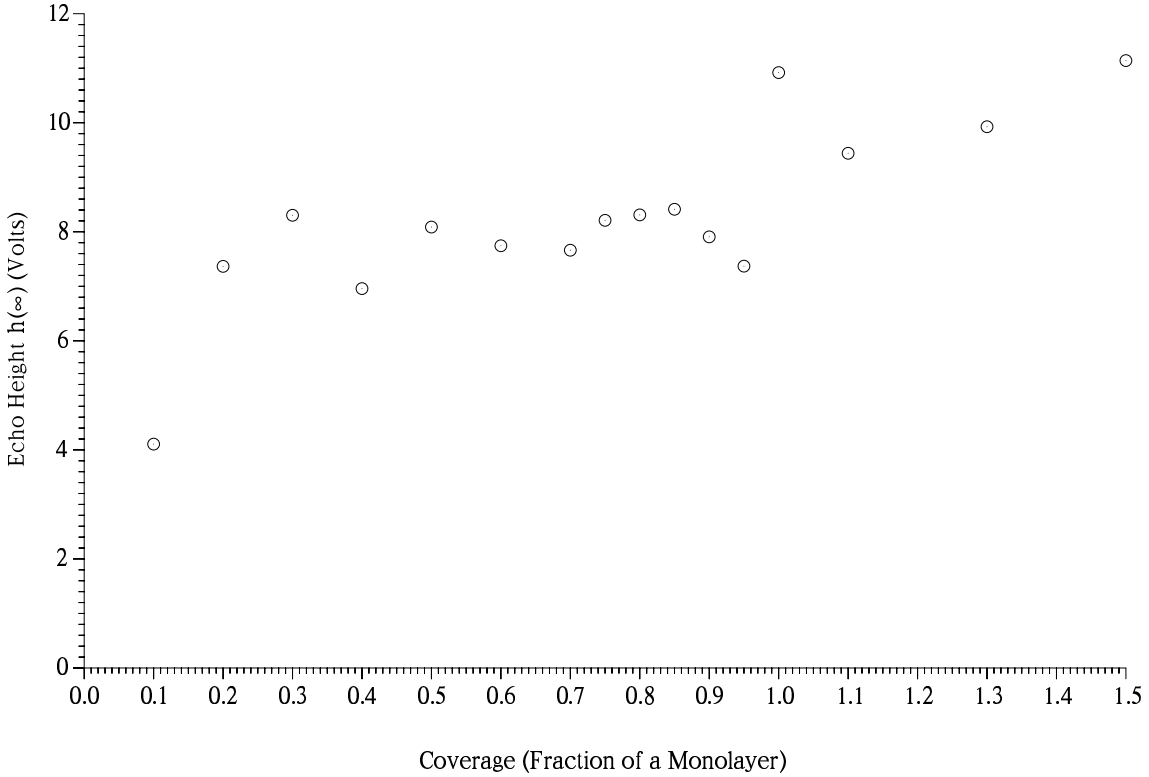

Figure 7.4.3.10,[11]B, 'D' from 'SD3' Fit vs Coverage, BN, Run#8, F=4.88MHz, T=1.1K

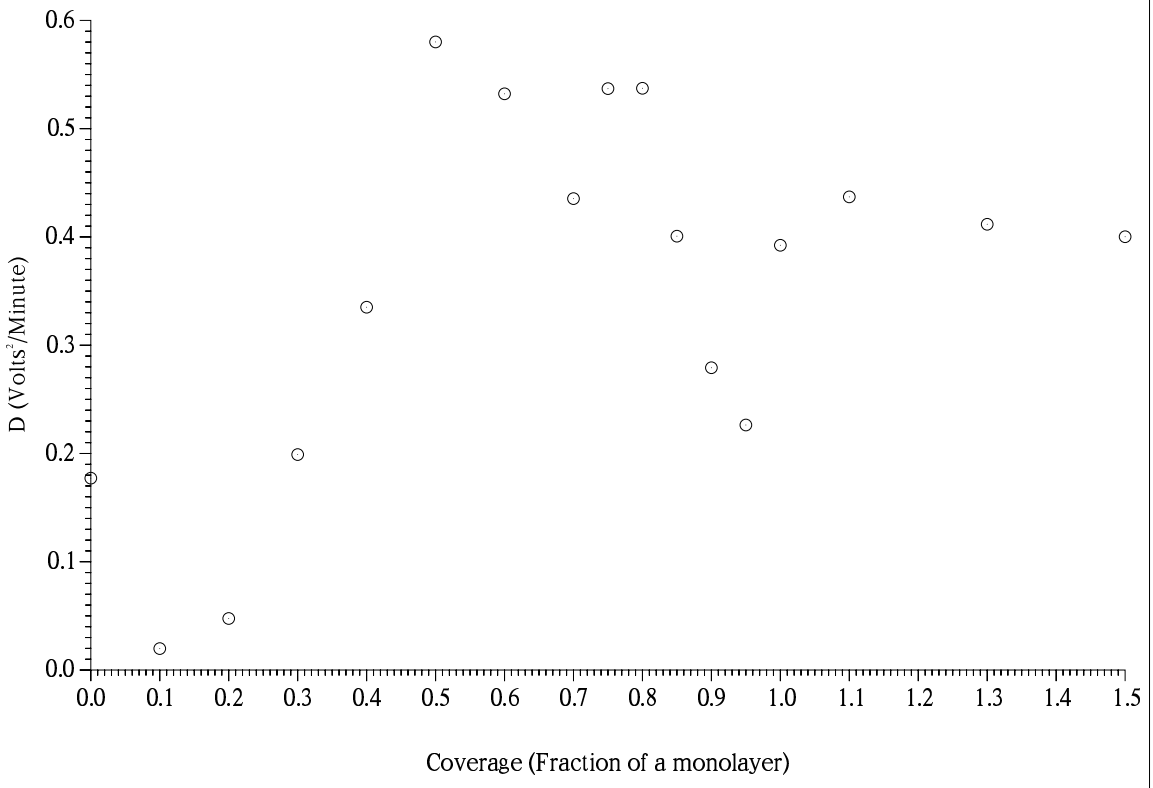

Figure 7.4.3.11,[11]B, h(0) & h(∞) from 'SD3' Fit vs Coverage, BN, Run#8, F=4.88MHz, T=1.1K

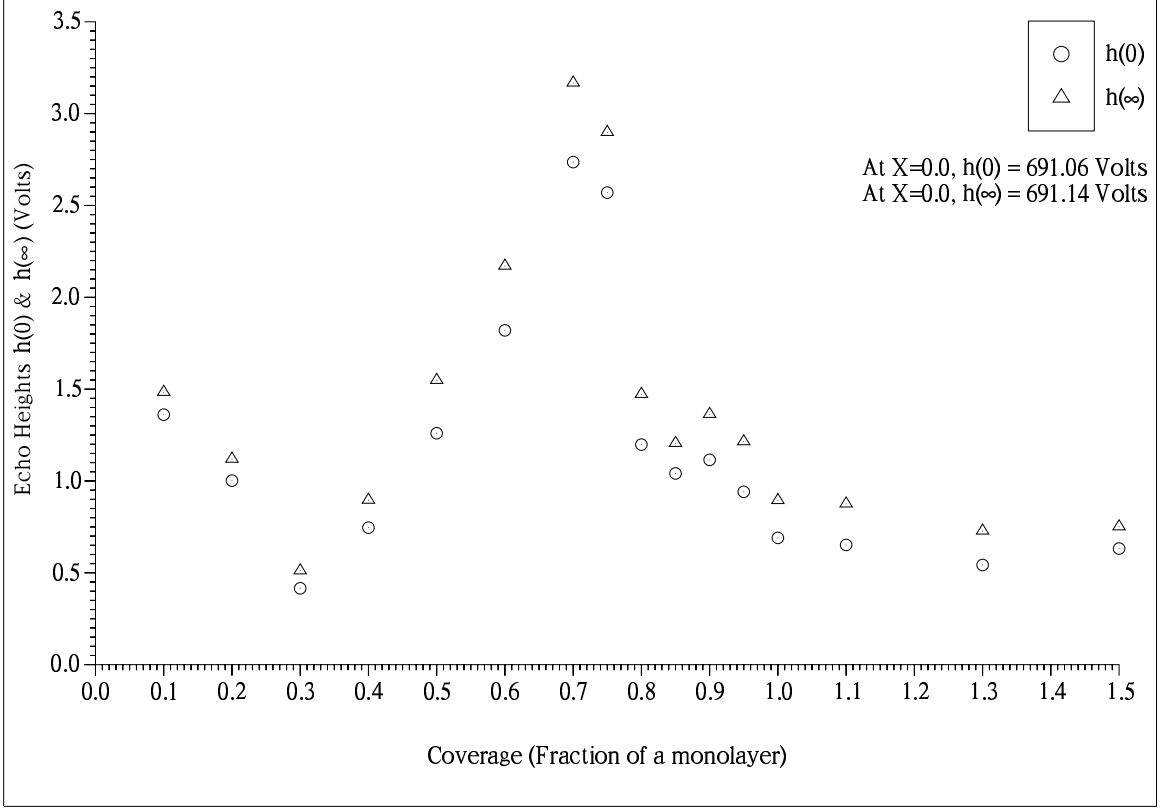

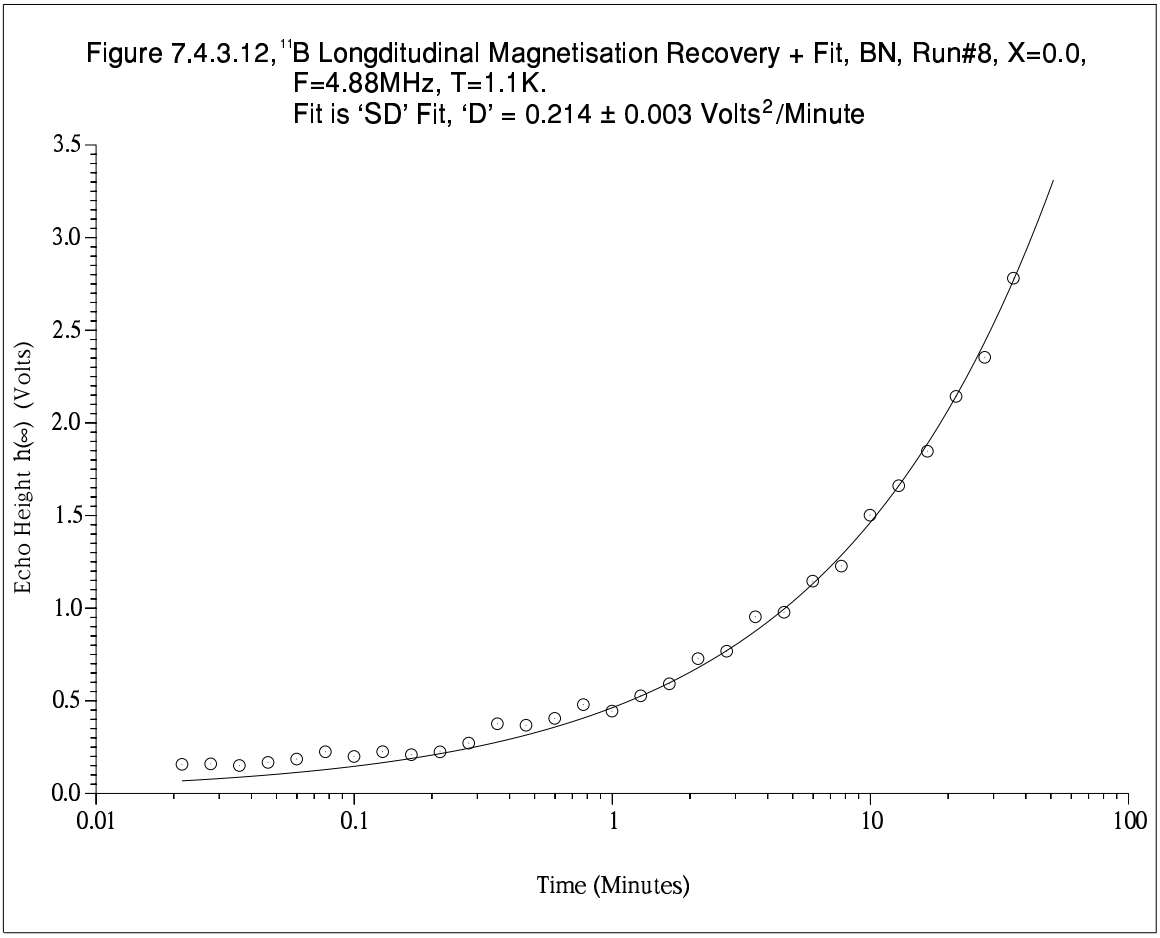

As coverage increases from X=0.1 to 0.3; the D contribution rises rapidly to 98.2% of the recovery at 35 minutes. T_1 has dropped substantially and $h(\infty)$ has fallen significantly. The following explanation is applied; Additional ^{3}He spins have gone into the basal-plane 2D gas. Their rapid motion precludes them relaxing themselves, relying instead on the solid edge-film. These 2D gas spins do have an effect on ^{11}B relaxation however, playing the same role as bulk liquid ^{3}He does in the DLX6000 experiments in which the beads were immersed in the liquid **[147]**, the adsorbed solid ^{3}He layer relaxing the bulk liquid whose rapid motion prevents self-relaxation. The substrate ^{19}F relaxation rate is also much enhanced over the monolayer value. This is because the bulk liquid in effect increases the size of the adsorbed solid monolayer's Zeeman bath. Rapid solid-layer↔bulk-liquid particle exchange ensures the two phases remain in mutual equilibrium **[152]**. Figure 7.4.3.13 shows a schematic diagram of the model. Compare with figure 3.5.3.2.

Figure 7.4.3.13, The Direct $^{19}F(^{11}B)-^{3}He$ Coupling Mechanism with Additional Bulk−Liquid (*2D Gas*) Component.

(DLX6000 specific components shown in standard typeface, BN specific in *italic*.)

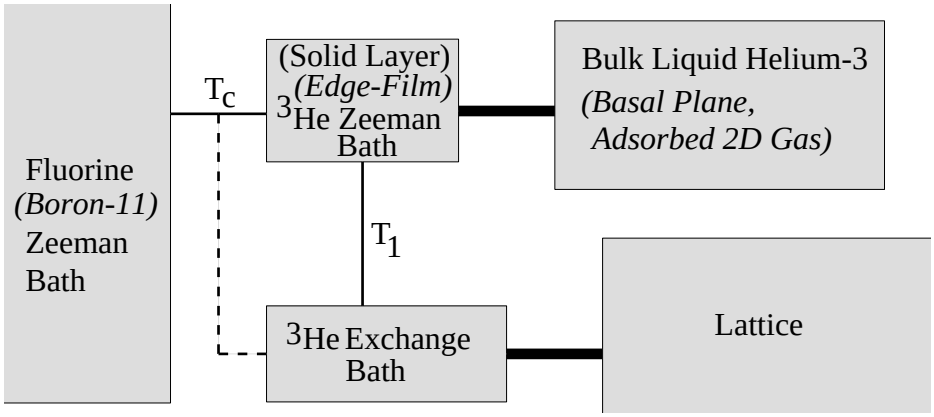

For more information see reference **147**. Returning to BN, at X=0.3 (cf. X=0.1) after the destruction of the ^{11}B longitudinal magnetisation; Edge-sites ^{11}B spins recover via the solid edge-film. The solid edge-film spins are assisted by the additional 2D gas spins' magnetisation which flows via the edge-film to the ^{11}B spins refreshing their magnetisation. This takes place at short times, times of the order of T_c in the above figure but $\ll$ the ^{11}B spin diffusion time for interior spins to be reached from the edge-sites. This mechanism is responsible for the >2× fall in ^{11}B T_1 and the increase in $(Dt)^{½}$ as more ^{11}B spins are able to recover. ^{11}B recovery from the lattice via the ^{3}He exchange bath is not helped however because the edge-film now has the additional responsibility of recovering the 2D gas spins' thermal equilibrium magnetisation from the lattice. Therefore at long times when the 2D gas *magnetisation reservoir* is *empty* the exponential edge-film contribution to ^{11}B recovery is small. This is shown by the reduction in $h(\infty)$ as X=0.1→0.3. Notice that the fall is approximately linear in X, the signature of an *Augmentation Factor* related process.

As coverage rises from X=0.3→0.5 the situation changes because registered spins start to appear on the exposed basal-planes. Consequently the exponential surface process contribution now increases as shown by $h(\infty)$. At 35 minutes it accounts for 25% of the recovery when X=0.5. T_1 continues to fall as all additional spins add to the effective size of the ^{3}He Zeeman reservoir and registered spins strengthen the links with both the lattice (ie. decreasing the figure 7.4.3.13 model's 'T_1') and the substrate spins (ie. decreasing the model's 'T_c'). With the better magnetisation transport to the crystallite's interiors via basal-plane surfaces the absolute size of the $(Dt)^{½}$ contribution increases as diffusion limited interior spins recover sooner. The spin diffusion journey to

the crystallite centres is of course much shorter and quicker via the basal-planes (see §7.3.2).

X=0.5→0.75. Here the situation is less clear. Additional ^{3}He spins go into the 2D gas and registry. At X=0.75 we assume the 2D gas component has vanished (see figure 7.4.3.1 for example) leaving registered spins on the exposed basal-planes plus a small number of non-edge-sites heterogeneous solid spins due to inadequate annealing. The exponential surface process contribution $h(\infty)$ continues to increase as far as 0.7 monolayers (where the exponential fits have their T_1 minimum), reaching 44% at 35 minutes. This is expected as registering increases. Significantly $h(\infty) \propto X$ for $0.3 \leqslant X \leqslant 0.7$ suggesting the registered population grows proportionally to coverage as inferred on Grafoil **[206]** (See also §7.2.3.2). In a change to the previous trend the $(Dt)^{½}$ contribution falls slightly over X=0.5→0.7 and T_1 rises a little over X=0.5→0.75. A clue to a possible reason for the change is provided by the 'SD3' T_1 which uniquely has no discontinuity at X=0.7, the abrupt change occurring instead at perfect registry, X=0.75; As discussed above the position of the minimum in T_1 is known to display some frequency dependence. The figure 7.4.3.13/3.5.3.2 model's T_1 and T_c represent sampling the motion via spectral densities at different frequencies (equations 2.2.16, 8.3−8.5) and will therefore have ($\omega_x\tau_c \approx 1$) minima at different motional speeds τ_c. As perfect registry is approached FMR relaxation is thought to surpass and dominate the homonuclear process for ^{3}He. That is $T_1 < T_c$ gives way to $T_c < T_1$. This provides a potential explanation for the 'SD3' T_1 behaviour since it, in contrast with the other plots in figure 7.4.3.7 only reflects and therefore better represents changes in relaxation at the surfaces. In reality as shown in chapter 8 the BN/^{3}He system is much more complicated than these simple models imply. It is likely the change at X=0.5 stems from a change in dominance of one term(s) over others in the heteronuclear (or even a combination of both) processes rather than simply from a homonuclear to heteronuclear mechanism. Another likely contributing factor to the changes at X=0.5 is a change-over from edge-sites to basal-plane dominated FMR relaxation which occurs once sufficient registered spins are present. The very limited change in D over $0.5 \leqslant X \leqslant 0.75$ suggests that maximum FMR relaxation efficiency of ^{11}B spins has been reached at X=0.5 (eg. 'SD3' T_1/figure 7.4.3.7) but that a decreasing number of residual interior spins' recoveries are still spin diffusion limited at long times.

Above X=0.75 the exponential surface process contribution $h(\infty)$ falls off rapidly to a constant level near monolayer. T_1 has a maximum near monolayer then a slow rise and D has a minimum similarly close to monolayer followed by a constant

level. Comparing the 'SD3' T_1 with the ^{3}He T_1 coverage dependence data (figures 7.2.1.2 and 7.4.3.3) for X>0.75 reveals the same features albeit at a slightly higher coverage, suggesting similar explanations − Namely the onset of second layer promotion at X≈0.9 reducing the incommensurate solid's density increase as far as maximum first layer density at X=1.0 (§7.2.1). Overall, the situation is complicated here with several unanswered questions. For example; (1) Why do second layer 2D gas spins not enhance the ^{11}B relaxation rate as first layer low coverage 2D gas spins do for the edge-film? (2) What role does the edge-film play at X≫0.75 where ^{11}B relaxation via the exposed basal-planes is inefficient? (3) Why does the T_1 maximum occur at X=1.0 but the D minimum at X=0.95?

Many of the unexplained features/outstanding questions probably originate in the ^{3}He coupling with other substrate spins. There is no reason to suppose that ^{11}B is the only substrate isotope to couple with ^{3}He or even necessarily the dominant one. Indeed, chapter 8 shows it is unlikely to be the dominant one, potentially relegating ^{11}B spins to more of an observer of the substrate↔^{3}He magnetisation flows than a major participant.

7.5 The Argon Isotherm

As discussed in the introduction to the chapter an Argon adsorption isotherm was performed to get a second estimate for the BN sample's surface area. It was done at liquid nitrogen temperature. A continuous entry technique was used in which Argon was admitted continuously but very slowly to the sample allowing the adsorbed film to build up quasi-statically. The advantages are a semi-unattended experiment and very high resolution. Over the ~72 hours the isotherm took approximately 4 layers were admitted and 39206 sets of measurements were made.

Referring to figure 4.1.2.1, Druck head#2 monitors the gas pressure in the gas handling system's 18.5cm^3 capacity standard volume while head#1 monitors the sample line pressure. Between these two halves of the gas handling system a precision Hoke 'Micro Mite' needle valve was used to set the sample admission rate. The Druck control/ display unit was specially modified to allow remote selection of the heads by computer. Running in a loop, the ISOTHERM program operates by selecting and reading, via the Prema DVM, each head in turn and logging the results to disc. With each set of pressures the temperature was logged using POTREG in monitor mode (see §4.2.4.1) and the pot Allen-Bradley thermometry resistor.

Due to the small size of the standard volume 6 refills were needed in the course of the experiment leading to small discontinuities in the isotherm. Unfortunately the isotherm was not exactly isothermal! The temperature drifted downwards by ~8K during the experiment, according to the thermometry system. It had been assumed active temperature regulation for T=77K would not be needed with the *helium bath* filled with liquid nitrogen, opened to the filled un-pumped pot and the IVC+OVC containing exchange gas (see figure 4.1.1.1). The temperature fall is believed to have been caused by oxygen dissolved in the nitrogen preferentially evaporating as the experiment proceeded. Oxygen boils at 90K under atmospheric pressure.

To calculate the amount of gas adsorbed in the isotherm the sample chamber dead volume must be known. It was found from a room temperature ^{4}He isotherm. Its low binding energy together with the high temperature make adsorption negligible. The sample chamber dead volume, including the sample filling line (figure 4.1.1.1) is 0.67cm^3.

The BET model was used to determine the Argon monolayer. Despite its faults [214] the model is widely used (see references in §3.3 for example) and gives respectable results. The BET equation, used to fit the experimental data is,

$$N_a(p) = A \frac{C(p/p_0)}{[1-(p/p_0)]\,[1-(p/p_0)+C(p/p_0)]} \qquad 7.5.1$$

where,

- $N_a(p)$ is the number of moles adsorbed as a function of sample pressure p.
- A is the number of moles/layer.
- C is the adsorption energy of the first layer relative to higher layers.
- p_0 is the saturated vapour pressure (SVP) at the experimental temperature.

Instead of abandoning the data because of temperature drift the following salvaging procedure was adopted: Accept that p_0 cannot be treated as a known constant and make it an adjustable parameter, an average value of which is to be estimated in the fitting process. Justifying this are; (1) The vapour pressure at the end of the isotherm was ~250mbar which is the (bulk) Argon SVP at 77K. We therefore assume this is the base temperature, the dissolved Oxygen having boiled off and that with almost 4 layers present the behaviour must be close to that of the bulk condensate. The value of p_0 obtained should be largely determined here where $(p/p_0)\rightarrow 1$ and $N_a(p)\rightarrow\infty$. (2) Fortunately, the temperature drift was small around the monolayer point where $(p/p_0)\ll 1$ and $(Cp/p_0)\approx 1$ which is where A is largely determined providing $C\gg 1$. Also, the adsorbed population should be little affected because the temperature drift was small compared to the Ar/BN binding energy, E=1077K **[116]**.

The results of the NLLSQ fit to equation 7.5.1 ('BET2' fit in listing 6.3.2.1) are,

A = 0.91 ± 0.01 mmoles/layer, ≡ 21.8 ± 0.3 cm^3 Argon/layer at STP…

C = 35.1 ± 0.3. …See also §7.2.1/X=0.75.

p_0 = 340.5 ± 0.2 mbar.

Figure 7.5.1 shows the isotherm plot scaled by A and p_0 together with the fit. Also included are the corresponding temperatures. Some of the smaller temperature *steps* are due to the poor temperature coefficient of resistance of the thermometry resistor at liquid nitrogen temperatures coupled with digitisation error in the SHE bridge (§4.2.4). The larger *steps* occurred as the nitrogen level fell (or was topped up) uncovering or recovering sections of the cryostat (figure 4.1.1.1), altering thermal conduction into the cryostat/sample chamber. The resolution and accuracy of the thermometry resistor's

Figure 7.5.1, Coverage vs Sample Pressure, BN, Argon Isotherm, with Temperature Drift and 'BET2' Fit Shown.

NB: Standard Volume {Re}fill#n Shown in Circles.

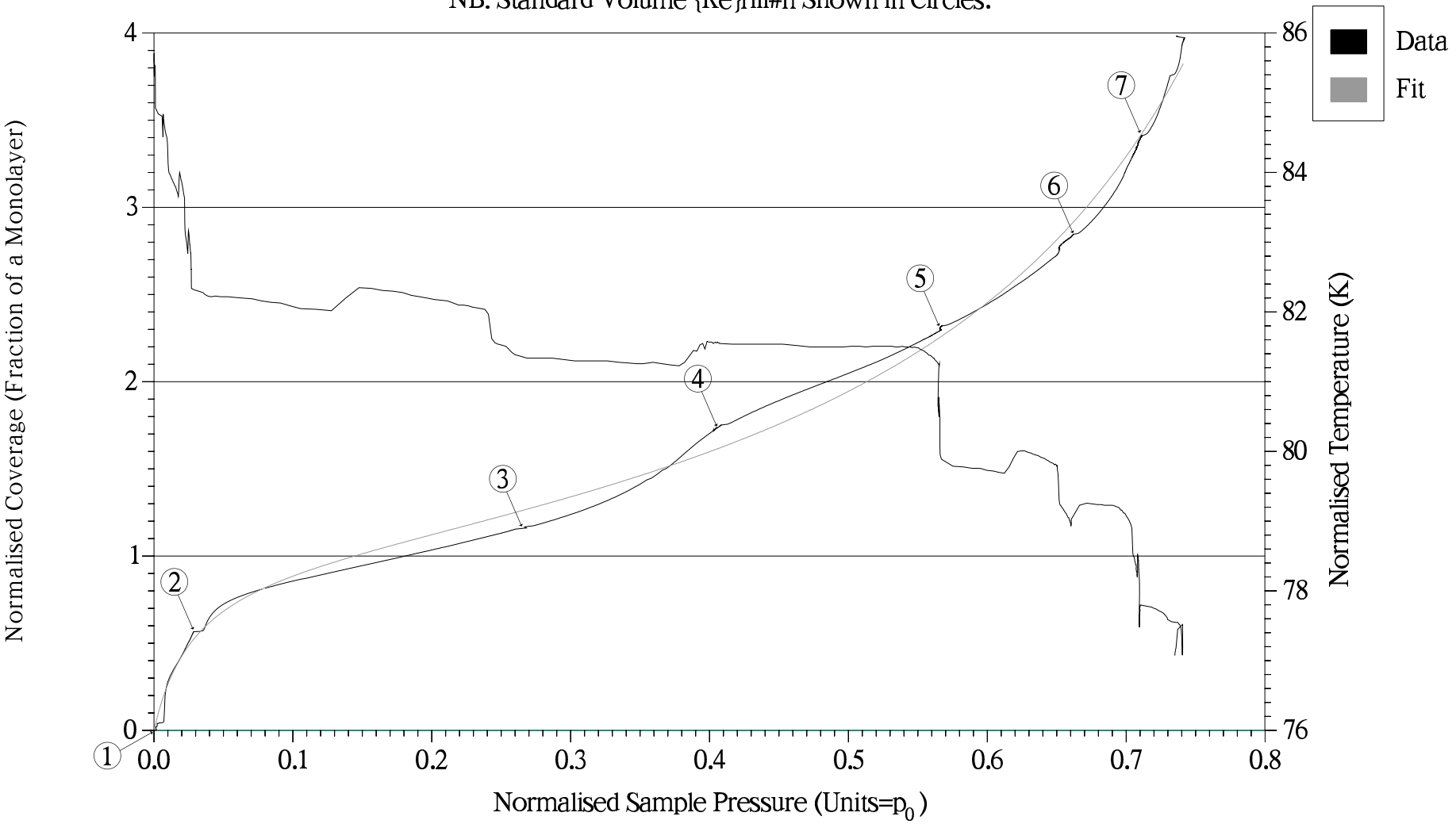

Figure 7.5.2, Coverage vs Sample Pressure, Low Coverages, BN, Argon Isotherm, with Temperature Drift and 'BET2' Fit Shown.

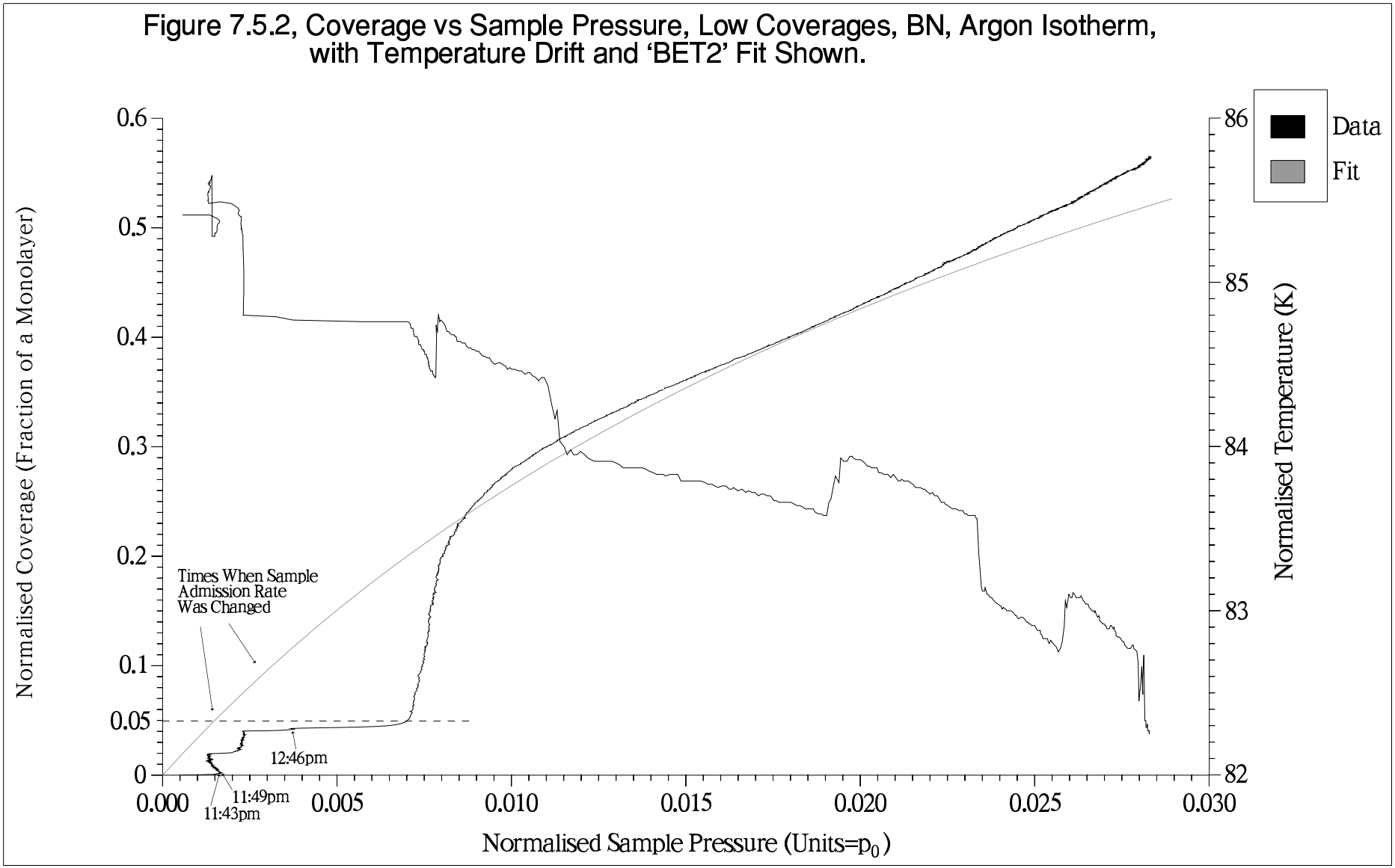

calibrations at '77K' from the, single calibration point taken at that temperature, 4.2K and room temperature (see §4.2.4.1) are obviously fairly limited. Deviations from the isotherm fit are doubtless due in part to temperature drift. There are signs of phase transitions not described by the BET model; The feature around X=0.6, if not entirely an artifact of the refill, could indicate a melting transition. However, this seems unlikely given its temperature and coverage [98]. The other feature around X=1.75, if not purely an artifact, probably indicates 3rd layer promotion as seen in reference **112** but at a lower coverage (further below X=2) due to the higher temperature here.

Figure 7.5.2 is an expanded view of the low coverage portion of the isotherm. The nearly vertical feature at X=0.05 is attributed to the higher binding energy edge-sites surface having been filled. See also figure 3.3.2 where Krypton was used. At still lower coverages there are some smaller features. Some are undoubtedly due to changes in the sample admission rate which was being optimised in the very early stages of the experiment. Temperature changes may also have had an effect. However the step between X=0.02→0.04 does not obviously appear to correspond to any of these changes. Instead it probably indicates a distinct stage in the build up of the edge-film. Maybe there are more than one distinct edge adsite with different binding energies. See §1.10.2 on Grafoil.

7.6 Summary And Conclusions Of The Data

7.6.1 Introduction

Figure 7.6.1 shows the proposed phase diagram for ^{3}He on hexagonal BN. Some of the phase boundaries are highly speculative, particularly those in the commensurate-incommensurate solid transition region. This is mainly due to the very course coverage grid w.r.t. the phase features. For example neither the X=0.8 or 0.9 T_2 temperature dependence give any useful idea of how the 3 temperature regions of the X=0.85 data (figure 7.2.2.40) appear and disappear with coverage.

7.6.2 The Edge-Film

Evidence for the edge-film is overwhelming:− The low temperature T_1 and T_2 values for low coverages are orders of magnitude smaller than expected for a 2D gas − Augmentation factor relaxation for $X \leqslant 0.3$ − The Argon isotherm showing 5% of the surface area consists of distinct higher energy sites − The observation of phase transitions not seen on substrates such as Mylar where a broadly similar fraction of the surface is heterogeneous but the distribution of the heterogeneity over the surface is random − The BN adsorption literature discussed in §3.3. Inferring from the T_2 maxima and minima data (§7.2.3.1), the edge-film is a tightly bound, exchange modulated solid with increasing thermally activated motion at higher temperatures. It is thought to melt somewhere above $T \approx 6$K with the bulk of the melt desorbing at $T \geqslant 8.5$K.

7.6.3 Low Coverages, $X \leqslant 0.3$

A combination of the fixed 5% edge-film and basal-plane 2D gas operates here. Relaxation is dominated by the edge-film. At low temperatures and coverages T_2 is temperature independent due to relaxation by exchange motion in the solid edge-film. At higher temperatures and coverages T_2 becomes influenced/dominated by the non dipolar PMI/fluid mechanism as ^{3}He spins relax in the substrate's *dirty wall* electronic impurity fields. Desorption reimposes dipolar relaxation as spins are largely removed from the reach of the dirty BN surfaces only to give way to the PMI/fluid mechanism again at the highest temperatures (ie. the T_2 desorption maximum) once the ^{3}He spin↔BN surface *visit rate* is high enough. A $1/T_1 \propto \sqrt{T}$ (2D) gas law relation demonstrates the presence of the 2D gas. An abrupt change of slope in the plots at a particular higher temperature confirms desorption as a 3D gas component appears. A deep minimum in T_1 with temperature at around 5K occurs once sufficient thermal activation is present in the solid

Figure 7.6.1, Proposed Phase Diagram for Helium-3 on Hexagonal BN.

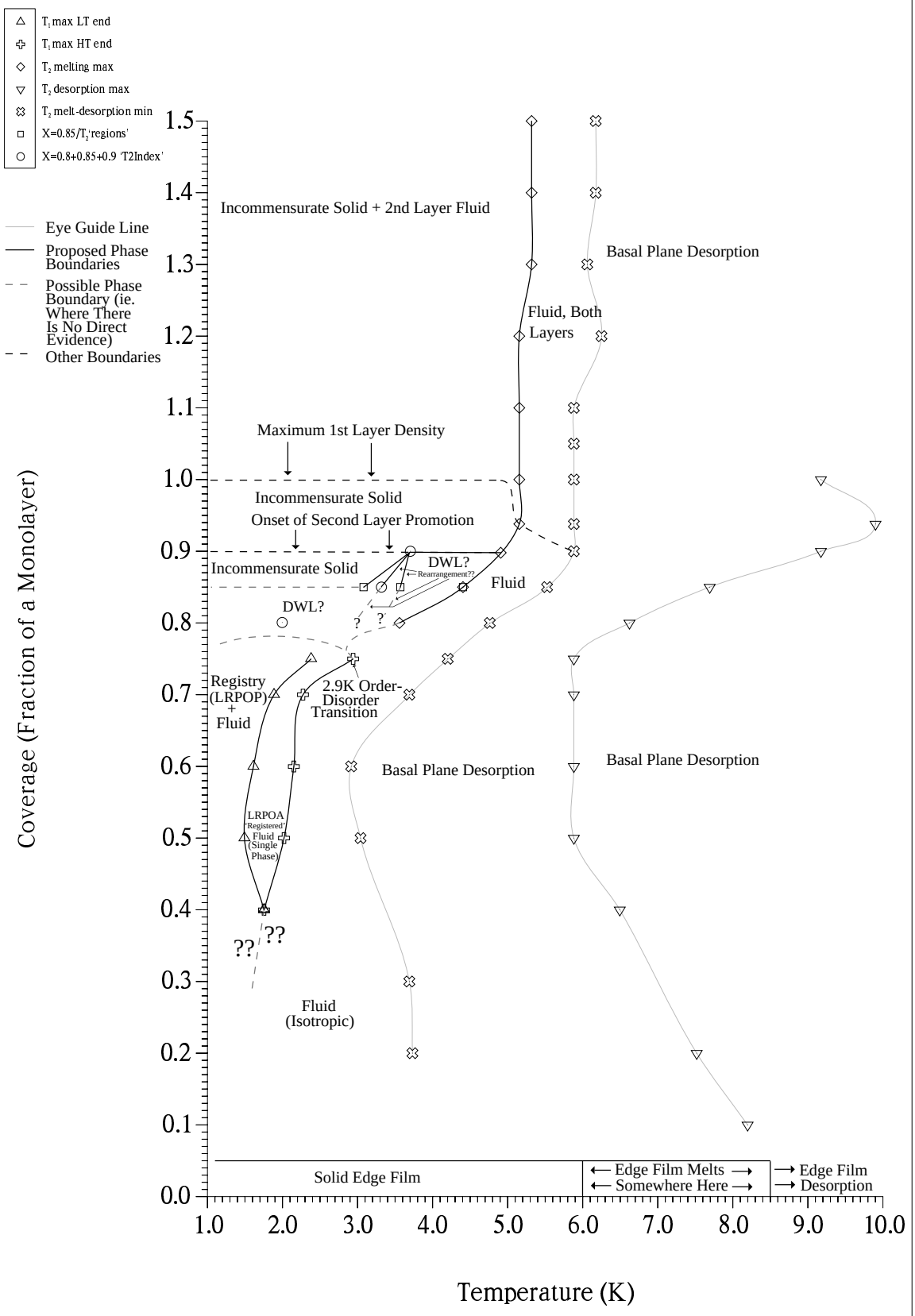

edge-film to fulfil an $\omega_x\tau_c\approx1$ condition. $T_1^{min} \propto X$ (actually extending over all coverages) shows augmentation factor relaxation by the edge-film must be responsible for producing the minimum. Extrapolating back to X=0.05 gives T_1^{min} = 7.9mS which constitutes very efficient relaxation. This could be due to homonuclear relaxation in the very dense edge-film or more probably heteronuclear relaxation via multiply adsorbed spins in the edge-film. See the change in ^{11}B 'SD3' T_1 in figure 7.4.3.7 for example as X=0.0→0.1, even though $T \ll T^{min}$. *Sub-region* behaviour in both indices which is believed to stem from thermal effects in the solid (at these coverages, the edge-film) decreases as the solid:fluid ratio falls.

7.6.4 Intermediate Coverages, $0.4 \leqslant X \leqslant 0.75$

The onset of registering has dramatic effects on both relaxation processes. The augmentation factor relaxation signature disappears and both low temperature relaxation times fall as coverage increases towards X=0.75. In the case of T_2 localisation of ^{3}He spins together with partial suppression of exchange by the substrate potential wells contribute to the increase in relaxation rate with the loss of motional narrowing. T_1 falls as the spatial and motional changes on registering greatly enhance relaxation of the longitudinal magnetisation. The ^{11}B T_1 *vs* X data, the short 44.9mS ^{3}He T_1 (T=1.1K, F=4.5MHz) compared with Grafoil at perfect registry and its super-exponentiality strongly suggest the mechanism is dominantly heteronuclear dipolar. The low temperature frequency dependence for registered spins has a distinct minimum at 4.5MHz − an inexplicable feature in terms of homonuclear relaxation. The conclusion drawn from the coverage and frequency dependence data is that a ^{3}He spin which has been localised by a BN basal-plane hexagon undergoes exceptionally efficient mutual spin flip-flops with its 3 nearest neighbour Boron or Nitrogen spins on that hexagon and that the residual ^{3}He−^{3}He exchange motion in the registered configuration is able to generate maximum relaxation efficiency at 4.5MHz. Data taken at 4.5MHz therefore provides a probe uniquely sensitive to the presence registered spins. NB: This mechanism is discussed in detail in Chapter 8 and leads us to infer that it is the ^{14}N spins and their quadrupole frequency which is responsible for this unique 4.5MHz behaviour.

Low temperature T_2 *vs* X data at $X \leqslant 0.3$ suggests the onset of registering occurs a little below X=0.3. By how much in unclear. In particular it is not known if the registry+fluid coexistence phase exists down zero basal-plane coverage. From heat capacity data on Grafoil the fluid is thought to be stable against registering below $X\approx0.4$ for both helium isotopes **[31,36]**. NMR data (figure 1.10.1) on Grafoil possesses a similar

turnover in relaxation times at similar coverages. Due to the uncertainty in the onset coverage the phase boundary line has been deliberately left ambiguous in figure 7.6.1.

At 0.4 monolayers there is a sharp maximum in T_1 with temperature at T=1.8K where the registered component is thermally destroyed. At higher coverages the maxima broaden to form plateaux. These plateaux are believed to indicate formation of a single phase, intermediate between the registered+fluid coexistence and the (isotropic) fluid. It has been labelled the LRPOA (*long-range-positional-order-absent*) or registered fluid − The idea being the registered solid patches of the low temperature coexistence phase which possessed long range positional order (LRPOP) have given way to a single phase which has both fluid (liquid?) and registered characteristics. It lacks the substrate imposed positional order of the coexistence patches but does possess a high degree of bond orientational order in which a ^{3}He spin has a good chance of being found in a registered position. For this reason the LRPOA phase T_1 is thought to still relax dominantly via the substrate like the coexistence patches albeit with less efficiency. The phase boundaries in figure 7.6.1 are delimited by the two plateaux ends. See figure 7.2.2.29.

T_2 which is not driven by the cross relaxation still reflects the temperature induced LRPOP→LRPOA→isotropic fluid transitions although to a much lesser degree. A weak maximum in T_2 with T and the corresponding minimum in 'T2Index' lie within the low temperature shoulder of the T_1 plateaux where the LRPOP→LRPOA transition is proposed to take place. The 'T2Index' minimum indicates a peak in relaxation multiplicity at the centre of the LRPOP→LRPOA transition where both components are maximally present. The slow fall in T_2 above the maximum is produced by the slight additional mobility of the LRPOA phase which leads to a small increase in relaxation via the PMI/fluid mechanism.

'T1Index' rises with falling temperature as the effective registered population increases. At lower temperatures and higher coverages large *sub-region* behaviour features occur, indicating details of the LRPOP↔LRPOA transition. This is probably due to the film breaking up into separate domains. As perfect registry is approached the 'T_1' relaxation becomes super-exponential at low temperatures. This is thought to be a consequence of 2D effects in which spin diffusion in a plane results in a long tailed correlation function decaying as t^{-1} combined with strong heteronuclear relaxation dominated by an adiabatic-like contribution.

In general all of the maximum/minimum features discussed above increase in size and clarity as coverage increases to X=0.75 and the registered component becomes

increasingly dominant. At X=0.75 the data is clear enough to observe the 2.9K order-disorder transition in both T_1 and T_2 temperature data. T_2 and 'T2Index' data show that it is our LRPOA→isotropic fluid transition which corresponds to the accepted (ie. 3K on Grafoil) order-disorder transition − The sharp fall in T_2 and its index with temperature above the transition are due to PMI/fluid relaxation taking over as spin mobility rapidly increases with the attendant loss of order.

Above the T_1 plateaux temperatures a $1/T_1 \propto \sqrt{T}$ law usually operates as expected for the isotropic fluid. X=0.7 and X=0.75 data clearly show the ^{3}He magnetisation depression effects of coupled relaxation with substrate spins.

It has been thought for some time that the phase transitions of helium on graphite may be in the same universality class as the 2D three-state Potts model. Ecke, Shu, Sullivan and Vilches **[32]** have placed ^{4}He/graphite heat capacity data on a phase diagram for this model allowing them to locate the tricritical point (TCP) which delimits the three phases involved. These are the low temperature registered+fluid coexistence, the fluid and the 'commensurate' phase. Figure 7.6.2 reproduces their phase diagram.

Figure 7.6.2, The Low Coverage Phase Diagram for Helium-4 on Graphite due to Ecke et.al.

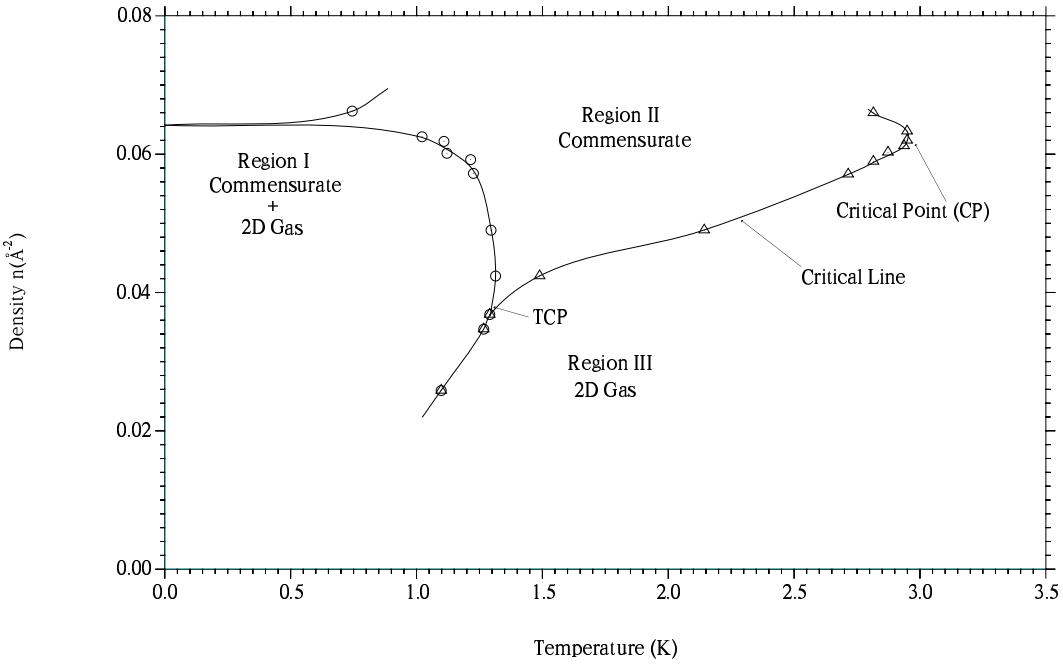

Despite some obvious differences and the sparser BN data is seems plausible to suggest the BN LRPOA phase and Ecke's Graphite 'commensurate' phase might be the same and that the ^{3}He/BN system is also in this universality class. Ecke's description of this phase

as “commensurate with vacancies” is consistent with our LRPOA *registered fluid* where a ^{3}He spin has an enhanced probability of being in a registered position. The ^{3}He/BN phase diagram places the TCP somewhere near X=0.4,T=1.8K which is broadly similar to Ecke's X=0.34,T=1.3K bearing in mind the resolution of the BN data grid.

7.6.5 The Commensurate-Incommensurate Transition Region, $0.75 \leqslant X \leqslant 0.9$

Potentially the most complicated region of the phase diagram, the sparse coverage grid of the data makes it the least well understood and the resolution of the proposed phase boundaries very poor. The inferences drawn are necessarily highly speculative and should be treated as such.

As mentioned in §1.8.7 concerning ^{3}He/Grafoil Greywall **[31]** described this region in terms of a set of coexistence phases composed of combinations of fluid, incommensurate solid, $\sqrt{3} \times \sqrt{3}$ R30 registered and two possible configurations of a 2/5 occupancy registered phase. Lauter, Godfrin, Frank and Schildberg reinterpreted the data in terms of domain wall phases as shown in figure 7.2.2.39. Domain wall models have also been applied to H_2, HD and D_2 on graphite **[210]**. A domain wall interpretation is preferred here since it provides a potential explanation for multiple phase transitions in temperature with those phase transitions able to occur at or above the order-disorder transition temperature. The later is particularly clear with D_2/Graphite **[215,210]** where the order-disorder transition occurs at 18.2K and the highest coverage DWL exists up to 22.8K. Multiple phase transitions are clearly shown in the BN T_2 data at 0.85 monolayers (figure 7.2.2.40). In §7.2.2/X=0.85 the three regions below the melting-maximum were first suggested might be incommensurate solid, DWL and isotropic fluid. The main drawback was how then to interpret the T_2 *melting-maximum* when the isotropic fluid had already formed, given the successful explanation of the T_2 melting-maximum in the high coverage incommensurate solid as the signature of the incommensurate solid→isotropic fluid melting transition. The alternative explanation presented in §7.2.2/X=0.85 proposed both region 2 (3.03K$\leqslant T \leqslant$3.57K) and region 3 (3.57K$\leqslant T \leqslant$4.55K) as DWL phase(s) in which some unspecified structural rearrangement takes place at the inter-region boundary. This model is preferred and is used in figure 7.6.1. Further possible indicators of structural rearrangement within region 2 at 3.33K and at 3.70K at X=0.9 and maybe at 2K at X=0.8 are from minima in ‘T2Index’ where a maximally two component system at the rearrangement-transition produces a peak in two component relaxation. Recapping, in this scheme at;

- X=0.8; The DWL present at 1.1K *melts* to the isotropic fluid at the T_2 melting-maximum. Possibly some structural rearrangement at 2K.
- X=0.85; The incommensurate solid present at 1.1K transforms to the DWL at 3.03K, undergoes multiple structural rearrangement at higher temperatures and *melts* to the isotropic fluid at the T_2 melting-maximum.
- X=0.9; The incommensurate solid present at 1.1K exists up to 3.70K where it enters an incommensurate solid/DWL borderline region, *melting* to the isotropic fluid at the T_2 melting-maximum.

Hysteresis of the relaxation times, particularly T_2 and its index in the double temperature-sweep data seems to be confined to those coverages and temperatures where the DWL is proposed − It abruptly disappears at X>0.9 where the incommensurate solid melts directly to the isotropic fluid. A domain wall phase with a tendency to structurally rearrange with temperature, needing an *energy of rearrangement* to do so might be expected to display some hysteresis with temperature sweep direction. Other evidence that the regions of the phase diagram labelled DWL are qualitatively different from the incommensurate solid are (1) the anomalous shift at X=0.85 of the low temperature T_1 minimum in T at 10.7MHz where it has moved up into the region 2 DWL and (2) the non-activation law relation followed by T_2 in the rise to the melting-maximum at X=0.8 − In the incommensurate solid an activation law is followed.

7.6.6 The Incommensurate Solid and Second Layer Fluid

The incommensurate solid exists at low temperatures at X=0.85 and X=0.9. At X=0.938 and above the first layer incommensurate solid melts directly to the isotropic fluid. As density increases towards maximum first layer density at X=1.0 where the low temperature T_2 minimum is, the temperature of the T_2 melting-maximum and the activation energy measured in the rise to that maximum, both rise rapidly to monolayer plateaux. The low temperature T_2 maximum at X=1.2 is thought to be due to interlayer exchange effects. ‘T2Index’ tends to show more low temperature *noisiness* with increasing coverage as far as the monolayer where second layer 2D gas spins increasingly mask the cause, namely the proposed thermal breakup of the incommensurate solid film into patches. T_1 continues to produce the three minima in T first seen at X=0.8. These minima move to higher temperatures as far as their monolayer plateaux with decreasing motion and increasing density in the solid first layer. The onset of second layer promotion at low temperatures occurs at 0.9 monolayers on the *maximum-first-layer-density=monolayer-coverage* coverage scale used in this work.

7.6.7 The T_2 Maxima and Minima

A set of T_2 maxima/minima occur as a function of temperature. Essentially there are 3 features;

(1) All coverages display the desorption-maximum. It is the highest temperature feature, occurring between 5.9K and ~11K. It is thought to indicate dipolar relaxation which increases T_2 with temperature, giving way to the non-dipolar PMI/fluid mechanism as the desorbed spins' visit-rate to substrate embedded PMIs rises. Melting and desorption temperatures or temperature limits for the edge-film have been inferred from the desorption-maximum data. See §7.2.3.1 for details.

(2) The melt-desorption-minimum, the next highest temperature feature occurs when rapidly diffusing fluid spins from the melted solid/DWL, relaxing via the PMI/fluid mechanism regain dipolar dominance as desorption removes them from the surface embedded electronic impurities. In the discussions of §7.2.3.1 the concept has been generalised to include minima produced by lower coverage, non-melt 2D gas/fluid spins. A solid edge-film is inferred for temperatures encompassed by this feature ($2.9\text{K} \leqslant T \leqslant 6\text{K}$) from the data. Limited variation in T_2 with coverage at this minimum is consistent with the non-dipolar mechanism interpretation.

(3) The melting-maximum is the lowest temperature feature. It marks melting of the incommensurate solid (or DWL at intermediate coverages). Melting occurs once a critical vacancy concentration is reached. Like the desorption-maximum the melting-maximum occurs when the rapid increase in motional speed accompanying the loss of order at melting causes dipolar relaxation to give way to the PMI/fluid mechanism.

7.6.8 The T_1 Minima

In general three separate minima occur in temperature. Only the highest T one is present below 0.8 monolayers. All are believed to be dipolar in nature and are formed when suitable $\omega_x\tau_c \approx 1$ conditions are met. Their individual characteristics are summarised as follows, from highest to lowest temperature:−

(1) Due to relaxation in the edge-film − Augmentation factor relaxation of all other spins − Very efficient relaxation, $T_1^{\min}(X \equiv 0.05) = 7.9\text{mS}$ − Probably dominantly heteronuclear relaxation.

(2) Due to relaxation in dense basal-plane fluid − Augmentation factor

relaxation of second layer fluid spins at higher coverages − Much less efficient relaxation than at minimum (1) − Homonuclear relaxation (see §8 for justification).

(3) Occurs at or below the T_2 melting-maximum, therefore due to relaxation in the solid (or DWL) basal-plane film − Augmentation factor relaxation of second layer fluid at higher coverages − Heteronuclear relaxation (see §8 for justification).

7.6.9 Activation Energy Data

Activation energy data was extracted from the $T_{1,2}$ temperature dependence data wherever an activation law was at least approximately valid. This was in the rise to the; T_2 melting-maximum, desorption-maximum and on both sides of the dominant T_1 minimum. From these data the; vacancy+tunnelling creation energy in the high coverage solid, analogous quantity for the solid edge-film, desorption energy of the dense basal-plane melt fluid and the vacancy creation energy in the registered phase were determined or at least rough-estimated.

7.6.10 Frequency Dependence of the Data

This comprises two sets of data. Both relaxation time's temperature dependence were measured as a function of frequency at 0.938 monolayers in one set. In the other both relaxation times were measured at 1.1K as a function of frequency for coverages, $0.4 \leqslant X \leqslant 1.0$.

The X=0.938 T_2 data was frequency independent at low temperatures as expected for dipolar relaxation. At higher temperatures, maximally at 8.5K (in the desorption-maximum) there is a clear minimum in frequency at 6.9MHz. Observation of this frequency dependence rather than the expected $1/T_2 \propto F_0$ or $1/T_2 \propto F_0^2$ suggests the $\exp -t^3$ 'CP' decays seen at these temperatures must be due to relaxation by diffusion in the static field inhomogeneities and not in BN diamagnetic fields. The frequency dependent contribution to the relaxation is small, being ~8% at 8.5K. The cause of the minimum is not certain but see 7.2.2/X=0.938.

The X=0.938 T_1 data frequency dependence is summarised below. Where data trends were able to be characterised they point towards dipolar but probably both homonuclear and heteronuclear dipolar relaxation:

- $3 \times T_1^{\min}$ *vs* F plots show a $T_1^{\min}$ *-linear-in-* F law but not going through the origin. cf. $T_1^{\min} = \omega_0/m_2$ for homonuclear relaxation. The slope of the

plot is highest for the higher T minima.

- The temperature-of-occurrence of the minima is essentially independent of frequency within experimental error.
- T_1 *vs* $1/T$ plots:− The 3 minima become progressively more distinct as F=2.7MHz→8.6MHz. At 10.7MHz they are abruptly subsumed into a single broad minimum.
- T_1 *vs* F linear law fit plots:−
  - − Slope is large at low temperatures, consistent with $\omega_x\tau_c>1$ limit.
  - − Slope is small and approximately constant at mid range temperatures where minima occur. Consistent with $\omega_x\tau_c\approx1$. Eg. in the case of homonuclear relaxation a T_1^{min} *vs* ω_0 plot has a $slope=m_2^{-1}=const.$
  - − F=0 Intercept is small at low temperatures.
  - − F=0 Intercept is comparable to the frequency dependent part at mid-range temperatures but linear law fits are poor.

T_2 does show some frequency dependence at low temperatures. A system with homonuclear dipolar relaxation at temperatures well below the T_1 minimum where the 10/3 effect operates, should be independent of frequency. There are two separate features to consider here: (1) At X=0.75 registered spins produce a maximum at 4.5MHz which corresponds to the very similar minimum in T_1 and must therefore be related to the same heteronuclear processes. (2) At X=0.8 and to a lesser degree at X=0.85 where the lowest-T T_1 minimum occurs at low temperatures (figure 7.2.3.8) T_2 increases with frequency (figure 7.2.4.6) as expected for relaxation near the 10/3 effect or a heteronuclear analogue [47]. Above X=0.85 T_2 is frequency independent within experimental error.

In general T_1 increases at least linearly fast with frequency at low temperatures as expected for dipolar relaxation in a 2D system. At X=0.7 and 0.75 heteronuclear relaxation by registered spins generates a minimum at 4.5MHz as an aberration in the otherwise smooth increase. Linear and exponential law fits have been applied to the high coverage T_1 *vs* frequency data where appropriate. The results reinforce a non-homonuclear dipolar interpretation.

7.6.11 Boron-11 NMR Related Work

This section summarises the work of Runs#7 and #8 where $^3He\leftrightarrow^{11}B$ cross-relaxation was investigated.

- Double resonance experiments at X=0.5 produced some weak evidence for ^{3}He−^{11}B spin flipping.
- ^{11}B T_1 *vs* temperature data also taken at X=0.5 showed a maximum at 5.1K where the ^{3}He T_1 minimum is. The picture remains very unclear however due to poor data quality. The case for ^{11}B heteronuclear relaxation being responsible for producing the ^{3}He T_1 minimum remains unproven.
- ^{11}B T_2 *vs* temperature data at X=0.5 gave some evidence for motional narrowing of surface ^{11}B spins by mobile ^{3}He spins at higher temperatures. Again data quality was not good and conclusions not firm.
- Magnetic susceptibility data derived from the ^{11}B longitudinal magnetisation recoveries, as a function of temperature showed Curie's law was obeyed as expected. Comparison of the ^{11}B and ^{3}He susceptibilities have allowed the penetration depth into the BN crystallite edge-sites *plane* of the proposed ^{3}He-edge-film-mediated ^{11}B magnetisation recoveries to be estimated.
- Using NMR field sweep measurements the quadrupolar frequency of ^{11}B in hexagonal BN has been obtained from the first order powder pattern of the ^{11}B spins. F_Q = 1.47MHz.
- A second set of 1.1K ^{3}He relaxation-times *vs* coverage data revealed the effects of insufficient annealing. In general T_2 was shortened and T_1 was lengthened as solid heterogeneous *clumps* of spins on the basal-planes disrupted registering and incommensurate solid formation.
- A set of 1.1K ^{11}B relaxation-times *vs* coverage data was taken and the following inferred;
  - T_2 revealed broadening of the ^{11}B (surface spins) NMR line by ^{3}He spin local fields. Maximum broadening was at registry.
  - T_1 displayed a deep minimum at registry verifying the previous assumption that 'T_1' relaxation of registered ^{3}He spins is dominated by cross-coupled relaxation with substrate spins. The effects of cross relaxation in possibly determining the precise position of the minimum have been discussed. ^{11}B recoveries were further analysed by decomposition into an exponential ^{3}He mediated surface-process component and a crystallite interior spin-diffusion limited one. A comparison was drawn between the submonolayer BN system involving ^{11}B−^{3}He cross relaxation, the

solid edge-film plus low coverage basal-plane 2D gas −and− the analogous bulk liquid ^{3}He+DLX6000 system involving ^{19}F−^{3}He cross relaxation, a solid ^{3}He surface layer plus bulk liquid ^{3}He respectively.

7.6.12 The Nitrogen Temperature Argon Isotherm

This was done to get a better/second estimate of the surface area of the BN sample. Despite problems with temperature drift the following were observed/obtained; A BET surface area of 81±1 m^2 − Some evidence for multilayer phase transitions − 5% of the surface area is on the crystallite's edges − Some evidence for two distinct sets of sites within the edge area with different binding energies. Using the mass of the BN sample, total surface area and the 5% edge fraction permitted the size and geometry of an average BN particle to be estimated. This was vital in explaining the strong FMR relaxation observed at registry (see §7.2.2/X=0.75).

Chapter 8
Models For Coupled Relaxation

8.1 Introduction

Motivation: Chapter 3 and Chapter 7 treated coupled relaxation with a very simple phenomenological model in which the homonuclear and heteronuclear interactions were represented by two relaxation times 'T_1' and 'T_c'. However coupled dipolar relaxation has been studied from first principles along with the homonuclear case from the early days of the field [47]. Chapters 1 and 2 describe how successful the detailed theory of homonuclear dipolar relaxation has been in explaining the observed features of experimental NMR data in single isotope spin systems − in particular ^{3}He relaxation in 2D/adsorbed systems [70]. The purpose of this chapter is to apply the theory of coupled dipolar relaxation to the ^{3}He/BN system with a view to understanding in some detail the features of the experimental data.

No theory of coupled relaxation in 2 dimensions has been developed so 3D correlation functions etc. are used here. 2D effects are discussed later. In a simple system the time evolution of the magnetisations of the two coupled spin systems after a disturbance, as they return to thermal equilibrium, is given by,

$$\frac{dM_x}{dt} = -\rho_1\left[M_x - M_x^{\infty}\right] + \sigma_1\left|\frac{\gamma_x}{\gamma_y}\right|\left[M_y - M_y^{\infty}\right] \qquad 8.1$$

$$\frac{dM_y}{dt} = -\left(\rho_2 + 1/T_1\right)\left[M_y - M_y^{\infty}\right] + \sigma_2\left|\frac{\gamma_y}{\gamma_x}\right|\left[M_x - M_x^{\infty}\right] \qquad 8.2$$

where M_y and M_x are the two magnetisations. Only the *y* spins are considered to have an appreciable spin-lattice relaxation rate here. T_1 is the homonuclear spin-lattice contribution to the *y* spins recovery and is given by equation 2.2.16. ρ_n describe the relaxation of the spins towards their own equilibrium magnetisation and the σ_n, the relaxation towards the other spins equilibrium magnetisation. They are given by,

$$\rho_1 = \frac{1}{3}J_0(\omega_y - \omega_x) + J_1(\omega_x) + 2J_2(\omega_y + \omega_x) \qquad 8.3$$

$$\rho_2 = \frac{1}{3} J_0(\omega_y - \omega_x) + J_1(\omega_y) + 2J_2(\omega_y + \omega_x) \qquad 8.4$$

$$\sigma_1 = \sigma_2 = \frac{1}{3} J_0(\omega_y - \omega_x) + 2J_2(\omega_y + \omega_x) \qquad 8.5$$

The spectral densities are those of Cowan presented in §2.2 except that the cluster $\hbar^2\gamma^4(\mu_0/4\pi)^2<1/r_{ij}^6>$, essentially the second moment of the NMR line is replaced by $\hbar^2\gamma_y^2\gamma_x^2(\mu_0/4\pi)^2<1/r_{y\text{-}x}^6>$ and is effectively the heteronuclear analogue of the homonuclear second moment − ie. a measure of the strength of the interaction. γ_y and γ_x are the gyromagnetic ratios of the two spin species and $r_{y\text{-}x}$ is the internuclear separation of the *x* and *y* spins. The ω_x and ω_y are the Larmor frequencies of the two spin species. M_x^∞ and M_y^∞ are the equilibrium magnetisations of the two spin systems.

For a ^{3}He adsorbed system three groups of spins have to be considered − the ^{3}He film spins, the substrate surface spins to which they couple and the substrate's interior spins. Following Geng et. al **[147]**, equations 8.1 and 8.2 become,

$$\frac{dM_s}{dt} = -\rho_1\left[M_s - M_s^\infty\right]\left(\frac{N_s^s}{N_s}\right) + \sigma_1\left|\frac{\gamma_s}{\gamma_{He}}\right|\left[M_{He} - M_{He}^\infty\right]\left(\frac{N_s^s}{N_{He}}\right) \qquad 8.6$$

$$\frac{dM_{He}}{dt} = -\left(\rho_2 + 1/T_1\right)\left[M_{He} - M_{He}^\infty\right] + \sigma_2\left|\frac{\gamma_{He}}{\gamma_s}\right|\left[M_s - M_s^\infty\right]\left(\frac{N_{He}}{N_s}\right) \qquad 8.7$$

M_s is the substrate magnetisation, M_{He} the ^{3}He film magnetisation, N_{He} is the number of ^{3}He spins, N_s^s, the number of substrate surface spins and N_s the total number of substrate spins. Rewriting equations 8.6 and 8.7 as,

$$\frac{dy}{dt} = -a_1\left[y - y(\infty)\right] - a_2\left[x - x(\infty)\right] \qquad 8.8$$

$$\frac{dx}{dt} = -b_1\left[y - y(\infty)\right] - b_2\left[x - x(\infty)\right] \qquad 8.9$$

where,

$M_{He} \equiv y$, $M_s \equiv x$,

$$a_1 \equiv + \left(\rho_2 + 1/T_1\right)$$

$$a_2 \equiv - \sigma_2 \left|\frac{\gamma_{He}}{\gamma_s}\right| \left(\frac{N_{He}}{N_s}\right)$$

$$b_1 \equiv - \sigma_1 \left|\frac{\gamma_s}{\gamma_{He}}\right| \left(\frac{N_s^s}{N_{He}}\right)$$

$$b_2 \equiv + \rho_1 \left(\frac{N_s^s}{N_s}\right)$$

The solutions **[216]** describing the recovery of the magnetisations are,

$$y(t) - y(\infty) = A_1 \exp(-r_1 t) + A_2 \exp(-r_2 t) \qquad 8.10$$

$$x(t) - x(\infty) = B_1 \exp(-r_1 t) + B_2 \exp(-r_2 t) \qquad 8.11$$

where the recovery rates are given by,

$$r_1 = \frac{a_1 + b_2 + \sqrt{(a_1 - b_2)^2 + 4a_2 b_1}}{2} \qquad 8.12$$

$$r_2 = \frac{a_1 + b_2 - \sqrt{(a_1 - b_2)^2 + 4a_2 b_1}}{2} \qquad 8.13$$

Treating the A_n as arbitrary constants of integration, the B_n are given by,

$$B_n = \left(\frac{r_n - a_1}{a_2}\right) A_n, \quad n = 1, 2 \qquad 8.14$$

It is instructive to compare these results with the simpler and more easily comprehensible liquid Hydrogen Fluoride system described by Abragam **[47]**. The two coupled spins are ^1H and ^{19}F in HF. There is an additional scaler coupling term due to intermolecular chemical exchange. It has the effect of reducing the system to,

$$a_1 = b_2 = \rho, \quad a_2 = b_1 = \sigma \qquad 8.15$$

which leads to,

$$r_1 = \rho + \sigma, \quad r_2 = \rho - \sigma \tag{8.16}$$

and,

$$B_1 = A_1, \quad B_2 = -A_2 \tag{8.17}$$

Immediately after a 180° pulse to the *y* spins, at t=0,

$$y(0) - y(\infty) = -2y(\infty) = A_1 + A_2 \tag{8.18}$$

$$x(0) - x(\infty) = 0 = B_1 + B_2 = A_1 - A_2, \; A_1 = A_2 = -y(\infty) \tag{8.19}$$

giving solutions,

$$y(t) - y(\infty) = -y(\infty)\,(\exp -[\rho-\sigma]t \; + \; \exp -[\rho+\sigma]t) \tag{8.20}$$

$$x(t) - x(\infty) = +y(\infty)\,(\exp -[\rho-\sigma]t \; - \; \exp -[\rho+\sigma]t) \tag{8.21}$$

which are Abragam's results.

Now, returning to the adsorbed system, after a 180° pulse to the *y* spins at t=0 equations 8.18 and 8.19 again describe the magnetisations. The B_n are given by equation 8.14 and the A_n become,

$$A_1 \; = \; 2y(\infty)\left[\frac{r_2 - a_1}{r_1 - r_2}\right] \tag{8.22}$$

$$A_2 \; = \; -2y(\infty)\left[\frac{r_1 - a_1}{r_1 - r_2}\right] \tag{8.23}$$

allowing solutions $y(t) - y(\infty)$ and $x(t) - x(\infty)$ to be written down.

From a practical point of view equations 8.10 and 8.11 describe a complicated system making it cumbersome for theoretical modelling and fitting to the experimental data. While producing theoretical models to look for ^{3}He double minima in τ_c for example, it is inconvenient to have to deal simultaneously with two relaxation rates r_1 and r_2. Moreover, given the absence of any true double-exponential-relaxation

experimental data and the consequent fact that the spin-lattice relaxation data fits have all been made to yield a single relaxation time 'T_1' or 'T_1(1/e)', makes r_1 and r_2 awkward to fit with. Also, r_1 and r_2 are both functions of four distinct relaxation rate terms, a_1, a_2, b_1 and b_2 which are themselves functions of ρ_1, ρ_2, T_1, $\sigma_{1,2}$, N_{He}, N_s and N_s^s. Clearly a means of combining r_1 and r_2 into a single relaxation time for the *y* spins magnetisation and simplifying the system is needed to make it usable. The T_1(ave) measure gives an average relaxation time from r_1 and r_2 by weighting each by their respective amplitudes,

$$\frac{1}{T_1(\text{ave})} = \frac{r_1 A_1}{A_1 + A_2} + \frac{r_2 A_2}{A_1 + A_2} \qquad 8.24$$

and elegantly fulfils the above criteria: Substituting the above formulae into equation 8.24 gives,

$$\frac{1}{T_1(\text{ave})} = a_1 = \rho_2 + \frac{1}{T_1} \qquad 8.25$$

It is interesting to compare this approximation with that used by Schuhl et. al. **[150]** and Geng et. al. **[147]** for ^{3}He and ^{19}F in DLX6000. Both authors reduce the full model of equations 8.6, 8.7 and components to the simple 'T_c' and 'T_1' model of figure 3.5.3.2 by approximating T_1(homonuclear) ≡ 'T_1' and $\rho_1 = \rho_2 = \rho = \sigma \equiv 1/$'$T_c$'. Both authors worked at sufficiently high frequencies such that $\omega_{expt}\,\tau_c^{exchange} \gg 1$. Schuhl et. al. knowing the $J_n(\omega)$ are smoothly decaying functions of ω obtain $\rho_1 = \rho_2 = \rho = \sigma \equiv 1/$'$T_c$' by assuming $J_0(\omega_F - \omega_{He})$ in equations 8.3−8.5 dominate all the other terms. However this is not a valid assumption since ^{3}He has a negative gyromagnetic ratio (see Appendix 1) which leads to $J_2(\omega_F + \omega_{He})$ being the dominant term and $\rho_1 = \rho_2 = \rho \neq \sigma$. Geng et. al.'s assumption also seems doubtful due to a dropped sign in their equation 11c − c.f. Abragam **[47]**/treatment of HF.

In this work much lower Larmor frequencies were used than in the DLX6000 studies so all the spectral terms in equations 8.4 and 2.2.16 have been retained.

An expression for the heteronuclear analogue of the homonuclear spin-spin relaxation time T_2 (equation 2.2.17) also exists. It describes the decay of the transverse magnetisation of the *y* spins as they relax in the local fields of the *x* spins. Using the same spectral densities as equations 8.3−8.5,

$$\frac{1}{T_2^y} = \frac{2}{3}J_0(0) + \frac{1}{6}J_0(\omega_y - \omega_x) + \frac{1}{2}J_1(\omega_y) + J_1(\omega_x) + J_2(\omega_y + \omega_x) \qquad 8.26$$

8.2 Development of the Model

Having obtained a manageable expression in T_1(ave) the next step was to develop models possessing the key characteristics of the experimental ^{3}He data. These are;

- The low temperature (long τ_c) fall-off in T_1 at X=0.75 and 4.5MHz.
- The minimum in frequency at 4.5MHz observed at X=0.75.
- The basal plane T_1 double minima in temperature occurring for $X \geqslant 0.8$ and over frequencies 2.7MHz$\leqslant F \leqslant$10.7MHz which scale 'correctly' in temperature with coverage.
- The smoothly increasing T_1-in-frequency behaviour seen for $X \geqslant 0.8$.

A key question the models have to address is which of the four isotopes (see Appendix 1) in naturally abundant BN couple with the ^{3}He spins to produce the observed ^{3}He relaxation data? The 1% abundant ^{15}N has been ignored due to its tiny proportion. The 20% abundant ^{10}B is not immediately favoured either on account of its low relative abundance, small gyromagnetic ratio, large spin moment and hence multiple quadrupolar splitting of its NMR line. This leaves ^{11}B and ^{14}N. ^{11}B ($\boldsymbol{I}$=3/2) was the preferred candidate in the discussions of §7 since its gyromagnetic ratio is larger and its quadrupole frequency in hexagonal BN is known from the literature and confirmed by measurements in this work (see §7.4.2) − Most importantly it is small compared to the applied fields/^{11}B Larmor frequencies used in this work − allowing it to be treated in the high field limit in which the quadrupolar interaction is only a perturbation splitting the NMR line **[47]**. In contrast the ^{14}N ($\boldsymbol{I}$=1) Larmor frequency is only 0.43MHz when the ^{3}He F_0=4.5MHz and its quadrupole moment is much larger. Unfortunately no measurement of the ^{14}N quadrupole frequency in hexagonal BN could be found in the literature. It has however, been measured for solid molecular nitrogen **[217]** and is 3.49MHz. It seems plausible to suppose that hexagonal BN with its polarised B−N bond might produce an EFG at the ^{14}N nucleus large enough to give a ^{14}N F_Q of a few MHz.

The first approach was to try to obtain an analytic expression for the occurrence of T_1 minima in τ_c by solving for $(dT_1(\text{ave})/d\tau_c) = 0$. However the solutions become

prohibitively complicated, even for the Reduce computer Algebra system running on a Convex C3840 supercomputer. All subsequent model investigations were done numerically in FORTRAN by varying the dependants of T_1(ave) and observing how T_1(ave) varies with τ_c and frequency. These model investigations and their results are summarised here;

- Models 1−5 treat ^{3}He coupled relaxation with ^{11}B.

  Features are; Varied m_2^{ht} and frequency (ie. field). Tried both with and without quadrupolar splitting of the ^{11}B line. The ^{11}B resonance(s) were treated as one would treat a mixture of separate spin-½ species − as in the 'fictitious spin-½ formalism' **47**. NB: m_2^{ht} is the heteronuclear analogue of the second moment of the NMR line. ie. $m_2^{ht}=\hbar^2\gamma_{He}^2\gamma_B^2(\mu_0/4\pi)^2<1/r_{He\text{-}B}^6>$ and defines the strength of the heteronuclear interaction. The homonuclear second moment is $m_2^{hm}=\hbar^2\gamma_{He}^4(\mu_0/4\pi)^2<1/r_{He\text{-}He}^6>$. The relative intensities of the ^{11}B NMR satellite lines (figure 2.1.2) were taken account of. Both 2D (with $\beta=0^o$ & $\beta=90^o$) and 3D spectral densities were tried. A word about the 2D spectral densities is needed: This is not an attempt to retreat the work of Cowan **70** for heteronuclear relaxation − a massive undertaking given all the angular factors etc. involved. Instead the spectral density formulae of §2.2.2 for a triangular lattice 2D solid have been pressed into service. Clearly this makes some dubious approximations, eg. the ^{3}He−^{11}B bond angle does not lie in the substrate plane as the ^{3}He−^{3}He bond does. It should however give an indication of the effects of two-dimensionality on the system − eg. that of the low frequency divergence of the spectral densities when compared with 3D models − This is all that is intended.

  Results; Only those models with quadrupolar splitting produced double minima in τ_c which were restricted to $1.1\text{MHz}\leqslant F\leqslant 1.6\text{MHz}$ − ie. to frequencies of the order of the splitting frequency.

  Conclusion; ^{11}B coupled relaxation cannot account for the $X\geqslant 0.8$ double

minima which occur for 2.7MHz⩽F⩽10.7MHz at least not with this simple model.

- Models 6−9,11 &17 treat ^{3}He coupled relaxation with ^{14}N.

  Features are; The ^{14}N quadrupole frequency F_Q was set at 4.5MHz with the quadrupole transitions treated as a fictitious spin-½. 2D and 3D spectral densities were tried both with and without powder averaged Zeeman splittings of the ^{14}N quadrupolar line. Varied m_2^{ht} and looked for double minima in τ_c.

  Conclusion; Double minima do occur but only over the frequency range 3.7MHz⩽F⩽5.7MHz and with a gap at F≈4.5MHz. Figure 8.2.1 shows a set of T_1 *vs* τ_c curves for the model over a range of frequencies. NB: m_2^{hm}=1. Comparing figure 8.2.1 with the X=0.75 experimental data (figures 7.2.2.31 and 8.5.1) we see the model displays the correct low temperature/long τ_c fall-off at 4.5MHz and the double minimum for F⩬4.5MHz. Looking at the longest τ_c in the frequency direction, the model has clearly reproduced the minimum in frequency at 4.5MHz as $J_2(\omega_{He}+\omega_N) \rightarrow J_2(0)$.

- Models 10 &12 treat coupling of ^{3}He with ^{11}B and ^{14}N together.

  Features; Instead of a full treatment involving three mutually coupled differential equations with one for each spin magnetisation, the ^{11}B Larmor or ^{14}N quadrupolar resonance has been just ‘tacked on’ to the model for simplicity − ie. a second ρ_2 term for the extra spin is appended to equation 8.25. This approximation assumes the two substrate spins do not couple significantly with each other of course. The purpose of these models is to investigate the effect of the two dominant substrate spins present together to see if there is an effect beyond a purely additive one.

  Conclusion; The results are only a combination of previous models − Double T_1 minima in τ_c are restricted to 1.1MHz⩽F⩽1.6MHz and 3.7MHz⩽F⩽5.7MHz.

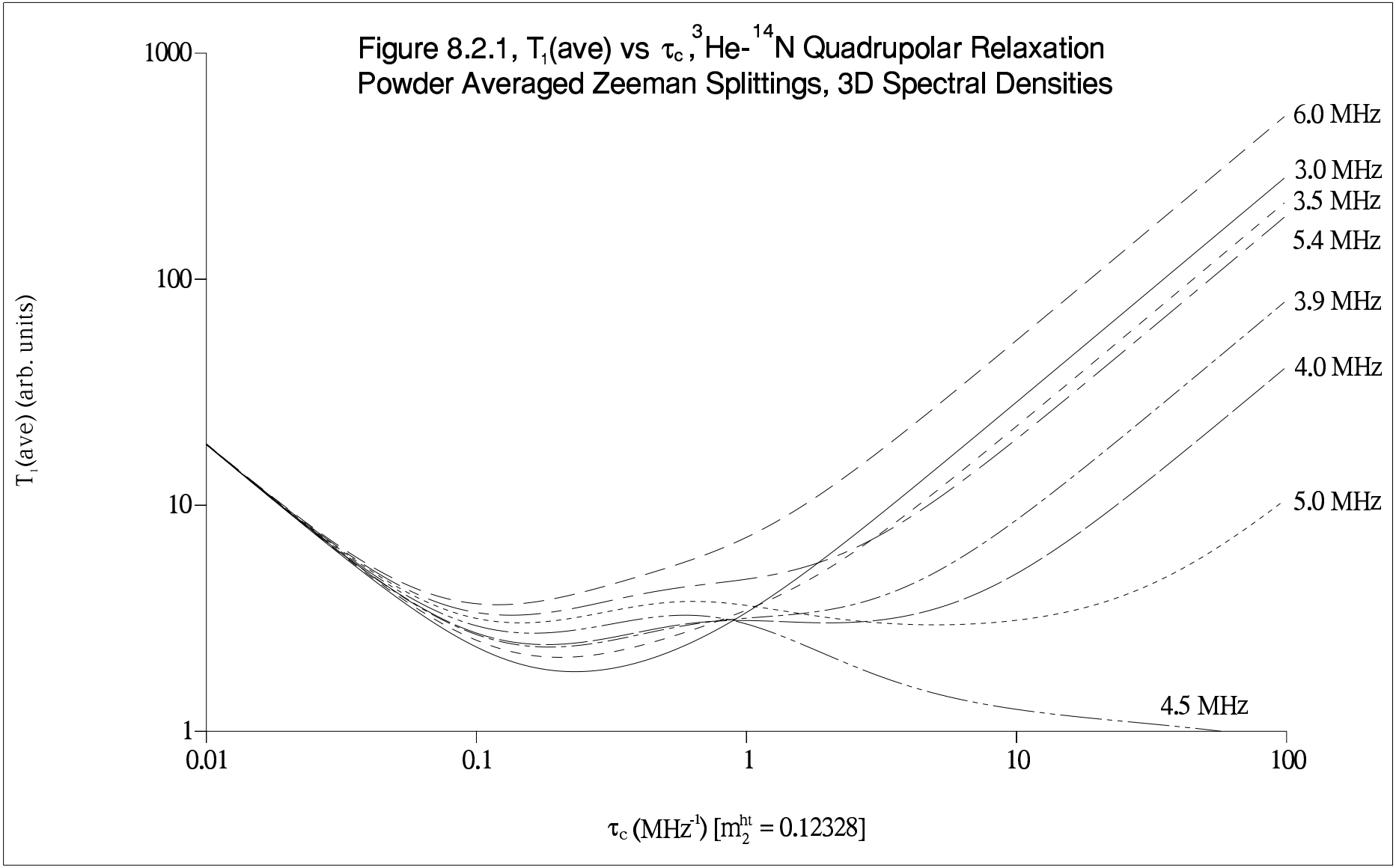
Figure 8.2.1, T1(ave) vs τc, 3He-14N Quadrupolar Relaxation
Powder Averaged Zeeman Splittings, 3D Spectral Densities
1000
100
10
1
T1(ave) (arb. units)
0.01
0.1
1
10
100
τc (MHz-1) [m2ht = 0.12328]
6.0 MHz
3.0 MHz
3.5 MHz
5.4 MHz
3.9 MHz
4.0 MHz
5.0 MHz
4.5 MHz

- Models 14−16 also treat $^{14}N-^{3}He$ coupled relaxation but include an additional empirical ^{14}N contribution at twice the ^{14}N quadrupole frequency (ie. at 2 × 4.5MHz).

  Rational: There is a small dip in the ^{3}He T_1 frequency profile at 2 × 3.49MHz in addition to the main minimum at 3.49MHz (the solid molecular nitrogen quadrupole frequency) in the ^{3}He on N_2 on CaF_2 work of Van Keuls et. al. **218**,**219**. These models attempt to emulate the effect of that double frequency resonance.

  Conclusion; Double minima in τ_c occur for 3.7MHz⩽*F*⩽5.5MHz and 8.5MHz⩽*F*⩽10.0MHz and does not solve the restricted frequency range-of-occurrence of double-minima problem. Model 15 like models 10 and 12 additionally include an ^{11}B Larmor frequency contribution and similarly produced double minima for 1.1MHz⩽*F*⩽1.6MHz, 3.8MHz⩽*F*⩽5.3MHz and 8.5MHz⩽*F*⩽10.0MHz.

- Models 19,20 & 23 treat $^{14}N-^{3}He$ coupling where the EFG at the ^{14}N nucleus is asymmetric.

  Rational; Hexagonal BN with its planar structure (figure 3.2.1) has trigonal symmetry in the plane **83**,**84** giving it cylindrical symmetry about the B−N bond axis which produces the EFG. The question arises as to whether the ^{14}N spins in the surface basal planes could experience an additional EFG component out of the surface plane due to the adsorbed $^{3}He-^{14}N$ 'bond' breaking the symmetry of the EFG at the ^{14}N nucleus? This is possible but seems unlikely due to the low polarisability of the helium atom.

  Features; The models use 3D spectral densities with and without the Zeeman splitting (actually shifting since there is no degeneracy in the asymmetric case) of the quadrupole line. The asymmetric EFG splits the degenerate $-1\leftrightarrow0$ and $0\leftrightarrow+1$ transitions to give three frequencies ω_{yz}, ω_{xz} and ω_{xy} as described is reference **47/p.251**.

  Conclusion; Double minima in τ_c occur over a wider overall range of frequencies for certain values of η the asymmetry

parameter (§2.1). Typically 1.3MHz⩽*F*⩽6.5MHz. However there are gaps in frequency unlike the experimental data with the low frequency bunch (typically around 1MHz) being due to the low frequency ω_{xy} term. Also, T_1 @minimum#1 (the shorter τ_c minimum) increases with frequency but T_1 @minimum#2 is anomalous and does not. Removing the ω_{xy} contribution does not eliminate the anomalous behaviour.

• Models 21 & 22 attempt to emulate the case of $^{14}N-^{3}He$ relaxation where the substrate or film is inhomogeneous. This is done by averaging the spectral densities over a distribution of τ_c about the nominal value. 3D spectral densities are used.

Conclusion; There is no evidence that the spread of τ_c's assist double minima to occur at higher frequencies, eg. *F*>5.7MHz.

• Models 24−30 treat $^{14}N-^{3}He$ relaxation and introduce the $\tau_c^{Jhm\_sf}$ scaling factor.

Rational; Although both the ^{3}He homonuclear and ^{3}He−substrate cross relaxation channels are modulated by the same motion − namely motion in the helium film, the two mechanisms do

Figure 8.2.2, Helium-3 in the $\sqrt{3} \times \sqrt{3}$ R30 Registered Structure adsorbed on Hexagonal Boron Nitride.

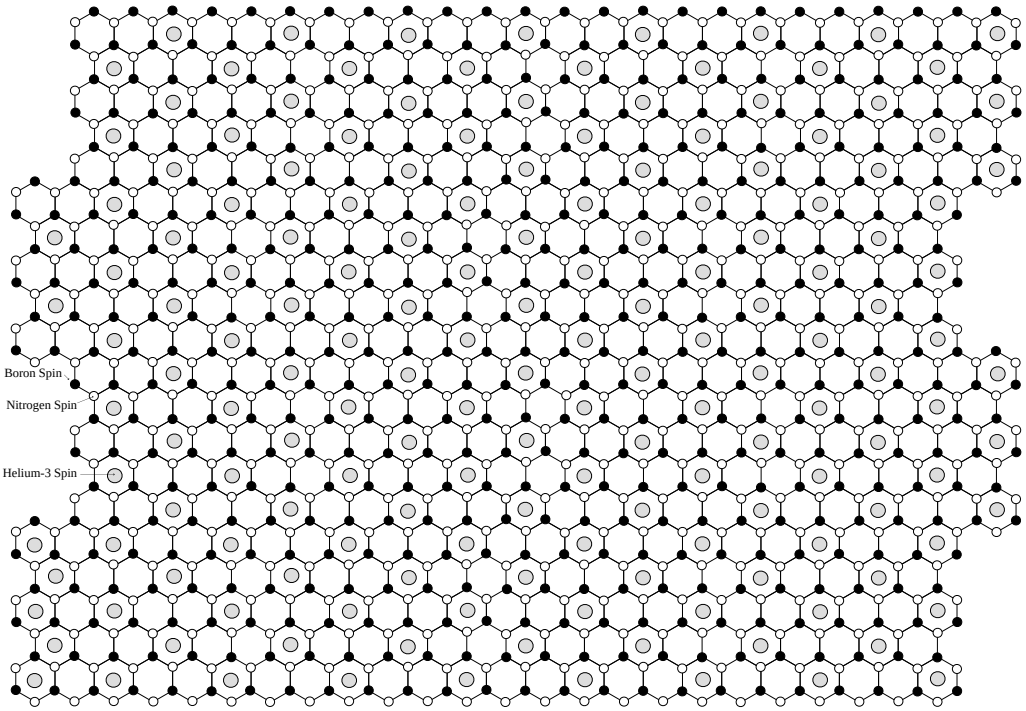

not necessarily experience the same motional speed. Consider a helium spin in figure 8.2.2 diffusing across the BN surface. At this coverage it is evident the ^{3}He spins will typically pass over several substrate spins, with the opportunity for mutual spins flips, in the time needed to encounter and flip via another ^{3}He spin. $\tau_c^{Jhm\_sf}$ describes this feature of the system. It is the factor τ_c is multiplied by before being used in evaluating T_1 in equation 8.25 via equation 2.2.16.

Features; 3D spectral densities used. Models produced both with and without Zeeman splitting of the quadrupolar line.

Results; For suitable values of $\tau_c^{Jhm\_sf}$, $\tau_c^{Jhm\_sf} \leqslant 0.01$ and $\tau_c^{Jhm\_sf} \geqslant 10$ double minima occur for all ^{3}He Larmor frequencies F, $2.7 \leqslant F \leqslant 10.7$MHz tested except where $F \approx 4.5$MHz where a gap can occur as discussed before due to the long time τ_c fall-off as $\omega_{He}+\omega_N \rightarrow 0$. Using a lower value for the ^{14}N F_Q eg. 3.0MHz or 1.5MHz also yield double minima over the above frequency range. In particular using $F_Q \ll 2.7$MHz, eg. F_Q=1.5MHz gives an unbroken set of double minima over the range $2.7 \leqslant F \leqslant 10.7$MHz. Figure 8.2.3 shows ^{3}He T_1 *vs* τ_c for a range of frequencies − correctly displaying the characteristics of the $X \geqslant 0.8$ experimental T_1 *vs* $1/T$ data. Figure 8.2.4 shows the model can produce T_1 at the minima linear in frequency data too. At the high temperature/short τ_c minimum#1 T_1(ave) *vs* F almost goes though the origin as expected for this homonuclear dominated minimum. Eg. T_1@minimum = ω_0/m_2 in the usual homonuclear dipolar relaxation case. The heteronuclear dominated minimum#2 is a straight line for most of the frequency range, deviating only as $F \rightarrow F_Q$=1.5MHz. Figure 8.2.5 shows the effect on the minima of varying m_2^{hm} − the high T/short τ_c minimum#1 rapidly deepens as m_2^{hm} is increased as expected while the lower T minimum#2 is little affected. In the physical system m_2^{hm} and m_2^{ht} will increase together as coverage is raised of course. Adding in Zeeman splitting

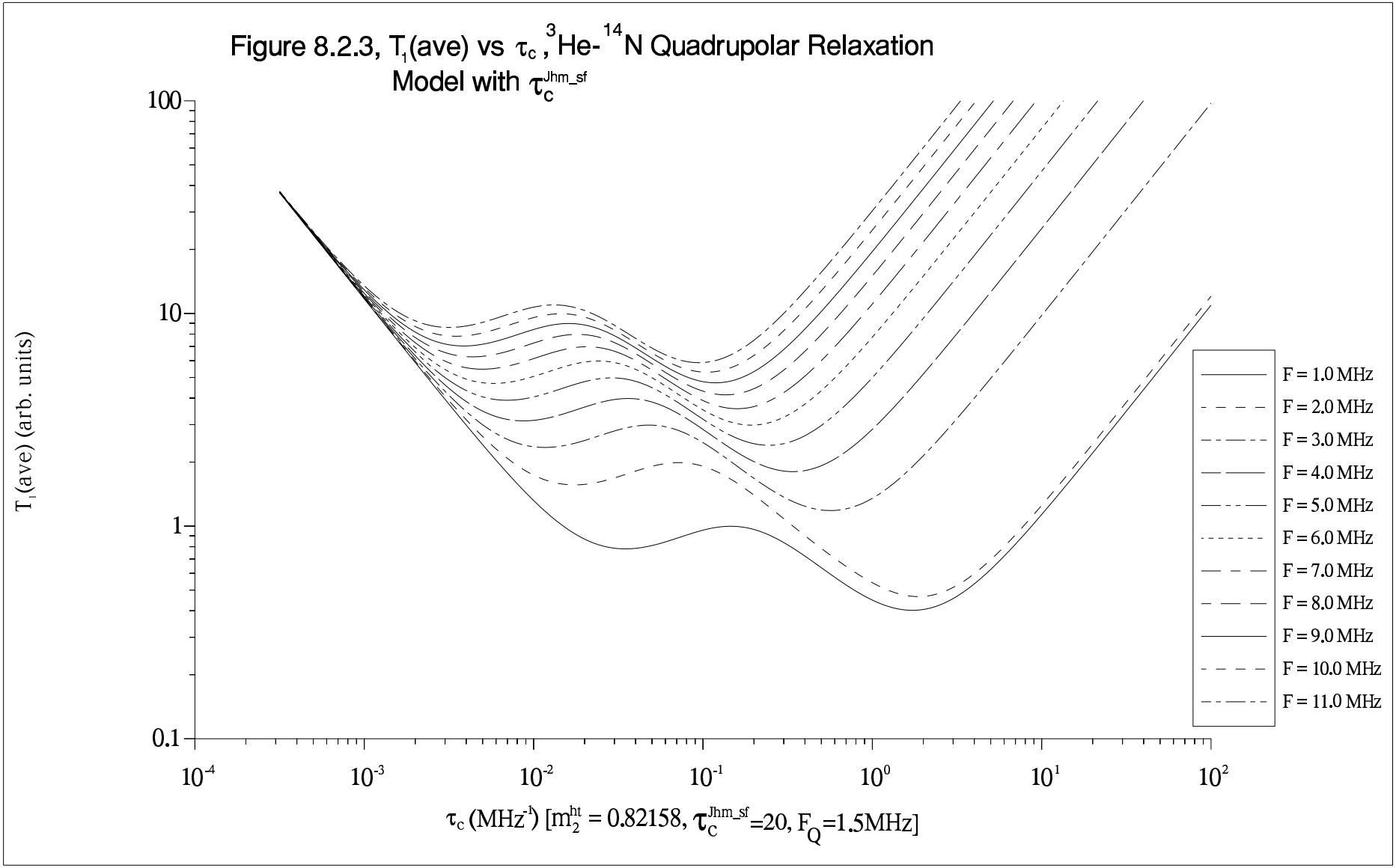
Figure 8.2.3, T_1(ave) vs τ_c, ^{3}He-^{14}N Quadrupolar Relaxation
Model with $\tau_c^{Jhm\_sf}$
100
10
1
0.1
T_1(ave) (arb. units)
10^{-4}
10^{-3}
10^{-2}
10^{-1}
10^{0}
10^{1}
10^{2}
τ_c (MHz^{-1}) [m_2^{ht} = 0.82158, $\tau_c^{Jhm\_sf}$=20, F_Q=1.5MHz]
F = 1.0 MHz
F = 2.0 MHz
F = 3.0 MHz
F = 4.0 MHz
F = 5.0 MHz
F = 6.0 MHz
F = 7.0 MHz
F = 8.0 MHz
F = 9.0 MHz
F = 10.0 MHz
F = 11.0 MHz

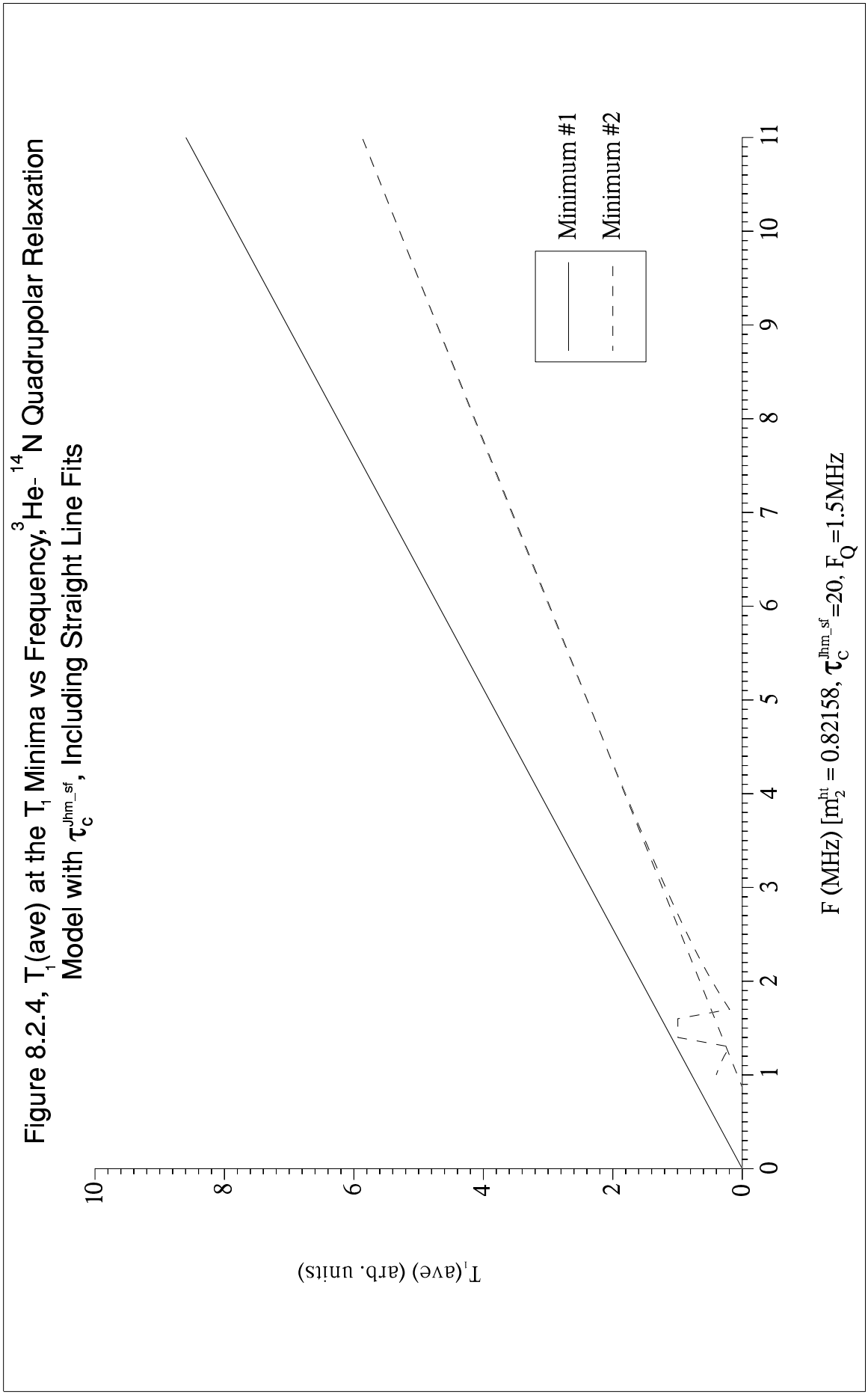
Figure 8.2.4, T_1(ave) at the T_1 Minima vs Frequency, ^{3}He-^{14}N Quadrupolar Relaxation
Model with $\tau_c^{Jhm\_sf}$, Including Straight Line Fits
T_1(ave) (arb. units)
F (MHz) [m_2^{ht} = 0.82158, $\tau_c^{Jhm\_sf}$=20, F_Q=1.5MHz
Minimum #1
Minimum #2
0
2
4
6
8
10
0
1
2
3
4
5
6
7
8
9
10
11

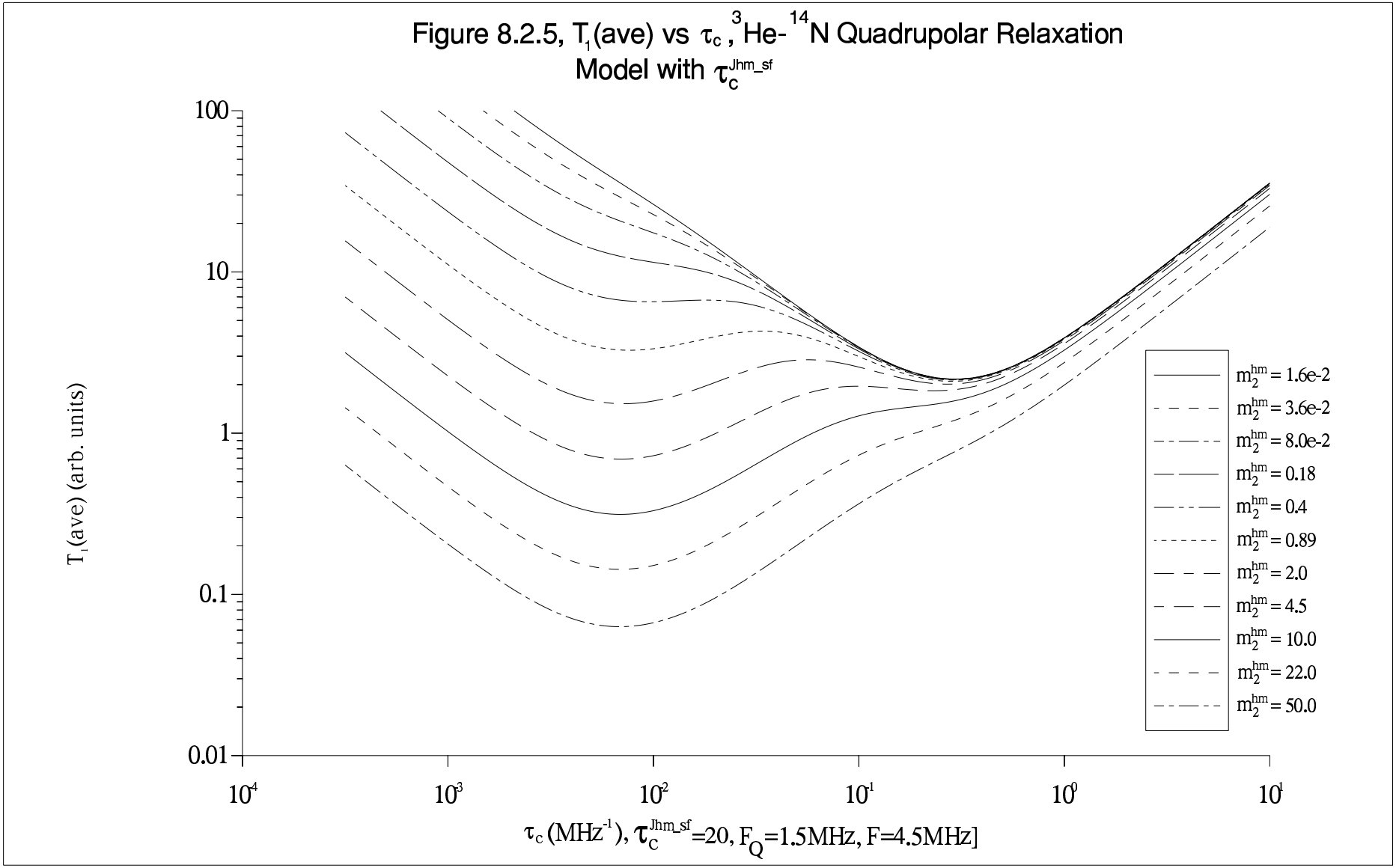
Figure 8.2.5, T_1(ave) vs τ_c, ^{3}He-^{14}N Quadrupolar Relaxation Model with $\tau_c^{Jhm\_sf}$
T_1(ave) (arb. units)
100
10
1
0.1
0.01
10^{-4}
10^{-3}
10^{-2}
10^{-1}
10^{0}
10^{1}
τ_c (MHz^{-1}), $\tau_C^{Jhm\_sf}$=20, F_Q=1.5MHz, F=4.5MHz]
m_2^{hm} = 1.6e-2
m_2^{hm} = 3.6e-2
m_2^{hm} = 8.0e-2
m_2^{hm} = 0.18
m_2^{hm} = 0.4
m_2^{hm} = 0.89
m_2^{hm} = 2.0
m_2^{hm} = 4.5
m_2^{hm} = 10.0
m_2^{hm} = 22.0
m_2^{hm} = 50.0

of the ^{14}N line has little effect other than slightly reducing the range of occurrence of double minima. Finally, model 30 treats ^{11}B−^{3}He relaxation simply by substituting the ^{14}N quadrupole frequency by the ^{11}B Larmor frequency, $F_Q = \gamma_B B_0$. This gives a very similar set of double minima since the equivalent F_Q=1.9MHz. Naturally, the frequency dependence will be quite different.

Conclusion; Introducing $\tau_c^{Jhm\_sf}$ unlike previous modifications to the basic model allows the models to correctly reproduce the four key features of the experimental data laid out at the beginning of this section. Therefore all the following models for fitting the experimental data incorporate it.

8.3 Data Fitting Models

The next step was to produce fitting models for use with the Marquardt-Fletcher non-linear least squares fitting software so that experimental data could be fitted to the models, the model parameters extracted and used to interpret the physics of the experimental system. Fit models to treat T_1 frequency dependence data at a single temperature have been produced, as have fit models for T_1 temperature dependence or combined temperature dependence + frequency dependence datasets. The main difference between the earlier fit models developed and later ones is in the way the temperature dependence is handled. Initially a simple activation law was used to describe the change in τ_c with T but physical changes such as melting and layer promotion make this often an indifferent approximation. So, later models build on and enhance the activation law in various ways. Below are listed all the fitting models currently provided by the NLLSQ_MODEL program which was developed for the purpose. The fit model's name, features, adjustable parameters and rationale for developing are each summarised. NB: For convenience the units used are; ‘times/ MHz^{-1}’, ‘frequencies/MHz’, ‘energies/Kelvin’, ‘Rates/MHz and ‘temperatures/Kelvin’

Listing 8.3.1, Temperature and Frequency Dependence Fitting Models

- Model 0: Features; Fits T_1(ave) to τ_c, F_Q is the ^{14}N quadrupole frequency
  Parameters; $\tau_c^{Jhm\_sf}$, m_2^{hm}, m_2^{ht} & F_Q
  Rationale; Testing purposes only.

- Model 2: Features; Fits T_1(ave) to temperature T. Treats homonuclear relaxation only. Correlation time $\tau_c=\tau_0\exp(E_a/T)$. τ_0 is the inverse activation attempt rate and E_a the Activation energy. See also §1.10.4.
  Parameters; τ_0, m_2^{hm} & E_a
  Rationale; Testing only

- Model 3: Features; Fits T_1(ave) to temperature T. Treats homonuclear relaxation only. Includes the low temperature temperature independent exchange rate $1/\tau_c^{ex}$. Correlation time τ_c is, $1/\tau_c = 1/\tau_c^{ex} + 1/\tau_c^{t}$. $\tau_c^{t}=\tau_0\exp(E_a/T)$.
  Parameters; τ_0, m_2^{hm}, E_a & τ_c^{ex}
  Rationale; Testing only, illustrates the need to include the exchange contribution in temperature dependence data.

- Model 5: Features; Fits T_1(ave) to temperature T. Treats homonuclear and heteronuclear relaxation. τ_c as above.
  Parameters; τ_0, $\tau_c^{Jhm\_sf}$, m_2^{hm}, m_2^{ht}, F_Q, E_a & τ_c^{ex}
  Rationale; Simplest model treating both homonuclear and heteronuclear relaxation.

- Model 5B: Features; As Model 5 but replaces τ_0 with $R_{\tau 0}$ & τ_c^{ex} with $R_{\tau cex}$ where $R_{\tau 0} = 1/\tau_0$ & $R_{\tau cex} = 1/\tau_c^{ex}$
  Parameters; $R_{\tau 0}$, $\tau_c^{Jhm\_sf}$, m_2^{hm}, m_2^{ht}, F_Q, E_a, $R_{\tau cex}$ & const(optional)
  Rationale; Substitutions make programming the functions simpler and use the more natural rates in place of times. The const parameter optionally adds in a frequency independent (ie. non dipolar) component to T_1. The motivation is to test improvements to fit quality, particularly in the frequency domain, which might be achieved by taking into account a non dipolar mechanism such as relaxation by PMIs. The optional const parameter can be added to T_1 as a simple constant, (T_1(total) = T_1(dipolar) + const) or as a relaxation rate, $1/T_1$(total) = $1/T_1$(dipolar) + 1/const.

- Model 5B_2D:
  Features; As Model 5B but uses 2D spectral densities as described in §8.2
  Parameters; $R_{\tau 0}$, $\tau_c^{Jhm\_sf}$, m_2^{hm}, m_2^{ht}, F_Q, E_a, $R_{\tau cex}$ & const(optional)
  Rationale; Compare with Model 5B. Can 2D effects (eg. low frequency divergence) explain the data?

- Model 5B_11B:
  Features; As Model 5B but treats ^{11}B–^{3}He relaxation by replacing the ^{14}N F_Q with the ^{11}B Larmor frequency, $\gamma_B B_0$
  Parameters; $R_{\tau 0}$, $\tau_c^{Jhm\_sf}$, m_2^{hm}, m_2^{ht}, E_a, $R_{\tau cex}$ & const(optional)
  Rationale; Investigate if ^{11}B–^{3}He relaxation could explain the data.

- Model 5B_wq2_11B:
  Features; As Models 5B & 5B_11B but with the $^{11}B-^{3}He$ contribution (m_2^{ht2}) an addition to the ^{14}N one.
  Parameters; $R_{\tau 0}$, $\tau_c^{Jhm\_sf}$, m_2^{hm}, m_2^{ht}, F_Q, E_a & $R_{\tau cex}$, m_2^{ht2} & const(optional)
  Rationale; Investigate if $^{11}B-^{3}He$ + $^{14}N-^{3}He$ relaxation could explain the data, in particular improve fit quality in the frequency direction.

- Model 5B_wq2:
  Features; As Model 5B_wq2_11B but with the additional contribution (m_2^{ht2}) a second quadrupole (frequency F_{Q2}) rather than a ^{11}B Larmor one.
  Parameters; $R_{\tau 0}$, $\tau_c^{Jhm\_sf}$, m_2^{hm}, m_2^{ht}, F_Q, E_a, $R_{\tau cex}$, m_2^{ht2}, F_{Q2} & const(optional)
  Rationale; Investigate if $^{14}N-^{3}He$ + a second (eg. the ^{11}B quadrupole line) coupled relaxation pathway could explain the data, in particular improve fit quality in the frequency direction.

- Model 6: Features; As Model 5B but with an 'index' power term 'i' added to the activation law, $\tau_c^t=\tau_0 \exp(E_a/T)^i$
  Parameters; $R_{\tau 0}$, $\tau_c^{Jhm\_sf}$, m_2^{hm}, m_2^{ht}, F_Q, E_a, $R_{\tau cex}$, i & const(optional)
  Rationale; Attempt to better model effectively a range of activation energies which change over T. c.f. the 'T1Index' & 'T2Index' fits of §7 which successfully modelled a range of relaxation times during the course of sub-exponential decays.

- Model 6_2D:
  Features; As Model 6 but uses 2D spectral densities as described in §8.2
  Parameters; $R_{\tau 0}$, $\tau_c^{Jhm\_sf}$, m_2^{hm}, m_2^{ht}, F_Q, E_a, $R_{\tau cex}$, i & const(optional)
  Rationale; See Models 6 & 5B_2D.

- Model 6_11B:
  Features; As Model 6 but treats $^{11}B-^{3}He$ relaxation by replacing the ^{14}N F_Q with the ^{11}B Larmor frequency, $\gamma_B B_0$
  Parameters; $R_{\tau 0}$, $\tau_c^{Jhm\_sf}$, m_2^{hm}, m_2^{ht}, E_a, $R_{\tau cex}$ & i
  Rationale; See Models 6 & 5B_11B.

- Model 7: Features; As Model 5B but using a double activation law $1/\tau_c^t = R_{\tau 0\_a} \exp(-E_{a\_a}/T) + R_{\tau 0\_b} \exp(-E_{a\_b}/T)$
  Parameters; $R_{\tau 0\_a}$, $R_{\tau 0\_b}$, $\tau_c^{Jhm\_sf}$, m_2^{hm}, m_2^{ht}, F_Q, E_{a_a}, E_{a_b}, $R_{\tau cex}$ & const(optional)
  Rationale; Attempt to better model effectively a range of activation energies which change over T. eg. the 2D solid and its melt.

- Model 7_2D:
  Features; As Model 7 but uses 2D spectral densities as described in §8.2
  Parameters; $R_{\tau 0\_a}$, $R_{\tau 0\_b}$, $\tau_c^{Jhm\_sf}$, m_2^{hm}, m_2^{ht}, F_Q, E_{a_a}, E_{a_b}, $R_{\tau cex}$ & const(optional)
  Rationale; See Models 7 & 5B_2D.

- Model 7_11B:
  Features; As Model 7 but treats $^{11}B-^{3}He$ relaxation by replacing

the ^{14}N F_Q with the ^{11}B Larmor frequency, $\gamma_B B_0$
Parameters; $R_{\tau 0\_a}$, $R_{\tau 0\_b}$, $\tau_c^{Jhm\_sf}$, m_2^{hm}, m_2^{ht}, E_{a_a}, E_{a_b} & $R_{\tau cex}$
Rationale; See Models 7 & 5B_11B.

- Model 8: Features; A combination of Models 6 & 7 comprising a double activation law with 'index' modifications.
  $1/\tau_c^t = R_{\tau 0\_a}\exp(-E_{a\_a}/T)^{i1} + R_{\tau 0\_b}\exp(-E_{a\_b}/T)^{i2}$
  Parameters; $R_{\tau 0\_a}$, $R_{\tau 0\_b}$, $\tau_c^{Jhm\_sf}$, m_2^{hm}, m_2^{ht}, F_Q, E_{a_a}, E_{a_b}, $R_{\tau cex}$, $i1$, $i2$ & const(optional)
  Rationale; A further attempt to better model effectively a range of activation energies which change over T. eg. the 2D solid and its melt.

- Model 8_2D:
  Features; As Model 8 but uses 2D spectral densities as described in §8.2
  Parameters; $R_{\tau 0\_a}$, $R_{\tau 0\_b}$, $\tau_c^{Jhm\_sf}$, m_2^{hm}, m_2^{ht}, F_Q, E_{a_a}, E_{a_b}, $R_{\tau cex}$, $i1$, $i2$ & const(optional)
  Rationale; See Models 8 & 5B_2D.

- Model 8_11B:
  Features; As Model 8 but treats ^{11}B–^{3}He relaxation by replacing the ^{14}N F_Q with the ^{11}B Larmor frequency, $\gamma_B B_0$
  Parameters; $R_{\tau 0\_a}$, $R_{\tau 0\_b}$, $\tau_c^{Jhm\_sf}$, m_2^{hm}, m_2^{ht}, E_{a_a}, E_{a_b}, $R_{\tau cex}$, $i1$ & $i2$
  Rationale; See Models 8 & 5B_11B.

- Model 9: Features; Implements an activation law which is switchable in T about a switching temperature T_{switch}.
  $1/\tau_c = S_{w1}\,R_{\tau 0\_1}\exp(-E_{a\_1}/T) + S_{w2}\,R_{\tau 0\_2}\exp(-E_{a\_2}/T)$
  For $T<T_{switch}$, $S_{w1}=1$ & $S_{w2}=0$
  For $T\geqslant T_{switch}$, $S_{w1}=0$ & $S_{w2}=1$
  Parameters; $R_{\tau 0\_1}$, $R_{\tau 0\_2}$, $\tau_c^{Jhm\_sf}$, m_2^{hm}, m_2^{ht}, F_Q, E_{a_1}, E_{a_2} & $R_{\tau cex}$
  Rationale; Attempts to model the situation where two quite separate regimes each with distinct activation law parameters exist in T – eg. a solid and its melt. T_{switch} is entered by the user and is not a fitted parameter. Performance of this model was very poor due to the unphysical discontinuity at T_{switch} and its non-adjustability by the fitting procedure and it was never used.

- Model 10: Features; τ_c as Model 9 but with the S_{wn} controlled as follows;
  $S_{w1} = 1/(1+\exp(a[T-T_{switch}])$ & $S_{w2} = 1-S_{w1}$
  Parameters; $R_{\tau 0\_1}$, $R_{\tau 0\_2}$, $\tau_c^{Jhm\_sf}$, m_2^{hm}, m_2^{ht}, F_Q, E_{a_1}, E_{a_2}, $R_{\tau cex}$, a, T_{switch} & const(optional)
  Rationale; Attempts to model the situation where two quite separate regimes each with distinct activation law parameters exist in T – eg. a solid and its melt. The changeover between the two activation law regimes is controlled by the NLLSQ_MODEL program via the T_{switch} parameter which is now adjustable. The software enforces continuity across the boundary and the cross-over region between the two activation laws is now finite in T, its width being controlled by the a parameter.

- Model 10_2D:
  Features; As Model 10 but uses 2D spectral densities as described

in §8.2

Parameters; $R_{\tau 0\_1}$, $R_{\tau 0\_2}$, $\tau_c^{Jhm\_sf}$, m_2^{hm}, m_2^{ht}, F_Q, E_{a_1}, E_{a_2}, $R_{\tau cex}$, a, T_{switch} & const(optional)

Rationale; See Models 10 & 5B_2D.

- Model 10_11B:

  Features; As Model 10 but treats ^{11}B–^{3}He relaxation by replacing the ^{14}N F_Q with the ^{11}B Larmor frequency, $\gamma_B B_0$

  Parameters; $R_{\tau 0\_1}$, $R_{\tau 0\_2}$, $\tau_c^{Jhm\_sf}$, m_2^{hm}, m_2^{ht}, E_{a_1}, E_{a_2}, $R_{\tau cex}$, a, T_{switch} & const(optional)

  Rationale; See Models 10 & 5B_11B

- Model 10_wq2_11B:

  Features; As Models 10 & 10_11B but with the ^{11}B–^{3}He contribution (m_2^{ht2}) an addition to the ^{14}N one.

  Parameters; $R_{\tau 0\_1}$, $R_{\tau 0\_2}$, $\tau_c^{Jhm\_sf}$, m_2^{hm}, m_2^{ht}, F_Q, E_{a_1}, E_{a_2}, $R_{\tau cex}$, a, T_{switch} m_2^{ht2} & const(optional)

  Rationale; Investigate if ^{11}B–^{3}He + ^{14}N–^{3}He relaxation could explain the data, in particular improve fit quality in the frequency direction.

- Model 10_wq2:

  Features; As Model 10_wq2_11B but with the additional contribution (m_2^{ht2}) a second quadrupole (frequency F_{Q2}) rather than a ^{11}B Larmor one.

  Parameters; $R_{\tau 0\_1}$, $R_{\tau 0\_2}$, $\tau_c^{Jhm\_sf}$, m_2^{hm}, m_2^{ht}, F_Q, E_{a_1}, E_{a_2}, $R_{\tau cex}$, a, T_{switch}, m_2^{ht2}, F_{Q2} & const(optional)

  Rationale; Investigate if ^{14}N–^{3}He + a second (eg. the ^{11}B quadrupole line) coupled relaxation pathway could explain the data, in particular improve fit quality in the frequency direction.

- Model 11: Features; As Model 10 but with three separate activation law regimes in T.

  $1/\tau_c = S_{w1}\, R_{\tau 0\_1} \exp(-E_{a\_1}/T) +$
  $S_{w2}\, R_{\tau 0\_2} \exp(-E_{a\_2}/T) +$
  $S_{w3}\, R_{\tau 0\_3} \exp(-E_{a\_3}/T)$.

  The S_{wn} are controlled as follows;
  $F_{n1} = 1/(1+\exp(a_1[T-T_{switch\_1}])$,
  $F_{n2} = 1/(1+\exp(a_2[T-T_{switch\_2}])$,
  $S_{w1} = F_{n1}$, $S_{w2} = F_{n2}-F_{n1}$ & $S_{w3} = 1-F_{n2}$

  Parameters; $R_{\tau 0\_1}$, $R_{\tau 0\_2}$, $R_{\tau 0\_3}$, $\tau_c^{Jhm\_sf}$, m_2^{hm}, m_2^{ht}, F_Q, E_{a_1}, E_{a_2}, E_{a_3}, $R_{\tau cex}$, a_1, a_2, T_{switch_1}, T_{switch_2} & const(optional)

  Rationale; Attempts to model the situation where three quite separate regimes each with distinct activation law parameters exist in T – eg. a solid, its melt and a partially desorbed system. The changeover between the three activation law regimes is controlled by the NLLSQ_MODEL program via the T_{switch_1} and T_{switch_2} adjustable parameters. The software enforces continuity across the two boundaries and the width of the two cross-over regions between the three regimes in T is controlled by the a_1 and a_2 parameters.

- Model 11_2D:

  Features; As Model 11 but uses 2D spectral densities as described in §8.2

Parameters; $R_{\tau 0\_1}$, $R_{\tau 0\_2}$, $R_{\tau 0\_3}$, $\tau_c^{Jhm\_sf}$, m_2^{hm}, m_2^{ht}, F_Q, E_{a_1}, E_{a_2}, E_{a_3}, $R_{\tau cex}$, a_1, a_2, T_{switch_1}, T_{switch_2} & const(optional)
Rationale; See Models 11 & 5B_2D.

Listing 8.3.2, Frequency Dependence only Fitting Models

- Model F: Features; As Model 5B but without T dependence, eg. $1/\tau_c = const = R_{\tau cex}$ at low temperatures.
  Parameters; $\tau_c^{Jhm\_sf}$, m_2^{hm}, m_2^{ht}, F_Q & $R_{\tau cex}$
  Rationale; Simplest model treating both homonuclear and heteronuclear relaxation in frequency dependence.

- Model F_11B:
  Features; As Model 5B_11B but without T dependence, eg. $1/\tau_c = const = R_{\tau cex}$ at low temperatures.
  Parameters; $\tau_c^{Jhm\_sf}$, m_2^{hm}, m_2^{ht} & $R_{\tau cex}$
  Rationale; Investigate if $^{11}B-^{3}He$ relaxation could explain the frequency dependence data.

- Model F_2D:
  Features; As Model 5B_2D but without T dependence, eg. $1/\tau_c = const = R_{\tau cex}$ at low temperatures.
  Parameters; $\tau_c^{Jhm\_sf}$, m_2^{hm}, m_2^{ht}, F_Q & $R_{\tau cex}$
  Rationale; Compare with model F. Can 2D effects (eg. low frequency divergence) explain the frequency dependence data?

- Model F_2D_11B:
  Features; As Models F_2D and F_11B
  Parameters; $\tau_c^{Jhm\_sf}$, m_2^{hm}, m_2^{ht} & $R_{\tau cex}$
  Rationale; Compare with above models. Can a combination of 2D effects (eg. low frequency divergence) and $^{11}B-^{3}He$ relaxation explain the frequency dependence data?

Notes: The software implementing the models in listing 8.3.1 and 8.3.2 include several other important features, including;

- Apply upper and lower limits to the values F_Q can take to aid convergence and prevent silly results. In particular a lower limit of 0.05MHz was used for most of the temperature dependence containing datasets since extrapolation in frequency to much lower values (eg. $F_Q \ll 2.7$MHz) by the algorithm cannot produce sensible values and can cause ill conditioning in the numerical calculations.

- Optionally enforce the occurrence of double minima in T_1 in T at specified frequency/frequencies − ie. reject fits which do not generate double minima.

- Perform a 'Log fit'. Ie. Instead of fitting to T_1 *vs* T data, fit to log(T_1) *vs* T. Using log(T_1) tends to emphasize the T_1 minima as features in the T_1 *vs* 1/T plots at the expense of the less interesting data at the extremities of temperature, in particular the data at $T \gg T$(T_1-minima) where T_1 is largest.

8.4 Trials of the Data Fitting Models

Before embarking on a systematic fitting of all the experimental data the relative usefulness of the fitting model functions of listings 8.3.1 and 8.3.2 was evaluated in an extensive set of trials − the idea being to obtain a manageably small set of fitting models with the best performance to apply to the full set of experimental data. In doing these trials some useful general points about fitting the data were elucidated − eg. the applicability of 2D effects to the data. Most of the trials were performed using data at X=0.9 where the film is incommensurate solid and melts in a simple way. The main points of the trials are summarised here.

- Comparing Models 5B, 6, 7, 8 & 10, the fit quality improves markedly as 5B→6→7→8→10. Model 5B followed by Model 10 are the most reliable in the sense of consistently giving sensible fits to the data. Figure 8.4.1 shows an example of these fits.
- Model 11 can produce closer fits than Model 10 but has the drawback of being much more sensitive to the initial guess parameters values it is supplied with.
- Comparing Models 5B, 6, 7, 8 & 10 with 5B_11B, 6_11B, 7_11B, 8_11B & 10_11B and using all available data at X=0.9, ie. 4.5MHz and 2.7MHz temperature dependence + 1.1K and 4.2K frequency dependence combined:− The *_11B fits were inferior in all respects − suggesting ^{3}He−^{11}B relaxation does not explain the X>0.75 data even though the lack of minima in frequency indicates the effective substrate frequency must be <2.7MHz.
- Comparing the frequency dependence only models using X=0.9/1.1K data results in; F Fit ⇒ reasonable, F_11B ⇒ very poor, F_2D ⇒ best and F_11B_2D ⇒ very poor. The F_2D fits tend to be best where T_1 is linear in frequency, in accordance with the work of Cowan **[68]**, but can be temperamental.

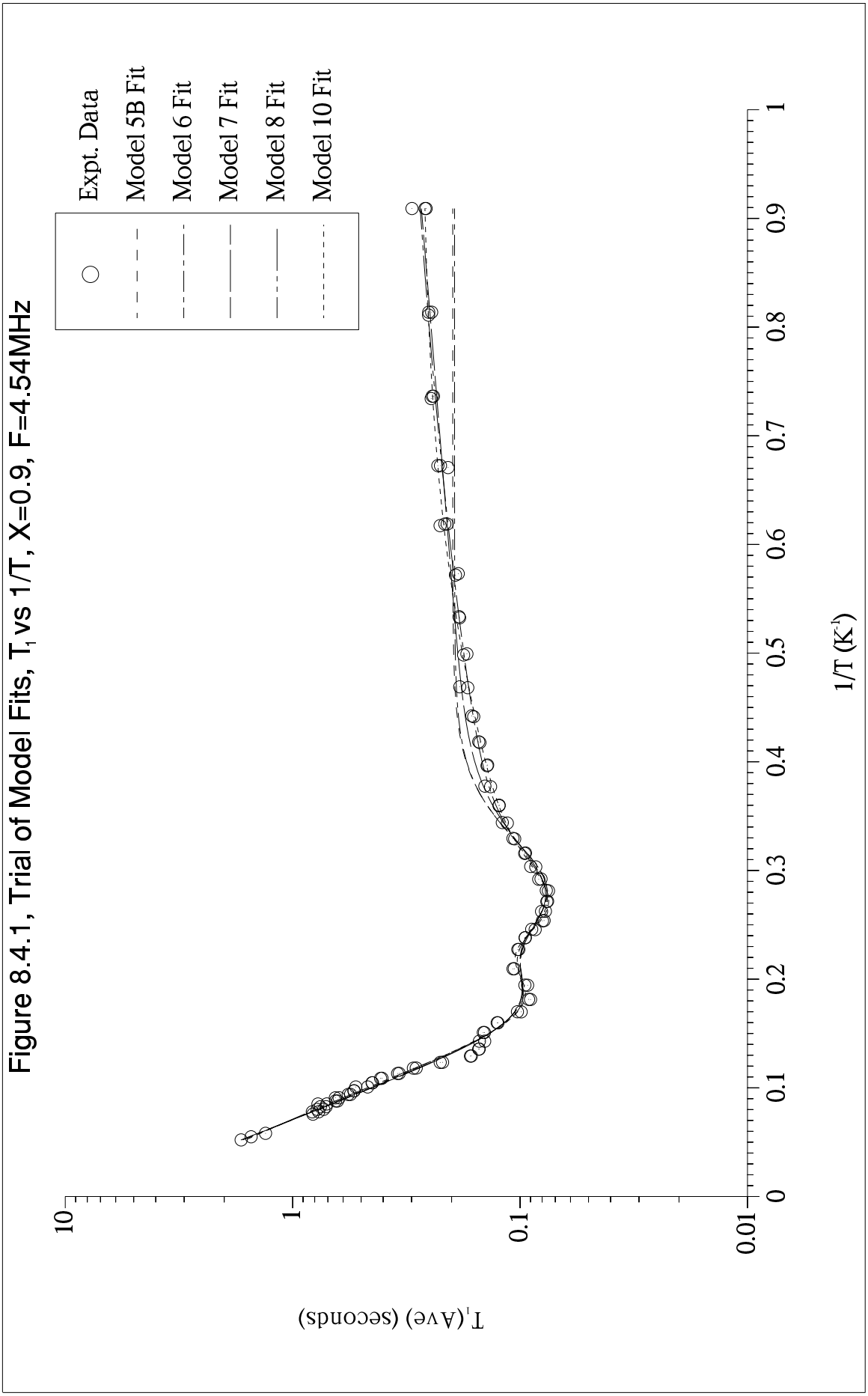
Figure 8.4.1, Trial of Model Fits, T1 vs 1/T, X=0.9, F=4.54MHz
Expt. Data
Model 5B Fit
Model 6 Fit
Model 7 Fit
Model 8 Fit
Model 10 Fit
T1(Ave) (seconds)
10
1
0.1
0.01
0
0.1
0.2
0.3
0.4
0.5
0.6
0.7
0.8
0.9
1
1/T (K-1)

- Using the log-fit feature gives much improved fitting through double minima.
- On comparing Models 5B, 6, 7, 8 & 10 with 5B_2D, 6_2D, 7_2D, 8_2D & 10_2D usually worse results are produced by the *_2D fits, implying that at elevated temperatures where layer promotion etc. operates, 2D effects which might be significant at low T in a localised film, are not apparent.
- Investigating adding a constant term to T_1(ave) brought marginal improvements in fit quality. The improvement was biggest at the Model 5B end of the list of models and least at the Model 10 end. Adding the constant as a relaxation time rather than as a relaxation rate gave the best results. Conclusion: Adding a frequency independent contribution to T_1(ave) does little to correct the model's less-than-perfect fitting performance/suitability in frequency.
- Comparison of the Model 5B, 5B_wq2 & 5B_wq2_11B fits and their Model 10 series counterparts:− The extra substrate quadrupole or ^{11}B Larmor frequency contributions add little or nothing to overall fit quality. Moreover they tend to worsen the fit in the frequency direction − the one thing it might have been hoped they would improve. Conclusion: Appealing to extra substrate resonance frequencies does not appear to cure the models' deficiencies. However it must be borne in mind that for X>0.75 data, all of the important substrate frequencies probably occur < 2.7MHz and therefore involve extrapolation below the experimental frequency range, thereby exacerbating the vagaries of the NLLSQ fitting process.

As a result of the above trials, all of the temperature dependence and combined temperature + frequency dependence datasets have been fitted using models 5B and 10 with the log-fit option and no constant term. Frequency dependence data has mostly been fitted to all four frequency dependence only models of listing 8.3.2 since they are are comparatively simple to use but on many occasions they (particularly F_11B and F_2D_11B) gave silly results which were ignored. Model F fits were nearly always used.

8.5 Fitting the Data to the Models

This section treats the fits to the data at each coverage in turn. Selected data+fits are plotted and their fit parameters given together with a discussion of the

points raised by the fit. Where available, sets of data have been combined to form compound datasets for fitting to − the idea being to furnish the fitting software with extra information (eg. adding frequency dependence data to temperature dependence data to help the software converge to a sensible value of a particular, especially, frequency-dependent fit parameter, eg. F_Q). Three compound datasets have been defined. They are labelled '*ALL*', '*ALL_1100*' and '*EVERYTHING*' for convenience. '*ALL*' comprises all of the 4.5MHz temperature dependence data − up and down temperature sweep T_1 measurements. '*ALL_1100*' comprises the '*ALL*' dataset plus the 1.1K frequency data where the 1.1K data uses either 'T_1' or '$T_1(1/e)$' values. The '*EVERYTHING*' dataset contains all available data at that coverage − typically the '*ALL*' 4.5MHz temperature + 2.7MHz temperature + 1.1K frequency + 4.2K frequency dependence data. Progressing from '*ALL*'→'*ALL_1100*'→'*EVERYTHING*' datasets tends to give more stable , sensible values to some fit parameters (eg. F_Q) at the expense of overall fit quality due to the inadequacies of the models.

***X*=0.75,** Figure 8.5.1 plots the '*ALL*' dataset fit. The raw results from the NLLSQ_MODEL software follow. A couple of words about them: (1) Too much concern should not be given to the error bars values − The rather large numbers are due to general compromises made in applying these simple models to the experimental data and probably also to the way they are estimated, (see §6.3.2) rather than a general failure of the model to fit the data by locating the global minimum. (2) The parameter listed as 'wq' is synonymous with $2 \times F_Q$.

The Model 10 fits are the by far the closest, following the data throughout. However it must be remembered the large minimum at 7.6K through which the 10 fits have fit is due to the edge-film and is therefore an artifact in this context. The Model 5B fit puts its minimum around 4.3K where the 'true' basal-plane minimum is − see figure 7.2.3.8. All the fits show the low temperature fall-off due to $F_Q \approx 4.5$MHz, especially Model 10 fits where the $R_{\tau cex} \rightarrow 0$ suggesting exchange has been all but suppressed by the substrate lattice potentials. Listing 8.5.1 shows some non-uniqueness in F_Q from the Model 10 fits. Whatever the precise actual value of F_Q the $\tau_c^{Jhm\_sf} \sim 1$ fit does show how strong the effect of relatively weak heteronuclear relaxation when $J_2(\omega_{He}+\omega_N) \rightarrow J_2(0)$ can be from its m_2^{ht} value.

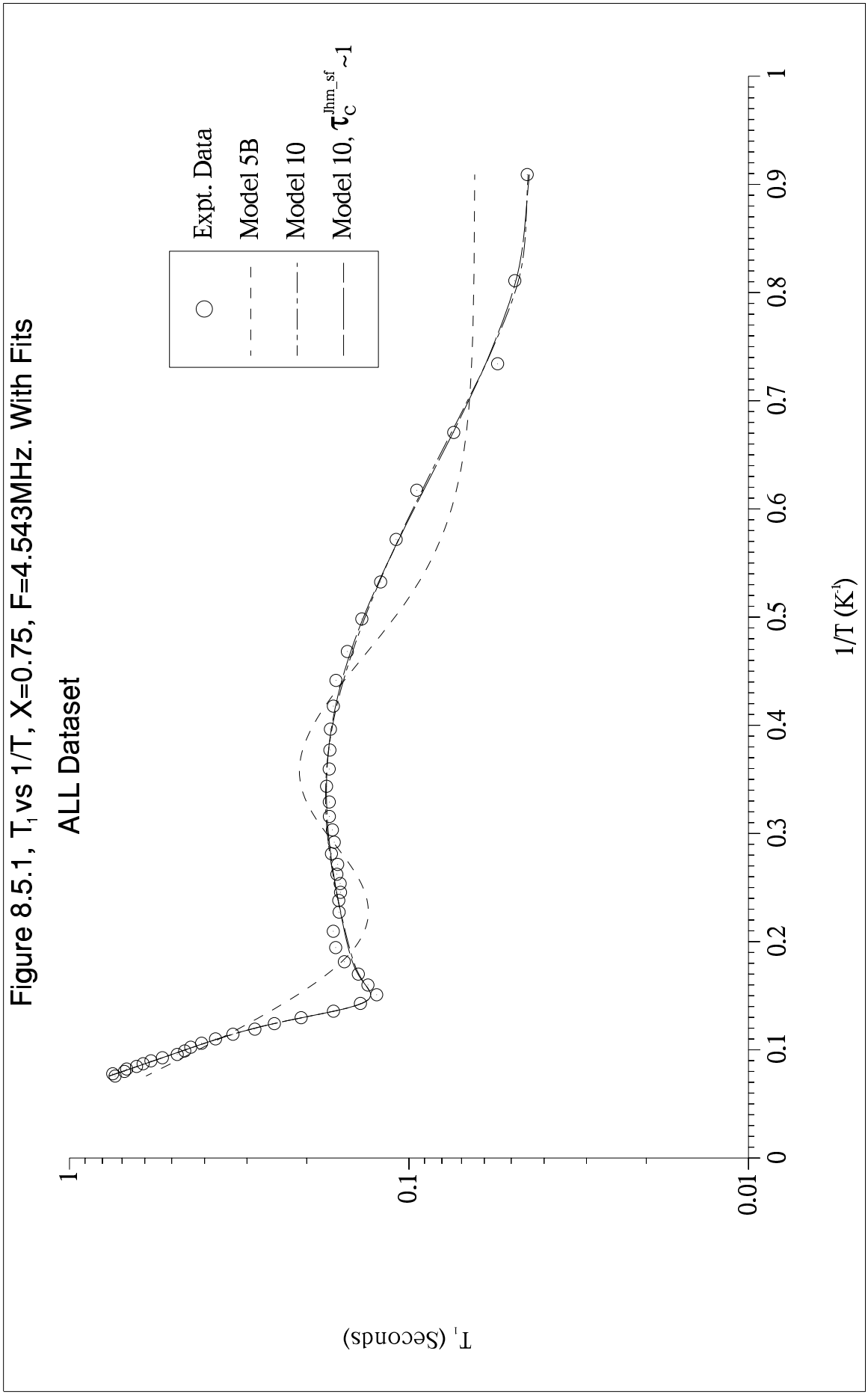
Figure 8.5.1, T_1 vs 1/T, X=0.75, F=4.543MHz. With Fits
ALL Dataset
Expt. Data
Model 5B
Model 10
Model 10, $\tau_C^{lhm\_sf}$ ~1
T_1 (Seconds)
1/T (K^{-1})
1
0.1
0.01
0
0.1
0.2
0.3
0.4
0.5
0.6
0.7
0.8
0.9
1

Listing 8.5.1, NLLSQ_MODEL Results for *X*=0.75, *ALL* Dataset

```
Model 5B Fit
Sum of squares at convergence:    2.32839748

Fitted parameters;

rt0      =    1936.64     +/-    4437.46
tcjhm_sf =    8.85902     +/-    20.2640
m2hm     =    22.8786     +/-    2.11204
m2ht     =    7.81209     +/-    15.0645
wq       =    9.07229     +/-    252.266
Ea       =    15.2794     +/-   0.827626
rtcex    =    1.04335     +/-    2.93013


Model 10 Fit
Sum of squares at convergence:   0.511769030E-01

Fitted parameters;

rt0_1    =    100.859     +/-    38.1833
rt0_2    =    5047.96     +/-    2014.43
tcjhm_sf =    10.7197     +/-    4.19210
m2hm     =    22.6790     +/-   0.444902
m2ht     =    13.2080     +/-    4.56614
wq       =    10.2767     +/-   0.412182
Ea_1     =    5.78289     +/-   0.303962
Ea_2     =    21.9693     +/-   0.694474
rtcex    =   0.151948E-06 +/-   0.202056
a        =    2.22190     +/-   0.266704
Tswitch  =    7.25495     +/-   0.649215E-01


Model 10 Fit
Sum of squares at convergence:   0.430800197E-01

Fitted parameters;

rt0_1    =    8.01493     +/-    96.7502
rt0_2    =    478.287     +/-    6036.32
tcjhm_sf =    1.03618     +/-    13.3179
m2hm     =    22.0819     +/-    4.49281
m2ht     =    1.99644     +/-    23.7397
wq       =    8.90681     +/-    2.11320
Ea_1     =    4.98978     +/-   0.441852
Ea_2     =    21.8097     +/-   0.671748
rtcex    =   0.192273E-11 +/-   0.282311E-01
a        =    2.14269     +/-   0.224750
Tswitch  =    7.24281     +/-   0.615558E-01
```

Figure 8.5.2 shows some Model F fits to the frequency data. Only Model F fits gave sensible results. The fits correctly reproduce the minimum at 4.5MHz. Note however that $\tau_c^{Jhm\_sf} < 1$ for these fits.

Listing 8.5.2, NLLSQ_MODEL Results for *X*=0.75, Frequency data

```
Model F Fit
Sum of squares at convergence:   0.709223242E-02

Fitted parameters;

tcjhm_sf =   0.137296E-01 +/-   0.262294
m2hm     =    34.1296     +/-    568.508
```

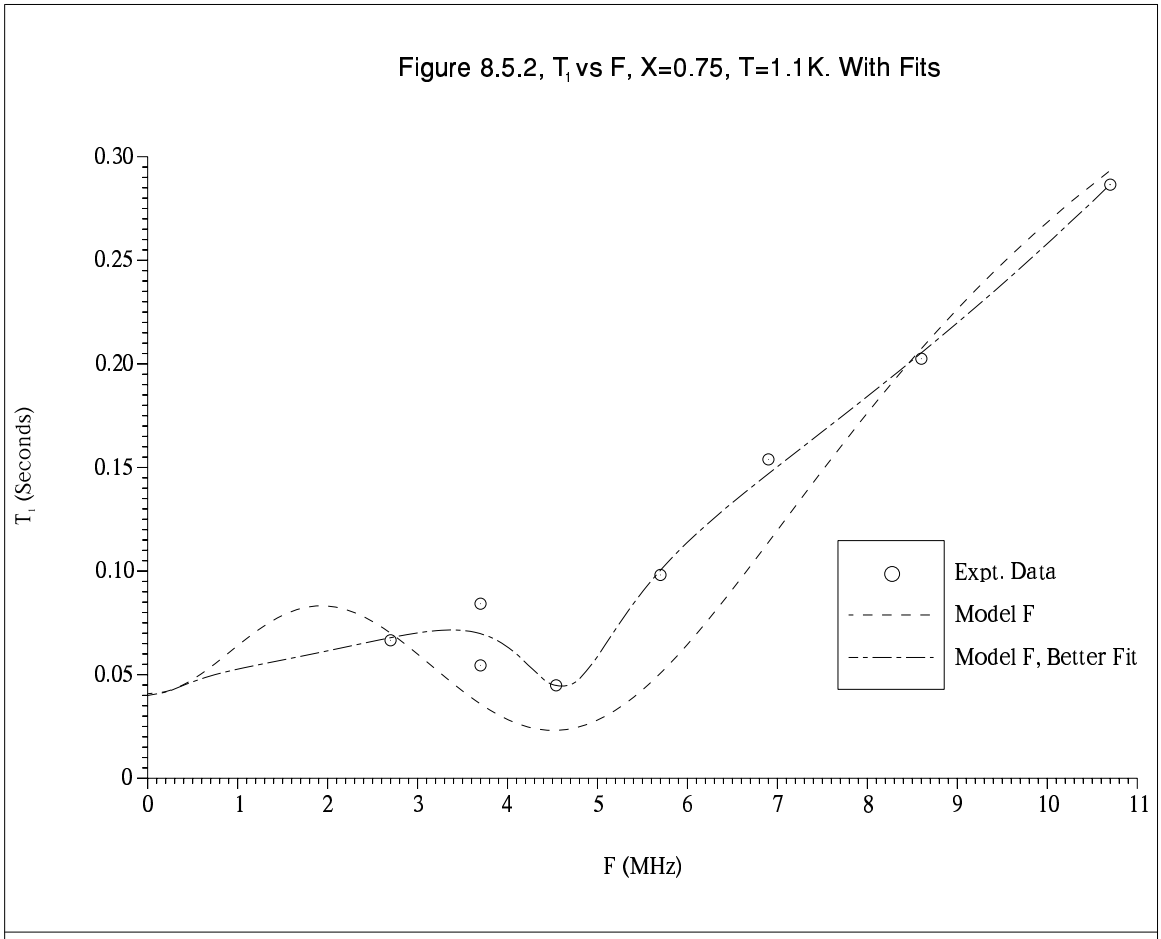
Figure 8.5.2, T_1 vs F, X=0.75, T=1.1K. With Fits
T_1 (Seconds)
0.30
0.25
0.20
0.15
0.10
0.05
0
0
1
2
3
4
5
6
7
8
9
10
11
F (MHz)
Expt. Data
Model F
Model F, Better Fit

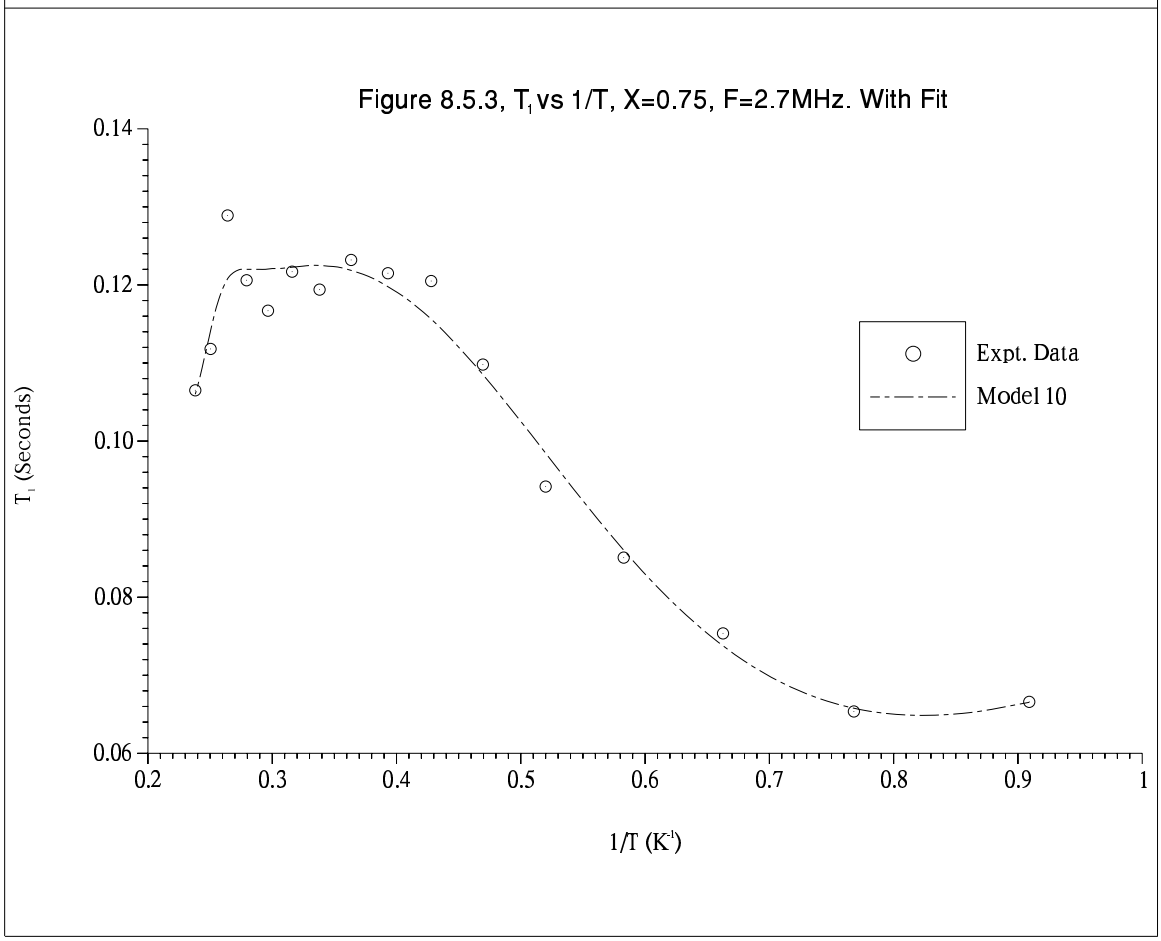
Figure 8.5.3, T_1 vs 1/T, X=0.75, F=2.7MHz. With Fit
T_1 (Seconds)
0.14
0.12
0.10
0.08
0.06
0.2
0.3
0.4
0.5
0.6
0.7
0.8
0.9
1
1/T (K^{-1})
Expt. Data
Model 10

```
m2ht     =    20.1196     +/-    10.6317
wq       =    9.03230     +/-   0.829798
rtcex    =    1.00652     +/-    1.04472


Model F Fit
Sum of squares at convergence:   0.506125089E-03

Fitted parameters;

tcjhm_sf =   0.571583E-01 +/-   0.207062E-01
m2hm     =    31.0063     +/-    3.03972
m2ht     =    3.15828     +/-    1.20774
wq       =    9.23964     +/-   0.438435
rtcex    =   0.483310     +/-   0.215860
```

Figure 8.5.3 shows the Model 10 fit to the 2.7MHz 1.1<T<4.2K temperature dependence data over which only one minimum occurs. Model 5B did not produce a good fit. It does show the steep low temperature fall-off at 4.5MHz has become a shallow minimum as $J_2(\omega_N+2.7\text{MHz}) \ll J_2(\omega_N+4.5\text{MHz})$. Listing 8.5.3 shows a sensible value for F_Q was obtained despite the Larmor frequency being $\ll F_Q$ and the absence of any frequency dependence data.

Listing 8.5.3, NLLSQ_MODEL Results for X=0.75, F=2.7MHz Data

```
Model 10 Fit
Sum of squares at convergence:   0.122771821E-01

Fitted parameters;

rt0_1    =    12.5751     +/-    146.274
rt0_2    =    14986.4     +/-    875743.
tcjhm_sf =    2.50633     +/-    30.6755
m2hm     =    15.9389     +/-    31.8337
m2ht     =    4.16530     +/-    33.6736
wq       =    5.96521     +/-    4.64558
Ea_1     =    5.20810     +/-    6.21410
Ea_2     =    32.7515     +/-    243.323
rtcex    =   0.123575     +/-    1.29677
a        =    6.59865     +/-    65.7085
Tswitch  =    3.67933     +/-    2.84930
```

Figures 8.5.4 and 8.5.5 plot the temperature and frequency dependence for the *ALL_1100* dataset fits. The temperature dependence is compromised a little at low temperatures by the frequency data but has the same general form. The frequency dependence's dip has become broader and shallower but significantly is still there − Significantly, because as listing 8.5.4 indicates $\tau_c^{Jhm\_sf} > 1$ showing that $\tau_c^{Jhm\_sf} > 1$ (which for reasons to be discussed in §8.6 is preferred to $\tau_c^{Jhm\_sf} < 1$) is compatible with a T_1 dip in F.

Figure 8.5.4, T_1 vs 1/T, X=0.75, With Fits, ALL_1100 Dataset, F=4.543MHz/T=1.1K [T_1 Data]

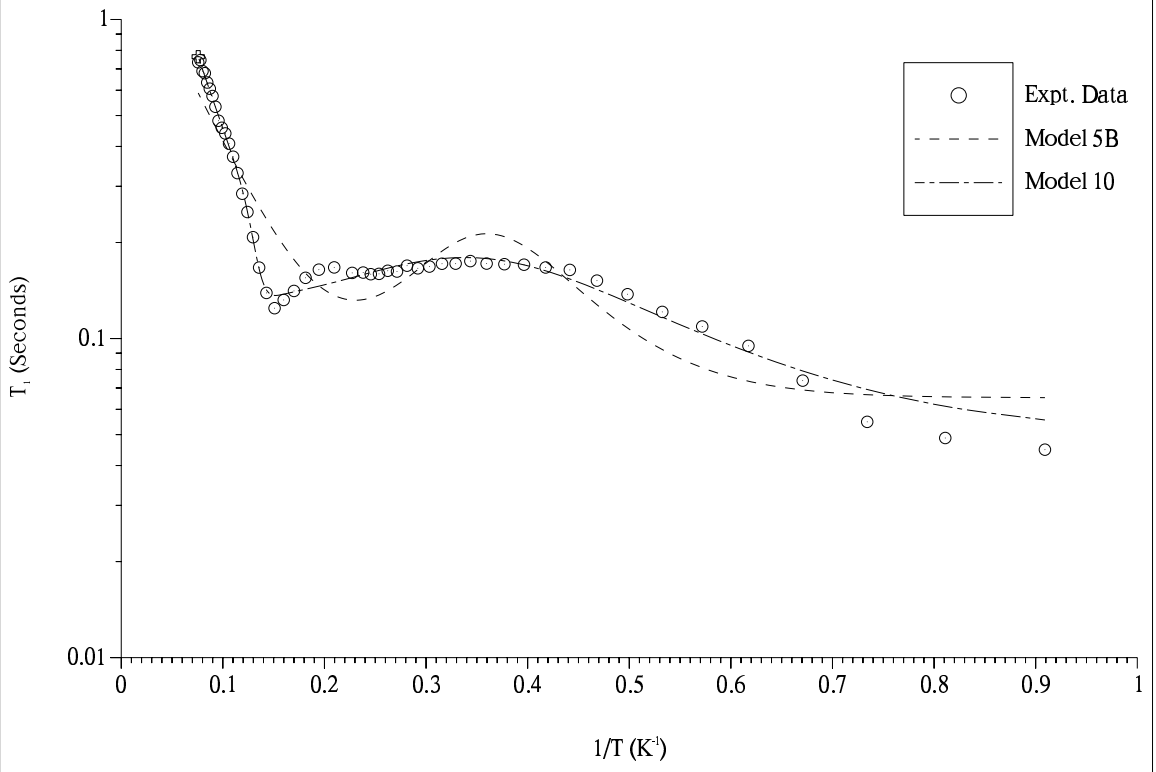

Figure 8.5.5, T_1 vs F, X=0.75, With Fits, ALL_1100 Dataset, F=4.543MHz/T=1.1K [T_1 Data]

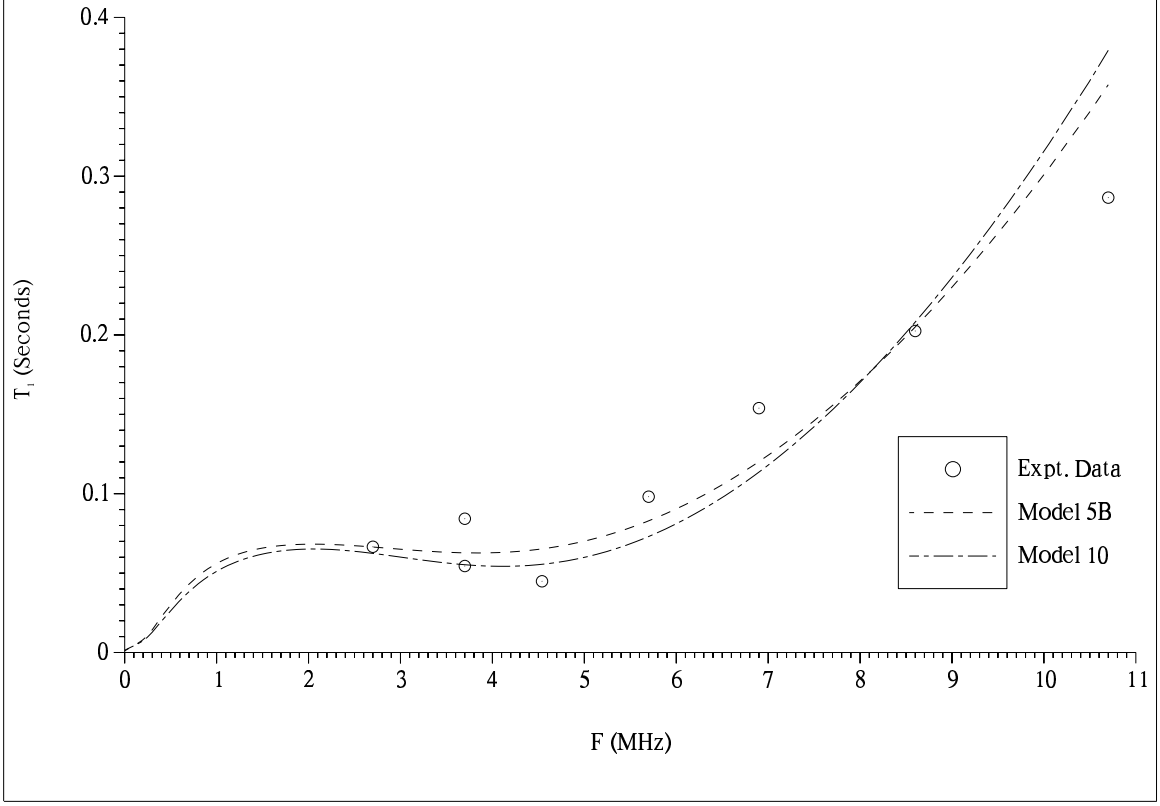

Figure 8.5.6, T_1 vs 1/T, X=0.75, With Fits, EVERYTHING Dataset, F=4.543MHz/T=1.1K [T_1 Data]

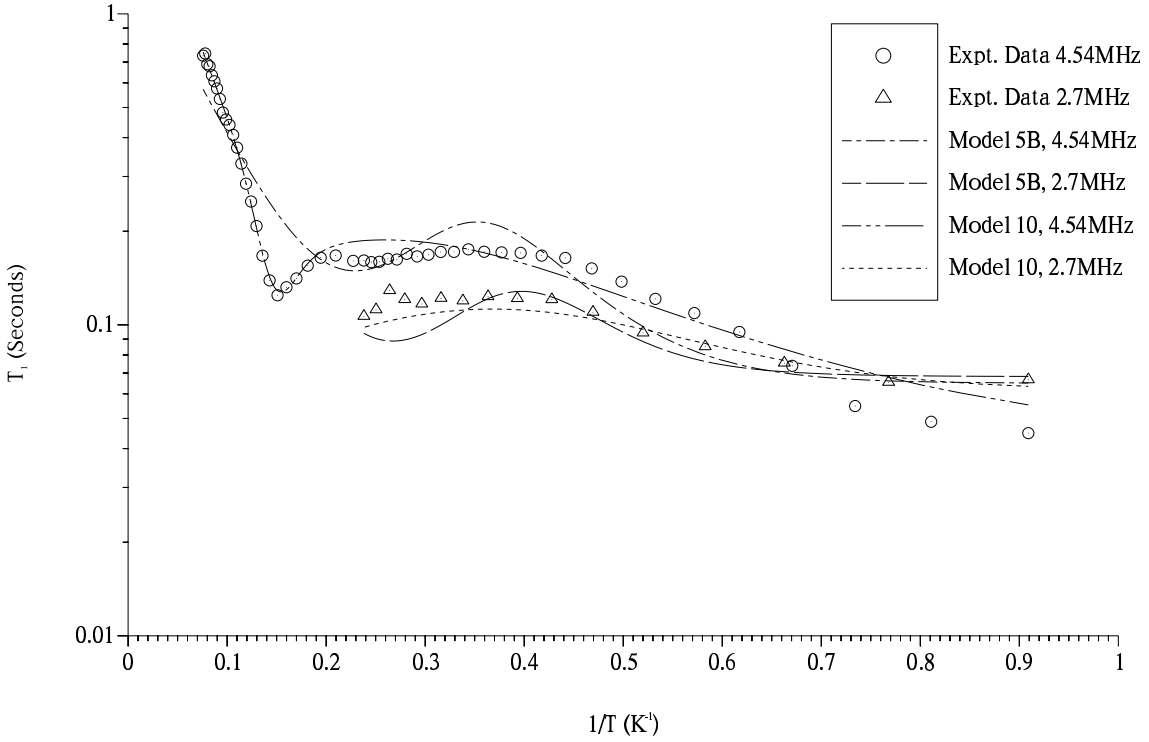

Figure 8.5.7, T_1 vs F, X=0.75, With Fits, EVERYTHING Dataset, F=4.543MHz/T=1.1K [T_1 Data]

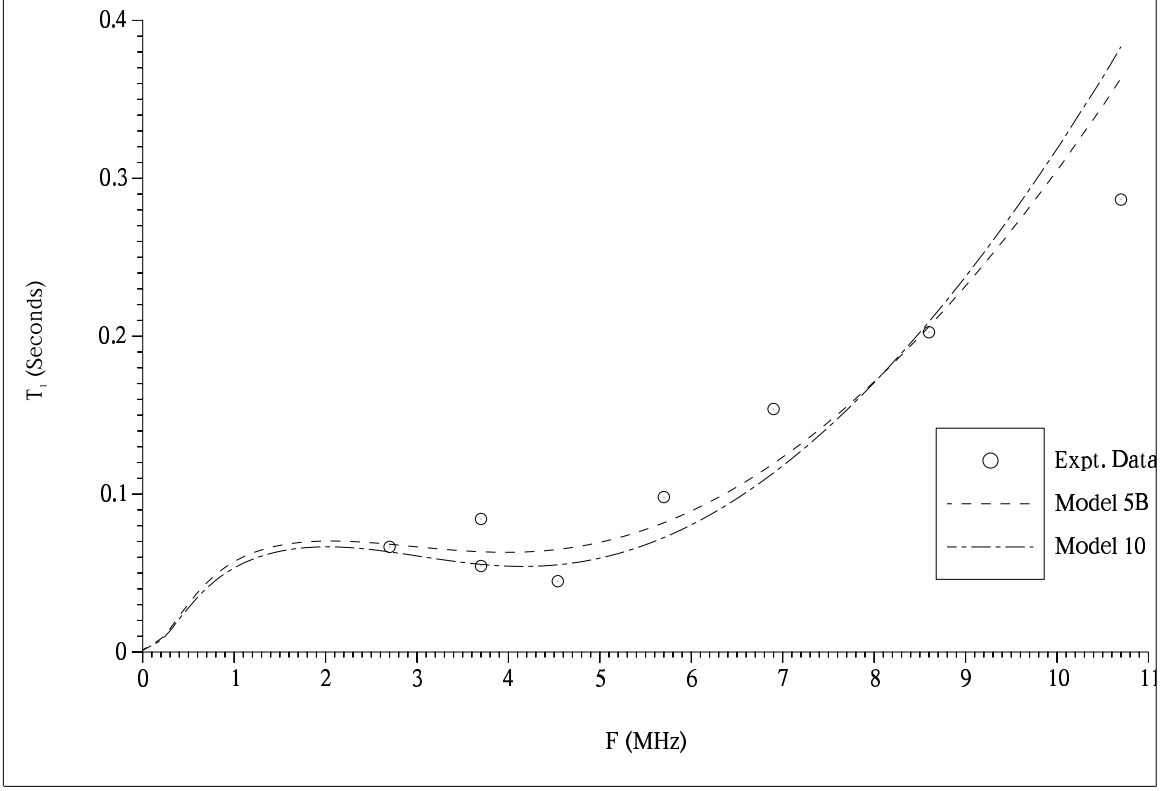

Listing 8.5.4, NLLSQ_MODEL Results for *X*=0.75, *ALL_1100* Dataset

```
Model 5B
Sum of squares at convergence:    2.87821580

Fitted parameters;

rt0      =    5167.79     +/-    1410.01
tcjhm_sf =    24.5719     +/-    4.43818
m2hm     =    23.0046     +/-    1.30399
m2ht     =    19.2080     +/-    1.64379
wq       =    8.37293     +/-   0.804092
Ea       =    14.8894     +/-   0.682133
rtcex    =    2.92734     +/-   0.338539

Model 10
Sum of squares at convergence:   0.727097463

Fitted parameters;

rt0_1    =    262.131     +/-    75.4799
rt0_2    =    7276.68     +/-    1863.16
tcjhm_sf =    16.2408     +/-    1.69444
m2hm     =    21.4992     +/-    1.33794
m2ht     =    19.7483     +/-   0.749208
wq       =    8.61739     +/-   0.316351
Ea_1     =    7.34649     +/-   0.659003
Ea_2     =    22.0493     +/-    2.45560
rtcex    =    2.17308     +/-   0.196228
a        =    2.49963     +/-    1.28811
Tswitch  =    7.42130     +/-   0.230986
```

Figures 8.5.6 and 8.5.7 plot the temperature and frequency dependence for the *EVERYTHING* dataset fits and are very similar to the *ALL_1100* fits. The 2.7MHz temperature dependence fit has produced a minimum in about the expected place for the 2.7MHz experimental points. It is evident from the compound datasets that the model/ experimental-data mismatch is largest at the lowest temperatures. A combination of 2D angular effects and the dominance of exchange motion over thermally activated vacancy tunnelling in a localised film at these temperatures seem a plausible explanation. Listing 8.5.6 gives the fit parameters.

Listing 8.5.6, NLLSQ_MODEL Results for *X*=0.75, *EVERYTHING* Dataset

```
Model 5B Fit
Sum of squares at convergence:    3.46750516

Fitted parameters;

rt0      =    3509.58     +/-    776.108
tcjhm_sf =    20.9502     +/-    2.93611
m2hm     =    20.0087     +/-   0.932210
m2ht     =    18.8551     +/-    1.10343
wq       =    8.55329     +/-   0.497093
Ea       =    14.0847     +/-   0.580682
rtcex    =    2.85859     +/-   0.281694
```

```
Model 10 Fit
Sum of squares at convergence:    1.08455565

Fitted parameters;

rt0_1    =    92.2565     +/-    22.2524
rt0_2    =    8063.95     +/-    2887.93
tcjhm_sf =    19.6367     +/-    1.77682
m2hm     =    23.4834     +/-    1.48606
m2ht     =    19.6465     +/-   0.646386
wq       =    8.67936     +/-   0.259322
Ea_1     =    5.42429     +/-   0.613445
Ea_2     =    20.0109     +/-    3.41633
rtcex    =    1.80428     +/-   0.286020
a        =    1.35717     +/-   0.358498
Tswitch  =    7.15823     +/-   0.385422
```

***X*=0.8,** Figure 8.5.8 plots the '*ALL*' dataset fit. Careful weighting of the data encompassing the minima ensures that it correctly fits the 1.233K and the 3.5K minima avoiding the temperature up-sweep/down-sweep hysteretic feature and the edge-film minimum. See §7.2.2/*X*=0.8, figures 7.2.2.37 and 7.2.3.8 for further details. Listing 8.5.7 gives the fit parameters.

Listing 8.5.7, NLLSQ_MODEL Results for *X*=0.8, *ALL* Dataset

```
Model 5B fit
(High temperature expt. data removed)
Sum of squares at convergence:   0.771200630E-01

Fitted parameters;

rt0      =    265.670     +/-    64.5990
tcjhm_sf =    8.04651     +/-    2.20593
m2hm     =    31.1333     +/-   0.121321
m2ht     =    15.3197     +/-    3.52841
wq       =    3.85172     +/-    2.06127
Ea       =    5.32611     +/-   0.130868
rtcex    =   0.172060E-07 +/-   0.127631

Model 10 Fit
Sum of squares at convergence:   0.396886420

Fitted parameters;

rt0_1    =    247.943     +/-    208.427
rt0_2    =    2587.21     +/-    2225.55
tcjhm_sf =    4.55446     +/-    3.86548
m2hm     =    31.2617     +/-   0.767260
m2ht     =    9.38750     +/-    5.76526
wq       =    6.50289     +/-    1.87399
Ea_1     =    6.54454     +/-   0.165922
Ea_2     =    20.0570     +/-   0.502752
rtcex    =   0.293590     +/-   0.124680
a        =    3.47835     +/-   0.315024
Tswitch  =    8.15884     +/-   0.340544E-01
```

Figure 8.5.9 shows the good quality Model F fit to the frequency data. Only Model F gave sensible results. Note that $\tau_c^{Jhm\_sf} < 1$ as at *X*=0.75. F_Q=0.05MHz, the software's imposed artificial lower frequency limit, which qualitatively accords with the

Figure 8.5.8, T_1 vs 1/T, X=0.8, F=4.54MHz. With Fits
ALL Dataset

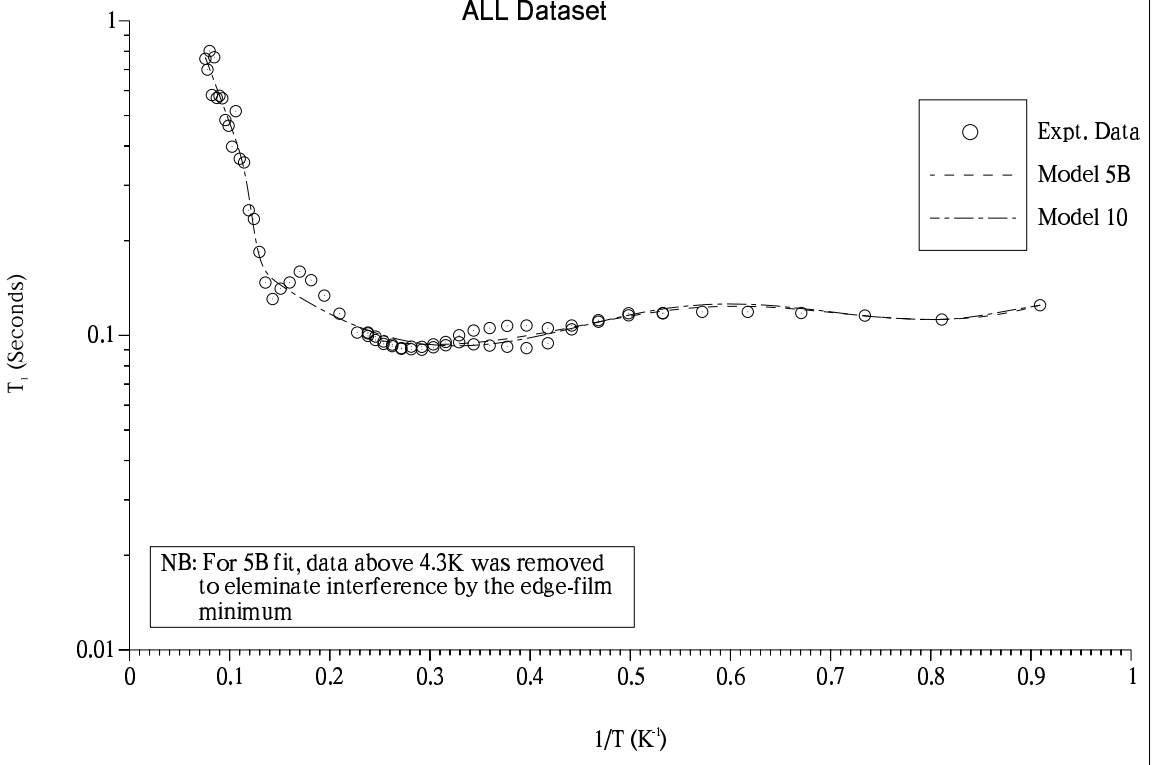

Figure 8.5.9, T_1 vs F, X=0.8, T=1.1K. With Fit
[T_1 Data]

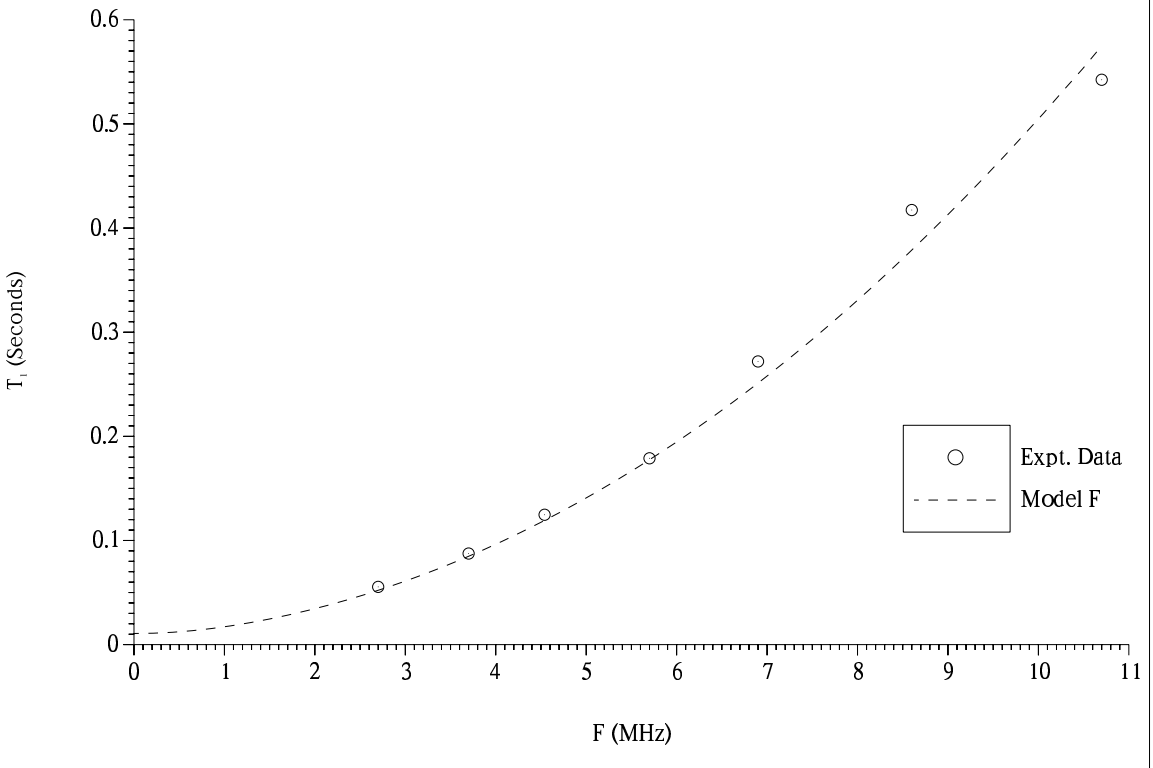

smoothly increasing frequency profile − in stark contrast with X=0.75.

Listing 8.5.8, NLLSQ_MODEL Results for X=0.8, Frequency [T_1 Data] data

```
Model F Fit
Sum of squares at convergence:   0.301961347E-02

Fitted parameters;

tcjhm_sf =   0.326389     +/-    31.7606
m2hm     =    19.2359     +/-    4298.62
m2ht     =    21.3463     +/-    1081.57
wq       =   0.100000     +/-    425.318
rtcex    =    1.09464     +/-    208.643
```

Figure 8.5.10 shows the Model 5B fit to the 2.7MHz 1.1<T<4.2K temperature dependence. The fit possesses only one minimum. It is possible the lowest T three points do describe a minimum but did not convince the model fit. Model 10 did not produce a good fit. Assuming the model fit is correct and there is no low temperature minimum, the low temperature fall-off in T_1 accords with the X=0.8, $F_Q \ll 4.5$MHz interpretation suggesting it should in fact be ~2.7MHz giving $J_2(\omega_N + 2.7\text{MHz}) \sim J_2(0)$. Listing 8.5.9 shows this is so and is in reasonable agreement with the F_Q obtained from the 4.5MHz *ALL* dataset.

Listing 8.5.9, NLLSQ_MODEL Results for X=0.8, F=2.7MHz Data

```
Model 5B Fit
Sum of squares at convergence:   0.200026109E-01

Fitted parameters;

rt0      =    452.234     +/-    5982.77
tcjhm_sf =    3.13852     +/-    51.3720
m2hm     =    25.9622     +/-    16.0665
m2ht     =    9.51823     +/-    86.5684
wq       =    5.33665     +/-    1203.84
Ea       =    13.2809     +/-    22.7213
rtcex    =    1.42036     +/-    22.902
```

Figures 8.5.11 and 8.5.12 plot the temperature and frequency dependence for the *ALL_1100* dataset fits. It was not possible to find a good Model 10 fit but the Model 5B fit compares with that of figure 8.5.8/5B showing there is little in the way of a temperature/frequency compromise. Listing 8.5.10 shows $\tau_c^{\text{Jhm\_sf}} > 1$ in contrast with the frequency dependence data alone fit − as was the case at X=0.75 − again showing $\tau_c^{\text{Jhm\_sf}} > 1$ can and does produce sensible simultaneous frequency/temperature fits. Listing 8.5.10 gives a reasonable value of F_Q, $F_Q \ll 4.5$MHz but still ~ the low MHz.

Figure 8.5.10, T_1 vs 1/T, X=0.8, F=2.7MHz, With Fit

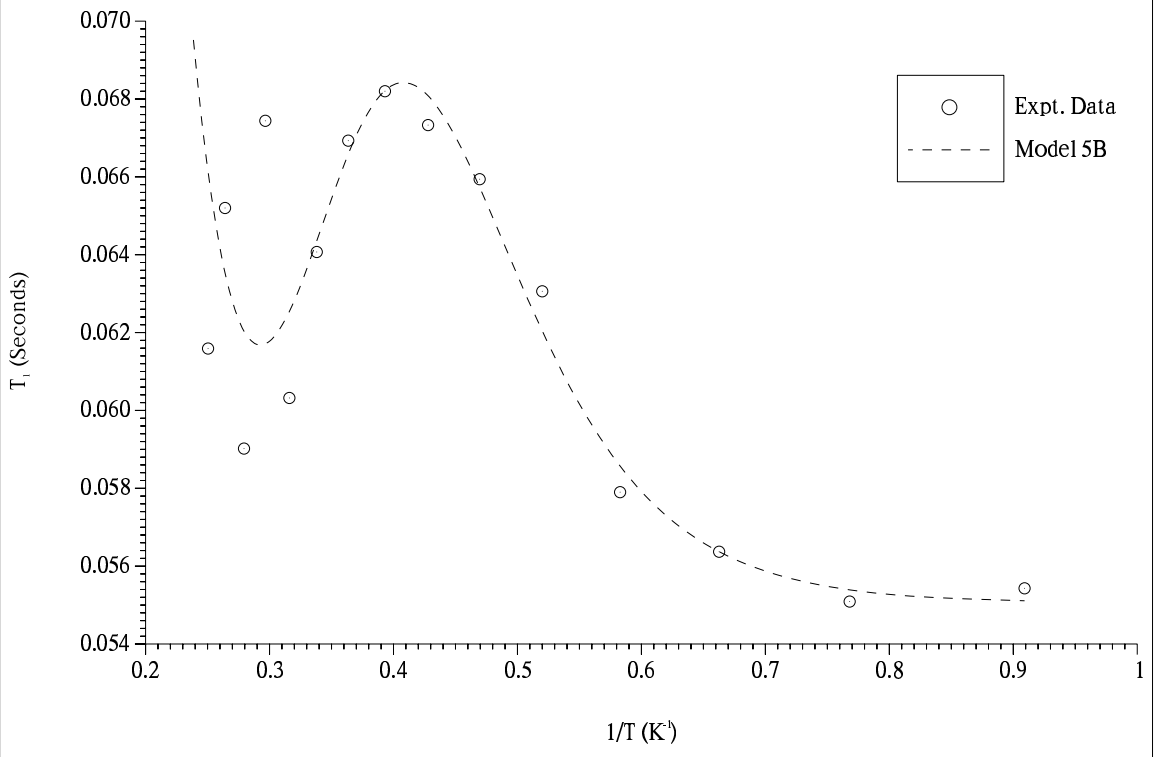

Figure 8.5.11, T_1 vs 1/T, X=0.8, With Fit, ALL_1100 Dataset, F=4.54MHz/T=1.1K [T_1 Data]

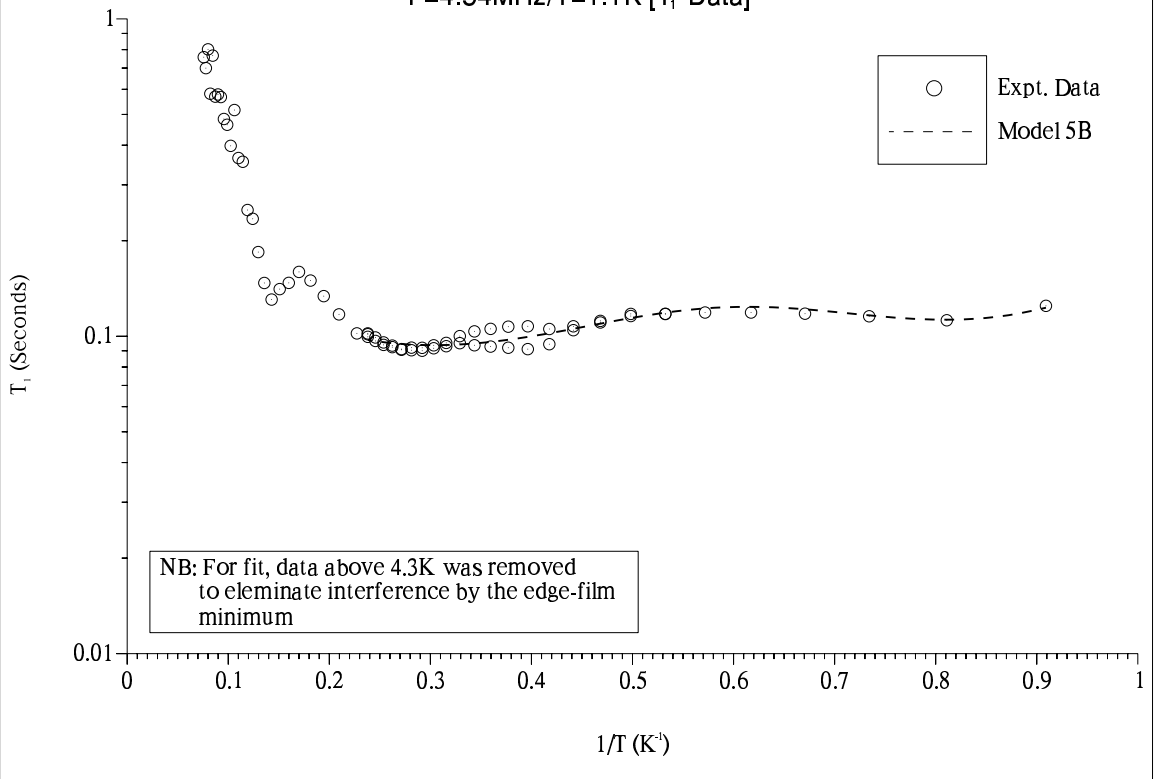

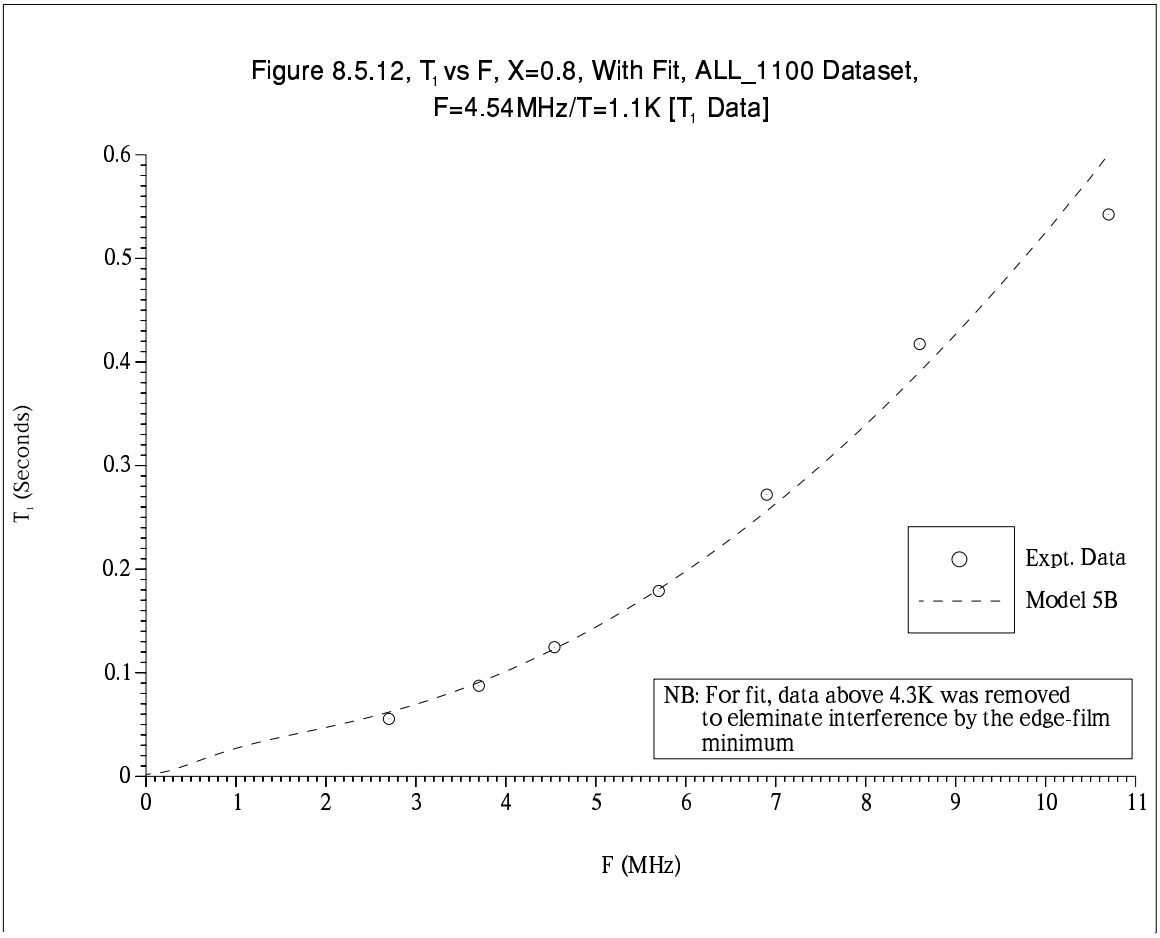

Note that $R_{\tau cex} \rightarrow 0$ suggesting the exchange contribution to the motion is still small.

Listing 8.5.10, NLLSQ_MODEL Results for *X*=0.8, *ALL_1100* Dataset

```
Model 5B fit
Sum of squares at convergence:   0.159247984

Fitted parameters;

rt0      =    287.890     +/-    13.8465
tcjhm_sf =    9.36626     +/-   0.131844
m2hm     =    31.1251     +/-   0.987801E-01
m2ht     =    17.5685     +/-   0.105615
wq       =    2.31538     +/-   0.645603E-01
Ea       =    5.10005     +/-   0.929915E-01
rtcex    =   0.331435E-07 +/-   0.107882
```

Figures 8.5.13 and 8.5.14 plot the temperature and frequency dependence for the *EVERYTHING* dataset fits. At 4.5MHz the temperature dependence fits are very similar to the *ALL_1100* fits. The 2.7MHz temperature fit is poor, due in part to the greater weighting in the fitting process received by the more numerous 4.5MHz data and the lower quality of the 2.7MHz points. Listing 8.5.11 gives the fit parameters. F_Q and

Figure 8.5.13, T_1 vs 1/T, X=0.8, With Fits, EVERYTHING Dataset, F=4.54MHz/T=1.1K [T_1 Data]

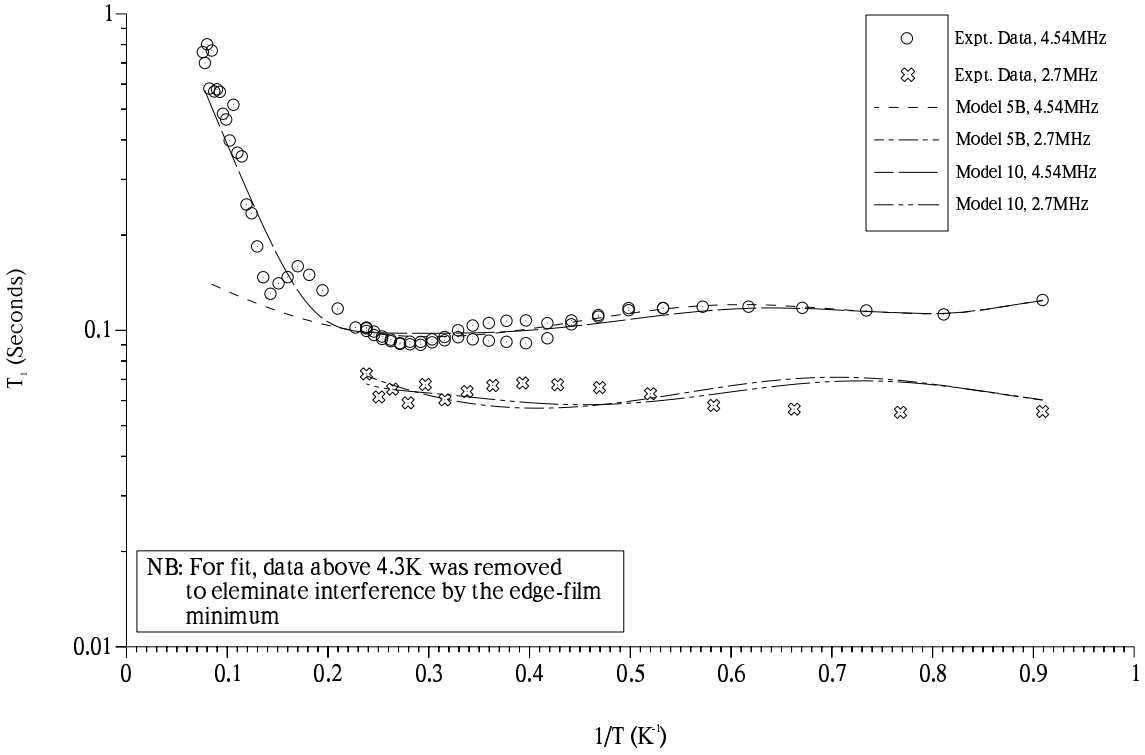

Figure 8.5.14, T_1 vs F, X=0.8, With Fits, EVERYTHING Dataset, F=4.54MHz/T=1.1K [T_1 Data]

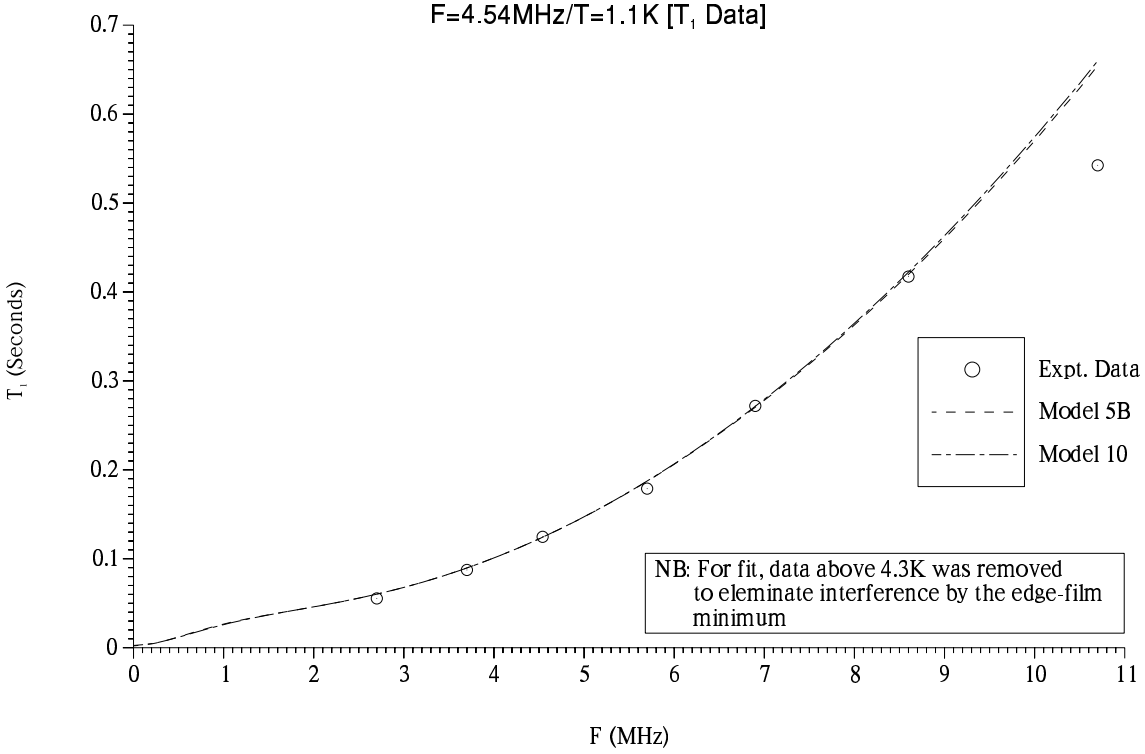

$R_{\tau cex}$ are similar to the *ALL_1100* dataset fits.

Listing 8.5.11, NLLSQ_MODEL Results for *X*=0.8, *EVERYTHING* Dataset

```
Model 5B Fit
Sum of squares at convergence:   0.407035206

Fitted parameters;

rt0      =    222.018     +/-    12.3913
tcjhm_sf =    7.88460     +/-   0.159716
m2hm     =    30.1776     +/-   0.140400
m2ht     =    16.4382     +/-   0.145424
wq       =    2.87760     +/-   0.815596E-01
Ea       =    4.90380     +/-   0.112003
rtcex    =   0.483347E-06 +/-   0.131449

Model 10 Fit
Sum of squares at convergence:   0.389502454

Fitted parameters;

rt0_1    =    301.219     +/-    536.014
rt0_2    =    2362.91     +/-    68006.1
tcjhm_sf =    6.73511     +/-   0.249113
m2hm     =    28.9124     +/-   0.144945
m2ht     =    15.7692     +/-   0.227908
wq       =    3.05128     +/-   0.880791E-01
Ea_1     =    5.19752     +/-    2.02038
Ea_2     =    18.0143     +/-    142.319
rtcex    =   0.360870E-06 +/-    1.19652
a        =    1.36123     +/-    6.42341
Tswitch  =    3.60501     +/-    2.59756
```

***X*=0.85,** Figure 8.5.15 plots the 4.54MHz *ALL* dataset, 2.82 and 10.7MHz data together with their separate fits. The fits are good but give widely differing parameters (listing 8.5.12), demonstrating model/experiment data misfit coupled with the absence of frequency dependent information.

Listing 8.5.12, NLLSQ_MODEL Results for *X*=0.85, Separate Fits.

```
10.7MHz data, Model 5B Fit
Sum of squares at convergence:   0.138681120

Fitted parameters;

rt0      =    533.950     +/-    5751.33
tcjhm_sf =    8.50990     +/-    100.150
m2hm     =    38.7904     +/-    5.73417
m2ht     =    5.47632     +/-    44.2183
wq       =    9.60702     +/-    166.469
Ea       =    5.73051     +/-    3.76581
rtcex    =   0.131229E-03 +/-    5.56439

4.5MHz, ALL Dataset, Model 5B Fit
Sum of squares at convergence:    4.35060739

Fitted parameters;

rt0      =    4393.82     +/-    981.110
```

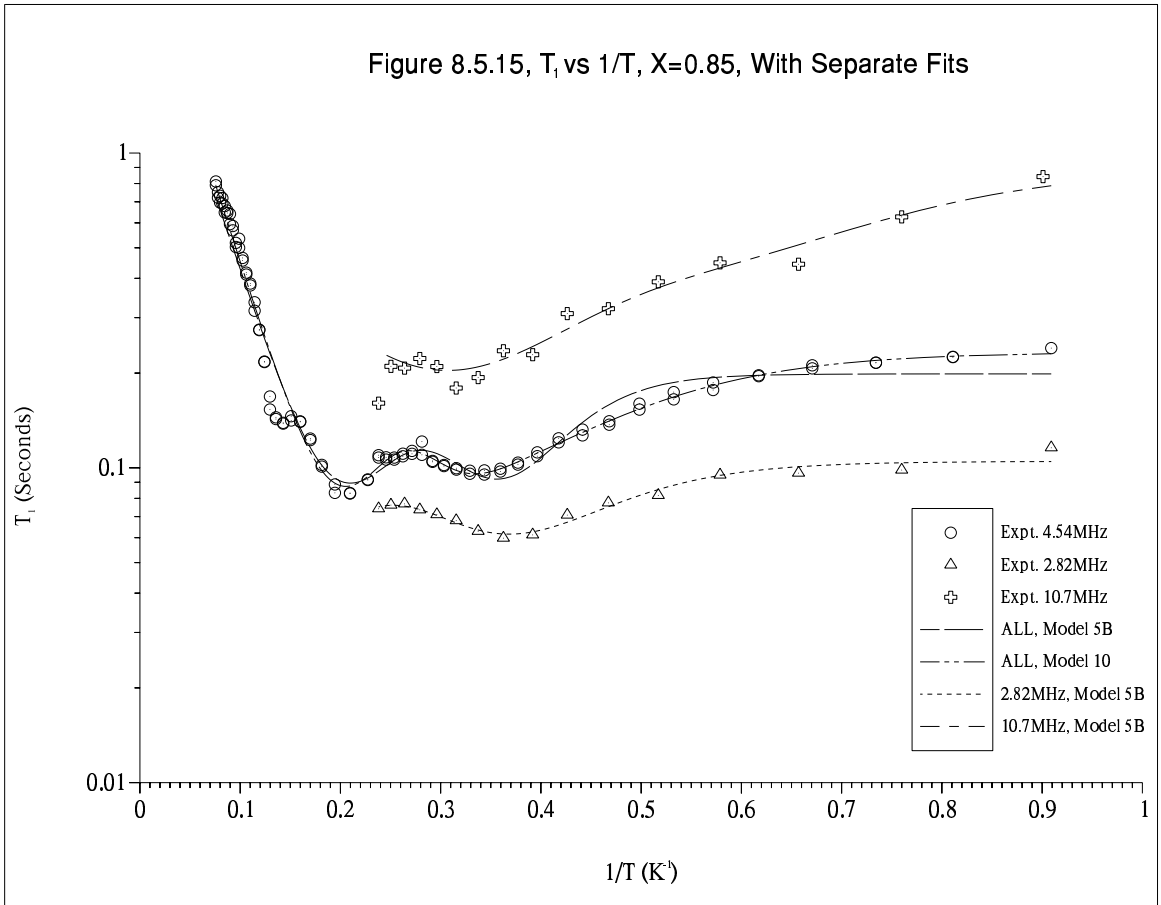
Figure 8.5.15, T1 vs 1/T, X=0.85, With Separate Fits
T1 (Seconds)
1/T (K-1)
Expt. 4.54MHz
Expt. 2.82MHz
Expt. 10.7MHz
ALL, Model 5B
ALL, Model 10
2.82MHz, Model 5B
10.7MHz, Model 5B

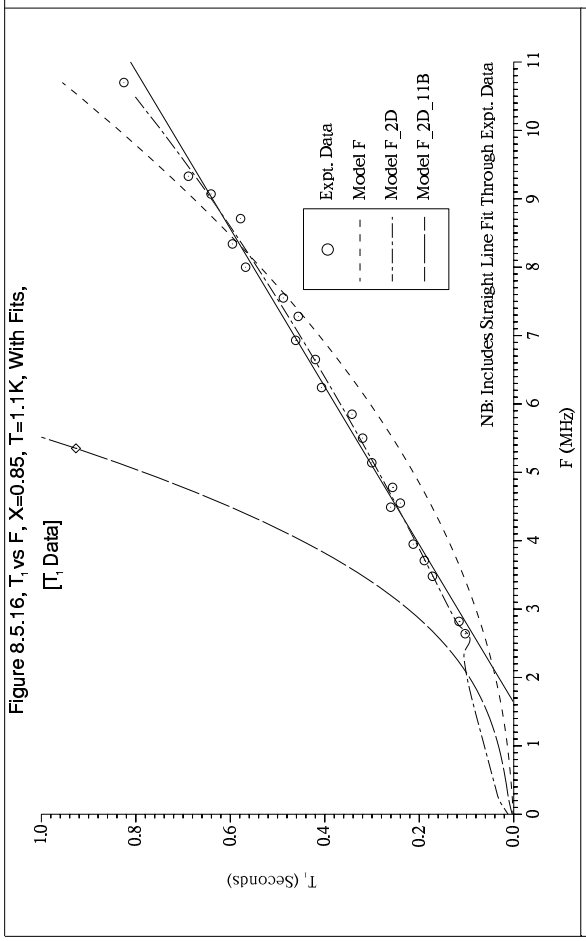
Figure 8.5.16, T1 vs F, X=0.85, T=1.1K, With Fits,
[T1 Data]
Expt. Data
Model F
Model F_2D
Model F_2D_11B
NB: Includes Straight Line Fit Through Expt. Data
F (MHz)
T1 (Seconds)

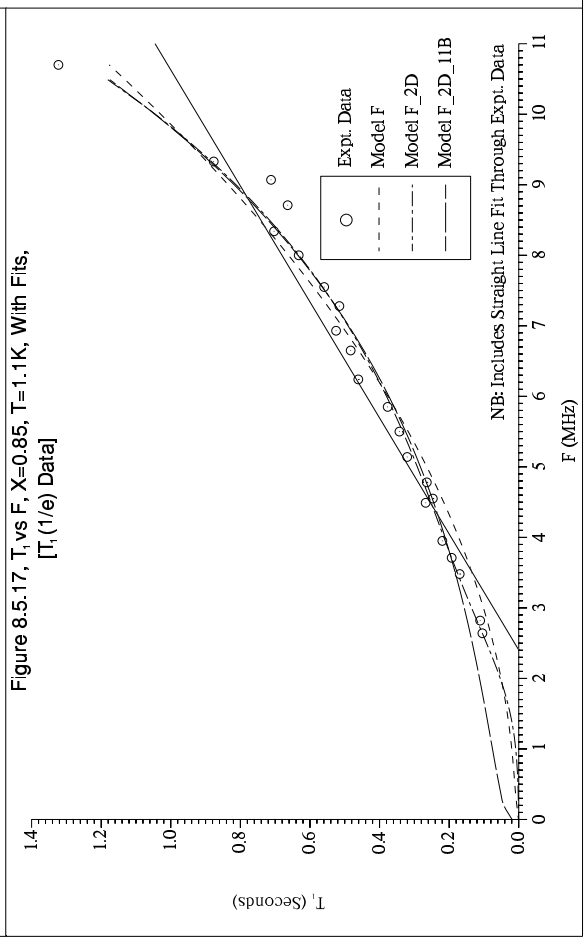
Figure 8.5.17, T1 vs F, X=0.85, T=1.1K, With Fits,
[T1 (1/e) Data]
Expt. Data
Model F
Model F_2D
Model F_2D_11B
NB: Includes Straight Line Fit Through Expt. Data
F (MHz)
T1 (Seconds)

```
tcjhm_sf =    6.84674     +/-    1.57207
m2hm     =    32.2472     +/-   0.342131
m2ht     =    15.0727     +/-    2.65892
wq       =    5.56451     +/-   0.845888
Ea       =    21.9817     +/-   0.162951
rtcex    =   0.486770     +/-   0.129240

2.82MHz Data, Model 5B Fit
Sum of squares at convergence:   0.228026434E-01

Fitted parameters;

rt0      =    284.526     +/-    8393.18
tcjhm_sf =    25.5475     +/-    892.348
m2hm     =    58.1781     +/-    644.383
m2ht     =    24.3785     +/-    751.901
wq       =   0.100000     +/-    340.233
Ea       =    13.1951     +/-    5.45182
rtcex    =   0.966618     +/-    31.5094
```

Figures 8.5.16 and 8.5.17 illustrates several fits to the frequency dependence data. Numerically, the best fits are the F_2D ones, particularly in figure 8.5.16 where the experimental data follows a linear law. However the F fit parameters are probably more reliable.

Figures 8.5.18 and 8.5.19 plot the temperature and frequency dependence for the *EVERYTHING* dataset fits. There is good experiment/fit agreement at 4.54 and 2.82MHz but at 10.7MHz model T_1 are $\gg$ the experimental data. Figure 8.5.19 suggests the 10.7MHz point may be anomalous. The $T_1(1/e)$ frequency data presented here, with its *faster-than-linear-law* form at 1.1K gives marginally better overall fits than the T_1 data, particularly at low T. Listing 8.5.13 gives the fit parameters. In contrast with the 0.8 monolayers data (listing 8.5.11) $F_Q \rightarrow 0$ and $R_{\tau cex}$ is now finite. Higher coverages continue with these characteristics.

Listing 8.5.13, NLLSQ_MODEL Results for X=0.85, *EVERYTHING* Dataset

```
Model 5B Fit
Sum of squares at convergence:    10.9704325

Fitted parameters;

rt0      =    4620.18     +/-    269.174
tcjhm_sf =    10.7850     +/-   0.352088
m2hm     =    30.5116     +/-   0.307951
m2ht     =    25.3429     +/-   0.507515
wq       =   0.100001     +/-   0.286897
Ea       =    19.5214     +/-   0.166181
rtcex    =    1.17913     +/-   0.238260E-01


Model 10 Fit
Sum of squares at convergence:    7.87148414

Fitted parameters;
```

Figure 8.5.18, T_1 vs 1/T, X=0.85, With Fits, EVERYTHING Dataset, T=1.1K [T_1 (1/e) Data]

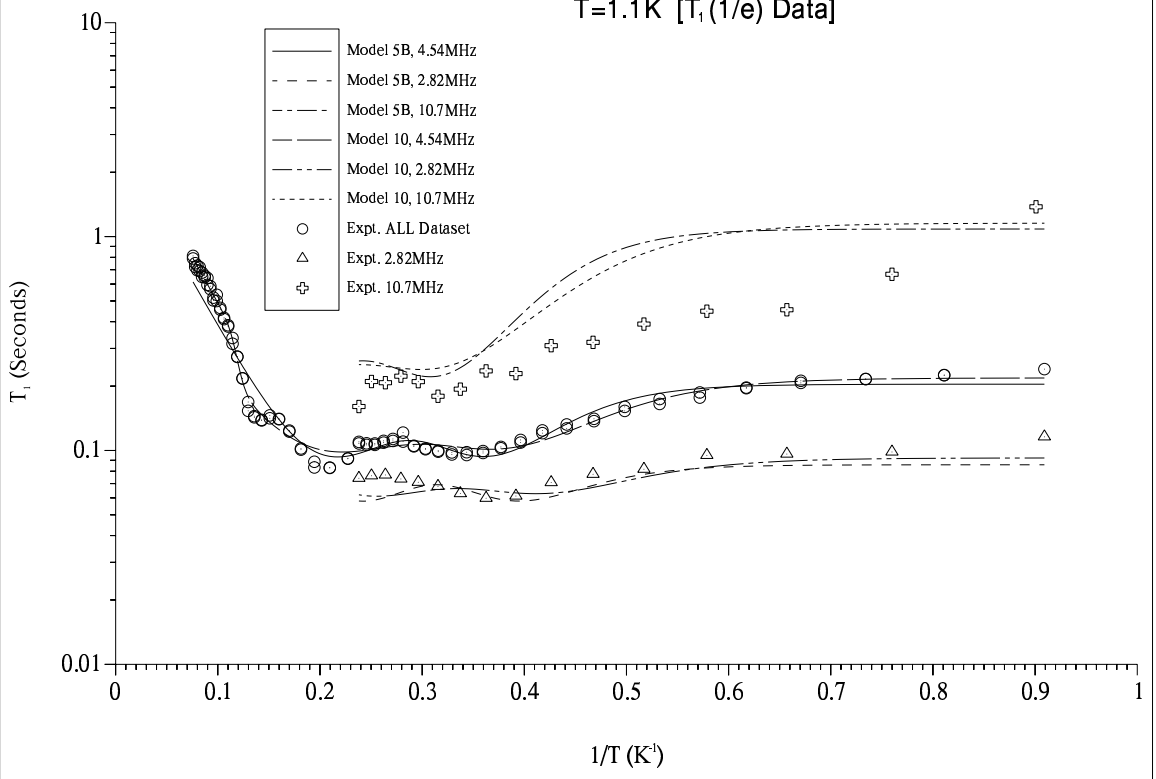

Figure 8.5.19, T_1 vs F, X=0.85, With Fits, EVERYTHING Dataset, T=1.1K [T_1 (1/e) Data]

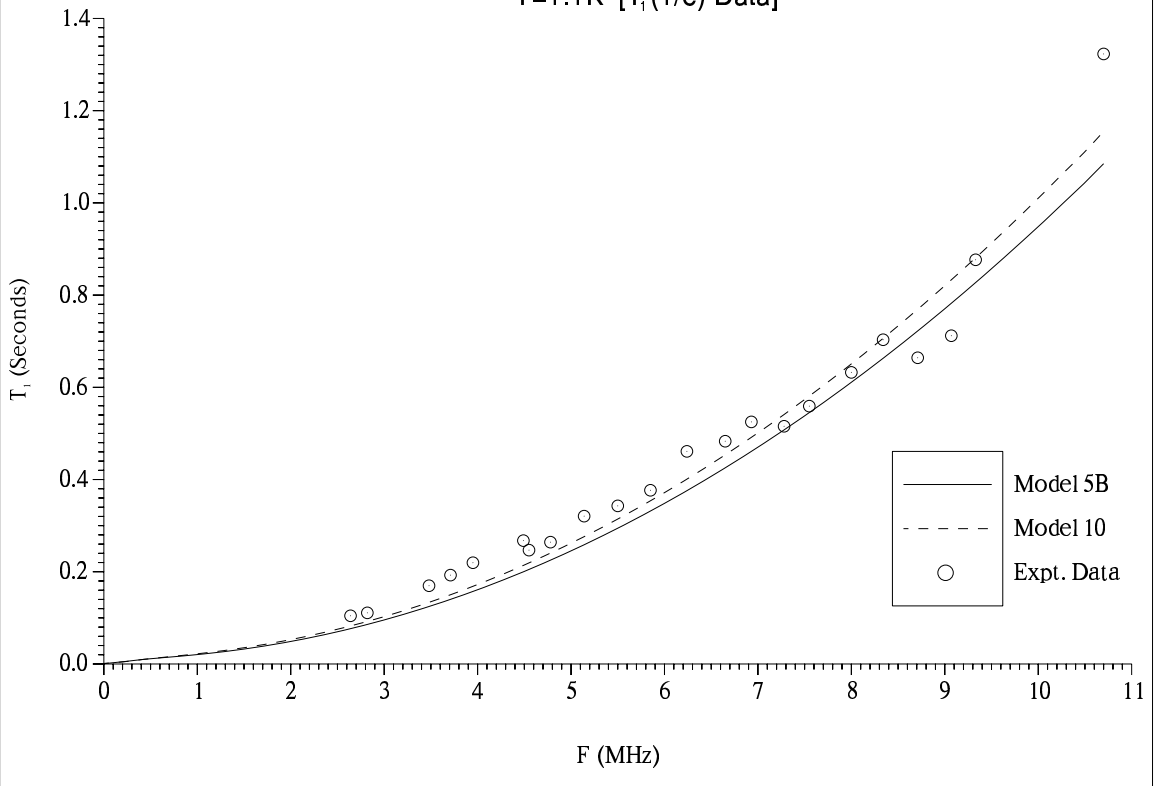

```
rt0_1    =    1080.95     +/-    96.7309
rt0_2    =    3791.00     +/-    610.840
tcjhm_sf =    7.20899     +/-   0.281864
m2hm     =    27.5702     +/-   0.328589
m2ht     =    21.6815     +/-   0.452180
wq       =   0.100000     +/-   0.264477
Ea_1     =    14.8355     +/-   0.240658
Ea_2     =    19.9570     +/-    1.71990
rtcex    =    1.24926     +/-   0.236792E-01
a        =    3.29769     +/-   0.880552
Tswitch  =    8.39756     +/-   0.115752
```

***X*=0.9,** Figure 8.5.20 plots the 4.54MHz *ALL* dataset data together with the fits. The fits are good, especially Model 10. Listing 8.5.14 gives the parameters.

Listing 8.5.14, NLLSQ_MODEL Results for *X*=0.9, *ALL* Dataset

```
Model 5B Fit
Sum of squares at convergence:    1.40919212

Fitted parameters;

rt0      =    6191.60     +/-    4869.85
tcjhm_sf =    5.75749     +/-    4.43801
m2hm     =    28.0273     +/-    2.02990
m2ht     =    20.7180     +/-    12.1922
wq       =    4.86692     +/-    3.61321
Ea       =    27.5276     +/-   0.569818
rtcex    =   0.456044     +/-   0.421629

Model 10 Fit
Sum of squares at convergence:   0.447691413

Fitted parameters;

rt0_1    =    2.77356     +/-    33.0473
rt0_2    =    8104.98     +/-    92560.9
tcjhm_sf =    10.5506     +/-    121.192
m2hm     =    27.7622     +/-   0.778656
m2ht     =    31.7965     +/-    365.452
wq       =   0.100000     +/-    205.738
Ea_1     =    2.98404     +/-   0.761456
Ea_2     =    22.8061     +/-    1.57083
rtcex    =   0.513768     +/-    6.14855
a        =   0.519189     +/-   0.579429E-01
Tswitch  =    6.06487     +/-   0.614037
```

The frequency dependence fits are similar to *X*=0.85 with the best fit being to the T_1(1/e) -*faster-than-linear-law*- data.

Figures 8.5.21 and 8.5.22 plot the the temperature and frequency dependence for the *EVERYTHING* dataset fits. Experiment/fit agreement is reasonable with the minima being located at both frequencies but at 2.7MHz the model T_1 are $\ll$ the experimental data. As at 0.85 monolayers the T_1(1/e) frequency data with its *faster-than-linear-law* form at 1.1K gives marginally better overall fits than does the T_1 data, particularly at low *T*. At 4.2K the data closely follows a linear frequency law as the straight line fit in figure 8.5.22 demonstrates. Listing 8.5.15 gives the fit parameters.

Figure 8.5.20, T_1 vs 1/T, X=0.9, F=4.54MHz, With Fits
ALL Dataset

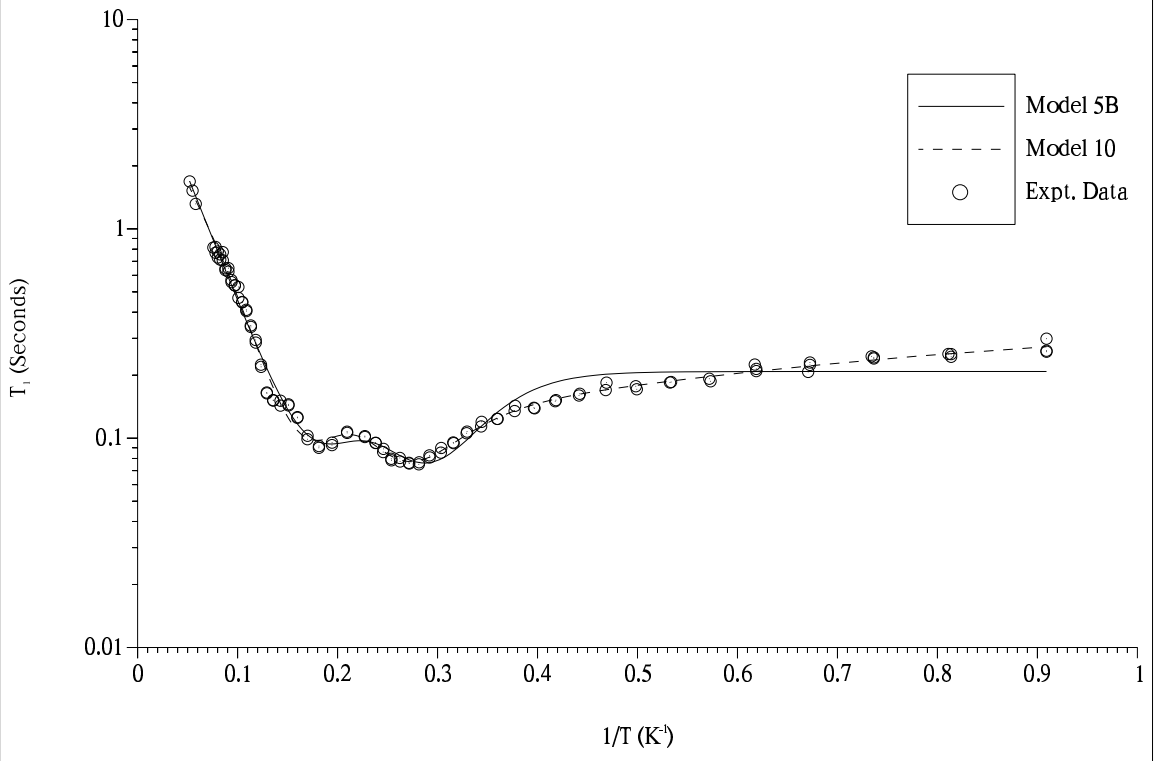

Figure 8.5.21, T_1 vs 1/T, X=0.9, With Fits, EVERYTHING Dataset,
T=1.1K [T_1 (1/e) Data]

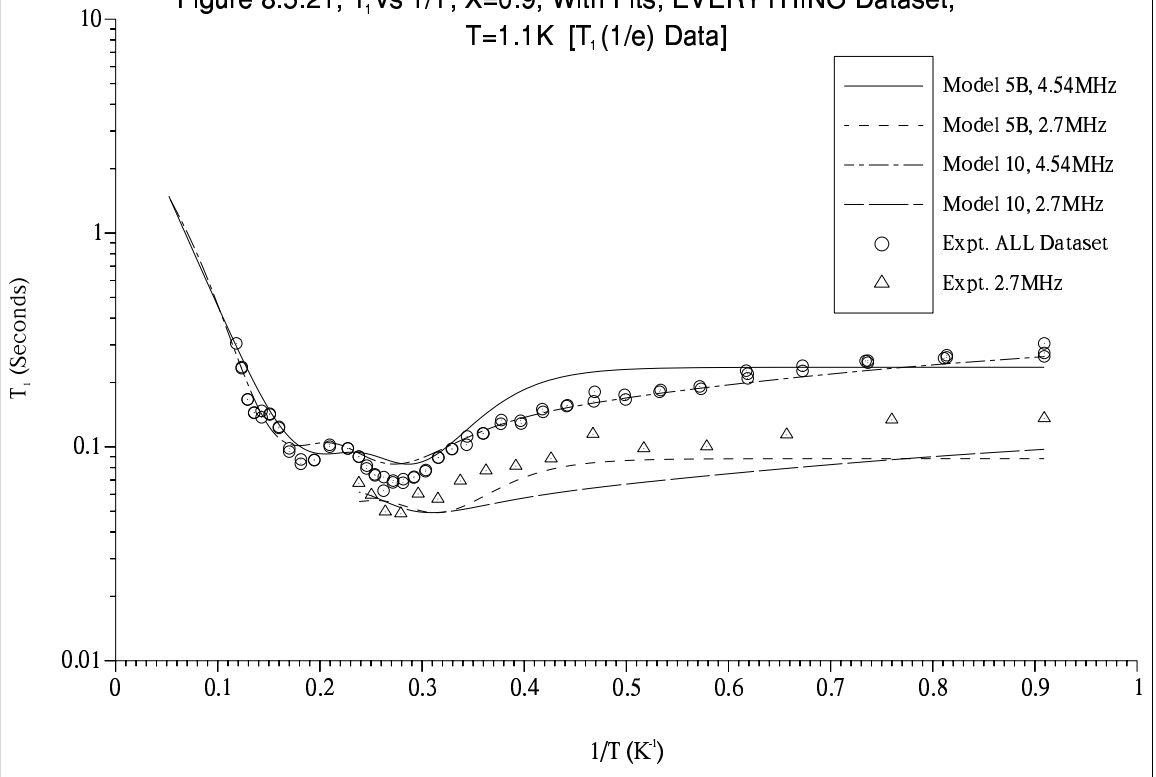

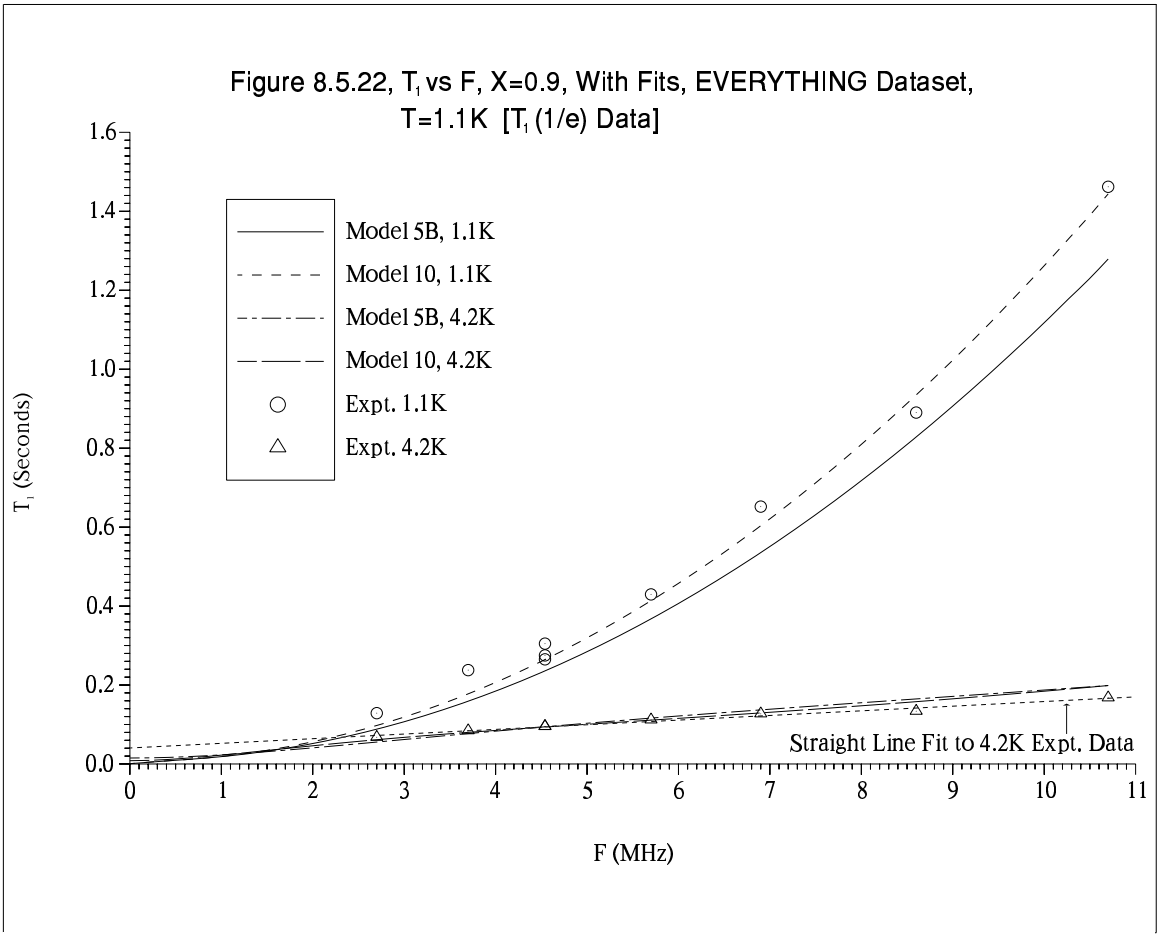

Like the 0.85 monolayers data (listing 8.5.13) $F_Q \rightarrow 0$ and $R_{\tau cex}$ is finite.

Listing 8.5.15, NLLSQ_MODEL Results for *X*=0.9, *EVERYTHING* Dataset

```
Model 5B Fit
Sum of squares at convergence:    3.52227490

Fitted parameters;

rt0      =    5914.87     +/-    973.503
tcjhm_sf =    7.12155     +/-   0.728371
m2hm     =    27.8894     +/-    1.41693
m2ht     =    27.6034     +/-    1.56611
wq       =   0.100000     +/-   0.500274
Ea       =    24.9688     +/-   0.548615
rtcex    =   0.898612     +/-   0.451607E-01

Model 10 Fit
Sum of squares at convergence:    2.46469900

Fitted parameters;

rt0_1    =    3.32437     +/-    1.59606
rt0_2    =    5148.55     +/-    1567.82
tcjhm_sf =    8.79255     +/-    1.28101
m2hm     =    25.9926     +/-    1.50579
m2ht     =    28.8880     +/-    1.33619
wq       =   0.100000     +/-   0.429993
Ea_1     =    3.07331     +/-    1.33377
Ea_2     =    19.8457     +/-    2.63037
rtcex    =   0.582097     +/-   0.158052
```

```
a        =   0.488704     +/-   0.603710E-01
Tswitch  =    7.26216     +/-   0.879993
```

***X*=0.938,** Figures 8.5.23−8.5.29 plot the temperature dependence data together with the individual fits at each frequency. The fits are good, especially Model 10, demonstrating the model's ability to describe the data, including the double minima for frequencies far from the usual 4.5MHz experimental frequency. Listing 8.5.16 gives the parameters. Values of F_Q vary widely due to the absence of frequency dependence data supplied to the NLLSQ software. The E_{a_2} value for the 10.7MHz (figure 8.5.29) fit is obviously silly, concurring with the 5B fit in suggesting no true double minimum occurs at this frequency.

Listing 8.5.16, NLLSQ_MODEL Results for *X*=0.938, Individual Data

```
2.7MHz Data, Model 5B Fit
Sum of squares at convergence:   0.650708767

Fitted parameters;

rt0      =    9682.04     +/-    12031.3
tcjhm_sf =    7.55299     +/-    9.23971
m2hm     =    24.1437     +/-    3.47242
m2ht     =    24.8799     +/-    25.7025
wq       =    2.35395     +/-    4.89964
Ea       =    30.6801     +/-    1.43778
rtcex    =   0.367647     +/-   0.602512

2.7MHz Data, Model 10 Fit
Sum of squares at convergence:   0.294241233

Fitted parameters;

rt0_1    =    6.93536     +/-    55.2728
rt0_2    =    6899.81     +/-    50357.5
tcjhm_sf =    5.05467     +/-    35.6592
m2hm     =    18.4545     +/-    6.69958
m2ht     =    14.1459     +/-    84.3076
wq       =    6.83529     +/-    9.84308
Ea_1     =    10.5200     +/-    2.81413
Ea_2     =    34.0422     +/-    1.59404
rtcex    =   0.139581     +/-    1.01621
a        =    1.66624     +/-    3.93478
Tswitch  =    4.11085     +/-    2.61188

3.7MHz Data, Model 5B Fit
Sum of squares at convergence:    1.30337050

Fitted parameters;

rt0      =    6972.49     +/-    22525.8
tcjhm_sf =    4.37625     +/-    13.7952
m2hm     =    29.8075     +/-    6.71341
m2ht     =    15.4800     +/-    34.8057
wq       =    4.66290     +/-    8.25316
Ea       =    30.0229     +/-    1.08346
rtcex    =   0.340831     +/-    1.13556


3.7MHz Data, Model 10 Fit
```

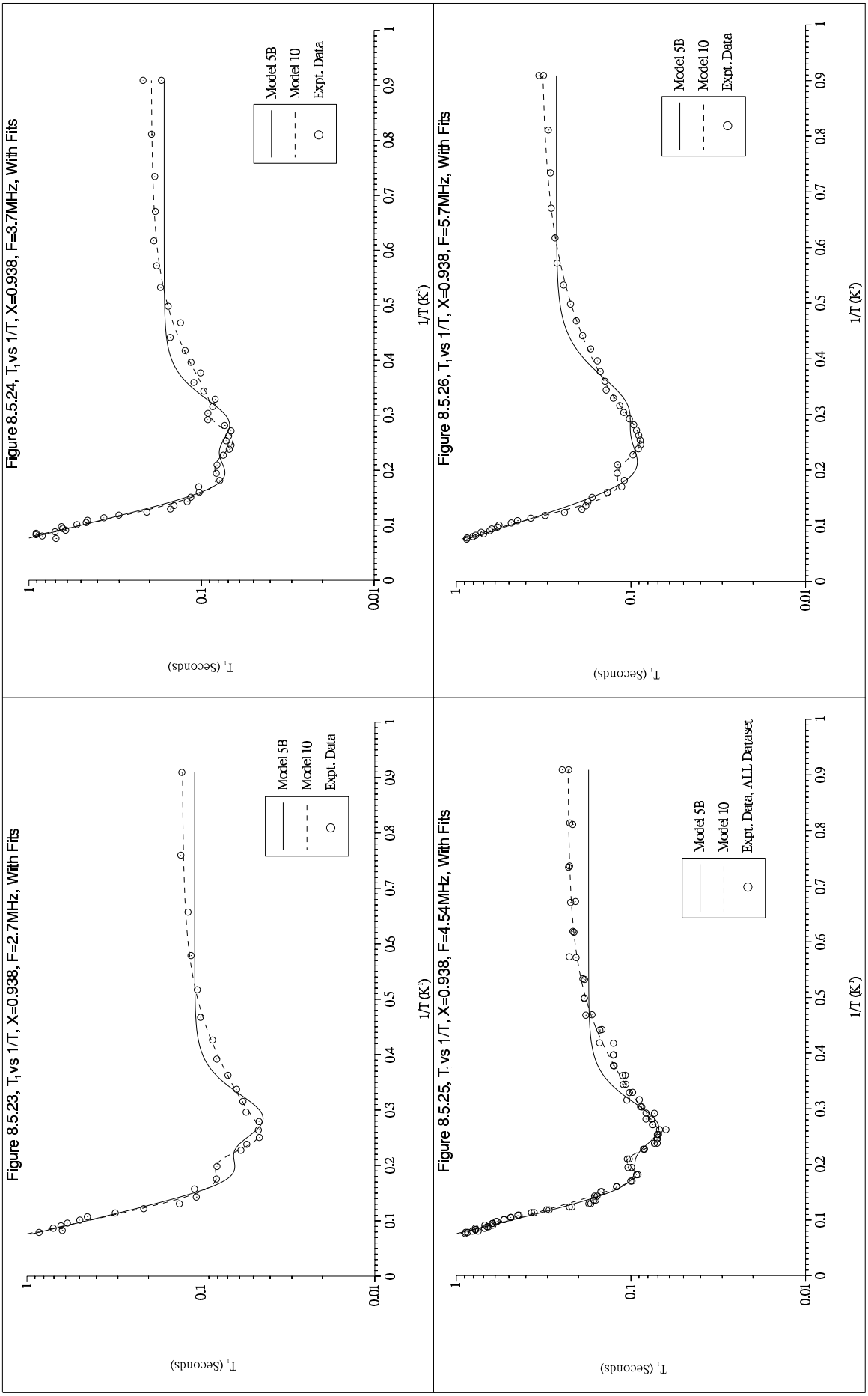
Figure 8.5.24, T1 vs 1/T, X=0.938, F=3.7MHz, With Fits
Figure 8.5.26, T1 vs 1/T, X=0.938, F=5.7MHz, With Fits
Figure 8.5.23, T1 vs 1/T, X=0.938, F=2.7MHz, With Fits
Figure 8.5.25, T1 vs 1/T, X=0.938, F=4.54MHz, With Fits
Model 5B
Model 10
Expt. Data
Expt. Data, ALL Dataset
T1 (Seconds)
1/T (K-1)

Figure 8.5.27, T_1 vs 1/T, X=0.938, F=6.9MHz, With Fits

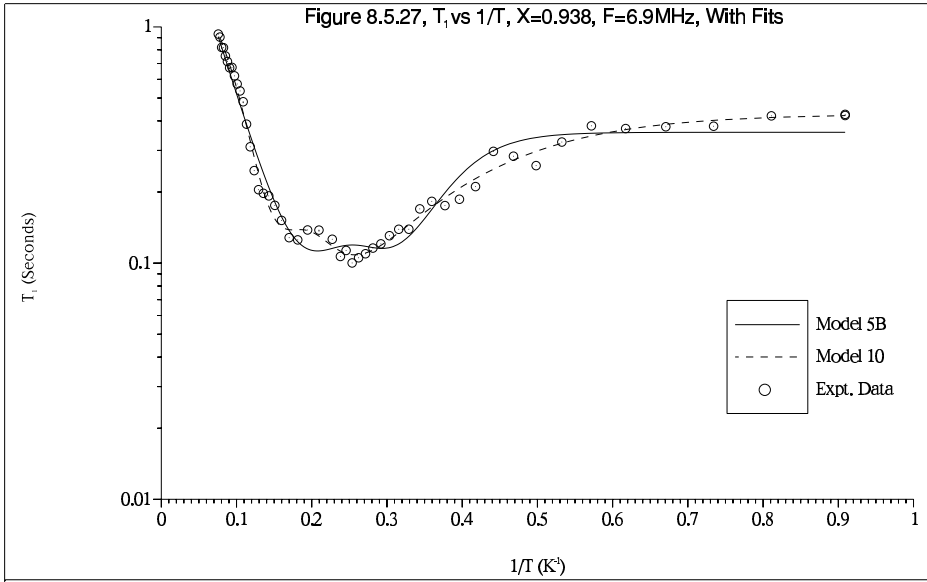

Figure 8.5.28, T_1 vs 1/T, X=0.938, F=8.6MHz, With Fits

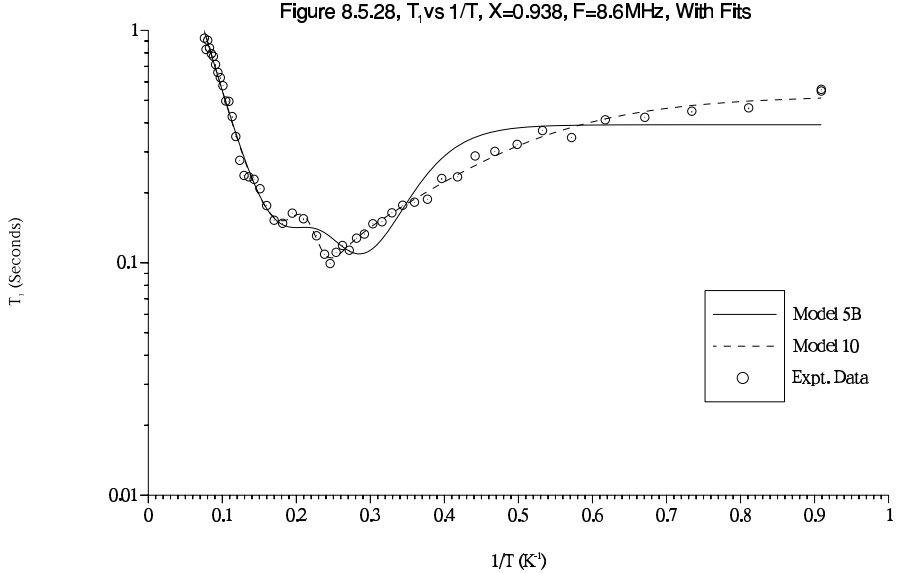

Figure 8.5.29, T_1 vs 1/T, X=0.938, F=10.7MHz, With Fits

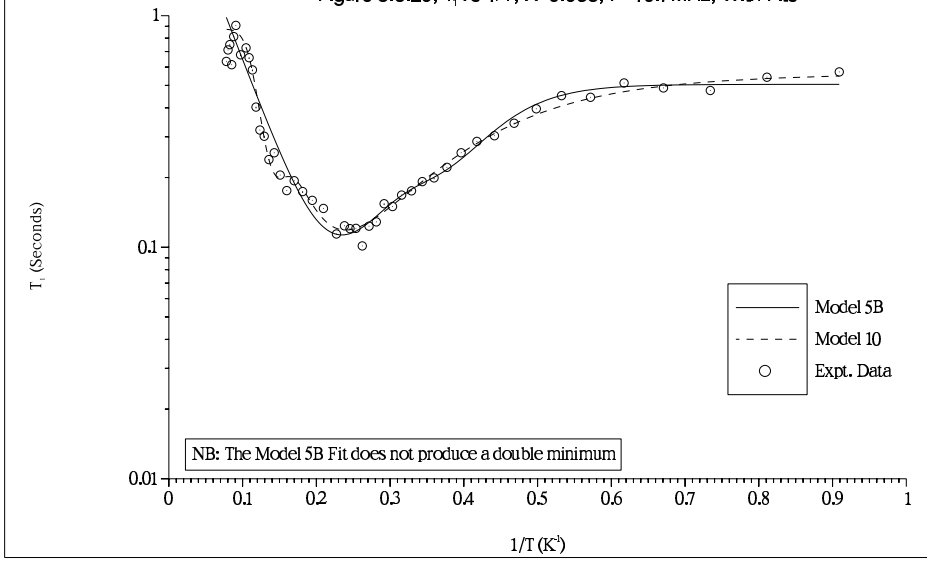

Figure 8.5.30, T_1 vs F, X=0.938, T=1.1K, With Fits
[T_1 Data]

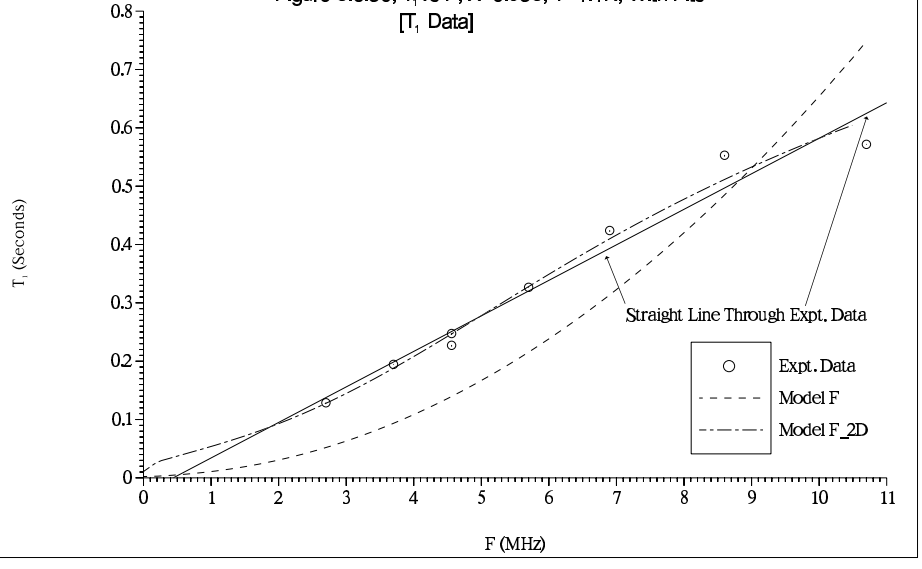

```
Sum of squares at convergence:   0.690492966

Fitted parameters;

rt0_1    =    29.7542     +/-    71.8532
rt0_2    =    14345.6     +/-    26209.5
tcjhm_sf =    7.54703     +/-    13.6288
m2hm     =    25.4972     +/-    2.56702
m2ht     =    26.7703     +/-    43.0220
wq       =    1.40259     +/-    17.7529
Ea_1     =    10.4350     +/-    2.39508
Ea_2     =    33.2336     +/-   0.951897
rtcex    =   0.595207     +/-    1.38736
a        =    8.73609     +/-    12.0710
Tswitch  =    3.30628     +/-   0.169908


4.54MHz ALL Dataset, Model 5B Fit
Sum of squares at convergence:    4.55779768

Fitted parameters;

rt0      =    10307.7     +/-    1179.17
tcjhm_sf =    7.19279     +/-   0.895955
m2hm     =    26.4331     +/-   0.255068
m2ht     =    29.7617     +/-    3.45132
wq       =    2.68172     +/-    1.31933
Ea       =    30.2895     +/-   0.262424
rtcex    =   0.766860     +/-   0.144923


4.54MHz ALL Dataset, Model 10 Fit
Sum of squares at convergence:    1.72109687

Fitted parameters;

rt0_1    =    10.5230     +/-    3.51027
rt0_2    =    7849.81     +/-    2324.31
tcjhm_sf =    6.75220     +/-    1.98265
m2hm     =    29.6692     +/-   0.241206
m2ht     =    18.8658     +/-    4.77628
wq       =    6.09558     +/-   0.974901
Ea_1     =    9.99756     +/-   0.363539
Ea_2     =    27.1560     +/-   0.271292
rtcex    =   0.248340     +/-   0.870261E-01
a        =    2.01982     +/-   0.106721
Tswitch  =    5.07835     +/-   0.569144E-01


5.7MHz Data, Model 5B Fit
Sum of squares at convergence:   0.756032582

Fitted parameters;

rt0      =    3072.95     +/-    12403.8
tcjhm_sf =    3.13722     +/-    12.3160
m2hm     =    35.8364     +/-    10.2200
m2ht     =    14.9858     +/-    39.2905
wq       =    6.97993     +/-    16.1637
Ea       =    23.2442     +/-   0.808116
rtcex    =   0.533580     +/-    2.17373


5.7MHz Data, Model 10 Fit
Sum of squares at convergence:   0.173190165

Fitted parameters;

rt0_1    =    13.9591     +/-    48.4152
rt0_2    =    5896.42     +/-    11846.4
tcjhm_sf =    7.47216     +/-    16.1718
m2hm     =    26.8489     +/-    1.53971
```

```
m2ht     =    29.5054     +/-    62.6905
wq       =    2.95083     +/-    33.0924
Ea_1     =    7.27775     +/-   0.975164
Ea_2     =    23.0756     +/-    3.53277
rtcex    =   0.673590     +/-    2.34293
a        =   0.740944     +/-   0.195118
Tswitch  =    6.11852     +/-   0.860566


6.9MHz Data, Model 5B Fit
Sum of squares at convergence:   0.820205238

Fitted parameters;

rt0      =    3606.45     +/-    11877.3
tcjhm_sf =    3.52180     +/-    11.2814
m2hm     =    35.1457     +/-    8.89724
m2ht     =    17.0395     +/-    37.4320
wq       =    8.28328     +/-    17.0702
Ea       =    23.4283     +/-   0.937581
rtcex    =   0.544241     +/-    1.86650


6.9MHz Data, Model 10 Fit
Sum of squares at convergence:   0.248088632

Fitted parameters;

rt0_1    =    21.6629     +/-    114.014
rt0_2    =    3531.93     +/-    10630.6
tcjhm_sf =    7.24984     +/-    22.7768
m2hm     =    27.7178     +/-    1.82672
m2ht     =    30.6428     +/-    94.9085
wq       =    2.41601     +/-    67.4571
Ea_1     =    8.13620     +/-    2.27435
Ea_2     =    15.9777     +/-    5.28294
rtcex    =   0.834843     +/-    3.89062
a        =   0.701763     +/-   0.785469E-01
Tswitch  =    7.68799     +/-   0.911223


8.6MHz Data, Model 5B Fit
Sum of squares at convergence:    1.05733505

Fitted parameters;

rt0      =    8050.87     +/-    8373.65
tcjhm_sf =    6.71337     +/-    7.02788
m2hm     =    33.6482     +/-    3.66859
m2ht     =    34.6472     +/-    31.2968
wq       =    5.32967     +/-    18.4464
Ea       =    24.8821     +/-    1.29481
rtcex    =   0.978485     +/-    1.40047


8.6MHz Data, Model 10 Fit
Sum of squares at convergence:   0.191166641

Fitted parameters;

rt0_1    =    6.95230     +/-    330.714
rt0_2    =    3280.14     +/-    152082.
tcjhm_sf =    7.94772     +/-    371.086
m2hm     =    26.2744     +/-    1.78339
m2ht     =    41.4941     +/-    1940.45
wq       =   0.100000     +/-    1597.10
Ea_1     =    4.36527     +/-    1.44474
Ea_2     =    14.1367     +/-    5.30091
rtcex    =   0.832016     +/-    39.7369
a        =   0.673805     +/-   0.722999E-01
Tswitch  =    7.72588     +/-   0.934398
```

```
10.7MHz Data, Model 5B Fit
Sum of squares at convergence:    2.74099204

Fitted parameters;

rt0      =    3949.18     +/-    45896.0
tcjhm_sf =    2.83868     +/-    32.5760
m2hm     =    60.9092     +/-    19.9219
m2ht     =    10.6161     +/-    80.7431
wq       =    13.9323     +/-    74.7849
Ea       =    19.2500     +/-    1.06486
rtcex    =    1.04735     +/-    11.7067


10.7MHz Data, Model 10 Fit
Sum of squares at convergence:    1.71377964

Fitted parameters;

rt0_1    =    18.9310     +/-    110.359
rt0_2    =    1045.42     +/-    3138.41
tcjhm_sf =    7.30881     +/-    23.6637
m2hm     =    30.4423     +/-    5.61152
m2ht     =    31.0427     +/-    93.3039
wq       =    12.2419     +/-    39.2302
Ea_1     =    9.56078     +/-    4.40965
Ea_2     =   0.310049E-06 +/-    9.62666
rtcex    =   0.503093     +/-    2.20908
a        =    1.37170     +/-   0.295148
Tswitch  =    8.41448     +/-   0.567730
```

Figure 8.5.30 shows the 1.1K frequency behaviour. The data is 'T_1' data but is very similar to the 'T_1(1/e)' data in both being close to linear in F − that is apart from the apparently anomalous 10.7MHz point, the cause of which is unknown. As expected the F_2D fit is best able to model the linear law.

Figures 8.5.31 and 8.5.32 plot the the temperature and frequency dependence for the *EVERYTHING* dataset fits, which at this coverage comprise all frequencies measured over $1.1 \leqslant T \leqslant 13.2$K. Qualitatively, the temperature fits display the same characteristics as the data but for the highest and lowest frequencies there is a systematic discrepancy − For $F \rightarrow 2.7$MHz T_1(model) < T_1(expt.) and $F \rightarrow 10.7$MHz T_1(model) > T_1(expt.) for all T. This implies there is a significant non-dipolar contribution to T_1(expt.). Appending a frequency independent relaxation rate/time term to the fit as discussed in §8.3 and §8.4 made only a marginal improvement. This is not surprising since candidates for a non-dipolar mechanism such as relaxation via PMIs are likely to be strong a function of temperature. On the frequency axis the fit is compromised by the inability of the model to accurately describe the linear frequency law coupled with the anomalous 1.1K/10.7MHz point. At higher T, around the T_1 minima T_1 is a weaker function of frequency resulting in closer data−model correspondence. Note: T_1(1/e) data and fit is very similar to the T_1 data and fit presented here. Listing 8.5.17 gives the fit parameters. Again, particularly with the closer Model 10 fit $F_Q \rightarrow 0$ and $R_{\tau cex}$ is finite.

Figure 8.5.31, T_1 vs 1/T, X=0.938, With Model 5B Fit, EVERYTHING Dataset
[T_1 Data]

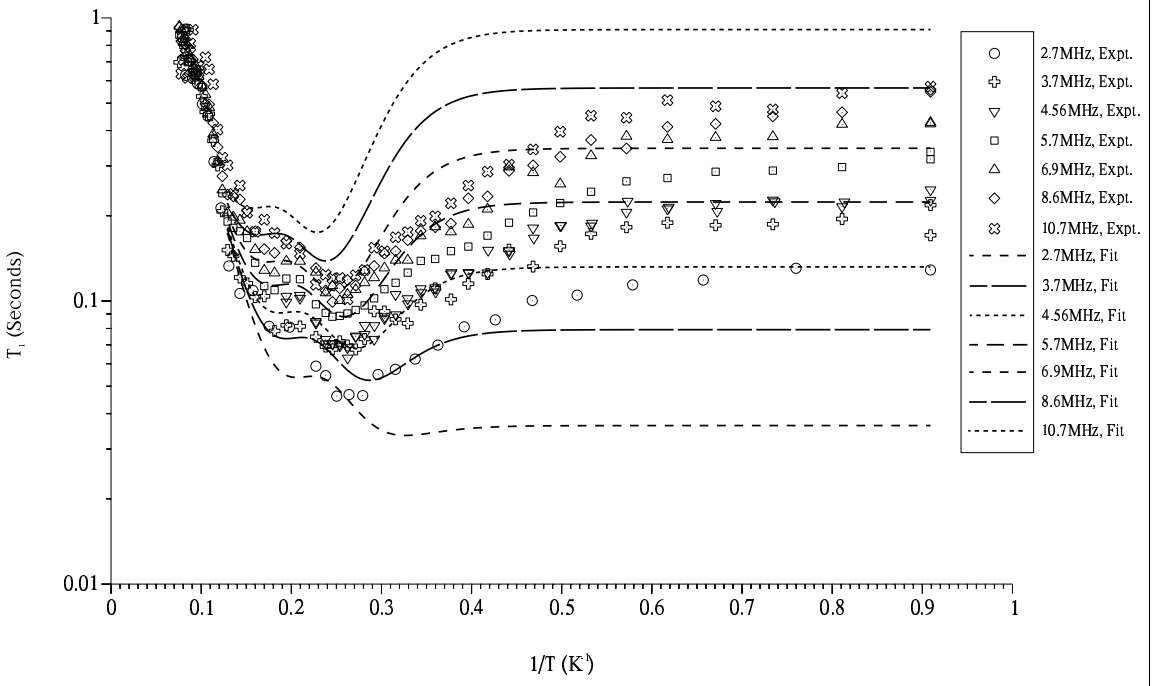

Figure 8.5.32, T_1 vs F, X=0.938, With Model 5B Fit, EVERYTHING Dataset
[T_1 Data]

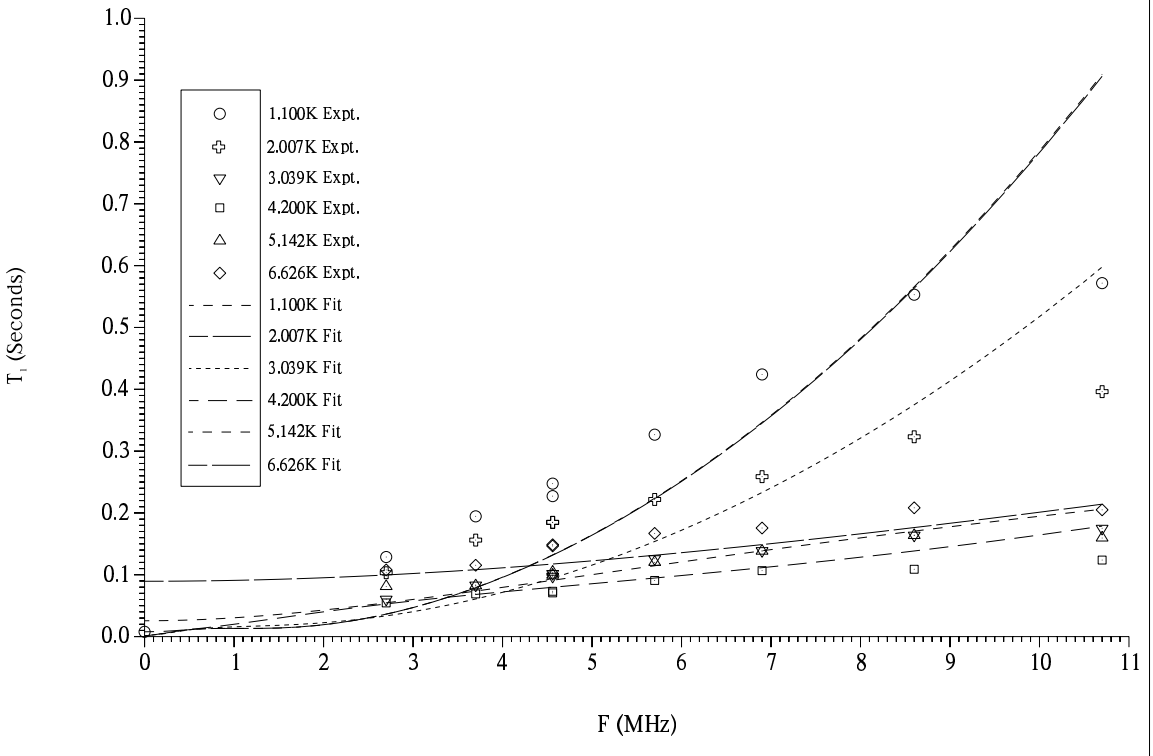

Listing 8.5.17, NLLSQ_MODEL Results for X=0.938, *EVERYTHING* Dataset

```
Model 5B fit
Sum of squares at convergence:    69.5502989

Fitted parameters;

rt0      =    8568.54     +/-    2382.51
tcjhm_sf =    7.44274     +/-    1.24500
m2hm     =    28.4255     +/-    2.01096
m2ht     =    30.0150     +/-    1.93319
wq       =    2.78247     +/-   0.260187
Ea       =    29.3198     +/-    1.06690
rtcex    =    1.01882     +/-   0.619089E-01


Model 10 Fit
Sum of squares at convergence:    28.5561890

Fitted parameters;

rt0_1    =    22.0409     +/-    34.7404
rt0_2    =    8116.77     +/-    6682.31
tcjhm_sf =    6.58937     +/-    1.35339
m2hm     =    29.7723     +/-    2.26399
m2ht     =    29.1497     +/-    2.08857
wq       =   0.100001     +/-   0.598566
Ea_1     =    4.89422     +/-    1.35672
Ea_2     =    25.0557     +/-    8.77938
rtcex    =   0.569889     +/-   0.127649
a        =   0.265157     +/-   0.270885
Tswitch  =    4.38490     +/-    9.52113
```

Figures 8.5.33 and 8.5.34 respectively plot the temperatures of occurrence and T_1 values at the two T_1 minima as a function of frequency. See also figures 7.2.2.53 and 7.2.2.54. As noted in §7.2.2/X=0.938 the experimental temperature-of-occurrence changes little with frequency. The model values increase with frequency as expected, by only about 1K over the range 2.7<F<10.7MHz, which is reasonable within experimental error given the models do not properly/at all take account of melting/desorption in the film or the non-dipolar relaxation component. Model T_1's at the T_1 minima increase linearly in F to a very good approximation as expected for dipolar relaxation, ($T_1^{\min} = \omega_0/m_2$, in the homonuclear case). Moreover for the Model 10 minima where $F_Q \rightarrow 0$ the plots effectively go through the origin too, showing heteronuclear relaxation can display this feature of homonuclear relaxation providing $0 \leftarrow F_Q \ll F_0$. In the Model 5B plot where $0 \nleftarrow F_Q \ll F_0$ for minimum#1, the lower T, longer τ_c minimum which for $\tau_c^{\text{Jhm\_sf}} > 1$ is the heteronuclear one, extrapolates to a significant negative offset, a consequence of the F_Q~1.4MHz produced in this fit. The $T_1^{\min\#1,2}$ *vs* F slopes represent the two dipolar interaction strengths, roughly ($1/m_2^{\text{ht}}$) and ($1/m_2^{\text{hm}}$) respectively − So it is likely that both experimental slopes being less than their model counterparts plus the

Figure 8.5.33, Temperature of T_1 Minima vs F, X=0.938, With Fit, EVERYTHING Dataset, [T_1 Data]

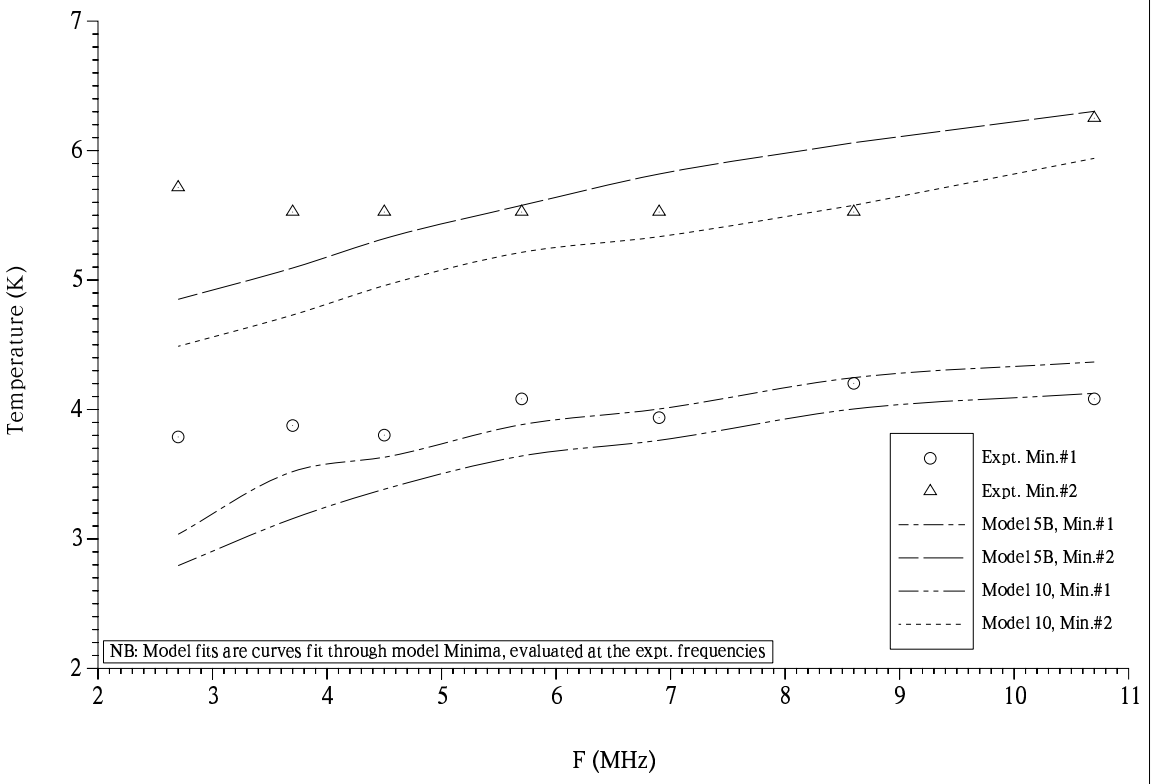

Figure 8.5.34, T_1 at T_1 Minima vs F, X=0.938, With Fit, EVERYTHING Dataset, [T_1 Data], Including Straight Line Fits

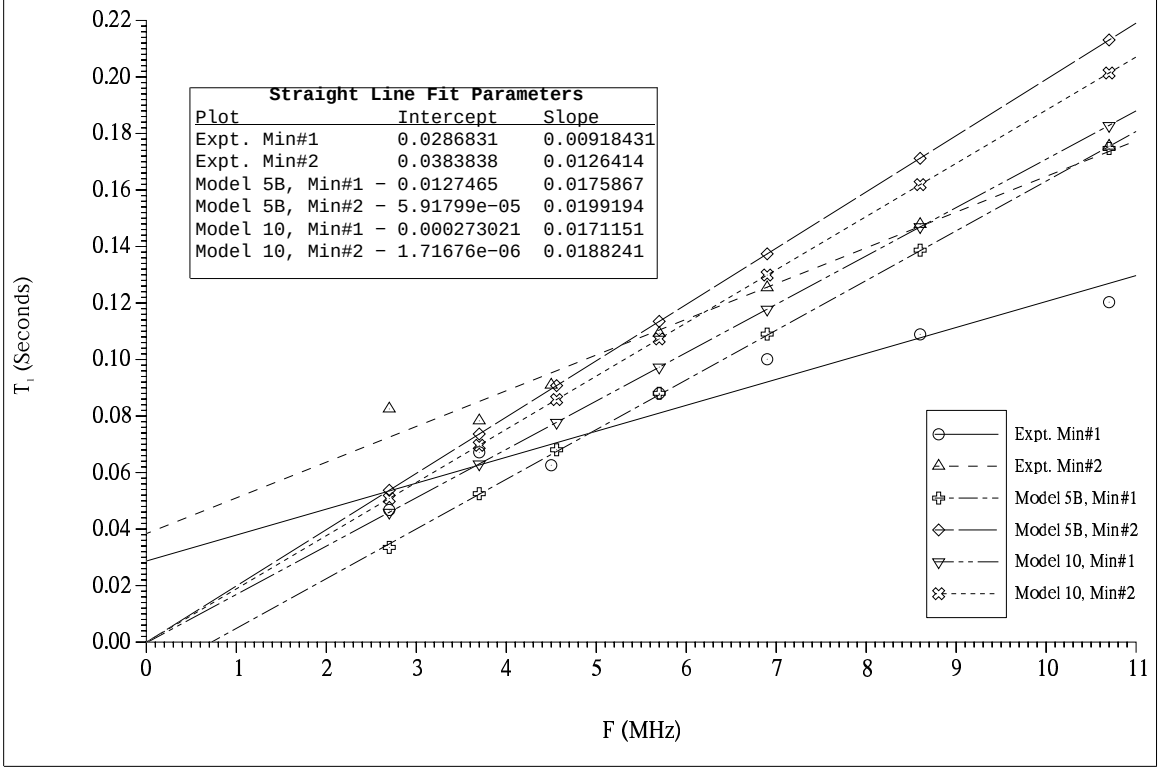

positive F=0 contribution to the experimental T_1 values is due to non-dipolar relaxation.

Figures 8.5.35 and 8.5.36 respectively plot the Slope and Intercept of the T_1-vs-F straight line fits against Temperature. See also figures 7.2.2.62 and 7.2.2.63. At low temperatures the model slopes are significantly bigger than those of the experimental data. As with the $T_1^{\min\#1,2}$ *vs* F slopes this is most probably due to the model fits underestimating the total relaxation of the system due to them not taking account of the non-dipolar component. If this explanation is correct, there should be a much greater difference between the experiment/model F=0 intercepts than the experiment/model slopes since the non-dipolar component should be frequency independent and therefore with a perfect data analysis method only the F=0 intercept would be affected. Here the figures show this is so. At mid-range temperatures where the T_1 minima occur, dipolar relaxation becomes stronger allowing it to dominate the non dipolar component, the F=0 intercept$\rightarrow$0 and the slope becomes small as the fast side (ie. where T_1 is frequency independent in 3 dimensions) of the T_1 minimum is approached.

***X*=1.0,** Figure 8.5.37 plots the temperature dependence data together with the models 5B and 10 fits. The fits are good, especially Model 10. Figures 8.5.38 and 8.5.39 plot the *ALL_1100* dataset temperature and frequency fits. Again, the temperature fits are good, especially Model 10, except at low temperatures where the 1.1K frequency dependence data has compromised the fit a little. Figure 8.5.38 shows why. The 3D models are unable to describe very well the T_1-linear-in-F 1.1K frequency data. In contrast Model F_2D provides a good fit the frequency data, underlining the point made in §8.4 that 2D characteristics appear to be applicable in the low temperature solid but at higher temperatures where layer promotion etc. occur, 2D characteristics diminish and 3D models are able to give good descriptions. 'T_1(1/e)' 1.1K data is also linear in F and very similar to the 'T_1' data presented here. Listing 8.5.18 contains the X=1.0 fit parameters.

Listing 8.5.18, NLLSQ_MODEL Miscellaneous Results for X=1.0.

```
ALL Dataset, Model 5B Fit
Sum of squares at convergence:    4.04525849
Fitted parameters;

rt0      =    10296.4     +/-    1838.78
tcjhm_sf =    6.57835     +/-    1.22671
m2hm     =    26.2600     +/-   0.305162
m2ht     =    27.5137     +/-    4.69403
wq       =    1.92550     +/-    2.26883
Ea       =    30.8742     +/-   0.257669
```

Figure 8.5.35, Slope (of T_1 vs Frequency) vs T, X=0.938, With Fit Data, EVERYTHING Dataset, [T_1 Data]

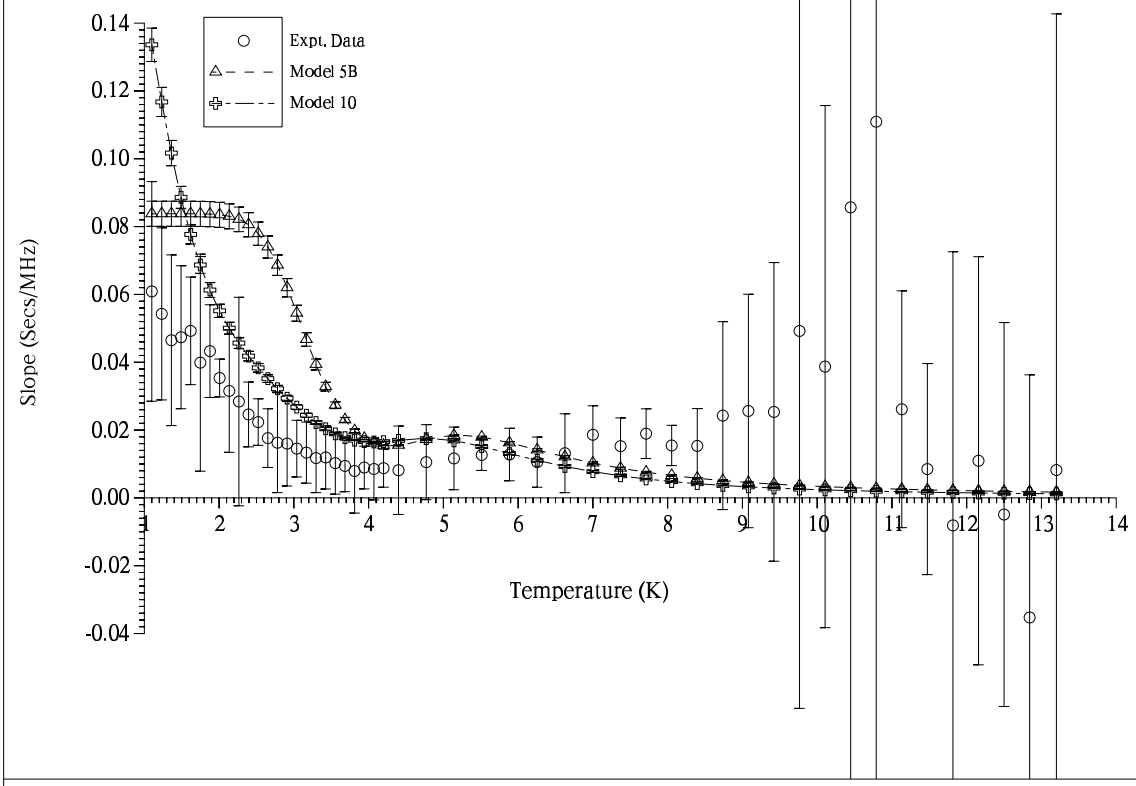

Figure 8.3.36, Intercept (of T_1 vs Frequency) vs T, X=0.938, With Fit Data, EVERYTHING Dataset, [T_1 Data]

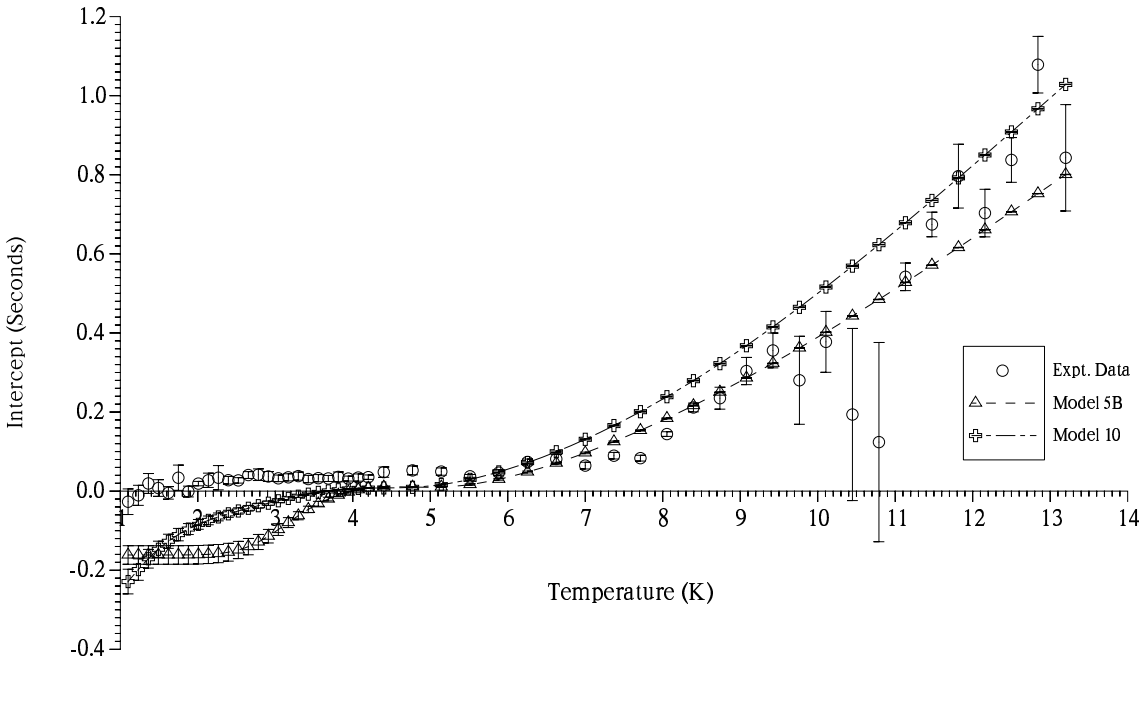

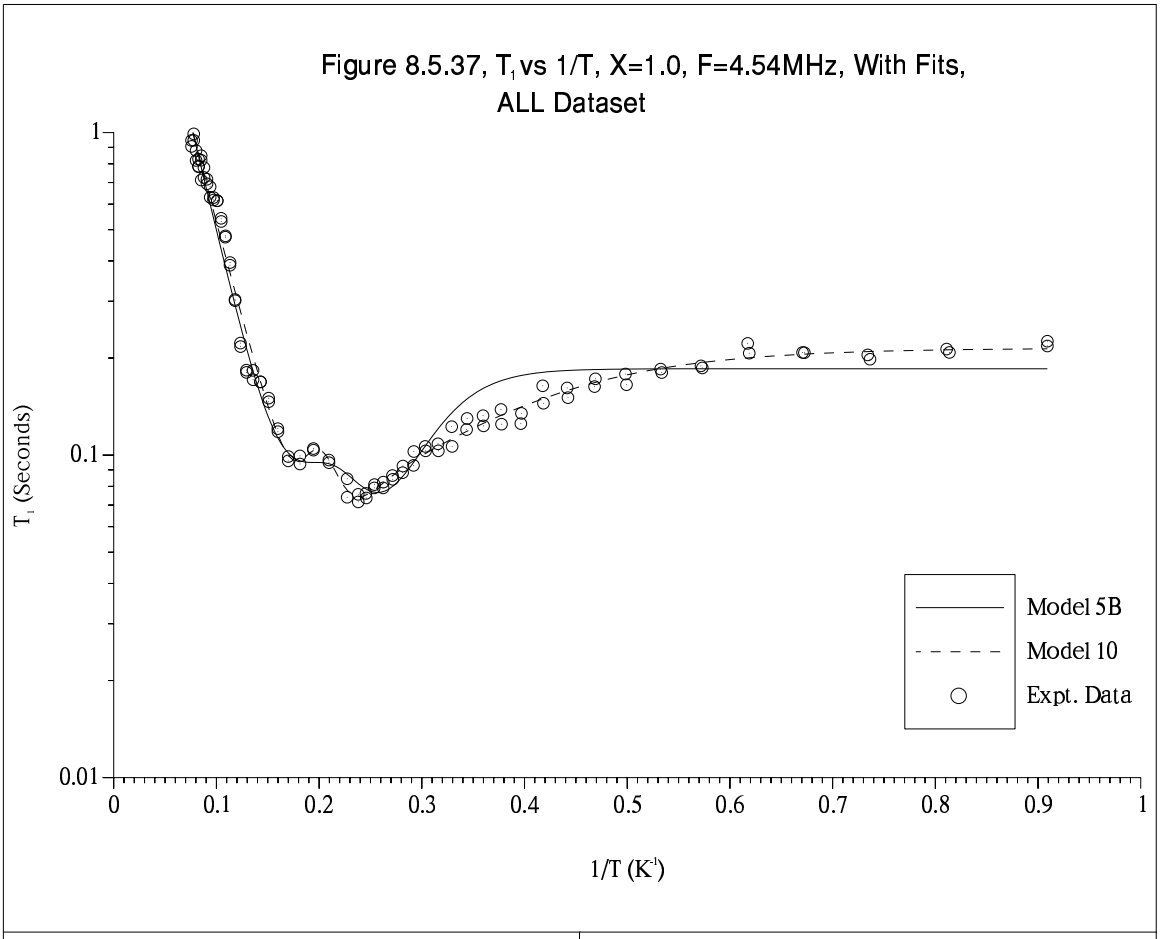
Figure 8.5.37, T1 vs 1/T, X=1.0, F=4.54MHz, With Fits, ALL Dataset
T1 (Seconds)
1/T (K-1)
Model 5B
Model 10
Expt. Data

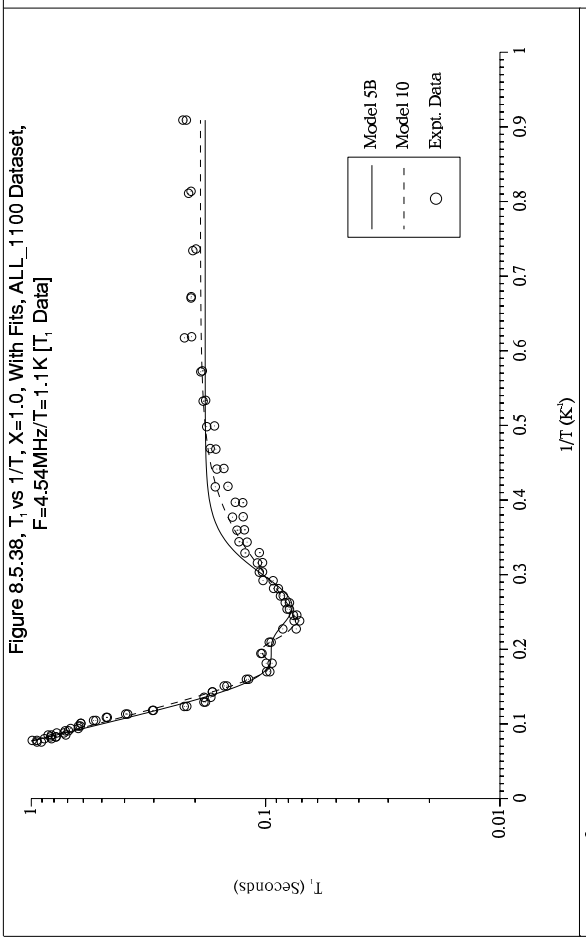
Figure 8.5.38, T1 vs 1/T, X=1.0, With Fits, ALL_1100 Dataset, F=4.54MHz/T=1.1K [T1 Data]
T1 (Seconds)
1/T (K-1)
Model 5B
Model 10
Expt. Data

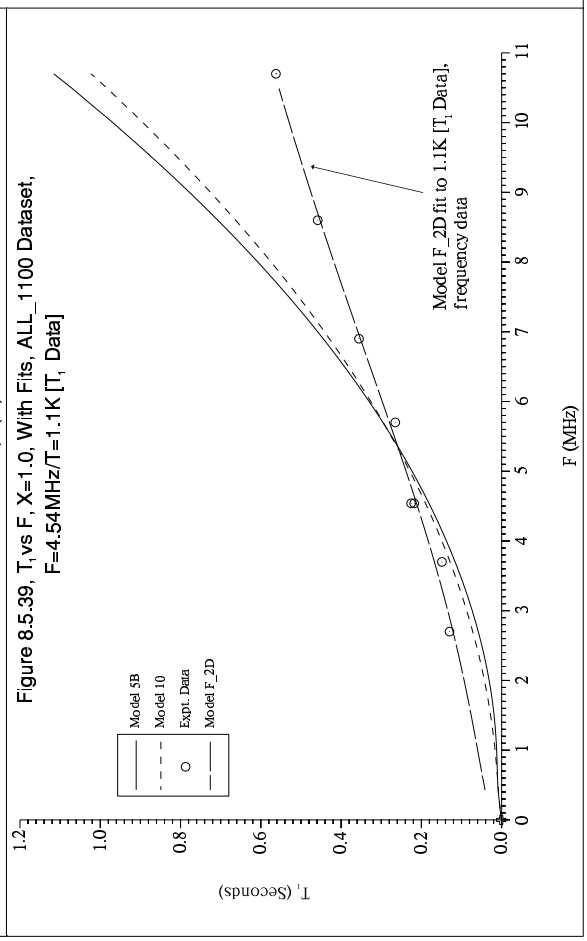
Figure 8.5.39, T1 vs F, X=1.0, With Fits, ALL_1100 Dataset, F=4.54MHz/T=1.1K [T1 Data]
T1 (Seconds)
F (MHz)
Model 5B
Model 10
Expt. Data
Model F_2D
Model F_2D fit to 1.1K [T1 Data], frequency data

```
rtcex    =   0.897935     +/-   0.234824


ALL Dataset, Model 10 Fit
Sum of squares at convergence:    34.5962098

Fitted parameters;

rt0_1    =    2.76108     +/-    10.6888
rt0_2    =    2001.08     +/-    4415.86
tcjhm_sf =    10.6073     +/-    27.0422
m2hm     =    18.5471     +/-    2.45713
m2ht     =    29.1213     +/-    74.8141
wq       =    2.82921     +/-    28.2488
Ea_1     =    3.33554     +/-    1.88107
Ea_2     =    19.4923     +/-    5.53078
rtcex    =   0.874716     +/-    3.69122
a        =    1.27962     +/-   0.448760
Tswitch  =    7.27517     +/-   0.787129


ALL_1100 Dataset, Model 5B Fit
Sum of squares at convergence:    5.51441559

Fitted parameters;

rt0      =    10290.7     +/-    558.684
tcjhm_sf =    6.59455     +/-   0.215320
m2hm     =    26.3315     +/-   0.244072
m2ht     =    27.6463     +/-   0.569137
wq       =    1.72956     +/-   0.261851
Ea       =    30.8145     +/-   0.216429
rtcex    =   0.949434     +/-   0.283659E-01


ALL_1100 Dataset, Model 10 Fit
Sum of squares at convergence:    2.43176531

Fitted parameters;

rt0_1    =    125.123     +/-    24.4270
rt0_2    =    15468.0     +/-    827.101
tcjhm_sf =    11.2612     +/-   0.382382
m2hm     =    28.6012     +/-   0.285885
m2ht     =    32.6958     +/-   0.696604
wq       =   0.100001     +/-   0.368167
Ea_1     =    15.5689     +/-   0.661820
Ea_2     =    28.5200     +/-   0.355440
rtcex    =   0.984940     +/-   0.219722E-01
a        =    2.32243     +/-   0.173612
Tswitch  =    5.31236     +/-   0.518962E-01


1.1K T1 Frequency Dependence Data, Model F_2D Fit
Sum of squares at convergence:   0.902014881E-03

Fitted parameters;

tcjhm_sf =    9.44541     +/-    153.231
m2hm     =    36.4594     +/-    131.732
m2ht     =    44.4105     +/-    78.4883
wq       =   0.100000     +/-    792.861
rtcex    =    37.9331     +/-    661.285
```

8.6 The Question of $\tau_c^{Jhm\_sf} < 1$ Fits

Depending on the guess-values supplied to the NLLSQ_MODEL software, fits with $\tau_c^{Jhm\_sf} < 1$ are sometimes produced, moreover for some Model F frequency

dependence fits $\tau_c^{Jhm\_sf} < 1$ is the software's preferred result. Whatever physical problems there might be with such results, it is desirable to investigate whether a set of consistently sensible fits to a variety of data can be obtained with $\tau_c^{Jhm\_sf} < 1$ and how that fit quality compares with the more usual $\tau_c^{Jhm\_sf} > 1$ result. To this end a set of trials were performed. X=0.85 was used since the two minima in T are both very distinct:

(1) *ALL* dataset data with and without the two minima emphasized/weighted ×200 were tried. The weighting ensures the fit goes as closely as possible through the two minima at the potential expense of a poorer fit through the lower temperature points. Result: The $\tau_c^{Jhm\_sf} < 1$ were poorer than $\tau_c^{Jhm\_sf} > 1$.

(2) Separate *EVERYTHING* dataset trials incorporating 'T_1' and 'T_1(1/e)' 1.1K frequency dependence data produced $\tau_c^{Jhm\_sf} < 1$ fits with slightly lower *sum-of-squares* values than $\tau_c^{Jhm\_sf} > 1$ but the $\tau_c^{Jhm\_sf} > 1$ fits looked better overall − that is the model misfit appeared more evenly spread over the temperature/frequency range.

(3) Using *ALL_1100* dataset data, separately incorporating 'T_1' and 'T_1(1/e)' 1.1K frequency dependence with the *ALL* 4.54MHz low temperature points emphasized/ weighted ×20 gave mixed results for $\tau_c^{Jhm\_sf}$ >1 &<1 best *sum-of-squares* values but all were broadly similar.

(4) As (3) but with the 1.1K frequency dependence data also emphasized/ weighted ×20. Following the rationale of (3) the purpose of this dataset was to give the $\tau_c^{Jhm\_sf} < 1$ fits a further chance to demonstrate if they could better fit the 1.1K frequency data where, as §8.5 shows, model/data discrepancies are most noticeable. For the 'T_1' incorporated dataset the results were mixed, for the 'T_1(1/e)' one the $\tau_c^{Jhm\_sf} < 1$ fits were a little better.

The general conclusion is: There is no evidence $\tau_c^{Jhm\_sf} < 1$ fits can give consistently better fits. Therefore the assumption is they cannot be a good physical representation of the data.

8.7 The Model Fit Parameters *vs* Coverage

This section presents the Model Fit parameters ($R_{\tau 0,}$ $\tau_c^{Jhm\_sf}$, m_2^{hm}, m_2^{ht}, F_Q, E_a and $R_{\tau cex}$) obtained over the coverage range $0.75 \leqslant X \leqslant 1.0$ and discusses them with a view to better understanding the coupled relaxation in the film. *ALL* dataset data exists for $0.75 \leqslant X \leqslant 1.5$, the *ALL_1100* dataset extends over $0.75 \leqslant X \leqslant 1.1$ and *EVERYTHING* dataset data over $0.75 \leqslant X \leqslant 0.938$. Naturally for the higher coverages, in particular X>1.0 the second layer fluid is present which the models discussed in this chapter ignore. While

bearing this in mind, together with the fact that most of the T_1 relaxation takes place in the solid first layer, it is useful to include these high coverages here to help elucidate any trends in the high coverage data.

8.7.1 $R_{\tau 0}$ − The Vacancy Tunnelling Attempt Rate

Figure 8.7.1.1 plots $R_{\tau 0}$ *vs* X. $R_{\tau 0}$ increases approximately linearly with coverage as far as X=0.9 where maximum first layer density at the elevated temperatures effective in the model fits occurs. Then $R_{\tau 0}$ slowly tails off as T_1 decreases with the slowly increasing relaxation burden imposed by the growing second layer. The increase in the tunnelling attempt rate to 0.9 monolayers is presumed to be due to ^{3}He spins coming closer together, making the probability of tunnelling greater. The energy required to actually tunnel a vacancy E_a is a separate issue.

8.7.2 $\tau_c^{Jhm\_sf}$ − The Correlation Time Scaling Factor

Figure 8.7.2.1 plots $\tau_c^{Jhm\_sf}$ *vs* X. It is evident the Model 10 fits do not produce very reproducible results. This is due to the ability of the two regimes ($T>T_{switch}$ and $T<T_{switch}$) to follow physical changes (eg. melting) in the film very closely which can strongly affect the resultant $\tau_c^{Jhm\_sf}$. Also, the *ALL_1100* and *EVERYTHING* datasets (not shown here) show reduced reproducibility too since the extra components compromise the temperature dependence fits which provide the best method for estimating $\tau_c^{Jhm\_sf}$, primarily via the relative locations of the two minima. With the Model 5B fits the trend is a linear decrease in X for X=0.75→0.9, where layer promotion occurs. At higher coverages $\tau_c^{Jhm\_sf}$ is roughly constant as expected for an unchanging solid or fluid completed monolayer/underlayer.

Theoretically how should $\tau_c^{Jhm\_sf}$ scale with coverage? For homonuclear relaxation the correlation time is, essentially, $\tau_c^{hmn} = a^2/2D$, where a is the average ^{3}He−^{3}He internuclear distance and D is the diffusion constant describing whatever motion is present. Given $a = 1/\sqrt{X}$, we have, $\tau_c^{hmn} \propto 1/X$. The heteronuclear correlation time, the average time needed for a ^{3}He spin to diffuse to a place where the local field it experiences due to substrate spins is significantly changed is, $\tau_c^{htn} = c^2/2D$, where c is the average in-plane ^{3}He−Substrate internuclear distance. Here, for simplicity, the assumption is being made that the system is flat − that is the ^{3}He and surface layer substrate spins all lie in a plane. This allows us to define an effective *coverage* of substrate spins X_s for which $c = 1/\sqrt{X_s}$, giving $\tau_c^{htn} \propto 1/X_s$. Using figure

Figure 8.7.1.1, $R_{\tau 0}$ vs X, From Model Fits, ALL dataset

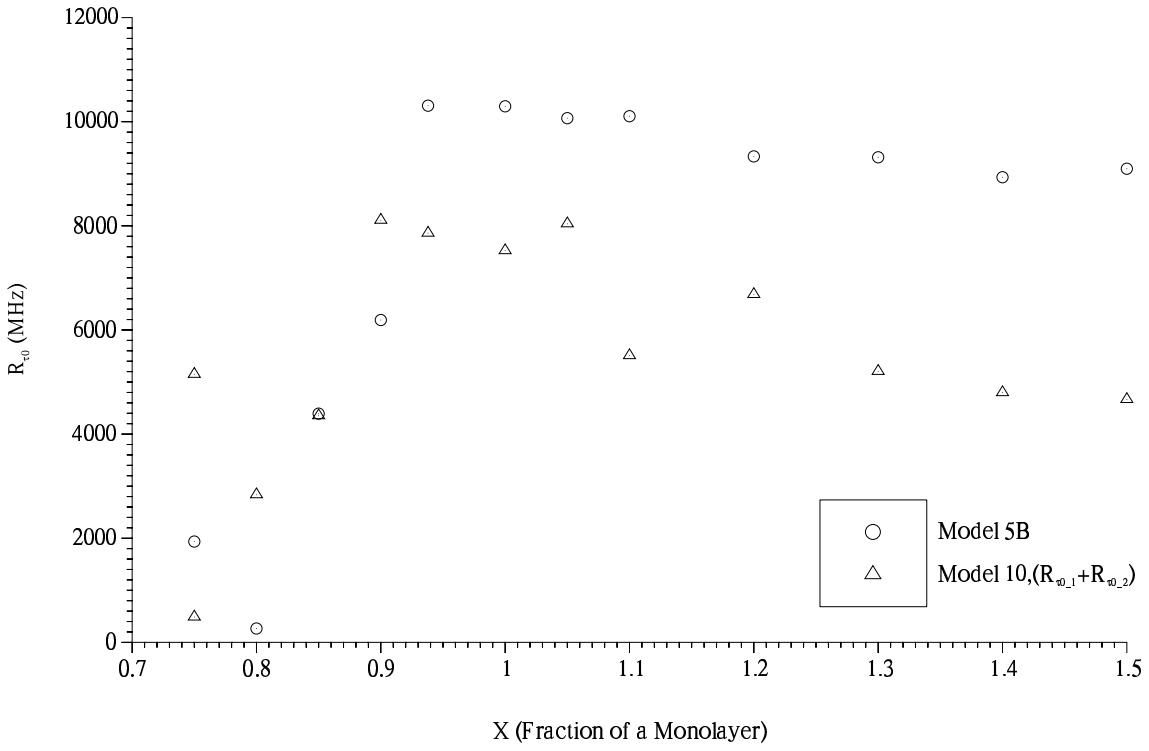

Figure 8.7.2.1, $\tau_c^{Jhm\_sf}$ vs X, From Model Fits, ALL Dataset

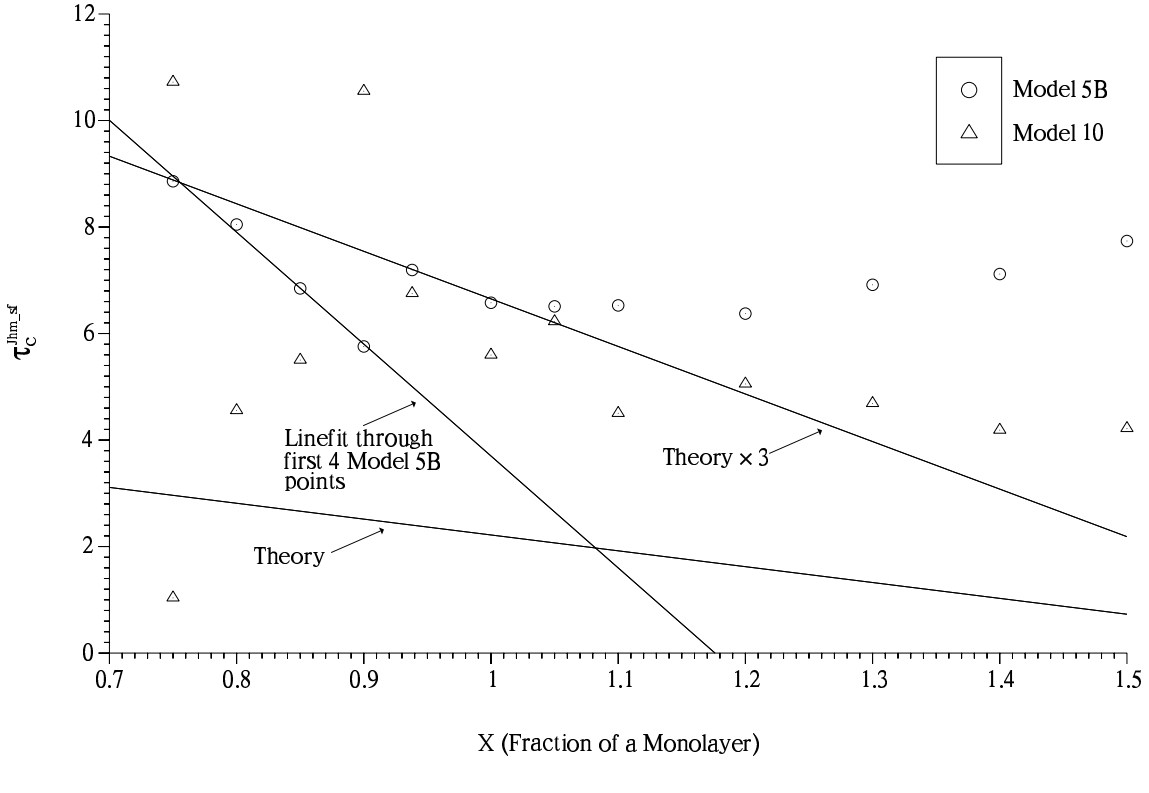

8.2.2 it is evident that at registry, where X=0.75 the ratio of ^{14}N:^{3}He spins is 3:1 giving X_s = 2.25 monolayers for the nitrogen (or equally the boron) spins. Therefore,

$$\tau_c^{jhm\_sf} = \frac{\tau_c^{hmn}}{\tau_c^{htn}} = \frac{a^2}{c^2} = \frac{(1/X)}{(1/X_s)} = \frac{2.25}{X} \qquad 8.7.2.1$$

Giving at;

- X=0.75, $\tau_c^{Jhm\_sf}$ = 3.0, [The experimental figure is 9 − 3× bigger)
- X=0.9, $\tau_c^{Jhm\_sf}$ = 2.5, [The experimental figure is 5.8 − 2.3× bigger)
- X=1.0, $\tau_c^{Jhm\_sf}$ = 2.25, [The experimental monolayer plateau at 6.6 − 3× bigger)

So how can the experimental $\tau_c^{Jhm\_sf}$ being a factor of ~3× bigger than theory be explained? Counting in the boron spins only brings the figure up to 6×. An additional explanation involves layer promotion/desorption since promoted/desorbed ^{3}He spins are no longer available to the short ranged FMR interaction − reducing the first layer coverage X, increasing the value of $\tau_c^{Jhm\_sf}$ in equation 8.7.2.1. The X=0.05 edge-sites film is also a factor in reducing the effective coverage since it should be subtracted from X. Another explanation involves the microscopic nature of the motion: The concept of diffusion used in obtaining the τ_c's is a long time phenomenon but the times of interest in defining $\tau_c^{Jhm\_sf}$ are short. Here the detailed nature of the microscopic motion (exchange and/or thermally activated vacancy tunnelling) and the substrate spin geometry, which will likely be correlated may be able to significantly reduce τ_c^{htn}, increasing $\tau_c^{Jhm\_sf}$.

8.7.3 m_2^{hm} − The (homonuclear) Second Moment

The homonuclear second moment describes the strength of the homonuclear dipolar interaction. Figure 8.7.3.1 plots m_2^{hm} *vs* X. How should m_2^{hm} vary as a function of X? Recalling $m_2^{hm}=\hbar^2\gamma_{He}^4(\mu_0/4\pi)^2<1/r_{He\text{-}He}^6>$, $<r_{He\text{-}He}> \propto 1/\sqrt{X}$, $\therefore$ $m_2^{hm} \propto X^3$. Even where the data increases with coverage, over X=0.75→0.85 that increase is slower even than a linear law. A little thereafter m_2^{hm} decreases approximately linearly with X. The most likely explanation is that for X=0.75→0.85 layer promotion/desorption slows the increase of m_2^{hm} from the expected X^3 law as some of the additional ^{3}He spins enter the second layer and desorbed gas where they contribute nothing to relaxation and hence to m_2^{hm}, instead burdening the first layers spins with relaxing them. Above 0.85 monolayers a greater proportion of the spins enter the second layer/desorbed gas causing relaxation efficiency to turn over and decline. The graph shows that extrapolating back to the end of the approximately linear region whose existence implies all additional spins enter the

Figure 8.7.3.1, m_2^{hm} vs X, From Model Fits

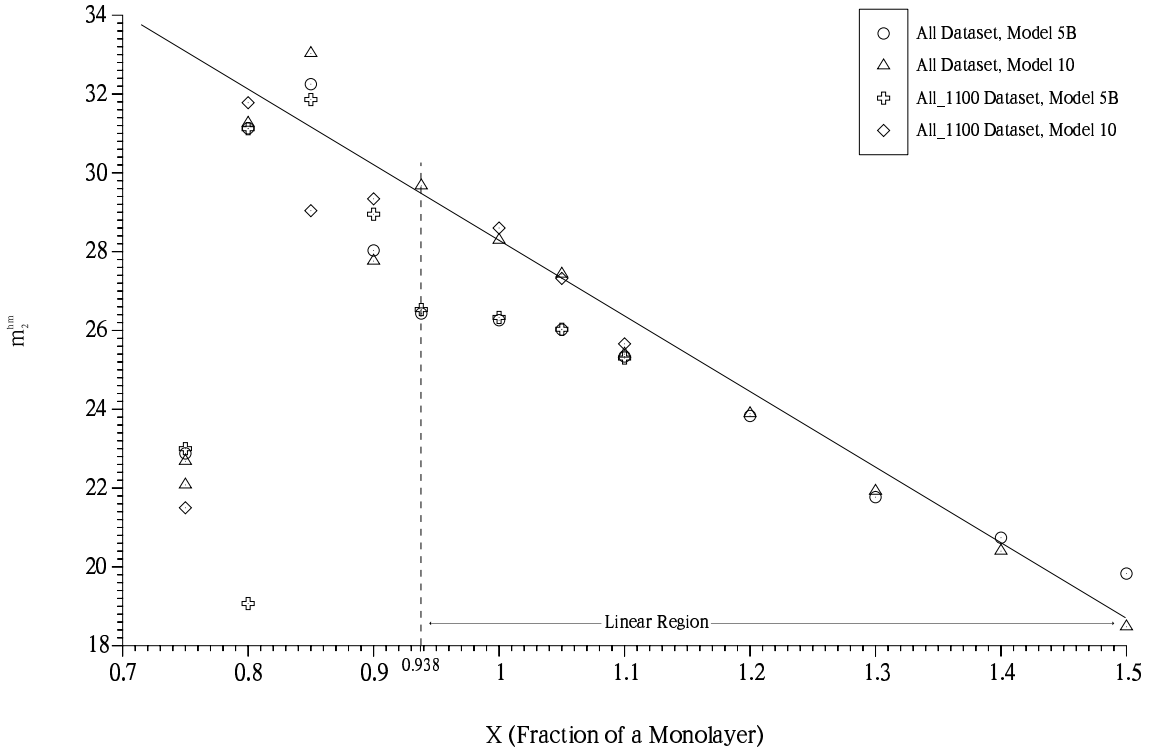

Figure 8.7.4.1, m_2^{ht} vs X, From Model Fits, ALL Dataset

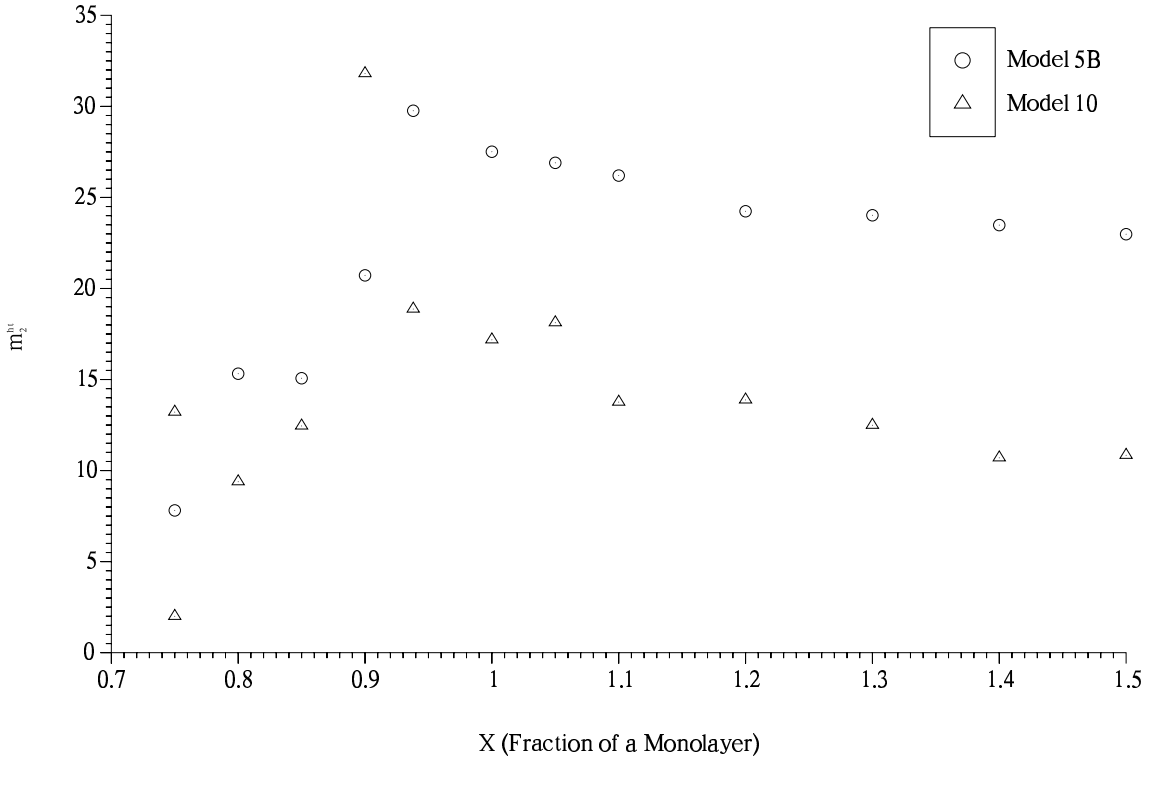

second layer/desorbed gas, shows that X=0.938 is the cut-off point after which all additional spins do enter the second layer/desorbed gas − that is maximum first layer density. The reason for this relatively low coverage is because the models do not take account of layer promotion/desorption as temperature rises − Both m_2^{hm} and m_2^{ht} are assumed to be constant in temperature − which experimentally they patently are not. Without independent information on higher layer and desorbed spin populations or energies of promotion as a function of X etc. this is an unavoidable limitation of the models. As a basic confidence test, the calculated rise in m_2^{hm} over 0.75→0.85 monolayers where layer promotion/desorption will be smallest, is consistent with the data in figure 8.7.3.1 − $(0.85^3/0.75^3) \sim 1.46 \sim (33/22)$. The reason for the apparently anomalous Model 10 point at X=0.9 and the plateau-like region around X=1 in the Model 5B points in unclear. However the Model 10 fits are preferred since they produce better numerical fits to the data and do not cause artifact features in m_2^{hm} and m_2^{ht}, c.f. some other parameters such as $\tau_c^{Jhm\_sf}$. This is because m_2^{hm} and m_2^{ht} represent the strengths of the two dipolar interactions which depend in a simple way on T_1 throughout the T_1 *vs* T dataset.

8.7.4 m_2^{ht} − The (heteronuclear) 'Second Moment'

m_2^{ht} is the heteronuclear analogue of the second moment of the homonuclear NMR line. It describes the strength of the heteronuclear dipolar interaction. Figure 8.7.4.1 plots m_2^{ht} *vs* X. We need to know theoretically how should m_2^{ht} vary a a function of X? The situation is not as simple as in the case of m_2^{hm}. There are two limiting regimes which can be considered:

(1) If the adsorbed ^{3}He spins in the film are a large distance d from the BN surface (where *large* means large compared to the substrate spins interatomic separation b, then m_2^{ht} will be defined by d and be independent of b.

(2) If the ^{3}He spins were to be <u>on</u> the BN surface, that is coplanar with the substrate's surface-layer spins then the system could be regarded as a single film comprising ^{3}He, nitrogen and boron spins. This is the approximation used to estimate $\tau_c^{Jhm\_sf}$. In this limit we expect $m_2^{ht} \propto X^3$, since $<r_{He-S}> \propto 1/\sqrt{X}$ where He−S is the ^{3}He−substrate spin internuclear separation c, in the plane. In this limit m_2^{ht} naturally has the same coverage dependence as m_2^{hm}.

In reality (2) could not exist and the system must lie between the two limits and m_2^{ht} increase with coverage but at a slower rate than X^3. However the system has the

potential for m_2^{ht} to change in a much more complicated and even discontinuous fashion w.r.t. X due to geometrical correlations between the ^{3}He film's spins and those of the substrate, as coverage increases and phase changes take place in the film. As a hypothetical but simple (and admittedly energetically unlikely) example, consider figure 8.7.4.2 where the registered film has undergone a short creep such that a ^{3}He spin moves to be directly over a nitrogen spin. Two of the three nitrogen spins on the hexagon having an adsorbed helium spin have lost their nearest ^{3}He neighbour status but the third spin is now much closer to the ^{3}He providing $d<c$. Given the $m_2^{ht} \propto <1/r_{He\text{-}N}^6>$ relation a big jump in m_2^{ht} occurs.

The fitted m_2^{ht} shows a fast but erratic rise to a peak at 0.9−0.938 monolayers followed by a slow asymptotic fall towards second layer completion. The form of the rise is consistent with the above arguments but the surprising thing is the size of the increase − a factor of 3.9× (Model 5B) and 16× (Model 10). On an X^3 law 1.73 and 1.96 respectively are expected. As in the m_2^{hm} case the slow fall off of m_2^{ht} with X is believed to be due to the relaxation burden placed on the first layer ^{3}He spins by the additional second layer/desorbed gas spins which in turn slow the recovery of the substrate spins.

Figure 8.7.4.3 plots the Model 5B m_2^{hm} and m_2^{ht} values together for comparison. It is evident that at and above the monolayer the two interaction strengths are very similar with homonuclear relaxation unsurprisingly being affected relatively a little more by the second layer/desorbed gas at high coverages. At and above the monolayer a first layer incommensurate solid solid should exist and geometric correlation effects should therefore be minimal. This supports the idea that, comparing the m_2^{hm} and m_2^{ht} rises with X, the later, greater magnitude and erratic rise of m_2^{ht} is due to geometric correlation effects − occurring as it does in the intermediate coverage/mixed phase region of the phase diagram where any such effects should be most noticeable.

8.7.5 F_Q− The Substrate Quadrupolar Frequency

Naïvely, one would not expect the substrate quadrupole frequency to be affected by the helium film at all. However the quadrupole frequency inferred here is not necessarily the same quantity that would be measured in a conventional NQR on Boron Nitride experiment. Instead the ^{3}He spins act as a microscopic probe of the system and couple with the quadrupolar energy levels they encounter in their local environments. As mentioned earlier, a possible explanation for the coverage dependence of the quadrupole frequency is the change in EFG at the ^{14}N nucleus due to the polarisation of the ^{14}N−^{3}He adsorption ‘bond’ which would change with the orientation of the ^{3}He adatom with

Figure 8.7.4.2, Helium-3 in the $\sqrt{3} \times \sqrt{3}$ R30 Registered Structure Adsorbed on Hexagonal Boron Nitride. Shown Here Undergoing a Hypothetical Short Ranged Creep.

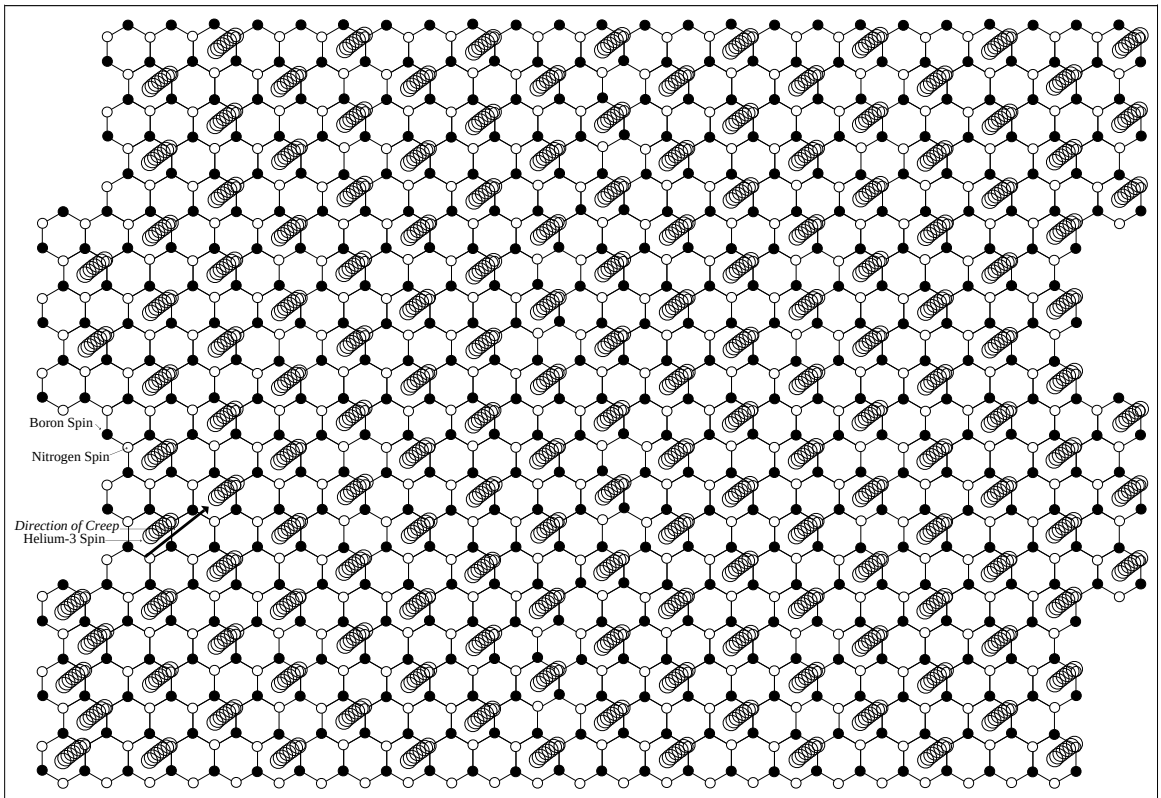

Figure 8.7.4.3, m_2^{hm} and m_2^{ht} together vs X, From Model 5B Fits, ALL Dataset

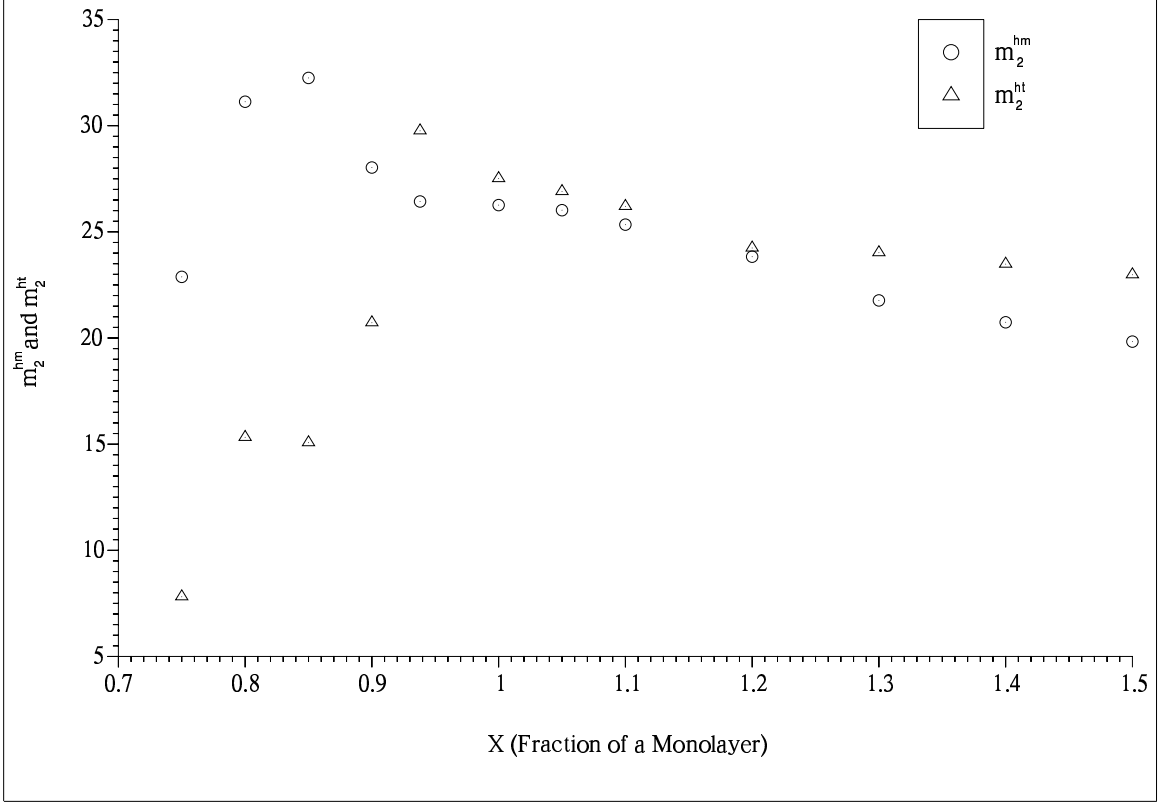

respect to the substrate crystalline axes. The low polarisability of the ^{3}He atom however, makes this an unlikely candidate.

Before further theorising it is useful to examine the fit data. Figure 8.7.5.1 shows Models 5B and 10 fits to both *ALL* and *ALL_1100* datasets. With the exception of X=0.75 where T_1 falls at low temperatures as motion slows (figure 8.5.1) and the $J_2(\omega_{He}+\omega_Q)\rightarrow J_2(0)$ term of equation 8.4 for ρ_2, probably aided by 2D effects, dominates relaxation − there is significant ambiguity in the estimates for F_Q. Introducing the 1.1K frequency dependence data helps considerably since any instances of F_Q falling within the frequency range of the experimental data ($2.7\leqslant F\leqslant 10.7$MHz) should show up as dip or inflection in frequency which the fitting algorithm will will 'lock onto'. This clearly occurs at X=0.75, verifying the temperature dependence data alone result. Conversely if no such feature occurs in the 1.1K frequency data the algorithm is lead to infer F_Q must lie outside the experimental frequency range, in practice that it lies < 2.7MHz. Here the actual values can be a little meaningless due to the algorithm having to extrapolate in frequency, possibly to frequencies well below the lowest experimental ones. Some arbitrariness in these F_Q is therefore inevitable. The best results tend to come from the Model 10/*ALL_1100* dataset giving the closest fits in the temperature direction and qualifying them in the 1.1K frequency domain. They show F_Q ~4.3MHz at 0.75 monolayers, falling to ~1MHz at X=0.8. Thereafter F_Q falls to a very low value (ie.$\ll$2.7MHz), arbitrarily limited to 0.05MHz by the NLLSQ_MODEL software to aid convergence. The *EVERYTHING* dataset fits give very similar results to the *ALL_1100* ones.

Working on the assumption that at the applied field used in most of this study the ^{14}N signal will be a single quadrupole line with the Zeeman splitting only smearing out the line a little, some points can be made and a possible explanation for the data produced: For so-called pure quadrupole resonance in zero field there is no preferred direction in space and the resonant frequency is independent of crystal orientation **[47,p.249]**. In an NQR experiment the intensity of the quadrupole resonance does however, vary with the angle the applied RF field makes to the EFG symmetry axis. It is a maximum at 90^o and a minimum at 0^o **[220,p.7]**. Accepting the ^{14}N F_Q cannot change as a function of orientation (preventing structural changes in the ^{3}He film from effectively re-orientating the ^{14}N nucleus and changing the ^{14}N F_Q seen from the ^{3}He spins' frame of reference), could the <u>intensity</u> of the ^{3}He−^{14}N coupling depend on the relative position of the ^{3}He spin? If so could the X=0.75→0.8→… fall off in F_Q be explained as follows? :− Assume F_Q of ^{14}N in BN is ~4.5MHz. The maximum intensity

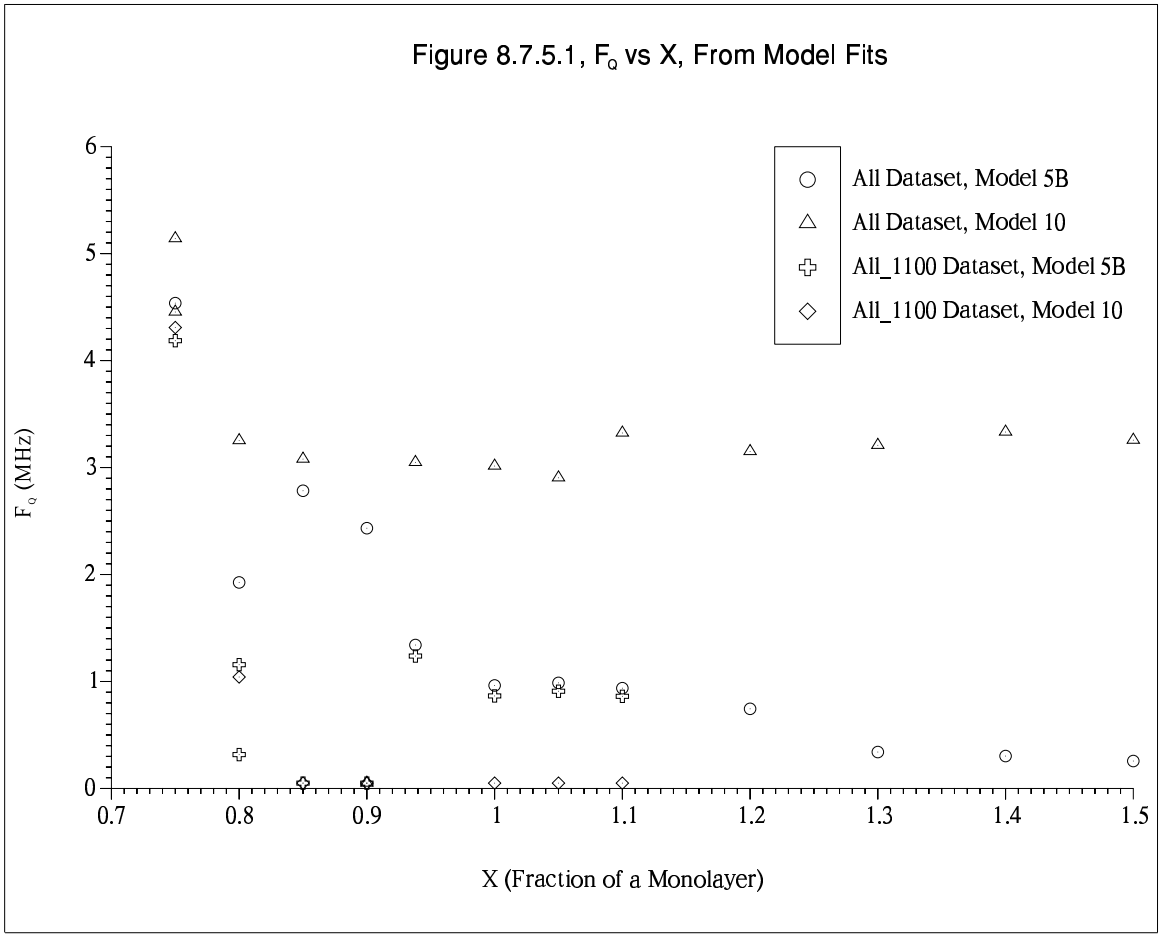

of the $^{14}N-^{3}He$ coupling then occurs at registry due to the unique configuration in which all of the ^{3}He spins are located at a hexagon centre where they will have the maximum $3 \times {}^{14}N$ nearest-neighbour spins all of which are in the arrangement closest to the optimum 90^{o} $^{3}He-^{14}N$ 'bond' axis to $^{11}B-^{14}N$ bond (and crystalline EFG) axis in-plane angle as shown in figure 8.7.5.2.

Figure 8.7.5.2, Helium-3 Spin Adsorbed on a BN Basal Plane Hexagon Centre

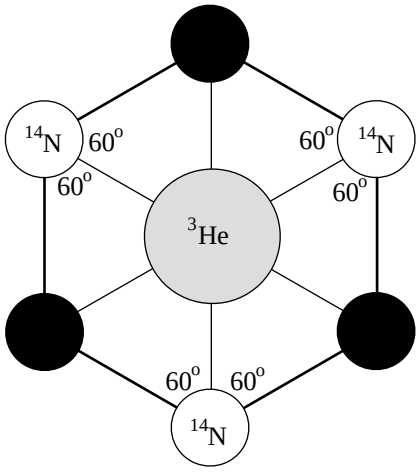

This will be particularly effective if the ^{3}He−substrate plane distance *d*, is small due to the localising effect of the substrate potential wells. As coverage rises and ^{3}He spins move away from the hexagon centres, the intensity of the ^{14}N−^{3}He relaxation falls-off and other substrate frequencies dominate. Assuming the 4.5MHz/*X*=0.75 effects are due to ^{14}N F_Q ~4.5MHz, then since these other frequencies will be much lower, the values of F_Q obtained from the fitting process, effectively an average over those frequencies, will fall too as figure 8.7.5.1 shows. T_1 rises as figure 7.2.1.2 demonstrates due the the less efficient transfer of magnetisation to the substrate even though m_2^{ht} rises as shown in figures 8.7.4.1 and 8.7.4.3 as the average ^{3}He−substrate spin separation decreases with increasing *X*. What then might these other frequencies be? Figure 8.7.5.3 illustrates the more important ones. Nitrogen-14 and Boron-10 are both presented in the low field limit, where it is valid. The shading indicates line broadening due to Zeeman splitting of their degenerate $m=\pm n\leftrightarrow\pm(n-1)$ quadrupole transitions and is given by **47**,

$$F^{\mp n\leftrightarrow\mp(n-1)} = F_Q \pm \gamma B_0 \cos\theta \qquad 8.7.5.1$$

where θ is the angle between the axes of the crystalline EFG and the applied field. The ^{10}B frequencies are estimated from the measured ^{11}B F_Q (1.47MHz) by assuming the EFG '*eq*' at the ^{10}B nucleus is the same as for ^{11}B. The relative quadrupole moments '*eQ*' are given in Appendix 1 and the estimated quadrupole frequencies for ^{10}B are then given by,

$$F_Q = \frac{3e^2qQ}{4hI(2I-1)}(2|m|-1) \qquad 8.7.5.2$$

for the $\pm m\leftrightarrow\pm(m-1)$ transition.

Boron-11 is given in the high field limit where it is valid. For convenience it is shown as three distinct frequencies which should be a good approximation given the powder pattern for the first order splittings of an ***I***=3/2 species (figure 2.1.2). In the low field limit its splittings become more complicated − there are five lines, the four α, α', β and β' plus a low frequency transition **47**. This regime occurs for frequencies below $\gamma_{He}B_0$ = 4.5MHz and is not considered here. As a guide to the eye, the dashed box indicates our main area of interest − around the ^{3}He 4.5MHz field. Note: Figure 8.7.5.3 ignores the signs of the gyromagnetic ratios and e^2qQ quadrupole coupling constants on

Figure 8.7.5.3, Diagram Illustrating Proposed Resonant Frequencies as a Function of Applied Field for Helium-3 on Hexagonal BN

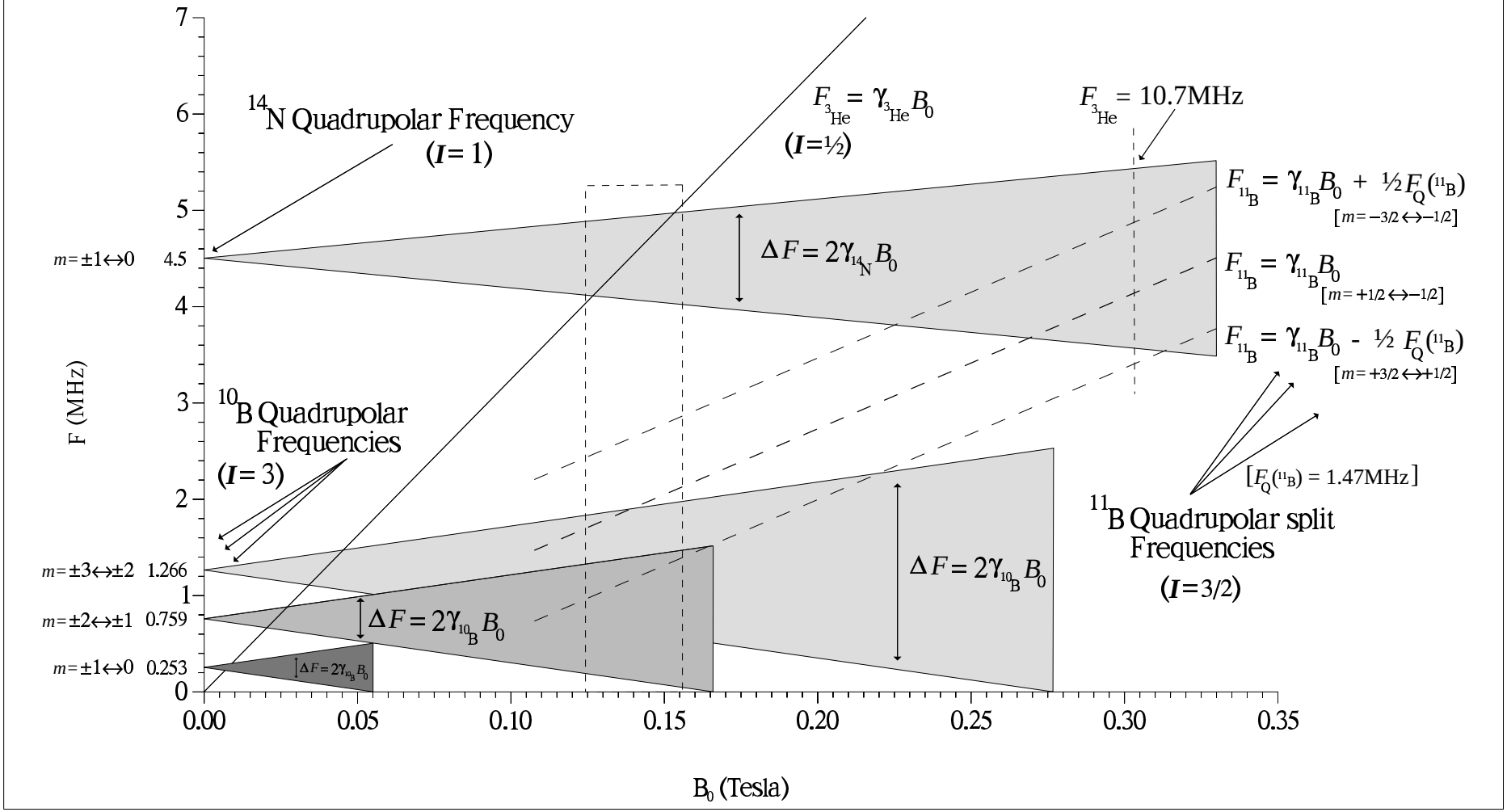

the basis that whatever the actual signs of the two frequencies ω_x and ω_y, either $J_0(\omega_y - \omega_x) \rightarrow 0$ or $J_2(\omega_y + \omega_x) \rightarrow 0$ will be fulfilled for ρ_2 (equation 8.4) at the frequency crossing points. For ^{3}He resonant at 4.5MHz the figure indicates that the frequency transitions available for ^{3}He to couple with, other than ^{14}N are; the three × ^{11}B splittings centred on 2.64, 1.90 and 1.17MHz plus the Zeeman broadened $\pm3 \leftrightarrow \pm2$ and $\pm2 \leftrightarrow \pm1$ ^{10}B quadrupolar ones centred on 1.266 and 0.759MHz. The ^{11}B transitions are the preferred candidates, having the higher frequencies (ie. closer to ^{3}He frequency) and 4 × the isotopic relative abundance. Also and more importantly, being due to Zeeman rather than quadrupolar levels, they will not have the same ^{3}He−Substrate 'bond' -to- B−N bond axis angle intensity relation as ^{14}N is proposed to have. It is not clear what effect the Zeeman splitting of the ^{10}B levels, which is relatively speaking much larger than for ^{14}N owing to their larger gyromagnetic ratio plus smaller quadrupole frequencies, will have on the proposed orientational intensity-of-coupling relation for ^{10}B with ^{3}He. If it were to be significantly different it could allow the ^{10}B levels to play a significant role in the fall-off of fitted F_Q with X as X=0.75→1.0. In passing its also worth pointing out that in the ^{3}He−^{14}N cross relaxation work of Van Keuls et. al. **[218,219]** the Zeeman spread of ^{14}N orientations inferred from the ^{3}He data was significantly narrower than predicted on a powder average.

If the ^{14}N F_Q is ~4.5MHz the question arises as to why the the resonance was not seen at zero field given the good ^{3}He signals at X=1 and the fact that $N(^{14}\text{N})/N(^3\text{He}@X=1)$ is more than 2 orders of magnitude? Van Keuls found the ^{14}N quadrupole resonance hard to detect in his solid nitrogen layers. The bulk ^{14}N T_1 may be long and its T_2 short. Moreover, even if a ^{3}He layer gives a usably short relaxation time to the ^{14}N surface spins, unless the bulk ^{14}N spin diffusion time is comparably short, only those surface layer ^{14}N spins, a tiny fraction of the total, will be visible. Further factors conspiring to make signal detection difficult are; the combined intensity of the $\boldsymbol{I}$=1 degenerate $\pm1 \leftrightarrow 0$ lines measured in a pulse-NMR experiment being only a factor $\sqrt{2}/4$ of that obtained from an equivalent $\boldsymbol{I}$=½ species **[85]**, the Zeeman broadening on top of that and the reduced tipping angle. With the spectrometer RF pulse amplitude B_1 and pulse duration τ set to apply a 90° pulse to resonant ^{3}He spins at 4.5MHz, we have $\gamma_{He} B_1 \tau = \pi/2$. Treating the ^{14}N spins with their proposed F_Q=4.5MHz using the fictitious spin-½ formalism **[47]**, they will be tipped an angle $[I(I+1) - |m|(|m|-1)]^{½} \gamma_N B_1 \tau = \sqrt{2}\gamma_N B_1 \tau$. Substituting $B_1 \tau = \pi/2\gamma_{He}$, gives the tipping angle $\sqrt{2}\gamma_N \pi/2\gamma_{He} = 0.211$ radians ≡ 12°. Compared to ^{3}He, only a fraction $\sin(12^o) \equiv 21\%$ of the magnetisation is tipped into the transverse plane where it can be detected as an FID.

8.7.6 E_a− The Activation Energy

The fitted activation energies are in reasonable agreement with the directly obtained values discussed in §7.2.3.3. Figure 8.7.6.1 shows the Model 5B fit values together with the directly obtained T_2 melting and desorption maximum ones. Fit E_a's show the same basic features as the T_2 melting maximum data − namely a rise to a near plateau at X=1.0 followed by a very slow fall-off above one monolayer. Fitted E_a values occurring between the two T_2 measures is consistent with the dominant features of the T_1 data, namely the two minima, falling between the T_2 melting and desorption maxima in temperature. See figure 7.2.3.7. Notice the apparently anomalous point at X=0.8. figure 8.7.6.2 includes some Model 10 fit data. This model with its two separate temperature regimes shows the Model 5B fit was uniquely dominated by a low temperature features at X=0.8 − Its E_a value is very close to the Model 10 E_{a_1} with E_{a_2} being consistent with the general Model 5B and Model 10 E_{a_2} trend. The low temperature feature in question is the 1.233K minimum (see figures 7.2.2.37 and 7.2.3.8). It is also likely the simplistic Model 5B's fitting inadequacies are exacerbated at X=0.8 by the complex nature of the film and by its phase transitions with temperature.

8.7.7 $R_{\tau cex}$ or J − The Exchange Frequency

$R_{\tau cex}=1/\tau_c^{ex}$,$\tau_c^{ex}$ is the correlation time in the low temperature limit where thermally activated vacancy tunnelling is suppressed and exchange motion dominates. $R_{\tau cex}$ is therefore expected to be proportional to J, the Heisenberg two particle exchange frequency. See §2.2.2. The NLLSQ_MODEL software was supplied with frequencies in units of MHz. $R_{\tau cex}$ therefore has units of $(10^6/2\pi) \times \sec^{-1}$. Using $J=0.267/\tau_c$, we have,

$$J = 0.04249 \times 10^6 \times R_{\tau cex} \ (\sec^{-1}) \qquad 8.7.7.1$$

It is useful to compare the BN J values with those obtained from Grafoil. Figures 8.7.7.1 and 8.7.7.2 do this. The Grafoil data is from reference **60**. In order to plot the Grafoil data with the BN data it was necessary to rescale the Grafoil coverages to those of BN. This has been done using the following three criteria; (1) Arrange for the Grafoil registry coverage (0.61 of a Grafoil monolayer) to appear at X=0.75 on the BN scale where registry on BN occurs. The point being that the occurrence of ordering rather than the absolute areal density is what matters here. In any case, using the lattice parameter a=2.50Å for BN and 2.46Å on Grafoil shows there is only a small difference in basal

Figure 8.7.6.1, E_a vs X, From Model 5B Fits Together With Values Obtained Directly From T_2 maxima

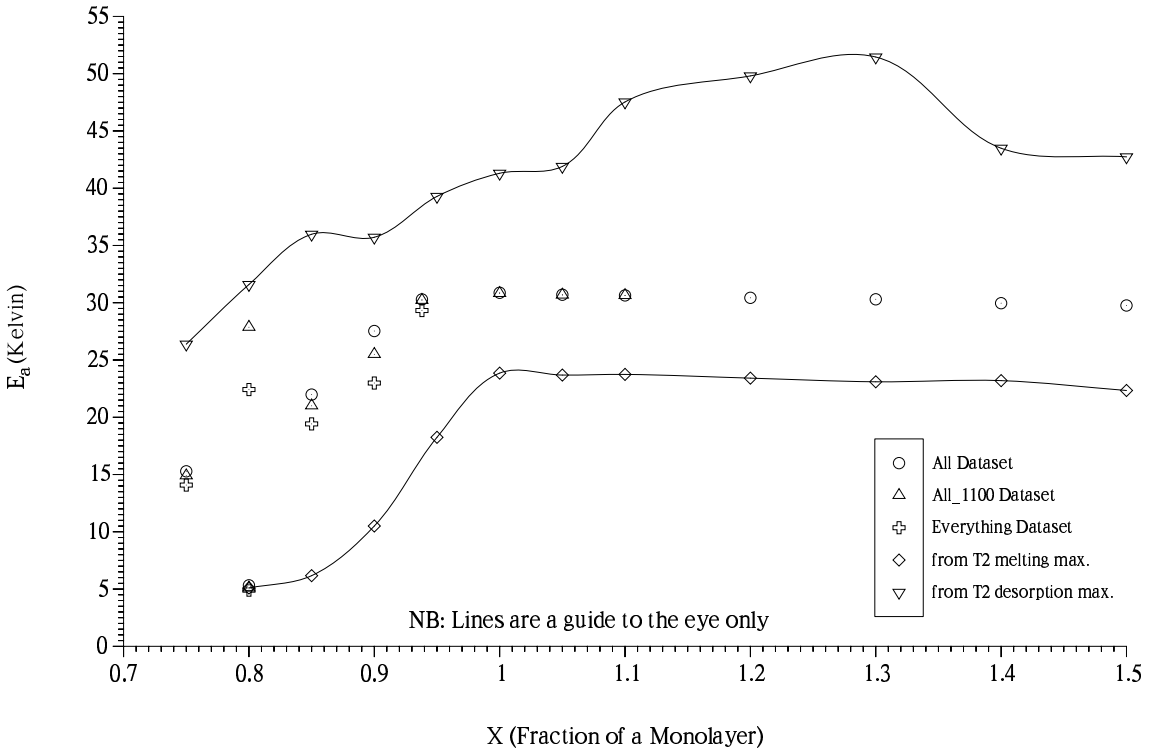

Figure 8.7.6.2, E_a vs X, From Model Fits, ALL Dataset

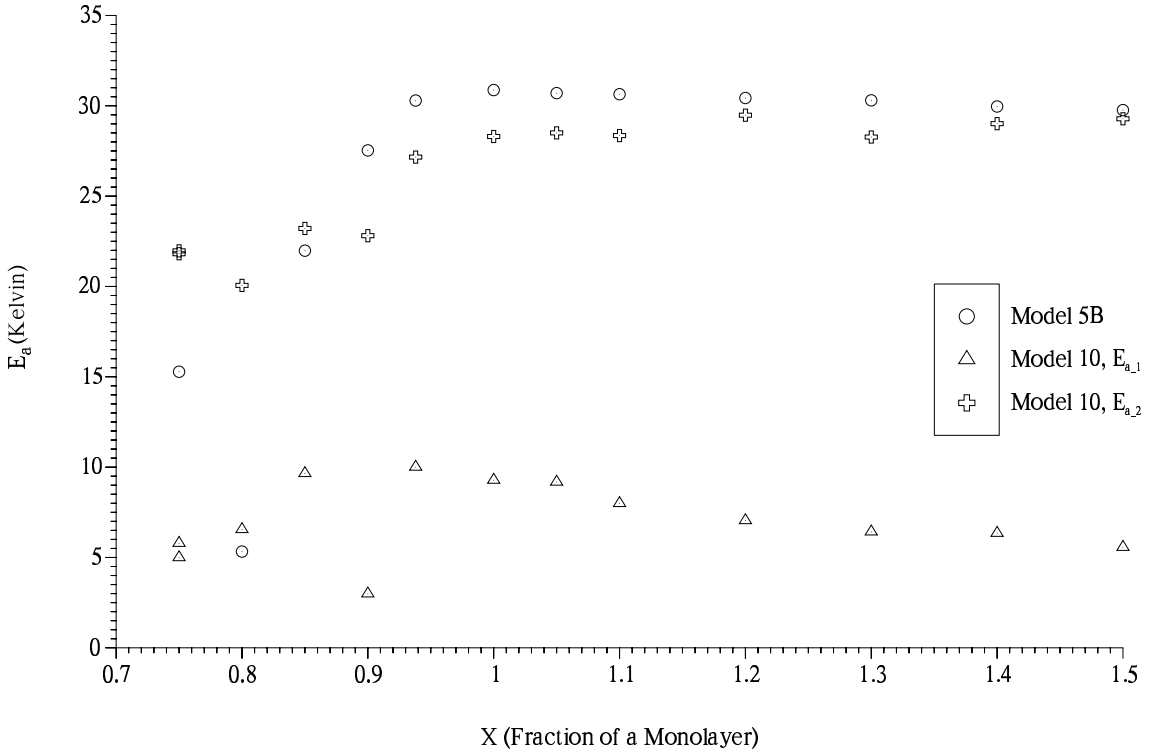

plane hexagon area for BN − $(2.50/2.46)^2$ = 1.033 ~3.3% more, hence 3.3% less helium coverage at BN registry than on Grafoil. (2) Take account of the 0.05 monolayer edge-film present on BN. (3) Arrange for the absolute coverage scales to converge to coincidence in the incommensurate solid, at maximum first layer density on BN, ie. at X=1.0. Therefore,

$$X^{\text{BN-Scale}} = 0.05 + 0.7 \times \left\{ \frac{1.0}{0.61} \times \left[1 + \left(\frac{X^{\text{Grafoil}} - 0.61}{1 - 0.61} \right) \times 0.033 \right] \times X^{\text{Grafoil}} \right\} \quad 8.7.7.2$$

which gives X=1 on Grafoil at X=1.198 on the BN scale.

It is clear from the figures that the Grafoil exchange frequencies are larger than the BN ones − by up to three orders of magnitude. Only at Grafoil maximum first layer density are they similar. Also in contrast with the Grafoil J's which fall rapidly with coverage in reasonable agreement with theoretical estimates due to Roger **[94]** based on three-particle spin exchange, the BN values change very little. This is not particularly surprising given the narrower coverage range of existence of the incommensurate solid plus the greater low temperature layer promotion in the approach to maximum first layer density which affects the derived T_1's and J's. See phase diagram, figure 7.6.1. Unfortunately this precludes getting out an estimate for the Gruneisen constant. Of the two fits, Model 10 values are preferred since they produce significantly better fits to the T_1 *vs* $1/T$ data at low T (see §8.4 and §8.5) and do show a slight decrease with X over the incommensurate solid coverages. The model fits have produced some very small values of exchange frequency at X=0.75 and 0.8 − see figure 8.7.7.1. Without taking these numbers too literally they do suggest that within the ability of the experimental T_1 measurement-probe and the model extrapolation to low-T to produce reliable first layer film motional speed values, exchange has been all but suppressed by registry. The most disquieting aspect of the data is the much-smaller-than-expected values of J in the incommensurate solid. One would expect BN to produce larger exchange frequencies than Grafoil due to its smaller binding energy and resultant lower film density. Maybe the BN incommensurate solid is not a triangular lattice or different n-particle exchange processes operate etc… Some reassurance comes from comparing BN and Grafoil T_2 values (§8.8.3, figures 8.8.3.1 and 8.8.3.2). With BN T_2's dominated by their homonuclear adiabatic $J_0(0)$ contribution, heteronuclear relaxation can effectively be ignored and the T_2's should be identical. However despite easier thermal activation on BN and the residual additional local-field relaxation component on Grafoil, the BN T_2's

Figure 8.7.7.1, J vs X, From BN ALL Dataset and Grafoil Data

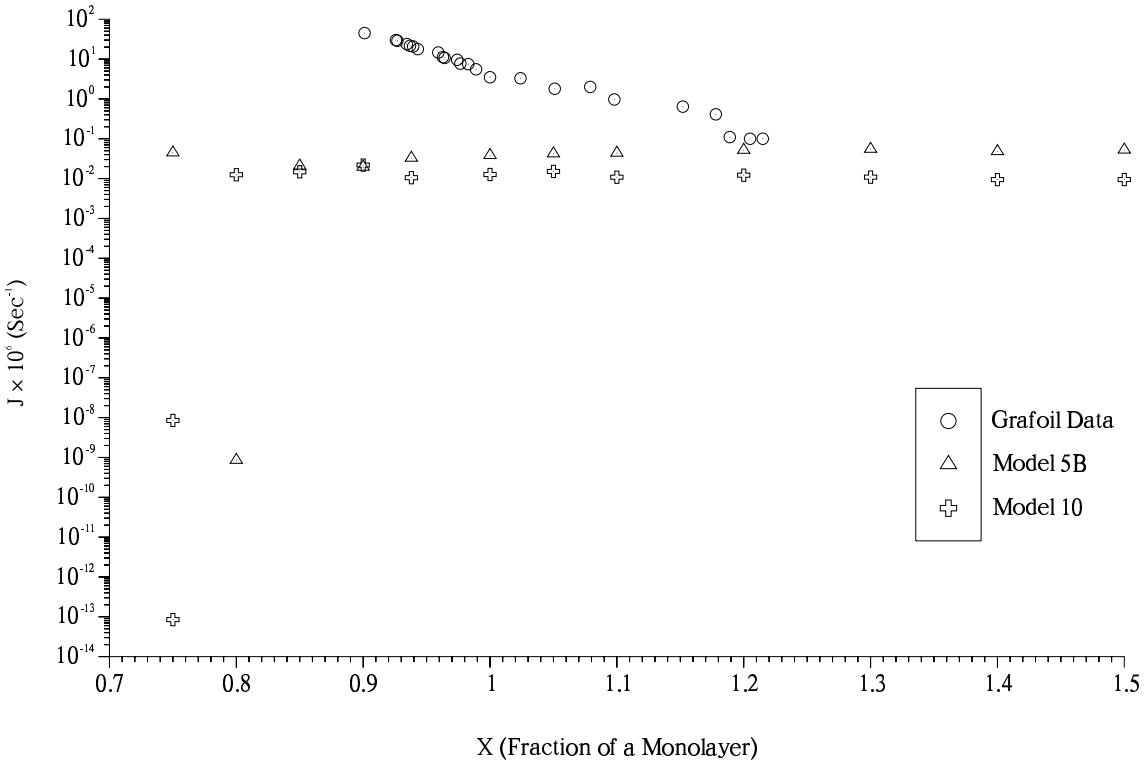

Figure 8.7.7.2, J vs X, From BN ALL Dataset and Grafoil Data, Main Body of Data on an Expanded Scale

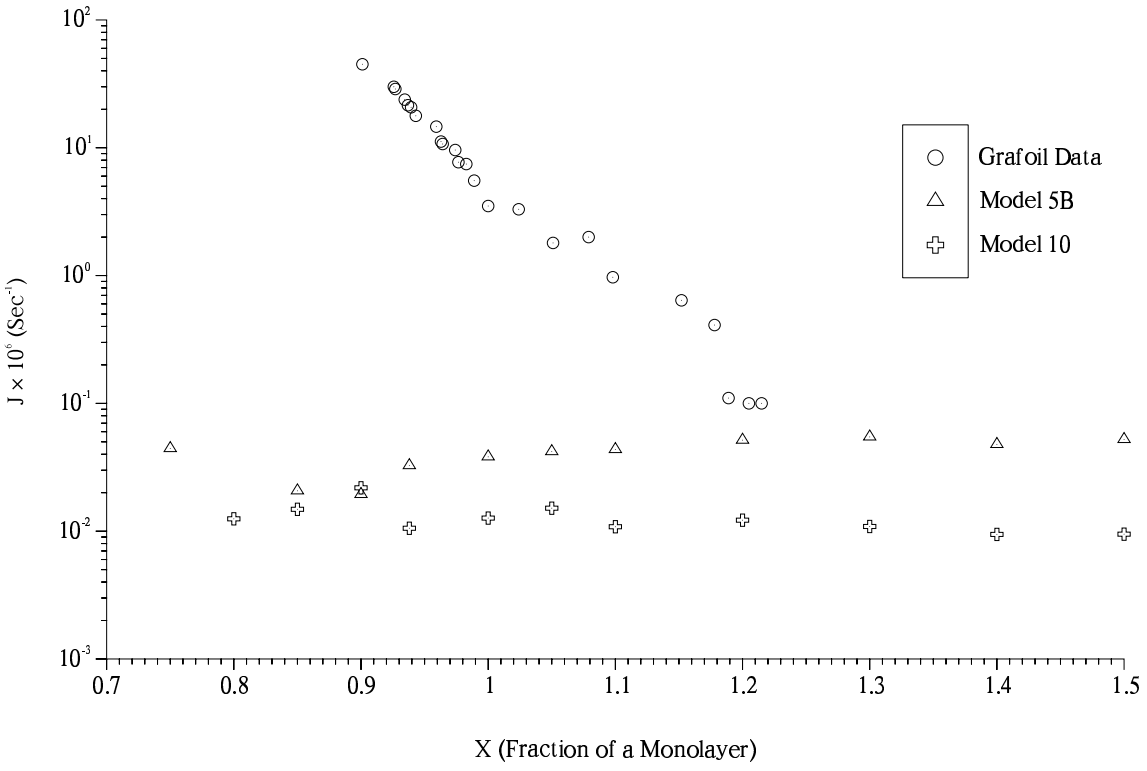

are much lower indicating slower exchange.

8.8 The Decomposition of the Relaxation Times

This section discusses the fitted relaxation times in terms of their homonuclear and heteronuclear components. The motivation is in part to compare the BN data with Grafoil data which lacks the heteronuclear relaxation channel which affects BN ^{3}He T_1 so strongly. Equation 8.25 describes the decomposition of the ^{3}He T_1: The homonuclear, heteronuclear and total relaxation rates are respectively given by $1/T_1$, ρ_2 and $1/T_1$(ave) where $1/T_1$ is given by equation 2.2.16 and ρ_2 by equation 8.4. The homonuclear contribution to the ^{3}He spin-spin relaxation time is T_2 (equation 2.2.17), the heteronuclear contribution is given by T_2^{He} (equation 8.26) and the total relaxation rate is the sum of the two component relaxation rates.

8.8.1 T_1 Decomposition *vs* X − Comparison with Grafoil

Figures 8.8.1.1 and 8.8.1.2 show the decomposition. According to the model it is evident that for all coverages on BN, T_1 is dominated by heteronuclear relaxation. With the Grafoil coverages re-scaled via equation 8.7.7.2 to the BN coverage scale, the X=0.8 (F=5MHz) T_1 minimum appears at 0.97 of a BN monolayer. Even if the BN/re-scaled Grafoil exchange frequencies were identical it is likely an X~0.97 homonuclear T_1 minimum on BN would be obscured by second layer promotion, being so close to the monolayer. It is therefore entirely unsurprising that no T_1 minimum in coverage is seen on submonolayer BN.

Comparing Grafoil with BN T_1 data and bearing in mind that both BN T_1 components will have been increased beyond their naïvely expected values by layer promotion at coverages close to the monolayer, some points can be made: (1) At registry the overwhelming dominance of heteronuclear relaxation is clear. (2) Homonuclear relaxation appears significantly less efficient on BN than on Grafoil. Although heteronuclear relaxation dominance results in a relatively poor estimate for the homonuclear component, that the homonuclear BN T_1's $\gg$ Grafoil T_1's is consistent with the proposed BN $J \ll$ Grafoil J values. The Model 5B/10 and *ALL_1100* and *EVERYTHING* datasets all give very similar results.

8.8.2 T_1 Decomposition *vs* $1/T$

Two sets of plots are given; Figures 8.8.2.1−8.8.2.6 plot the fits for the

condensed film coverages together by component and figures 8.8.2.7−8.8.2.18 plot the components and experimental data together for each coverage separately. As already noted the Model 10 fits are generally significantly better than the 5B ones. The fact that the lower temperature minimum is the heteronuclear one is nicely illustrated in these plots. It is a consequence of the models having $\tau_c^{Jhm\_sf} > 1$. It leads to the general conclusion that the low temperature data is dominated by heteronuclear relaxation and the high temperature data by homonuclear relaxation. Figures 8.8.2.1 and 8.8.2.2 which show the total T_1 fits, illustrate the way the minima bunch up in temperature as activation energy rises with coverage. See figure 7.2.3.11 for E_a *vs* X plot. Finally it is necessary to recall a point made in §8.5/X=0.75 concerning the Model 10 fit at X=0.75: The minimum at 6.6K to which the model has clearly fit is in fact the high temperature minimum due to relaxation in the edge-film. This results from the greater ability of Model 10 to track what are effectively artifacts in the data coupled with the minute size of the 'true' minimum at 3.7K. See §7.2.3.2 for details.

8.8.3 T_2 Decomposition *vs* X − Comparison with Grafoil

Figures 8.8.3.1 and 8.8.3.2 plot the components of the spin-spin relaxation time together with the experimental T_2 and Grafoil T_2 data. The Grafoil data is coverage-rescaled to the BN scale. The T_2 components are calculated as described above in §8.8 and the fit parameter values used are from the T_1 data fits. It is evident that the discrepancies between the T_2(total) and T_2(expt.) are much greater than in the corresponding T_1 fits/plots. The most likely explanation is that T_1 is dominated by its heteronuclear contribution and so tends to produce relatively poor estimates for the homonuclear component but T_2 is dominated by its homonuclear $J_0(0)$ adiabatic term as the breakdown of the T_2(total) relaxation times shows.

Comparing the BN and Grafoil experimental data, two observations can be made: (1) Over $0.8 \leqslant X \leqslant 1.0$, $T_2(\text{BN}) < T_2(\text{Grafoil})$ which is consistent with the interpretation of §8.7.7 that the ^{3}He exchange frequencies are lower on BN than Grafoil. (2) $T_2(\text{Grafoil}) \ll T_2(\text{BN})$ at their respective maximum first layer densities even with BN's additional heteronuclear relaxation pathway. This reaffirms the idea that the ^{3}He on Grafoil monolayer is more dense than that on BN. Note: The Grafoil diamagnetic local-field contribution can be ignored at the monolayer **[60]**.

Figure 8.8.1.1, T_1 vs X Decomposition, From BN Model 5B Fits, ALL Dataset with Grafoil Data, T=1.1K

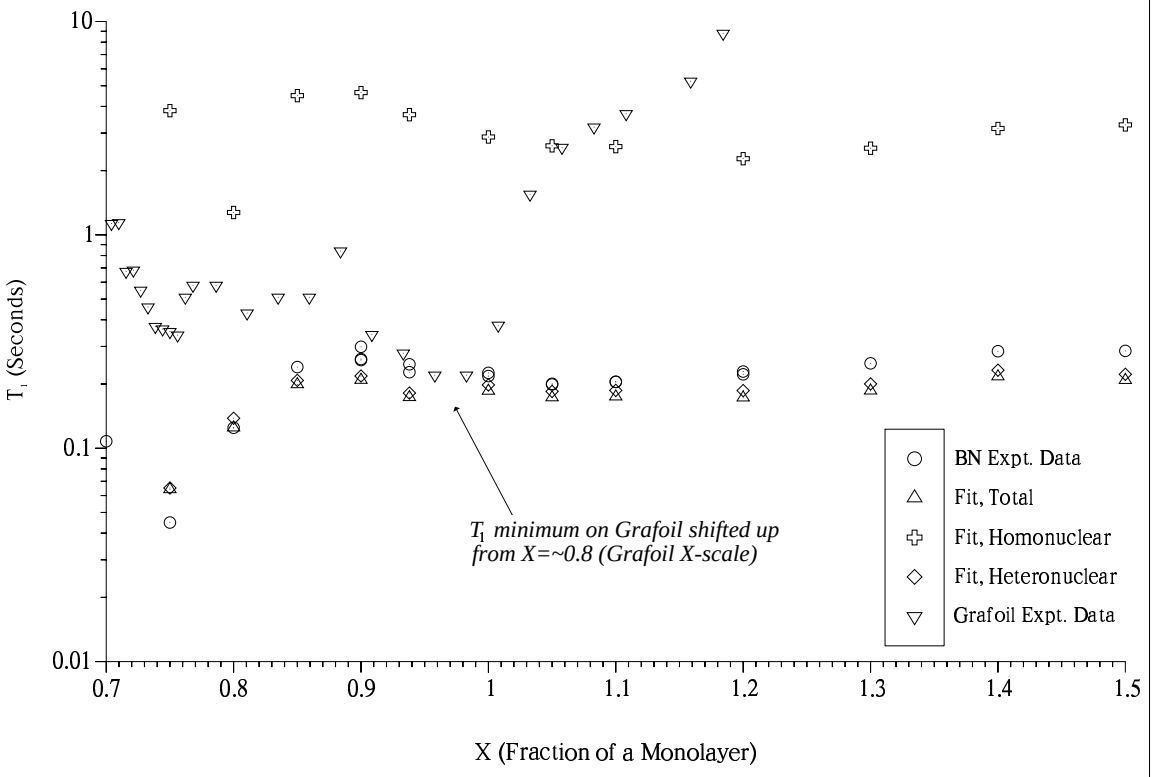

Figure 8.8.1.2, T_1 vs X Decomposition, From BN Model 10 Fits, ALL Dataset with Grafoil Data, T=1.1K

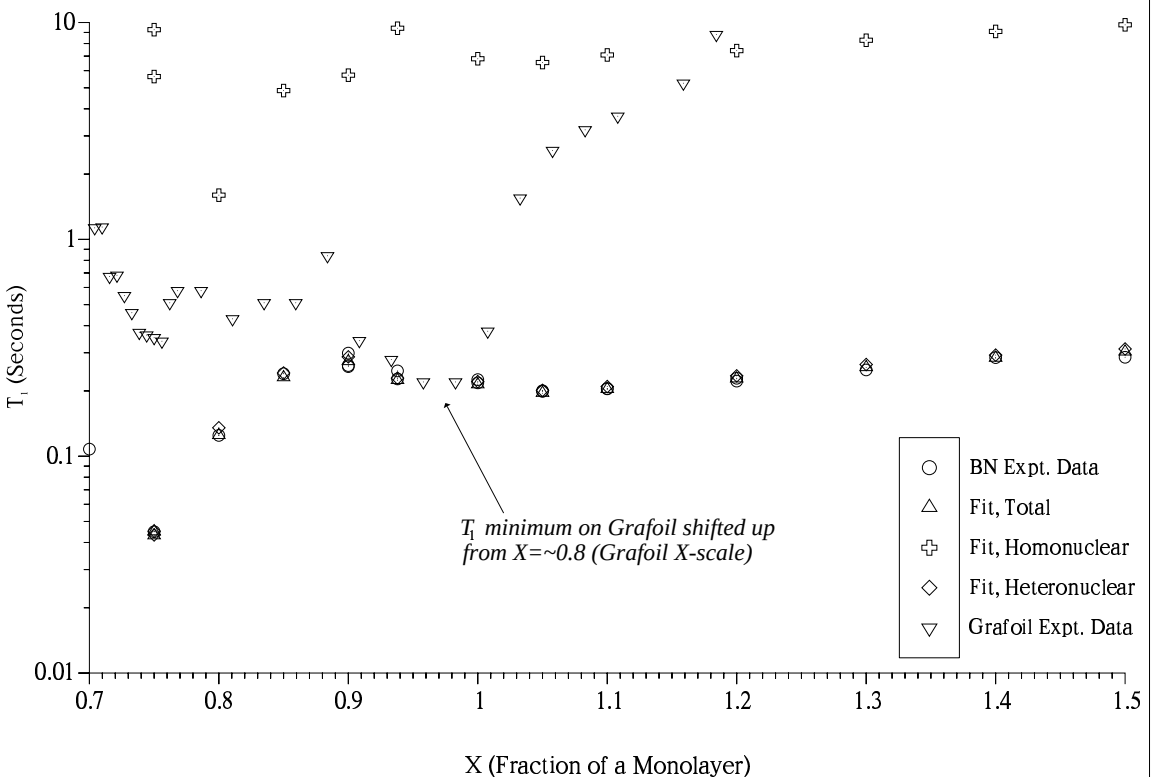

Figure 8.8.2.1, T_1 (total) vs 1/T, From Model 5B Fits, ALL Dataset

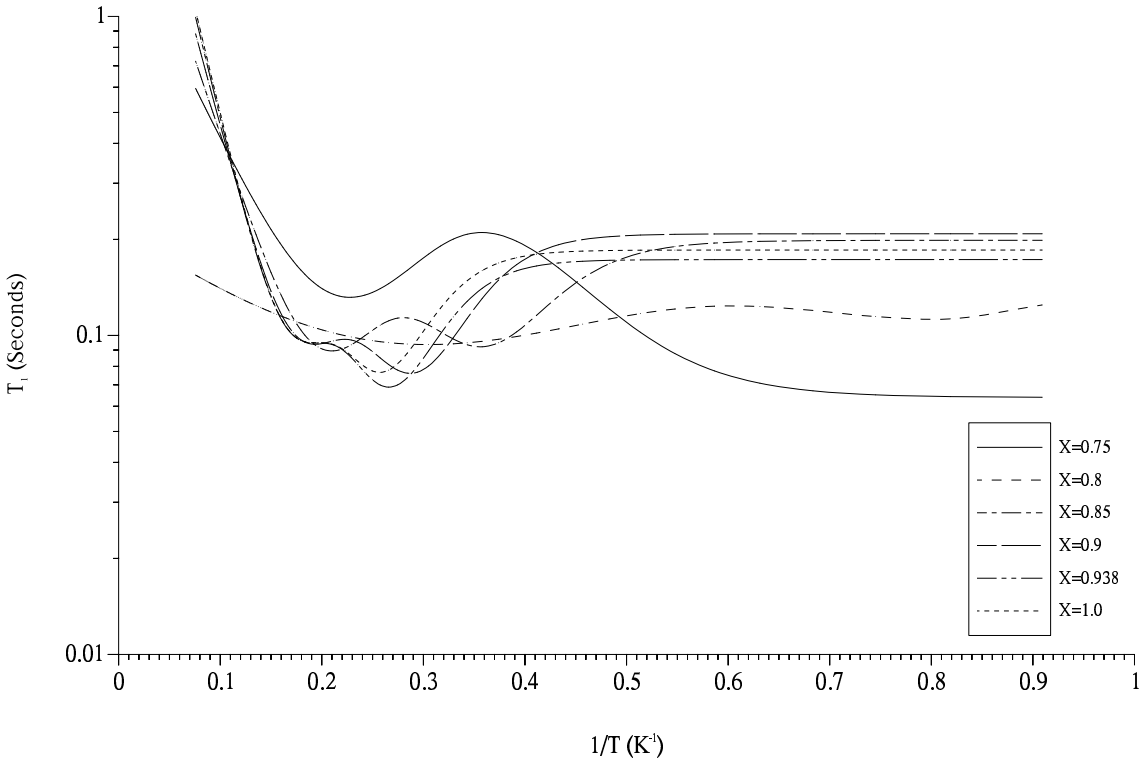

Figure 8.8.2.2, T_1 (total) vs 1/T, From Model 10 Fits, ALL Dataset

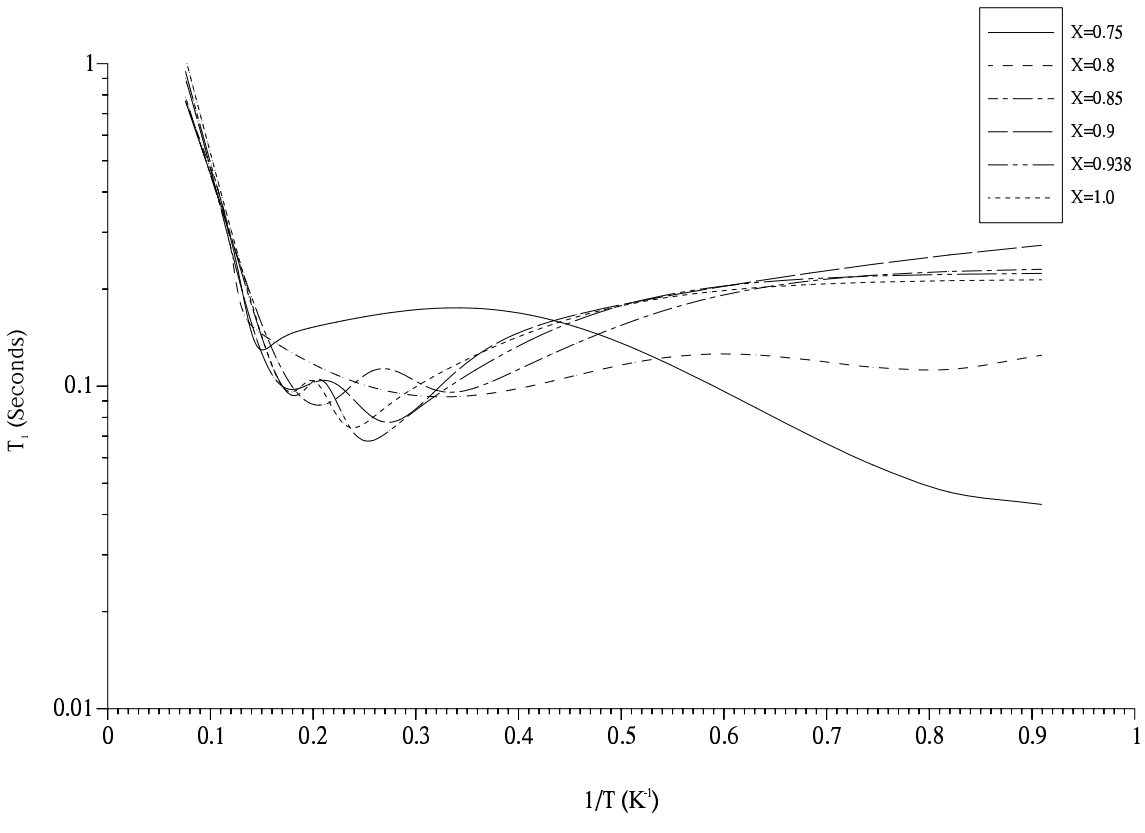

Figure 8.8.2.3, T_1 (homonuclear) vs 1/T, From Model 5B Fits, ALL Dataset

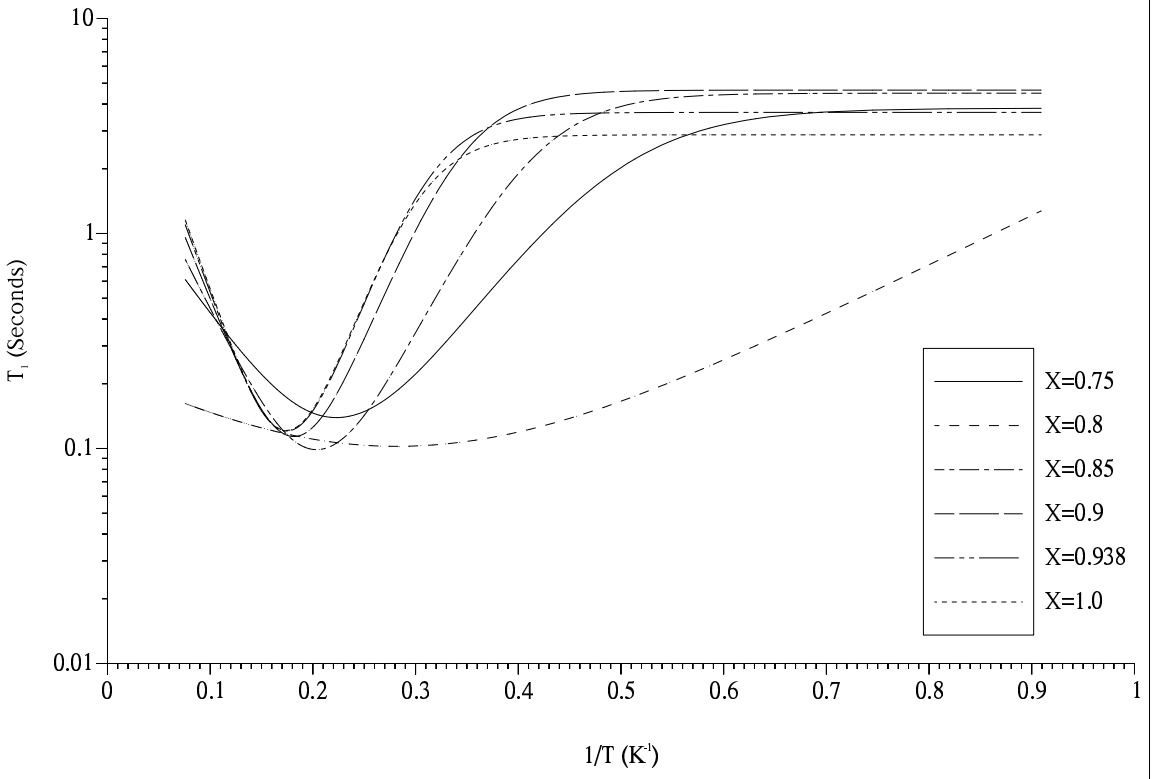

Figure 8.8.2.4, T_1 (homonuclear) vs 1/T, From Model 10 Fits, ALL Dataset

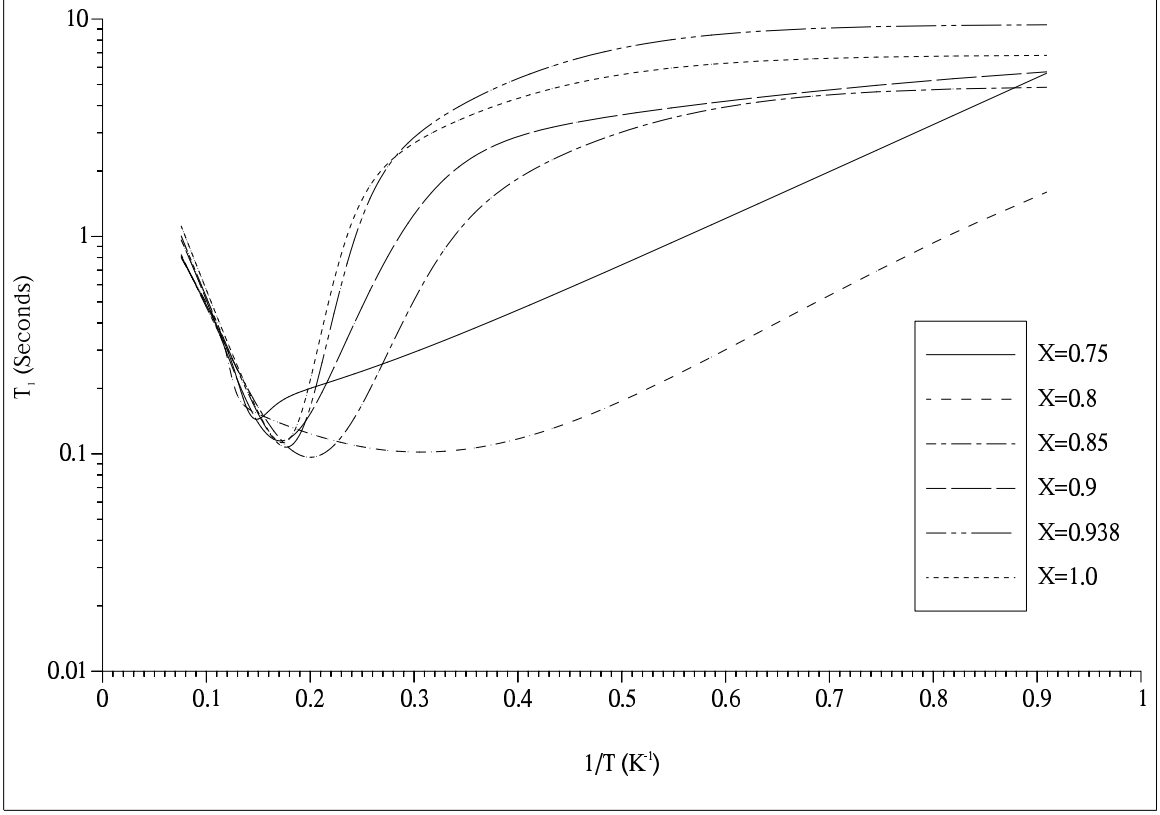

Figure 8.8.2.5, T_1 (heteronuclear) vs 1/T, From Model 5B Fits, ALL Dataset

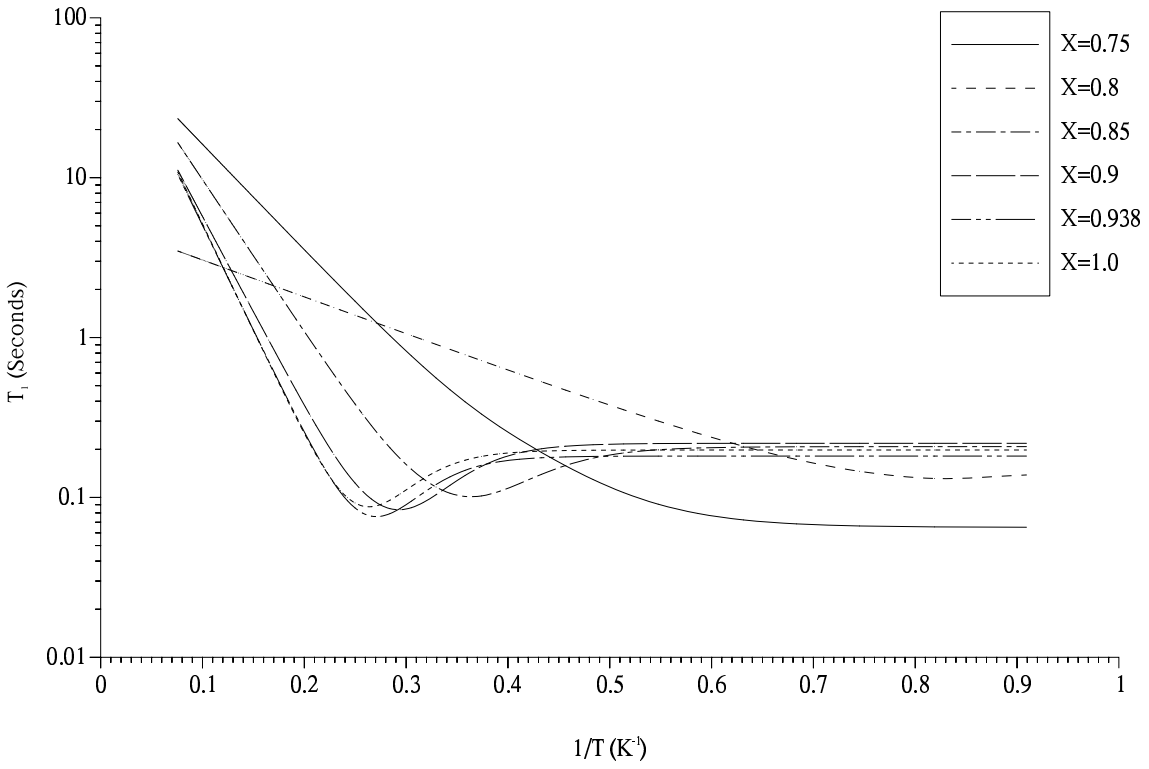

Figure 8.8.2.6, T_1 (heteronuclear) vs 1/T, From Model 10 Fits, ALL Dataset

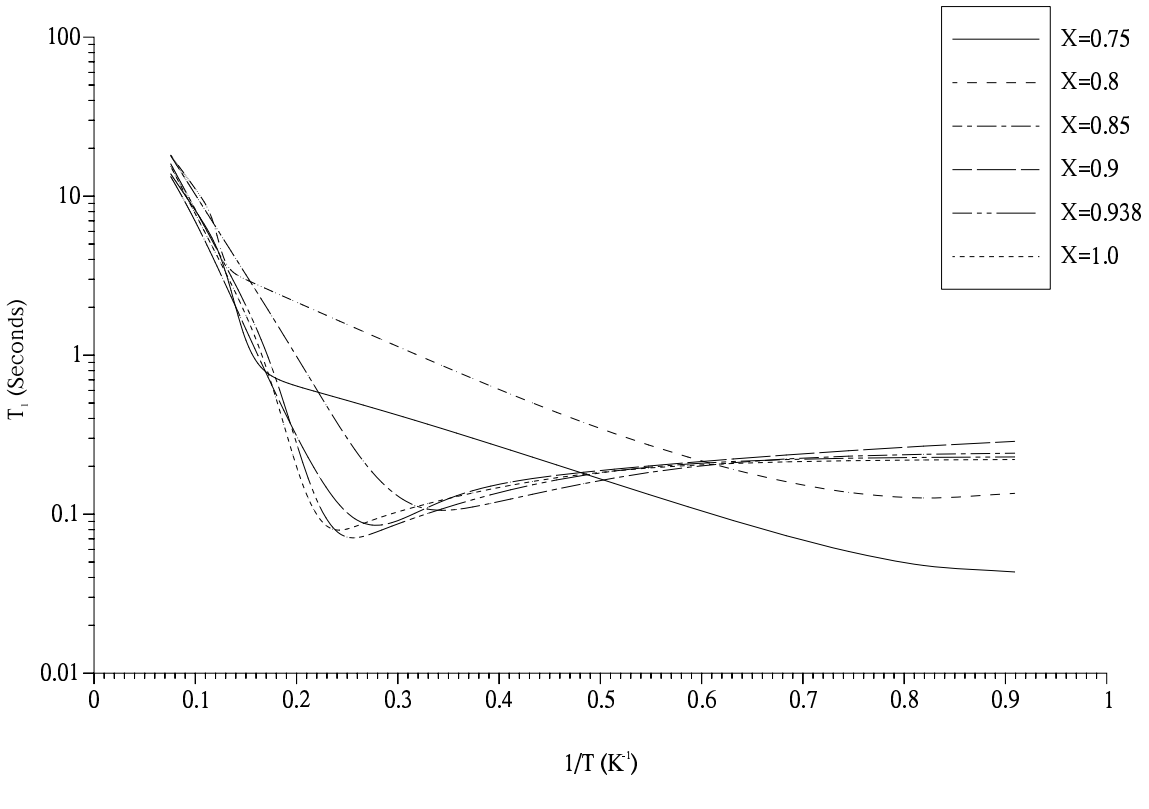

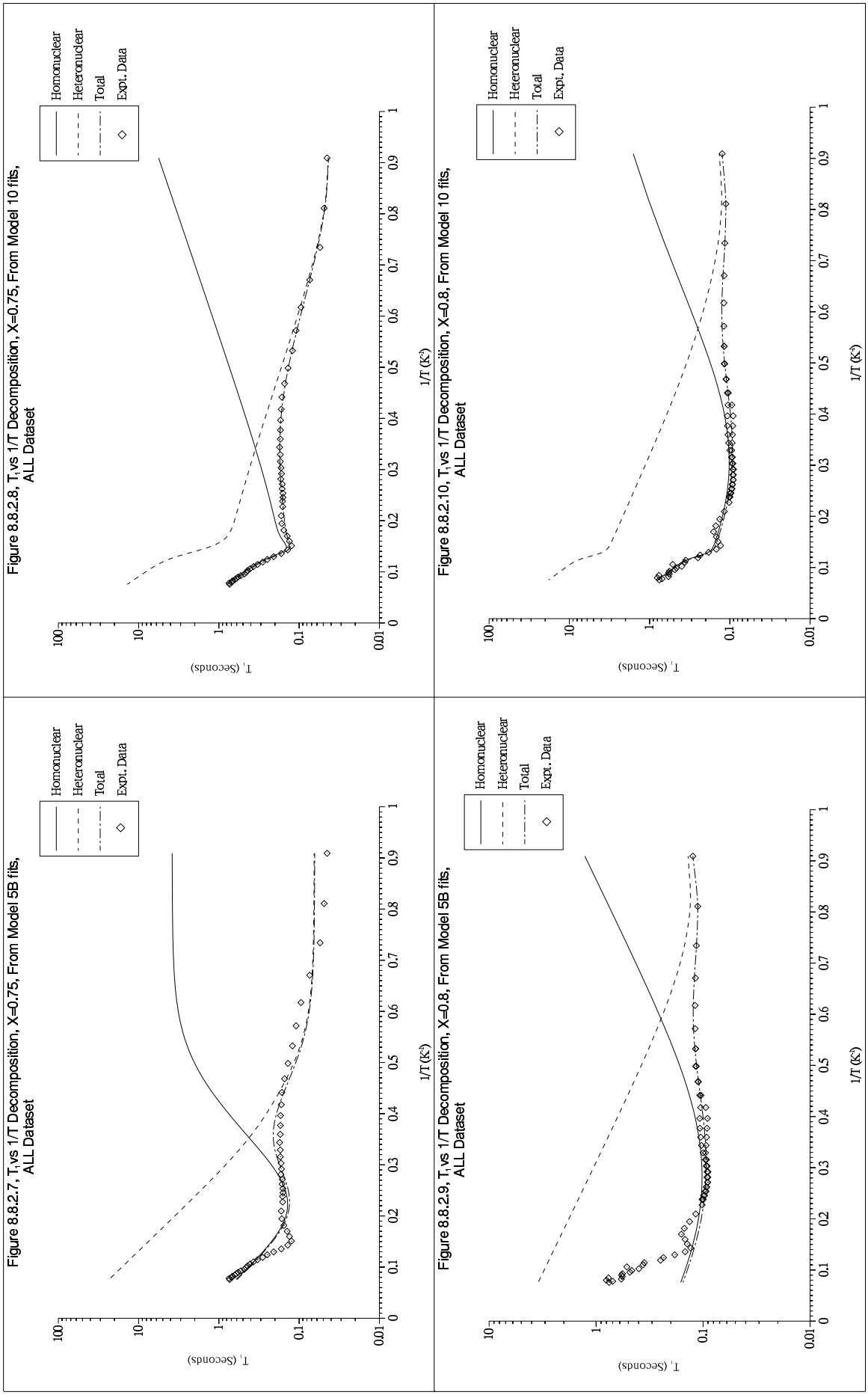
Figure 8.8.2.8, T1vs 1/T Decomposition, X=0.75, From Model 10 fits, ALL Dataset
Homonuclear
Heteronuclear
Total
Expt. Data
T1 (Seconds)
1/T (K-1)
Figure 8.8.2.10, T1vs 1/T Decomposition, X=0.8, From Model 10 fits, ALL Dataset
Figure 8.8.2.7, T1vs 1/T Decomposition, X=0.75, From Model 5B fits, ALL Dataset
Figure 8.8.2.9, T1vs 1/T Decomposition, X=0.8, From Model 5B fits, ALL Dataset

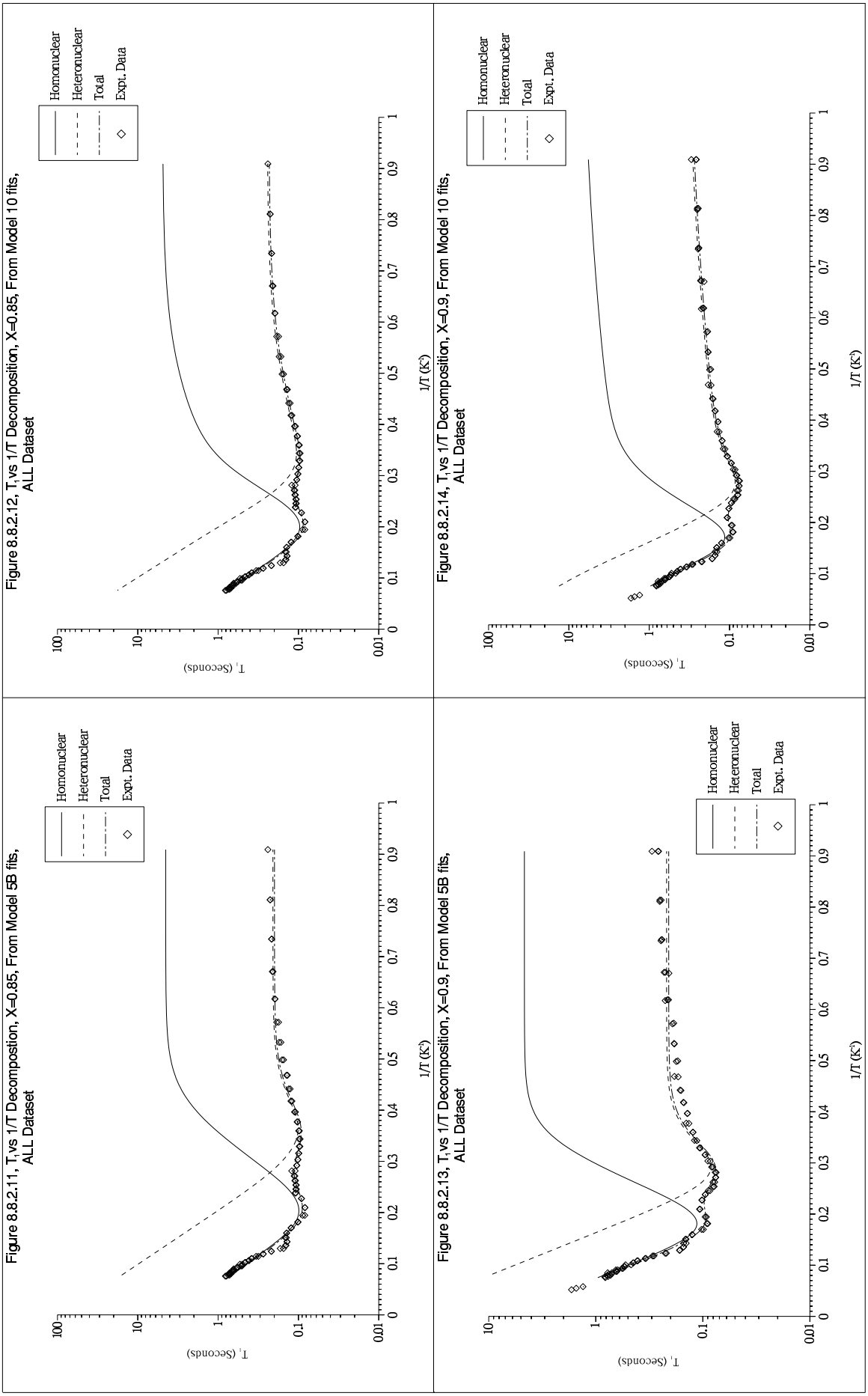

Figure 8.8.2.11, T1vs 1/T Decomposition, X=0.85, From Model 5B fits, ALL Dataset

Figure 8.8.2.12, T1vs 1/T Decomposition, X=0.85, From Model 10 fits, ALL Dataset

Figure 8.8.2.13, T1vs 1/T Decomposition, X=0.9, From Model 5B fits, ALL Dataset

Figure 8.8.2.14, T1vs 1/T Decomposition, X=0.9, From Model 10 fits, ALL Dataset

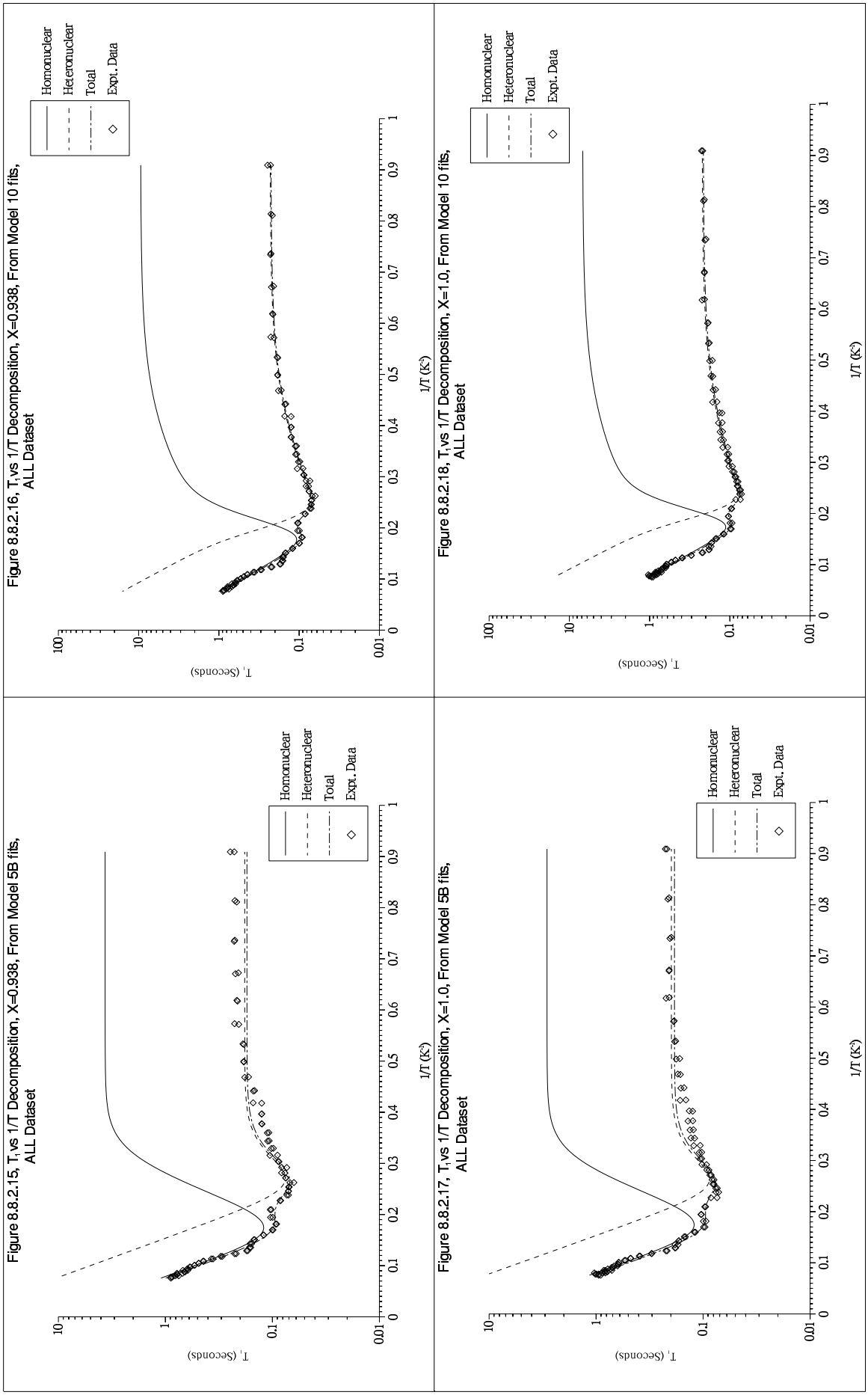

Figure 8.8.2.16, T_1 vs 1/T Decomposition, X=0.938, From Model 10 fits, ALL Dataset

Figure 8.8.2.18, T_1 vs 1/T Decomposition, X=1.0, From Model 10 fits, ALL Dataset

Figure 8.8.2.15, T_1 vs 1/T Decomposition, X=0.938, From Model 5B fits, ALL Dataset

Figure 8.8.2.17, T_1 vs 1/T Decomposition, X=1.0, From Model 5B fits, ALL Dataset

8.8.4 T_2 Decomposition *vs* 1/*T*

For brevity only Model 10 fits are shown here. The Model 5B fits are broadly similar. Two sets of plots are included − as for T_1 *vs* 1/*T*; Figures 8.8.4.1−8.8.4.3 plot the fits for the condensed film coverages together by component and figures 8.8.4.4−8.8.4.9 plot the components and experimental data together for each coverage separately. NB: Bear in mind the effect of the *X*=0.75/Model 10 fit/edge-film T_1 minimum artifact on the high temperature T_2 fit data at *X*=0.75. The T_2 components are derived in the same way as §8.8.3/T_2 *vs X* and show similar discrepancies between T_2(total) and T_2(expt.) at low temperatures. As temperature rises these discrepancies become much larger, increasing to a factor of two orders of magnitude at 13.2K. This can be explained by non-dipolar relaxation at elevated temperatures. PMI/dirty wall relaxation has been used to explain the fall-off in T_2 after the melting and desorption maxima (§7.2.2) where a hike in motional speed occurs. Naturally it is at these temperatures where the discrepancies are greatest. Moreover, whatever 2D dynamics remain at these elevated temperatures, where desorption and layer promotion occur, will further shorten the experimental T_2's due to the inability of the dipolar hamiltonian in 2D to properly average out the dipolar local fields, even in the extreme narrowing regime, as compared with the 3D correlation functions/spectral densities used by the Model. It is noteworthy that at the higher coverages where activation energies are higher and motion consequently slower, the fits show the discrepancies becoming small and fairly constant in *T* as far as melting, consistent with the relaxation here being dipolar.

8.8.5 T_2 Decomposition *vs* Frequency

Figure 7.2.4.6 shows the experimental T_2 *vs F* plots for *X*=0.8 and above at 1.1K. Recalling §7.2.4.2, T_2 has a significant linear frequency dependence at *X*=0.8 (T_2 = 2.54 + 0.078 × *F*), which has fallen off substantially by *X*=0.85 (T_2 = 1.52 + 0.008 × *F*) and disappeared within experiment error at *X*⩾0.9. Since the T_2−*linear-in-F* relation is neither the theoretical or experimental frequency dependence displayed by ^{3}He on Grafoil due to the later's diamagnetism we want to know if a heteronuclear analogue of the T_2 frequency dependence produced around the region of the T_1 minimum, that is an analogue of the 10/3 effect, is produced by the Model. The occurrence of a T_1 minimum in *T* at low *T* (*T*=1.233K) at *X*=0.8, which given $\tau_c^{Jhm\_sf} > 1$ in the fits will be due to heteronuclear relaxation, suggests that it might. Figures 8.8.5.1−8.8.5.3 plot the frequency dependence of the fitted T_2 components and table 8.8.5.1 lists the results of

Figure 8.8.3.1, T_2 vs X Decomposition, From BN Model 5B fits, ALL Dataset with Grafoil Data, T=1.1K

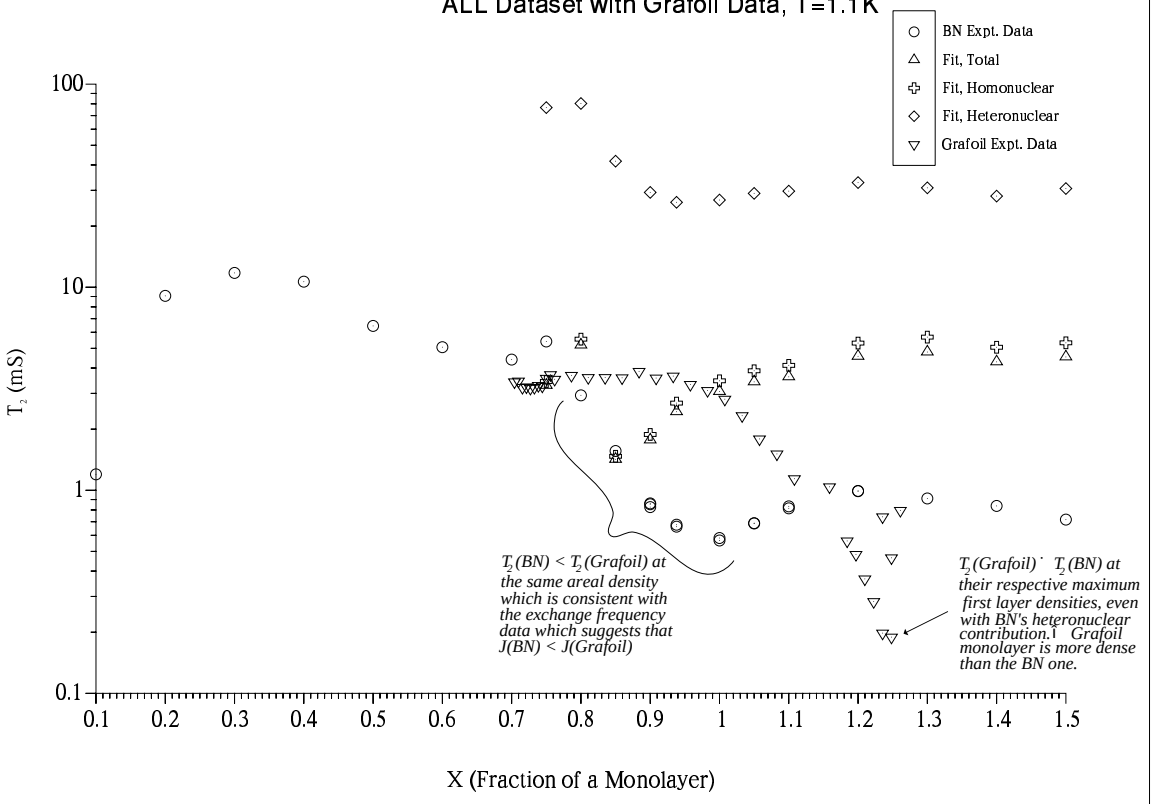

Figure 8.8.3.2, T_2 vs X Decomposition, From BN Model 10 fits, ALL Dataset with Grafoil Data, T=1.1K

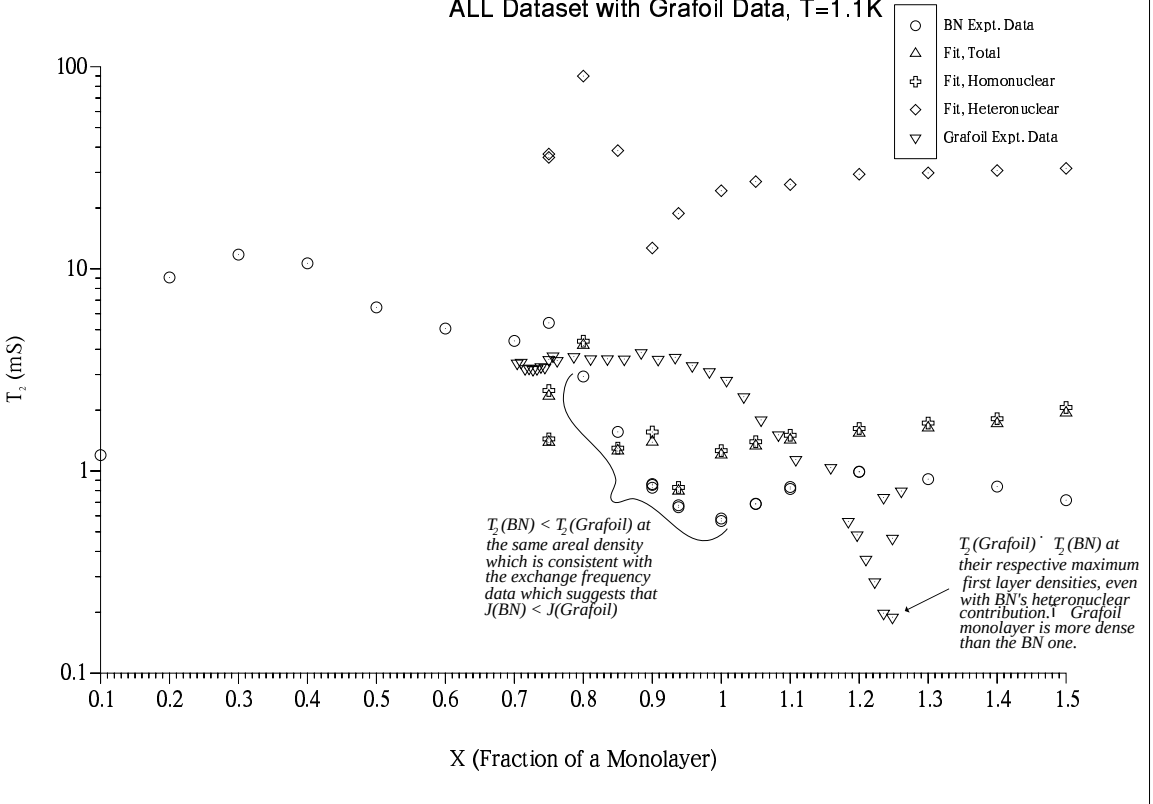

Figure 8.8.4.1, T_2 (total) vs 1/T, From Model 10 Fits, ALL Dataset

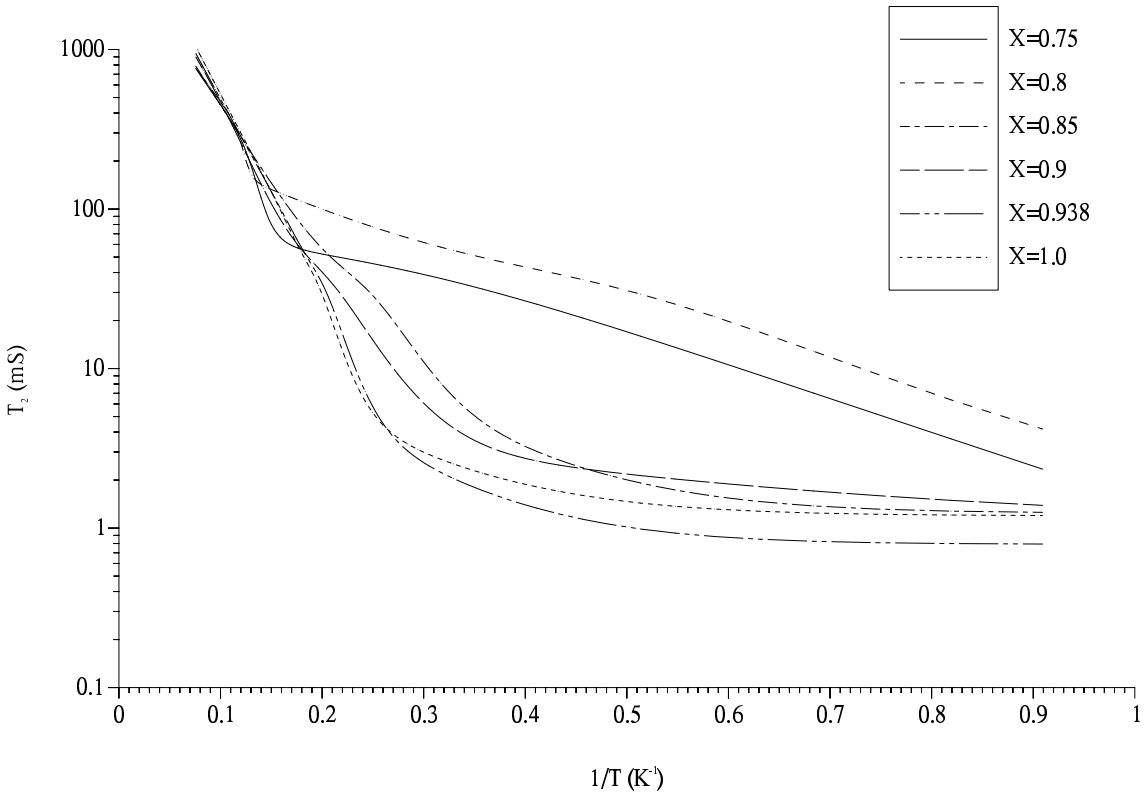

Figure 8.8.4.2, T_2 (homonuclear) vs 1/T, From Model 10 Fits, ALL Dataset

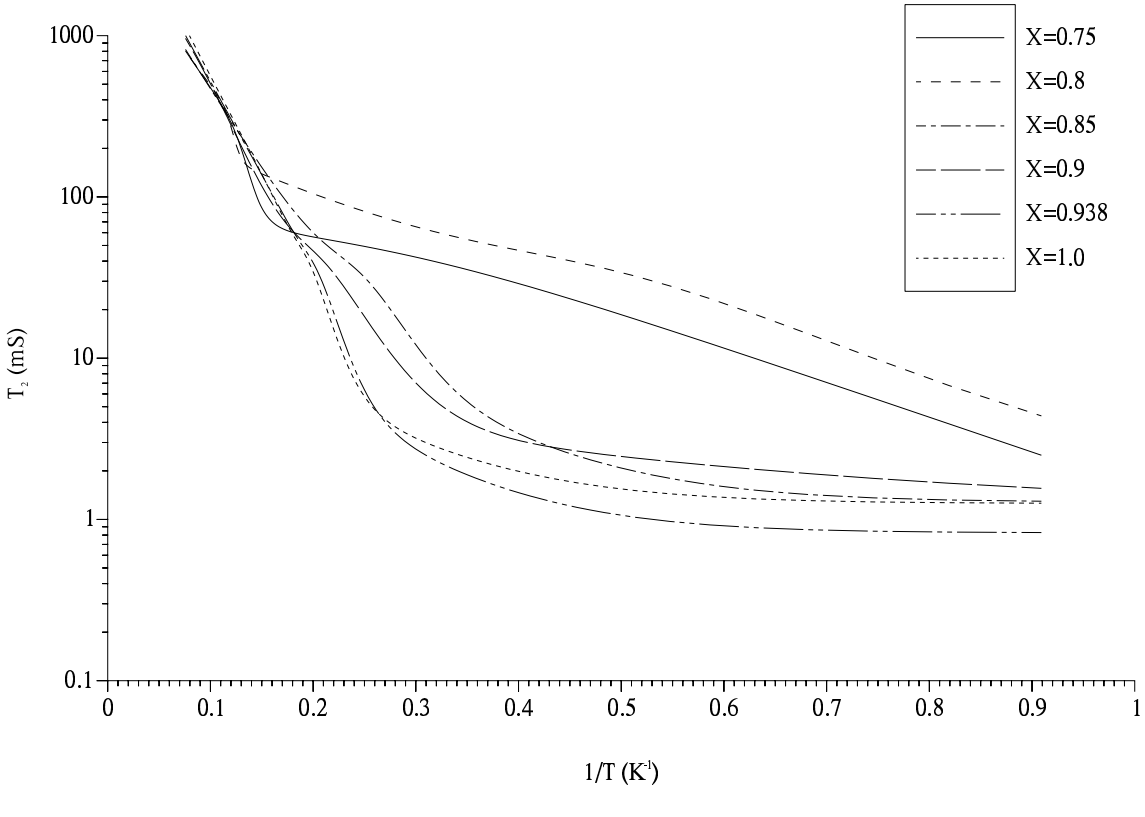

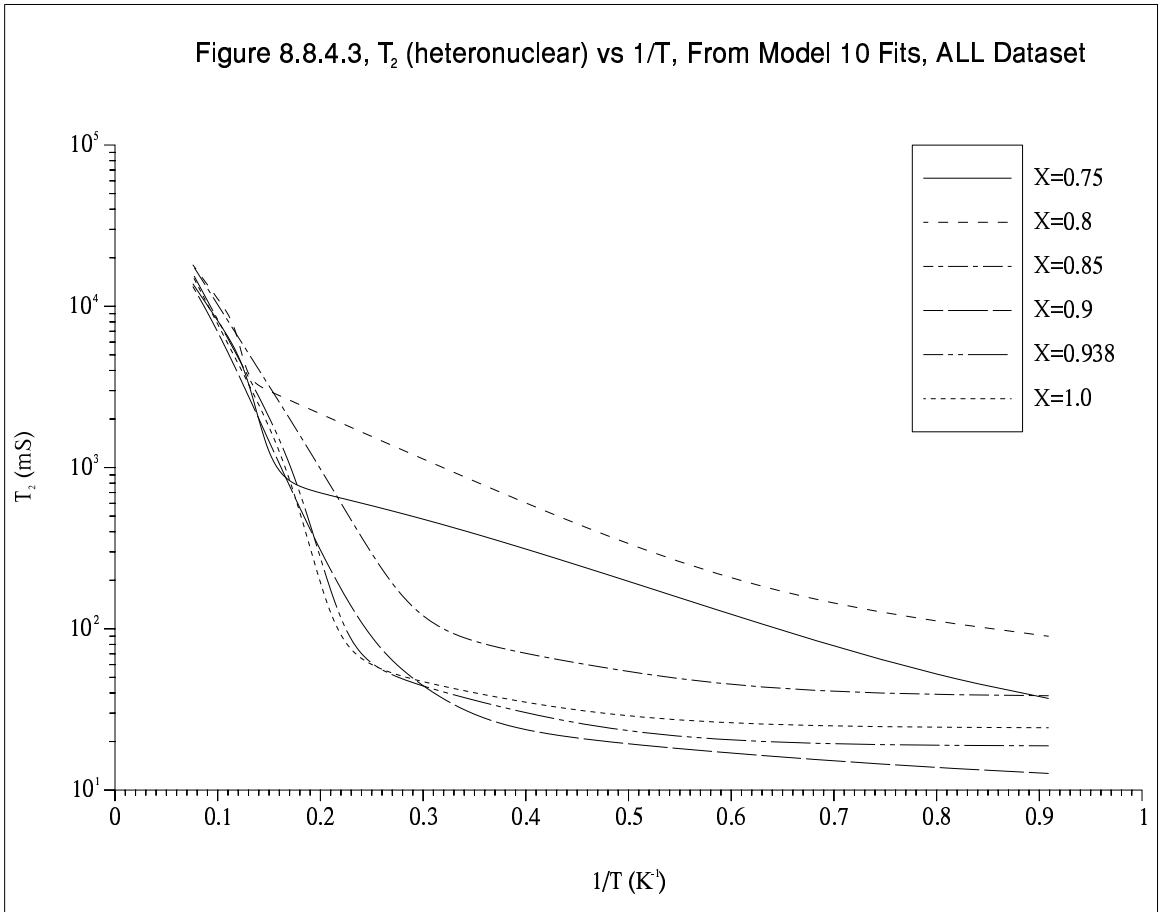
Figure 8.8.4.3, T2 (heteronuclear) vs 1/T, From Model 10 Fits, ALL Dataset
T2 (mS)
1/T (K-1)
X=0.75
X=0.8
X=0.85
X=0.9
X=0.938
X=1.0

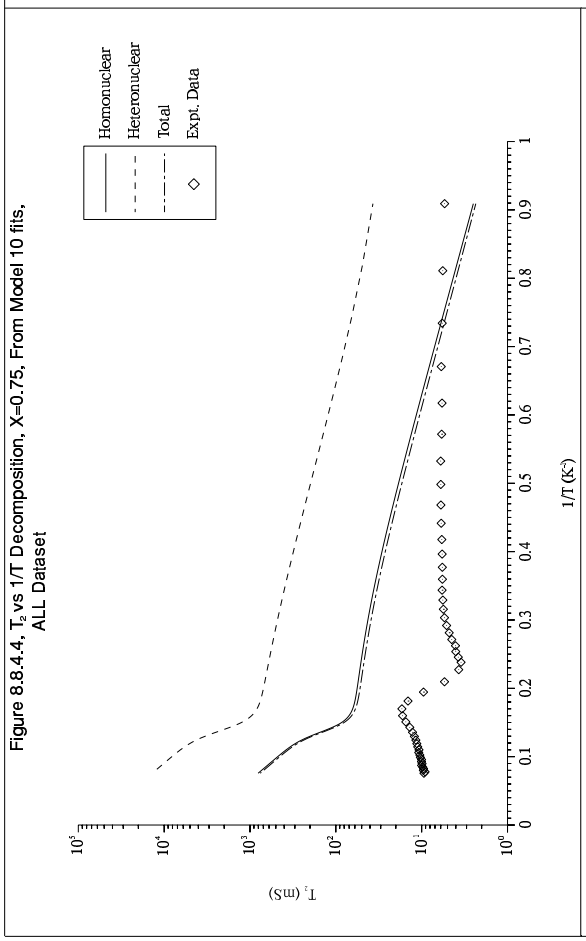
Figure 8.8.4.4, T2 vs 1/T Decomposition, X=0.75, From Model 10 fits, ALL Dataset
Homonuclear
Heteronuclear
Total
Expt. Data
T2 (mS)
1/T (K-1)

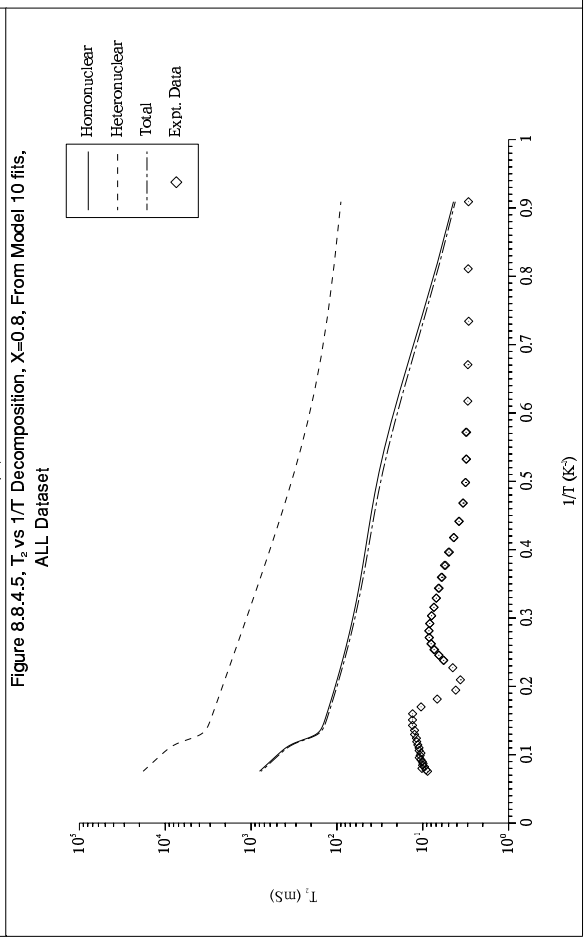
Figure 8.8.4.5, T2 vs 1/T Decomposition, X=0.8, From Model 10 fits, ALL Dataset
Homonuclear
Heteronuclear
Total
Expt. Data
T2 (mS)
1/T (K-1)

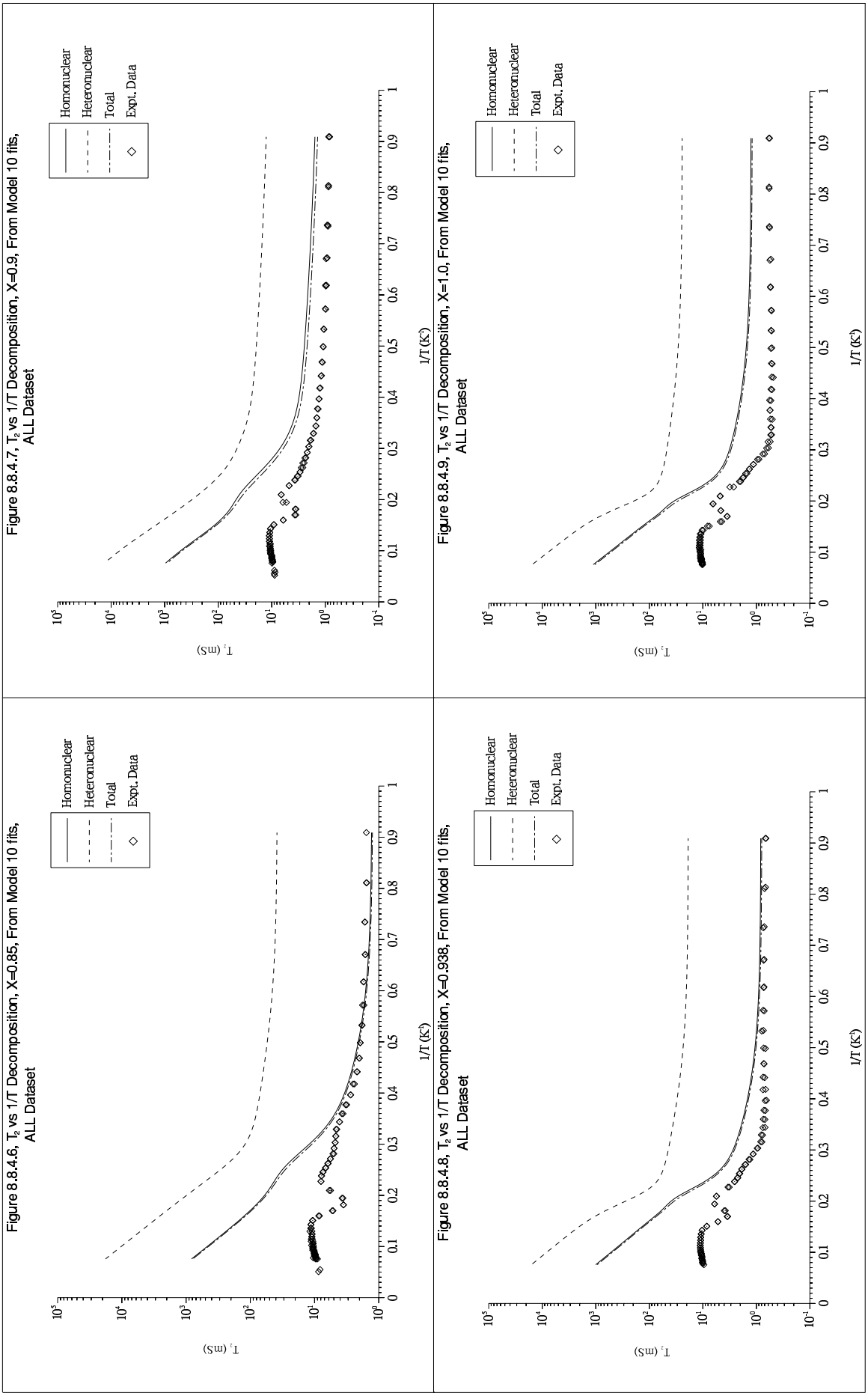

Figure 8.8.4.6, T_2 vs 1/T Decomposition, X=0.85, From Model 10 fits, ALL Dataset

Figure 8.8.4.7, T_2 vs 1/T Decomposition, X=0.9, From Model 10 fits, ALL Dataset

Figure 8.8.4.8, T_2 vs 1/T Decomposition, X=0.938, From Model 10 fits, ALL Dataset

Figure 8.8.4.9, T_2 vs 1/T Decomposition, X=1.0, From Model 10 fits, ALL Dataset

Figure 8.8.5.1, T_2(total) vs F, T=1.1K, From Model 10 fits, ALL_1100 Dataset

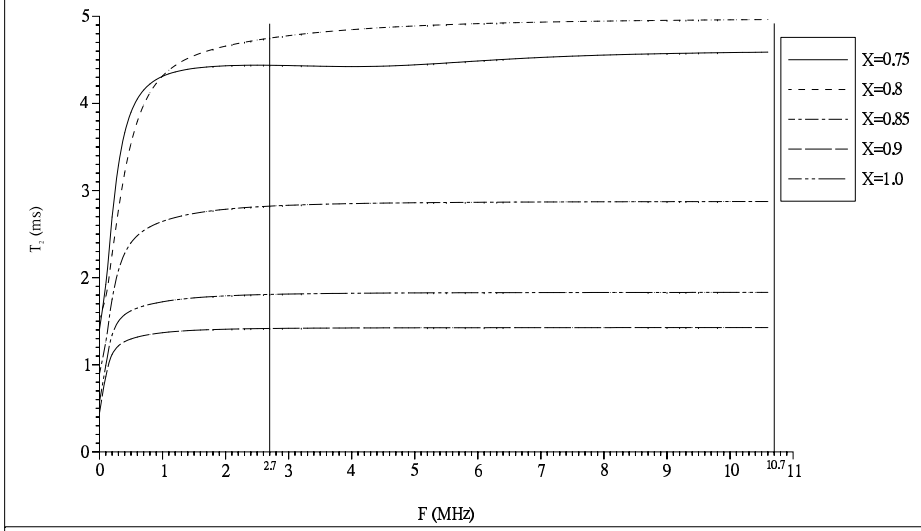

Figure 8.8.5.2, T_2(homonuclear) vs F, T=1.1K, From Model 10 fits, ALL_1100 Dataset

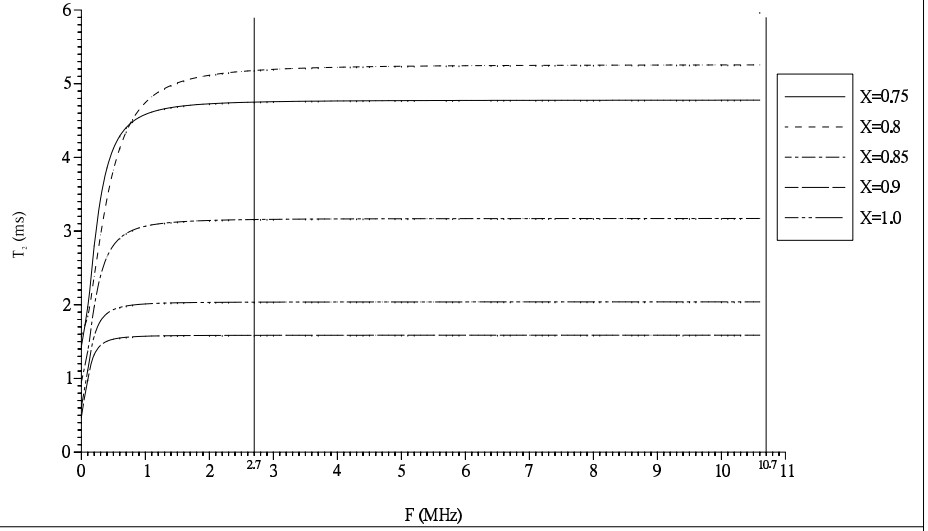

Figure 8.8.5.3, T_2(heteronuclear) vs F, T=1.1K, From Model 10 fit, ALL_1100 Dataset

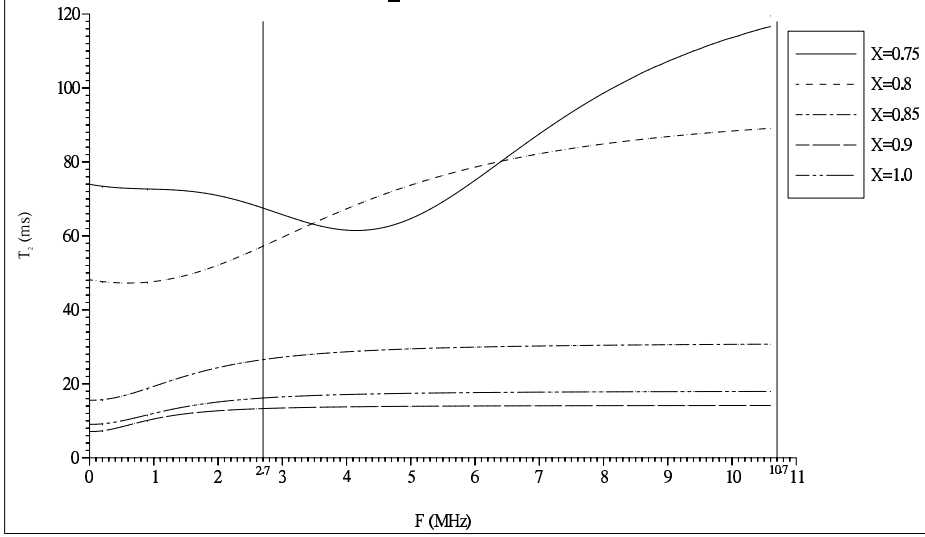

Table 8.8.5.1, Parameters from Straight Line Fits to the T_2 (components) *vs F* Fit Data

T_2 (total) vs F, Straight Line fit taken over 2.7-10.7MHz

X=0.75: T_2 = 4.33458 + 0.025808 × F
X=0.8: T_2 = 4.75743 + 0.022424 × F
X=0.85: T_2 = 2.82892 + 0.005021 × F
X=0.9: T_2 = 1.41842 + 0.000967 × F
X=1.0: T_2 = 1.81134 + 0.002196 × F

T_2 (homonuclear) vs F, Straight Line fit taken over 2.7-10.7MHz

X=0.75: T_2 = 4.75529 + 0.002399 × F
X=0.8: T_2 = 5.19372 + 0.006886 × F
X=0.85: T_2 = 3.15928 + 0.001279 × F
X=0.9: T_2 = 1.58576 + 0.000149 × F
X=1.0: T_2 = 2.03609 + 0.000339 × F

T_2 (heteronuclear) vs F, Straight Line fit taken over 2.7-10.7MHz

X=0.75: T_2 = 30.6951 + 8.19756 × F
X=0.8: T_2 = 52.6421 + 3.85449 × F
X=0.85: T_2 = 26.9467 + 0.41680 × F
X=0.9: T_2 = 13.4445 + 0.07835 × F
X=1.0: T_2 = 16.392 + 0.17237 × F

straight-line fits to those plots, evaluated over $2.7 \leqslant F \leqslant 10.7$MHz for comparison with the experimental straight-line fits of figure 7.2.4.6. *ALL_1100* dataset/Model 10 fit data has been used here for maximum 1.1K experimental frequency data contribution together with the closest fits. The total and homonuclear plots look very similar and their data are dominated by and have broadly similar F=0, frequency independent contributions. However the T_2(total) frequency dependent contribution is >3× larger than in the homonuclear case at X=0.8. Moreover, the X=0.8 T_2(total) frequency dependent term is 4.5× that at X=0.85 and that in turn is 5× the 0.9 monolayer figure which compares passably with the experimental X=0.8→0.9 factor of 9.8×. T_2(heteronuclear) *vs* F confirms that it is at X=0.8 where heteronuclear relaxation generates the strongest frequency dependence which all accords with the heteronuclear 10/3-type effect idea. Unfortunately, lack of plentiful experimental T_2 *vs* $1/T$ data on both sides of the 1.233K T_1 minimum in figure 7.2.2.26 and the shallowness of the minimum preclude direct observation of the heteronuclear 10/3 effect.

8.9 Conclusion to Chapter 8

Starting with the coupled differential equations, which are the analogues of the Bloch equations for spin-lattice relaxation, describing the time evolution of the two magnetisations, models have been progressively developed, culminating in the introduction of the $\tau_c^{Jhm\_sf}$ parameter, which quantitatively describe all the important features of the experimental ^{3}He on BN data − many of them unique to BN. This is remarkable given the simplicity of the models and the many approximations made in the course of their development. These approximations do help explain some of the model/ experimental data discrepancies. The more important ones are:

T_1(ave) as a function of τ_c treats the coupled-spins' double exponential relaxation as a single exponential, eliminating dependence on ρ_1, $\sigma_{1,2}$ and the number ratios of ^{3}He, substrate surface and interior spins. As the double exponential relaxation times and component amplitudes diverge the approximation degrades. Incidentally, the value of the stretched-exponential 'T1,2Index' fits lie in their sensitivity to such changes which the experimental T_1 measurement misses. The low temperature data in particular has a distribution of relaxation times due to relaxation on individual BN particles at different orientations in the powder. Associated with that, T_1(expt.) echo height *vs* time data whether fitted by a single or double exponential can only be an approximation to the double exponential relaxation stemming from coupled relaxation. The models do not treat layer promotion or desorption which are particularly important on BN and at

elevated temperatures. Treatment by the models, especially at low temperatures, of the data using 3D correlation functions/spectral densities can only be an approximation [70,75]. Even Model 10 only affords a crude approximation to the phase transitions in temperature by treating only the motional speed τ_c's change across the phase boundary − accompanying changes in film structure, internuclear separation, the hike in layer promotion etc. are all ignored. §7.2.2 shows how strongly relaxation via PMIs, particularly for T_2 increases with T at high temperatures, especially at melting and desorption but the models ignore this − ignoring non-dipolar relaxation altogether or treating it as constant in T. The models used to analyse all the data treat the substrate as a single frequency transition to which the helium-3 spins couple but figure 8.7.5.3 shows this can only be an approximation. Despite judicious cutting/weighting of the data to reduce the influence of the edge-film T_1 minimum at the lower post-registry coverages it is still likely to have some residual influence on the T_1 values and location-in-temperature of the second (ie. higher-T, homonuclear) minimum.

The least well understood part of the model results concerns the quantitative roles played in the ^{3}He relaxation by the various substrate isotopes. ^{14}N is believed to have an F_Q ~4.5MHz and be the dominant pathway for ^{3}He relaxation at registry. The ^{3}He film is known to relax though the ^{11}B spins from the ^{11}B T_1 data of §7.4.3.2, probably together with its splittings and those of ^{10}B too. They are thought to dominate the ^{14}N−^{3}He relaxation channel at higher coverages.

Figure 8.7.5.3 provides a potential explanation for the anomalous 10.7MHz points seen in the T_1 *vs* F plots at certain coverages − extrapolating the ^{3}He resonance line to 10.7MHz shows, at that field, all three ^{11}B quadrupolar splittings fall within the Zeeman split ^{14}N line, making interesting combinations of enhanced ^{14}N−^{11}B magnetisation transfer possible.

For simplicity the assumption has been made in this chapter that $F_Q(^{14}\text{N})$ is positive. However this need not be so. Given the +ve sign of the ^{14}N quadrupole moment in Appendix 1, if the EFG '*eq*' for ^{14}N in BN is −ve, F_Q will also be −ve as equation 8.7.5.2 shows and $J_0(F_Q - F_{He})$ will dominate $J_2(F_Q + F_{He})$, particularly when ^{14}N relaxation is dominant at registry. This does not have catastrophic consequences for the model since ρ_2 (equation 8.4) is symmetrical in the J_0 and J_2 terms within a factor of 6×. In two dimensions the different angular prefactors involved (see equations 2.2.24−2.2.26) may be significant. The same arguments, albeit with less importance here, also apply to the ^{10}B quadrupole frequencies.

Finally, observation of the heteronuclear analogue of the 10/3 effect is another

feature unique to this graphite structured adsorbed system.

Suggestions For Future Work

This section presents some suggestions for future work which might usefully be conducted in the light of this study. It has been divided into four sections, the first dealing with possible experiments, the second with enhancements to the experimental apparatus, the third with possible theoretical work and the fourth with some miscellaneous suggestions. For brevity a terse style had been adopted. They are presented in no particular order.

(A) Experimental Suggestions

(1) Take $T_{1,2}$ *vs* X data at 1K using a much finer coverage grid, paying particular attention to the C−IC transition region. Look at T_1 minimum and 'T1Index' peak at X=0.75. How large does the index become at the peak? Ensure good sample annealing. Take $T_{1,2}$ *vs* T data also using a finer coverage grid to study the registry/DWL/incommensurate solid/fluid etc. phase transitions.

(2) Investigate the possibility of obtaining/making a Grafoil-like exfoliated form of hexagonal BN for dipolar anisotropy studies. Keywords; exfoliation, chemical intercalation.

(3) Do X-ray or other scattering experiment (see §1.9) (but not neutron) to verify $\sqrt{3} \times \sqrt{3}$ R30 registered structure at X=0.75 and triangular lattice for the incommensurate solid.

(4) Do very low X ($X \leqslant 0.05$) NMR measurements to investigate the edge-film;

- $T_{1,2}$ *vs* $1/T$ @ $X<0.05$; Observe T_2-desorption-maximum temperature and T_1 minimum temperature and value.
- $T_{1,2}$ *vs* $1/X$ for $0<X \leqslant 0.05$ at T=1K and compare with the Grafoil results of references **61** & **62** and the argon isotherm step at X=0.05.

(5) Do controlled doping experiments with paramagnetic impurities eg. iron. Observe the effects on ^{3}He and substrate relaxation times. In particular;

What are the effects on the ^{3}He T_2 melting-maximum, melt-desorption-minimum and desorption-maximum? Quantitatively what are the relative effects on the ^{3}He T_1 and T_2?, compare with Fardis' data (§3.4.3). How much are the ^{11}B T_1 recoveries affected?

(6) Do ^{3}He NMR measurements at low frequencies ~1MHz where the ^{11}B quadrupolar splitting F_Q=1.47MHz should strongly modify ^{3}He−^{11}B cross relaxation.

(7) Do ^{3}He NMR measurements at high frequencies $F \gg 10$MHz where the substrate quadrupolar splittings should be negligible. Also how does such high frequency BN data compare with the high frequency DLX6000 data discussed in §3.5.3 and tabulated in table 7.2.2.1? Is $T_1 \propto F$ for $F \rightarrow 100$MHz as on DLX6000 (§3.5.3) or does T_1 diverge more rapidly as required for a system characterised by a single τ_c like Grafoil (§1.10.6)?

(8) Preplate the BN with ^{4}He, by degrees to test ^{3}He relaxation via the substrate. Verify Fardis' exponential T_1 relaxation with a full ^{4}He monolayer (§3.4.1) severing FMR relaxation. Investigate the cross relaxation due to the edge-film by measuring T_1 (maybe *vs* T also) *vs* X(^{3}He), progressively preplating with ^{4}He while maintaining X(total) $\leqslant 0.05$. Eliminating the strong edge-film ^{3}He−Substrate relaxation by preplating with 0.05 monolayers of ^{4}He, monitor the appearance of registered (^{3}He) spins on the basal-plane with coverage at X~0.3 by measuring T_1 *vs* X at 1K and 4.5MHz.

(9) Measure the ^{3}He nuclear magnetic susceptibility at low temperatures of the order of the 2D ^{3}He Fermi temperature for $X \leqslant 0.75$ to help determine the low temperature phase composition. The same technique could also be used to investigate the onset of second layer promotion.

(10) Measure $T_{1,2}$ *vs* F *vs* T at X=0.75. How does the low temperature frequency minimum/maximum (respectively) change as temperature rises above 1K and the registered phase disorders?

(11) Measure $T_{1,2}$ *vs* X using a much finer coverage grid as a function of temperature over mK<T⩽10K in the C−IC region to investigate the transition phases, discussed in §1.8.7 for Grafoil. eg. DWL, striped phases etc. See also suggestion (1)

(12) Do NMR studies with H_2, D_2 & HD adsorbed on BN and compare with the corresponding Grafoil work regarding the phase diagrams **[210,215]**.

(13) Re-analyse some registry ^{3}He/Grafoil T_1 data using the 'T1Index' fits. Are there any comparable changes in exponentiality to those seen on BN? This is not expected but it must be remembered that naturally abundant carbon does contain a small proportion of ^{13}C (1%) which has a spin, $\boldsymbol{I}$=½.

(14) Measure the ^{13}C T_1 *vs* X at 1K for ^{3}He on Grafoil. Is there any evidence for cross-relaxation? Especially, look at registry and the incommensurate solid T_1 minimum. ^{13}C−^{3}He cross relaxation does operate (§3.5.4) but ^{13}C does not relax like ^{19}F as might be expected in DLX6000 **[142]**. Could a ^{13}C enriched form of Grafoil or graphitised Carbon Black be obtained for such work?

(15) Look for an explanation of the X=0.938 T_2 *vs* F minimum at 6.9MHz. Does this occur at other coverages? − Do some measurements. How is the minimum affected by a deliberately applied field gradient?

(16) Measure T_1 *vs* T *vs* F in greater detail using a finer frequency and temperature grid at X=0.938. Examine the relative changes in the T_1 minima in T with F, in particular the increase in relative depth of the minima for F=2.7→8.6MHz followed by the change at 10.7MHz. See §7.2.2/X=0.938.

(17) There are significant qualitative differences between the NMR data obtained with sample chambers #3 and #4. Investigate the effects of the sample firing time and temperature − In particular their effects on edge-film area and basal-plane homogeneity.

(18) Directly measure the desorbed helium-3 spin population at higher temperatures from the sample line pressure reading. Compare with the analysis of §7.2.3.1

(19) Measure T_1 at 1K in the incommensurate solid on BN over a wider range of frequencies, for example over 3 decades as was done with DLX6000, (§3.5.3), where $T_1 \propto F$, ruling out a homogeneous film whose exchange motion is characterised by a single τ_c. Or, given the structural similarity, is the film consistent with a single τ_c like Grafoil [75] ? See also suggestions (6) and (7).

(20) Further investigate the T_2 dependencies around 1.1K and X=0.8. Are they consistent with a heteronuclear analogue of the 10/3 effect? Do they agree with the corresponding T_1 behaviour?

(21) Do $^{11}B-^{3}He$ double resonance cross flipping experiments at 1.1K and X=0.75. Do this also at $X \leqslant 0.05$ at the T_1 minimum in T. Is the effect visible?

(22) Does any direct inter-substrate-nuclei (eg. $^{11}B-^{14}N$) spin cross flipping occur at the surface, mediated by motion in the helium film? Do an experiment to test this idea.

(23) Do ^{11}B T_1 *vs* $1/T$ measurements using better equipment, eg. better S/N. (a) At X=0: Is there any temperature dependence? (b) At $X \leqslant 0.05$ for relaxation in the edge-film where a T~5K ^{3}He T_1 minimum is expected. (c) At X=0.75 for coupled relaxation on the basal-plane registered film as it goes through the order-disorder transition. (d) Over $0.85<X<0.9$ where the $3 \times {}^{3}He$ T_1 minima occur in T. Repeat these experiments with ^{14}N, ^{10}B and ^{15}N if possible.

(24) Repeat some of suggestions (23) with T_2 and look for motional narrowing of the substrate surface spins by motion in the ^{3}He film.

(25) Make CW NMR measurements preferably as a function frequency to

better estimate the quadrupolar frequency of ^{11}B and the other $\boldsymbol{I}>½$ substrate nuclei, in particular that of ^{14}N which does not appear to have been measured in hexagonal BN.

(26) Systematically investigate the effects of annealing time/temperature on the ^{3}He relaxation times. cf. §7.4.3.1

(27) Repeat the more detailed measurements of suggestion (1) for the ^{11}B relaxation times;

- − Look for motional narrowing of surface ^{11}B spins by ^{3}He via the ^{11}B T_2.
- − Preplating with X=0.05 ^{4}He, watch for the effect of the onset of registering with coverage on ^{11}B T_2 and T_1 at 1K. Further investigate via the 'SD3' T_1 measure. Compare the magnetic susceptibility as measured in figure 7.4.3.9, as a function of coverage with the ^{3}He edge-film-present case of figure 7.4.3.9.
- − Determine exactly where the ^{11}B minimum occurs in coverage at registry at 1K for fields $(2.7\text{MHz}/\gamma_{He}) \leqslant B_0 \leqslant (10.7\text{MHz}/\gamma_{He})$. In particular where does the minimum occur for F_0=4.54MHz × γ_{He}/γ_B? − at X=0.75 as for ^{3}He?
- − Repeat these measurements using ^{14}N, ^{10}B and ^{15}N if possible.

(28) Check the argon isotherm by re-doing it properly at constant temperature. Do the X=0.05 and X<0.05 features still appear? Repeat with some other suitable gases. Eg. Krypton and compare with figure 3.3.2 which also possessed a feature attributed to the edge-sites filling up.

(29) For comparison with the helium-on-graphite (homogeneous substrate, formation of distinct higher layers but no FMR relaxation) and DLX6000 (heterogeneous surface, no formation of distinct higher layers but strong FMR relaxation) work, do a multi-layer NMR study of ^{3}He on hexagonal BN using both the ^{3}He relaxation times and those of the substrate to explore the growth of higher layers leading to the onset of bulk liquid ^{3}He behaviour.

(30) Do a detailed heat capacity study of ^{3}He and/or ^{4}He submonolayer and multilayer films on hexagonal BN along the lines of the work on graphite summarised in §1.8.

(31) Do an NMR study, with particular reference to FMR relaxation, of ^{3}He adsorbed on cubic BN whose crystalline symmetry results in no EFG and therefore no quadrupolar splittings.

(32) Using a ^{3}He monolayer adsorbed on DLX6000 sample, measure the ^{3}He and ^{19}F T_1s against $1/T$ for T>1K and look for simultaneous minima. How does it compare with the BN data?

(33) Analyse some ^{19}F recoveries from ^{3}He on DLX6000 data using the 'SD3' fit. How do they compare with the ^{11}B recoveries presented in §7.4.3.2?

(34) Bearing in mind the difficulties mentioned in §8.7.5 make a serious effort to measure the ^{14}N quadrupole frequency on hexagonal BN and hopefully verify the F_Q ~4.5MHz inferred from the ^{3}He data, upon which so much of the explanations given depend.

(35) Use an alternative method, eg. heat capacity to obtain some independent measurements of the exchange frequency J in the ^{3}He-on-BN incommensurate solid and compare with the values from §8.7.7.

(B) Suggested Instrumental Enhancements

(1) Install the dilution refrigerator for the above lower temperature experiments.

(2) Modify the POTREG software to operate the pot pumping line solenoid valves, including the QSV as a binary array for finer graduation in pumping rate. That is, the pumping rate delivered by each valve is adjusted to increase approximately by a power of two with valve number.

Any number of valves may be on at once and each binary bit of the pumping rate number corresponds to a 'valve'. This will have the beneficial side effect of reducing the frequency of noisy QSV operations. See figure 4.1.2.1.

(3) The liquid helium consumption of the cryostat is currently larger by about 2 litres/day than it was in the past. Upgrades to the in-cryostat main magnet current supply leads may have been responsible. Therefore investigate thermal conduction into the cryostat with a view to saving liquid helium. The multiple parameter cryostat state monitoring ability of the system discussed in Chapter 4 should be useful. IR photography of the cryostat might also be valuable for revealing 'cold-spots' where the heat leak is greatest, eg. at the cryostat-top main magnet leads connector.

(4) Investigate measures to increase the performance of the NMR spectrometer;

- Replace the cryostat-top pre-amp with an in-cryostat 4K cooled one.
- Replace the frequency stepper unit with a miniature uniselector driven device, in the cryostat, alongside the cooled amplifier close to the NMR coil to avoid the signal degradation of the current system when moving away from the natural resonant frequency of the tank circuit. NB: We have obtained a number of potentially suitable uniselectors from a surplus electronics firm.
- Look into using DC SQUID detection for increased S/N performance, particularly valuable for low frequency work.
- Data taking where T_2^* is very short such as for Boron-11 is made difficult by the tank circuit ringdown time which is of the order of T_2^* even with the present ringdown damping measures. Investigate possible active-damping schemes; Consider developing an ADC→(dedicated microprocessor or computer unit)→DAC system where feedback is used to eliminate as much as possible of the ringdown from a few dummy pulse sequences (ie. with no signal present) preceding a set of spin-echo etc. measurements.

(5) Building on the work already done, automate spectrometer frequency changing.

(6) Consider replacing the TEK2230 oscilloscope with a more advanced model. Desirable additional features are; A 'soft' X & Y gain to allow the controlling computer to compensate for changes in signal height and length during a set of automatic measurements. A faster internal microprocessor since this appears to be the bottleneck in TEK2230 trace→IEEE-488 bus→Archimedes data transfers. It is this bottleneck which limits the overall data taking rate.

(7) Take steps to reduce or eliminate computer noise leaking into the spectrometer receiver section. Since computer noise from a machine in close physical or electrical proximity to the spectrometer is practically impossible to eliminate, the ideal solution would be to move the computer far enough away from the cryostat/spectrometer to eliminate RF pickup. The two could then be linked via optic fibre. A custom hardware/software interface at the computer end would encode/decode IEEE-488 and 1MHz bus read/write commands etc. for the optic fibre. At the spectrometer end a simple dedicated microprocessor based system in a well screened box would interface to the optic fibre, reconstituting IEEE-488 and 1MHz bus signals. Additionally, using a µP with a *CPU clock halt when inactive* facility (as used in laptop PCs for battery saving) would ensure there is no digital activity of any sort near the spectrometer except when commands are being sent across the optic fibre, further reducing the opportunity for correlated noise to get into the spectrometer. One of the Microchip 'PIC' family of RISC microcontrollers [221] would be ideal.

(8) Only 8 thermometry resistors can be selected under computer control at present. With the addition of the dilution fridge the bridge interface unit (figure 4.1.2.1) should be upgraded/replaced to allow automatic selection of many more resistors, n>20−30. Modification/replacement of the SHE conductance bridge to permit computer control of the bridge *range* and other front panel settings would be useful.

(9) Extra security measures against ‘hangs’ by the magnet controller would be desirable for better magnet/helium level protection. Suggest that instead of all accesses to the 2K hardware page driving the re-triggerable monostable, which can probably randomly occur quite easily when the OS has lost control of the CPU due to hardware misbehaviour, that accesses (possibly several specific sequential ones) to a specific memory location with specific data be used to hold-off timeout of the RTM.

(10) This entry lists some possible modifications to the cryostat ancillaries worth considering. The idea is to assist one set of unattended measurements to automatically follow another;

- Addition of solenoid valves to the gas handling system to allow computer controlled sample admission. Useful for example in a detailed set of 1K $T_{1,2}$ *vs* X data where the coverage must be increased many times in a relatively short period of time,
- Addition of a computer controlled solenoid valve linking the pot pumping line to the cryostat helium recovery line would assist cooling the pot after sample annealing (see §4.2.4.1).
- Replace the pot heater on/off computer control with a variable power one to permit T>4.2K measurements to automatically, efficiently follow $T\leqslant$4.2 ones. eg. A high heater power is used to boil-off the pot followed by a small but gradually increasing power to regulate temperature as T=4.2K→13.2K data taking proceeds.
- Computer controllable pot filling. This could be implemented by an in-cryostat solenoid valve on the pot filling line, leaving the needle valve to set the inflow rate. Alternatively, a solenoid valve switched continuous fill system might be useful.
- Computer logging of the return lines' gas meters to permit the controlling program to measure the cryostat helium boil off rate and more importantly the volume of helium gas returned from, hence liquid remaining in, the pot.

− Computer controlled helium transfers to assist uninterrupted data taking over weekends etc.

(11) Enhance the ARCONTROL6 software to make real-time decisions while data taking. Eg: Adjust the oscilloscope y-gain and number-of-averages etc. dynamically to best suit the signal size and S/N ratio. Discard traces corrupted by random glitches etc. Dynamically adjust the pulse generator delay etc. times to suit current relaxation times.

(C) Suggested Theoretical Work

(1) A theoretical study of heteronuclear dipolar relaxation in two dimensions along the lines of the homonuclear study of reference **70**.

(D) Other Suggested Improvements

(1) Enhance the ANALYSE software. Some spin-echoes which decay strongly sub-exponentially receive a less than ideal fit from the product function (equation 6.2.2). Although not a serious problem since all echoes in a particular dataset tend to be similarly affected, leaving relaxation times derived from the echo heights unaffected, it is undesirable. Providing a third fitting function of the *index* type should cure the problem.

(2) If a suitable package still does not exist, write a decent WIMP driven scientific graph plotting program.

(3) A replacement computer for experimental control and data analysis? As figure 4.1.2.1 shows the computer controlling the experiment is at the heart of the experimental setup. It is therefore essential that it works properly − that the system is fast, the software flexible to use and above all reliable. With the benefit of hindsight it was unwise to attempt to build a preemptively scheduled multitasking arrangement on a machine whose OS was not designed to support one − as the problems discussed in §4.2.4.2 make clear. A significant amount of data-taking and program debugging

time was lost due to the system hangs/crashes. A better approach might have been to try using the cooperative scheduler built into the RISC OS windowing environment. Obtaining sufficiently regular time-slices for the POTREG program to operate properly is the main problem. ARCONTROL6 as well as POTREG would have to be rewritten to run in the windowing environment, with particular care taken over the CPU time-slices used by ARCONTROL6, to achieve this. At best it is an inconvenient and inefficient way to use an OS whose scheduling arrangements were designed to give a fast response to intensively interactive programs running within the desktop windowing environment.

Computer technology − hardware and software date more rapidly than almost any other type of laboratory instrumentation. Bearing this in mind, and the time of writing (Late 1996) the following suggestions will be presented: It would be desirable to replace the current computer control system with something more suitable but what are the available options? Hardware-wise the options can be grouped into three classes, with attendant hardware and software choices;

(1) Keep the Archimedes.

− Advantages: Continue to have easy access to Acorn specific hardware − User Port and 1MHz bus.

(a) Continue to run RISC OS and rewrite POTREG and ARCONTROL6 software.

− Advantages: Least work involved.

− Disadvantages: As documented in this work.

(b) Run a version of the Unix™ operating system on the Archimedes.

− Advantages: A proper multitasking OS with preemptive scheduling.

− Options: (I) Use Risc iX a commercial but now obsolete version of Unix produced by Acorn Computers Ltd.

(II) With a more recent model Archimedes (eg. A5000) the free Linux version of Unix could be

run.

(III) With one of the most recent Risc-PC machines another free version of Unix, RiscBSD could be used.

(IV) Wait for Linux or RiscBSD to be ported to model A440 hardware or do the port.

(2) Replace the Archimedes with an 'IBM compatible' PC.

- Advantages: Wide choice of machines and software available, eg. for graph plotting, numerical analysis etc.
- Disadvantages: Need to abandon or modify user-port/ 1MHz bus driven hardware or build a PC interface card to emulate user-port and 1MHz bus protocols.

(a) Run Linux (or other free Unix) on the machine.

- Advantages: Huge amount of free software available or comes with the OS. Eg. Graphics libraries/toolkits to run under the X Windows System for displaying data in real time etc. etc. User support via the Internet from the international Linux user community for programming/installation/user etc. problems.
- Disadvantages: Significant amount of learning required to get the best out of OS of this size and complexity.

(b) Run a commercial Microsoft Windows™ based application specifically designed for controlling laboratory instrumentation and performing numerical analysis etc. such as National Instruments Corporation's Labview™ product.

- Advantages: Facilities to produce 'virtual instruments' in the WIMP environment (eg. oscilloscope, DVM) which interface to corresponding hardware instruments or interface card and permit extra features such

as FFT to be added in software.

- Disadvantages: Difficult to say with no first hand experience of the system but areas such as real time performance in time-critical applications such as pulse-generation, particularly if driving unintelligent hardware such as described in §4.2.5, would need to be investigated. It is also questionable whether the WIMP/object driven method of programming used by such systems is actually preferable to the traditional HLL/ text-editor method despite perhaps being superficially more appealing,

(3) Replace the Archimedes with a 'proper' workstation from Digital Equipment Corporation, Sun Microsystems, Hewlett Packard etc. running the OpenVMS™ or Unix operating systems.

- Advantages: A commercially supported, fully featured, multi-user OS.
- Disadvantages: More expensive than previous options. As with a PC, user-port and 1MHz emulation or modification of peripheral hardware needed.
- Of particular interest are the DEC VAX and Alpha/AXP machines which run the OpenVMS OS on which most of the data analysis software such as ANALYSE has been developed and run. VAX, a 32 bit CISC CPU, Digital's established processor had been in existence for 19 years and is very well supported by commercial and free software. Alpha/AXP, a 64 bit RISC processor has been available for four years. It is the fastest general purpose CPU available with some of the latest versions

(Alpha 21164) being clocked at 500MHz and also boasts the best price/performance ratio currently available [222]. There are reports [223] of a WIMP/X-windows driven package, broadly similar in function to National Instruments Corporation's Labview™ product, which is available for the AXP/OpenVMS platform − which could be an important factor in making choices between computer hardware.

From the point of view of a user responsible for controlling the experiment, analysing the experimental data, developing software and undertaking miscellaneous computing activities, potentially the most profound choice to be made is between a single-user OS such as Windows or RISC OS and a multi-user one, eg. Unix or OpenVMS, rather than between hardware platforms. With a multi-user OS a number of highly desirable features/possibilities become available together with a more secure working environment for the experiment's controlling software. Some of these are;

(a) Separate processes for POTREG and ARCONTROL6 etc. experimental controller software running at suitably elevated scheduling priorities.

(b) Remote login via *Telnet*/*Rlogin* from any other machine on Campus or anywhere on the Internet − eg. login from home to check/control experiment.

(c) Similarly, local or remote access through the X-windows graphical user-interface to monitor the state of the experiment and control it using WIMP based tools.

(d) Near real-time execution of ANALYSE or other raw-data analysis ‘number-crunching’ software on the same machine, running at a lower scheduling priority. This gives easy and immediate access to

the raw data produced by real-time data taking processes such as ARCONTROL6 and ensures the quickest automated availability of analysed data and eliminates the need to transfer raw data files to a separate machine for analysis.

(e) Availability of all the standard Internet servers, eg. FTP (file-transfer), NFS (remote mounting of local discs or directory trees), HTTP (Web protocol), SMTP (E-mail) etc. provides for easy automatic backup of files over the network, the easy availability of raw data files on more powerful remote machines should one be needed for analysis etc. etc., all without the need to disturb the experimental controller/data taking.

(f) Simultaneous access to the machine, by more than one user for general computing activities, again without interrupting data taking − eg. reading Usenet news, using E-mail, accessing the Web, developing software etc. etc.

(g) With experimental control functions running in separate processes there is no reason in principle why one machine should not simultaneously control several entirely separate experiments, without mutual interference, increasing the cost effectiveness of a multi-user system.

The author's personal preference, funds permitting, would be to use an OpenVMS workstation on grounds of familiarity and (high and low level) system security. Alternatively a fast PC running Linux might provide a less expensive but functionally similar solution. Ideally the machine would be located far enough away from the cryostat/spectrometer to eliminate RF pickup, on a separate mains supply and with an optic fibre linking the spectrometer and computer as suggested above. Using a WIMP driven package to run the experiment on such a system could make for a very

convenient alternative to purpose written programs such as ARCONTROL6. For spectrometer setting-up/manual data taking a simple character cell terminal such as a VT220 (which tend to be less serious RF radiators) or a PC running X-Windows (should a WIMP interface be needed) could be connected to the network or directly to the multi-user machine and placed next to the spectrometer for convenient access. Once setting up was complete, the terminal would be switched off and the experiment monitored/controlled from the workstation or elsewhere.

Appendix 1.

Appendix 1, Some NMR relevant data for selected spins [224].

Isotope	Natural Relative Abundance	Spin ($\hbar$)	Larmor Frequency (MHz/Tesla)	Quadrupole Moment $Q/10^{-28}$ m^2
^{1}H	99.985%	1/2	+42.5760	
^{2}H	0.015%	1	+6.5357	+0.00274
^{3}He	0.0001%	1/2	−32.4338	
^{10}B	19.6%	3	+4.574	+0.06
^{11}B	80.4%	3/2	+13.6595	+0.04
^{13}C	1.108%	1/2	+10.7054	
^{14}N	99.635%	1	+3.076	+0.07
^{15}N	0.0365%	1/2	−4.315	
^{19}F	100%	1/2	+40.0543	
^{29}Si	4.71%	1/2	−8.458	
^{169}Tm	100%	1/2	−3.47	

Appendix 2.

The ARCONTROL6 Software.

```
REM >arcontrol6
REM Load the IEEE library if not present
ON ERROR INSTALL “BAS488”
A%=FNservice_requested
ON ERROR PROCerror
REM T.Crane July 1988 Experimental controller
IF MODE <> 7 THEN MODE7
REM Revision History: 2-Jan-1989: Amended for 50Mhz Master Clock
REM                 : 2-Feb-1989: Amended for sep ch. for T1 180o pulse
REM                 : 2-Feb-1989: Amended to ensure ARM in user mode before LDM to return to BASIC
REM                 :10-Nov-1989: “LONG OFF” added to ensure TEK2230 gives short messages
REM                 : 2-Feb-1989: Amended to allow 4K tek traces
REM                 :28-Jun-1990: Added support for temperature logging & magnet controller
REM                 :01-Aug-1990: Mods to allow temperature control, conductance logging &
paroscientific gauge logging via HP5335A frequency counter, freq%->freq
REM                 :08-Aug-1990: Added Temperature control for T1, Log T1 delays & 5minute wait after
attaining required temperature
REM                 :16-AUG-1990: Bug-fix, moved pulse_offset%=1 inside temperature loop (also
PROCinit_scope_for_echoes)
REM                 :30-AUG-1990: Added SC Speer logging
REM                 :16-NOV-1990: Added Temperature control for FIDs
REM                 :17-NOV-1990: Bugfix for susp. CRO firmware bug, See Run book #1, P.162
REM                 :21-NOV-1990: Implemented reading instructions from file
REM                 :26-NOV-1990: Multi-string ‘*’ commands from file bugfix
REM                 :12-NOV-1990: Implemented gradient measurements (sequence$=“GRAD”)
REM                 :13-DEC-1990: Ensured sign of Temp_increment is correct
REM                 :17-DEC-1990: Implemented log field gradients
REM                 :18-DEC-1990: Added “gradient_log_fac” facility
REM                 :19-DEC-1990: Gradient voltage now read from Prema scanner
REM                 :21-DEC-1990: Added separate tolerances for 2K<T<2K to reduce 1/4SV actuations
REM                 :02-JAN-1991: Added check for correct Prema multiplexer ch.
REM                 :04-JAN-1991: PROCdelay now uses FOR-NEXT-LOOP not REP.U.TIME etc. or *fx19s (See
M&HD book#2, P.111), added debugging writes to FNprema
REM                 :08-JAN-1991: Modified timing in potreg-hang detection
REM                 :21-JAN-1991: Stopped using PROCdelay2 in Required_Temp_check for *fx138,0,x wait
override facility
REM                 :23-JAN-1991: Implemented better required temp check wait override facility
REM                 :30-JAN-1991: Stopped reading prema (He & N2) every trace
REM                 :19-FEB-1991: Stopped reading SCSP every trace
REM                 :25-APR-1991: Clarified appending of O/P file
REM                 :25-APR-1991: Added MC S/D checking facility
REM                 :30-MAY-1991: Added interactive ‘*’ command facility
REM                 :14-OCT-1991: Added nos_ave% facility from file
REM                 :17-OCT-1991: Added preload delay to bugfix hangs
REM                 :31-OCT-1991: Added interrupt mode operation (see M&HD book#2,p116)
REM                 :02-NOV-1991: Delays now displayed in uS,mS,Sec & Mins as appropriate
REM                 :06-NOV-1991: Tidied up the above displays
REM                 :12-DEC-1991: Added LOG T2 delays & initial T2 dummy pulse (for Rt<T1 situation)
REM                 :05-JAN-1992: Increased Trigger pulse from 2uS to 5uS to prevent trigger failure &
bugfixed limits on LOG delays
version$=“3.0.07 (Arc) (05-JAN-1992)”
interrupt_mode = FALSE
IEEE_tek_address=1
IEEE_prema_address=7
IEEE_arc_address=0
IEEE_magnet_controller_address=3
IEEE_hp5335a_address=3                  :REM !!! ### CAREFUL ### !!!
nmr_data%=0
No%=4
pulse_offset%=0
RTC_wait$=“TRUE”
update_specials_count%=0
aveorss$=“ ”
WHILE INSTR(“SsAa”,aveorss$)=0
INPUT “SINGLE SHOTS OR AVERAGE MODE  S/A ”aveorss$
ENDWHILE
PROCinit_IEEE_and_devices
acquisition_points%=FNacq_points
PRINTCHR$129;“ACQUISITION POINTS= ”;acquisition_points%
IF aveorss$=“S” OR aveorss$=“s” THEN
screen_length%= 9 + acquisition_points%
  ELSE
screen_length%= 9 + 2 * acquisition_points%
ENDIF
nos_ave%=1: REM Default nos shots = 1 ie. 1 shot mode
IF aveorss$=“A” OR aveorss$=“a” THEN INPUT“NUMBER OF AVERAGES ”nos_ave%
DIM channel$(No%)
DIM T1pulse%(7)
DIM T2pulse%(5)
DIM grad_pulse%(5)
DIM FIDpulse%(1)
DIM pulse%(2*No%-1)
DIM screen% screen_length%
DIM buffer% 80 :REM FOR OS_ReadVarVal
MC_current1$=“N/A”
INPUT “FREQUENCY (x 4) (MHz) ”freq
freq=freq/4
PRINT“FREQUENCY = ”;freq
PROCsetup_output_file
```

```
PROCsetup_pulse_generator
INPUT “SEQUENCE(s) ”sequence$
IF sequence$ = “T1” THEN
 PROCT1_input
 PROCT1
 PROCstop
ELSE
 IF sequence$ = “T2” THEN
  PROCT2_input
  PROCT2
  PROCstop
 ELSE
  IF sequence$ = “FID” THEN
   PROCFID_input
   PROCFID
   PROCstop
  ELSE
   IF sequence$ = “AUTO” THEN
    PROCauto
   ELSE
    IF sequence$ = “FILE” THEN
     PROCfile_sequence
    ELSE
     IF sequence$ = “GRAD” THEN
      PROCgrad_input
      PROCgrad
     ELSE
      PRINTCHR$129;“NO SUCH SEQUENCE, must be one of T1, T2, FID, AUTO, FILE or GRAD”
     ENDIF
    ENDIF
   ENDIF
  ENDIF
 ENDIF
ENDIF
PROCstop
END
:
DEFPROCfile_sequence
REM This procedure allows instructions to be read from a file
INPUT “INPUT FILE NAME ? ”sequence_file$
sfh%=OPENINsequence_file$
REPEAT
seq$=FNfile_readS(sfh%)
CASE seq$ OF
WHEN “T1” :PROCT1_from_file :PROCT1
WHEN “T2” :PROCT2_from_file :PROCT2
WHEN “FID”:PROCFID_from_file:PROCFID
ENDCASE
UNTIL EOF#sfh%
CLOSE#sfh%
ENDPROC
:
DEFPROCT1_from_file
PRINTCHR$129;“Reading T1 information from file”
nos_ave%=FNfile_readN(sfh%)
PRINT“Nos_ave% = ”;nos_ave%
ch_180=FNfile_readN(sfh%)
PRINT“180o pulse from Ch.2 by itself or from Ch.0 with rest from 0/2 = ”;ch_180
IF ch_180 <> 0 AND ch_180 <> 2 THEN PRINTCHR$129;“ERROR ch_180 MUST BE 0 OR 2”:PROCstop
REM P1 & P2 & P3 (uS)
T1pulse%(1)=FNfile_readN(sfh%)
T1pulse%(3)=FNfile_readN(sfh%)
T1pulse%(5)=FNfile_readN(sfh%)
PRINT“P1 = ”;T1pulse%(1);“ P2 = ”;T1pulse%(3);“ P3 = ”;T1pulse%(5)
REM Spin-Echo delay (uS)
T1pulse%(4)=FNfile_readN(sfh%)
PRINT“Spin-Echo delay (uS) = ”;T1pulse%(4)
REM LIN or LOG Delays, 0/1 ?
T1_logorlin$=FNfile_readS(sfh%)
IF T1_logorlin$ <> “LIN” AND T1_logorlin$ <> “LOG” THEN
 PRINTCHR$129;“T1_logorlin$ must be LOG or LIN”
 PROCstop
ELSE
PRINT“T1_logorlin$ = ”;T1_logorlin$
ENDIF
IF T1_logorlin$ = “LOG” THEN
 REM T1 Process Delays (uS); START, FINISH
 T1sta_del%=FNfile_readN(sfh%)
 T1fin_del%=FNfile_readN(sfh%)
 PRINT“T1 process delays; START = ”;T1sta_del%;“, FINISH = ”;T1fin_del%
 REM Number of logarithmic delay increments ?
 T1inc_del%=FNfile_readN(sfh%)
 PRINT“Number of logarithmic delay increments = ”;T1inc_del%
ELSE
 REM T1 Process Delays (uS); START, FINISH, INCREMENT
 T1sta_del%=FNfile_readN(sfh%)
 T1fin_del%=FNfile_readN(sfh%)
 T1inc_del%=FNfile_readN(sfh%)
 PRINT“T1 process delays; START = ”;T1sta_del%;“, FINISH = ”;T1fin_del%;“, INCREMENT = ”;T1inc_del%
ENDIF
REM Temperature at which to make measurement; START, STOP & INCREMENT
Temp_start=FNfile_readN(sfh%)
Temp_stop=FNfile_readN(sfh%)
Temp_increment=FNfile_readN(sfh%)
PRINT“Temperatures; START = ”;Temp_start;“, STOP = ”;Temp_stop;“, INCREMENT = ”;Temp_increment
REM Temperature regulation tolerance (mK)
Tolerance=FNfile_readN(sfh%)
Tolerance2=Tolerance
PRINT“Tolerance (regulation) = ”;Tolerance
```

```
REM In-range-checking tolerance (mK)
Tolerance_in_range_checking=FNfile_readN(sfh%)
PRINT"Tolerance (in-range-checking) = ";Tolerance_in_range_checking
REM Paroscientific gauge logging Y/N ?
ps_logging$=FNfile_readS(sfh%)
PRINT"Paroscientific gauge logging = ";ps_logging$
REM Log the sample-chamber resistor Y/N ?
scr_logging$=FNfile_readS(sfh%)
PRINT"Sample-chamber resistor logging = ";scr_logging$
REM Check for Magnet-Controller S/D Y/N ?
MCSD_checking$=FNfile_readS(sfh%)
PRINT"Magnet-Controller S/D Checking = ";MCSD_checking$
REM REPETITION TIME (centi-seconds)
T1reptim=FNfile_readN(sfh%)
PRINT"Repetition Time = ";T1reptim
REM WAIT AFTER CHECKING FOR REQUIRED TEMPERATURE
RTC_wait$=FNfile_readS(sfh%)
PRINT"Required Temperature Checking Wait = ";RTC_wait$
IF RTC_wait$ <> "TRUE" AND RTC_wait$ <> "FALSE" THEN  PRINT "RTC_wait ERROR":PROCstop
ENDPROC
:
DEFPROCT2_from_file
PRINTCHR$129;"Reading T2 information from file"
nos_ave%=FNfile_readN(sfh%)
PRINT"Nos_ave% = ";nos_ave%
REM P1 & P2 (uS)
T2pulse%(1)=FNfile_readN(sfh%)
T2pulse%(3)=FNfile_readN(sfh%)
PRINT"P1 = ";T2pulse%(1);" uS, P2 = ";T2pulse%(3);" uS"
REM Initial T2 dummy pulses?
T2_dummy_pulses$=FNfile_readS(sfh%)
IF T2_dummy_pulses$ <> "FALSE" AND T2_dummy_pulses$ <> "TRUE" THEN
 PRINTCHR$129;"T2_dummy_pulses$ must be TRUE or FALSE"
 PROCstop
ELSE
 PRINT"T2_dummy_pulses$ = ";T2_dummy_pulses$
ENDIF
IF T2_dummy_pulses$ = "TRUE" THEN T2_dummy_pulses%=TRUE ELSE T2_dummy_pulses%=FALSE
REM LIN or LOG Delays, 0/1 ?
T2_logorlin$=FNfile_readS(sfh%)
IF T2_logorlin$ <> "LIN" AND T2_logorlin$ <> "LOG" THEN
 PRINTCHR$129;"T2_logorlin$ must be LOG or LIN"
 PROCstop
ELSE
PRINT"T2_logorlin$ = ";T2_logorlin$
ENDIF
IF T2_logorlin$ = "LOG" THEN
 REM T2 Delays (uS); START, FINISH
 T2sta_del%=FNfile_readN(sfh%)
 T2fin_del%=FNfile_readN(sfh%)
 PRINT" Delays (uS) ; START = ";T2sta_del%;", FINISH = ";T2fin_del%
 REM Number of logarithmic delay increments ?
 T2inc_del%=FNfile_readN(sfh%)
 PRINT"Number of logarithmic delay increments = ";T2inc_del%
ELSE
 REM T2 Delays (uS); START, FINISH, INCREMENT
 T2sta_del%=FNfile_readN(sfh%)
 T2fin_del%=FNfile_readN(sfh%)
 T2inc_del%=FNfile_readN(sfh%)
 PRINT"Delays (uS); START = ";T2sta_del%;", FINISH = ";T2fin_del%;", INCREMENT = ";T2inc_del%
ENDIF
REM Temperatures & Tolerances
Temp_start=FNfile_readN(sfh%)
Temp_stop=FNfile_readN(sfh%)
Temp_increment=FNfile_readN(sfh%)
PRINT"Temperatures (mK); START = ";Temp_start;", FINISH = ";Temp_stop;", INCREMENT = ";Temp_increment
Tolerance=FNfile_readN(sfh%)
Tolerance2=Tolerance
PRINT"Tolerance (regulation) (mK) = ";Tolerance
Tolerance_in_range_checking=FNfile_readN(sfh%)
PRINT"Tolerance (in-range-checking) (mK) = ";Tolerance_in_range_checking
ps_logging$=FNfile_readS(sfh%)
PRINT"Paroscientific gauge logging = ";ps_logging$
scr_logging$=FNfile_readS(sfh%)
PRINT"Sample-chamber resistor logging = ";scr_logging$
MCSD_checking$=FNfile_readS(sfh%)
PRINT"Magnet-Controller S/D Checking = ";MCSD_checking$
T2reptim=FNfile_readN(sfh%)
PRINT"REPETITION TIME (centi-seconds) = ";T2reptim
REM WAIT AFTER CHECKING FOR REQUIRED TEMPERATURE
RTC_wait$=FNfile_readS(sfh%)
PRINT"Required Temperature Checking Wait = ";RTC_wait$
IF RTC_wait$ <> "TRUE" AND RTC_wait$ <> "FALSE" THEN  PRINT "RTC_wait ERROR":PROCstop
ENDPROC
:
DEFPROCFID_from_file
PRINTCHR$129;"Reading FID information from file"
nos_ave%=FNfile_readN(sfh%)
PRINT"Nos_ave% = ";nos_ave%
REM Length of 90o pulse
FIDpulse%(1)=FNfile_read(sfh%)
PRINT"P1 = ";FIDpulse%(1);" uS"
REM Temperatures & Tolerances
Temp_start=FNfile_readN(sfh%)
Temp_stop=FNfile_readN(sfh%)
Temp_increment=FNfile_readN(sfh%)
PRINT"Temperatures (mK); START = ";Temp_start;", FINISH = ";Temp_stop;", INCREMENT = ";Temp_increment
Tolerance=FNfile_readN(sfh%)
Tolerance2=Tolerance
```

```
PRINT“Tolerance (regulation) (mK) = ”;Tolerance
Tolerance_in_range_checking=FNfile_readN(sfh%)
PRINT“Tolerance (in-range-checking) (mK) = ”;Tolerance_in_range_checking
ps_logging$=FNfile_readS(sfh%)
PRINT“Paroscientific gauge logging = ”;ps_logging$
scr_logging$=FNfile_readS(sfh%)
PRINT“Sample-chamber resistor logging = ”;scr_logging$
MCSD_checking$=FNfile_readS(sfh%)
PRINT“Magnet-Controller S/D Checking = ”;MCSD_checking$
FIDreptim=FNfile_readN(sfh%)
PRINT“REPETITION TIME (centi-seconds) = ”;FIDreptim
REM WAIT AFTER CHECKING FOR REQUIRED TEMPERATURE
RTC_wait$=FNfile_readS(sfh%)
PRINT“Required Temperature Checking Wait = ”;RTC_wait$
IF RTC_wait$ <> “TRUE” AND RTC_wait$ <> “FALSE” THEN  PRINT “RTC_wait ERROR”:PROCstop
ENDPROC
:
DEFFNfile_readS(handle%)
REM Read a string from the input file
LOCAL string$,char%
string$=””
REPEAT
char%=BGET#handle%
IF char% <> ASC“*” THEN
 WHILE char% <> 10 AND char% <> ASC“,” AND char% <> 32 :REM <LF>, <SPACE> or comma separators
 string$=string$+CHR$char%
 char%=BGET#handle%
 ENDWHILE
ELSE
 REM Execute the string if it is a “*” command
 WHILE char% <> 10 :REM <LF> separator
 string$=string$+CHR$char%
 char%=BGET#handle%
 ENDWHILE
 PRINTCHR$7;CHR$129;“OS COMMAND: ”;string$
 OSCLI(string$)
 string$=””
ENDIF
UNTIL LEN(string$) >= 1
=string$
:
DEFFNfile_readN(handle%)
=VAL(FNfile_readS(handle%))
:
DEFPROCauto
REM At this stage automatic calling of PROCs T1, T2 & FID is handled
PRINTCHR$129;“AUTO SEQUENCE”
PROCT1_input:PROCT2_input:PROCFID_input :REM get I/P info
FOR sequence%=1 TO 3
CASE sequence% OF
WHEN 1:PROCT1
WHEN 2:PROCT2
WHEN 3:PROCFID
ENDCASE
NEXT sequence%
PROCstop
ENDPROC
:
DEFPROCstop
*shut
VDU7
STOP
ENDPROC
:
DEFPROCT1_input
PRINTCHR$129;“Enter T1 information”
REPEAT
INPUT “180o pulse from Ch.2 by itself or from ch.0 with rest 0/2 ”,ch_180
UNTIL ch_180 = 0 OR ch_180 = 2
INPUT “P1 & P2 & P3 (uS) ”T1pulse%(1),T1pulse%(3),T1pulse%(5)
INPUT “Spin-Echo delay (uS) ”T1pulse%(4)
REPEAT
INPUT “LIN or LOG Delays, LOG/LIN ? ”T1_logorlin$
UNTIL T1_logorlin$ = “LIN” OR T1_logorlin$ = “LOG”
IF T1_logorlin$ = “LOG” THEN
  INPUT ”T1 Process Delays (uS); START, FINISH ”T1sta_del%,T1fin_del%
  INPUT “Number of logarithmic delay increments ? ”T1inc_del%
ELSE
  INPUT “T1 Process Delays (uS); START, FINISH, INCREMENT ”T1sta_del%,T1fin_del%,T1inc_del%
ENDIF
INPUT “Temperatures (mK); START, FINISH, INCREMENT ”Temp_start,Temp_stop,Temp_increment
INPUT “Temperature regulation tolerance {t>2k } (mK) ”Tolerance
INPUT “Temperature regulation tolerance {t<2k } (mK) ”Tolerance2
INPUT “In-range-checking tolerance (mK) ”Tolerance_in_range_checking
INPUT “Paroscientific gauge logging Y/N ? ”ps_logging$
INPUT “Log the sample-chamber resistor Y/N ? ”scr_logging$
INPUT “Check for Magnet-Controller S/D Y/N ? ”MCSD_checking$
INPUT “REPETITION TIME (centi-seconds) ”T1reptim
ENDPROC
:
DEFPROCT1
sequence$=“T1”
No%=4
FOR I%=1 TO 7
pulse%(I%)=T1pulse%(I%)
NEXT I%
reptim=T1reptim
pulse%(6)=pulse%(4)
pulse%(7)=5: REM Trigger pulse = 5uS
```

```
REM Channel allocation; P1 & P2 & P3 − channel 0
REM P4 (trigger pulse) − channel 1
channel$(1)="0"
channel$(2)="0"
IF ch_180 = 0 THEN
channel$(3) = "0":REM Normal channel for this pulse
  ELSE
channel$(3) = "2":REM 180o pulse from separate channel to allow 90o phase shift
ENDIF
channel$(4)="1"
OSCLI ("POTREG SEL_R AUTO") :REM Make sure automatic resistor selection is enabled
Temp_increment=ABS(Temp_increment)*FNsgn(Temp_stop−Temp_start)
FOR Required_Temp=Temp_start TO Temp_stop STEP Temp_increment :REM −Temperatures
 IF Required_Temp >= 2000 THEN
 OSCLI ("POTREG SET_T "+STR$(Required_Temp)+" "+STR$(Tolerance)+" "+STR$(Tolerance_in_range_checking))
  ELSE

OSCLI ("POTREG SET_T "+STR$(Required_Temp)+" "+STR$(Tolerance2)+" "+STR$(Tolerance_in_range_checking))
 ENDIF
 PROCRequired_Temp_check :REM Check that the required temperature has been reached
 PROCinit_scope_for_echos
 pulse_offset%=1: REM Don't produce first pulse
 REM H(infinity) measurement
 reading%=1
 PRINTCHR$129;"H(Infinity), @ T = ";Required_Temp;"mK"
 pulse%(2)=T1sta_del%
 FOR shot_no%= 1 TO nos_ave%
  PROCrun (FALSE)
 NEXT shot_no%
 REM Now main T1 readings
 PRINTCHR$129;"Main T1 readings, @ T = ";Required_Temp;"mK"
 pulse_offset%=0: REM Restore the first pulse
 IF T1_logorlin$ = "LIN" THEN
   FOR pulse%(2)=T1sta_del% TO T1fin_del% STEP T1inc_del%: REM ---- Delays
    reading%=reading%+1
    FOR shot_no%= 1 TO nos_ave%: REM ------------------------------ Shot no.
     PROCrun (FALSE)
    NEXT shot_no%
   NEXT pulse%(2)
 ELSE
   FOR pulse_log=LOG(T1sta_del%) TO LOG(T1fin_del%) STEP ((LOG(T1fin_del%)−LOG(T1sta_del%))/
(T1inc_del%)): REM --- Delays
    pulse%(2)=10^pulse_log
    reading%=reading%+1
    FOR shot_no%= 1 TO nos_ave%: REM ------------------------------ Shot no.
     PROCrun (FALSE)
    NEXT shot_no%
   NEXT pulse_log
 ENDIF
NEXT Required_Temp
ENDPROC
:
DEFPROCT2_input
PRINTCHR$129;"Enter T2 information"
INPUT "P1 & P2 (uS) "T2pulse%(1),T2pulse%(3)
REPEAT
INPUT "T2 dummy pulses Y/N? " T2_dummy_pulses$
UNTIL T2_dummy_pulses$="Y" OR T2_dummy_pulses$="y" OR T2_dummy_pulses$="N" OR T2_dummy_pulses$="n"
IF T2_dummy_pulses$="Y" OR T2_dummy_pulses$="y" THEN
 T2_dummy_pulses%=TRUE
ELSE
 T2_dummy_pulses%=FALSE
ENDIF
REPEAT
INPUT "LIN or LOG Delays, LOG/LIN ? "T2_logorlin$
UNTIL T2_logorlin$ = "LIN" OR T2_logorlin$ = "LOG"
IF T2_logorlin$ = "LOG" THEN
  INPUT "Delays (uS); START, FINISH "T2sta_del%,T2fin_del%
  INPUT "Number of logarithmic delay increments ? "T2inc_del%
ELSE
  INPUT "Delays (uS); START, FINISH, INCREMENT "T2sta_del%,T2fin_del%,T2inc_del%
ENDIF
INPUT "Temperatures (mK); START, FINISH, INCREMENT "Temp_start,Temp_stop,Temp_increment
INPUT "Temperature regulation tolerance {t>2k } (mK) "Tolerance
INPUT "Temperature regulation tolerance {t<2k } (mK) "Tolerance2
INPUT "In−range−checking tolerance (mK) "Tolerance_in_range_checking
INPUT "Paroscientific gauge logging Y/N ? "ps_logging$
INPUT "Log the sample−chamber resistor Y/N ? "scr_logging$
INPUT "Check for Magnet−Controller S/D Y/N ? "MCSD_checking$
INPUT "REPETITION TIME (centi−seconds) "T2reptim
ENDPROC
:
DEFPROCgrad_input
REM Static gradient & temperature are varied
PRINTCHR$129;"Enter gradient information"
INPUT "P1 & P2 (uS) "grad_pulse%(1),grad_pulse%(3)
INPUT "Delay D1 (uS); "grad_pulse%(2)
REPEAT
INPUT "LIN or LOG Gradients, LOG/LIN ? "grad_logorlin$
UNTIL grad_logorlin$ = "LIN" OR grad_logorlin$ = "LOG"
IF grad_logorlin$ = "LOG" THEN
  INPUT "Grad. current; START, FINISH "gradient_current_start,gradient_current_stop
  INPUT "Number of logarithmic gradients values ? "gradient_current_steps%
  INPUT "Gradient log−rate factor ? "gradient_log_fac
ELSE
  INPUT "Grad. current; START, FINISH, NOS_STEPS
"gradient_current_start,gradient_current_stop,gradient_current_steps%
ENDIF
INPUT "Temperatures (mK); START, FINISH, INCREMENT "Temp_start,Temp_stop,Temp_increment
```

```
INPUT “Temperature regulation tolerance {t>2k } (mK) ”Tolerance
INPUT “Temperature regulation tolerance {t<2k } (mK) ”Tolerance2
INPUT “In−range−checking tolerance (mK) ”Tolerance_in_range_checking
INPUT “Paroscientific gauge logging Y/N ? ”ps_logging$
INPUT “Log the sample−chamber resistor Y/N ? ”scr_logging$
INPUT “Check for Magnet−Controller S/D Y/N ? ”MCSD_checking$
INPUT “REPETITION TIME (centi−seconds) ”grad_reptim
ENDPROC
:
DEFPROCT2
sequence$=“T2”
No%=3
FOR I%=1 TO 5
pulse%(I%)=T2pulse%(I%)
NEXT I%
reptim=T2reptim
pulse%(5)=5: REM Trigger pulse = 5uS
PROCinit_scope_for_echos
REM Channel allocation; P1 & P2 − channel 0
REM P3 (trigger pulse) − Channel 1
channel$(1)=”0”
channel$(2)=“0”
channel$(3)=“1”
OSCLI (“POTREG SEL_R AUTO”) :REM Make sure automatic resistor selection is enabled
Temp_increment=ABS(Temp_increment)*FNsgn(Temp_stop−Temp_start)
FOR Required_Temp=Temp_start TO Temp_stop STEP Temp_increment :REM −−−− Temperatures
 IF Required_Temp >= 2000 THEN
 OSCLI (“POTREG SET_T ”+STR$(Required_Temp)+“ ”+STR$(Tolerance)+“ ”+STR$(Tolerance_in_range_checking))
  ELSE
 OSCLI (“POTREG SET_T ”+STR$(Required_Temp)+“ ”+STR$(Tolerance2)+“
“+STR$(Tolerance_in_range_checking))
 ENDIF
 PROCRequired_Temp_check :REM Check that the required temperature has been reached
 PRINTCHR$129;“T2 Readings, @ T = ”;Required_Temp;“mK”
 reading%=0
 REM Send initial T2 dummy pulses is required
 IF T2_dummy_pulses% THEN
  pulse%(2)=T2sta_del%
  pulse%(4)=pulse%(2)
  reading%=1
  shot%=1
  PROCrun (TRUE)
 ENDIF
 IF T2_logorlin$ = “LIN” THEN
   FOR pulse%(2)=T2sta_del% TO T2fin_del% STEP T2inc_del%: REM −−−− Delays
    pulse%(4)=pulse%(2)
    reading%=reading%+1
    FOR shot_no%= 1 TO nos_ave%: REM ------------------------------ Shot no.
     PROCrun (FALSE)
    NEXT shot_no%
   NEXT pulse%(2)
 ELSE
   FOR pulse_log=LOG(T2sta_del%) TO LOG(T2fin_del%+1) STEP ((LOG(T2fin_del%)−LOG(T2sta_del%))/(T2inc
_del%−1)): REM −−− Delays
    pulse%(2)=10^pulse_log
    pulse%(4)=pulse%(2)
    reading%=reading%+1
    FOR shot_no%= 1 TO nos_ave%: REM ------------------------------ Shot no.
     PROCrun (FALSE)
    NEXT shot_no%
   NEXT pulse_log
 ENDIF
NEXT Required_Temp
ENDPROC
:
DEFPROCgrad
sequence$=“GRAD”
No%=3
FOR I%=1 TO 5
pulse%(I%)=grad_pulse%(I%)
NEXT I%
pulse%(4)=pulse%(2)
reptim=grad_reptim
pulse%(5)=5: REM Trigger pulse = 5uS
PROCinit_scope_for_echos
REM Channel allocation; P1 & P2 − channel 0
REM P3 (trigger pulse) − Channel 1
channel$(1)=”0”
channel$(2)=“0”
channel$(3)=“1”
OSCLI (“POTREG SEL_R AUTO”) :REM Make sure automatic resistor selection is enabled
Temp_increment=ABS(Temp_increment)*FNsgn(Temp_stop−Temp_start)
FOR Required_Temp=Temp_start TO Temp_stop STEP Temp_increment :REM −−−− Temperatures
 IF Required_Temp >= 2000 THEN
 OSCLI (“POTREG SET_T ”+STR$(Required_Temp)+“ ”+STR$(Tolerance)+“ ”+STR$(Tolerance_in_range_checking))
  ELSE

OSCLI (“POTREG SET_T ”+STR$(Required_Temp)+“ ”+STR$(Tolerance2)+“ ”+STR$(Tolerance_in_range_checking))
 ENDIF
 REM Initialise MC to 0.0 while the new temperature is reached
 PROCsetup_magnet_controller
 PROCadrandoutput (3,IEEE_magnet_controller_address,“SWITCH_HOLD_ON”)
 PROCadrandoutput (3,IEEE_magnet_controller_address,“COIL=0”)
 PRINTCHR$129;“SETTING MC TO 0.0”
 PROCadrandoutput (3,IEEE_magnet_controller_address,“CURRENT=0.0”)
 PROCRequired_Temp_check :REM Check that the required temperature has been reached
 PRINTCHR$129;“Gradient Readings, @ T = ”;Required_Temp;“mK”
 reading%=0
 IF grad_logorlin$ = “LIN” THEN
```

```
  FOR gradient_current=gradient_current_start TO gradient_current_stop STEP ((gradient_current_stop-
gradient_current_start)/(gradient_current_steps%-1))
   PRINTCHR$129;"GRADIENT CURRENT (MC)= ";gradient_current
   PROCsetup_magnet_controller
   PROCadrandoutput (3,IEEE_magnet_controller_address,"SWITCH_HOLD_ON")
   PROCadrandoutput (3,IEEE_magnet_controller_address,"COIL=0")
   PROCadrandoutput (3,IEEE_magnet_controller_address,"CURRENT="+STR$gradient_current)
   PRINTCHR$129;"Waiting for MC to get there"
   A%=0
   REPEAT
    PROCadrandoutput (3,IEEE_magnet_controller_address,"DAC?")
    MC_current1$=FNadrandinput (3,IEEE_magnet_controller_address,255)
    PROCdelay(20)
    PROCadrandoutput (3,IEEE_magnet_controller_address,"DAC?")
    MC_current2$=FNadrandinput (3,IEEE_magnet_controller_address,255)
    IF MC_current1$=MC_current2$ THEN A% +=1 ELSE A%=0
   UNTIL A% = 10
   PRINT;"MC now at ";MC_current1$
   gradient_voltage$=FNprema(3) :REM read prema for the gradient voltage
   reading%=reading%+1
   FOR shot_no%= 1 TO nos_ave%: REM ------------------------------ Shot no.
    PROCrun (FALSE)
   NEXT shot_no%
  NEXT gradient_current
 ELSE
 REM Logarithmic gradient currents
  FOR gradient_current2=LOG(gradient_current_start+gradient_log_fac) TO
LOG(gradient_current_stop+gradient_log_fac) STEP ((LOG(gradient_current_stop+gradient_log_fac)-
LOG(gradient_current_start+gradient_log_fac))/(gradient_current_steps%-1))
   gradient_current=10^gradient_current2 - gradient_log_fac
   PRINTCHR$129;"GRADIENT CURRENT [log] (MC)= ";gradient_current
   PROCsetup_magnet_controller
   PROCadrandoutput (3,IEEE_magnet_controller_address,"SWITCH_HOLD_ON")
   PROCadrandoutput (3,IEEE_magnet_controller_address,"COIL=0")
   PROCadrandoutput (3,IEEE_magnet_controller_address,"CURRENT="+STR$gradient_current)
   PRINTCHR$129;"Waiting for MC to get there"
   A%=0
   REPEAT
    PROCadrandoutput (3,IEEE_magnet_controller_address,"DAC?")
    MC_current1$=FNadrandinput (3,IEEE_magnet_controller_address,255)
    PROCdelay(20)
    PROCadrandoutput (3,IEEE_magnet_controller_address,"DAC?")
    MC_current2$=FNadrandinput (3,IEEE_magnet_controller_address,255)
    IF MC_current1$=MC_current2$ THEN A% +=1 ELSE A%=0
   UNTIL A% = 10
   PRINT;"MC now at ";MC_current1$
   gradient_voltage$=FNprema(3) :REM read prema for the gradient voltage
   reading%=reading%+1
   FOR shot_no%= 1 TO nos_ave%: REM ------------------------------ Shot no.
    PROCrun (FALSE)
   NEXT shot_no%
  NEXT gradient_current2
 ELSE
 ENDIF
NEXT Required_Temp
REM Set MC to 0.0 since measurements are finished
PROCsetup_magnet_controller
PROCadrandoutput (3,IEEE_magnet_controller_address,"SWITCH_HOLD_ON")
PROCadrandoutput (3,IEEE_magnet_controller_address,"COIL=0")
PRINTCHR$129;"SETTING MC TO 0.0"
PROCadrandoutput (3,IEEE_magnet_controller_address,"CURRENT=0.0")
ENDPROC
:
DEFPROCrun (dummy_run%)
REM This procedure sends the pulses and takes the data
IF sequence$ <> "FID" THEN
PROCdisplay_state (pulse%(2),shot_no%)
  ELSE
PRINTCHR$131;"SHOT NUMBER +";shot_no%
ENDIF
REM send pulses
REM If pulse-generator code already assembled just call it
IF dummy_run% PRINTCHR$129;"Dummy pulses..."
IF shot_no%>1 THEN
PRINTCHR$131;"RUNNING...."
CALL start
   ELSE
PROCpulse_generator
ENDIF
REM Repetition time routine
TIME=0
REPEAT
PRINTTAB(0,23)"REPETITION TIME = ";TIME
UNTIL TIME > reptim
IF dummy_run% THEN
 REM Reset the tek scope before proceeding
 CASE sequence$ OF
 WHEN "T1"   :PROCinit_scope_for_echos
 WHEN "T2"   :PROCinit_scope_for_echos
 WHEN "FID"  :PROCinit_scope_for_FIDs
 WHEN "GRAD" :PROCinit_scope_for_echos
 ENDCASE
 ENDPROC   :REM return immediately
ENDIF
REM If averaging is finished read in & dump the data to disk
IF shot_no%=nos_ave% THEN
 REM check tek is ready before extracting data
 PROCbusy_check (IEEE_tek_address)
 PROCtek_scope
```

```
 IF (aveorss$="A" OR aveorss$="a") THEN
  REM Reset scope after 'LIMIT' reached on average mode
  CASE sequence$ OF
  WHEN "T1"   :PROCinit_scope_for_echos
  WHEN "T2"   :PROCinit_scope_for_echos
  WHEN "FID"  :PROCinit_scope_for_FIDs
  WHEN "GRAD" :PROCinit_scope_for_echos
  ENDCASE
 ENDIF
ENDIF
ENDPROC
:
DEFPROCdisplay_state (delay%,shot_no%)
LOCAL display_state_str$
IF delay% < 1E3 THEN
 display_state_str$=LEFT$(STR$delay%,4)+" uS"
ELSE
 IF delay% < 1E6 THEN
  display_state_str$=LEFT$(STR$(delay%/1E3),4)+" mS"
 ELSE
  IF delay% < 60E6 THEN
   display_state_str$=LEFT$(STR$(delay%/1E6),4)+" Secs"
  ELSE
   display_state_str$=LEFT$(STR$(delay%/60E6),4)+" Mins"
  ENDIF
 ENDIF
ENDIF
PRINTCHR$131;"DELAY = ";display_state_str$;" SHOT# ";shot_no%
ENDPROC
:
DEFPROCinit_scope_for_echos
PRINTCHR$130;"SETTING UP OSCILLOSCOPE FOR SPIN ECHOS"
PROCsetup_scope
PROCadrandoutput (3,IEEE_tek_address,"ACQ TRIGC:"+STR$(acquisition_points% DIV 2)): REM set trigger to
center of screen
REM Set up sample mode OR average mode and sweep & weight settings
IF aveorss$="S" OR aveorss$="s" THEN
PROCadrandoutput (3,IEEE_tek_address,"ACQ CURR:SAM,NUM:0")
  ELSE
PROCadrandoutput (3,IEEE_tek_address,"ACQ CURR:AVE,WEI:"+STR$nos_ave%+",NUM:"+STR$nos_ave%)
ENDIF
PROCdelay (400): REM Small delay for tek to recover
PROCbusy_check (IEEE_tek_address) :REM Having initialised tek wait until it has recovered
ENDPROC
:
DEFPROCsetup_scope
PROCtimeout_on
PROCeos_out_1chr (10)
PROCeos_in_2chr (13,10)
PROCcontroller (IEEE_arc_address)
PRINTCHR$133;"TEK STATUS BYTE="FNserial_poll (IEEE_tek_address)
PROCadrandoutput (3,IEEE_tek_address,"LONG OFF"): REM Use short message format
ENDPROC
:
DEFPROCsetup_magnet_controller
PROCtimeout_on
PROCeos_out_1chr (13)
PROCeos_in_1chr (13)
PROCcontroller (IEEE_arc_address)
A%=FNserial_poll(IEEE_magnet_controller_address)
IF A% <> 0 THEN PRINT"MC STATUS= ";A%:VDU7:STOP
ENDPROC
:
DEFPROCtek_scope
PROCsetup_scope
PROCadrandoutput (3,IEEE_tek_address,"WFMPRE?")
wfmpre$=FNadrandinput (3,IEEE_tek_address,255)
PRINT"WFMPRE = ";wfmpre$
PROCadrandoutput (3,IEEE_tek_address,"CURVE?")
PROCadrandinputmem (2,IEEE_tek_address,screen%,screen_length%)
REM Obtain the readings from the Prema DMM
REM Don't update prema every trace to save time
IF (update_specials_count% MOD 10 = 0) THEN
 resch1$=FNprema (1)
 resch0$=FNprema (0)
ENDIF
REM Get the temperature of the selected resistor
SYS "OS_ReadVarVal","Potreg$Current_Temperature",buffer%,80,0 TO ,,nos%
temperature$=""
FOR count%=0 TO nos%-1
temperature$=temperature$+CHR$(buffer%?count%)
NEXT count%
PRINT"Temperature= ";temperature$
REM Get the conductance of the selected resistor
SYS "OS_ReadVarVal","Potreg$Current_Conductance",buffer%,80,0 TO ,,nos%
conductance$=""
FOR count%=0 TO nos%-1
conductance$=conductance$+CHR$(buffer%?count%)
NEXT count%
PRINT"Conductance= ";conductance$
REM Get the last temperature update time
SYS "OS_ReadVarVal","Potreg$Last_Update_Time",buffer%,80,0 TO ,,nos%
temperature_update_time$=""
FOR count%=0 TO nos%-1
temperature_update_time$=temperature_update_time$+CHR$(buffer%?count%)
NEXT count%
PRINT"Temperature update time= ";temperature_update_time$
REM Obtain frequencies from HP5335A if required
IF ps_logging$ = "Y" OR ps_logging$ = "y" THEN
```

```
PROCread_hp5335a_frequencies :REM Read the frequencies from the ps gauge
PRINThp5335a_cha$,hp5335a_chb$
  ELSE
hp5335a_cha$=“NOT IN USE”
hp5335a_chb$=“NOT IN USE”
ENDIF
IF scr_logging$ = “Y” OR scr_logging$ = “y” THEN
IF (update_specials_count% MOD 10 = 0) OSCLI (“POTREG ALT_R 6”)
REM Get the temperature of the sample−chamber resistor
SYS “OS_ReadVarVal”,“Potreg$Alternate_Temperature”,buffer%,80,0 TO ,,nos%
alternate_temperature$=“”
FOR count%=0 TO nos%−1
alternate_temperature$=alternate_temperature$+CHR$(buffer%?count%)
NEXT count%
PRINT“Temperature(SC Speer)= ”;alternate_temperature$
REM Get the conductance of the sample−chamber resistor
SYS “OS_ReadVarVal”,“Potreg$Alternate_Conductance”,buffer%,80,0 TO ,,nos%
alternate_conductance$=“”
FOR count%=0 TO nos%−1
alternate_conductance$=alternate_conductance$+CHR$(buffer%?count%)
NEXT count%
PRINT“Conductance(SC Speer)= ”;alternate_conductance$
  ELSE
alternate_temperature$=“NOT LOGGED”
alternate_conductance$=“NOT LOGGED”
ENDIF
REM DATA to disk:−
PRINTCHR$130;“DUMP DATA TO FILE”
CASE sequence$ OF
WHEN “T1”  :PROCdump_T1_info
WHEN “T2”  :PROCdump_T2_info
WHEN “FID” :PROCdump_FID_info
WHEN “GRAD”:PROCdump_grad_info
ENDCASE
PROCdump_string (wfmpre$):REM Waveform preamble
REM Transfer the waveform data to the output file
PRINTCHR$130;“DUMPING SCREEN TO DISK”
SYS “OS_GBPB”,2,nmr_data%,screen%,screen_length%
REM Periodically Check that Helium level as monitored by the Magnet−Controller
REM the Magnet−Controller is not low.
REM Bit 7 of status−byte is set if He−level is low
IF (update_specials_count% MOD 10 = 0) THEN
 IF MCSD_checking$ = “Y” OR MCSD_checking$ = “y” THEN
  PRINT “MAGNET S/D Checking”
  PROCsetup_magnet_controller :REM So he−level check becomes active
  PROCadrandoutput (3,IEEE_magnet_controller_address,“DAC?”)
  PRINT “DAC = ”;FNadrandinput (3,IEEE_magnet_controller_address,255)
  tmp%=FNserial_poll (IEEE_magnet_controller_address)
  PRINTCHR$133;“MC STATUS BYTE = ”;tmp%
  IF (tmp% AND 128) <> 0 THEN
   PRINTCHR$129;“** MAGNET S/D DETECTED AT ”;TIME$;“ **”
   PROCstop
  ENDIF
 ENDIF
ENDIF
update_specials_count%+=1
ENDPROC
:
DEFPROCdump_string (string$)
FOR A%=1 TO LEN(string$)
BPUT#nmr_data%,ASC(MID$(string$,A%,1))
NEXT
BPUT#nmr_data%,0: REM ‘0’ Terminates string
ENDPROC
:
DEFPROCdump_string2 (string$)
FOR A%=1 TO LEN(string$)
BPUT#nmr_data%,ASC(MID$(string$,A%,1))
NEXT
BPUT#nmr_data%,13: REM ‘<CR>’ Terminates string
ENDPROC
:
DEFFNprema (multiplexer_ch%)
REM If multiplexer_ch% is −ve then the front sockets are used
LOCAL result$
PROCsetup_prema:PRINT“1”;
REM The following commands are carried out a a lower level to allow the prema to keep up
REPEAT
 PROCatn_true:PRINT;“2”;
 PROCunlisten:PRINT;“3”;
 PROCtalk (IEEE_arc_address):PRINT;“4”;
 PROClisten (IEEE_prema_address):PRINT;“5”;
 PROCatn_false:PRINT;“6”;
 IF multiplexer_ch% >= 0 THEN
 PROCoutput (0,“VDA1T3C0M”+STR$(multiplexer_ch%)):PRINT;“7”; :REM Select a multiplexor channel &
disconnect front sockets
  ELSE
 PROCoutput (0,“VDA1T3MOC1”):PRINT;“8”;                    :REM Select the front sockets & switch
multiplexer off
 ENDIF
 PROCatn_true:PRINT;“9”;
 PROCunlisten:PRINT;“A”;
 PRINT;“a”;
 PROCdelay (300):PRINT;“B”;: REM CF Int time=1Sec
 PROClisten (IEEE_arc_address):PRINT;“C”;
 PROCtalk (IEEE_prema_address):PRINT;“D”;
 PROCatn_false:PRINT;“E”;
 result$=FNinput (0,31):PRINT;“F”;
 PROCatn_true:PRINT;“G”;
```

```
 PROCuntalk:PRINT;“H”;
 PROCatn_false:PRINT;“I”;
 PRINT result$
UNTIL  RIGHT$(result$,2) = “M”+STR$(multiplexer_ch%)
REM Now set auto-ranging OFF
PROCatn_true:PRINT;“J”;
PROCunlisten:PRINT;“K”;
PROCtalk (IEEE_arc_address):PRINT;“L”;
PROClisten (IEEE_prema_address):PRINT;“M”;
PROCatn_false:PRINT;“N”;
PROCoutput (0,“A0”):PRINT;“O”;
PROCatn_true:PRINT;“P”;
PROCunlisten:PRINT;“Q”;
PROCatn_false:PRINT;“R”;
REM “GO TO LOCAL” because Prema does not automatically
PROCgo_to_local (IEEE_prema_address):PRINT;“S”
=result$
:
DEFPROCsetup_prema
PROCtimeout_on
PROCeos_out_1chr (13)
PROCeos_in_1chr (13)
PROCcontroller (IEEE_arc_address)
PRINTCHR$133;“PREMA STATUS BYTE=”FNserial_poll (IEEE_prema_address)
ENDPROC
:
DEFPROCsetup_output_file
REM This procedure sets up the output data file
INPUT“DATA FILENAME (Data appended if file exists) ”file$
PRINTCHR$130;“OPEN DATA FILE”
nmr_data%=0
WHILE nmr_data%=0
nmr_data%=OPENUP file$ :REM The UG is wrong about this
REM Create data file if nonexistent
IF nmr_data%=0 THEN
 PRINT“Creating O/P file ”;file$
 OSCLI(“SAVE ”+file$+“ 0 0”)
ENDIF
ENDWHILE
IF EXT#nmr_data% > 0 THEN
 PRINTCHR$130;“END OF DATA FILE AT ”;EXT#nmr_data%;“ Bytes”
 PTR#nmr_data%=EXT#nmr_data%
ENDIF
ENDPROC
:
DEFPROCdelay (period)
REM This procedure waits for the specified time in centisecond units
LOCAL tmp% ,usercmd$
IF period > 30000 THEN PRINT “DELAY TOO BIG!”:VDU7:PROCstop
tmp%=INKEY(period)
IF tmp% = ASC“*” THEN
 PRINTCHR$7;CHR$129;“USER *COMMAND ”;CHR$130;
 INPUT “” usercmd$
 OSCLI (usercmd$)
 PRINTCHR$129;“RE-SCHEDULING DELAY”
 PROCdelay(period)
ENDIF
IF tmp% <> -1 AND tmp% <> ASC “*” THEN PRINTCHR$7;“KEY PRESSED”
ENDPROC
:
DEFPROCdelay2 (period)
REM This procedure waits for the specified time in centisecond units
LOCAL tmp%, tmp2%
tmp2%=528.8*period
FORtmp%=1TOtmp2%
NEXTtmp%
ENDPROC
:
DEFPROCsetup_pulse_generator
REM This procedure initialises the pulse generator system
REM Find the absolute location of the hardware
fred_offset%=0
SYS “I/O_Podule_Hardware” TO ,podule_base_addr
base_addr = podule_base_addr - &3C0000 + 4 * fred_offset%
REM Find the scaling factor for the current clock frequency
hardware_clock_factor=FNclock_frequency
REM Pulse generator register offsets
pulse_latch1=      0
pulse_latch2=      4 * 1
pulse_latch3=      4 * 2
pulse_latch4=      4 * 3
delay_latch1=      4 * 4
delay_latch2=      4 * 5
delay_latch3=      4 * 6
delay_latch4=      4 * 7
instruction_latch= 4 * 8
route_latch=       4 * 9
status_latch=      4 * 14
irq_reset=         4 * 14
REM Symbolic names for ARM registers
R_tmp=                     0
R_current=                 1
R_last=                    2
R_base_addr=               3
R_tmp2=                    4
REM Space for ARM code
armcode_size%=2000
DIM mc% armcode_size%
switch%=0
```

```
ENDPROC
:
DEFPROCpulse_generator
REM This procedure assembles and calls the ARM code which produces
REM the pulses
PRINTCHR$130;“ASSEMBLING CODE....”
REM Produce the code for the pulses
pulse_delay_sequence_no% = 0
generate_listing=FALSE
IF generate_listing THEN
 listing_par%=3
ELSE
 listing_par%=2
ENDIF
FOR pass%=0 TO listing_par% STEP listing_par%
P%= mc%
PROCirq_handler
[OPT pass%
.base_addr_store               EQUD base_addr
.interrupt_jump_addr           EQUD 0
.pulse_generation_finished_flag EQUD 0
.start
]
PROCinit_pulse_generator
REM Don’t assemble 1st pulse for a T1 H(inf)
FOR I%=pulse_offset%+1 TO No%
PROCpulse_delay (I%,pulse_offset%)
NEXT I%
NEXT pass%
REM Check that the assembled ARM code did not exceed the space reserved for it
IF P% > mc%+armcode_size% THEN PRINTCHR$7;CHR$129;“ARM CODE ACCESS VIOLATION!!”:PROCstop
:
REM Now call the assembled ARM code
counter%=0
PRINTCHR$131;“RUNNING....”
CALL start
ENDPROC
:
DEFFNconvert(value,type%)
REM Convert the pulse/delay/rep times into hardware units
LOCAL value%, max, min
REM Natural units=uS
IF type%=0 THEN IF value<140E-3 PRINTCHR$129;“PULSES >=140 nanoseconds !”:PROCstop
IF type%=1 THEN IF value<30 PRINTCHR$129;“DELAYS >=30 microseconds !”:PROCstop
value=value*hardware_clock_factor
IF value>&7FFFFFFF THEN
max=&7FFFFFFF/(hardware_clock_factor*60E6)
PRINTCHR$129;(value/hardware_clock_factor);“uS TOO BIG. MAX=”;max;“ minutes at this clock speed
!”:PROCstop
ENDIF
IF value<1 THEN
min=1/(hardware_clock_factor*1E-3)
PRINTCHR$129;(value/hardware_clock_factor);“uS TOO SMALL. MIN=”;min;“ nanoseconds at this clock speed
!”:PROCstop
ENDIF
value%=value
=value%
:
DEFFNroute(route$)
REM Work out the destinations for the pulses
REM Channel zero is now accepted
route%=0
FOR M%=1 TO LEN(route$)
IF ASC(MID$(route$,M%,1))>55 OR ASC(MID$(route$,M%,1))<48 THEN route%=1E6
route%=route%+2^(VAL(MID$(route$,M%,1)))
NEXT
IF route%>255 THEN PRINTCHR$129;“NO SUCH CHANNEL !”:PROCstop
=route%
:
DEFPROCinit_pulse_generator
REM This procedure initialises the pulse generator system
REM Only disable interrupts if in interrupt mode
IF NOT interrupt_mode THEN
[OPT pass%
   STMFD   R13!, {r0-r12 ,R14}                    ;Push registers onto BASIC stack
   SWI     “OS_EnterOS”                           ;Drive the CPU into SVC mode
   MOV     R_tmp, R15
   ORR     R_tmp, R_tmp, #((1<<26)+(1<<27))
   TEQP    R_tmp, #0                              ;Disable IRQs and FIQs
   ADR     R_tmp, base_addr_store
   LDR     R_base_addr, [R_tmp, #0]               ;Load R_base_addr with the physical base address
   MOV     R_last, #2                             ;Let “DIV2” status flag appear to be HI initially
]
 ELSE
[OPT pass%
   STMFD   R13!, {r0-r12 ,R14}                    ;Push registers onto BASIC stack
;
; First, claim the device vector for the pulse generator
;
   MOV     R0, #13                          ;Device number 13 is a/the I/O podule
   ADR     R1, irq_handler_addr             ;Address of IRQ handler routine
   MOV     R2, #0                           ;Value to be passed to IRQ handler in R12
   MOV     R3, #base_addr
   ADD     R3, R3, #status_latch            ;Pulse-generator interrupt flag register (status_latch)
   MOV     R4, #64                          ;Pulse-generator interrupt flag mask (status_latch bit#6)
   MOV     R5, #0                           ;Probably unnecessary, see PRM,Vol#1,pp.94-95
   SWI     “OS_ClaimDeviceVector”           ;Claim the device vector for the IRQ handler code
;
;
```

```
   SWI     “OS_EnterOS”                              ;Drive the CPU into SVC mode
   ADR     R_tmp, base_addr_store
   LDR     R_base_addr, [R_tmp, #0]                  ;Load R_base_addr with the physical base address
   ADR     R_tmp, pulse_generation_finished_flag     ;Initialise this flag to zero
   MOV     R_tmp2, #0
   STR     R_tmp2, [R_tmp, #0]
]
ENDIF
ENDPROC
:
DEFPROCload_pulse (pulse_width%)
REM This procedure loads the pulse
IF pass%=3 THEN PRINT“pulse_width% =”;pulse_width%
[OPT pass%
   MOV     R_tmp, #(pulse_width% AND &FF) <<16                    ;Byte 1 (LSB)
   STR     R_tmp, [R_base_addr, #pulse_latch1]
   MOV     R_tmp, #(pulse_width% AND &FF00) <<8                   ;Byte 2
   STR     R_tmp, [R_base_addr, #pulse_latch2]
   MOV     R_tmp, #(pulse_width% AND &FF0000)                     ;Byte 3
   STR     R_tmp, [R_base_addr, #pulse_latch3]
   MOV     R_tmp, #(pulse_width% AND &FF000000) >>8               ;Byte 4 (MSB)
   STR     R_tmp, [R_base_addr, #pulse_latch4]
]
ENDPROC
:
DEFPROCload_delay (delay_width%)
REM This procedure loads the delay
IF pass%=3 THEN PRINT“delay_width% =”;delay_width%
[OPT pass%
   MOV     R_tmp, #(delay_width% AND &FF) <<16                    ;Byte 1 (LSB)
   STR     R_tmp, [R_base_addr, #delay_latch1]
   MOV     R_tmp, #(delay_width% AND &FF00) <<8                   ;Byte 2
   STR     R_tmp, [R_base_addr, #delay_latch2]
   MOV     R_tmp, #(delay_width% AND &FF0000)                     ;Byte 3
   STR     R_tmp, [R_base_addr, #delay_latch3]
   MOV     R_tmp, #(delay_width% AND &FF000000) >>8               ;Byte 4 (MSB)
   STR     R_tmp, [R_base_addr, #delay_latch4]
]
ENDPROC
:
DEFPROCpreload
REM This procedure sends the preload pulse
[OPT pass%
   MOV     R_tmp, #2<<16                                          ;Set preload line LO
   STR     R_tmp, [R_base_addr, #instruction_latch]
   BL      preload_delay
   MOV     R_tmp, #3<<16                                          ;Set preload line HI
   STR     R_tmp, [R_base_addr, #instruction_latch]
   BL      preload_delay
   MOV     R_tmp, #2<<16                                          ;Set preload line LO again
   STR     R_tmp, [R_base_addr, #instruction_latch]
   BL      preload_delay
   BAL     preload_end
.preload_delay
; Delay to ensure (pre)load to counters lasts at least one
; clock cycle, even at 50KHz. This is a fix to hangs
; (delays of &FFFFFFFF counts), 17th Oct. 1991, TPC.
   MOV     R_tmp, #32
.delay_loop
   SUBS    R_tmp, R_tmp, #1
   BNE     delay_loop
   MOV     R15, R14
.preload_end
]
ENDPROC
:
DEFPROCstop_pulses
REM This procedure sends the stop signal
[OPT pass%
   MOV     R_tmp, #0
   STR     R_tmp, [R_base_addr, #instruction_latch]    ;Stop pulses
]
IF interrupt_mode THEN
[OPT pass%
   ADR     R_tmp, pulse_generation_finished_flag       ;Signal the foreground holding loop that pulse
   MOV     R_tmp2, #1                                  ;generation has finished
   STR     R_tmp2, [R_tmp, #0]
   LDMFD   R13!, {r0-r12 ,R15}                         ;Return from interrupt for the last time
]
ENDIF
ENDPROC
:
DEFPROCstart
REM This procedure sends the start signal
[OPT pass%
   MOV     R_tmp, #1<<16
   STR     R_tmp, [R_base_addr, #instruction_latch]               ;Start pulses
]
ENDPROC
:
DEFPROCwatch
IF NOT interrupt_mode THEN
REM This part of the procedure watches until it finds status flag “pulse” = LO
REM AND “DIV2” status flag = NOT last value of “DIV2”
[OPT pass%
.watch_loop
   LDR     R_current, [R_base_addr, #status_latch]                ;Check to see if “pulse” is LO
   ANDS    R_tmp, R_current, #1
   BNE     watch_loop
```

```
                                    ;So “pulse” status flag = LO
   EOR     R_tmp, R_current, R_last   ;EOR with corresponding bit in R_last
   ANDS    R_tmp, R_tmp, #2           ;Mask out the other bits
   BEQ     watch_loop                 ;Go back to watch_loop if “DIV2” last was same as “DIV2” current
   MOV     R_last, R_current          ;Make the current “DIV2” the ‘last’ “DIV2”
]
 ELSE
  REM Code to do 2 pass assembly locally to forward reference labels
  locp%=P%
  FOR temp_pass%=1 TO listing_par% STEP listing_par%-1
  IF pass%>0 AND temp_pass%=listing_par% THEN loc_pass%=pass% ELSE loc_pass%=0
  P%=locp%
  [OPT loc_pass%
   ADR    R_tmp, interrupt_code_passes_here              ;Set up the jump table for the interrupt code
   ADR    R_tmp2, interrupt_jump_addr                    ;to jump thru
   STR    R_tmp, [R_tmp2, #0]
  ]
 IF generate_listing THEN PRINT “pulse_delay_sequence_no%= ”;pulse_delay_sequence_no%
 IF pulse_delay_sequence_no% = 0 THEN pulse_delay_sequence_no% = P%
 IF pulse_delay_sequence_no% = P% THEN
  [OPT loc_pass%
.foreground_holding_loop                                ; ** This code is only assembled once **
   ADR    R_tmp, pulse_generation_finished_flag         ;This is the main interrupt mode holding loop
   LDR    R_tmp, [R_tmp, #0]             ;The main thread of control waits here after the first pulse+
   CMP    R_tmp, #0                      ;delay have been programmed until the complete pulse sequence
   BEQ    foreground_holding_loop        ;has been completed by the interrupt code.
   BAL    svc_exit_code                  ;Sequence finished, return to BASIC.
  ]
 ELSE
  [OPT loc_pass%
   LDMFD   R13!, {r0-r12 ,R15}                     ;Return from interrupt here
  ]
 ENDIF
  [OPT loc_pass%
.interrupt_code_passes_here
   ADR     R_tmp, base_addr_store                 ;Load R_base_addr with the physical base address
   LDR     R_base_addr, [R_tmp, #0]               ;again for the interrupt context code.
   STR     R_tmp, [R_base_addr, #irq_reset]       ;Write this location to clear IRQ condition
.watch_loop_irq_mode
   LDR     R_current, [R_base_addr, #status_latch]  ;Check to see if “pulse” is LO
   ANDS    R_tmp, R_current, #1                   ;ie. Wait here until pulse has timed out and delay
   BNE     watch_loop_irq_mode                    ;is executing before re-programming counters
  ]
 NEXT temp_pass%
ENDIF
ENDPROC
:
DEFPROCsend_route(route_no%)
REM This procedure sends the routing information for the next pulse
IF pass%=3 THEN PRINT “route_no%= ”;route_no%
[OPT pass%
   MOV     R_tmp, #route_no% <<16
   STR     R_tmp, [R_base_addr, #route_latch]                    ;Send routing byte
]
ENDPROC
:
DEFPROCreturn
REM This procedure returns to BASIC, going from SVC mode with
REM IRQs & FIQs disabled to user mode with both interrupts enabled
REM Additionally when in interrupt mode the interrupt handler is removed
REM from the the device vector.
IF interrupt_mode THEN
[OPT pass%
.svc_exit_code
   MOV      R_tmp, R15
   BIC      R_tmp, R_tmp, #(3+(1<<26)+(1<<27))        ;Return to USR with both interrupts enabled
   TEQP     R_tmp, #0
;
; Release the device vector now pulse generation is finished
;
   MOV     R0, #13                           ;Device number 13 is a/the I/O podule
   ADR     R1, irq_handler_addr              ;Address of IRQ handler routine
   MOV     R2, #0                            ;Value that was passed to IRQ handler in R12
   MOV     R3, #base_addr
   ADD     R3, R3, #status_latch             ;Pulse-generator interrupt flag register (status_latch)
   MOV     R4, #64                           ;Pulse-generator interrupt flag mask (status_latch bit#6)
   MOV     R5, #0                            ;Probably unnecessary, see PRM,Vol#1,pp.94-95
   SWI     “OS_ReleaseDeviceVector”          ;Release the device vector for the IRQ handler code
   LDMFD    R13!, {r0-r12 ,R15}
]
 ELSE
[OPT pass%
   MOV      R_tmp, R15
   BIC      R_tmp, R_tmp, #(3+(1<<26)+(1<<27))          ;Return to USR with both interrupts enabled
   TEQP     R_tmp, #0
   MOVNV    R_tmp, R_tmp                                ;Ensure ARM in user mode before LDM
   LDMFD    R13!, {r0-r12 ,R15}
]
ENDIF
ENDPROC
:
DEFFNclock_frequency
REM This function returns with the current clock settings
REM Returned frequencies are in MHz as time is uS
LOCAL result%, status_latch_offset%, exclk%
status_latch_offset%=fred_offset%+14
SYS “OS_Byte”,146,status_latch_offset%,result% TO ,,result%
IF (result% AND %10000) <> 0 THEN
PRINTCHR$7;CHR$133;“Clock Is External”
```

```
INPUT “External clock frequency (in MHz) ? ”exclk%
=exclk%
        ELSE
CASE (result% AND %1100) OF
WHEN    %0000: PRINTCHR$133;“Clock Is Internal at 50Mhz” :=50.0
WHEN    %0100: PRINTCHR$133;“Clock Is Internal at 5Mhz”  :=5.0
WHEN    %1000: PRINTCHR$133;“Clock Is Internal at 500Khz”:=0.5
WHEN    %1100: PRINTCHR$133;“Clock Is Internal at 50Khz” :=0.05
ENDCASE
ENDIF
ENDPROC
:
DEFPROCerror
REM This procedure handles errors
REPORT:PRINT “ at line ”ERL
*shut
VDU7
STOP
ENDPROC
:
DEFPROCpulse_delay (i%,recycle_offset%)
REM This procedure schedules the generation of the pulses and delays
REM See T.Crane Microcomputer development book (P.235)
REM If this is the first pulse use section [1]
IF (i%-recycle_offset%)=1 THEN PROCsection_1 (i%)
REM If this is the second pulse use section [2]
IF (i%-recycle_offset%)=2 THEN PROCsection_2 (i%)
REM If this is an intermediate pulse use section [I]
IF (i%-recycle_offset%)>2 THEN PROCsection_I (i%)
REM If this is the last pulse use section [F]
IF i%=No% THEN PROCsection_F
ENDPROC
:
DEFFNcalculate_pulse (pulse_no%)
REM This function returns the value of a pulse or zero if there is no
REM valid pulse for the pulse number
IF pulse_no% > No% THEN
=0
     ELSE
=FNconvert(pulse%(2*pulse_no%-1),0)
:
DEFFNcalculate_delay (delay_no%)
REM This function returns the value of a delay
REM If the end of the sequence has been reached then the final long delay
REM is returned otherwise zero is returned
IF delay_no% = No% THEN =&7FFFFFFF
IF delay_no% > No% THEN
=0
     ELSE
=FNconvert(pulse%(2*delay_no%),1)
:
DEFPROCsection_1 (i%)
REM This procedure schedules the generation of the first [and second]
REM pulses and delays
PROCload_pulse (FNcalculate_pulse(i%)): REM First pulse
PROCload_delay (FNcalculate_delay(i%)): REM First [and final] delay
PROCsend_route (FNroute(channel$(i%))): REM route for first pulse
PROCpreload : REM Preload the first pulse
REM Load the pulse latches with the 2nd pulse (If valid)
temp%=FNcalculate_pulse (i%+1)
IF temp%>0 THEN PROCload_pulse (temp%)
REM Load the delay latches with the 2nd delay (If valid)
temp%=FNcalculate_delay (i%+1)
IF temp%>0 THEN PROCload_delay (temp%)
REM Now send the start signal
PROCstart
REM Now watch for the 1st pulse to timeout
PROCwatch
ENDPROC
:
DEFPROCsection_2 (i%)
REM This procedure routes the second pulse and loads the 3rd pulse
REM (If valid)
PROCsend_route (FNroute(channel$(i%))) :REM i%=2; recycle_offset=0
temp%=FNcalculate_pulse (i%+1)
IF temp%>0 THEN PROCload_pulse (temp%)
REM Now watch for the 2nd pulse to timeout
PROCwatch
ENDPROC
:
DEFPROCsection_I (i%)
REM This procedure handles intermediate pulses/delays
REM Load the delays latches with D(n)
temp%=FNcalculate_delay (i%)
IF temp%>0 THEN PROCload_delay (temp%)
REM Load the pulse latches with P(n+1) (IF valid)
temp%=FNcalculate_pulse (i%+1)
IF temp%>0 THEN PROCload_pulse (temp%)
REM Send the routing byte for P(n)
PROCsend_route (FNroute(channel$(i%)))
REM Watch for P(n) to timeout
PROCwatch
ENDPROC
:
DEFPROCsection_F
REM This procedure produces the code which stops the counters and returns
REM to BASIC
PROCstop_pulses
PROCreturn
```

```
ENDPROC
:
DEFPROCdump_T1_info
REM This procedure dumps to disk the information peculiar to T1
PROCdump_string (“SEQUENCE=”+sequence$):   REM  (1) Sequence T1/T2 etc.
PROCdump_string (“READING=”+STR$reading%): REM  (2) Reading no
PROCdump_string (“NOS_AVE=”+STR$nos_ave%): REM  (3) Nos. averages
PROCdump_string (“DEL_VAL=”+STR$pulse%(2)):REM  (4) T1 Delay value
PROCdump_string (“EDL_VAL=”+STR$pulse%(4)):REM  (5) Echo delay value
PROCdump_optional_information:             REM  (6) Optional Information
ENDPROC
:
DEFPROCdump_T2_info
REM This procedure dumps to disk the information peculiar to T2
PROCdump_string (“SEQUENCE=”+sequence$):   REM  (1) Sequence T1/T2 etc.
PROCdump_string (“READING=”+STR$reading%): REM  (2) Reading no
PROCdump_string (“NOS_AVE=”+STR$nos_ave%): REM  (3) Nos. averages
PROCdump_string (“EDL_VAL=”+STR$pulse%(4)):REM  (4) Echo delay value
PROCdump_optional_information:             REM  (5) Optional Information
ENDPROC
:
DEFPROCdump_grad_info
REM This procedure dumps to disk the information peculiar to gradient measurements
PROCdump_string (“SEQUENCE=”+sequence$):        REM  (1) Sequence T1/T2 etc.
PROCdump_string (“READING=”+STR$reading%):      REM  (2) Reading no
PROCdump_string (“NOS_AVE=”+STR$nos_ave%):      REM  (3) Nos. averages
PROCdump_string (“EDL_VAL=”+STR$pulse%(4)):     REM  (4) Echo delay value
PROCdump_string (“GRAD_VL=”+gradient_voltage$): REM  (5) Gradient voltage
PROCdump_optional_information:                  REM  (6) Optional Information
ENDPROC
:
DEFPROCdump_FID_info
REM This procedure dumps to disk the information peculiar to FIDs
PROCdump_string (“SEQUENCE=”+sequence$):   REM  (1) FID etc.
PROCdump_string (“NOS_AVE=”+STR$nos_ave%): REM  (2) Nos. averages
PROCdump_string (“PUL_WID=”+STR$pulse%(1)):REM  (3) Pulse width
PROCdump_optional_information:             REM  (4) Optional Information
ENDPROC
:
DEFPROCdump_optional_information
REM This procedure dumps the Optional Information to disk
PROCdump_string2 (“OPTIONAL_INFORMATION”+“VERSION=”+version$)
PROCdump_string2 (“FREQUENCY=”+STR$freq)
PROCdump_string2 (“TIME=”+TIME$)
PROCdump_string2 (“PREMA ch0=”+resch0$)
PROCdump_string2 (“PREMA ch1=”+resch1$)
PROCdump_string2 (“T = ”+temperature$)
PROCdump_string2 (“T(req) = ”+STR$(Required_Temp))
PROCdump_string2 (“Tolerance {t>2k } = ”+STR$(Tolerance))
PROCdump_string2 (“Tolerance {t<2k } = ”+STR$(Tolerance2))
PROCdump_string2 (“Tolerance (for in−range checking)= ”+STR$(Tolerance_in_range_checking))
PROCdump_string2 (“T adjust time (min) = ”+STR$(Temp_adjust_time))
PROCdump_string2 (“T last update time = ”+temperature_update_time$)
PROCdump_string2 (“Conductance = ”+conductance$)
PROCdump_string2 (“HP5335A CH A = ”+hp5335a_cha$)
PROCdump_string2 (“HP5335A CH B = ”+hp5335a_chb$)
PROCdump_string2 (“T(SC Sp) = ”+alternate_temperature$)
PROCdump_string2 (“Conductance(SC Sp) = ”+alternate_conductance$)
PROCdump_string  (“MC_DAC = ”+MC_current1$)
ENDPROC
:
DEFPROCinit_scope_for_FIDs
PRINTCHR$130;“SETTING UP OSCILLOSCOPE FOR FIDS”
PROCsetup_scope
PROCadrandoutput (3,IEEE_tek_address,“ACQ TRIGC:16”): REM set trigger to LHS of screen, NB: See Run
book #1, P.162
REM Set up sample mode OR average mode and sweep & weight settings
IF aveorss$=“S” OR aveorss$=“s” THEN
PROCadrandoutput (3,IEEE_tek_address,“ACQ CURR:SAM,NUM:0”)
  ELSE
PROCadrandoutput (3,IEEE_tek_address,“ACQ CURR:AVE,WEI:”+STR$nos_ave%+“,NUM:”+STR$nos_ave%)
ENDIF
PROCdelay (400): REM Small delay for tek to recover
PROCbusy_check (IEEE_tek_address) :REM Having initialised tek wait until it has recovered
ENDPROC
:
DEFPROCFID_input
PRINTCHR$129;“Enter FID information”
INPUT “Temperatures (mK); START, FINISH, INCREMENT ”Temp_start,Temp_stop,Temp_increment
INPUT “Temperature regulation tolerance {t>2k } (mK) ”Tolerance
INPUT “Temperature regulation tolerance {t<2k } (mK) ”Tolerance2
INPUT “In−range−checking tolerance (mK) ”Tolerance_in_range_checking
INPUT “Paroscientific gauge logging Y/N ? ”ps_logging$
INPUT “Log the sample−chamber resistor Y/N ? ”scr_logging$
INPUT “Check for Magnet−Controller S/D Y/N ? ”MCSD_checking$
INPUT “P1 (uS) ”FIDpulse%(1)
INPUT “REPETITION TIME (centi−seconds) ”FIDreptim
ENDPROC
:
DEFPROCFID
sequence$=“FID”
No%=1
pulse%(1)=FIDpulse%(1)
reptim=FIDreptim
REM P1 is Trigger pulse
OSCLI (“POTREG SEL_R AUTO”) :REM Make sure automatic resistor selection is enabled
Temp_increment=ABS(Temp_increment)*FNsgn(Temp_stop−Temp_start)
FOR Required_Temp=Temp_start TO Temp_stop STEP Temp_increment :REM −Temperatures
 IF Required_Temp >= 2000 THEN
```

```
 OSCLI (“POTREG SET_T ”+STR$(Required_Temp)+“ ”+STR$(Tolerance)+“ ”+STR$(Tolerance_in_range_checking))
  ELSE
 OSCLI (“POTREG SET_T ”+STR$(Required_Temp)+“ ”+STR$(Tolerance2)+“
“+STR$(Tolerance_in_range_checking))
 ENDIF
 VDU7
 PROCRequired_Temp_check :REM Check that the required temperature has been reached
 VDU7
 PROCinit_scope_for_FIDs
 REM Channel allocation; P1 − channel 0
 channel$(1)=“0”
 PRINTCHR$129;“FID Reading”
 FOR shot_no%= 1 TO nos_ave%: REM ------------------------------ Shot no.
 PROCrun (FALSE)
 NEXT shot_no%
NEXT Required_Temp
ENDPROC
:
DEFPROCinit_IEEE_and_devices
REM This procedure initialises the IEEE interface and the devices
PRINT;“INITIALISING IEEE488 INTERFACE”
PROCinit
PRINT;“INITIALISING IEEE488 DEVICES”
PROCdevice_clear
PROCdelay(100) :REM Wait 1 second
PRINT;“IEEE488 SYSTEM INITIALISED”
ENDPROC
:
DEFPROCbusy_check (IEEE_device_address)
REM This procedure watches until the device’s busy bit is clear
LOCAL tmp%
REPEAT
tmp%=FNserial_poll (IEEE_device_address)
PRINTCHR$129;“TEK STATUS BYTE=”;tmp%
UNTIL tmp%<>16
ENDPROC
:
DEFFNacq_points
REM This function returns the number of points in the acquisition
REM This is either 1024 for 4096
PROCsetup_scope
PROCadrandoutput(3,IEEE_tek_address,“ACQ? POI”)
=VAL(MID$(FNadrandinput(3,IEEE_tek_address,255),9,4))
:
DEFPROCRequired_Temp_check
REM This procedure checks that the required temperature has been reached
REM It does this by looping until the system variable “Potreg$Temperature_In_Range” is found to be
TRUE 10 consecutive times, it then returns.
REM The system variable “Potreg$Last_Update_Time_Binary” is also checked to ensure Potreg s/w has not
hung
REM The “update_specials_count%” variable is zeroed here to ensure that the SCSP is read after the
temperature has changed
update_specials_count%=0
LOCAL tmp%, binary_update$
Temp_adjust_time=TIME
PRINTCHR$129;“T Range Checking at ”;TIME$;“ for ”;Required_Temp/1000;“K”;CHR$7‘
PROCdelay(1000) :REM 10 seconds for Potreg s/w to update
tmp%=1
binary_update$=“”
WHILE tmp%<6
SYS “OS_ReadVarVal”,“Potreg$Temperature_In_Range”,buffer%,80,0 TO ,,nos%
buffer%?nos%=13 :REM Terminate immediate string
CASE $buffer% OF
WHEN “TRUE”:  tmp%+=1
WHEN “FALSE”: tmp%=1
OTHERWISE PRINT “ERROR; Potreg$Temperature_In_Range= ”;$buffer%
ENDCASE
REM Now check the last update time
SYS “OS_ReadVarVal”,“Potreg$Last_Update_Time_Binary”,buffer%,80,0 TO ,,nos%
buffer%?nos%=13 :REM Terminate immediate string
IF $buffer% = binary_update$ THEN
PRINT;CHR$7;CHR$129;“Potreg hang detected at ”;TIME$
PROCdelay(600)
tmp%=1
  ELSE
PRINTTAB(0,23);CHR$129;TIME$;SPC(6);Required_Temp/1000;“K”: REM bottom of screen
ENDIF
binary_update$ = $buffer%
PROCdelay(1000) :REM 10 second delay to let things settle down
ENDWHILE
Temp_adjust_time=(TIME−Temp_adjust_time)/6000
IF RTC_wait$ = “TRUE” THEN
 PRINTCHR$129;“INKEY WAIT FOR 1st 5 MINUTES”;CHR$7
 PROCdelay(5*60*100)
 PRINTCHR$129;“INKEY WAIT FOR 2nd 5 MINUTES”;CHR$7
 PROCdelay(5*60*100)
 VDU7
ELSE
 PRINTCHR$129;“2 x 5 minute wait overridden”;CHR$7
ENDIF
ENDPROC
:
DEFPROCread_hp5335a_frequencies
REM This procedure reads both channels of the HP5335A frequency counter
REM This instrument is connected to the Paroscientific pressure gauge on the pot pumping line to allow
temperature calibration.
PRINTCHR$133;“HP5335A STATUS BYTE=”FNserial_poll (IEEE_hp5335a_address)
REM Now get the frequencies from the A & B ports of the HP5335A
PROCadrandoutput (0,IEEE_hp5335a_address,“FN1”)  :REM PORT A
```

```
hp5335a_cha$=FNadrandinput (0,IEEE_hp5335a_address,255)
PROCadrandoutput (0,IEEE_hp5335a_address,“FN17”) :REM PORT B
hp5335a_chb$=FNadrandinput (0,IEEE_hp5335a_address,255)
ENDPROC
:
DEFFNsgn(arg)
REM As SGN() built−in but cannot return 0
IF arg < 0 THEN = −1 ELSE = +1
:
DEFPROCirq_handler
REM This procedure creates the device driver code to handle the interrupt
REM generated by the pulse generator when the pulse+delay times out.
REM This code is only assembled when the S/W is working in interrupt mode.
IF interrupt_mode THEN
[OPT pass%
.irq_handler_addr
   STMFD    R13!, {r0−r12 ,R14}                  ;Push registers onto interrupt stack
   ADR      R_tmp, interrupt_jump_addr           ;Get address of jump table
   LDR      R_tmp, [R_tmp, #0]                   ;Get jump address & make PC jump to the address
   MOV      R15, R_tmp                           ;NB R15=destination, so PC bits only are transferred
]
ENDIF
ENDPROC
```

Appendix 3.

Appendix 3, The POTREG Software.

Appendix 3.1, The Main Program.

```
/* POTREG Temperature Controller Software */
/* Written in Acorn ANSI-C, Adapted from ISO-Pascal Software written for */
/* BBC Master Microcomputer */
/* (C) T.P.Crane Jan. 1988 */
/* Revised July 1989 & September 1989 to enable code to run in a relocatable
   module as a background task.
   Revised October 1989 to confine all FP arithmetic to one function to
   minimise the amount of code which may have to be altered due to FP/SVC
   incompatibility problems.
   Revised:            December 1989
   Revised:            May  1990, added "Potreg$Current_Conductance"
   Revised:            June 1990, corrected for -ve values from clock() in BAD DATA check
   Revised:            August 1990, (1) conductances supplied directly to absp() due to high T granularity
                                    (2) out-ranging now cuts out a local_temperature cf. (local_temperature +/- tolerance)
                                    (3) added dynamic selection of solenoid valve based on rate of fall of temperature
                                    (4) Now 3 calibration ranges for all resistors
                                    (5) Added "ALT_R" command for temporary resistor selection & T logging
   Revised:            November 1990, Added "in_range_checking_tolerance" to be used in in-range checking
   Revised:            December 1990, Asynchronous re-entry blocked, See M&HD Book #2, P.110
   Revised:            December 1990, Relay states softcopy introduced to stop spurious invocations (See. M&HD book#2, P.110)
   Revised:            January  1991, Enabled IRQs in absp ** experimental only **, See M&HD book #2, P.112, & disabled them
                                      Checked for -ve values from clock() in update_temperature
                                      Trying changing entry rate from once every 100cSec to 160cSec
   Revised             March 1991,    Trying changing entry rate from once every 160cSec to 200cSec
                                      Corrected problem causing H/W crash caused by div by 0 error in calculation of
                                      rate_of_fall_of_T which was caused by timing problem  (ie. when time_curr = -time_last)
   Note: All 'double' values outside function absp have been converted to
         'int', as a result all temperature are now in mK */

/******* GENERAL INFORMATION **********/
/* relay (0)   - heater */
/* relays (1-4) - true solenoid valves */
/* relays (5-7) - quarter swing valve positions */
/*                                                */
/* Bridge/Interface Addr.       Function          */
/* ======================       ========          */
/*      0                       Digit 1 (LSD)     */
/*      1                             2           */
/*      2                             3           */
/*      3                             4           */
/*      4                             5 (MSD)     */
/*      5                       Range setting     */
/*      6                       Excitation        */
/*      7                       Time constant     */
/*      8                       Resistor no.      */

/* Include the library definitions */
#include <stdio.h>
#include <ctype.h>
#include <setjmp.h>
#include <signal.h>
#include <time.h>
#include <stdlib.h>
#include <stddef.h>
#include <string.h>
#include "kernel.h"
#include "swis.h"

/* Define some useful macros */
#define  sign(x)              (((x)<0)?-1:(x?1:0))
#define  UNUSED(x)             (x = x)
#define  PRINTVAR(x)           printf (#x " = %d\n",x)
#define  PRINTPTR(x)           printf (#x " = 0x%p\n",x)
#define  PRINTHEX(x)           printf (#x " = 0x%x\n",x)

/* Include the pre-processor defined constants */
#define AVE_OVER 4                    /* Nos observations to "average rate_of_fall_of_T" over */
#define TWO_K   2000                  /* Change-over temperature for resistor calibrations */
#define HE_BP   4200                  /* Boiling point of 4He in mK */
#define nos_res  8
#define max_com_length  8
#define max_com_no  3
#define potsp  4
#define potab  5
#define potreg_interface_VIA_no  1      /* NOTE: Two VIAs are used in this software Address of Potreg VIA */
#define RB_VIA_no  2                    /* on IEU Address of Relay board VIA on IEU  */
#define IEU_latch  0xD0
#define register_b  0xC0
#define register_a  0xC1
#define ddrb  0xC2
#define ddra  0xC3
#define pcr  0xCC
#define res_no_type  8
#define solenoid_no_max  7
#define solenoid_no_min  1
#define no_relay_devices 8
#define bridge_fudge_factor  2
#define bridge_interface_digits  9
#define time_limit  2000        /* Value is in centi-seconds */

/* Now the type definitions */
typedef int             cal_type [res_no_type] [3] [3];
typedef enum            {AB,SP}  res_type;
typedef enum            {FALSE,TRUE}  boolean;
typedef enum            {COMMAND,ASYNCHRONOUS} execution_type;
typedef enum            {ALARM_NORMAL,
                         ALARM_BRIDGE_OVERFLOW,
                         ALARM_BAD_DATA,
                         ALARM_NOT_AUTO,
                         ALARM_FP_ERROR,
                         ALARM_ARAD,
                         ALARM_BADCLK,
                         ALARM_SPARE3};
typedef res_type        res_types [res_no_type];
typedef unsigned char   byte;

/* Now the variable declarations */
static int              relays_softcopy [no_relay_devices];
static int              async_reentry_attempt_count;
```

```
static int              in_range_checking_tolerance;
static int              sol_mod_factor_g;
static int              rate_of_fall_of_T;
static int              last_temperature;
static int              max_pumping_rate;
static int              min_pumping_rate;
static int              auto_ipr;
static int              auto_dpr;
static boolean          threaded = FALSE;
static int              current_conductance;
static int              global_private_word;
static clock_t          time_last;
static clock_t          time_curr;
static int              old_solenoid;
static int              solenoids_tolerance;
static int              solenoid_outrange_limit;
static int              heater_outrange_limit;
static boolean          solenoid_outrange;
static boolean          heater_outrange;
static int              local_temperature;
static int              temperature_sol_max_step;
static jmp_buf          start_env;                                      /* For the non-local jump used in error handling */
static clock_t          change_time;
static clock_t          invoke_time;
static clock_t          settling_time_factor;
static int              wrong_resistor;
static int              bridge_cache [bridge_interface_digits];
static cal_type         calibrations;
static res_types        resistor;
static int              set_temperature;
static int              tolerance;
static int              current_temperature;
static int              selected_resistor;
static boolean          autm;
static boolean          heater_enabled;
static boolean          solenoid_enabled [solenoid_no_max + 1];
static int              solenoid_range [solenoid_no_max];
static execution_type   execution_mode;
static boolean          system_initialised = FALSE;

int absp (int /*R*/, int /*ABorSP*/, int /*a*/, int /*b*/ , int /*korc*/);

void dump_variables (void)
/* This function dumps all the system global variables */
{
 int i,j,k;

 printf ("\n****** DUMP OF GLOBAL VARIABLES ******\n\n");
 for (i=0; i<no_relay_devices; i++) PRINTHEX (relays_softcopy [i]);
 PRINTVAR (async_reentry_attempt_count);
 PRINTVAR (in_range_checking_tolerance);
 PRINTVAR (sol_mod_factor_g);
 PRINTVAR (rate_of_fall_of_T);
 PRINTVAR (last_temperature);
 PRINTVAR (max_pumping_rate);
 PRINTVAR (min_pumping_rate);
 PRINTVAR (auto_ipr);
 PRINTVAR (auto_dpr);
 PRINTVAR (current_conductance);
 PRINTHEX (global_private_word);
 PRINTVAR (time_last);
 PRINTVAR (time_curr);
 PRINTVAR (old_solenoid);
 PRINTVAR (solenoids_tolerance);
 PRINTVAR (solenoid_outrange_limit);
 PRINTVAR (heater_outrange_limit);
 PRINTVAR (solenoid_outrange);
 PRINTVAR (heater_outrange);
 PRINTVAR (local_temperature);
 PRINTVAR (temperature_sol_max_step);
 PRINTPTR (start_env);
 PRINTVAR (change_time);
 PRINTVAR (invoke_time);
 PRINTVAR (settling_time_factor);
 PRINTVAR (wrong_resistor);
 for (i=0; i<bridge_interface_digits; i++) PRINTVAR (bridge_cache [i]);
 for (i=0; i<res_no_type; i++)
       for (j=0; j<3; j++)
             for (k=0; k<3; k++) printf ("calibrations [%d] [%d] [%d] = %d\n", i, j, k, calibrations [i] [j] [k]);
 for (i=0; i<res_no_type; i++) PRINTVAR (resistor [i]);
 PRINTVAR (set_temperature);
 PRINTVAR (tolerance);
 PRINTVAR (current_temperature);
 PRINTVAR (selected_resistor);
 PRINTVAR (autm);
 PRINTVAR (heater_enabled);
 for (i=1; i<=solenoid_no_max; i++) PRINTVAR (solenoid_enabled [i]);
 for (i=0; i<solenoid_no_max; i++)  PRINTVAR (solenoid_range [i]);
 PRINTVAR (execution_mode);
 PRINTVAR (system_initialised);
}


void log_error (char *message, execution_type execution_mode)

/* This function is responsible for error logging, it does the following:
   (1)  Writes the message if the system is not executing asynchronously
   (2)  Sets the system variable "Potreg$Last_Error to the message */

{
 char   workspace[256];
 char   *var_name_ptr = "Potreg$Last_Error";
 char   *new_line = "\n";
 _kernel_swi_regs       registers;
 if (execution_mode == COMMAND) printf ("%s\n",message);
 strcpy (workspace,message);                                    /* Copy message to temporary work area */
 strcat (workspace,new_line);                                   /* Put a <LF> on the end of the string as required by SWI */
 registers.r[0] = (int)var_name_ptr;
 registers.r[1] = (int)workspace;
 registers.r[2] = (int)strlen(workspace);                        /* Length of original string plus <LF>. */
 registers.r[3] = 0;
 registers.r[4] = 0;
 _kernel_swi(OS_SetVarVal, &registers, &registers);
}



int read_fred (int address_offset)

/* This function returns the byte at the address in FRED at the
   specified offset.
   Uses Osbyte 146 -Read a byte from FRED */
{
 _kernel_swi_regs       registers;
 registers.r[0] = 146;
 registers.r[1] = address_offset;
 _kernel_swi(OS_Byte, &registers, &registers);
 return (registers.r[2]);
```

```
}


void write_fred (int address_offset, int value)

/* This procedure writes the specified byte at the address in FRED at the
   specified offset
   Uses Osbyte 147 −Write a byte to FRED */

{
 _kernel_swi_regs       registers;
 registers.r[0] = 147;
 registers.r[1] = address_offset;
 registers.r[2] = value;
 _kernel_swi(OS_Byte, &registers, &registers);
 /* Disabled line below 28th Dec 1990,
 for (i=0;i<10;i++);  Waste ~ 10uS to allow h/w to keep up with s/w, to stop spurious multiple solenoid invocations */
}


void handshake_A (void)

/* This procedure does a LO to HI transition on CA2 to signal data valid */

{
 write_fred (pcr, 14);  /* Make sure CA2 = HI initially */
 write_fred (pcr, 12);  /* Set CA2 = LO                 */
 write_fred (pcr, 14);  /* Set CA2 = HI, for data valid */
}


void handshake_B (void)

/* This procedure does a LO to HI transition on CB2 to signal data valid */

{
 write_fred (pcr, 224); /* Make sure CB2 = HI initially */
 write_fred (pcr, 192); /* Set CB2 = LO                 */
 write_fred (pcr, 224); /* Set CB2 = HI, for data valid */
}


void consistency_enforce (int relay_no)

/* This procedure writes all 8 relays (except the one just written)
   which control the heater and the 7 solenoid valves, according to
   the values held in their softcopies.
   This has been done in an attempt to stop spurious relay invocations
   from recking temperature control.
   The relay board will be selected when this function is envoked. */

{
 int i;
 for (i=0;i<no_relay_devices;i++)
   if (i != relay_no)
     {
      write_fred (register_a, relays_softcopy[i]+i);             /* Switch relay n on or off (&10=off, &18=on) */
      handshake_A();                                             /* Handshake for data valid */
     }
}


void heater (char *action)

/* This procedure turns the heater on or off and enables or disables software
   control of the heater and alters the boolean variable 'heater_outrange'
   which determines whether or not the heater will be used at temperatures
   < 4.2K for a faster warm−up */

{
 void   all_devices (char *);   /* So this procedure can be forward referenced */
 int    previous_VIA_no;

 if (strcmp (action, "DISABLE") == 0)
    heater_enabled = FALSE;
    else  if (strcmp (action, "ENABLE") == 0)
    heater_enabled = TRUE;
    else  if (strcmp (action, "OUTRNG") == 0)
    heater_outrange = TRUE;
    else  if (strcmp (action, "NOOUTRNG") == 0)
        {
        heater_outrange = FALSE;
        all_devices ("OFF");
        }
    else  if (heater_enabled == TRUE)
        {
        previous_VIA_no = read_fred (IEU_latch);                        /* Save the previous VIA no */
        write_fred (IEU_latch, RB_VIA_no);                              /* Select the relay board */
        write_fred (ddra, 0xFF);                                        /* Use port A of this VIA, Set all lines = O/P */
        if (strcmp (action, "OFF") == 0)
                {
                write_fred (register_a, 0x10);                          /* Switch heater (=relay 0) off */
                handshake_A();                                          /* Handshake for data valid */
                relays_softcopy[0] = 0x10;                              /* Update the softcopy for the heater relay */
                consistency_enforce (0);                                /* Force other relays to be consistant with their sc */
                }
        else if (strcmp (action, "ON") == 0)
                {
                write_fred (register_a, 0x18);                          /* Switch heater on */
                handshake_A();                                          /* Handshake for data valid */
                relays_softcopy[0] = 0x18;                              /* Update the softcopy for the heater relay */
                consistency_enforce (0);                                /* Force other relays to be consistant with their sc */
                }
        else
        log_error ("HEATER ERROR !",execution_mode);
        write_fred (IEU_latch, previous_VIA_no);                        /* Restore previous VIA in the IEU */
        }
}


void solenoid_operate (int on_or_off, int solenoid_no)

/* This procedure actually operates the solenoids */

{
int     previous_VIA_no;

previous_VIA_no = read_fred (IEU_latch);                        /* Save the previous VIA no */
write_fred (IEU_latch, RB_VIA_no);                              /* Select the relay board */
write_fred (ddra, 0xFF);
write_fred (register_a, on_or_off + solenoid_no);               /* Switch solenoid n (= relay no n) on or off (&10=off, &18=on) */
handshake_A();                                                  /* Handshake for data valid */
relays_softcopy[solenoid_no] = on_or_off;                       /* Update the softcopy for the specified solenoid relay */
```

```
consistency_enforce (solenoid_no);                          /* Force other relays to be consistant with their sc */
write_fred (IEU_latch, previous_VIA_no);                    /* Restore the previous VIA in the IEU */
}


void solenoid (char *par1, char *par2)

/* This procedure turns the specified solenoid on or off and
   enables or disables software control of that solenoid and
   alters the boolean variable 'solenoid_outrange'
   which determines whether or not solenoid (1) will be used
   at temperatures > 4.2K for a faster cool-down */

{
 void   all_devices (char *);                                       /* So this procedure can be forward referenced */
 if (strcmp (par1, "OUTRNG") == 0)
        solenoid_outrange = TRUE;
  else if (strcmp (par1, "NOOUTRNG") == 0)
        {
        solenoid_outrange = FALSE;
        all_devices ("OFF");
        }
  else
        {
        int     solenoid_no;
        if (strcmp (par1, "ENABLE") == 0)
                {
                solenoid_no = atoi (par2);                          /* Check solenoid no. is in range */
                if (solenoid_no >= solenoid_no_min  &&  solenoid_no <= solenoid_no_max)
                solenoid_enabled [solenoid_no] = TRUE;
                else
                log_error ("SOLENOID NO. ERROR (enable) !",execution_mode);
                }
        else if (strcmp (par1, "DISABLE") == 0)
                {
                solenoid_no = atoi (par2);                                  /* Check solenoid no. is in range */
                if (solenoid_no >= solenoid_no_min  &&  solenoid_no <= solenoid_no_max)
                solenoid_enabled [solenoid_no] = FALSE;
                else
                log_error ("SOLENOID NO. ERROR (disable) !",execution_mode);
                }
        else if (strcmp (par1, "OFF") == 0)
                {
                solenoid_no = atoi (par2);                                  /* Check solenoid no. is in range */
                if (solenoid_no >= solenoid_no_min  &&  solenoid_no <= solenoid_no_max)
                        {
                        if (solenoid_enabled [solenoid_no] == TRUE)
                        solenoid_operate (0x10, solenoid_no);               /* Switch solenoid n (= relay no n) off */
                        }
                else
                log_error ("SOLENOID NO. ERROR (off) !",execution_mode);
                }
        else if (strcmp (par1, "ON") == 0)
                {
                solenoid_no = atoi (par2);                                  /* Check solenoid no. is in range */
                if (solenoid_no >= solenoid_no_min  &&  solenoid_no <= solenoid_no_max)
                        {
                        if (solenoid_enabled [solenoid_no] == TRUE)
                        solenoid_operate (0x18, solenoid_no);               /* Switch solenoid n (= relay no n) on */
                        }
                else
                log_error ("SOLENOID NO. ERROR (on) !",execution_mode);
                }
        else
        log_error ("SOLENOID ERROR !",execution_mode);
        }
}


void auto_ipr_modify (char *par1)

/* This procedure turns the automatic-increase-pumping-rate
   facility by setting a flag variable
*/

{
 if (strcmp (par1, "ON") == 0)
        auto_ipr = TRUE;
  else if (strcmp (par1, "OFF") == 0)
        auto_ipr = FALSE;
  else
        log_error ("AUTO_IPR UNRECOGNISED COMMAND !",execution_mode);
}


void auto_dpr_modify (char *par1)

/* This procedure turns the automatic-decrease-pumping-rate
   facility by setting a flag variable
*/

{
 if (strcmp (par1, "ON") == 0)
        auto_dpr = TRUE;
  else if (strcmp (par1, "OFF") == 0)
        auto_dpr = FALSE;
  else
        log_error ("AUTO_DPR UNRECOGNISED COMMAND !",execution_mode);
}


int current_resistor (void)

/* This function obtains the current resistor number directly from the bridge
   interface unit, enabling manually selected resistors to be used */

{
 return (bridge_cache [8]);
}


int time_constant (void)

/* This function obtains the current bridge time-constant
   directly from the bridge interface unit
   The value is in centi-seconds */
{
 int time_const;
 time_const = bridge_cache [7];
 /* printf ("TIME CONSTANT = %d\n", time_const); */
 switch (time_const)
        {
        case    1: return (30);
        break;
        case    2: return (100);
```

```
        break;
        case    4: return (300);
        break;
        case    8: return (1000);
        break;
        default  : return (1000);
        }
}


void sel_R_poke (int chosen_R)
/* This procedure actually pokes the selected resistor into the resistor latch */

{
 int previous_VIA_no;

 previous_VIA_no = read_fred (IEU_latch);                    /* Save previous VIA no */
 write_fred (IEU_latch, potreg_interface_VIA_no);            /* Select potreg VIA no */
 write_fred (register_a, 0xB0 + chosen_R);                   /* Select RESISTOR LATCH & Put resistor number on data lines */
 handshake_A();                                              /* Handshake for data-valid */
 write_fred (IEU_latch, previous_VIA_no);                    /* Restore previous VIA on the IEU */
}


void all_devices (char *instruction)

/* This procedure is used when one instruction is to
   be carried out on all seven solenoids and the heater */
{
 solenoid (instruction, "1");
 solenoid (instruction, "2");
 solenoid (instruction, "3");
 solenoid (instruction, "4");
 solenoid (instruction, "5");
 solenoid (instruction, "6");
 solenoid (instruction, "7");
 heater (instruction);
}


void sel_R (char *com1)

/* This procedure sends the selected resistor to the resistor latch if a
   resistor is specified or sets the boolean variable 'autm' to true if
   automatic pot resistor selection is used */

{
 int temp;
 change_time = clock();
 invoke_time = 0;
 rate_of_fall_of_T = 0;

 if (strcmp (com1, "AUTO") == 0)
        {
        autm = TRUE;
        all_devices ("ENABLE");
        }
  else
        {
        temp = atoi (com1);
        if (temp >= 0  &&  temp <= 7)
                {
                autm = FALSE;
                /* If "automatic" is not selected the solenoids and heater */
                /* are disabled by default */
                all_devices ("DISABLE");
                selected_resistor = temp;
                sel_R_poke (selected_resistor);
                }
        else
                {
                char tmp_string [255];                                  /* Temporary workspace */
                sprintf (tmp_string,"%d IS NOT A VALID RESISTOR",temp);
                log_error (tmp_string,execution_mode);
                }
        }
}


void alternate_r (char *com1)
/* This procedure temporarily selects another resistor, waits for the
   bridge to settle down, logs the following systems variables
   (Potreg$Alternate_Conductance & Potreg_Alternate_Temperature) and
   restores the previous resistor/state.
*/

{
 int tmp_autm, tmp_curres;
 char tmpstr [255];
 clock_t tmptime;
 void give_alternate_conductance(void);
 void give_alternate_temperature(void);
 int update_temperature (void);

 tmp_autm = autm;
 tmp_curres = current_resistor();
 sel_R (com1);
 tmptime = clock();
 while ((clock() - tmptime) < settling_time_factor * time_constant()); /* Wait for bridge to settle down */
 while (update_temperature());                                         /* Update readings from bridge until good value comes */
 give_alternate_conductance();                                         /* Update "Potreg$Alternate_Conductance" system variable. */
 give_alternate_temperature();                                         /* Update "Potreg$Alternate_Temperature" system variable. */
 if (tmp_autm == TRUE)
        sel_R ("AUTO");                                                /* Restore automatic resistor selection */
   else
        {
         sprintf (tmpstr,"%d",tmp_curres);                             /* Restore the previous resistor */
         sel_R (tmpstr);
        }
}


int conductance (void)

/* Note it is assumed at this stage that all the data in the <bridge cache>
   is good. Any bad data should have been rejected by the main program
   NB: The conductance result from this function is in mMhos * 1e6 */

{
 static int     multiplier2;     /* This has been done to prevent arithmetic exceptions which happen when the
                                    invalid bridge_range = 0 is detected.
                                    This can sometimes occur momentarily when the bridge range is changed */
 int    bridge_range;
 int    bridge_digits;
```

```
 bridge_range = bridge_cache [5];
 switch (bridge_range)                          /* bridge_cache[5] = bridge range switch */
        {                                       /* The position of the decimal point */
         case 1 : multiplier2 = 10;             /* is determined by the range setting */
         break;
         case 2 : multiplier2 = 100;
         break;
         case 4 : multiplier2 = 1000;
         break;
         case 8 : multiplier2 = 10000;
         break;
         default:
                {
                char tmp_string [255];                                          /* Temporary workspace */
                sprintf (tmp_string,"INVALID BRIDGE RANGE %d",bridge_range);
                log_error (tmp_string,execution_mode);
                }
         break;                                                                 /* this statement may be superfluous */
        }
  bridge_digits =      bridge_cache [0] +
                  10 * bridge_cache [1] +
                 100 * bridge_cache [2] +
                1000 * bridge_cache [3] +
               10000 * bridge_cache [4] + bridge_fudge_factor;
  return (bridge_digits*multiplier2);
}


void wrt_display_poke (int number)

/* This procedure actually pokes the data to the display */

{
 if (number <= 9)
        {
        /* printf ("WRT_DISPLAY_POKE number = %d\n", number); */
        write_fred (register_a, 0xD0 + number);                 /* Select SEND TO DISPLAY & Put digit number on data lines */
        handshake_A();                                          /* Handshake for data-valid & clock up digit-selector */
        }
 else
        {
        char tmp_string [255];                                  /* Temporary workspace */
        sprintf (tmp_string,"WRT_DISPLAY_POKE INVALID BCD VALUE !! %d",number);
        log_error (tmp_string,execution_mode);
        }
}


void wrt_display (int display_temperature)

/* This procedure writes the temperature to the display on the bridge interface unit.
   There are 4 digits on the interface unit.
   The digits which are sent sequentially appear on the display from left (LSD)
   to right (MSD).
   The 5th digit gives the place of the decimal point.
   The 1st digit send is ignored so a dummy digit is sent 1st
   Using an int O/P format "%04" gives a number which is right-justified,
   padded with zeros and with a minimum field-width (fw) of 4.
   Using this format the correct place for the dp (in a temperature in K
   from mK) is dp position = 8 - fw. The dp is located on the RHS of a
   digit and the rightmost digit in the display is designated 1.
   Following are some example numbers:
        dp position     number(mK)      fw      Display
             4          0002            4       0.002
             4          0026            4       0.026
             4          0261            4       0.261
             4          2612            4       2.612
             3          26123           5       26.12
             2          261234          6       261.2
             1          2612345         7       2612.
             0          26123456        8       2612    display overflows */
{
 int    dp;
 char   display_string [20];
 char   *ptr = display_string;
 int    previous_VIA_no;

 if (display_temperature < 0) display_temperature = 0;                  /* T < 0 is clearly nonsense */
 previous_VIA_no = read_fred (IEU_latch);                               /* Save previous VIA no */
 write_fred (IEU_latch, potreg_interface_VIA_no);                       /* Select potreg interface VIA */
 handshake_B();                                                         /* Reset the digit selector, on HI->LO transition */
 dp = 8 - sprintf (display_string, "%04d", display_temperature);        /* format = right-justified, zero-padded & min fw =4 */

 if (dp >= 0)                                                           /* Otherwise gross overflow */
        {
         wrt_display_poke (0);                                                  /* Send dummy digit to display */
         for (ptr=display_string+3; ptr>=display_string; ptr--)                 /* Write digits, LHS to RHS */
         wrt_display_poke (*ptr - '0');
         wrt_display_poke (dp);                                                 /* Not forgetting the decimal point ! */
        }
 write_fred (IEU_latch, previous_VIA_no);                               /* Restore previous VIA on the IEU */
}


int startup (char * startup_file)

/* This procedure is responsible for reading in the resistor calibrations
   from a file together with other miscellaneous information required by the
   program and initialises the system.
   NB: This function returns 0 to indicate successful completion */

{
 int    previous_VIA_no;
 int    res_no;
 int    T_range_no;
 int    cal_par_no;
 int    count;
 char   ch;
 FILE   *res_cal;

 res_cal = fopen (startup_file,"r");                                    /* Open file "res_cal" access=readonly */
 if (res_cal == NULL)
         {
          printf ("ERROR INPUT FILE %s COULD NOT BE FOUND!!\n\n",startup_file);
          return (1);                                                   /* Indicate error to caller */
         }
 for (res_no = 0; res_no < nos_res; res_no++)
        {
        if (res_no!=4 && res_no!=6 && res_no!=7)
        /* This is an Allen-Bradley resistor, read in the three sets of
           calibration data for 1<T<2K, 2<T<4.2K & T>4.2K */
                {
                resistor [res_no] = AB;
                for (T_range_no = 0; T_range_no <= 2; T_range_no++)
                        {
```

```
                        for (cal_par_no = 0; cal_par_no <= 2; cal_par_no++)
                                {
                                fscanf (res_cal, "%d", &calibrations  [res_no] [T_range_no] [cal_par_no]);
                                printf ("STARTUP (AB) Rkab %d %d %d %d\n", res_no, T_range_no, cal_par_no,
                                                                        calibrations [res_no] [T_range_no] [cal_par_no]);
                                }
                        }
                }
        else
                /* This is a Speer resistor, read in the three sets of
                   calibration data for 1<T<2K, 2<T<4.2K & T>4.2K */
                {
                 resistor [res_no] = SP;
                 for (T_range_no = 0; T_range_no <= 2; T_range_no++)
                        {
                         for (cal_par_no = 0; cal_par_no <= 2; cal_par_no++)
                                {
                                 fscanf (res_cal, "%d", &calibrations  [res_no] [T_range_no] [cal_par_no]);
                                 printf ("STARTUP (SP) RCAB %d %d %d %d\n", res_no, T_range_no, cal_par_no,
                                                                        calibrations [res_no] [T_range_no] [cal_par_no]);
                                }
                        }
                }
             fscanf (res_cal, "\n");                                        /* Go to the next line (hopefully !) */
        }

/* Now read in from the file the solenoid ranges...
   Temperatures in the range <solenoid_range[0] > to 4.2K are regulated by solenoid 1 (small though-put)
   Temperatures in the range <solenoid_range[0] > to <solenoid_range[1] > are regulated by solenoid 2 (larger through-put)
                .
                .
                .
   Temperatures in the range 0K to <solenoid_range[solenoid_no_max-2] > are regulated by solenoid <solenoid_no_max>
   (largest through-put)       */

for (count = 0; count <  solenoid_no_max-1; count++)
        {
        fscanf (res_cal, "%d", &solenoid_range [count]);
        printf ("STARTUP SRNGE %d %d\n", count, solenoid_range [count]);
        }
fscanf (res_cal, "\n");                                         /* Extra <CR> before fscanf(&ch) */
for (count = 1; count <= (solenoid_no_max); count++)
        {
        fscanf (res_cal, "%c\n", &ch);                          /* ...and the enable/disable   */
        printf ("STARTUP SE/D %d %c\n", count, ch);
        if (ch == 'T')                                          /*   status of the solenoids...*/
        solenoid_enabled [count] = TRUE;
        else if (ch == 'F')
        solenoid_enabled [count] = FALSE;
        else
                {
                char tmp_string [255];                                  /* Temporary workspace */
                sprintf (tmp_string,"ERROR IN RESISTOR CALIBRATION FILE S/E !");
                log_error (tmp_string,execution_mode);
                }
        }
fscanf (res_cal, "%c\n", &ch);
printf ("STARTUP HE/D %d %c\n", count, ch);
if (ch == 'T')
heater_enabled = TRUE;                                          /* ... and the heater */
 else if (ch == 'F')
heater_enabled = FALSE;
 else
        {
        char tmp_string [255];                                          /* Temporary workspace */
        sprintf (tmp_string,"ERROR IN RESISTOR CALIBRATION FILE H/E !");
        log_error (tmp_string,execution_mode);
        }

/* Read in the settling time factor which is the number of times
   the bridge time-constant is to be multiplied by to get the dead-time
   in solenoid/heater operation, which will be observed after a
   change such as a temperature change */
fscanf (res_cal, "%d", &settling_time_factor);
printf ("STARTUP SETTLING TIME %d\n", settling_time_factor);

/* Read in the 'temperature_sol_max_step' parameter which determines the
   biggest single fall (in mK) in temperature that will be (locally)
   requested for temperatures in the range  < 4.2 K */
fscanf (res_cal, "%d", &temperature_sol_max_step);
printf ("STARTUP TSMS = %d\n", temperature_sol_max_step);

/* Read in the heater and solenoid outrange limits which determine
   how low the temperature must be below the desired value for the
   heater to be used for a faster warm-up and how high the temperature
   must be above the desired value before the solenoid (1) will be used
   for a faster cool-down */
fscanf (res_cal, "%d", &heater_outrange_limit);
printf ("STARTUP HOL = %d\n", heater_outrange_limit);
fscanf (res_cal, "%d", &solenoid_outrange_limit);
printf ("STARTUP SOL = %d\n", solenoid_outrange_limit);

/* Read in the heater outrange status which determines if the heater
   can be used outside its normal range (ie. T > 4.2K) for a faster
   warm-up */
fscanf (res_cal, "\n");                                         /* Extra <CR> before fscanf(&ch) */
fscanf (res_cal, "%c\n", &ch);
printf ("STARTUP HE/OR %c\n", ch);
if (ch == 'T')
heater_outrange = TRUE;
 else if (ch == 'F')
heater_outrange = FALSE;
 else
        {
        char tmp_string [255];                                  /* Temporary workspace */
        sprintf (tmp_string,"ERROR IN RESISTOR CALIBRATION FILE H/OR !");
        log_error (tmp_string,execution_mode);
        }

/* Read in the solenoid outrange status which determines if the solenoid (1)
   can be used outside its normal range (ie. T < 4.2K) for a faster
   cool-down */
fscanf (res_cal, "%c\n", &ch);
printf ("STARTUP SOL/OR  %c\n", ch);
if (ch == 'T')
solenoid_outrange = TRUE;
 else if (ch == 'F')
solenoid_outrange = FALSE;
 else
        {
        char tmp_string [255];                                  /* Temporary workspace */
        sprintf (tmp_string,"ERROR IN RESISTOR CALIBRATION FILE S/OR !");
        log_error (tmp_string,execution_mode);
        }

/* Read in the solenoid's tolerance (in mK)
   This parameter is used to introduce some hysteresis
   into the switching between solenoids to prevent jitter
```

```
*/
 fscanf (res_cal, "%d\n", &solenoids_tolerance);
 printf ("STARTUP SOLTOL = %d\n", solenoids_tolerance);
/* Read the auto-increase-pumping-rate (auto_ipr) status */
 fscanf (res_cal, "%c\n", &ch);
 printf ("STARTUP AUTO_IPR STATUS  %c\n", ch);
 if (ch == 'T')
 auto_ipr = TRUE;
  else if (ch == 'F')
 auto_ipr = FALSE;
  else
        {
        char tmp_string [255];                                  /* Temporary workspace */
        sprintf (tmp_string,"ERROR IN RESISTOR CALIBRATION FILE AUTO_IPR STATUS !");
        log_error (tmp_string,execution_mode);
        }
/* Read the auto-decrease-pumping-rate (auto_dpr) status */
 fscanf (res_cal, "%c\n", &ch);
 printf ("STARTUP AUTO_DPR STATUS  %c\n", ch);
 if (ch == 'T')
 auto_dpr = TRUE;
  else if (ch == 'F')
 auto_dpr = FALSE;
  else
        {
        char tmp_string [255];                                  /* Temporary workspace */
        sprintf (tmp_string,"ERROR IN RESISTOR CALIBRATION FILE AUTO_DPR STATUS !");
        log_error (tmp_string,execution_mode);
        }
/* Read the maximum permissable pumping rate [ie. temperature fall] (in mK/Sec) */
 fscanf (res_cal,"%d", &max_pumping_rate);
 printf ("STARTUP MAX PUMPING RATE = %d\n", max_pumping_rate);
/* Read the minimum permissable pumping rate [ie. temperature fall] (in mK/Sec) */
 fscanf (res_cal,"%d", &min_pumping_rate);
 printf ("STARTUP MIN PUMPING RATE = %d\n", min_pumping_rate);
 fclose (res_cal);                                              /* Close the file */

 rate_of_fall_of_T = 0;
/* Now configure the ports A & B for the Bridge/display/Resistor Latch */
 previous_VIA_no = read_fred (IEU_latch);                       /* Save previous VIA number */
 write_fred (IEU_latch, potreg_interface_VIA_no);               /* Select potreg interface VIA no */
 write_fred (ddra, 0xFF);                                       /* Pa0 - Pa7, all outputs */
 write_fred (ddrb, 0x00);                                       /* Pb0 - Pb7, all inputs */
 write_fred (IEU_latch, previous_VIA_no);                       /* Restore previous VIA on the IEU */
 return (0);                                                    /* Indicate successful completion to caller */
}



int required_solenoid (int temperature)

/* This function returns the correct solenoid number for the set temperature */
/* Results are 1 <= required_solenoid <= 7 */

{
 int count;

 if (temperature > solenoid_range [0]) return (solenoid_no_min);
  else
 if (temperature < solenoid_range [solenoid_no_max-2]) return (solenoid_no_max);
  else
        {
         for (count = 2; count <= solenoid_no_max-1; count++)
         if (temperature < solenoid_range [count-2]  &&  temperature >= solenoid_range [count-1])
         return (count);
        }
 return (1);                    /* So functions cannot fail to return a value */
}


int solenoid_check (int solenoid_number, int sol_mod_factor)

/* This small function checks to see if the solenoid number argument plus
   the "sol_mod_factor" is a legal value, if not it returns the nearest legal
   value.
   Additionally, if a solenoid number change is about to take place
   all devices are switched off to ensure no solenoid valves are left
   on spuriously.
   NB: This call to "all_devices ("OFF")" now has sole responsibility in the
       s/w for switching off other solenoids when a change in pending.
*/

{
 solenoid_number += sol_mod_factor;
 if (solenoid_number < solenoid_no_min)
    solenoid_number = solenoid_no_min;                          /* Was too small */
 else
        if (solenoid_number > solenoid_no_max)
            solenoid_number = solenoid_no_max;                  /* Was too big, else OK */
 if (solenoid_number != old_solenoid)
    all_devices ("OFF");
 return (solenoid_number);
}



int required_solenoid_hysteresis (int temperature, int sol_mod_factor)

/* This function provides some hysteresis for the required_solenoid function
   This has been done to counteract jitter in the solenoids which would
   otherwise occur if the temperature was exactly on the boundary of two solenoid
   ranges.
   If the old (current) solenoid and the proposed solenoid are not the same a
   check is made to see if they just straddle a solenoid change-over boundary.
   If so, the old solenoid is returned.
   Otherwise the specified temperature is assumed to be well inside the
   solenoid's range and the proposed solenoid is returned
        Additionally, if possible the "sol_mod_factor" (-n,0,+n) will be
        incorporated into the solenoid number returned. */

{
 int    proposed_solenoid;

 proposed_solenoid = required_solenoid (temperature);
 if (proposed_solenoid != old_solenoid)
        if (required_solenoid (temperature + solenoids_tolerance) == required_solenoid (temperature - solenoids_tolerance))
        return (solenoid_check(proposed_solenoid,sol_mod_factor));
          else
        return (solenoid_check(old_solenoid,sol_mod_factor));
  else
 return (solenoid_check(old_solenoid,sol_mod_factor));
}


int locally_set_T (void)

/* This procedure provides a locally set temperature for the switching of the
   solenoids plus the heater and the resistor (potsp/potab) selection.
```

```
   The use of this temperature for the resistor selection may cause problems
   due to discontinuities across the calibration boundries in which case the
   'set_temperature' will have to be used.
   The current purpose for this routine is to allow the graduated stepping
   down in temperature through the solenoid ranges.
   If a local_temperature change is pending the devices are switched off in
   case a resistor change occurs */

{
 int    new_temperature;
 int    curr_temperature;
 if (current_temperature > HE_BP)
 curr_temperature = HE_BP;
   else
 curr_temperature = current_temperature;

 if (set_temperature < HE_BP)
        if ((curr_temperature - set_temperature) >= temperature_sol_max_step)
        new_temperature = curr_temperature - temperature_sol_max_step;
          else
        new_temperature = set_temperature;
   else
 new_temperature = set_temperature;
 return (new_temperature);
}



void set_T (char *com1, char *com2, char *com3)

/* This procedure sets the required temperature and tolerance both tolerances
   o "tolerance" is used for regulation purposes
   o  "in_range_checking_tolerance" is used for in-range checking */
 {
 int temp_t, temp_tol, temp_tol2;
 temp_t = atoi (com1);
 temp_tol = atoi (com2);
 temp_tol2 = atoi (com3);
 if (temp_t <= 0)
        {
        char tmp_string [255];                                          /* Temporary workspace */
        sprintf (tmp_string,"%d IS AN INVALID TEMPERATURE",temp_t);
        log_error (tmp_string,execution_mode);
        }
           else
 set_temperature = temp_t;
 if (temp_tol <= 0)
        {
        char tmp_string [255];                                          /* Temporary workspace */
        sprintf (tmp_string,"%d IS AN INVALID REGULATION TOLERANCE",temp_tol);
        log_error (tmp_string,execution_mode);
        }
           else
 tolerance = temp_tol;
 if (temp_tol2 <= 0)
        {
        char tmp_string [255];                                          /* Temporary workspace */
        sprintf (tmp_string,"%d IS AN INVALID IN-RANGE-CHECKING TOLERANCE",temp_tol2);
        log_error (tmp_string,execution_mode);
        }
           else
 in_range_checking_tolerance = temp_tol2;
 /* When the temperature is changed all the solenoids and the heater must be
    reset to OFF as the solenoids and the heater are "set_temperature" appointed */
 all_devices ("OFF");
 change_time = clock();
 invoke_time = 0;
}


int calculate_T (int resistor_no)

/* This function returns the temperature given the resistor number and the
   resistances,
   There are three cases to consider:-
   (1) If the current resistor is a Speer then just use the Speer function
   (2) If the current resistor is an Allen Bradley and
      (a) 2<T<4.2K use the first set of Allen Bradley calibration data
      (b) T>4.2K use the second set of Allen Bradley calibration data
   NOTE: It is better to use the 'set' rather than the 'current' temperature
         because this avoids the problems of discontinuities across the '4.2k'
         function calibration data switch-over boundary.
         Also note that 'resistance' is a function name
   NOTE: (14th Jan 1988) The 'locally_set' temperature is now being used
   NOTE: (15th Jan 1988) The 'set_temperature' is being used again
                         due to jitter. See T.P.C Microcomputer development
                         book page 181 */

{
 int calno;

 if (set_temperature < TWO_K)
        calno = 0;
   else
         if (set_temperature <= HE_BP)
        calno = 1;
           else
        calno = 2;

  current_conductance = conductance();
  if (resistor [resistor_no] == SP)      /* Speer selected, Note: 2nd arg ==1 => Use Speer FN */
  return (absp(current_conductance,1, calibrations [resistor_no] [calno] [0],
                                      calibrations [resistor_no] [calno] [1],
                                      calibrations [resistor_no] [calno] [2]));
        else  /* Allen Bradley selected, Note: 2nd arg ==0 => Use Allen-Bradley FN */
  return (absp(current_conductance,0, calibrations [resistor_no] [calno] [0],
                                      calibrations [resistor_no] [calno] [1],
                                      calibrations [resistor_no] [calno] [2]));
}



void give_temperature_inrange (void)
/* This procedure sends the string value TRUE or FALSE to the
   "Potreg$Temperature_In_Range" system variable depending on whether the
   current temperature is within the acceptable tolerance or not */

{
 char *var_name_ptr = "Potreg$Temperature_In_Range";
 _kernel_swi_regs registers;

 registers.r[0] = (int)var_name_ptr;
 registers.r[3] = 0;
 registers.r[4] = 0;
  if (abs(set_temperature - current_temperature) <= in_range_checking_tolerance)
        {
```

```
         char *TRUE_ptr = "TRUE\n";
         registers.r[1] = (int)TRUE_ptr;
         registers.r[2] = 5;                    /* Length of string terminated by <LF>. */
        _kernel_swi(OS_SetVarVal, &registers, &registers);
        }
          else
        {
         char *FALSE_ptr = "FALSE\n";
         registers.r[1] = (int)FALSE_ptr;
         registers.r[2] = 6;                    /* Length of string terminated by <LF>. */
        _kernel_swi(OS_SetVarVal, &registers, &registers);
        }
}


void give_alternate_temperature (void)

/* This procedure sends the current temperature to the
   "Potreg$Alternate_Temperature" system variable. */

{
 char   wrt_digit [256];
 char   *var_name_ptr = "Potreg$Alternate_Temperature";
 char   *new_line = "\n";
 _kernel_swi_regs       registers;
 int    nos_chars_op;

 nos_chars_op = sprintf (wrt_digit, "%d", current_temperature); /* 'Print' the temperature to the string 'digit' */
 strcat (wrt_digit,new_line);                                   /* Put a <LF> on the end of the string as required by SWI */
 registers.r[0] = (int)var_name_ptr;
 registers.r[1] = (int)wrt_digit;
 registers.r[2] = ++nos_chars_op;                               /* Length of original string plus <LF>. */
 registers.r[3] = 0;
 registers.r[4] = 0;
 _kernel_swi(OS_SetVarVal, &registers, &registers);
}


void give_temperature (void)

/* This procedure sends the current temperature to the
   "Potreg$Current_Temperature" system variable. */

{
 char   wrt_digit [256];
 char   *var_name_ptr = "Potreg$Current_Temperature";
 char   *new_line = "\n";
 _kernel_swi_regs       registers;
 int    nos_chars_op;

 nos_chars_op = sprintf (wrt_digit, "%d", current_temperature); /* 'Print' the temperature to the string 'digit' */
 strcat (wrt_digit,new_line);                                   /* Put a <LF> on the end of the string as required by SWI */
 registers.r[0] = (int)var_name_ptr;
 registers.r[1] = (int)wrt_digit;
 registers.r[2] = ++nos_chars_op;                               /* Length of original string plus <LF>. */
 registers.r[3] = 0;
 registers.r[4] = 0;
 _kernel_swi(OS_SetVarVal, &registers, &registers);
}


void give_alternate_conductance (void)

/* This procedure sends the current conductance to the
   "Potreg$Alternate_Conductance" system variable.
   This is in nMhos (ie. 1e-9 Mhos) */

{
 char   wrt_digit [256];
 char   *var_name_ptr = "Potreg$Alternate_Conductance";
 char   *new_line = "\n";
 _kernel_swi_regs       registers;
 int    nos_chars_op;

 nos_chars_op = sprintf (wrt_digit, "%d", current_conductance); /* 'Print' the conductance to the string 'digit' */
 strcat (wrt_digit,new_line);                                   /* Put a <LF> on the end of the string as required by SWI */
 registers.r[0] = (int)var_name_ptr;
 registers.r[1] = (int)wrt_digit;
 registers.r[2] = ++nos_chars_op;                               /* Length of original string plus <LF>. */
 registers.r[3] = 0;
 registers.r[4] = 0;
 _kernel_swi(OS_SetVarVal, &registers, &registers);
}


void give_conductance (void)

/* This procedure sends the current conductance to the
   "Potreg$Current_Conductance" system variable.
   This is in nMhos (ie. 1e-9 Mhos) */

{
 char   wrt_digit [256];
 char   *var_name_ptr = "Potreg$Current_Conductance";
 char   *new_line = "\n";
 _kernel_swi_regs       registers;
 int    nos_chars_op;

 nos_chars_op = sprintf (wrt_digit, "%d", current_conductance); /* 'Print' the conductance to the string 'digit' */
 strcat (wrt_digit,new_line);                                   /* Put a <LF> on the end of the string as required by SWI */
 registers.r[0] = (int)var_name_ptr;
 registers.r[1] = (int)wrt_digit;
 registers.r[2] = ++nos_chars_op;                               /* Length of original string plus <LF>. */
 registers.r[3] = 0;
 registers.r[4] = 0;
 _kernel_swi(OS_SetVarVal, &registers, &registers);
}


int read_bridge (void)

/* This procedure reads the digits from the bridge interface and places
   them in the 'bridge_cache'
   If any of the 9 data digits obtained was bad then a value of 1 is returned
   A bridge overflow condition returns 2
   Good data results in a 0 being returned
   Register variables are used here for speed */

{
 register int   previous_VIA_no;
 register int   digit_select;
 register int   accumulator;

 previous_VIA_no = read_fred (IEU_latch);                       /* Save previous VIA no */
 /* printf ("READ-BRIDGE Previous_VIA_no= %x\n",previous_VIA_no); */
 write_fred (IEU_latch, potreg_interface_VIA_no);               /* Install interface unit's VIA */
 for (digit_select = 1; digit_select <= 9; digit_select++)
        {
```

```
        write_fred (register_a, 0xE0 + digit_select);           /* Select GET BRIDGE DATA & put "digit" address on data lines */
        handshake_A();                                          /* Handshake for data-valid */
        accumulator = read_fred (register_b);                   /* Read the byte from the interface unit */
        /* printf ("READ_BRIDGE accumulator1 %d %x\n", digit_select, accumulator); */
        if ((accumulator & 0x10) == 0)                          /* BRIDGE OVERFLOW bit is clear => overflow condition */
                {
                write_fred (IEU_latch, previous_VIA_no);        /* Restore previous VIA before returning */
                return (2);
                }
        accumulator &= 0x0F;                                    /* Mask out the high nybble */
       /* printf ("READ BRIDGE accumulator2 %d %x\n", digit_select, accumulator); */
        if (accumulator > 0x09)                                 /* Data is invalid, so return with 1 */
                {
                write_fred (IEU_latch, previous_VIA_no);        /* Restore previous VIA before returning */
                return (1);
                }
        /* Data is OK so store it in the bridge_cache */
        /* printf ("READ_BRIDGE accumulator3 %d %x\n", digit_select, accumulator); */
        bridge_cache [digit_select-1] = accumulator;
        }
 /* The bridge_cache is now full with good data so return with 0 */
 write_fred (IEU_latch, previous_VIA_no);                       /* Restore previous VIA before returning */
 return (0);
}


int act (void)

/* This procedure carries out the interrupt driven functions of this temperature
   measurement/regulation software, which are;
   (1) - Get the temperature from the bridge
   (2) - Send it to the display
   (3) - Control the temperature through the pot solenoids/heater
   If the "could not select the required resistor" error occurs the return
   code is "1".
   If the current_temperature returned by calculate_T() is "0" (indicating an
   error in absp()) then "2" is returned.
   Otherwise "0" is returned */

{
 local_temperature = locally_set_T();                           /* Get the local temperature */
/*  printf ("ACT LOCAL TEMPERATURE = %d\n", local_temperature); */
 if (autm == TRUE)
        {                                                       /* Automatic temperature control of pot */
                                                                /* Check that actual & programmed resistors tally with each other */
        if (set_temperature <= 2000)
                {                                                       /* Use the pot Speer */
                if (current_resistor() == potsp)  wrong_resistor = 0;   /* Don't alarm if resistor has not */
                else                                                    /* yet has time to be altered by the front end */
                        {
                        wrong_resistor++;
                        sel_R_poke (potsp);
                        if (current_resistor() != potsp  &&  wrong_resistor > 1)
                                {
                                 log_error ("POT SPEER OVERRIDDEN !!",execution_mode);
                                 return (1);
                                }
                        }
                }
        else
                {                                                               /* Use the pot Allen Bradley as T > 2K */
                if (current_resistor() == potab) wrong_resistor = 0;            /* Don't alarm if resistor has not */
                else                                                            /* yet has time to be altered by the front end */
                        {
                        wrong_resistor++;
                        sel_R_poke (potab);
                        if (current_resistor() != potab  &&  wrong_resistor > 1)
                                {
                                 log_error ("POT ALLEN-BRADLEY OVERRIDDEN !!",execution_mode);
                                 return (1);
                                }
                        }
                }
        }

 /* Now calculate the current temperature from the bridge
    and send it to the display */

 current_temperature = calculate_T (current_resistor());
 if (current_temperature == 0) return (2);                              /* Flag an error ultimately from absp() */
/* printf ("CURRENT TEMPERATURE = %d current_resistor() = %d\n", current_temperature,current_resistor()); */
 wrt_display (current_temperature);

/* Now calculate the average rate of fall of T (in mK/Sec) over the most recent "AVE_OVER" observation
   o If > "max_pumping_rate" AND "auto_dpr" == TRUE AND current_temperature < 4.2K then the solenoid no. will be reduced if poss.
   o If < "min_pumping_rate" AND "auto_ipr" == TRUE AND current_temperature < 4.2K then the solenoid no. will be increased if poss.
*/
 if (abs(time_last) != abs(time_curr)) rate_of_fall_of_T =
                                      ((AVE_OVER-1)*rate_of_fall_of_T +
                                      100*(last_temperature-current_temperature)/(abs(time_curr)-abs(time_last)))/AVE_OVER;
 /* printf ("%d %d %d %d %d\n",rate_of_fall_of_T,last_temperature,current_temperature,time_curr,time_last); */
if (rate_of_fall_of_T > max_pumping_rate && auto_dpr == TRUE && current_temperature < HE_BP)
        {
         sol_mod_factor_g--;                                            /* Was too fast */
         rate_of_fall_of_T = sign(rate_of_fall_of_T)*(max_pumping_rate + 1);    /* prevent "rate_of fall_of_T" getting too big */
        }
 else
        {
         if (rate_of_fall_of_T < min_pumping_rate && auto_ipr == TRUE && current_temperature < HE_BP)
                sol_mod_factor_g++;                                     /* Was too slow */
         else
                sol_mod_factor_g = 0;                                   /* Was OK */
        }
 if (autm == TRUE)
        {                                                               /* Automatic temperature control of pot */
        /* Now operate the solenoids or heater if necessary */
        /* Note if settling_time < invoke_time, devices are not touched
           NB. See also 'change_time' */
        if (invoke_time > (settling_time_factor * time_constant()))
        {
        if (local_temperature <= HE_BP)
                {                                               /* T<=4.2K,  ===> ** Regulation NORMALLY by solenoids ** */
                if (current_temperature > local_temperature)
                        {
                        if (heater_outrange == TRUE) heater ("OFF"); /* If T=local_temperature (ie. middle of range) HTR=OFF */
                        if (current_temperature > (local_temperature + tolerance))
                                {                               /* Temperature too high, open required solenoid */
                                 switch (old_solenoid=required_solenoid_hysteresis (local_temperature,sol_mod_factor_g))
                                        {
                                        case 1: solenoid ("ON","1");
                                        break;
                                        case 2: solenoid ("ON","2");
                                        break;
                                        case 3: solenoid ("ON","3");
                                        break;
                                        case 4: solenoid ("ON","4");
                                        break;
```

```
                                        case 5: solenoid (“ON”,“5”);
                                        break;
                                        case 6: solenoid (“ON”,“6”);
                                        break;
                                        case 7: solenoid (“ON”,“7”);
                                        }
                                }
                        }
                           else
                        {
                         if (current_temperature < (local_temperature − tolerance))
                                {                                                       /* Temperature too low, close required solenoid */
                                 switch (old_solenoid=required_solenoid_hysteresis (local_temperature,sol_mod_factor_g))
                                        {
                                         case 1: solenoid (“OFF”,“1”);
                                         break;
                                         case 2: solenoid (“OFF”,“2”);
                                         break;
                                         case 3: solenoid (“OFF”,“3”);
                                         break;
                                         case 4: solenoid (“OFF”,“4”);
                                         break;
                                         case 5: solenoid (“OFF”,“5”);
                                         break;
                                         case 6: solenoid (“OFF”,“6”);
                                         break;
                                         case 7: solenoid (“OFF”,“7”);
                                        }

                                       /* Additionally if the variable ‘heater_outrange’ is TRUE and the current
                                          temperature is more than a factor ‘heater_outrange_limit’
                                          lower that the (locally) requested temperature then the
                                          heater will be used for a quick warm−up */
                                 if (heater_outrange == TRUE)
                                        if ((local_temperature − current_temperature) >= heater_outrange_limit)
                                        heater (“ON”);
                                }
                        }
                }
        else
                {                                       /* If temperature regulation is needed it will be the heater,T>4.2k */
                if (current_temperature < local_temperature)
                        {
                        if (solenoid_outrange == TRUE) solenoid (“OFF”,“1”); /* If T=local_temp. (ie. middle of range) SOL1=OFF */
                        if (current_temperature < (local_temperature − tolerance))
                                heater (“ON”);                                          /* Temperature too low, turn heater on */
                        }
                    else
                        {
                        if (current_temperature > (local_temperature + tolerance))
                                {
                                 heater (“OFF”);                                        /* Temperature too high, turn heater off */
                                 /* Additionally if the variable ‘solenoid_outrange’ is TRUE and the current
                                    temperature is more than a factor ‘solenoid_outrange_limit’
                                    higher that the (locally) requested temperature then solenoid (1)
                                    will be used for a quick cool−down */
                                 if (solenoid_outrange == TRUE)
                                 if ((current_temperature − local_temperature) >= solenoid_outrange_limit)
                                  solenoid (“ON”,“1”);
                                }
                        }
                }
        }
        else
        invoke_time = clock() − change_time;
        }
 last_temperature = current_temperature;
 return (0);                                                                            /* To indicate normal successful completion */
}



void fnerr (int status)
/* This function handles errors
   It logs the signal−type number and does a non−local
   jump from itself back to the main program,
   re−installing the environment that was in force when the
   program was started.
   signal−type = 2: Arithmetic Exception
   signal−type = 4: Escape condition    (NB: This should not affect a
   relocatable module) */
{
 switch (status)
        {
        case SIGFPE: log_error (“****** ERROR − Arithmetic Exception !!”,execution_mode);
        break;
        case SIGINT: ;                                                  /* ie. Escape condition detected so do nothing */
        break;
        default    : {                                                  /* Log any other exception */
                      char tmp_string [256];
                      sprintf (tmp_string,“****** ERROR Signal Type = %d”, status);
                      log_error (tmp_string,execution_mode);
                     }
        }
 longjmp (start_env, 26);
}



void potreg_finalisation (void)

 /* This function is called by the OS when the relocatable module is
    finalised
    It uses the OS_RemoveTickerEvent SWI to stop the OS calling the
    asynchronous_entry function which it does via the IRQ veneer
    function IRQ_MODE_asynchronous_entry. */

{
 _kernel_swi_regs registers;
 extern int IRQ_MODE_asynchronous_entry (_kernel_swi_regs *r, void *pw);
 registers.r[0] = (int)IRQ_MODE_asynchronous_entry;                     /* Pointer to routine to remove call to */
 registers.r[1] = global_private_word;                                  /* For consistency with OS_CallEvery */
 _kernel_swi(OS_RemoveTickerEvent, &registers, &registers);
 printf (“Potreg system finalised, Call to SWI OS_RemoveTickerEvent made\n”);
}



/* The main program used to start here */

int was_main (char * filename)
/* The possible argument is the name of the startup file */
{
 extern jmp_buf start_env;
 int status;
```

```
 printf (“POTREG STARTING\n”);

 /* Initial settings */
 async_reentry_attempt_count = 0;
 time_last = 0;
 change_time = clock();
 invoke_time = 0;
 old_solenoid = 1;
 local_temperature = HE_BP;
 set_temperature = HE_BP;                       /* mK */
 tolerance = 1000;                              /* mK */
 in_range_checking_tolerance = 1000;            /* mK */
 autm = TRUE;                                   /* Automatic temperature regulation of pot */
 current_temperature = HE_BP;
 wrong_resistor = 0;
 if (strlen (filename) != 0)       /* If no filename was given, use “RES_CAL” */
        {
         printf (“Reading from startup file %s\n”,filename);
         status = startup (filename);
        }
          else
        {
         printf (“Reading from default startup file RES_CAL\n”);
         status = startup (“RES_CAL”);
        }
if (status != 0) return (0);                            /* Return immediately if an error occurred */
all_devices (“OFF”);                                    /* Switch off the heater and all the solenoids */
if (setjmp (start_env) != 0) return (0);                /* Set up the non-local-jump position */
signal (SIGFPE, fnerr);                                 /* Handle arithmetic Exceptions (NB: These should be OK for async part) */
signal (SIGINT, fnerr);                                 /* Handle (suppress) Escape conditions */
 if (atexit(potreg_finalisation) != 0)                  /* Register the “potreg_finalisation” function to be called when the */
        printf (“ERROR COULD NOT REGISTER FINALISATION CODE\n”);       /* system finalises the relocatable module */
 system_initialised = TRUE;                             /* Indicates asynchronous operation may now begin */
 return (0);
}



void help (void)
/* This function writes out help information describing the commands the
   software understands */

{
 printf (“****** HELP INFORMATION For Potreg Utility ******\n\n”);
 printf (“       List Of Commands...\n”);
 printf (“BOOT [calibration filename] - Boot the system & read in calibration file\n”);
 printf (“SET_T <temperature>(mK) <tolerance>(mK) <acceptable tolerance>(mK)\n”);
 printf (“       - Sets (1); The temperature\n”);
 printf (“       - Sets (2); The tolerance used for temperature regulation\n”);
 printf (“       - Sets (3); The tolerance used for in-range checking\n”);
 printf (“SEL_R AUTO - Selects automatic selection of POT AB & Spear for\n”);
 printf (“             temperature regulation\n”);
 printf (“             - Other Effects: Enables all devices\n”);
 printf (“SEL_R <n> - Selects a resistor 0<=n<=7 in the cryostat\n”);
 printf (“           - Other Effects: Disables all devices\n”);
 printf (“HEATER DISABLE  - Disables the heater\n”);
 printf (“HEATER ENABLE   - Enables the heater\n”);
 printf (“HEATER OUTRNG   - Enables the use of the heater outside its normal\n”);
 printf (“                  range - ie. for T<4.2K, for quicker warming\n”);
 printf (“HEATER NOOUTRNG - Disables the use of the heater outside its normal\n”);
 printf (“                  operating range\n”);
 printf (“                  - Other Effects: Switches all devices off\n”);
 printf (“HEATER OFF      - Switches heater off, if enabled\n”);
 printf (“HEATER ON       - Switches heater on, if enabled\n”);
 printf (“SOLENOID OUTRNG      - Enables the use of the solenoid (0) outside its\n”);
 printf (“                       normal operating range. ie. for T>4.2 for quicker\n”);
 printf (“                       cooling\n”);
 printf (“SOLENOID NOOUTRNG    - Disables the use of the solenoid (0) outside its\n”);
 printf (“                       normal operating range\n”);
 printf (“                       - Other Effects: Switches all devices off\n”);
 printf (“SOLENOID ENABLE <n>  - Enables the use of the solenoid <n>, 1<=n<=7\n”);
 printf (“SOLENOID DISABLE <n> - Disables the use of the solenoid <n>, 1<=n<=7\n”);
 printf (“SOLENOID OFF <n>     - Switches off the solenoid <n>, 1<=n<=7, if enabled\n”);
 printf (“SOLENOID ON <n>      - Switches on the solenoid <n>, 1<=n<=7, if enabled\n”);
 printf (“DEV_STOP      - Causes all devices to be switched OFF & DISABLED\n”);
 printf (“ACT   - Read bridge/Update temperature/Control devices etc. NB: Obsolete\n”);
 printf (“DUMP  - Causes all global variables to be dumped\n”);
 printf (“AUTO_IPR ON  - Allow the dynamic increase of solenoid no. if fall of T too slow\n”);
 printf (“               This feature is only active for current temperature < 4.2K\n”);
 printf (“AUTO_IPR OFF - Disallow the dynamic increase of solenoid no.\n”);
 printf (“AUTO_DPR ON  - Allow the dynamic decrease of solenoid no. if fall of T too fast\n”);
 printf (“               This feature is only active for current temperature < 4.2K\n”);
 printf (“AUTO_DPR OFF - Disallow the dynamic decrease of solenoid no.\n”);
 printf (“ALT_R        - Temporarily select an alternate resistor, log T & Cond. from it\n”);
 printf (“HELP - Invoke this help script\n”);
}



_kernel_oserror *potreg_cmd (char *arg_string, int argc, int cmd_no, void *pw)
/* This function is called by the module header when a command is entered
   Only one command is recognised - “POTREG”
   All information is conveyed to the program as arguments to the command */
{
 int update_temperature (void);
 char   *ptr;
 char   *ptr1;
 char   *ptr2;
 char   *ptr3;
 char   empty [] = “”;
 char   workspace [256];
 UNUSED (pw);
 UNUSED (cmd_no);

/* Copy arg_string to workspace and append <NUL> to produce a valid C-string */
/* At the same time force any lower case characters to upper case for matching */
 ptr2 = workspace;
 for (ptr=arg_string; *ptr>=32; ptr++)
      {
       if (islower(*ptr)) *ptr2++ = *ptr & 0xDF;
          else
       *ptr2++ = *ptr;
      }
 *ptr2 = 0;
 ptr  = strtok (workspace,“ ”);
 if (argc >= 2)                                                 /* If this arg was not present set ptr1 to empty string */
 ptr1 = strtok (NULL,“ ”);
     else
 ptr1 = empty;
 if (argc >= 3)                                                 /* If this arg was not present set ptr2 to empty string */
 ptr2 = strtok (NULL,“ ”);
     else
 ptr2 = empty;
 if (argc >= 4)                                                 /* If this arg was not present set ptr3 to empty string */
 ptr3 = strtok (NULL,“ ”);
     else
 ptr3 = empty;
 execution_mode = COMMAND;                                      /* So O/P to the screen is allowed */
```

```
 threaded = TRUE;                                                    /* Indicate to asynchronous code that the program is threaded */
 if (strcmp (ptr, "BOOT") == 0) was_main (ptr1); else
 if (strcmp (ptr, "SET_T") == 0) set_T (ptr1, ptr2, ptr3); else
 if (strcmp (ptr, "SEL_R") == 0) sel_R (ptr1); else
 if (strcmp (ptr, "HEATER") == 0) heater (ptr1); else
 if (strcmp (ptr, "SOLENOID") == 0) solenoid (ptr1, ptr2); else
 if (strcmp (ptr, "DEV_STOP") == 0)     {
                                         all_devices ("ENABLE");
                                         all_devices ("OFF");
                                         all_devices ("DISABLE");
                                        } else
 if (strcmp (ptr, "ACT") == 0) update_temperature(); else
 if (strcmp (ptr, "HELP") == 0) help(); else
 if (strcmp (ptr, "AUTO_IPR") == 0) auto_ipr_modify (ptr1); else
 if (strcmp (ptr, "AUTO_DPR") == 0) auto_dpr_modify (ptr1); else
 if (strcmp (ptr, "ALT_R") == 0) alternate_r (ptr1); else
 if (strcmp (ptr, "DUMP") == 0) dump_variables(); else
 log_error ("BAD POTREG COMMAND !!",execution_mode);
 threaded = FALSE;                                    /* Indicate to asynchronous code that the program is no longer threaded */
 return (0);
}


void alarm_driver (int alarm_number, int bleeper)

 /* This function drives the alarm H/W in the bridge interface unit
    An addressable latch is used to hold the on/off state of the devices.
    There are 7 LEDs and a bleeper, the LED positions in the latch are
    described by the "ALARM_*" enum and the bleeper is at address 0 in the
    latch - currently only 4 alarm LEDs are allocated.
    See also T.Crane M&HD book 2, page 93...95.
    Whenever one of the alarm LEDs is activated the software activates the
    bleeper is as well. */

{
 int previous_VIA_no;

 previous_VIA_no = read_fred (IEU_latch);              /* Save previous VIA no */
 write_fred (IEU_latch, potreg_interface_VIA_no);      /* Select potreg VIA no */
 if (alarm_number == ALARM_NORMAL)
        {
         int i;
         for (i=0; i<8; i++)
                {
                 write_fred (register_a,0x70+i);       /* All is well so switch off all LEDs & bleeper */
                 handshake_A();                        /* Handshake for data valid */
                }
        }
                else
        {
         write_fred (register_a,0x78+alarm_number);    /* Switch on the LED to indicate this fault condition */
         handshake_A();                                /* Handshake for data valid */
         if (bleeper)
                {
                 write_fred (register_a,0x78);         /* Switch on the bleeper as well */
                 handshake_A();                        /* Handshake for data valid */
                }
        }
 write_fred (IEU_latch, previous_VIA_no);              /* Restore previous VIA on the IEU */
}


void update_time_stamp(void)
/* This function Updates the system variables "Potreg$Last_Update_Time"
   and "Potreg$Last_Update_Time_Binary" with the current time in ASCII and
   binary format respectively.
   This can be then be read by foreground tasks to determine the time of
   the last update and hence whether the Potreg software is working or
   not. */

{
 char   time_string [256];
 char   *var_name_ptr = "Potreg$Last_Update_Time_Binary";
 char   *var_name_ptr2 = "Potreg$Last_Update_Time";
 char   *new_line = "\n";
 _kernel_swi_regs       registers;
 int    nos_chars_op;
 time_t binary_time;

 time (&binary_time);                                                  /* Get the binary time */
 nos_chars_op = sprintf (time_string,"%d",binary_time);                /* Convert to int-string */
 strcat (time_string,new_line);                                        /* Put a <LF> on the end of the string as required by SWI */
 registers.r[0] = (int)var_name_ptr;
 registers.r[1] = (int)time_string;
 registers.r[2] = ++nos_chars_op;                                      /* Length of original string plus <LF>. */
 registers.r[3] = 0;
 registers.r[4] = 0;
 _kernel_swi(OS_SetVarVal, &registers, &registers);

 strcpy (time_string,ctime(&binary_time));                             /* Convert the binary time to ASCII textual time */
 strcat (time_string,new_line);                                        /* Put a <LF> on the end of the string as required by SWI */
 registers.r[0] = (int)var_name_ptr2;
 registers.r[1] = (int)time_string;
 registers.r[2] = strlen (time_string);                                /* Length of original string plus <LF>. */
 registers.r[3] = 0;
 registers.r[4] = 0;
 _kernel_swi(OS_SetVarVal, &registers, &registers);
}


int update_temperature (void)
/* This function is normally called asynchronously, about once a second and is
   responsible for overseeing the reading and displaying the temperature
   and controlling the heater and solenoid valve
   If an error occurs 1 is returned otherwise 0 is returned */

{
 int ret_val = read_bridge();
 int status = 0;
 time_curr = clock();
 if ((int)time_curr <= 0)
        {
         alarm_driver (ALARM_BADCLK,FALSE);                  /* Tell alarm H/W to flag bad clock() result error & return */
         log_error ("BAD CLOCK ERROR",execution_mode);
         /* ### return (1); ### */
        }
 if (ret_val == 0)
        {                                                              /* Data is OK so process it */
         int ret_val = act();
         time_last = time_curr;
         if (ret_val != 0)
                {
                 status = 1;
                 if (ret_val == 1)
                        {
                         alarm_driver (ALARM_NOT_AUTO,TRUE);                  /* Tell alarm H/W to flag wrong-resistor error */
                         log_error ("AB OR SP RESISTOR OVERRIDDEN",execution_mode);
                        }
```

```
                        else
                    {
                     alarm_driver (ALARM_FP_ERROR,TRUE);                    /* Tell alarm H/W to flag floating-point error */
                     log_error ("FLOATING POINT ERROR",execution_mode);
                    }
                }
                  else
                {
                 alarm_driver (ALARM_NORMAL,FALSE);                     /* Tell the alarm H/W to indicate no errors */
                 update_time_stamp();                                   /* Update "Potreg$Last_Update_Time" with current time */
                 give_temperature_inrange();                            /* Update "Potreg$Temperature_In_Range" system variable  */
                 give_conductance();                                    /* Update "Potreg$Current_Conductance" system variable. */
                 give_temperature();                                    /* Update "Potreg$Current_Temperature" system variable. */
                }
        }
   else
        {
         status = 1;
         if (ret_val == 1)
                {
                 if (abs(abs(time_curr) - abs(time_last)) >= time_limit)
                        {
                         log_error ("BAD DATA",execution_mode);
                         alarm_driver (ALARM_BAD_DATA,TRUE);
                        }
                }
           else
                {
                 log_error ("BRIDGE OVERFLOW",execution_mode);                  /* Since ret_val was 2, => bridge overflow */
                 alarm_driver (ALARM_BRIDGE_OVERFLOW,TRUE);
                }
        }
 return (status);                                                       /* Indicate an error occured */
}


int asynchronous_entry (_kernel_swi_regs *registers, void *pw)

/* This function is entered once a second to update the temperature
   Notes:       (1) It is entered in SVC mode.
                    OS_CallEvery is used in the initialisation code
                    (potreg_initialisation) to start the polling of this
                    function and potreg_finalisation is called (by C's
                    atexit function) when the module is finalised (ie.
                    RMKILL etc.)
                    NB: Polling is done indirectly via the cmhg irq veneer
                        (IRQ_MODE_asynchronous_entry).
                (2) It must not execute any of the temperature regulation
                    code until variables have been initialised by the
                    startup procedure - This is indicated by the
                    "system_initialised" variable.
                (3) This function returns non-0. This is necessary since
                    the code on called by OS_CallEvery has to behave like
                    IRQ code (ie. IRQ code as in by intercepting IrqV).
                    According to the "ANSI C Release 3" manual (p.386) this
                    function should return non-0 if the "interrupt" was
                    not for this handler
                (4) Experimental modification (25-Dec-1990!)
                    Double entrancy from interrupt code has been blocked,
                    as this is suspected as the cause of system hangs/crashes.
                    See "async_reentry_attempt_count" for evidence of
                    attempted asynchronous re-entry
                (5) Enabling interrupts after asynchronicity has been blocked,
                    this is for use in conjunction with interrupt mode operation
                    of arcontrol6 S/W. (Modification 29th October 1991) */
{
_kernel_swi_regs regs;
 UNUSED (pw);
 UNUSED (registers);
 if (system_initialised == TRUE)
        {
          if (threaded == FALSE)                                /* Only execute asynchronously if program is not already threaded */
                {
                 execution_mode = ASYNCHRONOUS;                     /* Indicates log_error may not write to the screen */
                 threaded = TRUE;                                   /* Indicate s/w is now asynchronously threaded */
                 _kernel_swi(OS_IntOn, &regs, &regs);               /* Enable interrupts now async operation blocked */
                 update_temperature();                              /* Call the code to update the temperature etc. */
                  _kernel_swi(OS_IntOff, &regs, &regs);             /* Disable interrupts before returning */
                 threaded = FALSE;                                  /* Indicate s/w is no longer asynchronously threaded */
                }
           else
                {
                 if (execution_mode == ASYNCHRONOUS)
                        {
                         alarm_driver (ALARM_ARAD,TRUE);        /* Flag Async-Reentry-Attempt-Detected on front panel */
                         async_reentry_attempt_count++;         /* Increment counter to leave record of event */

          }
                }
        }
 return (1);
}


_kernel_oserror *potreg_initialisation (char *cmd_tail, int podule_base, int r12_value)

 /* This function is called by the OS when the relocatable module is
    loaded.
    It uses the OS_CallEvery SWI to make the OS call the
    asynchronous_entry function once a second to update the temperature.
    NB: This is done indirectly via the cmhg IRQ veneer
        IRQ_MODE_asynchronous_entry */

{
 _kernel_swi_regs registers;
 extern int IRQ_MODE_asynchronous_entry (_kernel_swi_regs *r, void *pw);

 UNUSED(cmd_tail);
 UNUSED(podule_base);
 registers.r[0] = 200;                                                  /* Call every 200 centi-seconds */
 registers.r[1] = (int)IRQ_MODE_asynchronous_entry;                     /* Pointer to routine to call */
 registers.r[2] = global_private_word = r12_value;                      /* Workspace to be used by asynchronous code */
 _kernel_swi(OS_CallEvery, &registers, &registers);
 printf ("Potreg system initialised, Call to SWI OS_CallEvery made\n");
 return (0);
}
```

Appendix 3.2, The absp ‘C’ Source Code.

```
#include <limits.h>

#define ROOT10  3.16227766
#define C1      0.8690286
#define C3      0.2773839
#define C5      0.2543275
#define A1      1.1499196
#define A2      0.6774323
#define A3      0.2080030
#define A4      0.1268089
#define CALMUL  1000000

int absp (int conductance, int ABorSP, int a, int b, int korc)
/* Calculate a temperature in MK (int) from a conductance in nMhos (int).
   By confining FP arithmetic to this module assembly level hacking can be
   kept to a minimum
   Note: the a, b & korc parameters have (on entry) been multiplied by
         CALMUL to stop information loss on storing FP numbers in ints
   If the input resistance is illegal, then 0 is returned.
   Also, if values likely to cause a FP exception occur in the 10^X part
   of the Speer calculation then 0 is returned as well.
   Finally, if the return value whivh is casted into an int is too big for
   the int then 0 is returned */

{
 int    characteristic=0;
 double R;
 double tmp_R;
 double log10R;
 double accu;
 double tmp2;

   if (conductance > 0)         /* Check conductance is not 0 first */
      R = 1e9/conductance;
    else
      return (0);

/* Check that the resistance is in range.
   R cannot be too big since the double types used in the calculation can
   hold a much bigger number than (1/conductance) where the smallest value
   of conductance (an int) is 1 nMho.
   R must >= 2 since 1/log10(1) is illegal */

   if (R < 2) return (0);

/* Scale the resistance to the range 1<=R<=10 */
 for (tmp_R=R; tmp_R > 10; characteristic++) tmp_R /= 10;

/* Now calculate the log10 of the scaled R, See Approximations for Digital
   Computers by Hastings */

 accu = (tmp_R - ROOT10)/(tmp_R + ROOT10);
 log10R = characteristic + 0.5 + C1*accu +
                                 C3*accu*accu*accu +
                                 C5*accu*accu*accu*accu*accu;
 if (ABorSP == 0)
        {
         /* An Allen-Bradley resistor has been selected
            Multiply by 1000 to convert K to mK */

         tmp2 = 1000*CALMUL / (a + b*log10R + korc/log10R);

         /* If tmp2 is too big to cast to an int then return 0 */
         if (tmp2 < INT_MAX && tmp2 > -INT_MAX)
         return ((int)tmp2);
             else
         return (0);
        }
               else
        {
         /* A Speer was selected, so first calculate:-
            a + b*log10(R) + c/log10(R), then scale it to the range
            0<=tmp<=1 */

         double tmp;
         double ten_to_the_tmp;
         int scale = 0;
         int flag = 0;
         tmp = (a + b*log10R + korc/log10R)/CALMUL;
         if (tmp > 10 || tmp < -10) return(0);                          /* T>10^+/-10 is clearly stupid so return and flag eror */
         if (tmp >= 0)
                {
                 for (; tmp > 1; scale++) tmp -= 1;                     /* tmp +ve */
                }
                   else
                {
                 flag = 1;                                              /* tmp -ve */
                 for (tmp=0-tmp; tmp > 1; scale++) tmp -= 1;
                }
        /* Now work out the polynomial for 10**x, See Hastings for details */

         ten_to_the_tmp = 1 +
                         A1*tmp +
                         A2*tmp*tmp +
                         A3*tmp*tmp*tmp +
                         A4*tmp*tmp*tmp*tmp;
         ten_to_the_tmp *= ten_to_the_tmp;
         /* Now re-scale by multiplying by 10**scale */
         for (; scale > 0; scale--) ten_to_the_tmp *=10;

         /* If x was -ve then 10**x => 1/10**abs(x) */
         if (flag != 0) ten_to_the_tmp = 1/ten_to_the_tmp;

         /* Multiply by 1000 to convert K to mK */
         /* If tmp2 is too big to cast to an int then return 0 */
         tmp2 = 1000*ten_to_the_tmp;
         if (tmp2 < INT_MAX && tmp2 > -INT_MAX)
         return ((int)tmp2);
             else
         return (0);
        }
}
```

Appendix 3.3, The absp Assembly Language Code.

```
; generated by Norcroft RISC OS ARM C vsn 3.00 [Jul 12 1989]
a1 RN 0
a2 RN 1
a3 RN 2
a4 RN 3
v1 RN 4
v2 RN 5
v3 RN 6
v4 RN 7
v5 RN 8
v6 RN 9
sl RN 10
fp RN 11
ip RN 12
sp RN 13
lr RN 14
pc RN 15

f0 FN 0
f1 FN 1
f2 FN 2
f3 FN 3
f4 FN 4
f5 FN 5
f6 FN 6
f7 FN 7

    AREA |C$$code|, CODE, READONLY

        IMPORT  |__main|
|x$codeseg|
        B       |__main|

        DCB     &61,&62,&73,&70
        DCB     &00,&00,&00,&00
        DCD     &ff000008

        EXPORT  absp
absp
        STMFD   sp!, {v1 ,lr}
        MOV     ip, a4
        LDR     v1, [sp, #8]

;
; ** Code to change mode from SVC to USR with interrupts disabled follows **
;
        TEQP    pc, #&0000000        ; Enable interrupts and from SVC to USR
;####   TEQP    pc, #&8000000        ; Disable interrupts and from SVC to USR
        MOVNV   a1, a1               ; Allow ARM time to switch modes
        STR     sp, sp_USR_store     ; Save USR mode R13 & R14, otherwise USR
        STR     lr, lr_USR_store     ; mode interrupted code will crash
;
; NB: The values of lr_USR & sp_USR are irrelevant here as they are not used
;
        MOV     a4, #0
        MOV     lr, a4
        CMPS    a1, #0
        BLE     |L000274.J46.absp|
        FLTD    f0, a1
        LDFD    f1, [pc, #L0000f0-.-8]
```

```
        DVFD    f0, f1, f0
        CMFE    f0, #2
        BLT     |L000274.J46.absp|
        CMFE    f0, #10
        BLE     |L000058.J11.absp|
|L000048.J10.absp|
        DVFD    f0, f0, #10
        ADD     lr, lr, #1
        CMFE    f0, #10
        BGT     |L000048.J10.absp|
|L000058.J11.absp|
        LDFD    f2, [pc, #L0000f8-.-8]
        SUFD    f3, f0, f2
        ADFD    f0, f0, f2
        DVFD    f0, f3, f0
        FLTD    f2, lr
        ADFD    f3, f2, #0.5
        LDFD    f2, [pc, #L000100-.-8]
        MUFD    f2, f0, f2
        ADFD    f3, f3, f2
        LDFD    f2, [pc, #L000108-.-8]
        MUFD    f2, f0, f2
        MUFD    f2, f2, f0
        MUFD    f2, f2, f0
        ADFD    f3, f3, f2
        LDFD    f2, [pc, #L000110-.-8]
        MUFD    f2, f0, f2
        MUFD    f2, f2, f0
        MUFD    f2, f2, f0
        MUFD    f2, f2, f0
        MUFD    f0, f2, f0
        ADFD    f0, f3, f0
        CMPS    a2, #0
        BNE     |L000128.J15.absp|
        FLTD    f2, v1
        DVFD    f3, f2, f0
        FLTD    f2, ip
        MUFD    f2, f2, f0
        FLTD    f0, a3
        ADFD    f0, f2, f0
        ADFD    f0, f3, f0
        DVFD    f0, f1, f0
        LDFD    f1, [pc, #L000118-.-8]
        CMFE    f0, f1
        BGE     |L000274.J46.absp|
        LDFD    f1, [pc, #L000120-.-8]
        CMFE    f0, f1
        BLE     |L000274.J46.absp|
        B       |L000244.J48.absp|
L0000f0
        DCFD    1e9
L0000f8
        DCFD    3.16227766
L000100
        DCFD    0.8690286
L000108
        DCFD    0.2773839
L000110
        DCFD    0.2543275
L000118
        DCFD    2147483647.0
L000120
        DCFD    -2147483647.0
|L000128.J15.absp|
```

```
        MOV     a1, a4
        MOV     a2, a4
        FLTD    f1, v1
        DVFD    f2, f1, f0
        FLTD    f1, ip
        MUFD    f1, f1, f0
        FLTD    f0, a3
        ADFD    f0, f1, f0
        ADFD    f1, f2, f0
        LDFD    f0, [pc, #L00018c-.-8]
        DVFD    f0, f1, f0
        CMFE    f0, #10
        BGT     |L000274.J46.absp|
        MNFD    f1, #10
        CMFE    f0, f1
        BLT     |L000274.J46.absp|
        CMFE    f0, #0
        BLT     |L000194.J26.absp|
        CMFE    f0, #1
        BLE     |L0001b4.J33.absp|
|L000178.J28.absp|
        SUFD    f0, f0, #1
        ADD     a1, a1, #1
        CMFE    f0, #1
        BGT     |L000178.J28.absp|
        B       |L0001b4.J33.absp|
L00018c
        DCFD    1000000.0
|L000194.J26.absp|
        MOV     a2, #1
        MNFD    f0, f0
        CMFE    f0, #1
        BLE     |L0001b4.J33.absp|
|L0001a4.J34.absp|
        SUFD    f0, f0, #1
        ADD     a1, a1, #1
        CMFE    f0, #1
        BGT     |L0001a4.J34.absp|
|L0001b4.J33.absp|
        LDFD    f1, [pc, #L00024c-.-8]
        MUFD    f1, f0, f1
        ADFD    f2, f1, #1
        LDFD    f1, [pc, #L000254-.-8]
        MUFD    f1, f0, f1
        MUFD    f1, f1, f0
        ADFD    f2, f2, f1
        LDFD    f1, [pc, #L00025c-.-8]
        MUFD    f1, f0, f1
        MUFD    f1, f1, f0
        MUFD    f1, f1, f0
        ADFD    f2, f2, f1
        LDFD    f1, [pc, #L000264-.-8]
        MUFD    f1, f0, f1
        MUFD    f1, f1, f0
        MUFD    f1, f1, f0
        MUFD    f0, f1, f0
        ADFD    f0, f2, f0
        MUFD    f0, f0, f0
        CMPS    a1, #0
        BLE     |L000218.J40.absp|
|L000208.J39.absp|
        MUFD    f0, f0, #10
        SUB     a1, a1, #1
        CMPS    a1, #0
```

```
        BGT     |L000208.J39.absp|
|L000218.J40.absp|
        CMPS    a2, #0
        MVFNED  f1, #1
        DVFNED  f0, f1, f0
        LDFD    f1, [pc, #L00026c-.-8]
        MUFD    f0, f0, f1
        LDFD    f1, [pc, #L000118-.-8]
        CMFE    f0, f1
        BGE     |L000274.J46.absp|
        LDFD    f1, [pc, #L000120-.-8]
        CMFE    f0, f1
        BLE     |L000274.J46.absp|
|L000244.J48.absp|
        FIXSZ   a1, f0
;
; ** Change mode back to SVC before exiting **
;
        LDR     sp, sp_USR_store     ; Restore USR mode R13 & R14
        LDR     lr, lr_USR_store     ; before returning
        SWI     &16                  ; SWI OS_EnterOS
        LDMFD   sp!, {v1 ,pc}^
L00024c
        DCFD    1.1499196
L000254
        DCFD    0.6774323
L00025c
        DCFD    0.2080030
L000264
        DCFD    0.1268089
L00026c
        DCFD    1000.0
|L000274.J46.absp|
        MOV     a1, a4
;
; ** Change mode back to SVC before exiting **
;
        LDR     sp, sp_USR_store     ; Restore USR mode R13 & R14
        LDR     lr, lr_USR_store     ; before returning
        SWI     &16                  ; SWI OS_EnterOS
        LDMFD   sp!, {v1 ,pc}^

sp_USR_store
        %       4                    ; Store for USR mode R13
lr_USR_store                         ; Store for USR mode R14
        %       4

    AREA |C$$data|

|x$dataseg|


    END
```

Appendix 4.

Appendix 4, Magnet Controller Software.

This appendix shows one of the three assembler source code modules which drive the IEEE-488/GPIB interface.

```
                    TTL IEEE Sub-System1
                    MODULE IEEE488_01
; The module contains some of the code for the IEEE488 sub-system which
; uses the Texas Instruments TMS9914 GPIB Adapter.
; See Data Manual for details of IC.
;
; This section defines the symbols the linker must resolve for the module
; Zero page symbols:
IEEE_talker_ptr         EXZ
general_purpose_ptr1_I  EXZ
;
; Main memory symbols:
IEEE_int_mask0          EXT
IEEE_int_mask1          EXT
IEEE_external_address   EXT
IEEE_address_reg        EXT
IEEE_auxiliary_cmd      EXT
IEEE_talker_default_msg EXT
BO_IRQ_handler          EXT
IEEE_SPR_softcopy       EXT
IEEE_serial_poll        EXT
msg_or_number_flag      EXT
IEEE_int_status1        EXT
IEEE_DCAS_flag          EXT
LF_heater_Main          EXT
main_coil_htr_control   EXT
control_shim_htrs       EXT
selected_coil           EXT
auto_control_handler    EXT
reset_activator         EXT
mode_flag               EXT
phase_flag              EXT
phase_internal_flag     EXT
IEEE_address_status     EXT
LF_manual_key           EXT
KH_ctrl_manual          EXT
clear_old_input_buffer  EXT
display_latch_OA_flag   EXT
IEEE_data_in            EXT
IEEE_buffer_age_flag    EXT
IEEE_buffer_data_ptr    EXT
IEEE_buffer_size        EXT
set_IEEE_SPR_bits       EXT
IEEE_buffer             EXT
shutdown_confirmed      EXT
clear_NVM_confirmed     EXT
turn_swald_on           EXT
turn_swald_off          EXT
turn_hold_on            EXT
turn_hold_off           EXT
set_coil                EXT
set_temp_coil           EXT
set_I                   EXT
set_start_I             EXT
set_stop_I              EXT
set_sweep_time          EXT
query_swald             EXT
query_hold              EXT
query_cycle_phase       EXT
query_coil              EXT
query_heater            EXT
query_mode              EXT
query_DAC               EXT
query_latch             EXT
query_version           EXT
query_last_message      EXT
LF_swald_key            EXT
LF_hold_key             EXT
IEEE_INT0_flag          EXT
IEEE_INT1_flag          EXT
LF_lockout              EXT
;
;-------------------------
;
DEBUGGING_FLAG          EQU 0                               ; Flag to switch in debugging code (0=OFF,1=ON)
;
;-------------------------
;
; *** This Section Defines The Instrument's Serial Poll Bit Designations ***
; Bit no.       Meaning
;   0           Can't understand command (eg. if this command was received  "SHUTDOXN")
;   1           Bad command argument (eg. if this command was received "CURRENT=10.PQR")
;   2           Argument range error ie. some non-syntactical problem with command argument (eg. "CURRENT=100000.1" [amps])
;   3           "SHE" Shim already heated error since only 1 shim may be heated at once
;   4           Busy bit, this is set when the instrument is busy such as during the shutdown process
;   5           Non-Volatile-memory error, the NVM checksum test failed
;   6           IEEE standard defined rsv (Request SerVice) bit
;   7           He-4 level bit (0=normal,1=level low)
;
;-------------------------
;
```

```
; ** Local Program Data follows **
; This is the IEEE output message terminator for the device, that is it is
; appended to any message output by this unit.
; Note: The unit will accept any control character (ASCII 0 to 31) as a
;       message terminator on input.
IEEE_OP_termination_ch  GEQU 13
;
;-------------------------
;
; Set up the symbols for the bit fields of the interrupt status registers
; and interrupt mask registers.
MAC     = %00000001     ; Enable interrupt on my address change
RLC     = %00000010     ; Enable interrupt on remote/local change
SPAS    = %00000100     ; Enable interrupt on serial poll active state
END     = %00001000     ; Enable interrupt on EOI with ATN false
BO      = %00010000     ; Enable interrupt on byte output
BI      = %00100000     ; Enable interrupt on byte input

IFC     = %00000001     ; Enable interrupt on interface clear
SQR     = %00000010     ; Enable interrupt on service request
MA      = %00000100     ; Enable interrupt on my address
DCAS    = %00001000     ; Enable interrupt on device clear active state
APT     = %00010000     ; Enable interrupt on address pass through
UCG     = %00100000     ; Enable interrupt on unidentified command
ERR     = %01000000     ; Enable interrupt on incomplete source handshake
GET     = %10000000     ; Enable interrupt on group execute trigger
;
;-------------------------
;
; Subroutine to initialise the IEEE488 device after a hard or soft reset
; So set up the device as required then clear the reset condition
; First set up the interrupt mask registers which determine which types of
; conditions will cause the device to issue an interrupt request (IRQ).
; Finally set up the "IEEE_talker_ptr" to point to the default talker
; message.
initialise_IEEE488      ENT
                        BLOCK
int_mask0_value         = RLC + SPAS + BO + BI                  ; The currently implemented
int_mask1_value         = DCAS + IFC                            ;  interrupt types

                        lda #int_mask0_value
                        sta IEEE_int_mask0                      ; Set up the interrupt mask registers
                        lda #int_mask1_value
                        sta IEEE_int_mask1
                        lda IEEE_external_address               ; Read address from DIP switches
                        and #%00011111                          ; Mask for 5 bit address
                        sta IEEE_address_reg                    ; Inform TMS9914 of its address
                        stz IEEE_auxiliary_cmd                  ; Clear software reset condition
                        ldx #>IEEE_talker_default_msg           ; Initialise "IEEE_talker_ptr" to point
                        ldy #<IEEE_talker_default_msg           ;  to the default talker message so it will be O/P if the instrument
                        stx IEEE_talker_ptr + 0                 ;  is talked without a preceeding request for a response.
                        sty IEEE_talker_ptr + 1
                        rts
;
;-------------------------
;
; This subroutine is the primary interrupt handler for the TMS9914
; GPIB/IEEE488 interface adapter.
; It is responsible for determining the cause of the interrupt and
; handling it.
; Currently the following interrupts are handled;
; (1)   BI      - Byte In
;               A byte has arrived in the data-in register and is
;               available for reading.
; (2)   BO      - Byte Out
;               The TMS9914 is ready to accept a byte to be sent out in
;               its data-out register.
;               When the TMS9914 enters Talker mode this interrupt is
;               given to prompt loading of the 1st byte
; (3)   SPAS    - Serial Poll Active State
;               The controller has Serial Polled the TMS9914 which had set
;               the rsv bit.
;               The software must clear the rsv bit and any others which
;               serial polling should clear in the serial poll register.
;               The "msg_or_number_flag" is also cleared so that the unit
;               will return from displaying the error message associated
;               with the BRK that set the rsv bit in the SPR to displaying
;               the "input_buffer" which will be empty.
; (4)   RLC     - Remote local Change
;               A Remote to Local or Local to remote change has taken
;               place.
;               Note:   Stopping a local to remote change here in the case
;                       of a shutdown taking place or remote-lockout(TPC)
;                       being in force is not necessary since this is
;                       already prevented with the 'dai' command and the
;                       'rtl'(c/s=1) respectively.
; (5)   DCAS    - Device Clear Active State
;               The controller has sent a Device-Clear command to the
;               TMS9914.
;               On receipt the code winds down the DACs (but does not
;               touch any coils which are energised but not heated) and
;               activates the H/W-reset-under-software-control facility
;               which completely resets the system.
;               See the "DCAS_IRQ_handler" subroutine for details.
; (6)   IFC     - An Interface Clear has been received
;               The System Controller has sent an Interface Clear command.
;               The instrument responds by performing a software reset on
;               the TMS9914 and then going through the IEEE initialisation
;               routine "initialise_IEEE488".
;
; Note: Since the interrupt flag registers are cleared on reading they
;       must be stored in memory flag after reading. The handler routines
;       must then be called until all the enabled interrupt's bits in the
;       flags are clear, where each handler must clear its bit in the flag
;       when called.
; On Entry:     The INT STATUS 0 register is in X
service_IEEE_IRQ        ENT
                        BLOCK
;
; First, set up the "IEEE_INT0_flag" with the contents of the INT STATUS 0
; register ORRed with the flag's previous contents. This ensures that any
; pending interrupt will be serviced sooner or later.
;
                        txa
                        ora IEEE_INT0_flag                      ; Let IEEE_INT0_flag:=(old)IEEE_INT0_flag OR INT STATUS 0
                        and #int_mask0_value                    ; Mask out the INT0, INT1 & non-enabled bits in INT MASK 0
```

```
                        sta IEEE_INT0_flag                  ; Save the register interrupt bits in memory
                        tax
                        and #BI                             ; Was it BI ?
                        beq :not_BI
                        txa
                        and #(255 - BI)                     ; Clear the BI bit now that the BI handler is about to be entered
                        sta IEEE_INT0_flag                  ; Re-save the register interrupt bits in memory
                        IF DEBUGGING_FLAG
                        LDA #"I"                            ; ## Debugging only
                        STA &7CFF                           ; ## Debugging only
                        STA &7CFC                           ; ## Debugging only
                        FI
                        jsr BI_IRQ_handler                  ; Yes so handle it
                        ldx #0
                        bra service_IEEE_IRQ                ; Recurse with X=0 to service any remaining interrupt bits
:not_BI
                        txa
                        and #BO                             ; Was it BO ?
                        beq :not_BO
                        txa
                        and #(255 - BO)                     ; Clear the BO bit now that the BO handler is about to be entered
                        sta IEEE_INT0_flag                  ; Re-save the register interrupt bits in memory
                        IF DEBUGGING_FLAG
                        LDA #"O"                            ; ## Debugging only
                        STA &7CFF                           ; ## Debugging only
                        STA &7CFA                           ; ## Debugging only
                        FI
                        jsr BO_IRQ_handler                  ; Yes so handle it
                        ldx #0
                        bra service_IEEE_IRQ                ; Recurse with X=0 to service any remaining interrupt bits
:not_BO
                        txa
                        and #SPAS                           ; Was it SPAS ?
                        beq :not_SPAS
                        txa
                        and #(255 - SPAS)                   ; Clear the SPAS bit now the SPAS handler is about to be entered
                        sta IEEE_INT0_flag                  ; Re-save the register interrupt bits in memory
                        IF DEBUGGING_FLAG
                        LDA #"S"                            ; ## Debugging only
                        STA &7CFF                           ; ## Debugging only
                        STA &7CFB                           ; ## Debugging only
                        FI
                        lda IEEE_SPR_softcopy               ; Get the value of the SPR
                        and #%00010000                      ; Mask to clear all bits except the busy-bit
                        sta IEEE_serial_poll                ; Update IEEE SPR and softcopy
                        sta IEEE_SPR_softcopy
                        stz msg_or_number_flag              ; Clear the error message that set rsv from display
                        ldx #0
                        bra service_IEEE_IRQ                ; Recurse with X=0 to service any remaining interrupt bits
:not_SPAS
                        txa
                        and #RLC                            ; Was it RLC ?
                        beq :not_RLC
                        txa
                        and #(255 - RLC)                    ; Clear the RLC bit now that the RLC handler is about to be entered
                        sta IEEE_INT0_flag                  ; Re-save the register interrupt bits in memory
                        IF DEBUGGING_FLAG
                        LDA #"R"                            ; ## Debugging only
                        STA &7CFF                           ; ## Debugging only
                        STA &7CFE                           ; ## Debugging only
                        FI
                        jsr RLC_IRQ_handler                 ; Yes so handle it
                        ldx #0
                        bra service_IEEE_IRQ                ; Recurse with X=0 to service any remaining interrupt bits
:not_RLC
;
; Now, set up the "IEEE_INT1_flag" with the contents of the INT STATUS 1
; register ORRed with the flag's previous contents. This ensures that any
; pending interrupt will be serviced sooner or later.
;
:service_INT1_IRQs
                        lda IEEE_int_status1
                        ora IEEE_INT1_flag                  ; Let IEEE_INT1_flag:=(old)IEEE_INT1_flag OR INT STATUS 1
                        and #int_mask1_value                ; Mask out the non-enabled bits in INT MASK 1
                        sta IEEE_INT1_flag                  ; Save the register interrupt bits in memory
                        tax
                        and #DCAS                           ; Was it DCAS ?
                        beq :not_DCAS
                        txa
                        and #(255 - DCAS)                   ; Clear the DCAS bit now that the DCAS handler is about to be entered
                        sta IEEE_INT1_flag                  ; Re-save the register interrupt bits in memory
                        IF DEBUGGING_FLAG
                        LDA #"D"                            ; ## Debugging only
                        STA &7CFF                           ; ## Debugging only
                        STA &7CFD                           ; ## Debugging only
                        FI
                        jsr DCAS_IRQ_handler                ; Yes so handle it
                        lda #0
                        bra :service_INT1_IRQs              ; Recurse with A=0 to service any remaining interrupt bits in reg 1
:not_DCAS
                        txa
                        and #IFC                            ; Was it IFC ?
                        beq :not_IFC
                        txa
                        and #(255 - IFC)                    ; Clear the IFC bit now that the IFC handler is about to be entered
                        sta IEEE_INT1_flag                  ; Re-save the register interrupt bits in memory
                        IF DEBUGGING_FLAG
                        LDA #"F"                            ; ## Debugging only
                        STA &7CFF                           ; ## Debugging only
                        STA &7CF9                           ; ## Debugging only
                        FI
                        jmp IFC_IRQ_handler                 ; Yes so handle it
:not_IFC
                        rts                                 ; Return since all interrupts have been serviced
;
;-------------------------
;
; This subroutine handles the Interface Clear interrupt which is caused by
; the system controller sending the IFC command.
; The actions of this subroutine are as follows:
; (1)   Perform a software reset on the TMS9914
; (2)   Wait briefly
; (3)   Call the "initialise_IEEE488" subroutine to re-initialise the
;       TMS9914.
IFC_IRQ_handler         ENT
                        lda #128
```

```
                        sta IEEE_auxiliary_cmd                  ; Do the software reset
                        nop                                     ; Brief wait
                        nop
                        nop
                        jmp initialise_IEEE488                  ; Initialise the TMS9914
;
;-------------------------
;
; This subroutine handles the Device Clear interrupt.
; It is caused by the controller sending a Device Clear command on the
; bus.
; The Device Clear is implemented here to do 2 things, Wind down both DACs
; and Initiate a H/W reset.
; In Detail the procedure is as follows;
; (1)   Ensure 'swald' & 'hold' are deasserted since these could stop the
;       DACs being wound down.
; (2)   Switch ALL heaters OFF (H/W + LED flags)
; (3)   Set "selected_coil"=0 (for main coil DAC)
; (4)   Set flags (see below)
; (5)   Set "IEEE_DCAS_flag" =1 to indicate (internally) device clear is
;       in progress and the next task (see below for details) to be done.
; (6)   Call "auto_control_handler"
;       .
;       .       Thread of control through "goto_quiescent" using
;       .       "IEEE_DCAS_flag"
;       .
; (7)   Set "selected_coil"=1 (for shim coils DAC)
; (8)   Set flags (see below)
; (9)   Set "IEEE_DCAS_flag" =2 to indicate (internally) device clear is
;       in progress and the next task (see below for details) to be done.
; (10)  Call "auto_control_handler"
;       .
;       .       Thread of control through "goto_quiescent" using
;       .       "IEEE_DCAS_flag"
;       .
; (11)  Activate H/W reset
; Notes: (a)    These flags are set up as follows;
;               "mode_flag"=0,
;               "phase_flag"=2,
;               "phase_internal_flag"=0.
;               They are identical to those used in "KH_ctrl_manual" when
;               it does a MANUAL to AUTOMATIC change when the heater is
;               ON.
;               These flag setting cause "auto_control_handler" to assume
;               (falsely in this case) that the switch on the currently
;               selected coil is open and to close it using the standard
;               delays and to wind the DAC down to zero at the FAST rate
;               in NORMAL mode.
;               Fooling "auto_control_handler" like this allows ALL the
;               switches to be closed simultaneously with the standard
;               delays (before & after) and the DAC wound down without
;               writing extra code specially to do the job.
; Notes: (b)    The thread of control is maintained though the device
;               clear operation by re-entering this subroutine from
;               "goto_quiescent".
;               "goto_quiescent" is the last stage in the winding down of
;               the coil and is supervised by "auto_control_handler".
;               This behaviour in "goto_quiescent" and the behaviour when
;               this subroutine is entered is governed by the value of
;               "IEEE_DCAS_flag" as follows;
;                       This subroutine
;                       [0]     Enter this subroutine at stage (1)
;                       [1]     Enter this subroutine at stage (7)
;                       [2]     Enter this subroutine at stage (11)
;                       "goto_quiescent"
;                       [0]     Just RTS as normal
;                       [<>0]   Call this subroutine
;
DCAS_IRQ_handler        ENT
                        BLOCK
                        lda IEEE_DCAS_flag                      ; How far through the procedure are we ?
                        beq :enter_at_stage1
                        cmp #1
                        beq :enter_at_stage7
                        cmp #2
                        beq :enter_at_stage11
                        rts                                     ; This should never happen
:enter_at_stage1
; (1)
                        stz LF_swald_key                        ; Ensure 'swald' is deasserted
                        stz LF_hold_key                         ; Ensure 'hold' is deasserted
; (2)
                        stz LF_heater_Main                      ; Turn off the LED to indicate main coil heater is OFF
                        stz main_coil_htr_control               ; Turn the main coil heater relay OFF.
                        lda #0                                  ; Turn off all the shim heaters & their LEDs
                        ldx #10
:loop
                        jsr control_shim_htrs
                        dex
                        bne :loop
; (3)
                        stz selected_coil                       ; Set "selected_coil"=0 (for main coil DAC)
; (4)
                        jsr set_flags                           ; Set these flags up
; (5)
                        lda #1
                        sta IEEE_DCAS_flag                      ; Set this flag to mark the position across interrupt calls
; (6)
                        jmp auto_control_handler                ; Call this routine to wind the main coil DAC down
:enter_at_stage7
; (7)
                        ldx #1
                        stx selected_coil                       ; Set "selected_coil"=1 (for shim coils DAC)
; (8)
                        jsr set_flags                           ; Set these flags up
; (9)
                        lda #2
                        sta IEEE_DCAS_flag                      ; Set this flag to mark the position across interrupt calls
; (10)
                        jmp auto_control_handler                ; Call this routine to wind the shim coils DAC down
:enter_at_stage11
; (11)
                        lda #&FF
                        sta reset_activator
                        stz reset_activator                     ; Invoke the hardware reset (write a 1 followed by a 0)
                        rts                                     ; NB: This will probably never be executed!
```

```
;
;--------------------------
;
; This small subroutine set these flags up as follows for the DCAS routine
set_flags
                        BLOCK
                        stz mode_flag
                        lda #2
                        sta phase_flag
                        stz phase_internal_flag
                        rts
;
;--------------------------
;
; This subroutine handles the Remote/Local change interrupt.
; It is caused when a change from remote to local or vice versa takes
; place.
; When remote is selected the following are cleared;
; (a)   "msg_or_number_flag" -  So that the "input_buffer" is displayed
; (b)   "input_buffer" -        So the input display will appear blank
; (c)   "display_latch_OA_flag- So the latch display displays the
;                               currently selected latch.
; This subroutine is responsible for checking if 'manual' mode is in force
; and if so calling "KH_ctrl_manual" to force 'automatic control'.
; Note: If remote lockout(TPC) is in force this point should never be
;       reached.
; Note: The update of the "LF_local_key" & "LF_lockout" LEDs is done in
;       modules "MPLE" and "KHRT1".
; Note: 'manual' mode does not exist under IEEE control.
RLC_IRQ_handler
                        BLOCK
                        lda IEEE_address_status
                        bmi :now_remote
                        stz LF_lockout                          ; This is a remote to local change, so extinguish lockout LED in
                        rts                                     ;  case it was on (LLO) as gtl => local *without* remote-lockout
:now_remote
                        lda LF_manual_key                       ; Is the unit in the 'manual' or 'automatic' mode ?
                        beq :automatic_mode
                        jsr KH_ctrl_manual                      ; Manual mode so change to automatic
:automatic_mode
                        stz msg_or_number_flag                  ; Clear this flag
                        jsr clear_old_input_buffer              ; Clear the "input_buffer"
                        stz display_latch_OA_flag               ; Clear this flag
                        rts
;
;--------------------------
;
; This subroutine is responsible for servicing the BI interrupt which
; occurs when an incoming data byte from the IEEE bus is detected.
; When the byte arrives 4 possible states of affairs exist;
; (1)   The IEEE input termination character (any char < ASCII 32) has
;       been received.
;       The contents of the buffer are then processed
; (2)   The "IEEE_buffer_age_flag" is set which means that the data
;       currently in the "IEEE_buffer" is old (ie. already used) and must
;       be cleared before any new data is entered.
;       After clearing the byte is entered at position 0
; (3)   The "IEEE_buffer" is full so the character received cannot be
;       entered.
;       This is interpreted as the "command not recognised" error (bit 0
;       of SPR).
; (4)   There are already some bytes in the buffer, "IEEE_buffer_age_flag"
;       is not set and the buffer is not full.
;       Therefore the byte is entered at the next empty
;       position.
BI_IRQ_handler
                        BLOCK
                        lda IEEE_data_in                        ; Get the byte which just arrived
                        cmp #32                                 ; Is this a terminating control character ?
                        bcs :continue
; (1)
                        ldx #&FF
                        stx IEEE_buffer_age_flag                ; Set this flag since buffer is about to be processed & is now 'old'
                        lsr display_latch_OA_flag               ; Zero this flag (in 2 goes) since "TEMP_COIL=" is only temporary
                        lsr display_latch_OA_flag               ; This (ie. the 2) is necessary since the flag must remain non-zero
                        lsr display_latch_OA_flag               ;   after BOTH the "TEMP_COIL=" & "LATCH?" commands if the
                        lsr display_latch_OA_flag               ;   temporarily selected coil's latch value is to be read
                        jmp process_IEEE_buffer                 ; Process the data in the "IEEE_buffer"
:continue
; (2)
                        ldx IEEE_buffer_age_flag                ; Is the data in the "IEEE_buffer" old (ie. already used) ?
                        beq :not_old
                        stz IEEE_buffer_data_ptr                ; Yes, so zero the data pointer so next ch will be entered at pos. 0
                        stz IEEE_buffer_age_flag                ; Clear this flag since the cleared buffer is now 'fresh'
:not_old
; (3)
                        ldx IEEE_buffer_data_ptr
                        cpx IEEE_buffer_size                    ; Is the buffer already full ?
                        bcc :not_full
                        ldx #&FF                                ; Yes, so set the "IEEE_buffer_age_flag" since the data is useless
                        stx IEEE_buffer_age_flag

                        brk                                     ; Flag an error since this should not happen
                        DFB     21                              ; Error number
                        ASC     "IBO"                           ; "Ieee Buffer Overflow" error
                        DFB     0

                        lda #%01000001                          ; Code to set "command not recognised" bit(0) & rsv bit in IEEE SPR
                        jmp set_IEEE_SPR_bits                   ; Update SPR
:not_full
; (4)
                        cmp #"a"                                ; Force any lower case characters to uppercase to ease checking
                        bcc :not_LC_char
                        cmp #"z"+1
                        bcs :not_LC_char
                        and #&DF
:not_LC_char
                        sta IEEE_buffer,X                       ; Store the byte at the next free position in the "IEEE_buffer"
                        inx
                        stx IEEE_buffer_data_ptr                ; Increment the data pointer to point to the next position
                        rts
;
;--------------------------
;
; This subroutine parses and processes the data in the "IEEE_buffer".
; There are 3 groups of commands that the instrument understands - they
```

```
; are listed below together with a brief description;
; ** GROUP (a) –        –– Singular Commands ––
;                       These commands have no data appended to them and
;                       require no response on the bus from the unit.
; (1a)  SHUTDOWN –              Causes all magnet coils to be wound down
; (2a)  CLEAR_NVM –             Clears the Non–Volatile memory in the unit
; (3a)  SWITCH_HOLD_ON –        Asserts the 'switch–hold' function
; (4a)  SWITCH_HOLD_OFF –       De–asserts the 'switch–hold' function
; (5a)  HOLD_ON –               Asserts the 'hold' function
; (6a)  HOLD_OFF –              De–asserts the 'hold' function
;
; ** GROUP (b) –        –– Singular commands with a variable suffix ––
;                       These commands have a data field appended to them
;                       and do not require a response on the bus from
;                       the unit.
; (1b)  COIL=<x> –              Selects a coil in the unit, 0 <= x <= 10
; (2b)  TEMP_COIL=<x> –         Temporarily causes the latch for this coil
;                               to be displayed (instead of for the
;                               currently selected coil) until 2 new IEEE
;                               commands are received.
; (3b)  CURRENT=<f> –           Instructs the unit to go to the specified
;                               (floating point number [amps]) current.
; (4b)  START_CURRENT=<fp> –    Programs the specified start (floating
;                               point number [amps]) current for a sweep
;                               operation.
; (5b)  STOP_CURRENT=<fp> –     Programs the specified stop (floating
;                               point number [amps]) current for a sweep
;                               operation.
; (6b)  SWEEP_TIME=<fp> –       Programs the specified sweep time
;                               (floating point number [seconds]) for a
;                               sweep operation and starts the sweep.
;
; ** GROUP (c)          –– Interrogative Commands ––
;                       These commands have no data field and do not
;                       program any action but request a response over the
;                       bus from the instrument.
;                       They all end in a query character (?) to signify
;                       this.
; (1c)  SWITCH_HOLD? –          Inquires if 'switch–hold' is asserted for
;                               the current coil.
;                               Possible responses:– "TRUE" or "FALSE"
; (2c)  HOLD? –                 Inquires if 'hold' is asserted for the
;                               current coil.
;                               Possible responses:– "TRUE" or "FALSE"
; (3c)  CYCLE_PHASE? –          Inquires which cycle phase the unit is
;                               currently in.
;                               Possible responses:– "1","2","3","4" or
;                               "0" if dormant.
; (4c)  COIL? –                 Inquires which coil is currently selected
;                               Possible responses:– "0","1" thru. "10"
; (5c)  HEATER? –               Inquires if the heater for the currently
;                               selected coil is on.
;                               possible responses:– "TRUE" or "FALSE"
; (6c)  MODE? –                 Inquires which mode the unit is in
;                               Possible responses:– "NORMAL" or "SWEEP"
; (7c)  DAC? –                  Requests the unit to return a
;                               floating–point number string [amps] of the
;                               current in the DAC (ie. power supply)
;                               for the currently selected coil.
; (8c)  LATCH? –                Requests the unit to return a
;                               floating–point number string [amps] of the
;                               current in the latch (ie. energised coil)
;                               for the currently selected coil or
;                               temporarily selected coil (ie. using the
;                               "TEMP_COIL=" command above).
; (9c)  VERSION? –              Requests the unit to return the
;                               version number/assembly date string for
;                               the software.
; (10c) LAST_MESSAGE? –         Requests the unit to return the last
;                               informational or error message.
;
; The following section defines the IEEE command look up table.
; All device dependant character string commands the unit understands are
; in this table.
; The format of the tables is as follows;
;       The table starts at address "IEEE_command_table" and is
;       terminated by the last character in each string having its top bit
;       set.
;       Each entry in the table is formed as shown;
;       <command–string–to–lookup> Note: The top bit of the last byte is
;                                         set using the DC data directive.
;       LSB of handler routine for the command
;       MSB of handler routine for the command
IEEE_command_table      ENT
        DC      "SHUTDOWN"                                      ; (1a)
        DW      shutdown_confirmed
        DC      "CLEAR_NVM"                                     ; (2a)
        DW      clear_NVM_confirmed
        DC      "SWITCH_HOLD_ON"                                ; (3a)
        DW      turn_swald_on
        DC      "SWITCH_HOLD_OFF"                               ; (4a)
        DW      turn_swald_off
        DC      "HOLD_ON"                                       ; (5a)
        DW      turn_hold_on
        DC      "HOLD_OFF"                                      ; (6a)
        DW      turn_hold_off
        DC      "COIL="                                         ; (1b)
        DW      set_coil
        DC      "TEMP_COIL="                                    ; (2b)
        DW      set_temp_coil
        DC      "CURRENT="                                      ; (3b)
        DW      set_I
        DC      "START_CURRENT="                                ; (4b)
        DW      set_start_I
        DC      "STOP_CURRENT="                                 ; (5b)
        DW      set_stop_I
        DC      "SWEEP_TIME="                                   ; (6b)
        DW      set_sweep_time
        DC      "SWITCH_HOLD?"                                  ; (1c)
        DW      query_swald
        DC      "HOLD?"                                         ; (2c)
        DW      query_hold
        DC      "CYCLE_PHASE?"                                  ; (3c)
        DW      query_cycle_phase
        DC      "COIL?"                                         ; (4c)
        DW      query_coil
```

```
        DC      “HEATER?”                               ; (5c)
        DW      query_heater
        DC      “MODE?”                                 ; (6c)
        DW      query_mode
        DC      “DAC?”                                  ; (7c)
        DW      query_DAC
        DC      “LATCH?”                                ; (8c)
        DW      query_latch
        DC      “VERSION?”                              ; (9c)
        DW      query_version
        DC      “LAST_MESSAGE?”                         ; (10c)
        DW      query_last_message
        DFB     0                                       ; Zero <NUL> byte to terminate command lookup table
;
process_IEEE_buffer
                        BLOCK
                        ldx #>IEEE_command_table        ; Set up a pointer to the start of the command table
                        ldy #<IEEE_command_table
                        stx general_purpose_ptr1_I + 0
                        sty general_purpose_ptr1_I + 1
                        ldx #0                          ; Counter through “IEEE_buffer”
                        ldy #0                          ; Counter (LSB) through “IEEE_command_table”
:loop_main
                        lda (general_purpose_ptr1_I),Y
                        beq :end_of_table
                        pha                             ; Temp store for data byte from command lookup table
                        and #%01111111                  ; Mask out top bit since this indicates the last character in a word
                        cmp IEEE_buffer,X
                        bne :goto_next_entry            ; If bytes did not match go to start of next entry
                        pla                             ; Bytes matched but is this the end of the entry ?
                        bmi :end_of_entry               ; If this branch is taken the the command is found
                        inx                             ; Increment the X to next location in “IEEE_buffer”
                        cpx IEEE_buffer_data_ptr        ; Is this end of the data in the “IEEE_buffer” ?
                        beq :goto_next_entry2           ; If so, data in “IEEE_buffer” was too short, so goto next entry
                        jsr increment_Y                 ; Increment the Y to next location in “IEEE_command_table”
                        bra :loop_main
:goto_next_entry
                        pla                             ; Restore stack-pointer
:goto_next_entry2
;
; This section of code locates the beginning of the next entry in the look
; up table
;
:loop2
                        lda (general_purpose_ptr1_I),Y  ; First find the end of the current entry
                        bmi :end_of_current_entry
                        jsr increment_Y
                        bra :loop2
:end_of_current_entry
                        ldx #2                          ; End of current entry found, increment 3 bytes to start of next one
:loop_3
                        jsr increment_Y
                        dex
                        bpl :loop_3
                        ldx #0                          ; Start comparing again at beginning of “IEEE_buffer”
                        bra :loop_main                  ; Pointer => start of next entry in table, so go back to main loop

:end_of_entry
;
; This section of code is entered when the string in “IEEE_buffer” matched
; the current command in the lookup table.
; On Entry:     X is the offset to the last character of the command in
;               the “IEEE_buffer”
;               “(general_purpose_ptr1_I),Y” points to the last character
;               of the command entry in the lookup table.
;
                        jsr increment_Y                 ; Increment pointer to LSB of jump address in lookup table
                        lda (general_purpose_ptr1_I),Y  ; Get LSB of jump address from lookup table for command found
                        pha
                        jsr increment_Y                 ; Increment pointer to MSB of jump address in lookup table
                        lda (general_purpose_ptr1_I),Y  ; Get MSB of jump address from lookup table for command found
                        sta general_purpose_ptr1_I + 1  ; Setup MSB of indirect jump address
                        pla
                        sta general_purpose_ptr1_I + 0  ; Setup LSB of indirect jump address
                        inx                             ; Increment X so offset is to command’s data argument (if any)
                        jmp (general_purpose_ptr1_I)    ; Jump to the handler routine
:end_of_table
;
; This code is executed when the end of table (<NUL> byte) is detected.
; This means that the command received over the IEEE bus was not
; recognised.
; The response of the unit is to Set the “command not recognised” bit(0) &
; rsv bit in IEEE SPR and flag an error in the normal way.
;
                        brk                             ; Flag an error since this should not happen
                        DFB     22                      ; Error number
                        ASC     “CNR”                   ; “Command Not Recognised” error
                        DFB     0

                        lda #%01000001                  ; Code to set “command not recognised” bit(0) & rsv bit in IEEE SPR
                        jmp set_IEEE_SPR_bits           ; Update SPR
;
;-------------------------
;
; This small subroutine increments the pointer through the
; “IEEE_lookup_table”.
; If incrementing the Y causes it to wrap around to 0
; the MSB of “general_purpose_ptr1_I” is increased by 1 unit.
increment_Y
                        BLOCK
                        iny
                        beq :inc_MSB_of_ptr
                        rts
:inc_MSB_of_ptr
                        inc general_purpose_ptr1_I + 1  ; Increment the MSB of this pointer
                        rts
                        END
```

Glossary of Computing/Electronics Terms

A

Application Workspace

- Under RISC OS, the main memory area, reserved for user applications, eg. text editors/DTP packages etc.

ARM Procedure Call Standard

- Describes how the CPU's registers/ the stack etc. must be presented when a subroutine (procedure) is called. Ensures a procedure written in one compiled language may call one written in another.

Assembly Language

- A low level computer language in which there is a one-to-one correspondence between a machine code instruction and its assembler representation.

B

Batch Job

- A means of running a job on a multi-user computer away from a terminal. Input data/commands are read from a command file and the output goes to a log file. Ideal for processing large data analysis jobs.

C

Chip-Enable

- Logic signal sent to a chip to make it accessible to the CPU/etc.

CISC

- Complex Instruction Set Computer: A CPU architecture in which speedy operation relies on providing special instructions for most kinds of data manipulation. c.f. RISC.

Context-Switching

- A simple form of multitasking.

Cooperative Scheduling

- A simple form of computer scheduling. It relies on each task voluntarily handing back control to the machine after doing some work. c.f. preemptive scheduling.

D

DRAMs

- Dynamic Random Access Memory: A low cost/high capacity form of memory used in computers for main memory. It is based on capacitor-charge technology and requires periodically ‘refreshing’.

E

Escaping

- Modify the function of a particular code to indicate the code(s) which follow are to be interpreted differently. Eg. In a text-only medium set aside the ASCII code for “A” to indicate the two codes which follow represent an arbitrary hexadecimal number instead of a text character, “A03” then translates to the hexadecimal control code 3. It provides a means for transmitting any ASCII code (0−255) over a text-only medium.

Ethernet

- A high speed RF/serial link and protocol for computer networking.

Exceptions

- An efficient method for handling errors generated by programs within an operating system.

H

Hangs

- A computer which has completely seized up due to a fault condition the OS was not designed to cope with. It will not respond to any input and usually needs to be completely reset or power-cycled.

Hardware Vector

- Memory location in a CPU's memory map to which the thread of control passes under certain pre-defined hardware conditions, eg. reset, interrupt. The locations are fixed by the CPU's manufacturer and cannot be changed.

High Level Language

- A computer language in which instructions for addition/ subtraction/multiplication etc. etc. exist in a simple easy-to-understand form. They bear little resemblance to the machine code instructions to which they will ultimately be translated by the computer. c.f. a low level language such as assembler. Examples are; FORTRAN, C, Basic and Pascal.

I

Interpreter

- A computer program which executes the users' program on a line-by-line basis. c.f. a compiler which converts the users' program to machine code in its entirety, the resultant machine code 'executable image' being run later. The most commonly used interpreted language is BASIC.

IRQ-Veneer

- Part of the Acorn RISC OS C package. It is responsible for switching between the ARM's SVC and IRQ modes during interrupt handling in C coded relocatable modules.

L

Link Register

- Register R14 in the ARM architecture. It is used instead of external stack memory, for speed, during subroutine calls to hold the to-be-returned-to memory address.

Logical Memory

- Under the RISC OS architecture it refers to RAM memory, access to which is mediated by the MEMC memory controller chip. This makes the RAM memory map effectively fluid under the control of the OS and is used for context switching in the multitasking windowing environment.

Logical Names

- Under the OpenVMS operating system Logical Names can be defined and used to refer to certain objects such as files. A simple form of inter-process communication is enabled by translating a logical name in one process which was defined in

another.

M

Make Facility

- A application originally provided on Unix but now available under RISC OS and many other OSs. It automates re-compiling/linking etc. of executable programs from their source code.

Microcode

- A code interpreter contained within a CISC CPU which actually executes the CPU's instructions. It is responsible for a significant proportion of the time taken by such a CPU to execute programs.

MIPS

- Millions of Instructions executed Per Second. A crude measure of a CPU's performance.

Multi-Tasking

- An arrangement in which a computer's OS gives the impression of running several programs or tasks at once by rapidly slicing up and allocating chunks of the CPU's time between them.

N

NFS

- Network File System: An Internet program/OS addition which allows one computer to remote mount another's file system and treat the files on it as though they were held locally.

O

Object Code

- A code intermediate between source code and machine code. It is produced by a compiler or in some cases an assembler. A linker is then required to fill-in any unresolved addresses etc. to produce the machine code the computer will actually execute.

Offline

- Not currently in communication with the computer. eg. A printer not available to a computer for printing or a machine being used for data analysis which is not currently connected to the data taking machine.

OS-Vectors

- Entities provided by an OS such as RISC OS to which code may be attached such that the code is executed under certain conditions or at certain times. eg. code attached to a timer interrupt OS-vector will be executed periodically at a fixed interval, when the timer times out.

P

Packet

- A discrete chunk of data, usually comprising a header (which incorporates a checksum for data integrity) and the actual data. Typically used for sending data over a network connection.

Paged In

- Relates to the situation where one or more logical or virtual memory addresses can be made to appear at (ie. be mapped to) corresponding

physical address locations. If a particular logical/virtual address{-range} is mapped to the relevant physical addresses those addresses are said to be paged-in.

Pages

- For the purposes of multitasking/ scheduling the logical or virtual memory address space is divided up into chunks of the same size. These chunks are referred to as pages. Typical sizes are; on DEC VAX 512bytes and Acorn A440 32Kbytes.

Pipe-Lining

- A parallelising technique for speeding the operation of CPUs. While one instruction is being executed future instructions are being decoded or read-in to the CPUs registers.

Preemptive Scheduling

- A scheduling system in which the OS enforces the time each task/ process is permitted to use the CPU for. At the end of the processes' ‘quantum’ the scheduler interrupts it and transfers the CPU to execute another task/process. c.f. cooperative scheduling.

Process

- The basic unit under which multiuser OS's such as VMS and Unix are used. ie. A logged-in user exists on the system as a process.

Program Counter

- The register inside a CPU which contains the memory address of the currently executing instruction.

Programmers Model

- A model of a CPU etc.'s registers and hardware components from the point of view of a programmer.

R

Refresh

- See DRAMs

Registers

- Memory cells inside a CPU or other microprocessor support chip.

Relocatable Module

- Acorn RISC OS term: A specially written machine code program which resides in a memory area reserved for the purpose. It interfaces with the OS and is intended to provide extensions to the OS. For flexibility much of the OS outside the kernel is coded as RMs. Typical applications for an RM are the BASIC interpreter and an Ethernet packet driver.

RISC

- Reduced Instruction Set Computer: A CPU architecture in which speedy operation relies on a small but highly optimised set of instructions. Operations which are less common and therefore have no instruction to execute them are still rapidly carried out using a combination of the fast lower level instructions. c.f. CISC.

Rlogin

− Remote Login: An Internet protocol enabling remote interactive login to a multiuser system. By default a username/ User-ID and password are not required or prompted for. See also Telnet.

Run Time Library

− A machine code library of subroutines for executable programs to call − that is they are called from within the program at run time as opposed to being incorporated during linking.

S

SCSI

− Small Computer Systems Interface. A fast parallel bus interface standard and protocol enabling computers large and small to be connected to peripheral devices. Typical devices are hard disk drives and optical scanners.

Serial Line/Port

− A two-wire + handshake lines system for connecting computers to other computers/printers etc. It is a slow connection but almost all computers possess one.

Sideways RAM

− Acorn BBC Model computer term: To augment the 64Kbytes directly addressable memory available on the 65C02 processor, a system in which the top-but-one memory quadrant can be mapped to one of up to 16 × 16K RAMs (or ROMS) was developed. With the main memory map traditionally represented vertically the 16 × 16K memories were represented horizontally − ie. sideways.

Stack

− A region of memory reserved for a CPU to use as scratch space, on a first-in last-out sequential basis. A common use is to hold the program counter during subroutine calls in the CISC architecture.

SWI

− SoftWare Interrupt: An instruction on the ARM processor. Executing it causes the program's thread of control to pass though the ARM's SWI hardware vector to code within the OS. That code identifies the service required by the program from the OS via the contents of the ARMs registers and forwards the thread of control to the relevant part of the OS or relocatable module which provides the service before returning control to the program which executed the SWI.

SYS

− The RISC OS BASIC interpreter's software interface to the ARM's SWI instruction.

System Clock

− An oscillator which drives the CPU and is responsible for all timing in the computer/micro-processor system.

System Variable

− RISC OS term: It is analogous to an OpenVMS *logical name*.

T

Tar

− Tape ARchive. The Unix OS's program for backing up discs to tape. The Tar format describes the flattened disc directory structure and file headers format as they appear in the byte stream which is written to the tape.

Task

− The entity in which a program is run in a multitasking environment.

TCP/IP

− Transmission Control Protocol/ Internet Protocol. The protocol used for many Internet applications. Eg. Telnet.

Telnet

− An Internet protocol enabling remote interactive login to a multiuser system. A Username/ User-ID and password is usually required. See also Rlogin.

Thread

− The path of control running though a program executing in a task. A multitasking environment can be said to be multi-threaded.

U

Usenet

− The Internet News distribution system.

User Port

− An 8-bit parallel I/O port provided on Acorn machines.

V

VLSI

− Very Large Scale Integration. A chip with a very large number of transistors on it. A typical example is a CPU.

VMS Process

− See Process.

W

WIMP

− Windows Icons Mouse and Pointer: The Windowing/desktop computer user-interface provided by/under RISC OS, Microsoft Windows, the X-Window System etc.

Workstation

− A fast multiuser desktop based computer with a large high definition monitor intended to be used mainly by a single user working at the machine in the WIMP environment (usually the X-window System) provided. Many interactive terminal etc. sessions can be run simultaneously in the WIMP display.

X

The X-Window System

− A WIMP system typically found on workstations running Unix, OpenVMS etc. Dedicated 'X-terminals' also permit a user to access a remote Unix, OpenVMS etc. machine via the X-Window interface. The X-Terminal is responsible for running the display on its monitor but the applications executing under it run on the remote machine.

Glossary of Physics Terms

1

10/3 Effect

- The ten-thirds effect. For very fast spin motion (extreme narrowing regime) $\omega_0\tau_c \ll 1$, $1/T_1 = 1/T_2 = (10/3)\, m_2\tau_c$. Compare equation 2.2.17 in the $\omega_0\tau_c \ll 1$ regime [where $J_0(0) \sim J_1(\omega_0) \sim J_1(2\omega_0)$] with it in the motional narrowing regime, $\omega_0\tau_c > 1$ [where $J_1(\omega_0) \sim J_1(2\omega_0) \sim 0$].

9

90° & 180° Pulses

- Pulse sequences to rotate the longitudinal and transverse magnetisations in the rotating frame by those angles. See §2.1 for application.

A

Adatom

- An adsorbed gas atom.

Adsorption

- Gas atoms adhering to a solid surface due to the nett attractive potential of that surface. See page 1.

Adiabatic Relaxation Processes

- Magnetic relaxation processes involving no exchange of energy with another system. There are no nett spin-flips. E.g. the first term of equation 2.2.17.

Aldrich Powder

- A fluorocarbon polymer having an irregular structure. Manufacturer: Aldrich Chemical Co.

Annealing

- In the context of adsorbed systems, the sample chamber is heated until the sample desorbs and is then slowly cooled to ensure uniform re-adsorption occurs.

Arrhenius/Activation Law

- $\exp(-E_a/kT)$ Boltzmann law describing behaviour of systems such as those with thermally activated vacancy tunnelling.

Augmentation Factor Model

- Model explaining $T_{1,2} \propto X$ experimental law. Briefly, a small adsorbed solid component relaxes a larger fluid component incapable of self-relaxation. See §7.2.1/ $0.1 \leqslant X \leqslant 0.3$ on page 117.

B

Basal Planes

- The main exposed hexagonal adsorption surface on BN. c.f. Edge Sites.

BET Model

- A simple model for an adsorption isotherm. See §7.5.

Binding Energy

- Characteristic energy associated with an adsorbate+adsorber pair for the binding of the adatoms to the substrate.

Broadening [(In-)Homogeneous]

− A number of mechanisms exist which contribute to the width of an NMR line. Some are; dipole-dipole†, inhomogeneous applied magnetic field‡, quadrupole effects‡. They can be classified as homogeneous† or inhomogeneous‡ mechanisms. A homogeneous mechanism contributes equally to all part of the line. For an inhomogeneous one, the various parts of the line can potentially be attributed to different 'parts' of the mechanism, eg. the profile of an applied magnetic field and the shape of the line. Techniques such as spin-echoes can be used to eliminate an inhomogeneous contribution to relaxation.

C

C−IC Region

− Commensurate−Incommensurate solid transition region of the phase diagram.

Chapter 8 Combined Dataset Names

- *ALL* − All 4.5MHz temperature dependence $T_{1,2}$ data (ie. up-sweep & down-sweep datasets).
- *ALL_1100* − The *ALL* dataset plus the 1.1K $T_{1,2}$ frequency dependence data.
- *EVERYTHING* − Every $T_{1,2}$ dataset taken at that coverage.

Chapter 8 Data Fitting Models Names

− See §8.3 and listings 8.3.1 & 8.3.2 for details.

- Test purposes only: 0,2,3,5.
- Temperature+Frequency: 5B,5B_2D,5B_11B,5B_WQ2_11-B,5B_WQ2; 6,6_2D,6_11B; 7,7_2D,7_11B; 8,8_2D,8_11B; 9; 10,10_2D,10_11B,10_WQ2_11B,-10_WQ2; 11.
- Frequency Only: F, F_11B, F_2D,F_2D_11B.

Correlation Functions (dipolar)

− Autocorrelation functions of the dipolar Hamiltonian describing the effects of motion on the dipolar interaction. See §2.2.

Coupled Relaxation

− System containing two different spin species where the recovery of the magnetisations are governed by two coupled first-order differential equations. eg. ^{11}B/^{3}He & ^{19}F/^{3}He. See §8.1.

Coverage

− Fraction of a complete layer (monolayer).

CP Relaxation

− Labelled 'Carr-Purcell' relaxation. A fit designed to deal with spin-echo relaxation which has an additional $\exp(-t^3)$ component due to unbounded diffusion in a field gradient. The fit is to $h(t)=h(0)\exp(-t/T_2 - Ct^3)$. See also $\mathrm{Exp}(-t^3)$ Law and Listing 6.3.2.1.

Critical Point

− A critical point on the phase diagram of a critical model. Eg. the temperature above which a bulk gas will not condense or the temperature at which a registered film disorders.

CW NMR

− Continuous Wave NMR. The

sample is irradiated continuously with a low-level RF magnetic field, in contrast with Pulse NMR where brief pulses of high intensity RF magnetic fields are used.

D

Debye Model

- A simple thermodynamic model of a solid.

Desorption

- Opposite of Adsorption. Adsorbed spins will detach from the adsorbing surface and return to the surrounding gas at a temperature sufficiently high to overcome the substrate binding energy.

Dimensional Incompatibility

- Mismatch between the lattice parameters of a localised adsorbed film and those of the underlying substrate mesh.

Dipole−Dipole (Dipolar) Relaxation

- Spin relaxation mechanism involving only nuclear dipole moments. In an ideal NMR system this is the only mechanism. Some non-dipolar mechanisms encountered are due to Grafoil local field and PMIs.

Dirty Wall Relaxation

- See PMI/2D Gas Relaxation.

DLX6000 Microspheres

- A solid lubricant material consisting of 0.2μm diameter spherical beads of a fluorocarbon polymer. Manufacturer: E.I. Dupont DeNemours and Co. See also Aldrich Powder.

Domain Wall Phase(s)

- 2D solid phase(s) formed when mutually incompatible registered patches (domains) meet one another. 'Walls' of adatoms of varying topology and thickness result. See figure1.8.3.1 as a visual aid.

Double Resonance experiment

- Experiment on system with coupled magnetic relaxation (see also FMR) in which one spin system is perturbed while the other is monitored.

$(Dt)^{½}$ Law

- Spin-diffusion limited magnetisation recovery law for bulk insulating materials.

DWL

- Domain Wall Liquid. 2D phase formed by melting of (Solid) Domain Wall Phases. The walls of the mutually incompatible registered domains are deemed to move. See also Domain Wall phase and figure 7.2.2.39.

E

Edge Sites & Edge Film

- BN crystallites possess a distinct higher-binding-energy edge area to which gas atoms preferentially adsorb, forming the Edge Film. c.f. basal planes.

EFG

- Electric Field Gradient. An EFG '*eq*' exists at all crystalline/ molecular sites with less than cubic symmetry.

Exchange

- Quantum mechanical form of motion in which spins exchange places in spin-space.

Exp($-t^3$) Law

- Spin-Echo relaxation law due to unbounded diffusion of spins in a static magnetic field gradient, G. Relaxation $\propto \exp(-D\gamma^2G^2t^3/12)$.

F

Fictitious Spin−½ Formalism

- Useful method for treating other splitting mechanisms (eg. electric quadrupolar) as if they were the Zeeman splitting of a spin−½ species.

FID

- Free Induction Decay. The precessing magnetisation signal observed after a 90º pulse in a pulsed NMR experiment.

FMR Effect

- Due to Friedman, Millet and Richardson. Coupled magnetic relaxation between nuclear spins in a substrate and a quantum adsorbate. eg. $^{19}F + {}^{3}He$. See §3.5.

G

Grafoil

- A commercially produced form of exfoliated graphite. Exfoliated graphite has been chemically treated to expand apart its layers which exposes them, yielding a much larger basal plane area for adsorption.

Grafoil Local Fields

- Strong anisotropic diamagnetic fields produced by Grafoil platelets.

Gruneisen Ratio/Constant

- In the context of exchange modulated solid helium−3 systems it refers to $\mathrm{d}\,ln(J)/\mathrm{d}\,ln(X)$ and should be the same for all substrates, providing exchange frequency depends only on density.

H

Henry's Law

- Physical chemistry law describing amount of dissolved gas in a liquid being proportional to the partial pressure of that gas above the liquid in a closed equilibrium system. Generalised in adsorbed systems to an adsorption isotherm displaying a linear relation.

Heterogeneity (of substrate)

- Imperfections in the exposed adsorbing surface. Typically such regions have a higher binding energy and adatoms will preferentially be adsorbed there as a dense solid.

Heteronuclear Dipolar Interaction

- Dipolar interaction between spins of different species.

Heteronuclear 'T_2'

- Time constant/relaxation process describing the relaxation/ dephasing of the spins of one species by the dipole local fields of those of another. See equation 8.26.

Hole Burning

- Description of the effect of saturation by an intense applied RF field on an inhomogeneously broadened NMR line − The line literally appears to have a 'hole' burned into it.

Homonuclear Dipolar Interaction

- Dipolar interaction between spins of the same species.

I

Incommensurate (solid) Phase

- Phase in which the film's adatoms are not aligned with those of the substrate. See also Registered Phase.

Index of Relaxation

- A quantitative measure of the degree of non-exponentiality of a relaxation process. Writing, $h(t)=h(0)\exp(-t^i/T_2)$, 'i' is the *index* of relaxation. $i<1$ is sub-exponential relaxation, $i>1$ is super-exponential relaxation and $i=1$ signifies exponential relaxation. See also Super−/Sub− Exponential relaxation.

Isotherm (adsorption)

- A plot of gas pressure measured over an adsorber/substrate *against* the quantity of gas added, performed at constant temperature. An important use is to locate the monolayer coverage.

Isotropic Fluid

- A fluid having no internal structure. c.f. the hexatic fluid of the KTHNY theory.

IVC & OVC

- Inner Vacuum Can and Outer Vacuum Can. See figure 4.1.1.1.

K

KTHNY

- Due to Kosterlitz, Thouless, Halperin, Nelson and Young. A theory of melting in 2 dimensions. (Kosterlitz−Thouless theory).

L

Larmor Frequency

- Frequency of precessing magnetic moments in a magnetic field. $\omega_0=\gamma B_0$.

Lattice

- A generic NMR term, it describes all the non-spin degrees of freedom in the system. For historical reasons (NMR in solids where the motion = lattice vibrations) is is known as the *lattice*.

Lattice Gas

- Adsorbed system in which the adatoms are in a regular arrangement w.r.t. the substrate. eg. a registered phase.

Lattice Ordering Transition

- Critical model transition in which

an ordered lattice (eg. a registered film) is thermally disordered to leave an isotropic fluid.

Linear Programming (LP)

- Regression technique suited to systems where there is a high degree of non-uniqueness in the model fit. See §6.4.

Litz Wire

- Wire composed of a number of strands of enamelled wire twisted together to reduce the skin-effect. At radio frequencies the lower effective resistance permits higher *Q* tank circuits to be fabricated.

Logarithmic Divergence

- The excess low frequency motional component inherent in low dimensional systems results in a low frequency logarithmic divergence in the reduced dipolar spectral density function $j_0(\omega)$. c.f. 3D systems where the $J_n(\omega)$ are frequency independent at low ω. See §2.2 for details.

LRPOA & LRPOP

- Long Range Positional Order Absent and Long Range Positional Order Present: Terms coined to describe proposed phases in the intermediate coverage region of the ^{3}He/BN phase diagram in analogy with the KTHNY theory. LRPOP refers to the low temperature phase where long range positional order is proposed to exist amongst the registered spins and is imposed by the substrate. At intermediate temperatures that phase is proposed to to lose its long range positional order to be replaced by a 'registered fluid' where a ^{3}He spin has an enhanced probability of being found in a registered position and in analogy with KTHNY's hexatic phase is proposed to still possess 'bond' orientational order. A suggestion is made that this proposed phase may be the same as the 'commensurate with vacancies' phase proposed by another author **[32]**. See also figure 7.6.2.

M

Monolayer

- The first complete layer of adsorbate. There are several prescriptions for defining precisely where the first layer is deemed to be complete. This work uses maximum-first-layer-density as the monolayer definition. Within the course coverage grid used this is where the 1.1K T_2 minimum in coverage occurs and is also where the point-B isotherm point is. Note: Most of the Grafoil work encountered in the literature uses the onset-of-second-layer-promotion as the definition of monolayer.

Motional Narrowing

- Motional narrowing of the NMR line from its broad rigid lattice value occurs because the spins 'see' only an average of their neighbour's dipole fields (which give the line its width) during the Larmor period.

N

New growth Solid

- Localised ^{3}He spins which appear on the basal planes of BN at coverages $\gg$ the 5% edge-film.

They are believed to consist of registered spins in the $\sqrt{3} \times \sqrt{3}$ R30 configuration.

NLLSQ

− Non Linear Least SQuares fitting. An algorithm for determining the best fit to a mathematical model which is non-linear in its adjustable parameters. Also the name of a FORTRAN program developed for this work. See §6.3.1.

NLLSQ_MODEL

− Name of the Non-linear least squares fitting program developed to fit the experimental data to the Chapter 8 data fitting models.

'Noise' & 'Noisy' behaviour

− Special term coined to describe the erratic behaviour of the ^{3}He/BN temperature dependence data where 'Sub-region Behaviour' trends vary more often than every two points.

NQR

− Nuclear Quadrupole Resonance. It is similar to NMR except the splittings of the nuclear energy levels are produced by the interaction of a crystalline/ molecular EFG with a nuclear quadrupole moment.

O

Order−Disorder (O−D) Transition

− See Lattice Ordering Transition.

Orientational Order.

− A residual form of order left in a localised adsorbed film after positional order has been lost. It features in the KTHNY theory.

P

Preferential Sites

− Adsorption sites with a higher binding energy where adatoms will preferentially be adsorbed. See also Edge−Sites & Heterogeneity.

PMIs

PMI/Fluid Relaxation

PMI/2D Gas Relaxation

− ParaMagnetic Impurities. Electron paramagnetic impurities such as Iron embedded in the substrate or sample chamber walls can produce a strong unwanted source of relaxation due to their large (typically 1000× a nuclear moment) electronic moments. In particular fast moving adsorbed Fluid or 3D Gas ^{3}He spins are strongly relaxed. See also Dirty Wall Relaxation.

Point A Isotherm

− The point on an adsorption isotherm's coverage axis where the linear portion is extrapolated back to zero pressure.

Point B Isotherm

− The point on an adsorption isotherm where the linear portion starts to deviate from a linear law. See figure 4.1.1.1.1.

Powder Average/Powder Pattern

− In a powder sample crystallites will be present at all orientations. The

observed relaxation times/ quadrupolar splittings etc. will be an average over the distribution of orientations. Patterns such as figure 2.1.2 result.

Q

QSV

- Quarter Swing Valve. The large valve on the cryostat's helium-4 pot pumping line. See figure 4.1.2.1.

Quadrupole Frequency/Splitting

- Frequency of precessing magnetic moments due to the interaction of a nuclear quadruple moment with a molecular EFG. See equation 8.7.5.2. If a suitably large magnetic field is applied the NMR line can be split by the quadrupolar interaction. See also NQR.

R

Registered Phase

- Localised phase in which the film's adatoms are aligned with those of the substrate. Also known as a *commensurate* phase. See figure 1.8.3.1.

Rigid Lattice

- NMR concept: A solid with insufficient internal (thermal or other) motion to enter the motional narrowing regime. $T_1 \to \infty$ & $T_2 \to 1/\sqrt{m_2}$.

Robertson's Mechanism

- Mechanism describing $1/T_2 \propto \omega_0^2$ law in relation to relaxation due to bounded diffusion of fluid ^{3}He spins in Grafoil diamagnetic fields. See page 13.

'Rule of Thumb', NMR

- Simple expression for T_2 in the motional narrowing regime. $1/T_2 = m_2\tau_c$.

S

SD3 Fit.

- Fitting function developed to model magnetic recovery of ^{11}B spins. It comprises an exponential recovery term plus a spin-diffusion limited $(Dt)^{½}$ one. It is,

$h(t) = h(0)\exp(-t/T_1) + h(\infty) + (Dt)^{½}$

Second Moment (Of the NMR line)

- Indicator of the strength of the dipolar interaction and of the width of the NMR line.

Solid Patches

- Localised patches of higher density adsorbate formed at substrate sites with a higher binding energy. See also Preferential Sites & Edge Sites.

Spectral Density Functions (dipolar)

- Functions describing the power density of the motion modulating the dipolar interaction as a function of frequency. They are the fourier transforms of the dipolar correlation functions.

Spin Cross Flipping

- A feature of strong coupled relaxation in a two-spin system. Disturbing the magnetisation of one spin system results in the magnetisation of the other flipping. See figure 7.3.1.1.

Spin-Echo

− Pulse NMR technique used to refocus transverse magnetisation with a 180º pulse. Useful to remove imperfect magnet contribution to relaxation. See page 23.

Striped Phases

− See Domain Wall Phase(s).

Sub−/Super− Exponential Relaxation

− Relaxation process proceeding slower/faster than an exponential law. See also *index* of relaxation.

Sub-region Behaviour

− Term coined to describe a phenomenon seen in the ^{3}He/BN temperature dependence data in which a certain trend is followed by the data for a few points in T, changes, follows another trend for a few points and changes again etc. etc. Such behaviour occurs within larger features of the data which describe more profound changes in the film such as phase transitions. See also 'Noise' and page 138 text.

Substrate

− Solid material used to form the adsorbed film on.

T

$\sqrt{T}$ Law

− A relaxation Times $\propto\sqrt{T}$ relation is the signature of relaxation due to the thermal motion of a spins in a 2D or 3D gas.

T_1, T_2 & T_1 minima

− T_1 : Spin-Lattice relaxation time. Characteristic time for spins to recover their (longitudinal) magnetisation from the non-spin degrees of freedom (collectively known as the *lattice*) in the system. Energy is transferred.
− T_2 : Spin-Spin relaxation time. Characteristic time for spins' transverse magnetisation to decay away via a precessional dephasing process. No energy is transferred.
− T_1 minimum: A maximum in relaxation efficiency ($1/T_1$) occurs when the time characteristic of the motion in the system (τ_c) rises or falls to fulfil a $\omega_0\tau_c\sim1$ condition where ω_0 is the Larmor frequency.

T1Index & T2Index Fits

− NLLSQ fits to the $h(t)=h(0)\exp(-t^i/T_1)+h(\infty)$ and $h(t)=h(0)\exp(-t^i/T_2)$ forms. See Listing 6.3.2.1 for the form of the T1, T2, Twoexp, Twoexp2 and Carr-Purcell (CP) fits as provided by the NLLSQ program.

T_1 Plateaux

− In the intermediate coverage region of the ^{3}He/BN phase diagram T_1 possesses flat-topped maxima (plateaux) in T − See figure 7.2.2.29. These are proposed to delimit the proposed LRPOA phase. See LRPOA & LRPOP entry.

'T_1' & 'T_1(1/e)' Datasets

− Datasets comprising values of the T_1 relaxation time (*vs T, F, X* etc.) obtained by fitting echo-height *vs* time data to single & double exponentials respectively. In the

later case T_1(1/e) is the time the fitted relaxation profile takes to recover by a factor of 1/e.

T_2 Desorption Maximum (D-max)

- The highest temperature maximum in the T_2 temperature dependence. It is proposed to be due to a change of relaxation mechanism from dipolar to 2D gas/PMI as desorption increases the ^{3}He−PMI visit rate.

T_2 Melt-Desorption Minimum (MD-min)

- The minimum in the T_2 temperature dependence. It is proposed to be due to a change of relaxation mechanism from PMI/ Fluid to dipolar as desorption begins to remove the fluid melt spins from the influence of PMIs embedded in the substrate.

T_2 Melting Maximum (M-max)

- The lowest temperature maximum in the T_2 temperature dependence. It is proposed to be due to the change of relaxation mechanism from dipolar to PMI/Fluid as melting in the localised film increases the adatom mobility enough for PMI/Fluid relaxation to dominate.

Three State Potts Model

- A critical model, a generalisation of the 2D Ising model.

Tri-critical Point

- A critical point on the phase diagram of a critical model. It delimits 3 different phases.

U

Universality Class

- A class of statistical mechanical systems displaying the same critical behaviour.

V

Virial Coefficient Theory

- A theory of imperfect gases generalised from the ideal gas law, $PV=NRT$, to $PV=NRT + A + BT + CT^2 + \ldots$ where A,B,C etc. are the virial coefficients. The most important is the second virial coefficient (ie. B) theory.

Z

Zeeman Bath/Reservoir

- Energy reservoir of spins due to their Zeeman splitting. eg. figures 3.5.3.2 & 7.4.3.13.

Glossary of Symbols

$\sqrt{3} \times \sqrt{3}$ R30 ..The commonest registered structure on graphitic substrates.

B_0 .....Applied static magnetic field in NMR experiment.

B_1 .....Applied RF magnetic field in an NMR experiment. It is applied perpendicular to B_0.

C .....Heat capacity (C/Nk).

D .....Diffusion constant.

E_a .....The film's activation energy. See Glossary of Physics Terms.

eq .....Crystalline/molecular Electric Field Gradient (EFG).

eQ .....Nuclear quadrupole moment.

F .....Frequency (Hz).

F_0 .....Larmor frequency.

F_{scale} .....Exponential T_1 law parameter. See §7.2.4.1 & page 257 for details.

F_Q .....Quadrupole frequency.

F(t).....Spin-Spin relaxation function. See §2.2.

G .....Magnetic field gradient.

g(t) .....Reduced dipolar auto-correlation function (2D systems). See §2.2.

G(t) .....Dipolar auto-correlation function. See §2.2.

$H(0)$, $h(0)$.....Initial value of the magnetisation after a pulse.

$H(\infty)$, $h(\infty)$....Equilibrium value of the longitudinal magnetisation.

I.....Spin angular momentum.

J .....The Exchange frequency.

j(ω) .....Reduced dipolar spectral-density function (2D systems). See §2.2.

J(ω) .....Dipolar spectral-density function. See §2.2.

L(t).....Spin-Lattice relaxation function. See §2.2.

m_2.....The Second Moment of the NMR line.

max & min .....Superscripts. eg. T^{max}, T_1^{min}, T_2^{max} indicates the temperature of a maximum feature in temperature, the value of T_1 at a minimum and the value of T_2 at a maximum feature respectively.

n.....Adsorbed film density (number of atoms/unit area).

Q .....Tuned circuit quality factor. eg. $R=Q\omega L$. Q is also the approximate number of cycles the tank circuit rings after a pulse.

r .....Internuclear separation of spins. eg. r_{ij} is the separation of the ith & jth spin in an ensemble.

T.....Temperature.

T_1 & T_2 .....Relaxation times, See Glossary of Physics Terms.

$T_1(0)$.....Exponential T_1 law parameter. See §7.2.4.1 & page 257 for details.

T_1(1/e).....Estimate for T_1. The (echo-height,time) data is fitted by a double exponential. This measure is the time taken for the fitted curve to decay by a factor of 1/e.

T_1(ave).....Estimate for T_1. The (echo-height,time) data is fitted by a double exponential. This measure is the weighted average of the two relaxation times from the fit. See equation 8.24.

T_2^*.....Relaxation time obtained from an FID − as T_2 but without contribution due to imperfect magnet removed.

T_2(1/e).....Estimate for T_2. See T_1(1/e) for details.

T_2(ave).....Estimate for T_2. See T_1(ave) for details.

T_2c, T_2t, T_3c ..2D, critical & triple point temperatures plus 3D

critical point temperature.

T_c^*, T_c^{**}.....The two KTHNY transition temperatures.

$T^{D\text{-}max}$ .....See Glossary of Physics

$T^{MD\text{-}min}$ ....Terms.

$T^{M\text{-}max}$ ..... " " " " "

T_{sd}.....Spin Diffusion time. See figure 3.5.3.1.

X .....Coverage (fraction of a monolayer).

X_s .....Effective coverage of substrate spins.

β.....Angle substrate-normal makes to applied magnetic field B_0 in 2D system.

γ .....Gyromagnetic ratio.

η.....Asymmetry parameter (in quadrupole systems).

τ_0.....Tunnelling attempt time in a system with thermally activated vacancy tunnelling. This symbol is also used to refer to the 'microscopic time' − effectively the correlation time in a diffusive system.

τ_c.....Correlation time, the time taken for a spin to move to a place where the magnetic environment it experiences has changed significantly.

χ.....Magnetic susceptibility.

ω .....Angular frequency (radians/sec).

ω_0.....Larmor frequency.

ω_x.....Miscellaneous frequency (eg. a substrate frequency + ^{3}He Larmor frequency).

Simple Coupled Relaxation Model Parameters

Parameters defined in figure 3.5.3.1.

T_1^i.....^{3}He spin-lattice relaxation time.

$T_1^{intrinsic}$.....Intrinsic relaxation time of bulk substrate (^{19}F) spins.

T_1^{is}.....Substrate (^{19}F) surface spins −to− ^{3}He spins coupling time.

T_1^s.....Substrate (^{19}F) surface spins spin-lattice relaxation time.

Parameters defined in figure 3.5.3.2 & 7.4.3.13.

R .....The relative decrease in the ^{3}He magnetisation on saturation of the substrate spins.

T_1 .....^{3}He Zeeman−Exchange bath coupling time.

T_c .....Substrate spins −to− ^{3}He Zeeman bath coupling time.

Chapter 8 Data Fitting Model Parameters

E_a .....The film's activation energy. See Glossary of Physics Terms.

F_Q .....The effective substrate nuclear quadrupole frequency.

m_2^{hm} .....(homonuclear) second moment. The strength of the homonuclear dipolar interaction.

m_2^{ht} .....(heteronuclear) 'second moment'. The strength of the heteronuclear dipolar interaction.

$R_{\tau 0}$.....Vacancy tunnelling attempt rate.

$R_{\tau cex}$ .....$=1/\tau_c^{ex}$, where τ_c^{ex} is the correlation time due to exchange motion. It is proportional to the exchange frequency *J*.

$\tau_c^{Jhm\_sf}$.....Correlation time scaling factor. See equation 8.7.21. It is the ratio of the correlation time modulating the homonuclear dipolar interaction to that modulating the heteronuclear one.

ρ_1, ρ_2, σ_1, σ_2 .Relaxation rate terms describing coupled relaxation. See §8.1.

a, a_1, a_2, E_{a_1}, E_{a_2}, E_{a_3}, E_{a_a}, E_{a_b}, i, $i1$, $i2$, F_{Q2}, m_2^{ht2}, $R_{\tau 0\_1}$, $R_{\tau 0\_2}$, $R_{\tau 0\_3}$, $R_{\tau 0\_a}$, $R_{\tau 0\_b}$, T_{switch}, T_{switch_1},

T_{switch_2}.....Additional model specific Chapter 8 data fitting model parameters. See §8.3 for details.

References

(**1**) D.M. Young and A.D. Crowell, "Physical Adsorption of Gases", (Butterworths, 1962).
(**2**) J.G. Dash, "Two dimensional Matter", Scientific American, **228**, 30, (May 1973).
(**3**) M.G. Richards from "Phase Transitions in Surface Films", eds. J.G. Dash and J. Ruvalds, (Plenum Press, 1980).
(**4**) S.Ross and W.W.Pultz, J. Colloid and Interface Science, **13**, 397, (1958).
(**5**) M.H. Polley, W.D. Schaeffer and W.R. Smith, J. Phys. Chem., **57**, 469, (1953).
(**6**) A. Thomy and X. Duval, J. Chim. Phys. Physiochem. Biol., **66**, 1966, (1969).
(**7**) B. Cowan, W.J. Mullin and E. Nelson, J.L.T.P., **77**, 181, (1989).
(**8**) J.G. Dash, Phys. Reports, **38**, 177, (1978).
(**9**) J.G. Dash and M. Schick, from "The Physics of Liquid and Solid Helium", Part II, eds. K.H. Bennemann and J.B. Ketterson, (John Wiley and son, 1978).
(**10**) S. Ross and W.W. Pultz, J. Colloid Science, **13**, 397, (1958).
(**11**) K.J. Strandburg, Rev. Mod. Phys. **60**, 161, (1988), (and references therein).
(**12**) J.M. Kosterlitz and D.J. Thouless, J. Phys. C, **6**, 1181, (1973).
J.M. Kosterlitz and D.J. Thouless, 373, from "Progress in Low Temperature Physics", VII-B, Ed. D.F. Brewer (North Holland, Amsterdam, 1978).
B.I. Halperin and D.R. Nelson, Phys. Rev. Lett., **41**, 121, (1978).
D.R. Nelson and B.I. Halperin, Phys. Rev. B, **19**, 2457, (1979).
A.P. Young, Phys. Rev. B, **19**, 1855, (1979).
(**13**) N. Dupont-Pavlovsky, C. Bockel and A. Thomy, Surf. Sci., **160**, 12, (1985).
(**14**) A.D. Migone, Z.R. Li and M.H.W. Chan, Phys. Rev. Lett., **53**, 810, (1984).
(**15**) M. Nielsen, J. Als-Nielsen, J. Bohr, J.P. McTague and D.E. Moncton, Phys. Rev. B, **35**, 1419, (1987).
(**16**) K.L. D'Amico, J. Bohr, D.E. Moncton and D. Gibbs. Phys. Rev. B, **41**, 4368, (1990).
(**17**) Q.M. Zhang and J.Z. Larese, Phys. Rev. B, **43**, 938, (1991).
(**18**) M. Bretz, J.G. Dash, D.C. Hickernell, E.O. McClean and O.E. Vilches, Phys. Rev. A, **8**, 1589, (1973).
(**19**) R.L. Elgin and D.L. Goodstein, Phys. Rev. A, **9**, 2657, (1974).
(**20**) H. Godfrin, from "Excitations in 2D and 3D Quantum Fluids", eds. A.G.F. Wyatt and H.L. Lauter, (Plenum Press, 1991).
(**21**) D.S. Greywall and P.A. Busch, Phys. Rev. Lett., **67**, 3535, (1991).
(**22**) S.V. Hering and O.E. Vilches, from "Monolayer and Submonolayer Helium Films", eds. J.G. Daunt and E.Lerner (Plenum Press, 1973).
(**23**) M. Bretz and J.G. Dash, Phys. Rev. Lett., **26**, 963, (1971).
(**24**) M. Bretz, G.B. Huff and J.G. Dash, Phys. Rev. Lett., **28**, 729, (1972).
(**25**) M. Schick from "Phase Transitions in Surface Films", eds. J.G. Dash and J. Ruvalds, (Plenum Press, 1980).
(**26**) M. Nielsen, J.P. McTague and W. Ellenson, J. de Phys. **38**, C4 Supp. 10, (1977).
(**27**) C.E. Campbell and M. Schick, Phys. Rev. A., **3**, 691, (1971).
Phys. Rev. A, **5**, 1919, (1972).
(**28**) S.V. Hering, S.W. van Sciver and O.E. Vilches, J.L.T.P., **25**, 793, (1976).
(**29**) R. Feile, H. Wierchert and H.J. Lauter, Phys. Rev. B, **25**, 3410, (1982).
(**30**) J.G. Dash and M. Bretz, J.L.T.P., **9**, 291, (1972).
(**31**) D.S. Greywall, Phys. Rev. B, **41**, 1842, (1990).
(**32**) R.E. Ecke, Q.S. Shu, T.S. Sullivan and O.E. Vilches, Phys. Rev. B, **31**, 448, (985).
(**33**) F.C. Motteler, Ph.D. Thesis, University of Washington, (1986).
(**34**) R.E. Ecke and J.G. Dash, Phys. Rev. B, **28**, 3738, (1983).

(**35**) S.B. Hurlbut and J.G. Dash, Phys. Rev. Lett., **53**, 1931, (1984).
Phys. Rev. Lett., **55**, 2227, (1985).
(**36**) D.S. Greywall, Phys. Rev. B, **47**, 309, (1993).
(**37**) H.J. Lauter, H. Godfrin, V.L.P. Frank and H.P. Schildberg, Physica B, **165-166**, 597, (1990).
(**38**) O.E. Vilches, Ann. Rev. Phys. Chem., **31**, 463, (1980).
(**39**) J.J. Lander and J. Morrison, Surf. Sci., **6**, 1, (1967).
(**40**) J.K. Kjems, L. Passell, H. Taub, J.G. Dash and A.D. Novaco, Phys. Rev. B, **13**, 1446, (1976).
(**41**) P.M. Horn, R.J. Birgeneau, P. Heiney and E.M. Hammonds, Phys. Rev. Lett., **41**, 961, (1978).
(**42**) J.A. Venables, H.M. Kramer and G.L. Price, Surf. Sci., **55**, 373, (1976).
(**43**) G. Boato, P. Cantini and R. Tatarek, Phys. Rev. Lett., **40**, 887, (1978).
(**44**) H. Shechter, J. Suzanne and J.G. Dash, Phys. Rev. Lett., **37**, 706, (1976).
(**45**) J. Suzanne, J.P. Coulomb and M. Bienfait, Surf. Sci., **40**, 414, (1973).
(**46**) J.G. Dash, J. Suzanne, H. Shechter and R.E. Peierls, Surf. Sci., **60**, 411, (1976).
(**47**) A. Abragam, "Principles of Nuclear Magnetism", (Oxford University Press, 1986).
(**48**) M. Santini, M. Girera and G. Careri, Phys. Lett. **5**, 102, (1963).
(**49**) G. Careri, M. Santini, and G. Signorelli from "Low Temperature Physics", Proc. LT9, **A**, 364, (Plenum Press, 1965).
(**50**) P. Monod, J.A. Cowen, Internal Report #000571, from the "Service de Physique du Solide et de Magnetic Résonance Magnétique Centre D'Etudes Nucléaires de Saclay", (Paris 1966).
(**51**) H.T. Weaver, J. Phys. Chem. Solids., **34**, 421, (1972).
(**52**) D.F. Brewer, D.J. Creswell and A.L. Thompson, Proc. LT12, 157, (Acad. Press of Japan, Tokyo, 1970).
(**53**) D.J. Creswell, D.F. Brewer, and A.L. Thompson, Phys. Rev. Lett., **29**, 1144, (1972).
(**54**) A.L. Thompson, D.F. Brewer and Y. Goto, Proc. LT14, **1**, 463, (North Holland, Amsterdam, 1975).
(**55**) R.J. Rollefson, Phys. Rev. Lett., **29**, 410, (1972).
(**56**) D.P. Grimmer and K. Luczszynski, J.L.T.P., **26**, 19, (1977).
(**57**) D.P. Grimmer and K. Luczszynski, J.L.T.P., **30**, 153, (1978).
(**58**) N. Ganguli and K.S. Krishman, Proc. Roy. Soc. London, Ser. A, **177**, 168, (1941).
(**59**) R.L. Siddon and M. Schick, Phys. Rev. A, **9**, 907, (1974).
(**60**) L. Abou-El-Nasr, Ph.D. Thesis, University of London, (1989).
(**61**) A.J. Kent, Ph.D. Thesis, University of London, (1985).
(**62**) B.P. Cowan and A.J. Kent, Phys. Lett., **106A**, 54, (1984).
(**63**) J.R. Owers-Bradley, B.P. Cowan, M.G. Richards and A.L. Thompson, Phys. Lett. **65A**, 424, (1978).
(**64**) K. Satoh and T. Sugawara, J.L.T.P., **38**, 37, (1980).
(**65**) B. Robertson, Phys. Rev., **151**, 273, (1966).
(**66**) W.J. Mullin, D.J. Creswell and B.P. Cowan, J.L.T.P., **25**, 247, (1976).
(**67**) R. Chapman and M. Bloom, Can. J. Phys., **52**, 861, (1976).
(**68**) B.P. Cowan, J.L.T.P., **50**, 135, (1983).
(**69**) N. Bloembergen, E.M. Purcell and R.V. Pound, Phys. Rev., **73**, 679, (1948).
(**70**) B.P. Cowan, J. Phys. C, **13**, 4575, (1980).
(**71**) M.G. Richards, Proc. LT15, Supp. 8, J. de Phys., **39**, C6, 1342, (1978).
(**72**) B. Cowan, L. Abou-El-Nasr and M. Fardis, Proc. LT18, Supp. 26-3, Jap. J. Appl. Phys., **26**, 307, (1987).
(**73**) H.C. Torrey, Phys. Rev., **97**, 3, (1954).
(**74**) M.G. Richards, Adv. Mag. Res., **5**, 305, (1971).
(**75**) B. Cowan, L. Abou-El-Nasr, M. Fardis and A. Hussain, Phys. Rev. Lett., **58**, 2308,

(1987).
(**76**) M. Fardis, Ph.D. Thesis, University of London, (1990).
(**77**) B. Cowan, L. Abou-El-Nasr and M. Fardis, Proc. LT18, Supp. 26-3, Jap. J. Appl. Phys., **26**, 309, (1987).
(**78**) D.S. Greywall and P.A. Busch, Phys. Rev. Lett., **60**, 1860, (1988).
(**79**) R.E. Rapp and H.Godfrin, Phys. Rev. B, **47**, 12004, (1993).
(**80**) A. Widom, J.R. Owers-Bradley and M.G. Richards, Phys. Rev. Lett., **43**, 1340, (1979).
(**81**) E.L. Hahn, Phys. Rev., **80**, 580, (1950).
(**82**) M.H. Cohen and F. Reif, "Solid State Physics", **5**, 321, (Academic Press, 1957).
(**83**) A.H. Silver and P.J. Bray, J. Chem. Phys., **32**, 288, (1960).
(**84**) P.S. Marchetti, D. Kwon, W.R. Schmidt, L.V. Interrante and G.E. Maciel, Chem. Mater., **3**, 482, (1991).
(**85**) E. Fukushima and S.B.W. Roeder, "Experimental Pulse NMR - A Nuts and Bolts Approach", (Addison-Wesley, 1981).
(**86**) M.B. Khusidman and V.S. Neshpor, Zh. Struk. Khim., **12**, 1094, (1971) [English Trans.].
(**87**) B.P. Cowan, J. Phys. C, **10**, 3383, (1977).
(**88**) A. Avogadro and M. Villa, J. Chem. Phys., **16**, 2359, (1977).
(**89**) A.A. Kokin and A.A. Izmeslev, Russ. J. Phys. Chem., **39**, 309, (1965).
(**90**) A. Landesman, Ann. Phys. Paris, **8**, 53, (1973).
(**91**) R. Kubo and K. Tomita, J. Phys. Soc. Japan, **9**, 888, (1954).
(**92**) R. Kubo, J. Phys. Soc. Japan, **17**, 1100, (1962).
(**93**) A.G. Redfield, Phys. Rev., **116**, 315, (1959).
(**94**) M. Roger, Phys. Rev. B, **30**, 6432, (1984).
(**95**) R. Thompson, from "Progress in Boron Chemistry", 2, 187, Eds. R. Brotherton and H. Steinberg, (Pergamon Press, 1970).
(**96**) "BIDS" online computer access to the Institute of Scientific Information's "Science Citation Index" at the University of Bath. (http://www.bids.ac.uk).
(**97**) M.T. Alkhafaji and A.D. Migone, Phys. Rev. B, **45**, 8767, (1992).
(**98**) M.T. Alkhafaji and A.D. Migone, Phys. Rev. B, **43**, 8741, (1991).
(**99**) T.B. Gavrilova, A.V. Kiselev, I.V. Parshina and T.M. Roshchina, Colloid Journal of the USSR, **48**, 3627, (1986).
(**100**) J.C. Delachaume, M. Coulon and L. Bonnetain, Surf. Sci., **133**, 365, (1983).
(**101**) J.P. Laheurte, J.C. Noiray, M. Obadia and J.P. Romagnan, Surf. Sci., **22**, 330, (1982).
(**102**) A. Patrykiejew, M. Jaroniec and A.W. Marczewski, Thin Solid Films, **76**, 247, (1981).
(**103**) Y. Grillet and J. Roquerol, J. Colloid and Interface Science, **77**, 580, (1980).
(**104**) C. Bockel, A. Thomy and X. Duval, Surf. Sci., **90**, 109, (1979).
(**105**) M. Matecki, A. Thomy and X. Duval, Surf. Sci., **75**, 142, (1978).
(**106**) A.C. Levy, T.R. Rybolt and R.A. Pierotti, J. Colloid and Interface Science., **70**, 74, (1979).
(**107**) J. Regnier, A. Thomy and X. Duval, J. Colloid and Interface Science, **70**, 105, (1979).
(**108**) H.E. Thomas, R.N. Ramsey and R.A. Pierotti, J. Chem. Phys. **59**, 6163, (1973).
(**109**) M. Matecki, A. Thomy and X. Duval, C. R. Acad. Sc. Paris, 274, C-15, (3rd Jan 1972).
(**110**) R.N. Ramsey, H.E. Thomas, R.A. Pierotti, J. Phys. Chem. **76**, 3171, (1972).
(**111**) R.A. Pierotti and R.E. Smallwood, J. Colloid and Interface Science, **22**, 469, (1966).
(**112**) R.A. Pierotti, J. Phys. Chem. **66**, 1810, (1962).
(**113**) R.A. Pierotti, J. Chem. Phys., **36**, 2515, (1962).

(**114**) S. Ross and W.W. Pultz, J. Colloid and Interface Science, **13**, 397, (1958).
(**115**) G. Curthoys and P.A. Elkington, J. Phys. Chem. **71**, 1477, (1966).
(**116**) X. Zhang and T.R. Rybolt, J. Colloid and Interface, Science, **50**, 575, (1992).
(**117**) M.D. Evans, N. Patel and N.S. Sullivan, J.L.T.P., **89**, 653, (1992).
(**118**) A.D. Migone, A.T. Alkhafaji, G. Vidali and M. Karimi, **47**, 6685, (1993).
(**119**) M.D. Evans and N.S. Sullivan, J.L.T.P., **100**, 551, (1995).
(**120**) M.D. Evans and N.S. Sullivan, J.L.T.P., **100**, 535, (1995).
(**121**) K. Kim, J.R. Bodart and N.S. Sullivan, Cryogenics, **36**, 311, (1996).
(**122**) K. Morishige, K. Inoue and K. Imai, Langmuir, **12**, 4889, (1996).
(**123**) M. Fanciulli and M. Corti, Phys. Rev. B, **52**, 11872, (1995).
(**124**) K. Kim, J.R. Bodart, N.S. Sullivan, Czech. J. Phys., **46**, 515, (1996).
(**125**) T. Shibata, Y. Murakami, T. Watanuki and H. Suematsu, Czech. J. Phys., **46**, 1931, (1996).
(**126**) M. Karimi and G. Vidali, Phys. Rev. B, **36**, 7576, (1987).
(**127**) M. Karimi and G. Vidali, Phys. Rev. B, **34**, 2794, (1986).
(**128**) A. Patrykiejew, M. Jaroniec and A.W. Marczewski, Chemica Scripta. **22**, 136, (1983).
(**129**) B. McCarrol and R.P. Messmer, Surf. Sci., **27**, 451, (1971).
(**130**) R.A. Pierotti and J.C. Petricciani, J. Phys. Chem., **64**, 1596, (1960).
(**131**) Online computer access to “Chemical Abstracts”, the American Chemical Society, via ESA-QUEST database system, (http://www.esrin.esa.it/htdocs/esairs/overview.html).
Online computer access to INSPEC literature search database system (http://hplus.harvard.edu/alpha/INS.html).
(**132**) R. Groβe and B. Boddenberg, Zeitschrift für Physikalische Chemi Neue Folge, **152**, 12, (1987).
(**133**) B. Boddenberg and V. Grundke, Zeitschrift für Naturforschung **46A**, 211, (1991).
(**134**) A. Patrykiejew, Thin Solid Films, **76**, 241, (1981).
(**135**) S. Ross and I. Morrison, Surf. Sci., **52**, 103, (1975).
(**136**) B.P. Cowan and A.J. Kent, J.L.T.P., **57**, 589, (1984).
(**137**) R.S. Pease, Acta. Cryst., **5**, 356, (1952).
(**138**) J. Zupan, M. Komac and D. Kolar, J. Appl. Phys., **41**, 5337, (1970).
(**139**) L.J. Friedman, P.J. Millet and R.C. Richardson, Phys. Rev. Lett., **47**, 1078, (1981).
(**140**) E.I. Dupont DeNemours and Co., Wilmington, DE 19898.
(**141**) R.C. Richardson, Physica B, **126**, 298, (1984).
(**142**) L.J. Friedman, T.J. Gramila and R.C. Richardson, J.L.T.P., **55**, 83, (1984).
(**143**) Y.J. Brown, J.L.T.P., **60**, 183, (1985).
(**144**) L.J. Friedman, P.J. Millet and R.C. Richardson, Physica B, **108**, 837, (1981).
(**145**) O. Gonen and J.S. Waugh, Physica A, **156**, 219, (1987).
(**146**) A. Schuhl, F.B. Rasmussen and M. Chapellier, J.L.T.P., **57**, 483, (1984).
(**147**) Q. Geng, M. Olsen and F.B. Rasmussen, J.L.T.P., **74**, 369, (1989).
(**148**) M. Chapellier, J. de Phys. Lett., **43**, 16, (1982).
(**149**) M. Chapellier, G. Dreyfus, H. Alloul and J. Cowen, Proc. LT17, **2**, 747, (Elsevier Science, 1984).
(**150**) A. Schuhl, S. Maegawa, M.W. Meisel and M. Chapellier, Phys. Rev. B, **36**, 6811, (1987).
(**151**) A. Schuhl, F.B. Rasmussen and M. Chapellier, Proc. LT17, **2**, 749, (Elsevier Science, 1984).
(**152**) P.C. Hammel and R.C. Richardson, Phys. Rev. Lett., **52**, 1441, (1984).
(**153**) S. Maegawa, A. Schuhl, M.W. Meisel and M. Chapellier, Euro Phys. Lett., **1**, 83, (1986).
(**154**) S. Maegawa, A. Schuhl, M.W. Meisel and M. Chapellier, Proc. LT18, Supp. 26-3, Jap. J. Appl. Phys., **26**, 323, (1987).

(**155**) P.C. Hammel, P.L. Gonen and J.S. Waugh, Phys. Rev. B, **34**, 6543, (1986).
(**156**) Aldrich Chemical Co., Steinheim, Germany, No.18. 247-8.
(**157**) Q. Geng, M. Olsen and F.B. Rasmussen, Proc. LT18, Supp. 26-3, Jap. J. Appl. Phys., **26**, 329, (1987).
(**158**) O. Gonen, P.L. Kuhns, C. Zuo and J.S. Waugh, J. Mag. Res., **81**, 491, (1989).
(**159**) D.R. Swanson, D. Candela and D.O. Edwards, Proc. LT18, Supp. 26-3, Jap. J. Appl. Phys., **26**, 313, (1987).
(**160**) D.R. Swanson, D. Candela and D.O. Edwards, J.L.T.P., **72**, 213, (1988).
(**161**) P. Kuhns, O. Gonen and J.S. Waugh, J. Mag. Res., **82**, 231, (1989).
(**162**) F.W. van Keuls, T.J. Gramila, L.J. Friedman and R.C. Richardson, Physica B, **165-166**, 717, (1990).
(**163**) A.E. Egorov, F.L. Aukhadeev, M.S. Tagirov and M.A. Teplov, J.E.T.P. Lett., **39**, 585, (1985).
(**164**) J. Aubrey and A.A.V. Gibson, Phys. Rev. B, **39**, 3959, (1989).
(**165**) J.V. Gates and W.H. Potter, Proc. LT14, **4**, 5 (North Holland, 1975).
(**166**) Y. Hu, G.J. Stecher, T.J. Gramila and R.C. Richardson, Phys. Rev. B, **54**, 9639, (1996).
(**167**) B. Cowan, Measurement Science and Technology, **3**, 296, (1992).
(**168**) P. Cockerell, "ARM Assembly Language Programming", (MTC, UK, 1987).
(**169**) A and N van Someren, "Archimedes Operating System", (Dabs Press, 1988).
(**170**) "VL86C010 32-bit RISC MPU and Peripherals Users Manual", (Prentice Hall, 1989).
(**171**) "IEEE Standard Digital Interface for Programmable Instrumentation", ANSI/IEEE Std 488-1978 and Suppl., (USA, 1979).
(**172**) "IEEE-488 Interface Expansion for the Archimedes Computer", Intelligent Interfaces LTD, P.O. Box 80, Eastleigh, Hants. SO5 2AB, UK.
(**173**) "Rockwell 1985 Data Book, Semiconductor Products Division", Rockwell International Corporation, USA.
(**174**) J. Rouquerol, S. Partyka and F. Rouquerol, J. Chem. Soc. Faraday Trans., **73**, 306, (1977).
(**175**) "RISC OS Programmers Reference Manual", (Acorn Computers, 1989).
(**176**) "Archimedes I/O Podule Guide", (Acorn Computers, 1987).
(**177**) T.P. Crane and B.P. Cowan, Laboratory Microcomputer, **7**, 13, (1988).
(**178**) A.C. Rose-Innes, "Low Temperature Laboratory Techniques", (The English Universities Press, 1973).
(**179**) F.E. Hoare, L.C. Jackson and N. Kurti, "Experimental Cryophysics", (Butterworths, 1961).
(**180**) R.L. Rusby, J.L.T.P., **58**, 203, (1985).
(**181**) M. Farmer, "The Intensive C Course", (Chartwell-Bratt, 1987).
(**182**) B.W. Kernighan and D.M. Ritchie, "The C Programming Language", Second Edition, (Prentice Hall, 1988).
(**183**) C. Hastings, "Approximations For Digital Computers", (Oxford University Press, 1955).
(**184**) T.P. Crane and B.P. Cowan, Laboratory Microcomputer, **6**, 117, (1987).
(**185**) "Project 60969", 3T Superconducting Magnet, Oxford Instruments, Oxford, UK, (1990).
(**186**) "SPY2, Debugging Monitor and Utilities ROM", System Software LTD., 12 Collegiate Crescent Sheffield, UK, (1984).
(**187**) M. Plumbley, "BASIC ROM User Guide For the BBC Microcomputer and Acorn Electron", (Adder, 1985).
(**188**) "ADE+, Reference and Tutorial Guide", System Software LTD., 12 Collegiate Crescent Sheffield, UK, (1986).
(**189**) "TMS9914 GPIB Adapter Preliminary Data Manual", Texas Instruments LTD.,

(Sep. 1979).
(**190**) A. Dickens and M. Holmes, "The New Advanced User Guide for BBC Master, Compact, B, B+ and Electron", (Adder, 1987).
(**191**) A.G. Ray, Wireless World, PP.24-26,P.43, (Feb. 1984).
(**192**) "Data Converter Reference Manual", 1, Analog Devices, (1992).
(**193**) J.S. Murday, J. Mag. Res. **10**, 111, (1973).
(**194**) "VAX-PCA, Guide to VAX Performance and Coverage", Digital Equipment Corporation, Maynard Mass., USA, (1987).
(**195**) J. Wood, "Non-Linear Least Squares Methods for Parameter Estimation", EP6005, Private Communication, Queen Mary College, University of London, (1972).
(**196**) D.W. Marquardt, J. Soc. Indust. Appl. Math. **11**, 431, (1963).
(**197**) R. Fletcher, A.E.R.E. Report, R6799, Harwell, UK, (1971).
(**198**) B.P. Cowan, notes on "Regression Techniques", (April 1985, unpublished).
(**199**) N. Gastinel, "Linear Numerical Analysis", (Kershaw, London, 1983).
(**200**) R.E. Bellman, R.E. Kalaba and J.A. Lockett, "Numerical Inversion of the Laplace Transform", (Elsevier, 1966).
(**201**) K.P. Whittall and A.L. MacKay, J. Mag. Res., **84**, 134, (1989).
(**202**) K.P. Whittall, M.J. Bronskill and R.M. Henkelman, J. Mag. Res., **95**, 221, (1991).
(**203**) "NAG FORTRAN Library Manual, Mk.12", The Numerical Algorithmns Group LTD. Oxford, UK, (1987).
(**204**) J. Kärger, H. Pfeifer and W. Heink, Adv. Mag. Res., **12**, 1, (1988).
(**205**) P. Deschamps, J. Vaissière and N.S. Sullivan, Rev. Sci., Intrum., **48**, 664, (1977).
(**206**) J. Saunders, C.P. Lusher and B.P. Cowan, Phys. Rev. Lett., **64**, 2523, (1990).
(**207**) M.F. Secca and M.G. Richards, Proc. LT17, **2**, 741, (Elsevier Science, 1984).
(**208**) B.P. Cowan, D. Phil. Thesis, University of Sussex, (1976).
(**209**) B.P. Cowan, M.G. Richards, A.L. Thompson and W.J. Mullin, Phys. Rev. Lett., **38**, 165, (1977).
(**210**) H. Wierchert, Physica B, **169**, 144, (1991).
(**211**) J.R. Owers-Bradley, D. Phil. Thesis, University of Sussex, (1978).
(**212**) A.H. Silver and P.J. Bray, J. Chem. Phys., **29**, 984, (1958).
(**213**) C. Connor, J. Chang and A. Pines, Rev. Sci., Instrum. **61**, 1059, (1990).
(**214**) T.L. Hill, "An Introduction to Statistical Thermodynamics", (Addison-Wesley, 1962).
(**215**) H. Freimuth, W. Wierchert, H.P. Schildberg and H.J Lauter, Phys. Rev. B, **42**, 587, (1990).
(**216**) W.T. Martin and E. Reissner, "Elementary Differential Equations", (Addison-Wesley, 1956).
(**217**) J.R. Brookeman, M.M. McEnnan and T.A. Scott, Phys. Rev. B, **4**, 3661, (1971).
(**218**) F.W van Keuls, T.J. Gramila, L.J. Friedman and R.C. Richardson, Physica B, **165-166**, 717, (1990).
(**219**) F.W. van Keuls, Ph.D. Thesis, Cornell University, (1992).
(**220**) T.P. Das and E.L. Hahn, "Nuclear Quadrupole Resonance Spectroscopy", Solid State Physics, Supplement 1, (Academic Press, 1958).
(**221**) Microchip Technology Inc., (http://www.microchip.com).
(**222**) Digital Equipment Corp., (http://www.workstation.digital.com).
(**223**) L. Roobol, (roobol@kvi.nl), Private Communication, Kernfysisch Versneller Instituut, Groningen, The Netherlands, (http://www.kvi.nl), (1996).
(**224**) G.W.C. Kaye and T.H. Laby, "Tables of Physical and Chemical Constants", 14th Edition, (Longmans, 1973).